N° d'ordre: 40083

Université Lille 1

Ecole Doctorale « Sciences de la Matière, du Rayonnement et de l'Environnement »

Laboratoire « Géosystèmes » - UMR CNRS 8157

Thesis submitted to the Université Lille 1 for obtain the degree of Doctor of University

Speciality: « Geosciences, Ecology, Palaeontology and Oceanography »

Presented by

Jean Carlos MONTERO SERRANO
MSc. in Geochemistry, Universidad Central de Venezuela, Venezuela

---

Sedimentary and paleoclimate dynamics of the Gulf of Mexico during the last glacial cycle

---

Date of Approval: 20th November 2009, Villeneuve d'Ascq, France

Accepted on the recommendation of:

Christian ROBERT, Professor, CEREGE – Aix en Provence; **reporter**
Francis GROUSSET, Research director, OASU – Université Bordeaux 1; **reporter**
Benjamin FLOWER, Professor, USF – College of Marine Science, Florida; **examiner**
Laurent LABEYRIE, Professor, LSCE − CNRS, Gif-sur-Yvette; **examiner (Chair of Committee)**
Viviane BOUT-ROUMAZEILLES, Researcher − CNRS, Université Lille 1; **director**
Nicolas TRIBOVILLARD, Professor, Université Lille 1; **director**

N° d'ordre: 40083

Université Lille 1

Ecole Doctorale « Sciences de la Matière, du Rayonnement et de l'Environnement »

Laboratoire « Géosystèmes » - UMR CNRS 8157

Thesis submitted to the Université Lille 1 for obtain the degree of Doctor of University

Speciality: « Geosciences, Ecology, Palaeontology and Oceanography »

Presented by

Jean Carlos MONTERO SERRANO
MSc. in Geochemistry, Universidad Central de Venezuela, Venezuela

---

Sedimentary and paleoclimate dynamics of the Gulf of Mexico during the last glacial cycle

---

Date of Approval: 20th November 2009, Villeneuve d'Ascq, France

Accepted on the recommendation of:

Christian ROBERT, Professor, CEREGE – Aix en Provence; **reporter**
Francis GROUSSET, Research director, OASU – Université Bordeaux 1; **reporter**
Benjamin FLOWER, Professor, USF – College of Marine Science, Florida; **examiner**
Laurent LABEYRIE, Professor, LSCE − CNRS, Gif-sur-Yvette; **examiner (Chair of Committee)**
Viviane BOUT-ROUMAZEILLES, Researcher − CNRS, Université Lille 1; **director**
Nicolas TRIBOVILLARD, Professor, Université Lille 1; **director**

To my family,

To Jean-Alejandro,

"Mon père me disait toujours:
Mons fils soit prudent,
Quand je pense au futur,
Je n'oublis pas mon passé…!"

"My father always said me:
My sons are careful,
When I think on the future,
I do not forget my past…!"

Paulinho da viola, 1972

Acknowledgements

How does one condense three years of new experiences into a few paragraphs? Clear, many people supported my work scientifically and non-scientifically and I would like to thank them all.

For starters, I have been profoundly lucky to have two amazing advisors: Viviane Bout-Roumazeilles and Nicolas Tribovillard, I would like to thank for accepting me as a PhD student and supporting me throughout the time being in Lille. Thanks for taking time and having patience with me, for giving me motivation for continued efforts, and for introducing me into the "Paleoclimatology-world". I hope that our cooperation will continue.

In particular, I would like to thank my co-advisors Armelle Riboulleau and Aloys Bory (dear friend) for all the support, patience, understanding and motivating enthusiasm. Thomas Sionneau and Benjamin Flower are thanked for challenging discussions about the Gulf of Mexico.

I also want to acknowledge the rest of the members of my committee: Christian Robert, Francis Grousset, Benjamin Flower and Laurent Labeyrie, for their scientific contribution and constructive reviews.

We thank Yvon Balut, the Institut Paul-Emile Victor (IPEV), the officers and crew of the R/V Marion Dufresne and the IMAGES program for core collection.

Thanks to the technical and administrative staff of the Géosystèmes lab: Léa-Marie Emaille, Laurence Debeauvais, Deny Malengros, Philippe Recourt, Déborah Ponleve, Sylvie Regnier, Monique Gentric & Pascal Ciurlik. All the other people at the U.F.R. des Sciences de la Terre, Université Lille 1, who make this place great to work at.

I am grateful to François Baudin (Université Pierre et Marie Curie - Paris 6) and Geremie Letort (Institut Français du Pétrole, IFP) for performing the Rock-Eval analyses.

Thanks also to Richard Poore, Eric Grimm, Lee Nordt, Dirk Nürnberg, Martin Ziegler, Paul Mayewski and David Hodell for providing data.

Daniel Muhs, Michael Blum, Tammy Rittenour, Debra Willard and Nele Meckler are acknowledged for helpful insights and discussions at various points: evidences of a warmer last interglacial mid-continent North America (D.M.), Fluvial Evolution of the Mississippi River (M.B. & T.R.), Pollen distribution from NE North America (D.W.), and Holocene climate variability in the Mississippi catchment (N.M.); this thesis benefited greatly from their involvement.

Thanks also to Manuel Martínez (dear friend), Tommaso Tosiani, and Eduardo Carrillo for all the support and openness. I hope that our cooperation will continue.

I want to thank all my old and new colleagues in Sciences de la Terre from Université Lille 1: *Laurent Riquier, Skonieczny Charlotte, Aurélien Delabroye, Arnaud Bignon, Zhenxuan Li, Idrissa Karaboily, Aurélien Lacoste, Nicolas Sellier, Pitaksit Ditbanjong, Hélène Goubel, Louriño Cabana Beatriz, Kadlecova Milada, Jean-Philippe Ursule, Lefebvre Vincent, Minguely Bruno, Wane Ousmane, Marie Patin, Erika Araujo, Rodrigo Perovano, Oriol Ferrer*, who contributed in one way or the other to this work, most of it being company, lunch, provision with coffee or scientific discussions.

To "Dream Team" of Venezuelans in Sciences de la Terre, Lille: Maria Fernanda Romero, Melesio Quijada and Brenda Omaña thanks for its support and company, success for the future, always positive!

Acknowledgements

La Maison Bleue (**2006-2007**: *Tim De Buyser, Elisa Lacambra, Adriaan Coppens, Isabel Royo, Matthias Geeroms, Sibylle Delbecque, Valerie Jordan, Xavier Arumí, Marcelo DiMaria, Kilian Seitz, Anika Bührdel, Angelika Nesterski*), la Maison Bleue (**2007-2008**: *Aoife Nally, Gilles Scheen, Gonzalo Jiménez, Lina Martínez, Luis Arcas, Maria Swan, Olivia Barry, Alicia Payo, Marina Aguilera, Sorcha Hanratty*), la Maison Bleue (**2008-2009**: *Fadi Gebawi, Fanxi Delarue, Vivian Ferreira Paes, Jesús Barrientos Loaiza, Paula Rodriguez, Jie Xiao, Jose Galvez, Pascual Junquera, Pilar Almenar, and Ghirish Kumar*), and M. and Mme. Thomas, are all also thanked for the many ways in which they made life easier for me (and everyone else) every single day.

My cosmopolitan's friends (*Arnaud Augert, Cédric Dercy, Guillaume Thomas, Houssem Kasdallah, Geoffray Laumet, Francisca Redunante, Stoyan Ivanov, Iwona Krzyzanowska, Julien Sîeve, Flore Debout, Meryl Bultez, Nicolas Malaquin, Arnaud Moroy, Sandrine Pastor, Véro Flye Sainte Marie, Aurore Pic, Aurore and Boris Segbenou, Mahmoud Fatene, Floriane Robin, Natalia Szweda*), for their interest and for reminding me, that there is also a world outside science. To all you huge thanks for all the evenings with good football, parties, games (PES, FIFA), cocktails, dances (salsa, merengue, bachata, etc), dinners, and much more. Arnaud, Cédric, Guillaume and Houss, I estimate very much the help and advices that you offered to me.

Jhonny Mendoza, Bianca De Carvalho Pinheiro, Joselys Fermin, Paola Pertuz, Daniel Salazar, Igor García, Lucia Fermin, Roberto and Paulina for their support and the good times in the Lille, Paris, and beyond.

Ana Fermin and Lisandro Fermin, thanks for receiving me in Paris (October, 2006), helping me and supporting me throughout the time being in France. I consider them with my brothers. In spite of the time, I remember even your master lectures on statistics in the Central University of Venezuela (UCV) in Caracas (winter, 2003).

Cadenas family: Pedro, Lenys, Synel, Daniela and Pierina huge thanks for all the evenings with good food, company, hospitality, and to accept me as one more of the family. Pedro and Lenys thanks for cheering me up in difficult times.

Finally, cheers to all my friends in Venezuela (*Carlos Barrios, Germán Velásquez, Eduardo Barreto, Roberto Camacaro, Lisandro Moronta, Marcos Salinas, Jean Carlos Rodriguez, Viviana Lucero, Elvio Barco, Josefina Rodriguez, Nathalie Pérez, Geysi Palacios, Maicol Ochoa, Vannesa Bastos, Vikmar Kawka*), in spite of the distance, our friendship is continued maintaining throughout the time.

I am grateful to Sophie Algarte for your company, kindness, and by their warmhearted and love.

Last and most importantly, I want to thank my family (Montero, Serrano, Levy, Sanchez, Arvelo) for being there.

This thesis is dedicated to my son Jean-Alejandro (Mi Sol). We have been separated for a long time, but I hope that this effort gives its fruits in the future. Forgive me for not being in person to your side.

This PhD thesis was financially supported by: (1) the UMR Géosystèmes of the Université Lille 1 (France), and (2) the ***Program Alban****, the European Union Program of High Level Scholarships for Latin America, scholarship* ***No. E06D100913VE****.*

Table of Contents

List of figures

Chapter 1 - General introduction

Chapter 2 - The Pigmy Basin: core MD02-2553

Table of Contents

Table of Contents

Chapter 3 - The La Salle Basin: core MD02-2549

Table of Contents

Chapter 4 - Synthesis

Chapter 5 - Summary, main conclusions and outlook

List of tables

Chapter 2 - The Pigmy Basin: core MD02-2553

Chapter 3 - The La Salle Basin: core MD02-2549

Chapter 1

General introduction

1.1. Scientific background and motivation

Global climate changes are directly controlled by the activity of the thermohaline circulation (e.g., Rahmstorf, 2002, 2006). In the North Atlantic Ocean, the surface oceanic heat transfer from subtropical-tropical regions towards high-northern latitude is controlled by the hydrology of the Caribbean Sea (Fig. 1.1).

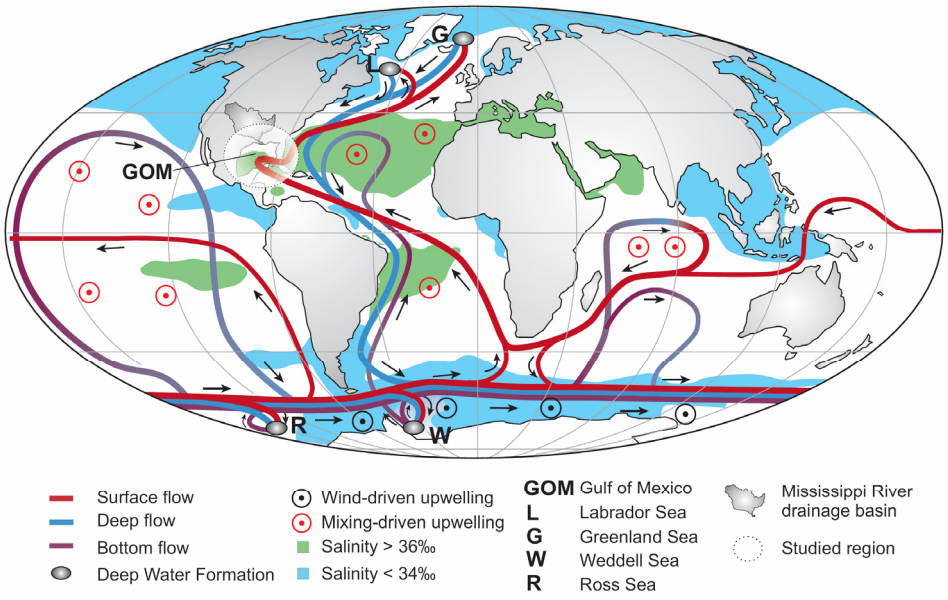

Fig. 1.1. Schematic representation of the global thermohaline circulation. Surface currents are shown in red, deep waters in light blue and bottom waters in dark blue (adapted from Rahmstorf, 2006).

Climate dynamic in the Caribbean region is seasonally modulated strongly by latitudinal migration of the Intertropical Convergence Zone (ITCZ) and the Atlantic Warm Pool (AWP, a large body of warm and salty water that in summer comprises the Gulf of Mexico, the Caribbean Sea, and the western tropical North Atlantic) (Poore et al., 2004; Ziegler et al., 2008). These characteristics results in a rainy season during northern hemispheric summer and a dry season during northern hemispheric winter. The warm tropical water masses originating from the Caribbean Sea flow into the Gulf of Mexico (GOM), via the Loop Current (Fig. 1.2). During their transit the hydrological properties of this warm water-mass are likely influenced by freshwater discharges from the Mississippi River (e.g.,

Nürnberg et al., 2008). This modified water mass then exits towards the North Atlantic Ocean and forms the Gulf Stream. Thus, tiny hydrological modifications occurring over the Caribbean region and GOM may affect the subpolar North Atlantic oceanography and consequently the NW-European climate (Fig. 1.1).

On this basis, the GOM is an important component of the global thermohaline circulation and consequently of the global climate system (Fig. 1.1). Therefore, this represents a key location to study the links between the subtropical hydrology and the high-latitude climatic variability. Additionally, it is the most important heat and moisture source toward central North America (Fig. 1.2). Warm/moist GOM air masses from the Caribbean Sea interact with dry/cold polar air masses from N/NW North America and form rainfall fronts. Long-term hydrographic changes in the GOM may thus have had a profound effect on both regional climate and moisture transport towards high northern latitudes ranging from orbital to sub-millennial time scales (e.g., Poore et al., 2003, 2004, 2005; Richey et al., 2007; Nürnberg et al., 2008). These aspects highlight the need for a better understanding of the relationships between freshwater inputs in the GOM (e.g., meltwater during deglaciation, runoff plus precipitations during the Holocene) and oceanic thermohaline circulation changes.

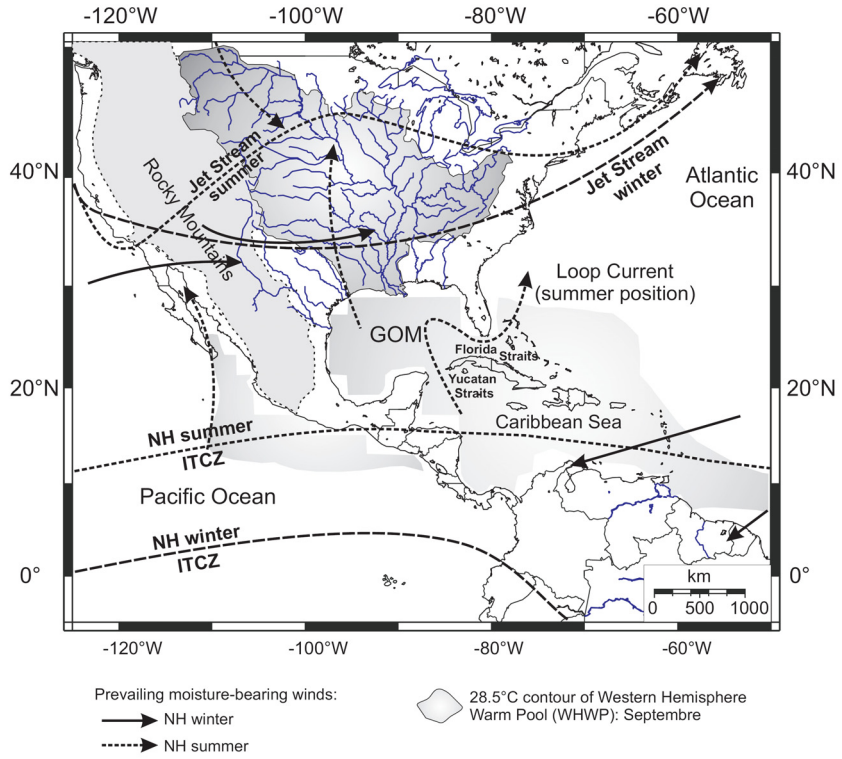

Fig. 1.2. Map showing the generalized position of the Intertropical Convergence Zone (ITCZ) for Northern Hemisphere (NH) winter and summer (adapted from Ziegler et al., 2008), the mean configuration of the middle-latitude jet stream during winter and summer regimes (adopted from Knox 2000, 2003), and 28.5°C contour of Western Hemisphere Warm Pool (Wang and Enfield, 2001). GOM: Gulf of Mexico.

North America was repeatedly covered by a massive sheet of ice during the Quaternary, the so-called Laurentide Ice Sheet (LIS). Numerical models reveal that during the last climatic cycle (since ~120 ka BP) the LIS experimented four periods of important expansion or growth phases (110, 90, 60 and 20 ka BP) interrupted by a major retreat phases between 27 and 30 ka BP (Marshall et al., 2000; Dyke et al., 2003, 2004). The LIS reached its maximum extension and elevation during the last glacial maximum (LGM: 26-20 ka BP; Peltier and Fairbanks, 2006), and then started to decrease (21-7 ka BP). Accordingly, there are several evidences that LIS meltwater discharges entered the GOM both (1) during deglaciation (e.g., Joyce et al., 1993; Aharon, 2003; Flower et al., 2004; Meckler et al., 2008; Sionneau et al., in revision), and (2) during intermediate ice volumes as during MIS 3 (Hill et al., 2006) and during some other intervals, e.g. Late Pleistocene to Early Pleistocene (Joyce et al., 1993). The timing and magnitude of LIS meltwater input to the GOM and/or meltwater diversion to the North Atlantic via the St. Lawrence River (e.g., Carlson et al., 2007), Hudson River (e.g., Donnelly et al., 2005), Arctic Ocean (e.g., Tarasov and Peltier, 2006) and the Hudson Strait (e.g., Broeker, 2006) may have influenced North Atlantic Deep Water (NADW) formation and hence regional to global climate. In particular, low-density meltwater from LIS and freshwater outburst from glacial Lake Agassiz may have inhibited deep convection in the North Atlantic and reduced northward heat transport, leading to regional cooling during the Younger Dryas, ca. 12.8-11.2 ka (e.g., Keigwin et al., 1991) and the 8.2 ka cool event (e.g., Kleiven et al., 2008).

Although the general history of LIS advance/retreat has been documented for North America, as well as its associate proglacial lake outbursts and meltwater outflows, and more recent Mississippi megafloods episodes (e.g., Knox, 2000, 2003; Rittenour et al., 2007; Bettis et al., 2008), the chronological resolution for terrestrial deposits (e.g., the Mississippi Valley) is lower than for marine counterparts on the continental margin (e.g., GOM). Besides, these climatic records are difficult to interpret on the North American continent because the glacier ice advance/retreat or megaflood induced erosion, which may modify and/or completely erase the original depositional signature. The GOM is strongly influenced by both marine sedimentary dynamics and continental erosion derived from of a large part of North America and brought to the Gulf mainly via the Mississippi River, which receives discharge from the Missouri and Ohio rivers and drains North America between the Appalachian and Rocky Mountains (Davies and Moore, 1970; Flocks and Swarzenski, 2007). Thus, hemipelagic sediment sequences deposited in the northern GOM are ideal for reconstructing continental

events because the terrestrial processes, though very subtle, recorded by siliciclastic sediments can be studied at high resolution, thanks to high sedimentation rates.

In this context, fluvial dynamics of the Mississippi River is both influenced by sediment load contributions and the hydrologic regime over midcontinent North America. During the Late Quaternary, the hydrological features of the GOM were strongly modified by the fluvial freshwater discharge of the Mississippi River resulting from two main climatic factors:

(1) Melting pulses of the LIS during glacial periods (e.g., Leventer et al., 1982; Joyce et al., 1993; Licciardi et al., 1999; Aharon, 2003; Flower et al., 2004; Sionneau et al., in revision).

(2) Episodes of high continental precipitation and large Mississippi River floods during interglacial times (e.g., Knox, 2000, 2003; Bettis et al., 2008).

As mentioned above, the LIS extension had continual fluctuations tuned to high-frequency climatic oscillations during the last climatic cycle (e.g., Dyke et al., 2003, 2004). The variations of the insolation controlled by the orbital parameters seem to constitute the first factor influencing the long-term evolution of the LIS (e.g., Huybers, 2006; Raymo et al., 2006). Its southern edge was especially unstable and reveals several retreat and advance phases related to decrease/growth phases of the ice-sheet. As a result of these successive phases of growth/decay, both the erosion zones and geometry of the continental areas drained by the Mississippi River changed considerably through time (e.g., Sionneau et al., in revision). These changes modified both the quantity and the nature of the terrigenous particles eroded and transported by the Mississippi River towards the GOM (Fig. 1.3). Consequently, the sediments in the GOM may record very precisely the changes in the geometry of the continental ice-sheet.

By contrast, during intervals of lower ice volume and more notably in the Holocene following the recession of the LIS (ca. 8 ka), the fluvial dynamics of the Mississippi River are controlled mainly by the position of precipitation belt over the North American continent, which is closely connected to the general location of the Jet Stream and Bermuda subtropical high (Forman et al., 1995; Pidwirny, 2006) and the resulting meridian moisture transfer towards the North American continent (Fig. 1.4). This rainfall front hovers between the north-western and eastern parts of the Mississippi River watershed.

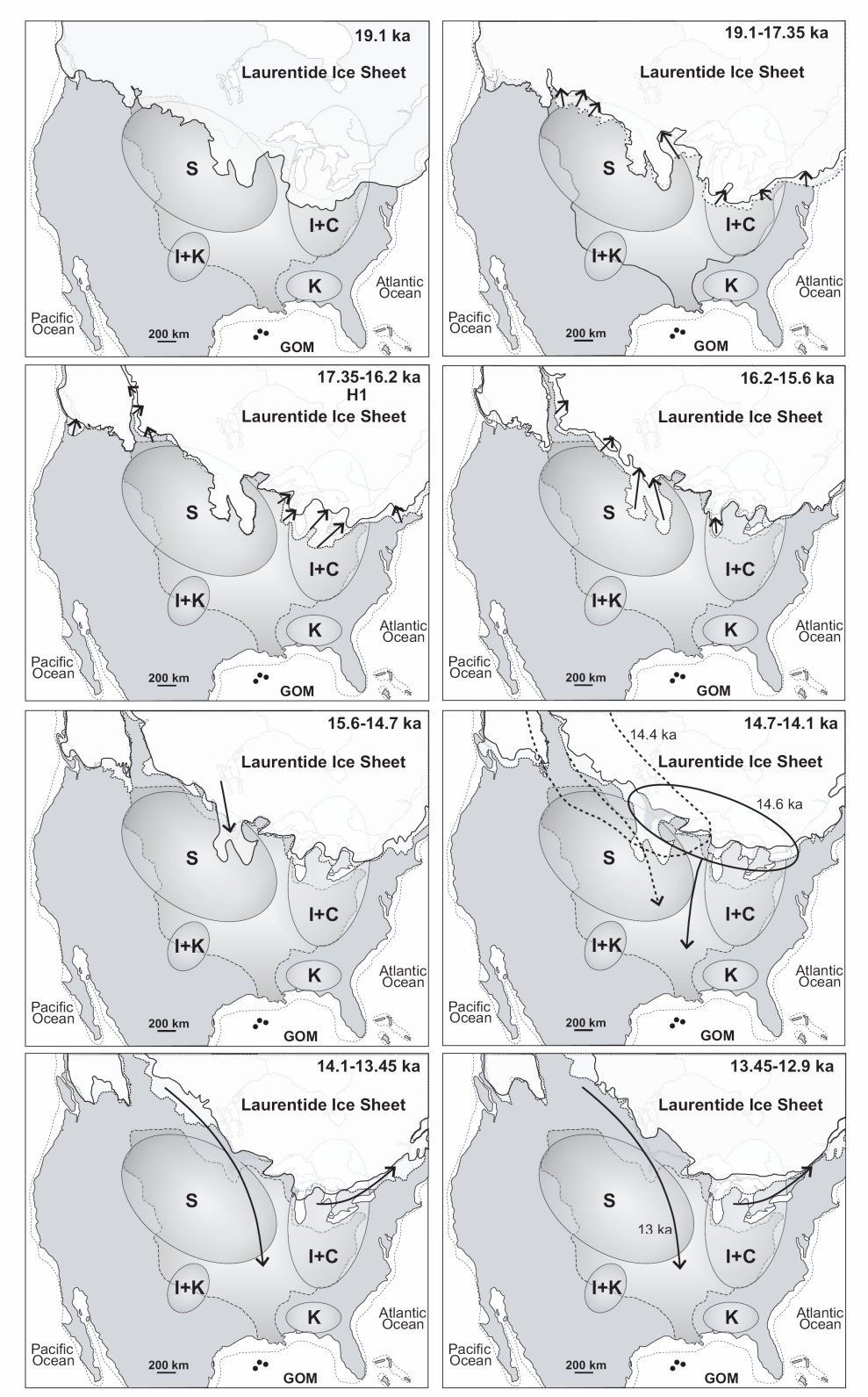

Fig. 1.3. Evolution of the southern margin of the LIS from 19.1 to 12.9 ka (adapted from Sionneau et al., in revision). Dotted and plain lines mark the position of the southern margin at the beginning and end of the interval respectively. White shaded areas correspond to important retreat of the margin over the time-slices. Solid and dotted arrows indicate drainage patterns of the LIS over the different time slices (Tarasov and Peltier, 2006). The letters S, I, C and K (standing for smectite, illite, chlorite and kaolinite, respectively) indicate areas where the bedrock/soils contain a clay-mineral assemblage markedly dominated by one clay species. GOM: Gulf of Mexico.

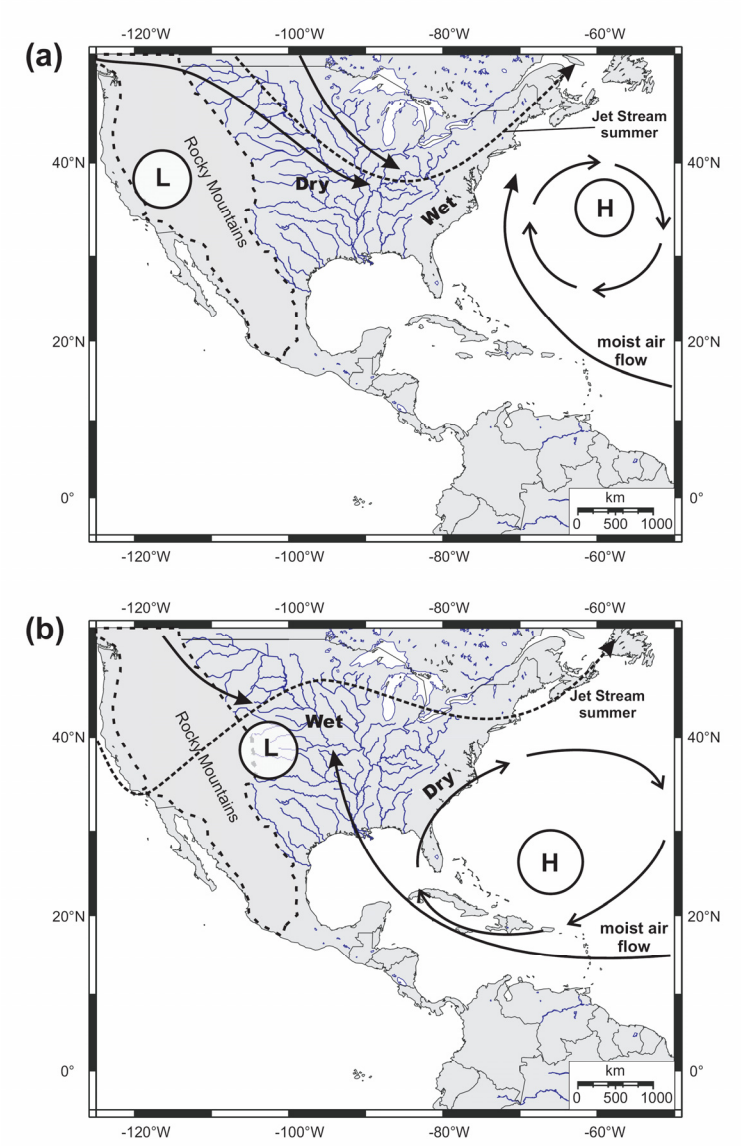

Fig. 1.4. Generalized reconstructions of regional atmospheric circulation patterns during the Holocene summer in the middle-latitude North America and their paleoclimatic implications (adapted from Forman et al., 1995; Liu and Fearn, 2000). (a) Configuration during predominant dry periods in central North America. (b) Configuration during predominant wet periods in central North America. The mean configuration of the middle-latitude Jet Streams (adapted from Knox 2000, 2003) denote the approximate boundaries of air masses from tropical, pacific and polar-source regions and locations of the areas with the main moisture transfers over the North American continent.

Investigations on the regional hydrologic responses to large-scale ocean-atmosphere circulation patterns in North America during the Holocene (e.g., Forman et al., 1995; Liu and Fearn, 2000; Knox, 2000, 2003; Harrison et al., 2003; Goman and Leigh, 2004) suggest that when the summer was relatively hotter than today (e.g., mid-Holocene thermal maximum, ca. 6 ka), the Jet Stream and the Bermuda High were situated to the south and northeast of their present-day positions, respectively, and moist air from the south Atlantic was pumped northward along the Atlantic coast of North America − as a result of the anticyclonic flow

around the southern and western flanks of the Bermuda High − producing an increase of the precipitations and floods in the eastern North America (Fig. 1.4a). In contrast, during relatively colder summers (e.g., Neoglacial cooling, since ca. 3 ka), the Jet Stream shifted to the north and the Bermuda High to the southwest, thereby pumping more moisture from the Caribbean region and the GOM toward the central North America, producing strong precipitations and floods in this region (Fig. 1.4b). The large flood episodes caused the massive erosion of alluvial plains and promoted the remobilization of fine-grained sediment and their mass transport, via the Mississippi River, toward the GOM (e.g., Brown et al., 1999). Consequently, the mineralogy, geochemistry and nature of terrigenous components transported by the Mississippi River during these floods are likely characteristics of the drainage areas.

An important aspect to extract of the previously discussed is that the mineralogy, geochemistry and nature of the terrigenous components transported by the Mississippi River toward the GOM during these climatic factors are characteristics of the drainage areas, where the bedrock/soils contain both different clay-mineral assemblages (Brown and Kennett, 1998; Sionneau et al., 2008) and geochemical signatures (Gustavsson et al., 2001; Grossman, 2009). Thus, the terrigenous fraction of GOM sediments may provide information in order to further investigate the variability of the Mississippi River discharges during the last climatic cycle. Indeed, both mineralogical and geochemical nature of this detrital fraction is characteristics of their source areas (e.g., Bout-Roumazeilles et al., 1999), and will help to reconstruct the variability of detrital provenance through time if their main sources are well identified and constrained. Their grain-size distributions will provide information on the fluvial discharge intensity and on erosion/flooding processes.

In this context, **Thomas Sionneau PhD-thesis** initiated this terrigenous approach in the northern GOM (Sionneau, 2008). One challenge was to calibrate the mineralogical proxy by distinguishing clay mineral provinces on the North American continent and producing **clay mineral distribution maps over the GOM** (Sionneau et al., 2008). Concurrently, the mineralogical signature of the main petrographic provinces from North America toward the GOM can be discriminated as follow: (1) the north-western Mississippi and Missouri rivers watershed characterized by high smectite content (2) the northeastern province mainly delivering illite and chlorite (3) the kaolinite-rich south-eastern part of the United States, and (4) the Brazos River and south-western Mississippi River watersheds dominated by illite and kaolinite (Fig. 1.3). Once this first crucial step has been achieved, it was then possible to use this approach on the sedimentary records from two intraslope basins, the Orca and Humphrey

Basin. The Orca basin is one example of interdomal intraslope basin as described by Bouma et al. (1986). The basin is isolated by upward diapirs that coalesced, preventing any deep-water entrance into the basin and favouring the initiation of ~200 meters-thick brine over its floor. Sedimentation is then mainly hemipelagic and displays very high accumulation rates (Flower et al., 2004). According to these characteristics, previous studies evidenced that the Orca basin is one of the best archive of the LIS melting history during the last glacial period and termination (Kennett and Shackleton, 1975; Leventer et al., 1982; Flower and Kennett, 1990; Flower et al., 2004). But so far, few studies concentrated on the detrital signal associated to these meltwater events. Sionneau et al. (in revision) evidenced the repetitive occurrences of peculiar clay mineral assemblages over the deglaciation, associated with specific fine-grained and cohesive particles. These smectite-rich intervals occurred simultaneously with major meltwater episodes previously described in the Orca Basin and referred as to meltwater flows (Aharon, 2003) or Meltwater Spike (Leventer et al., 1982; Brown et al., 1999; Flower et al., 2004). **Their mineralogical characteristics indicate that the detrital material associated with the meltwater events mainly originated from the northwestern Mississippi and Missouri watersheds, suggesting a preferential melting of the southwestern margin of the LIS during these events.** This finding confirms the time-step evolution of the LIS extent (Fig. 1.3) proposed by Dyke (2004).

A similar approach was tested on the MIS 3 interval. Similar alternations between smectite-rich intervals and illite and chlorite-rich interval were evidenced. When compared with the freshwater signal deduced from $\delta^{18}O$ and Mg/Ca analyses (Hill et al., 2006), the river discharges are characterized by illite and chlorite inputs within the clay mineral fraction. This result indicates that freshwater discharge during the last glacial were draining the northeastern Mississippi province rather than the northwestern smectite-rich province as it was the case for the deglacial meltwater events. **It suggests the MIS 3 freshwater discharges were thus originating from the Atlantic margin of the LIS rather than from its southwestern margin**. This is in agreement with the contemporaneous growth and destabilisation of the Atlantic and northeastern margin of the Labrador sector during climatic cooling evidenced by Bond and Lotti (1995). By contrast, the smectite-rich events are likely correlated with interstadials, and might then result from hydrological processes affecting the southwestern margin during these warm and moist climatic events. Indeed, the smectite enhanced supply may both results from melting of the southwestern margin of the LIS due to warmer climatic conditions or alternatively from enhanced precipitations over the area. In the absence of any significant meltwater evidence (i.e., in the $\delta^{18}O$ record), the second hypothesis is preferred so

far. Nevertheless, the chronostratigraphy is not so well constrained within MIS 3, with some uncertainties due to the influence of the reservoir age in an anoxic basin, and the sampling resolution needs to be improved in order to further investigate both hypotheses (Sionneau et al., 2009).

The core from Humphrey Basin evidenced some major sedimentary discrepancies likely resulting from mixed fluvial influences from the Mississippi river and the Brazos-Trinity system. The sedimentary filling of the basin is thought to be mainly controlled by eustatic forcing over the last climatic cycle as a result of a direct connection with the active Brazos system mainly during low-sea level. The main objectives were to produce an isotopic stratigraphy for this specific area and to be able to pinpoint any freshwater discharges in this remote area from the main Mississippi river plume. The results of Sionneau (2008) evidenced **unexpected major freshwater discharges during the termination II, with isotopic values up to** –2.5‰ at the MIS 6/5 transition. These freshwater discharges prevent us for using the isotopic record as a stratigraphic tool. But the occurrence of such event is intriguing in this area, evidencing major meltwater supply and raises the question of the role of the Brazos-Trinity system during termination II. **This question is still debating because the isotopic record also evidenced a major meltwater event around 14 ka, synchronous with the Meltwater Spike characterizing the Orca Basin**. Moreover, another meltwater event is also noticed during MIS 5a in core MD03-2641 and in nearby cores (MD03-2642; Mallarino et al., 2006), but it does not seem to affect the northeastern GOM.

1.2. Research objectives

In this framework, **this PhD-thesis will focus on two specific intraslope basins, Pigmy (core MD02-2553) and La Salle (core MD02-2549), located on the northwest continental slope of the GOM**, about 250-300 km southwest of the present-day Mississippi Delta (Fig. 1.5). These basins collect continuously a smoothed and averaged terrigenous supply from the North American continent and avoid local perturbations linked to the Louisiana slope depositional processes (Aharon, 2003, 2006). The sediment cores were taken during the 2002 PAGE (Paleoceanography of the Atlantic and Geochemistry) cruise of the research vessel Marion Dufresne, as part of the International Marine Past Global Changes Study (IMAGES) program.

In this view, these sedimentary records are likely appropriated to bring further information on the relationships between the high-latitude and the subtropical climates

through their respective impact on the continental hydrography (ice-sheet, precipitation and runoff) and atmospheric configuration (moisture transfer). **The initial objectives of this dissertation are to extract from the sedimentary records valuable information on the undergoing continental climatic conditions and their variations with time during the last climatic cycle with specific emphasis on rapid climatic variability and atmosphere-ocean coupling**. In order to fulfill the proposed objectives, the detrital signature of these cores was studied, setting emphasis on the clay mineral assemblage, and the chemical composition (organic and mineral) of the sediment.

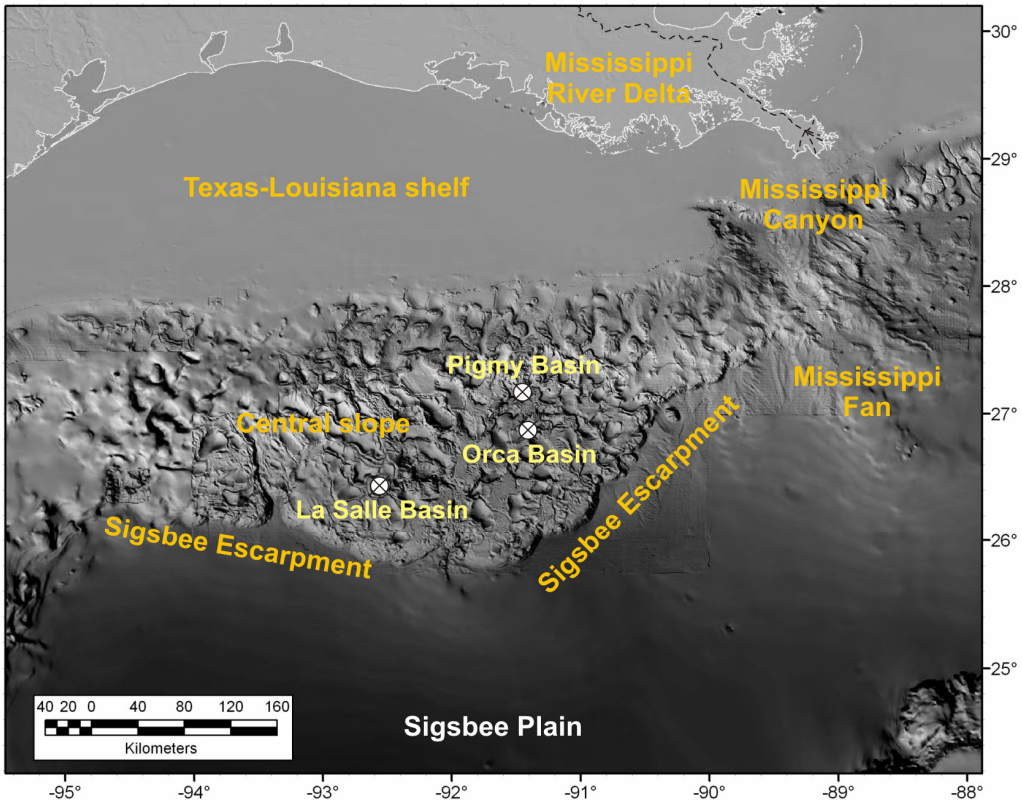

Fig. 1.5. Morphological map of the seafloor in the northern Gulf of Mexico (adapted from Tripsanas et al., 2007) showing locations of sediment cores MD02-2553 (Pigmy Basin), MD02-2552 (Orca Basin) and MD02-2549 (La Salle Basin).

1.3. The Gulf of Mexico − geological settings (intraslope basins)

Physiography

The GOM is a large oceanic basin connected with the Caribbean Sea through the Yucatan channel and with the tropical North Atlantic through the Florida Straits (Fig. 1.6). The GOM can be basically divided in 3 distinct sedimentological domains with contrasted characteristics: a carbonated province along the eastern and southern boundaries (Yucatan and Florida carbonated shelves; Fig. 1.6), a central area dominated by the present-day Mississippi

Canyon and Fan systems and a northern and western continental slopes where salt deformation is a dominant process (Twichell et al., 1996).

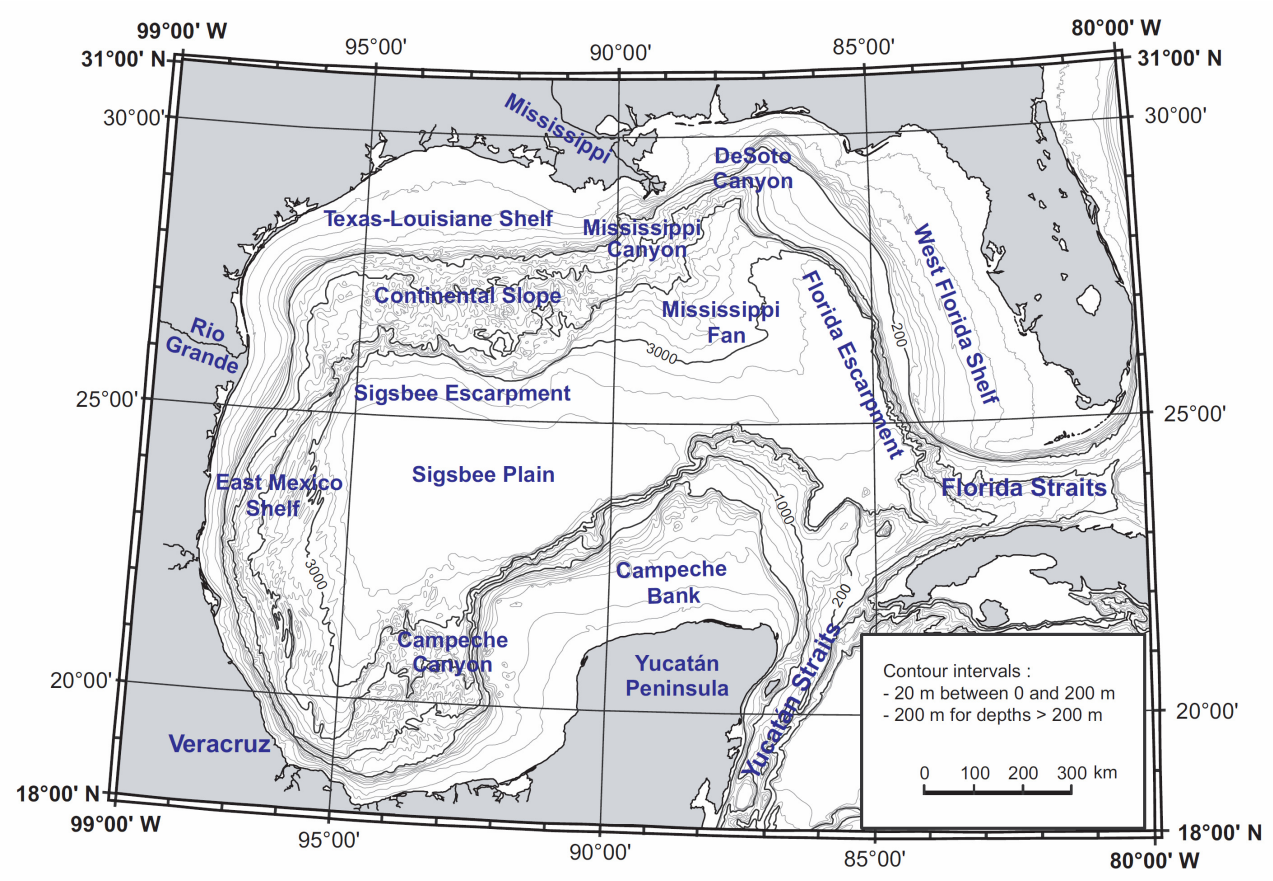

Fig. 1.6. General bathymetry and morphology of the Gulf of Mexico

The stratigraphy and structure of the continental slope are controlled from both terrigenous supply and salt- tectonic deformation partly resulting from the sedimentary load (Bryant et al., 1990; 1991; Uchupi, 1975). The physiography and bathymetry of the continental slope consists of numerous intraslope basins determined by shallow salt diapirs as a result of salt tectonics (Bryant et al., 1990; 1991; Pratson and Ryan, 1994). The intraslope basins from the GOM, which correspond to depression between salt diapirs display high variability, is shape, size and depth. The intraslope basins are classified in three distinct groups on the basis of the mechanisms leading to their formation (Bouma et al., 1981): interdomal basins, collapse basins and blocked canyons. The Orca basin is typically an interdomal basin whereas the Pigmy and La Salle basins are blocked canyons.

Sedimentary supply and the Mississippi River system

The sedimentation in the northwestern continental slope is mainly controlled by the discharge from the Mississippi River, while some particular domain may be locally influenced by other fluvial system as it is evidenced in the Brazos-Trinity system on the western part of the slope (Mallarino et al., 2006; Sionneau, 2008). Indeed, more than 20 major rivers (Rio Grande, Colorado, Apalachicola) reaches the GOM representing a freshwater discharge of 10.6 $x10^{11}$ m^3 per year with 65% from the Mississippi River alone. The present-day eastern position of the Mississippi River delta is supposed to have initiated during the last interglacial Marine Isotope Stage 5 or alternatively at the beginning of the last glaciation (Coleman et al., 1983; Bouma and Coleman, 1985; Bouma et al. 1985; Coleman, 1988). Before that migration, the Mississippi River was more than 300 km westward and its discharge was partly passing through the Bryant Canyon and/or the Eastern canyon system toward the GOM (Suter and Berryhill, 1985). When these two systems were active, i.e., during the development of the ancestral Mississippi delta, numerous gravity flows resulting from sediment failures or form hyperpcynal river plumes (Tripsanas et al., 2006) affected the sedimentation in the adjacent basins (e.g., La Salle Basin).

Oceanic circulation

As previously discussed, the Loop Current is the most important oceanic surface feature in the GOM. This surface current enters the northeastern part of the GOM as the ITCZ reaches its northward summer position, before to flow out toward tropical Atlantic through the Florida Straits (Fig. 1.2 and 1.7). This surface current shows a characteristic seasonal variability (e.g., Brunner, 1982; Sheinbaum et al., 2002) over imprinted on the glacial-interglacial variations.

The northern continental shelf is affected by a general east-west surface circulation forced by wind stress (Wang et al., 1998), which has also a strong seasonal component (Vastano et al., 1995). This peculiar surface pattern is responsible for the westward transportation of the main Mississippi River discharge from the delta front toward the Texas and Louisiana continental shelf and slope.

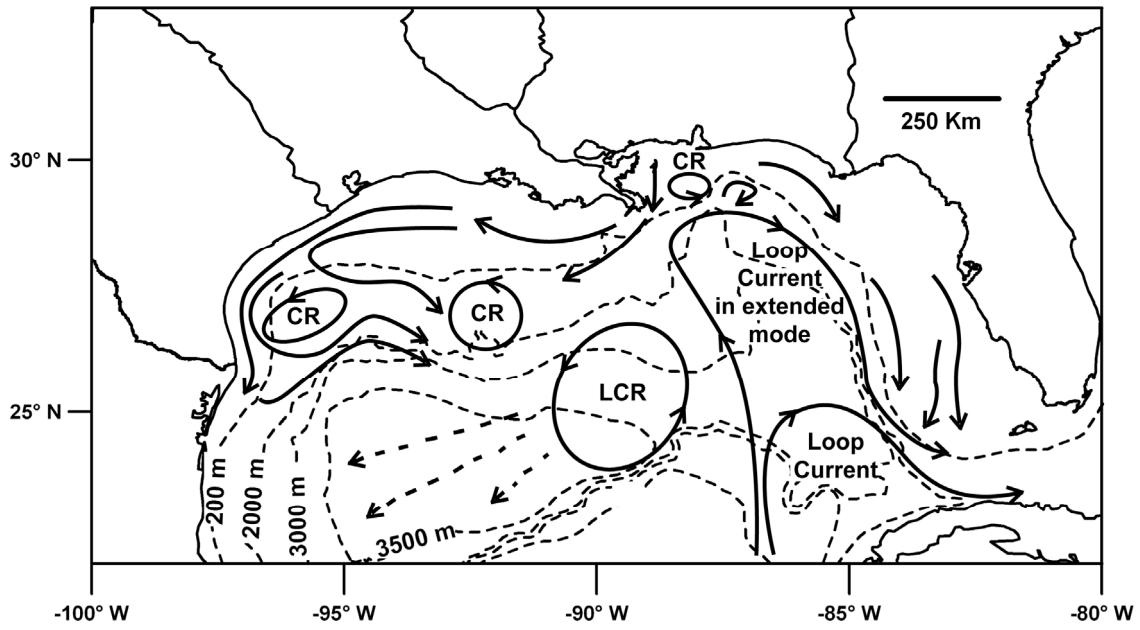

Fig. 1.7. Main surface oceanic features in the Gulf of Mexico (bold black arrows; adapted from Sionneau et al., 2008), including two different states of the Loop Current, Loop Current Rings (LCR) and Cyclonic Rings (CR). Dotted arrows represent propagation direction for LCR (Vukovich and Crissman, 1986).

Atmospheric configuration

The influence of the North American southwest monsoon may be recorded in the GOM sedimentation through its huge potential impact on precipitation intensity and distribution over the North American continent (Fig. 1.2). This phenomenon corresponds to the entrance of moisture from the GOM toward the southwestern part of North America during summer when the ITCZ and the AWP move northward (Higgins et al., 1997). The basic seasonality of this phenomenon is modulated by the lower-frequency variations linked with insolation (e.g., Poore et al., 2004, 2005).

1.4. Methods

1.4.1. Foraminifera picking

Initially, bulk samples were taken on selected core-depth intervals: 496-498, 516-518, 640-642, 775-778, 866-868 and 930-934 cm. Samples were sieved and prepared for the hand-picking procedure. Approximatively 300 specimens of monospecific planktonic *Globigerinoides ruber* (pink and white) were hand-picked from the >250µm fraction of selected intervals where foraminifera were sufficiently abundant (i.e., 30 mg of shells) to provide the amount of carbon necessary for ^{14}C AMS dating.

1.4.2. Clay mineralogy

X-Ray Diffraction analyses (XRD) were performed on 195 samples from core MD02-2553 and on 362 samples for core MD02-2549. Clay minerals (< 2µm) are identified by XRD following the protocol described in Bout-Roumazeilles et al. (1999). All samples were first decalcified with 0.2 M HCl. The excess acid was removed by repeated washing with distilled water and centrifugation. The clay-size fraction was separated by settling and centrifugation, and oriented on glass slides. The analyses were run on a Philips PW 1749 generator (copper anti-cathode, 40 Kv voltage, 25 mA intensity and 2theta/minute speed). Three XRD determinations were performed in routine, untreated sample ("normal" run), ethylene-glycol solvation for 12 h ("glycol" run) and heating at 490°C for 2 hours ("heated" run). The analyses were run from 2.49° to 32.49° 2theta for normal and glycol runs and from 2.49° to 14.49° 2theta for heated runs.

Each clay mineral is then characterized by its layer plus interlayer interval (d) as revealed by XRD analysis (Brown and Brindley, 1980). Identification of each clay mineral was mainly made according to the position of its basal reflection d (001) on the diagrams except for chlorite (002). Smectite (S) is characterized by a peak at 14Å on the normal run, which expands to 17Å after saturation in ethylene glycol and retracts to 10Å after heating. Illite (I) shows a basal peak at 10Å on the three tests. Chlorite (C) is characterized by peaks at 14 Å (001), 7Å (002), 4.75Å (003) and 3.53Å (004) on the three tests. Kaolinite (K) is characterized by peaks at 7Å (001) and 3.58Å (002) on the normal and glycol runs. Both peaks disappear or are strongly reduced after heating. Semi-quantitative estimation of clay mineral abundances is based on peak area measurements using the Macintosh MacDiff 4.2.5 software (Petschik, 2000). Clay mineral ratios [smectite/(illite + chlorite)] and kaolinite/ chlorite] were calculated in order to retrace the relative variations of the clay minerals. We used the peak areas to calculate the relative proportions of clay minerals and mineralogical ratios were determined using these percentiles. The error on both reproducibility of technical works and measurements is ± 5%.

1.4.3. Grain-size distribution

Grain-size analyses were carried out on 213 samples from core MD02-2553 and on 363 samples for core MD02-2549. Grain size determination were made on the carbonate-free fraction of the sediment using the principle of diffraction and diffusion of a monochromatic laser beam on suspended particles (Malvern Mastersizer 2000 laser diffractometer, red He-Ne laser, 632 and 466 nm wave lengths). The method is based on near-forward scattering of a

laser beam by particles in suspension. Measurements can range from 0.02 to 2000 µm with an obscuration comprised between 10 and 20 %. Sample preparation and optical settings for the Mastersizer 2000 generally followed Sperazza et al. (2004). Defloculation of the samples was done by successive washing with distilled water after decarbonatation of the sediments with 0.2 M HCl. Samples were split with a 2000 rpm stirrer and disaggregated by 40% ultrasonication (Hydro S dispersion cell) for >60 seconds during analysis. Sample quantity was adjusted in order to obtain a laser beam obscuration between 12 and 15%. We used a refractive index (RI) value of 1.544 (quartz) and an absorption value of 0.05. The distribution parameters reported here are: mode (µm, most frequent grain-size) and sediment grain-size composition (%) in clays (<2µm), silts (2–63 µm), and sands (>63µm). The Folk median value is the particle size corresponding to 50 % cumulated weight (Folk, 1980). Main descriptive parameters (mean and mode) are calculated in phi and converted in µm. According to their distinct behaviour during transport, two sub-fractions can be distinguished with the silt-size fraction: the cohesive–silts (2–10 µm) and non-cohesive silts (10–63 µm) (McCave et al., 1995). The cohesive fraction mainly deposits as aggregated material and is not further winnowed after deposition while the non-cohesive "sortable" silt refers to the fraction that can be removed/winnowed after deposition through hydrodynamic processes.

1.4.4. Bulk analyses: magnetic susceptibility, calcium carbonate, Rock-Eval pyrolysis and elemental analysis

Magnetic susceptibility.- Shipboard physical properties were not measured on core MD02-2553C[2] because the multisensor track was not adapted to the CASQ coring system. Magnetic susceptibility (MS) was thus measured at the Geosystèmes laboratory at the Université Lille 1. The massic low-field MS was measured on 194 samples, using a KLF-4 Agico apparatus. Remnant magnetization measurements were made on the three-axis using a magnetic field of 300 A/m with a step of 10 A/m. Each sample was measured three times and the mean of these measurements is reported here. The MS are normalized by dry mass and expressed as m^3/kg. Conversely, the MS from the core MD02-2549 was measured onboard with a 2cm-resolution (Labeyrie et al., 2005). The MS quantifies the ability of rock or sediment to be magnetized by a weak magnetic field according to the dia-, para- and ferromagnetic behaviour of the constituent minerals, their concentration and grain-size (Robinson, 1993). In the absence of diagenetic alteration, the MS can provide a record of the concentration in magnetic minerals within the sediments and reflects the bulk mineralogical changes induced by terrigenous input versus biogenic pelagic dilution (e.g., King, 1986).

Calcium carbonate.- Total inorganic carbon (TIC) content was determined as calcium carbonate ($CaCO_3$) on 194 samples from core MD02-2553 and on 205 samples for core MD02-2549. Prior to analysis, sediment samples were dried in a 40° oven and then finely ground. Next, the calcium carbonate (CaCO3) percentage was measured using a Bernard calcimeter (measuring the amount of CO_2 released by acid digestion, and based on standard samples of pure $CaCO_3$ – precision <5%).

Rock-eval pyrolysis.- Rock-eval pyrolysis was carried out on 157 samples from core MD02-2553 and on 57 samples for core MD02-2549. Total organic carbon (TOC, wt %), S2 peak (mg hydrocarbon per g sediment), Tmax (°C), and Hydrogen Index (HI, in mg hydrocarbon per g TOC) were determined by Rock-Eval pyrolysis with a Delsi Oil Show Analyser at the Université Paris 6, France. The pyrolysis program was adapted to recent sediments, starting with an isothermal stage of 3 min at 180°C. Then, the pyrolysis oven temperature was raised at 30°C/min to 600 °C, and held for 3 min at this temperature (see Espitalié et al., 1986 for procedural details and Disnar et al., 2008 for Rock-Eval use for Holocene sediments).

Elemental analysis.- Total carbon (TC), total sulfur (S_{total}) and total nitrogen (N_{total}) content were determined on 194 samples from core MD02-2553 and on 205 samples for core MD02-2549 using a Thermo Flash EA1112 CHNSO analyzer. About 1.5 to 2 mg of sample is introduced into a container, which is injected by an auto-sampler. In case of CHNS-determinations, approximately 5 mg vanadiumpentoxide is added to the sample as a combustion catalyst. 2,5-Bis(5-tert-butyl-benzoxazol-2-yl)thiophene (BBOT) is used as standard for the CHNS- determinations. The precision was better than 2% for TC, 4% for S_{total} and 5% for N_{total}, based on international standards and replicate samples.

For the upper 359 cm of the core MD02-2553 (79 samples) and for the entire sample set of the core MD02-2549, TOC was determined by subtracting inorganic carbon (TIC) concentrations from total carbon (TC) concentrations, because the TOC content obtained by Rock-Eval pyrolysis was studied at lower resolution. Both methods gave consistent results.

Though nitrogen may be present in the form of nitrate or ammonium in clay minerals, it is estimated that N_{total} mostly corresponds to organic nitrogen. With this assumption, the C/N ratio (TOC/N_{total}) was calculated to determine the origin of sedimentary organic matter (OM) (Jasper and Gagosian, 1990, Meyers, 1997 and Meckler et al., 2008). C/N ratios for OM of marine origin generally range from 4 to 10 because of the high protein content of lower organisms such as phytoplankton and zooplankton (e.g., Meyers, 1997). Higher plant-

derived OM gives higher C/N values than that of marine origin because it has a high percentage of nonprotein materials (e.g., C/N > 15; Meyers, 1997).

1.4.5. Elemental geochemistry

Major and trace element concentrations were determined at low-resolution, on 53 samples from core MD02-2553 and on 49 samples for core MD02-2549, by inductively coupled plasma optical emission spectrometry (ICP-OES) and inductively coupled plasma mass spectrometry (ICP-MS), at Activation Laboratories Ltd. (Ancaster, Canada). Samples were mixed with a flux of lithium metaborate ($LiBO_2$) and lithium tetraborate ($Li_2B_4O_7$), and fused in an induction furnace. Molten sample was immediately poured into a solution of 5% nitric acid (HNO_3) containing an internal standard, and mixed continuously until completely dissolved. Precision and accuracy are both better than 1-2% for major element, 5% for REE and 5-10% for the other elements, as checked by international standards and analysis of replicate samples. Elemental compositions and total REE are normalized to aluminum (Al) (see discussion about Al normalization in van der Weijden, 2002, and Tribovillard et al., 2006). In addition, trace metal (TM) concentrations are expressed in terms of enrichment factors (EF_{TM}) where the Al-normalized metal concentration is compared to the average shale values of Wedepohl (1971, 1991): $EF_{TM} = TM/Al_{sample} : TM/Al_{average\ shale}$. $EF_{TM}>1$ suggests enrichment relative to average shale but authigenic enrichments can be suspected when EF_{TM} exceed 5 (Tribovillard et al., 2006). Fractionation between light REE (LREE: La-Nd), middle REE (MREE: Sm-Gd) and heavy REE (HREE: Tb-Lu) is retraced by La/Yb and Gd/Yb normalized ratios (Lawrence et al., 2006). Al-normalized metal distributions are used as proxies of the detrital sediment sources, complementary to clay mineral proxies. In addition, the REE abundance patterns provide fingerprints associated with detrital fraction of the sediment which in turn represents the bulk composition and stands as proxy for the climate over the source area (e.g., Tanaka et al., 2007).

1.5. Thesis outline

The present thesis consists of four main chapters (Chapters 2 to 5). The sections 2.4.2, 2.4.3 and 3.4.2 follow the style and format of a scientific paper.

After this brief introductory chapter, **Chapter 2** is focused on the Pigmy Basin (core MD02-2553) in the northern GOM. **The sedimentary and geochemical evidence of deglacial megafloods in the northern GOM and, the large variations in the Mississippi**

River runoff over the course of the Holocene are presented and discussed. Firstly, this chapter will present a discussion on the origin and dynamics of **the main meltwater discharges to GOM (Meltwater Spike)**, in order to better constrain: (1) the connection between the LIS melting history and hydrological evolution of the GOM, and (2) the late deglacial and early Holocene paleoenvironmental and sedimentary changes in response to North American climate evolution. Secondly, **the Holocene sedimentological and geochemical records from the Pigmy Basin** are presented, and it is attempted to: (1) identify the variability of Mississippi River runoff throughout the Holocene, (2) document the main changes in precipitation distribution over North America, and (3) constrain the links between modifications of both high-latitude and sub-tropical domains, in order to propose synoptic scenarios or configurations of timely atmosphere-ocean-continent interactions during the Holocene.

Chapter 3 is concentrated on the La Salle Basin (core MD02-2549) in the northern GOM. This chapter will firstly present and discuss the **variability of terrigenous sediment provenance related to North American regional climate changes during the last climatic cycle**. Secondly, a first approach on the **changes in the atmosphere-ocean-continent interactions happened in response to interglacial climate variations (the Holocene versus the MIS 5e)** is discussed. These changes are reflected on the terrigenous transfers from the North American continent to the GOM, and they are summarized by two simple atmosphere-ocean coupling synoptic patterns. The results obtained in this chapter will provide a basis for improvement of atmospheric general circulation models that are critical for modelling of future climate.

The purpose of the **Chapter 4** is to present a **comparison on the long-term sedimentological signatures interpreted in the Pigmy and La Salle records** (Chapters 2 and 3) **with other sedimentological and geochemical records from the northern GOM** (transect from west to east). Thus, common patterns and discrepancies of these climate reconstructions are revealed, and therefore, the regional and local characters of paleoclimatic signatures interpreted in the Pigmy and La Salle basins are put in evidence.

To close this thesis, **Chapter 5** summarizes the most important findings of this research and provides an outlook for future works in the GOM. At the end of the dissertation, the entire data sets acquired are attached in the form of general appendix. Additionally **the abstract of the different papers, as co-author, are also attached in the general appendix. These papers are framed in the same context as this research**.

References

Aharon, P., 2003. Meltwater flooding events in the Gulf of Mexico revisited: Implications for rapid climate changes during the last deglaciation. Paleoceanography 18(4), PA1079. doi: 10.1029/2002PA000840.

Aharon, P., 2006. Entrainment of meltwaters in hyperpycnal flows during deglaciation superfloods in the Gulf of Mexico. Earth and Planetary Science Letters 241, 260-270.

Bettis, E.A., Benn, D.W., Hajic, E.R., 2008. Landscape evolution, alluvial architecture, environmental history, and the archaeological record of the Upper Mississippi River Valley. Geomorphology 101, 362-377.

Bond, G.C., Lotti, R., 1995. Iceberg discharges into the North Atlantic on millennial time scales during the last deglaciation. Science 267, 1005-1010.

Bouma, A.H., 1981. Depositional sequences in clastic continental slope deposits, Gulf of Mexico. Geo-Marine Letters 1, 115-121.

Bouma, A.H., Sterling, C.E., Coleman, J.M., 1985. Mississippi Fan, Gulf of Mexico. In: Bouma, A.H., Barnes, N.E., Normark, W.R. (Eds.), Submarine Fans and Related Sequences. Springer-Verlag, New York, pp. 143–150.

Bouma, A.H and Coleman, J., 1986. Intraslope basin deposits and relation to continental shelf, northern Gulf of Mexico. American Association of Petroleum Geologists Bulletin 9(70), p. 1178.

Bouma, A.H., Stelting, C.E., Leg 96 sedimentologists, 1986. Seismic stratigraphy and sedimentary processes in Orca and Pigmy Basin. In Initial Reports of the Deep-Sea Drilling Project. Leg 96. Bouma, A.H., Coleman, J.M., Meyer, A.W., et al., (Eds), Washington D.C., U.S. Government Printing Office. pp. 563-576 doi:10.2973/dsdp.proc.96.128.1986.

Bryant, W.R., Bryant, J.R., Feeley, M.R., Simmons, G.R., 1990. Physiographic and bathymetric characteristics of the continental slope, Northwest Gulf of Mexico. Geo-Marine Letters 10, 182–199.

Bryant, W.R., Lugo, J., Cordova, C. Salvador, A., 1991. Physiography and bathymetry, in Salvador, A., (Ed.), the Gulf of Mexico Basin, The Geology of North America, volume J. The geological Society of America, Boulder, 13-30.

Broecker, W.S., 2006. Was the Younger Dryas Triggered by a Flood?. Science 312, 1146-1148.

Brown, G., Brindley, G.W., 1980. X-ray diffraction procedures for clay mineral identification, in Brindley, G.W., Brown, G., (Eds.), Crystal Structures of Clay Minerals and their X-ray Identification. Mineralogical Society, London, pp. 305–359.

Brown, P.A., Kennett, J.P., 1998. Megaflood erosion and meltwater plumbing changes during last North American deglaciation recorded in Gulf of Mexico sediments. Geology 26, 599-602.

Brown, P., Kennett, J.P., Ingram, B.L., 1999. Marine Evidence for Episodic Holocene Megafloods in North America and the Northern Gulf of Mexico. Paleoceanography, 14(4), 498-510.

Brunner, C.A., 1982. Paleoceanography of surface waters in the Gulf of Mexico during the late Quaternary. Quaternary Research 17, 105–119.

Carlson, A.E., Clark, P.U., Haley, B.A., Klinkhammer, G.P., Simmons, K., Brook, E.J., Meissner, K.J., 2007. Geochemical proxies of North American freshwater routing during the Younger Dryas cold event. Proceedings of the National Academy of Sciences USA 104, 6556-6561

Coleman, J.M., Prior, D.B., Lindsay, J.F., 1983. Deltaic influences on shelf edge instability processes. In: Stanley, D.J., Moore, G.T. (Eds.), The Shelf Break, Critical Interface on Continental Margins. Society of Economic Paleontologists and Mineralogists Special Publication, vol. 33, pp. 121–137.

Coleman, J.M., 1988. Dynamic changes and processes in the Mississippi River delta. Geological Society of America Bulletin 100, 999-1015.

Davies, D.K., Moore, W.R., 1970. Dispersal of Mississippi sediment in Gulf of Mexico. Journal of Sedimentary Petrology 40, 339-349.

Disnar, J-R., Jacob, J., Morched-Issa, M., Lottier, N. and Arnaud, F., 2008. Assessment of peat quality by molecular and bulk geochemical analysis: Application to the Holocene record of the Chautagne marsh (Haute Savoie, France). Chemical Geology 254, 101-112.

Donnelly, J.P., Driscoll, N.W., Lloyd, E.U., Keigwin, D., Schwab, W.C., Thieler, E.R., Swift, S.A., 2005. Catastrophic meltwater discharge down the Hudson Valley: A potential trigger for the Intra-Allerød cold period. Geology 33, 89-92.

Drexler, J.W., Rose, W.I. Jr., Sparks, R.S.J., Ledbetter, M.T., 1980. The Los Chocoyos Ash, Guatemala: a major stratigraphic marker in middle America and in three ocean basins. Quaternary Research 13, 327-345.

Dyke, A.S., 2004. An outline of North American deglaciation with emphasis on central and northern Canada. In Ehlers, J., Gibbard, P.L., (Eds), Quaternary Glaciations - Extent and Chronology, Part II. Elsevier B.V., Amsterdam, pp. 373-424.

Dyke, A.S., Moore, A., Robertson, L., 2003. Deglaciation of North America. Geological Survey of Canada Open File, 1574. Online at http://geopub.nrcan.gc.ca/moreinfo_e.php?id=214399 (Revised 2009-05-26)

Espitalié, J., Deroo, G., and Marquis, F., 1986. La pyrolyse Rock Eval et ses applications, Revue de l'Institut Français du Pétrole 40(B), 755-784.

Folk, R.L.,1980. Petrology of Sedimentary Rocks, Hemphill, Austin, Texas, 182 p.

Forman, S.L., Oglesby, R., Markgraf, V., Stafford, T., 1995. Paleoclimatic significance of late Quaternary eolian deposition on the Piedmont and High Plains, central United States. Global and Planetary Change 11, 35-55.

Flower, B.P., Kennett, J.P., 1990. The Younger Dryas cool episode in the Gulf of Mexico. Paleoceanography 5(6), 949-961.

Flower, B.P., Hastings, D.W., Hill, H.W., Quinn, T.M., 2004. Phasing of deglacial warming and laurentide ice sheet meltwater in the Gulf of Mexico. Geology 32, 597-600.

Flocks, J., Swarzenski, P., 2007. Sediment collection from Orca and Pigmy Basins, Gulf of Mexico, and analyses for texture and trace-metal concentrations, July 2002, PAGE 127 Campaign. In: Winters, W.J., Lorenson, T.D., Paull, C.K. (Eds.), Initial Report of the IMAGES VIII/PAGE 127 Gas Hydrate and Paleoclimate Cruise on the RV Marion Dufresne in the Gulf of Mexico, 2–18 July 2002: U.S. Geological Survey Open-File Report 2004-1358, one DVD. Online at http://pubs.usgs.gov/of/2004/1358/. (Revised 2009-05-26)

Goman, M., Leigh, D.S., 2004. Wet early to middle Holocene conditions on the upper coastal plain of North Carolina. Quaternary Research 61, 256-264.

Gustavsson, N., Bølviken, B., Smith, D.B., Severson, R.C., 2001. Geochemical landscapes of the conterminous United States - New map presentations for 22 elements. U.S. Geol. Survey Prof. Paper, 1648. U.S. Department of the Interior.

Grossman, J., 2009. National Geochemical Atlas: The geochemical landscape of the conterminous United States derived from stream sediment and other solid sample media analyzed by the National Uranium Resource Evaluation (NURE) program. U.S. Geological Survey Open-File Report 98-622.
Online at http://tin.er.usgs.gov/geochem/about.php?group=Analyses+by+ICP%2FAcid+dissolution
(Revised 2009-05-29)

Harrison, S.P., Kutzbach, J.E., Liu, Z., Bartlein, P. J., Otto-Bliesner, B., Muhs, D.,Prentice, I. C., and Thompson, R. S., 2003. Mid-Holocene climates of the Americas: a dynamical response to changed seasonality. Climate Dynamics 20, 663-688.

Hill, H.W., Flower, B.P., Quinn, T.M., Hollander, D.J., Guilderson, T.P., 2006, Laurentide Ice Sheet meltwater and abrupt climate change during the last glaciation, Paleoceanography 21, PA1006, doi:10.1029/2005PA001186.

Higgins, R.W., Yao, Y., Wang, X.L., 1997. Influence of the North American monsoon system on the U.S. summer precipitation regime. Journal of Climate 10, 2600–2622.

Huybers, P.J., 2006. Early Pleistocene glacial cycles and the integrated summer insolation forcing. Science 313, 508-511.

Jasper, J.P. and Gagosian, R.B., 1990. The sources and deposition of organic matter in the late Quaternary Pigmy Basin, Gulf of Mexico. Geochimica et Cosmochimica Acta 54, 1117-1132.

Joyce, E.J., Tjalsma, L.R.C., Prutzman, J.M., 1993. North American glacial meltwater history for the past 2.3 m.y.: Oxygen isotope evidence from the Gulf of Mexico. Geology 21, 483-486.

Kennett, J.P. and Shackleton, N.J., 1975. Laurentide ice sheet meltwater recorded in Gulf of Mexico deep-sea cores. Science 188, 147-150.

Keigwin, L.D., Jones, G.A., Lehman, S.J., Boyle, E.A., 1991. Deglacial meltwater discharge, North Atlantic deep circulation, and abrupt climate change. Journal of Geophysical Research 96, 16811-16826.

King, J.W., 1986. Paleomagnetic and rock-magnetic stratigraphy of Pigmy Basin, Deep Sea Drilling Project Site 619, Leg 96. In Bouma, A. H., Coleman, J. M., Meyer, A. W., et al., Init. Repts. DSDP, 96: Washington (U.S. Govt. Printing Office), 677-684.

Kleiven, H.F., Kissel, C., Laj, C., Ninnemann, U.S., Richter, T.O. & Cortijo, E. 2008. Reduced North Atlantic deep water coeval with the glacial Lake Agassiz freshwater outburst. Science 319, 60–64.

Knox, J.C., 2000. Sensitivity of Modern and Holocene floods to climate change. Quaternary Science Reviews 19, 439- 457.

Knox, J.C., 2003. North American palaeofloods and future floods: Responses to climate change. In: K.J. Gregory and G. Benito, Editors, Palaeohydrology: Understanding Global Change, J. Wiley and Sons, Chichester (2003), pp. 143-164.

Labeyrie, L., Shipboard Scientific Party., 2005. MD127/IMAGES-IX PAGE Cruise Report, 2002. IPEV, in preparation.

Lawrence, M.G., Greig, A., Collerson, K.D., Kamber, B.S., 2006. Rare earth element and yttrium variability in South East Queensland waterways. Aquatic Geochemistry 12, 39-72.

Leventer, A., Williams, D.F., Kennett, J.P., 1982. Dynamics of the Laurentide ice sheet during the last deglaciation: evidence from the Gulf of Mexico. Earth and Planetary Science Letters 59, 11-17.

Licciardi, J.M., Teller, J.T., Clark, P.U., 1999. Freshwater routing by the Laurentide ice sheet during the last deglaciation. In Clark, P.U., et al., eds., Mechanisms of global climate change at millennial time scales. American Geophysical Union Geophysical Monograph 112, pp. 177-201.

Lisiecki, L.E., Raymo, M.E., 2005. A Pliocene-Pleistocene stack of 57 globally distributed benthic delta 18O records. Paleoceanography 20, PA1003, doi:10.1029/2004PA001071.

Liu, K.B., Fearn, M., 2000. Reconstruction of prehistoric landfall frequencies of catastrophic hurricanes in Northwestern Florida from lake sediment records. Quaternary Research 54, 238-245.

McCave, I.N., Manighetti, B., Robinson, S.G., 1995. Sortable silt and fine sediment size/composition slicing: parameters for palaeocurrent speed and palaeoceanography. Paleoceanography 10, 593–610.

Mallarino, G., Beaubouef, R.T., Droxler, A.W., Abreu, V., Labeyrie, L., 2006. Sea level influence on the nature and timing of a minibasin sedimentary fill (northwestern slope oft he Gulf of Mexico). American Association of Petroleum Geologists Bulletin 90, 1089-1119.

Marshall, S.J., Tarasov, L., Clarke, G.K.C., Peltier, W.R., 2000. Glaciological reconstruction of the Laurentide ice sheet: physical processes and modelling challenges. Canadian Journal of Earth Sciences 37, 769-793.

Marchitto, T.M., Wei, K.Y., 1995. History of Laurentide meltwater flow to the Gulf of Mexico during the last deglaciation, as revealed by reworked calcareous nannofossils. Geology 23, 779-782.

Meckler, A.N., C.J. Schubert, P.A. Hochuli, B. Plessen, D. Birgel, B.P. Flower, K.-U. Hinrichs, and Haug, G.H., 2008. Glacial to Holocene terrigenous organic matter input to sediments from Orca Basin, Gulf of Mexico- a combined optical and biomarker approach. Earth and Planetary Science Letters 272, 251-263.

Meyers, P.A., 1997. Organic geochemical proxies of paleoceanographic, paleolimnologic and paleoclimatic processes. Organic Geochemistry 27, 213-250.

Nürnberg, D., Ziegler, M., Karas, C., Tiedemann, R., Schmidt M.W., 2008. Interacting Loop Current variability and Mississippi River discharge over the past 400 kyr. Earth and Planetary Science Letters 272, 278-289.

Peltier, W.R., Fairbanks, R.G., 2006. Global glacial ice volume and Last Glacial Maximum duration from an extended Barbados sea level record. Quaternary Science Reviews 25, 3322-3337.

Petschick, R. 2000. MacDiff 4.2 Manual. MacDiff [Online]. Available from World Wide Web: http://www.geologie.uni-frankfurt.de/Staff/Homepages/Petschick/RainerE.html

Pidwirny, M., 2006. Global Scale Circulation of the Atmosphere. Fundamentals of Physical Geography, 2nd Edition. online at http://www.physicalgeography.net/fundamentals/7p.html (Revised 2009-05-29)

Poore, R.Z., Dowsett, H.J., Verardo, S., 2003. Millennial- to century-scale variability in Gulf of Mexico Holocene climate records. Paleoceanography 18, PA1048, doi:10.1029/2002PA000868.

Poore, R.Z., Quinn, T.M., Verardo, S., 2004. Century-scale movement of the Atlantic Intertropical Convergence Zone linked to solar variability. Geophysical Research Letters 31, L12214, doi: 10.1029/2004GL019940.

Poore, R.Z., Pavich, M.J., Grissimo-Mayer, H.D., 2005. Record of the North American monsoon from Gulf of Mexico sediment cores. Geology 33, 209-212.

Pratson, L.F., and Ryan, W.B.F., 1994. Pliocene to recent infilling and subsidence of intraslope basins offshore Louisiana. American Association of Petroleum Geologists Bulletin, 78:1483–1506.

Rahmstorf, S., 2006. Thermohaline Ocean Circulation, in Elias, S.A., (Ed.), Encyclopedia of Quaternary Sciences. Elsevier, Amsterdam, pp 1-10.

Rahmstorf, S., 2002. Ocean circulation and climate during the past 120,000 years. Nature 419, 207-214.

Raymo, M.E., Lisiecki, L., Nisancioglu, K., 2006. Plio-Pleistocene ice volume, Antarctic climate, and the global $\delta^{18}O$ record. Science 313, 492-495.

Richey, J.N., Poore, R.Z., Flower, B.P., Quinn, T.M., 2007. 1400 yr multiproxy record of climate variability from the northern Gulf of Mexico. Geology 35, 423-426.

Rittenour, T.M., Blum, M.D., Goble, R.J., 2007. Fluvial evolution of the lower Mississippi River valley during the last 100 k.y. glacial cycle: response to glaciation and sea-level change. Geological Society of America Bulletin 119, 586-608.

Robinson, S.G., 1993. Lithostratigraphic applications for magnetic susceptibility logging of deep-sea sediment cores: examples from ODP Leg 115. In Hailwood, E.A., and Kidd, R.B. (Eds.), High Resolution Stratigraphy. Geological Society, London, Special Publications, 70, 65-98.

Sionneau, T., 2008. Transferts Continent – Océan : Enregistrement du dernier cycle climatique par les sédiments terrigènes du Golfe du Mexique. PhD thesis, Université Lille 1. 377 p.
Online at http://tel.archives-ouvertes.fr/tel-00366377/fr/ (Revised 2009-05-29)

Sionneau, T., Bout-Roumazeilles, V., Bory, A., Tribovillard, N., Van Vliet-Lanoe, B., 2009. Influence des oscillations de Dansgaard-Oeschger sur la distribution, en Amérique du Nord, d'humidité provenant du Golfe du Mexique (28-45 ka cal BP) In: 12ème Congrès Français de Sédimentologie, Livre des résumés, Rennes.

Sionneau, T., Bout-Roumazeilles, V., Flower, B.P., Bory, A., Tribovillard, N., Kissel, C., Van Vliet-Lanoë, B., Montero-Serrano, J.C., in revision. On the provenance of freshwater pulses in the Gulf of Mexico during the last deglaciation: Evidence from grain size and clay mineralogy. Quaternary Research.

Suter, J.R., Berryhill Jr., H.L., 1985. Late Quaternary shelf-margin deltas, northwest Gulf of Mexico. American Association of Petroleum Geologists Bulletin 69, 77–91.

Sheinbaum, J., Candela, J., Badan, A., Ochoa, J., 2002. Flow structure and transport in the Yucatan Channel. Geophysical Research Letters, 29, doi: 10.1029/2001GL013990.

Sperazza, M., Moore, J.E., Hendrix, M.S., 2004. High-resolution particle size analysis of naturally occurring very fine-grained sediment through laser diffractometry. Journal of Sedimentary Research 74, 736-743.

Tanaka, K., Akagawa, F., Yamamoto, K., Tani, Y., Kawabe, I. & Kawai, T., 2007. Rare earth element geochemistry of Lake Baikal sediment: its implication for geochemical response to climate change during the Last Glacial/Interglacial transition. Quaternary Science Reviews 26, 1362-1368.

Tarasov, L., Peltier, W.R., 2006. A calibrated deglacial drainage chronology for the North American continent: evidence of an Arctic trigger for the Younger Dryas. Quaternary Science Reviews 25, 659-688.

Tribovillard, N., Algeo, T., Lyons, T.W., Riboulleau, A., 2006. Trace metals as paleoredox and paleoproductivity proxies: an update. Chemical Geology 232, 12-32.

Tripsanas, E.K., Bryant, W.R., Slowey, Kim, J.W., 2006. Marine Isotope Stage 6 Canyon and Spillover Deposits of the Bryant and Eastern Canyon Systems, Northwest Gulf of Mexico: Importance of Fine-Grained Turbidites on a Delta-Fed Prograding Slope. Journal of Sedimentary Research 76, 1012-1034.

Tripsanas, E.K., Bryant, W.R., Slowey, N.C., Bouma, A.H., Karageorgis, A.P., Berti, D., 2007. Sedimentological history of Bryant Canyon area, northwest Gulf of Mexico, during the last 135 kyr (Marine Isotope Stages 1-6): A proxy record of Mississippi River discharge. Palaeogeography Palaeoclimatology Palaeoecology 246, 137-161.

Twichell, D.C., Schwab, W.C., Kenyon, N.H., Lee, H.J., 1996. Breaching the levee of a channel on the Mississippi Fan. In: J.V. Gardner and D.C. Field M.E. Twichell, Editors, Geology of the United State's Seafloor, the View from Gloria, Cambridge University Press, Cambridge, pp. 85–96.

Uchupi, E., 1975. Physiography of the Gulf of Mexico and Caribbean Sea, in Nairm, A.E.M., Stehli, F.G., (Eds.), the ocean basins and margins, volume 3: The Gulf of Mexico and the Careibbean. Plenum Press, New York, 706p.

van der Weijden, C.H., 2002. Pitfalls of normalization of marine geochemical data using a common divisor. Marine Geology 184, 167-187.

Vastano, A.C., Barron, C.N., Shear, E.W., 1995. Satellite observations of the Texas current. Continental Shelf Research 15, 729–754.

Vukovich, F.M., Crissman, B.W., 1986. Aspects of warm rings in the Gulf of Mexico. Journal of Geophysical Research 91, 2645-2660.

Wang, W., Nowlin, W.D., Reid, R.O., 1998. Analyzed surface meteorological fields over the northwestern Gulf of Mexico for 1992–94: mean, seasonal, and monthly patterns. Monthly Weather Review 126, 2864-2883.

Wang, C., Enfield, D.B., 2001. The tropical Western Hemisphere warm pool. Geophysical Research Letters 28, 1635-1638.

Wedepohl, K.H., 1971. Environmental influences on the chemical composition of shales and clays. In: Ahrens, L.H., Press, F., Runcorn, S.K., Urey, H.C. (Eds.), Physics and Chemistry of the Earth. Pergamon, Oxford, pp. 305-333.

Wedepohl, K.H., 1991. The composition of the upper Earth's crust and the natural cycles of selected metals. In: Merian, E. (Ed.), Metals and Their Compounds in the Environment. VCH-Verlagsgesellschaft, Weinheim, pp. 3-17.

Ziegler M., Nürnberg D., Karas C., Tiedemann R., Lourens L.J., 2008. Persistent summer expansion of the Atlantic Warm Pool during glacial abrupt cold events. Nature Geoscience 1(9), 601-605.

Chapter 2

The Pigmy Basin: core MD02-2553

2.1. The Pigmy Basin – geological setting

The Pigmy basin is a small intraslope basin, 3.8 km to 7.5 km wide and 20 km long with a maximum water depth of ~2400m (Fig 2.1a). This basin is typically a blocked canyon intraslope basin formed by blockage of the thalweg of a submarine channel resulting from upward moving diapirs. It means that sediments deposited within the actual Basin are coarser in the axis of the basin and become finer (i.e.; clay) along the side of the diapirs. In that sense, the Pigmy Basin is very different from the Orca Basin, which is a typical interdomal basin (Bouma et al., 1986). The Orca Basin is a depression totally surrounded by bathymetric highs that prevent any coarser supply via bottom current and promote hemipelagic sedimentation. By contrast sedimentation within the Pigmy Basin is mainly hemipelagic but mass-deposit may occur. A previous survey of the Pigmy Basin by the R/V Gyre in 1996 revealed very steep walls, with slopes averaging 20° up to 50°. These very high angular values highlight the low stability of the walls that may be subjected to slumping or mass-flow (Bryant et al., 1990). According to these observations, the coring site was chosen in order to avoid the main mass-deposits.The core MD02-2553 was taken in the Pigmy Basin (Fig 2.1a). The coring target was determined on the basis of the 3.5 kHz seismic survey at 5 knots speed along the seismic profiles SP15 from point 1 (91.23E, 97.09N) to point 2 (91.23E, 27.12N) and SP16 from point 3 (91.26E, 27.10N) to point 4 (91.33E, 27.11N) (Fig 2.1b). The coring site is located at 27°11,01N and 091°25.00E at a water depth of 2259 meters (Fig 2.1). The main acoustic character alternates between parallel and semi-transparent seismic reflectors. These characteristics evidence at least 6 seismic units consisting of parallel reflectors overlying transparent or semi-transparent reflectors. All reflectors appear to be related to thin beds of silt / sand materials. The basin is filled by hemipelagic sediment interlayered with coarse-grained turbidites. The fill of the basin is asymmetric with draping seismic reflectors on the northwest side and abrupt termination of reflectors on the opposite side, while the sedimentary sequence expands northward. This asymmetry was previously interpreted as the results of faster upward moving of diapirs on the northwest side (Bouma et al., 1986).

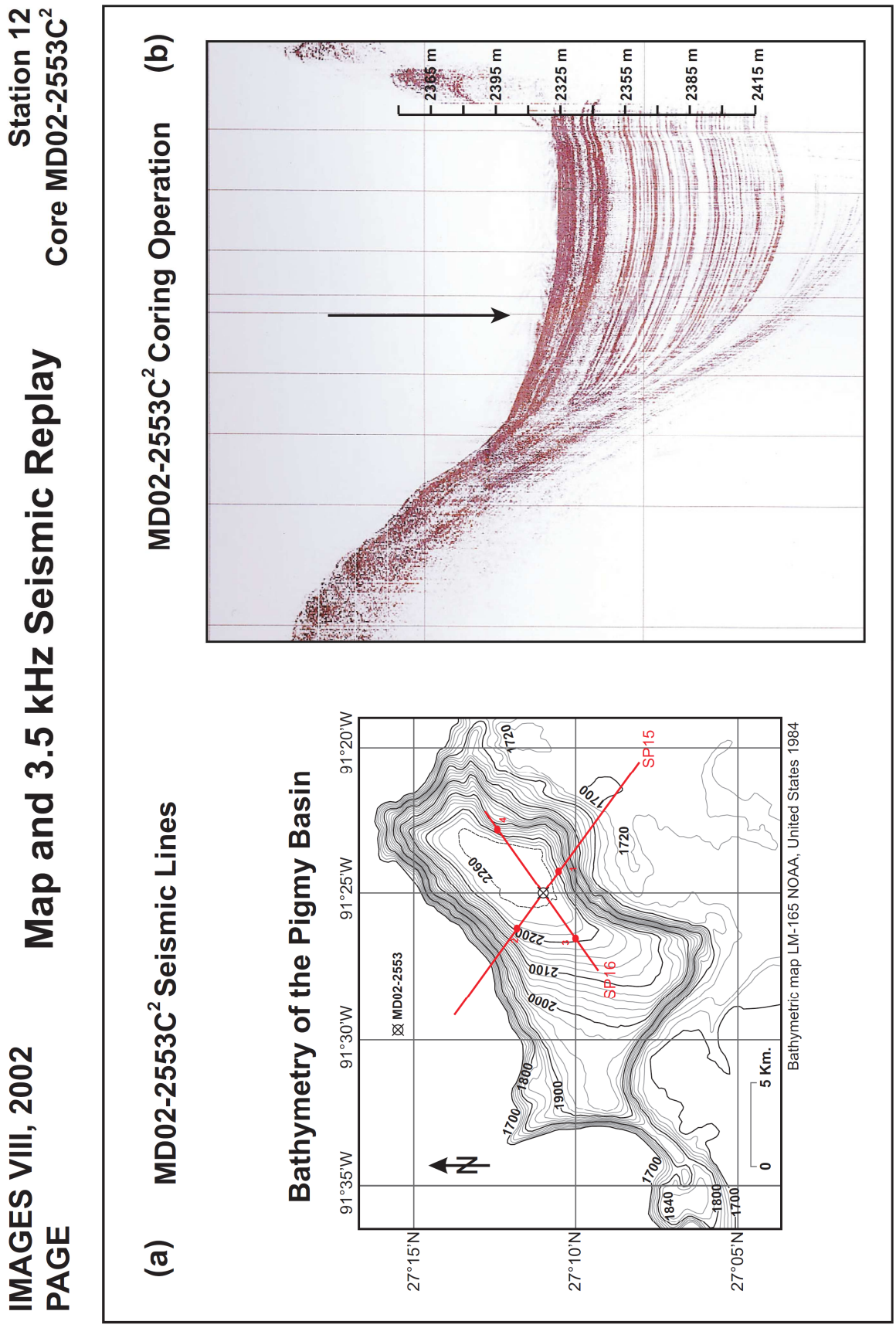

Fig. 2.1. (**a**) Bathymetric map of the Pigmy Basin showing location of sediment core MD02-2553, contours in meters. (**b**) Example of 3.5 kHz profile to the main axis of the Pigmy Basin.

The CASQ corer was used for this operation. This procedure allows recovering the sediment-water interface and prevents from any coring disturbance (i.e., stretching with the classic calypso corer in unconsolidated sediments or compression with classical gravity corer). Indeed the coring system developed by Yvon Balut (IPEV) penetrates slowly in the sediment without free-fall. This procedure allows to recover undisturbed sediment and to preserve both sedimentary structures and textures.

2.2. Material and sampling

The MD02-2553 core length is 1003 cm and coring operations were realized in good conditions. The uppermost part of the core is missing due to the sampling procedure of the CASQ corer using D-Tube.

2.2.1. Physical properties

The CASQ core was sampled using series of D-tubes. These tubes are larger than the liner commonly used for the Multisensor track analyses. For this reason, the sections were not analyzed using the shipboard multisensor-track. Spectral analysis (L*, a* and b*) of the core was carried out onboard the Marion Dufresne using a Minolta CM-2002 spectrophotometer, at a resolution of 2 cm.

The L* record is slightly higher (Fig. 2.2) on the upper 420 cm of the core suggesting an increased contribution of carbonate versus terrigenous supply. The L* also displays slightly higher values on the lowermost part of the core (950 – 1002 cm). By contrast lower L* values between 420 cm to 950 cm suggest an enhanced contribution of detrital supply versus carbonate content. The a* and b* channel records confirms the differences between the upper and lower parts of the core. It also highlights high a* values circa 425 cm and 625 cm delimitating a very homogenous interval (Fig. 2.2) and low a* values in the lowermost part of the core (around 975 cm).

2.2.2. Sedimentological description

The dominant lithologies consist of dark-yellowish brown, dark-grey, light-greenish grey, greenish grey and dark-greenish grey clay to silty-clay with foraminifera (Fig. 2.3 and 2.4). Bioturbation is observed throughout the core.

The uppermost part (top to 41 cm) of the core is characterized by dark yellowish coarser sediments corresponding to sandy - silty clay with foraminifera and coccolithes (Fig.

2.4). The core is characterized by the occurrence of darker laminated intervals between 625 and 655 cm, between 880 and 946 cm and between 981 cm and the base of the core.

Sand/silt layers, some of which displaying fining-upward sequences, are observed at 58-60 cm (sand layer with foraminifera), 115-116 cm (sand layer), 300-302 cm (fining upward sandy layer with foraminifera), 400-402 cm (foraminifera layer), 420-422 cm, 581-595 cm (normal graded foraminifera sequence) and 970-981 cm (series of 3 fining-upward foraminifera turbidites). These layers have been interpreted as small turbidites (Fig. 2.4).

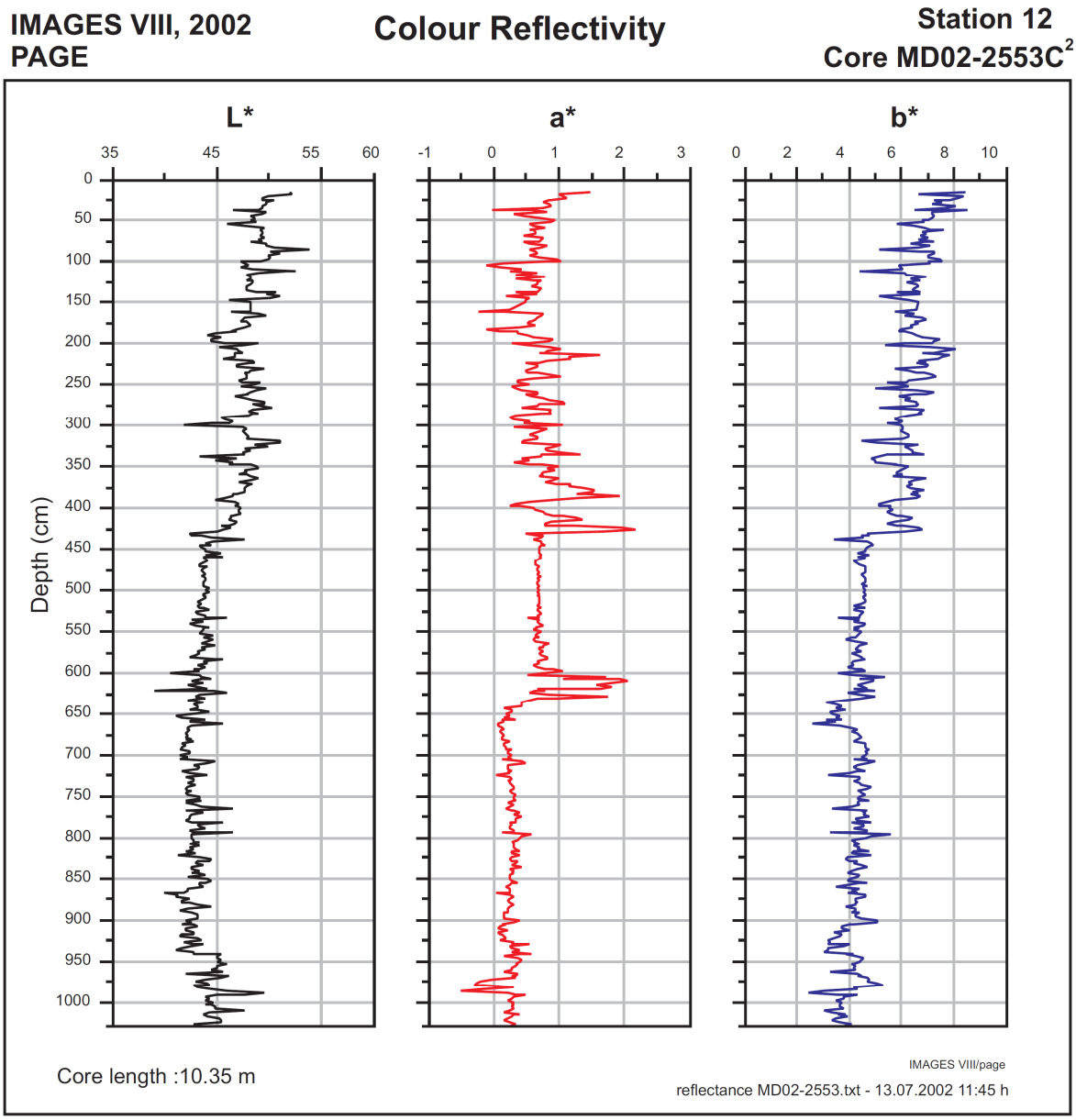

Fig. 2.2. Color reflectance parameters of the core MD02-2553 (Pigmy Basin). The L* denote lightness or luminance variation, a* denote red/green variation, and b* denote blue/yellow variation.

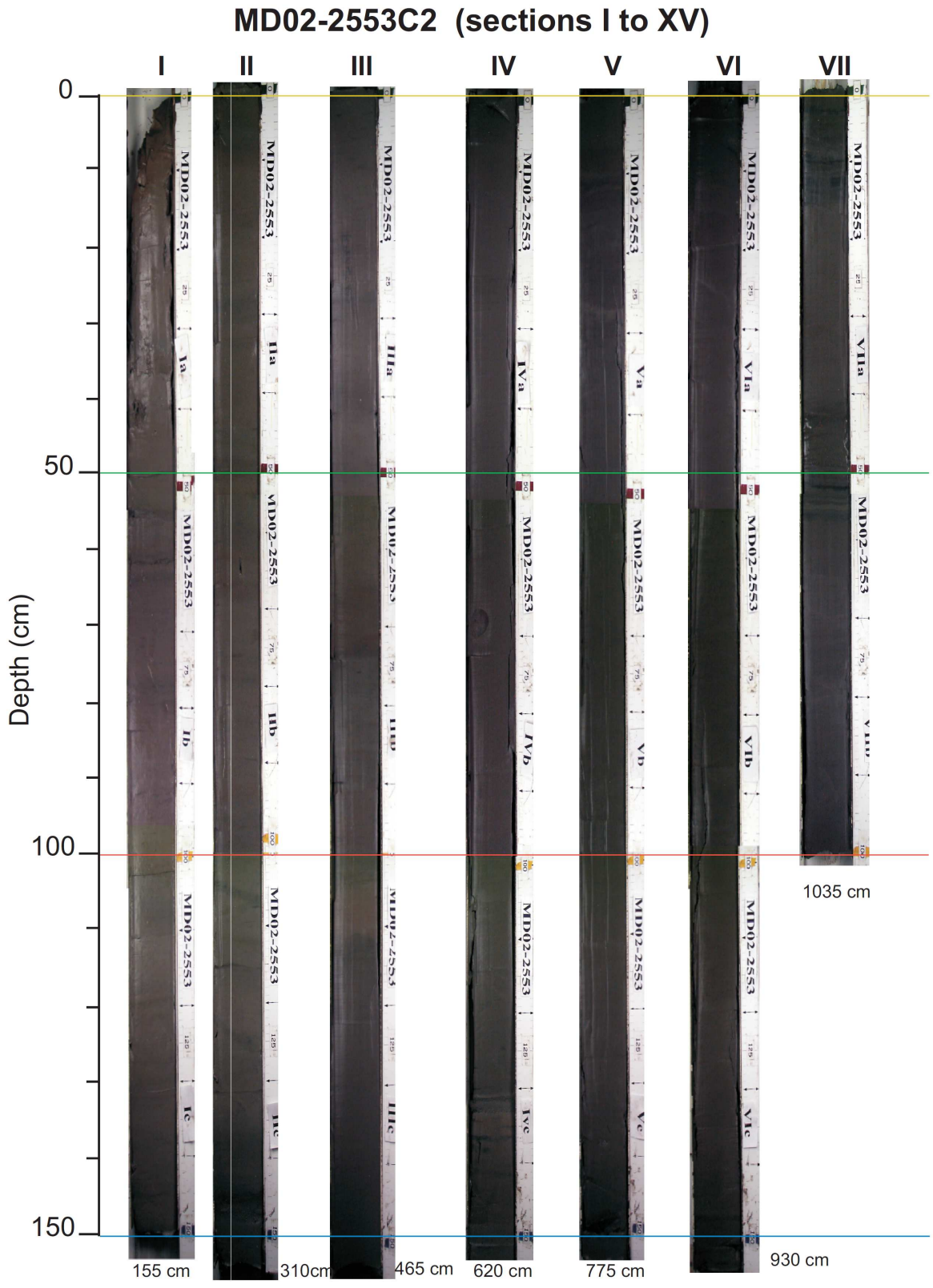

Fig. 2.3. Photomosaic of the box core MD02-2553 (Pigmy Basin). Brightness differences and contrasting angles in laminations are due to camera angle and lighting.

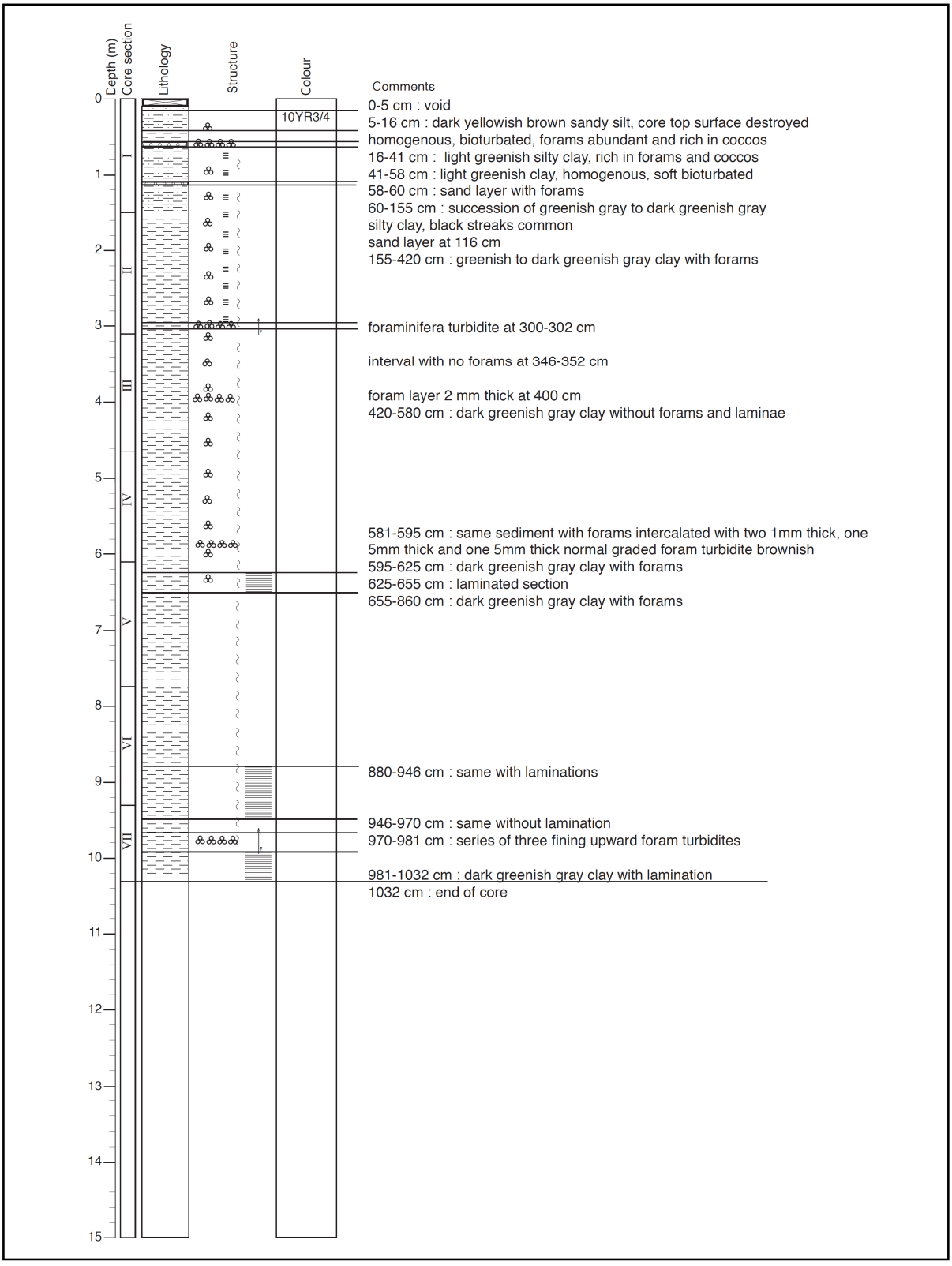

Fig. 2.4. Sedimentological descriptions from the core MD02-2553 (Pigmy Basin).

2.3. Results

2.3.1. Chronostratigraphy

The chronostratigraphy of core MD02-2553 is determined on 22 accelerator mass spectrometry (AMS) ^{14}C dates on foraminifera (Table 2.1; black squares in Fig. 2.5). The oldest 2 dates were generated in the frame of this thesis and measured on monospecific *Globigerinoides ruber* (both pink and white varieties) at the Poznan Radiocarbon Laboratory, Poland. The younger dates were carried out by Poore et al. (in press) and measured on mixed planktic foraminifers at the CAMS, Lawrence Livermore National Laboratory, USA. All ages were converted into calendar years with the CALIB software (Stuiver and Reimer, 1993, version 5.0.2; http://calib.qub.ac.uk/calib), using the calibration curve Marine04 (Hughen et al., 2004). All AMS ^{14}C ages were corrected using a constant reservoir age of 400 year ($\Delta R=0$) because it provides consistency with both modern values (Bard, 1988) and with previous paleoceanographic studies from the GOM (e.g., Flower et al., 2004; Meckler et al, 2008; Nürnberg et al., 2008).

In the lowermost section of the core (~350.5-1030 cm), core depth in centimeters was converted to calendar age by linear interpolation, because it is only had 4 main calibrated AMS ^{14}C ages at 350.5, 424.5, 640 and 932 cm (dotted line with blue squares in Fig. 2.5). Linear extrapolation from the radiocarbon date suggests that the age of the core base (~1030 cm) is approximately 15.1 ka (1 ka = 1000 cal yr BP), what indicates that the core MD03-2553 has recorded the last deglaciation period.

Contrastingly, in the upper core section (0-350.5 cm), core depth in centimeters was converted to calendar age by linear regression, because it is had 15 calibrated AMS ^{14}C ages relatively in line and an assumed zero-age at the core top (r^2=0.996; solid line in Fig. 2.5).

The calculated sedimentation rates range from about 200 to 397 cm/ka during the last deglaciation, while Holocene sedimentation rates is about 25-36 cm/ka (Table 2.1 and Fig. 2.5). The highest rates are associated with the glacial section and the meltwater pulse. The depth/age relationship also suggests continuous and uniform sedimentation over the past 12.9 ka.

Table 2.1. Radiocarbon ages for core MD02-2553.

Lab number or reference	Core depth (cm)	Species	^{14}C AMS Age (ka)	^{14}C Error (± year)	Calibrated age (median, ka BP)	Calibarted error (± year, 1 sigma)	Sedimentation rates (cm/ka)
	0		0		0	0	
	5.5		0.605	40	0.260	37	
	29.5		1.360	40	0.907	49	
	48.5		1.840	40	1.370	54	
	69.5		2.370	40	1.993	60	
	110		3.265	40	3.102	71	
	150.5		4.020	40	4.029	65	
	175.5		4.550	40	4.765	57	35.9
	200.5		5.075	40	5.428	50	
	210		5.155	40	5.523	43	
Poore et al. (in press)	235.5	Mixed planktic foraminifers	5.865	40	6.284	47	
	250.5		6.320	40	6.783	58	
	274.5		6.905	50	7.420	51	
	295.5		7.790	40	8.259	52	
	310		8.520	40	9.157	72	
	330.5		8.620	40	9.307	65	
	350.5		9.170	40	9.989	89	
	375.5		9.905	40	10.810	112	
	390.5		10.400	40	11.364	61	24.9
	409.5		10.888	40	12.529	81	
	424.5		11.455	40	12.956	44	
Poz-24558	640	*Globigerinoides ruber*	12.580	80	14.034	98	199.9
Poz-24559	932		12.960	80	14.769	195	397.3

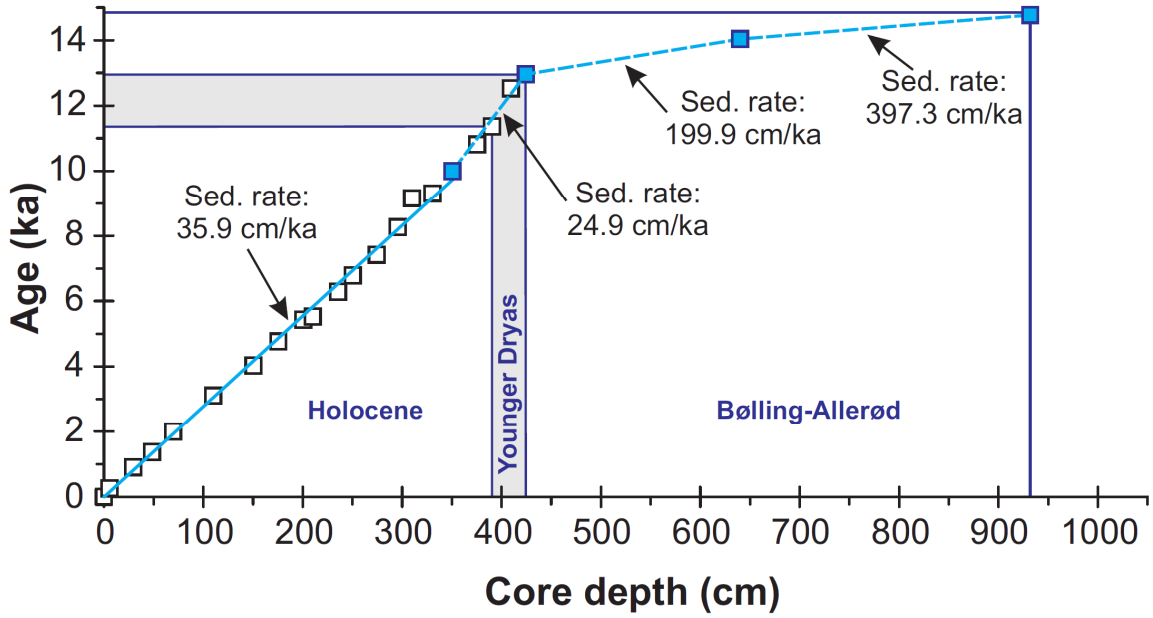

Fig. 2.5. Age model for core MD02-2553 based on 22 AMS ^{14}C dates from both *Globigerinoides ruber* and mixed planktic foraminifers, converted to calendar ages (see text). The dotted line with blue squares denotes the calibrated ages interpolated. The solid line shows the linear regression between calibrated ages.

The sedimentation rates obtained are in good agreement with sedimentation rates determined on (1) DSDP site 619 of the Pigmy Basin: 300 cm/ka in stage 2 and 92 cm/ka in stage 1 (Jasper and Gagosian, 1990), and (2) core MD02-2552 of the Orca Basin: ca. 215 cm/ka during the last deglaciation and ca. 65 cm/ka during the early Holocene (Sionneau et al., in revision) (Fig. 2.6). It is important to emphasize that discrepancies in the magnitude of the sedimentation rates observed in the different sedimentary records likely reflect uncertainties in the individual core chronologies. In the Pigmy Basin core, the distinct increases in linear sedimentation rates from about 25 to 397 cm/ka at about 12.9, 14 and 14.7 ka appear very large and abrupt, following a stair-step pattern (Fig. 2.6). However, the sedimentary observations of the core MD02-2553 do not reveal any sharp lithological breaks or evidences of hiatus or mass flow transport in these parts of the core, suggesting a rather continuous sedimentation. The decrease in sedimentation rates from 200 to 25 cm/ka at ca. 12.9 ka is consistent with a major reduction of meltwater flow (Licciardi et al., 1999; Teller et al., 2005; Tarasov and Peltier, 2005). This reduction is related to the formation of proglacial lakes, such as Lake Agassiz (Teller et al., 2005), which received and stored part of the terrigenous particles associated with the meltwater inputs from the northwestern margin of the LIS, before entering the Mississippi River.

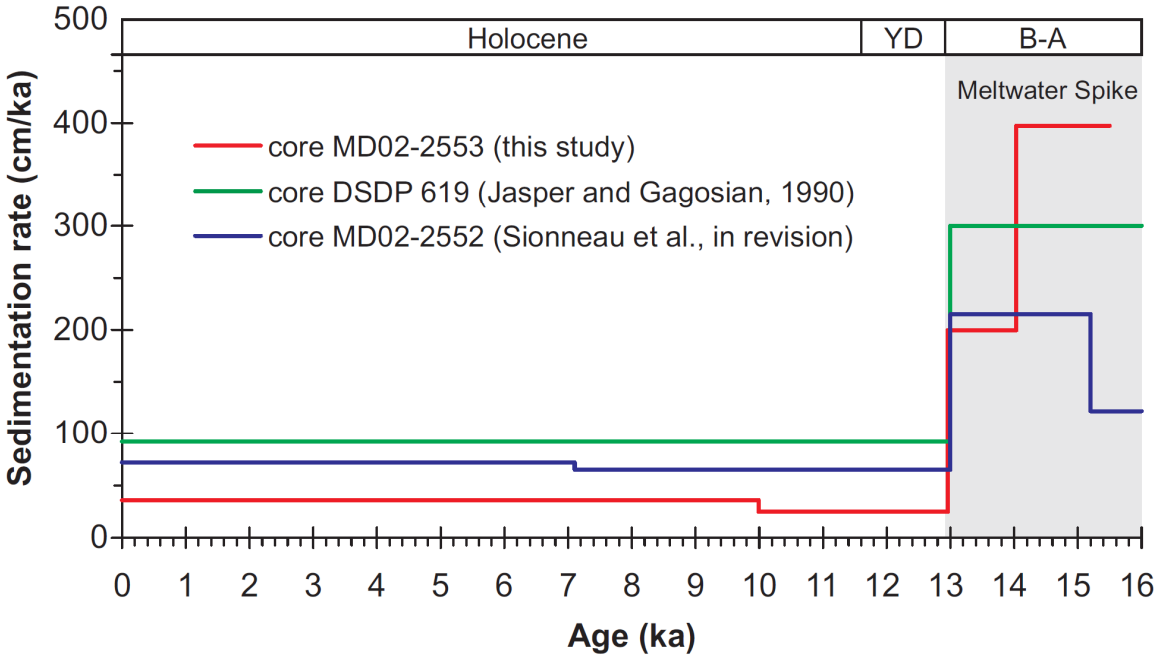

Fig. 2.6. Comparison of sedimentation rates of the Pigmy Basin (cores MD02-2553 and DSDP 619) and Orca Basin (MD02-2552) in the GOM. The Younger Dryas (YD) from 12.9 to 11.6 ka and Bølling-Allerød warming (B-A) from 15.4 to 12.9 ka are indicated.

2.3.2. Bulk analyses: magnetic susceptibility, calcium carbonate, elemental analysis and Rock-Eval pyrolysis

Magnetic susceptibility, calcium carbonate, elemental analyses were carried out on 194 samples, whereas the Rock-Eval pyrolysis was measured in 157 samples (where 123 samples correspond to deglacial interval).

Carbonate content is generally low (<12%) in the lowermost part of the core (15-12.9 ka, deglacial interval) and shows an upward increasing trend during the Holocene, where it reaches 24.5% (Fig. 2.8d). It is important to emphasize that the calcite dissolution processes, which could considerably affect the interpretations based on the concentrations of calcium carbonate ($CaCO_3$), is unlikely to have occurred as the core was collected at a water depth of 2,259 m which is above the calcitic lysocline (>4000 m in the Caribbean region; e.g., Vink et al., 2001). Further the excellent preservation of foraminiferal assemblages (e.g., Fig. 2.7) throughout the entire core (Poore et al., in press; this study) also confirms that calcium carbonate dissolution was negligible. Therefore, the calcium carbonate changes are mainly controlled by autochthonous biogenic productivity and terrigenous dilution. Similar results are reported in DeSoto Canyon (core MD02-2575; northeastern GOM) by Nürnberg et al. (2008).

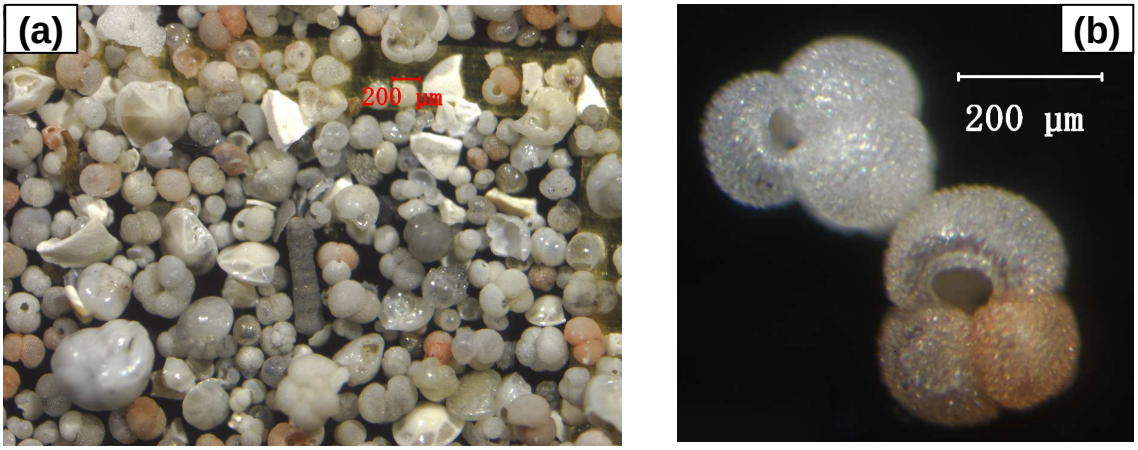

Fig 2.7. Photograph from the sample PB932 (14.8 ka) depicting (**a**) global foraminiferal assemblages and (**b**) the planktonic foraminifer *Globigerinoides rubber* (both pink and white varieties). Note that the specimens *Globigerinoides rubber* are the most abundant in (**a**).

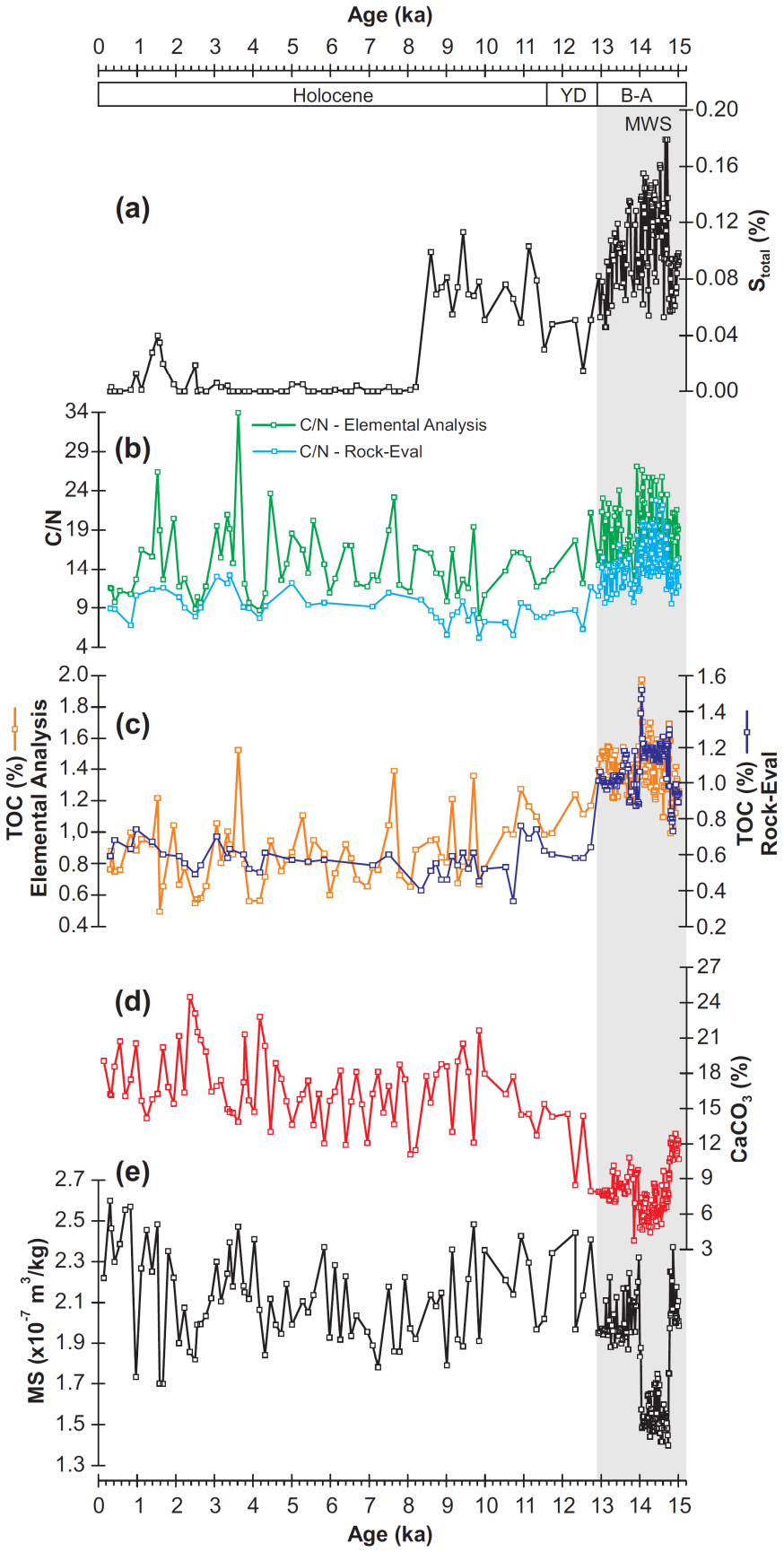

Fig. 2.8. Magnetic susceptibility (MS) distribution, carbonate ($CaCO_3$), TOC, S_{total} and concentrations (%), and C/N ratio. The Younger Dryas (YD) from 12.9 to 11.6 ka and Bølling-Allerød warming (B-A) from 15.4 to 12.9 ka are indicated. The meltwater spike (MWS) is indicated in shaded band.

The TOC determined by subtracting inorganic carbon concentrations from total carbon concentrations (elemental analysis), and the TOC obtained by Rock-Eval pyrolysis gave consistent results (Fig. 2.8b-c). The $TOC_{elemental\ analysis}$ obtained by subtraction is used in the Holocene interval, because the TOC content obtained by Rock-Eval pyrolysis was studied at lower resolution. The TOC content, obtained by Rock-Eval pyrolysis, ranges between 0.34 and 1.52% and C/N ratios range from 5.2 to 22.7. The TOC content, obtained by subtraction ranges from 0.49 to 1.98% and C/N ratio ranges from 7.7 to 33.9. Both TOC concentrations and C/N ratio show maximum values between 14.7 and 14 ka (meltwater spike) whereas the lowest values characterize the uppermost part of the core, Holocene interval (Fig. 2.8c). The used instrumental method in the elemental analysis only allowed the quantifying precise of the total sulfur (S_{total}) in the deglacial interval and early Holocene (15-8.6 ka). S_{total} content varies from 0.02 to 0.18%, with highest values during the meltwater spike (Fig. 2.8a).

MS displays a stair-step pattern during the main meltwater discharge episode (15-12.9 ka), with the lowest values between 14.7 and 14 ka which coincident with the interval of homogenous sediment (Fig. 2.8e). During the Holocene the MS fluctuates between 1.7 and 2.6 $x10^{-7}$ m^3/kg, with no remarkable changes.

The Rock Eval parameters (Tmax and HI) show little variations (Fig. 2.9). Tmax values ranges from 380 to 433°C and HI varies from 62 to 146 mg HC/g TOC. The TOC vs. S_2 and Tmax vs. HI crossplots together with C/N values (C/N>15; Fig. 2.8b) suggest predominantly immature type III OM, that is, of terrestrial origin.

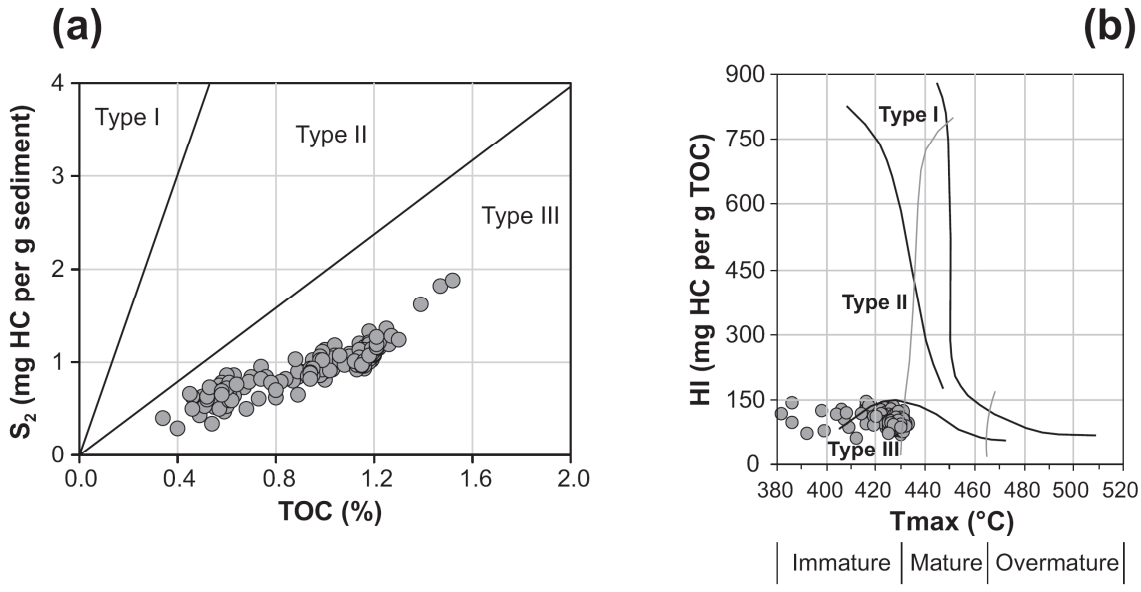

Fig. 2.9. Rock-Eval pyrolysis parameters. (**a**) TOC vs. S_2 and (**b**) Tmax vs. HI crossplot illustrating the origin and maturation states of the organic matter.

2.3.3. Grain size distribution

Grain-size analysis carried out on 213 samples indicates the sediments within Pigmy Basin are mainly composed of fine-grained cohesive silt (3.1µm<mode<5.2µm). All samples are characterized by a unimodal grain-size distribution. Vertical changes in the grain-size parameters of the sediment are illustrated in Fig. 2.10. More specifically, the sediments are composed of 49-70% cohesive-silt, 5-31% sortable-silt, 15-28% clay, and 0-58.2% sand. Intervals in the core with more of 10% of sand are interpreted as small turbidites (e.g., 29.7, 12, 20.3, 32.3, 58.2 ka in Fig. 2.10f). These small turbidites were removed from our calculations because they do correspond to instantaneous processes and will distort the stratigraphic distribution of the proxies.

The grain-size mode shows a slight coarsening-upward trend (Fig. 2.10a). The clay content is maximum in the lowermost part of the core (between 11 and 15 ka, deglacial interval) and shows an upward decreasing trend (Fig. 2.10e), whereas the cohesive-silt particles increase (Fig. 2.10d). The cohesive-silt/sortable-silt ratio is higher in the lowermost (14.7 to 12.9 ka; meltwater discharge episode) and uppermost (4 to 0 ka; late Holocene) parts of the core (Fig. 2.10b). The Younger Dryas (12.9-11.6 ka) is marked in the core MD02-2553 by increase in the clay-size particles (up to 27.5%), which also is reflected in the grain-size mode.

2.3.4. Clay mineral analysis

A total of 195 samples were analyzed by X-ray diffraction to determine the mineralogical assemblage of the Pigmy Basin sediments (core MD02-2553).

The clay fraction is composed of dominant smectite (63-86%, average 76%), and accessory illite (6-17%, average 11%), chlorite (2-11%, average 6%), and kaolinite (2-13%, average 8%) (Fig. 2.11). It may be is emphasized that the domination of smectite does not result from differential settling processes (Sionneau et al., 2008).

In general, the clay-mineral composition displays some characteristic oscillations between smectite-rich intervals (14.7-14, 8.1-6.8, 6.4-5.9, 4.9-3.6, 3.1-1.7 and 1-0.3 ka) and illite + chlorite-rich intervals (15-14.7, 14-12.9, 12.9-10, 6.8-6.4, 5.9-4.9, 3.6-3.1 and 1.7-1 ka) (Fig. 2.11a). It notices that the frequency of these oscillations increases during the Holocene.

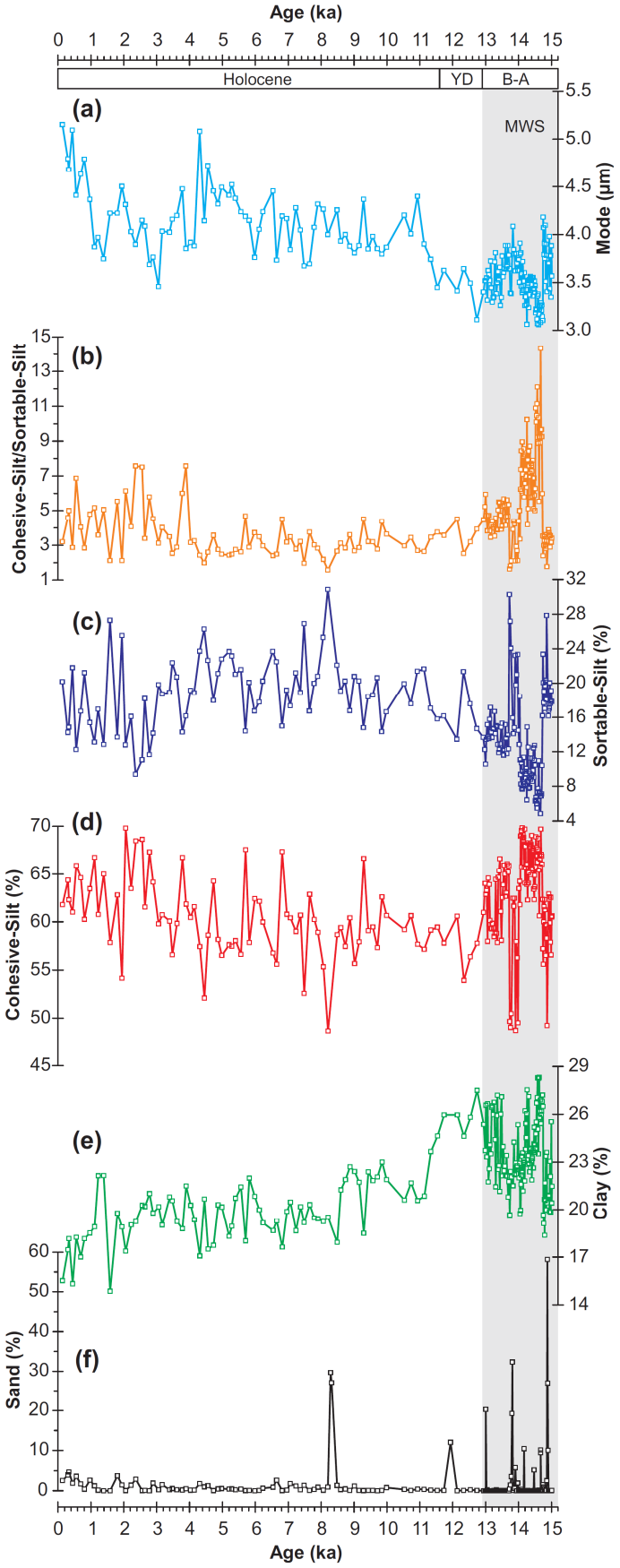

Fig. 2.10. Grain-size distributions (grain-size classes in %, and mode in µm) from Pigmy Basin (core MD02-2553). The Younger Dryas (YD) from 12.9 to 11.6 ka and Bølling-Allerød warming (B-A) from 15.4 to 12.9 ka are indicated. The meltwater spike (MWS) is indicated in shaded band.

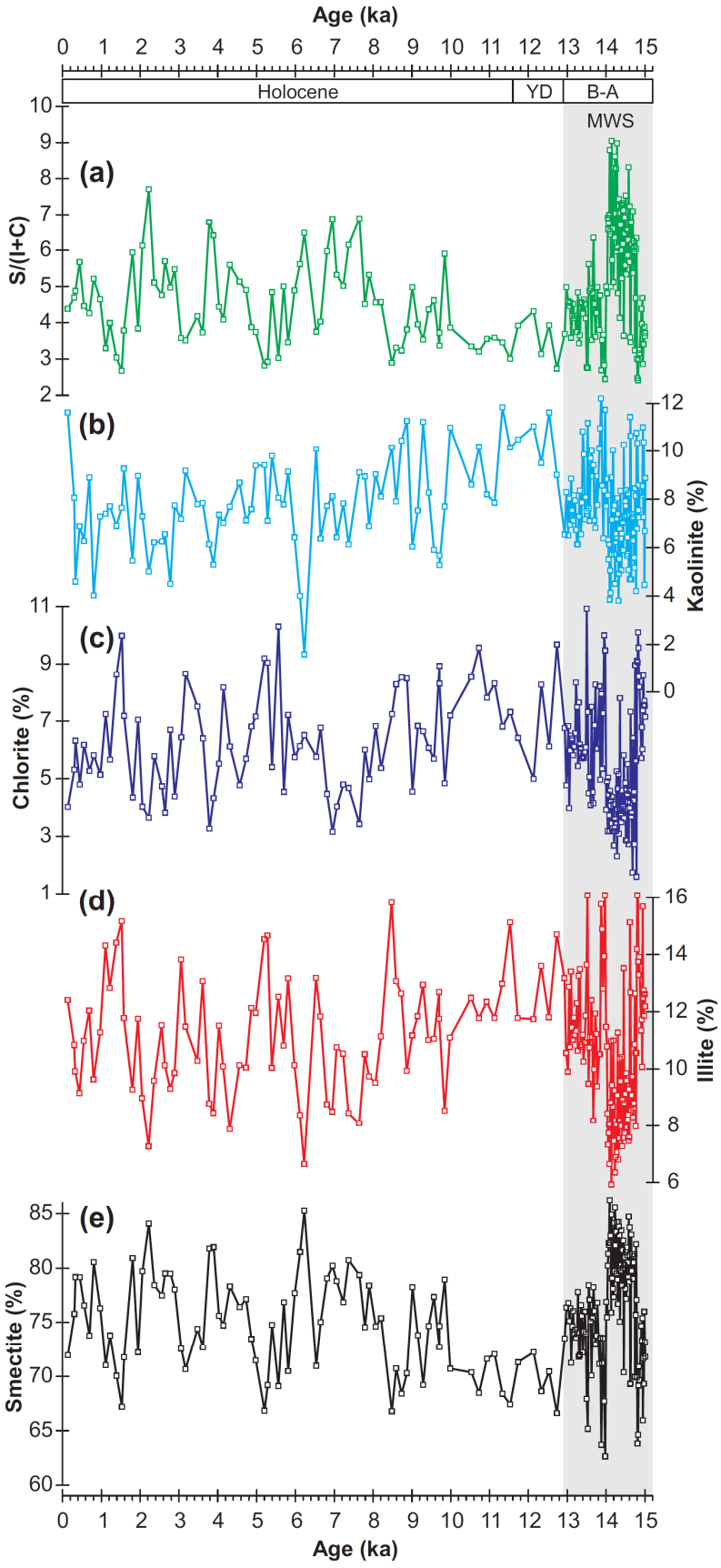

Fig. 2.11. Clay-mineral assemblages from Pigmy Basin (core MD02-2553). The Younger Dryas (YD) from 12.9 to 11.6 ka and Bølling-Allerød warming (B-A) from 15.4 to 12.9 ka are indicated. The meltwater spike (MWS) is indicated in shaded band.

In core MD02-2553, the main meltwater discharge episode (15-12.9 ka) is marked by the clay mineral assemblage by a stair-step pattern. In this interval, the smectite content displays highest values (up to 86%) between 14.7 and 14 ka and lowest values between 15-14.7 (up to 76%) and 14-12.9 ka (up to 78%). The clay fraction during the Younger Dryas (12.9-11.6 ka) is characterized by the increased contribution of illite (up to 13%), kaolinite (up to 10%) and chlorite (up to 7%) at the expense of smectite.

It is important to emphasize that in contrast to the others terrigenous proxies used in this study (Fig. 2.8 and Fig. 2.10), which increase or decrease markedly during the last deglaciation, the clay-mineral distributions display oscillations with similar magnitude between the last deglaciation and Holocene (Fig. 2.11). According to this observation, the variations in the clay mineral assemblage in the Pigmy Basin may be interpreted as changes in continental erosion and provenance through the last 15 ka.

2.3.5. Elemental geochemistry

Major- and trace-element analyses were carried out on 53 samples, taken on average at 20-cm stratigraphic intervals. Element concentrations were normalized to Al in order to exclude a dilution effect by varying carbonate contents.

Fig. 2.12 illustrates that the major and trace elements show little variations down core. However, the geochemical signature differs drastically in the lowermost parts of the core corresponding to the meltwater spike (14.7 to 14 ka). In this interval of the core, Al-normalized trace metal distributions are sometimes characterized by a synchronous stair-step pattern with low Mn/Al, Ca/Al, K/Al, Ba/Al, Th/Al, Y/Al, La/Al, Ce/Al, Co/Al, Ni/Al, Zn/Al, Cu/Al and total REE/Al ratios, and slightly high Si/Al, Fe/Al, Na/Al, V/Al and Mo/Al ratios compared to the Holocene (Fig. 2.12).

On the other hand, during mid- to late-Holocene the K/Al, Mg/Al, Ti/Al and Fe/Al ratios display relatively high variability (Fig. 2.12), which is consistent with the observed clay-mineral and grain-size (cohesive-silt/sortable-silt ratio) oscillations.

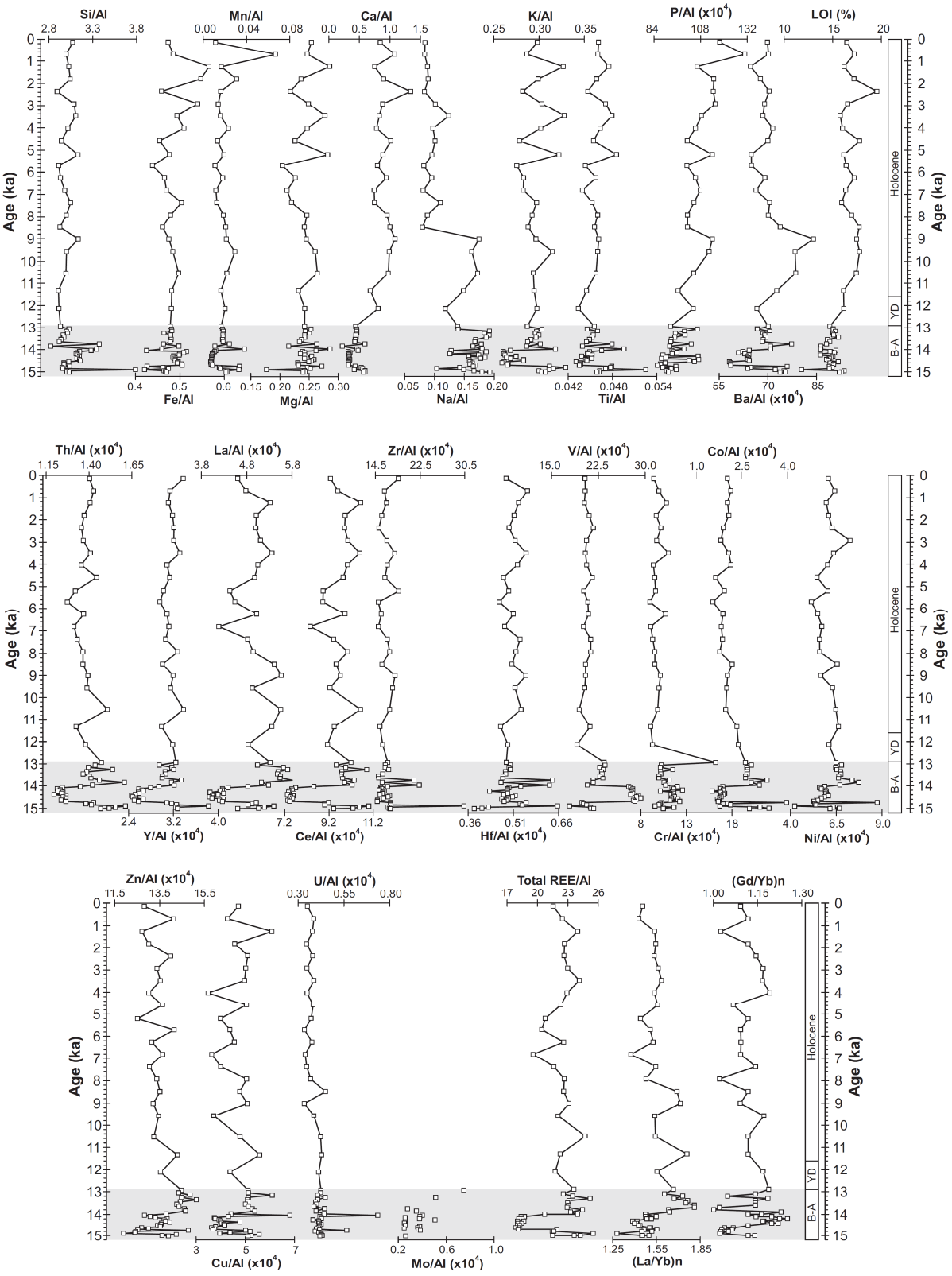

Fig. 2.12. Al-normalized elemental ratios: major, traces and rare earth (REE) elements. Note that the scale of the ratios is expanded. The suffix "n" denotes a NASC-normalized value (Gromet et al., 1984). LOI: Loss on Ignition. The Younger Dryas (YD) from 12.9 to 11.6 ka and Bølling-Allerød warming (B-A) from 15.4 to 12.9 ka are indicated. The meltwater spike is indicated in shaded band.

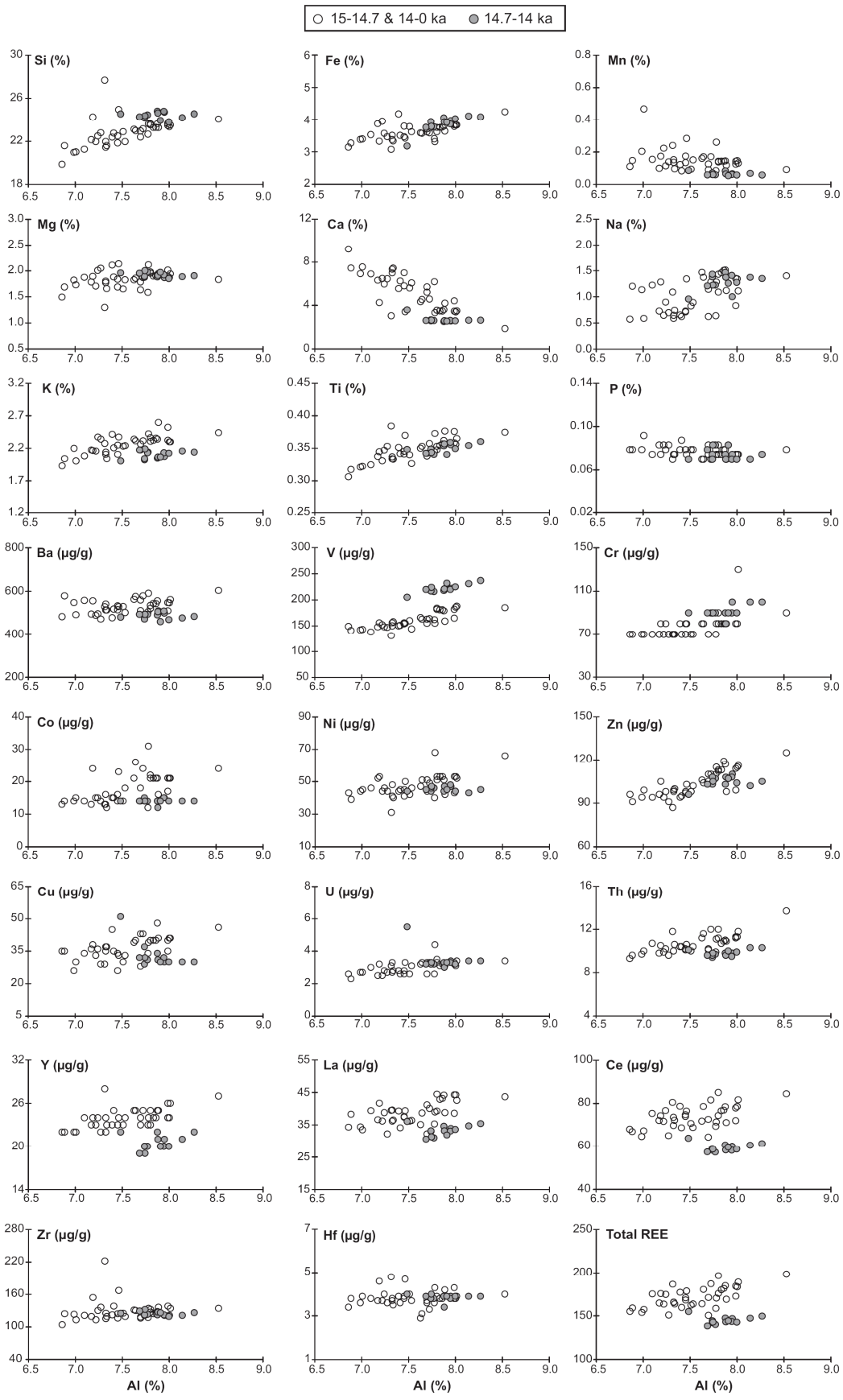

Fig. 2.13. Scatter plots of analyzed elements vs. Al concentrations. The samples that correspond to the meltwater spike are indicated in grey dots.

The peculiar geochemical character in the deglacial section of the core is also show on the scatter plots of metal vs. Al concentrations (Fig. 2.13), where major and trace elements show good correlation with Al concentrations, advocating to a detrital origin. Fig. 2.13 shows that the meltwater spike interval is slightly enriched in terrigenous elements such as Al, Si, Fe, Na and Ti, as well as in V, and slightly depleted in K and total REE. Furthermore, Ca, mainly associated with carbonates, shows a negative correlation with Al, suggesting a control by dilution process – that influx of more siliciclastics dilutes calcareous biogenic fraction and the metals associated with it. No relationship between Fe and Ni, Cu, Zn and Co was observed, evidencing no significant incorporation of the trace metals to iron sulfide (e.g., Tribovillard et al., 2006).

Trace-metal enrichment factors do not show any significant variations (average, 0.5 to 2.5), which also indicates that the redox sensitive and/or sulfide-forming trace metals (e.g., V, U, Mo, Cu, Ni, Co) are not authigenically enriched (EF_{TM}<5) (Fig. 2.14).

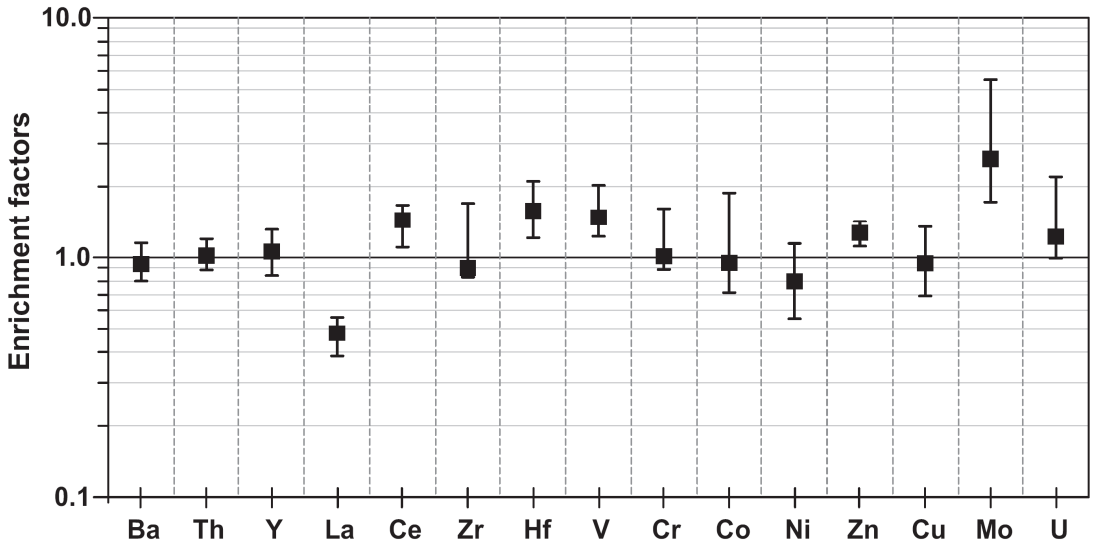

Fig. 2.14. Comparisons of the enrichment factor of selected trace metals of core MD02-2553 (Pigmy Basin). The extent line of the boxes corresponds to the range of values (min-max) and the boxes to the average value. The horizontal line EF = 1 indicates the value for which there is no enrichment/depletion with regards to average shale composition.

NASC–normalized REE patterns for Pigmy Basin sediment are shown in Fig. 2.15. The REE patterns exhibit variation typical of the NASC and do not show any striking features, except for a general slight enrichment in light REE (LREE: La-Nd) over heavy REE (HREE: Tb-Lu), evidenced also by the La/Yb and Gd/Yb distributions (Fig. 2.12). Ce and Eu anomalies (not shown) do not show any significant trend either. Lastly, the REEs patterns in the Pigmy Basin sediments exhibit a similar distribution to the Mississippi River suspended loads (Fig. 2.15).

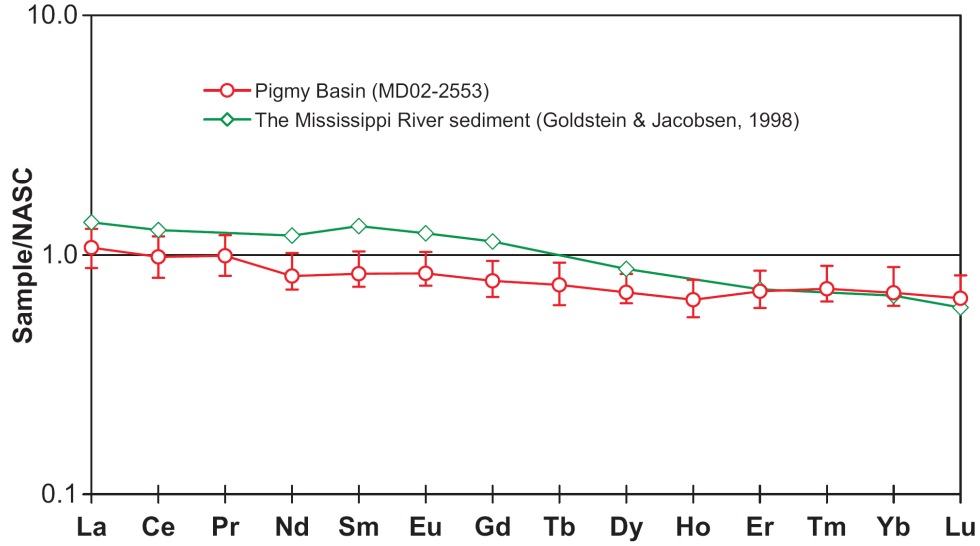

Fig. 2.15. Comparison of REE patterns between the averages of Pigmy Basin and Mississippi River sediments (Goldstein and Jacobsen, 1988; Elderfield et al., 1990). NASC values by Gromet et al. (1984) are used for normalization.

2.4. Interpretations and discussions

2.4.1. Sedimentary regimes over the last 15 ka in the Pigmy Basin (main findings, new insights)

Main characteristics of sedimentary regimes in the Pigmy Basin

The calcareous biogenic fraction in the Pigmy Basin sediments is relatively low ($CaCO_3$<25%) indicating that sedimentation is mainly ruled by the terrigenous supply over the entire interval being strictly detrital during the deglaciation (or meltwater spike) whereas significant autochthonous biogenic contribution is observed during the Younger Dryas and Holocene at the expense of the decreasing of terrigenous supply (Fig. 2.6-2.10). In addition, trace-metal enrichment factors suggest that the authigenic phases in the Pigmy Basin are negligible (Fig. 2.14). The C/N ratio (Fig. 2.8b) and Rock-Eval parameters (Fig. 2.9) suggest that the organic fraction is also mostly terrigenous, in agreement with similar findings obtained in the Pigmy Basin (core DSDP 619; Jasper and Gagosian, 1990) and in nearby the Orca Basin (Meckler et al., 2008; Tribovillard et al., 2008, 2009; Sionneau et al., in revision).

The absence of any significant REE fractionation when normalized to NASC in Pigmy Basin sediments indicates a highly-mixed detrital source. The similarity of REE distributions in Pigmy Basin sediments when compared with Mississippi River suspended loads (Goldstein and Jacobsen, 1988; Elderfield et al., 1990; Fig. 2.15) indicates the dominant influence of Mississippi River and weak contributions of other rivers (Mobile, Brazos and Atchafalaya). These results thus suggest that the Pigmy Basin mainly collects land-derived particles delivered by the Mississippi + Missouri river system that drains almost half of the conterminous USA. In other words, the Pigmy Basin is an appropriate recorder of the land-to-sea transfer, from North America to the GOM. Under this frame, any variation in sedimentation (e.g., changes in the nature of the terrigenous particles) is then likely to result from modifications of the erosional processes over the Mississippi River watersheds that are largely controlled by two main climatic factors:

(1) Meltwater discharges originating of the south margin of the LIS (Fig. 2.16), such as the meltwater spike, and proglacial lakes, during the deglaciation (e.g., Marchitto and Wei, 1995; Brown and Kennett, 1998; Aharon, 2003; Flower et al., 2004; Meckler et al., 2008; Sionneau et al., in revision).

(2) Successive migrations of the precipitation belt over North America (Fig. 2.17), and Mississippi megafloods episodes during the Holocene (e.g., Brown et al., 1999; Liu and Fearn, 2000; Knox, 2000, 2003).

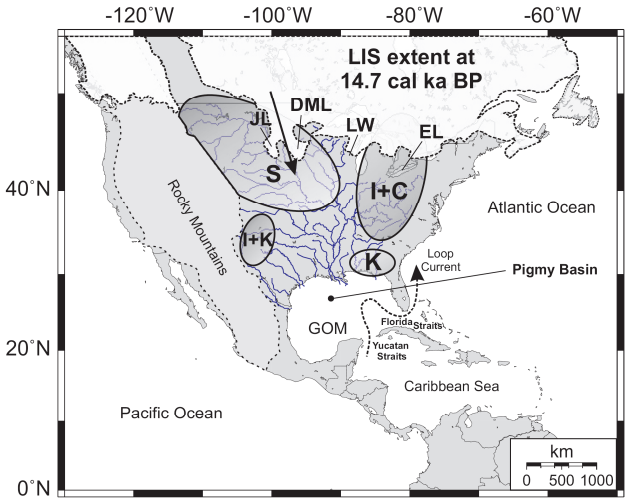

Fig. 2.16. Map of North America with the extent of the Laurentide Ice Sheet during the last deglaciation (14.7 ka) (Dyke, 2004) showing the main continental clay mineral provinces (Sionneau et al., 2008); S: smectite, I: illite, C: chlorite, K: kaolinite, GOM: Gulf of Mexico, JL: James glacial lobe, DML: Des Moines glacial lobe, LW: Lake Wisconsin, EL: Erie Lake.

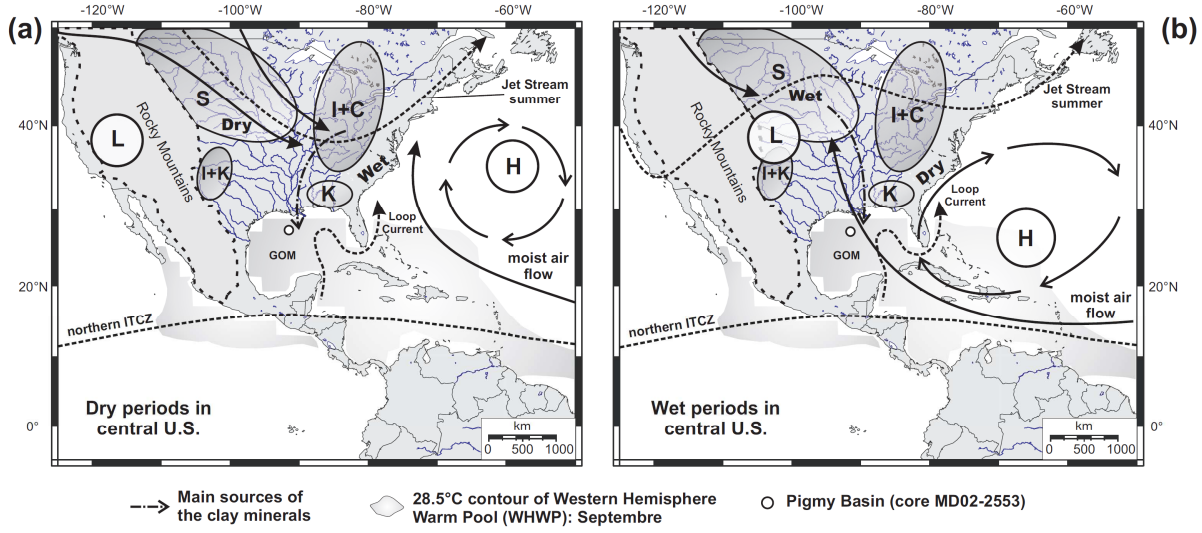

Fig. 2.17. Generalized reconstructions of regional atmospheric circulation patterns during the Holocene summer in the middle-latitude North America and their paleoclimatic implications (modified from Forman et al., 1995; Liu and Fearn, 2000). (**a**) Configuration during predominant dry periods in central North America. (**b**) Configuration during predominant wet periods in central North America. The Jet Streams denote the approximate boundaries of air masses from tropical, pacific and polar-source regions and locations of the areas with the main moisture transfers over the North American continent (adapted from Knox 2000, 2003). Main continental clay-mineral provinces over United States (Sionneau et al., 2008), main position of the Intertropical Convergence Zone (ITCZ) for Northern Hemisphere summer (adapted from Ziegler et al., 2008), and 28.5°C contour of Western Hemisphere Warm Pool (modified from Wang and Enfield, 2001) are also shown. The letters S, I, C and K stand for smectite, illite, chlorite and kaolinite, respectively.

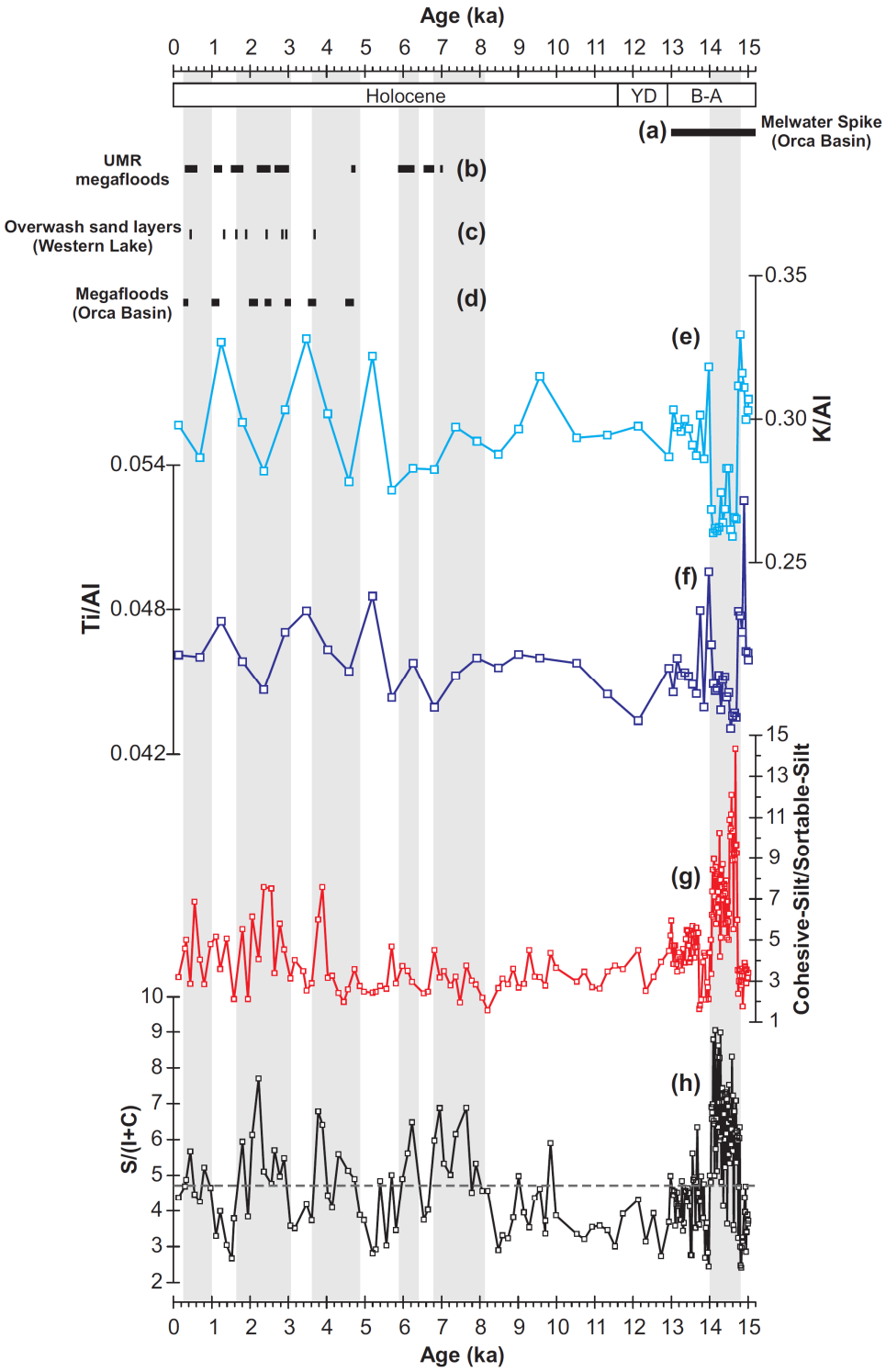

Fig. 2.18. Comparison of the main sedimentological and geochemical records of the Pigmy Basin with terrestrial and marine paleorecords of the GOM, Gulf Coast and central North America. (**a**) Meltwater spike interval; this interval is defined in the northern GOM by a major negative $\delta^{18}O$ excursion (-2.5‰) between 15.2 and 13 ka (Flower et al., 2004). (**b**) Upper Mississippi River (UMR) channel megafloods episodes (Knox, 2003). (**c**) Overwash sand layers from Western Lake, Gulf Coast (Liu and Fearn, 2000). (**d**) Megafloods on the Mississippi River identified by Brown et al. (1999) in the Orca Basin; Intervals punctuated by relatively coarse siliciclastic grain-size peaks, planktonic faunal turnovers, and negative $\delta^{13}C$ excursions of planktonic foraminifers *G. ruber* and *G. sacculifer*. Sedimentary records in the Pigmy Basin: (**e-f**) K/Al and Ti/Al ratios. (**g**) Cohesive-silt/Sortable-silt ratio. (**h**) smectite/(illite+chlorite) ratio. The smectite-rich intervals are indicated in shaded bands.

Recent studies (PhD thesis of Sionneau, 2008; Sionneau et al., in revision) proposed the use of clay mineralogy to track down the origin of the detrital material (and therefore of the main meltwater discharges and megafloods episodes) delivered to the GOM via the Mississippi River. Indeed during the last 15 ka, mineralogical and geochemical data both suggest that detrital sedimentation mainly results from the contributions of two different sources (Fig. 2.18 and 2.15). The first source is characterized by its high smectite content associated mainly with high V/Al ratio, whereas the second contributor is enriched in illite and chlorite with high Mg/Al, K/Al and Ti/Al ratios (Fig. 2.12 and 2.14). According to recently published clay-mineral distribution maps in and around the Mississippi River watershed (Sionneau et al., 2008), the first end-member corresponds to the northwestern Mississippi and Missouri rivers watershed province and the second one is likely the northeastern Great Lakes province (Fig. 2.19). On the other hand, the low correlation between the variations of illite and kaolinite (Pearson correlation coefficient: r = 0.31, n = 195; Fig. 2.20a) implies that the alternative illite-rich source area from the southwestern illite + kaolinite-rich province (Fig. 2.19) is not a possible candidate. In contrast, the relatively good correlation between illite and chlorite (Pearson correlation coefficient: r = 0.54, n = 195; Fig. 2.20b) indicates a common source for illite and chlorite, pointing out the northeastern province as the main contributor (Fig. 2.19). The respective contributions of smectite versus illite and chlorite are thus used to document the origin of the main detrital supply in the Pigmy Basin during the last 15 ka.

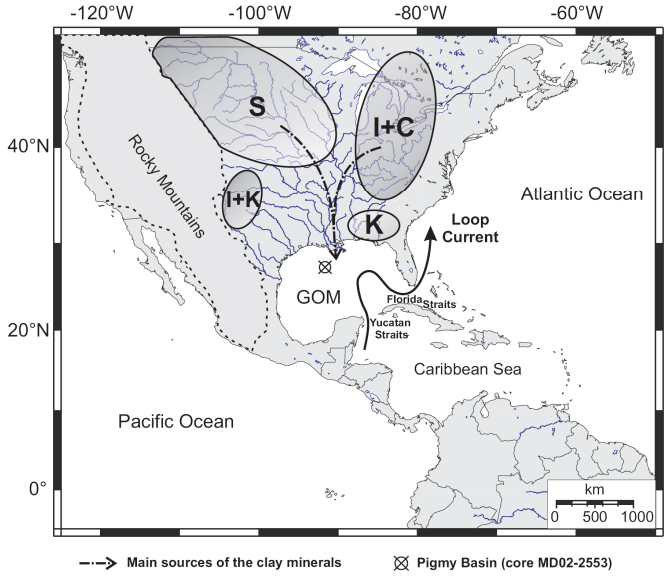

Fig. 2.19. Map showing the main continental clay-mineral provinces over United States (adapted from Sionneau et al., 2008). The letters S, I, C and K (standing for smectite, illite, chlorite and kaolinite, respectively) indicate areas where the bedrock/soils contain a clay-mineral assemblage markedly dominated by one clay species.

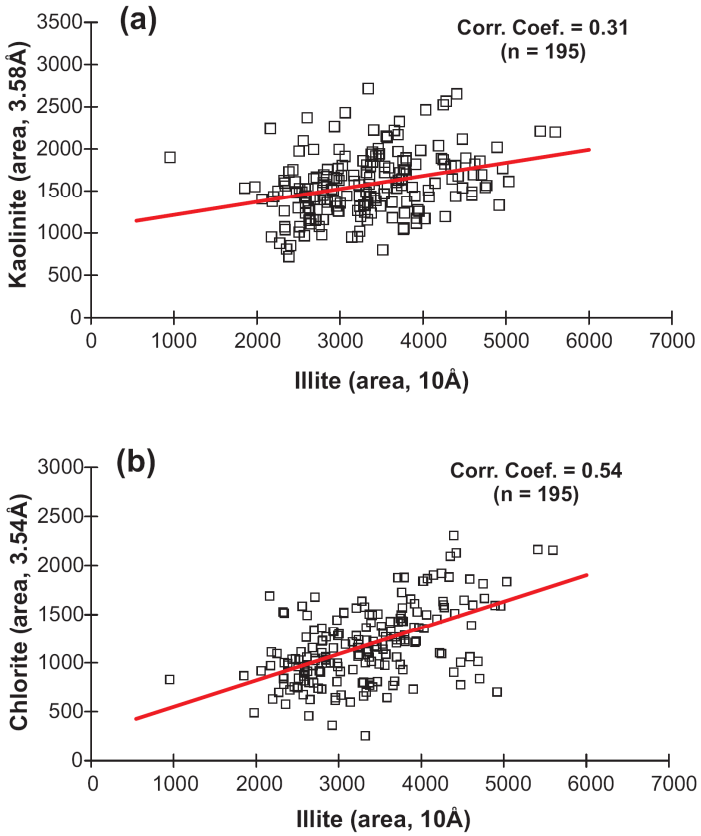

Fig. 2.20. The corresponding relationship between (**a**) illite vs. kaolinite and (**b**) illite vs. chlorite (in counts per second) for the full record of the Pigmy Basin (core MD02-2553). Corr. Coef. = Pearson correlation coefficient.

In addition, geochemical data compared with the Al-normalized metal concentrations from the Mississippi drainage area (Gustavsson et al., 2001; Grossman, 2009), give new evidences on the provenance of the detrital fraction. Thus, the elemental ratios in Pigmy Basin characterizing the smectite-rich intervals (mainly high V/Al ratios, and low Ti/Al, Th/Al, K/Al, La/Al, Y/Al and Total REE/Al ratios) are consistent with the hypothesis of specific supply from the northwestern part of the USA, while the elemental ratios observed in the illite- + chlorite-rich intervals (high Mg/Al, K/Al and Ti/Al ratios) reflect an increase contribution of the northeastern province.

The meltwater discharge interval (15-12.9 ka)

The variations of almost all the parameters measured in the core MD02-2553 from Pigmy Basin are synchronous with the main deglacial meltwater episode (so-called meltwater spike) described or modelled in previous marine or continental studies (e.g., Jasper and Gagosian, 1990; Knox, 1996; Marchitto and Wei, 1995; Brown and Kennett, 1998; Aharon, 2003; Flower et al., 2004; Rittenour et al., 2007; Meckler et al., 2008).

The meltwater discharge interval is marked in Pigmy Basin sediments by an increase in TOC and S_{total} concentrations and C/N ratio likely attributed to the higher sedimentation rates (about 200-397 cm/ka) that occurred at the time, and that resulted in the more efficient burial and preservation of terrigenous organic matter. This period of high meltwater supply is also linked with the occurrence of organic layers previously described in the northern GOM (e.g., Tripsanas et al., 2007; Meckler et al., 2008). The laminations observed in the lower part of the core MD02-2553 from Pigmy Basin may then correspond to (1) slight stratification in the deep part of the basin as described for the Orca Basin (Tribovillard et al., 2009), or (2) an enhanced oxygen consumption related to increased terrigenous particles flux (organic and mineral) (e.g., Leventer et al., 1983; Meckler et al., 2008). However, there are no geochemical evidences of strong modifications of the redox conditions in the Pigmy Basin that did not undergo oxygen-restricted conditions.

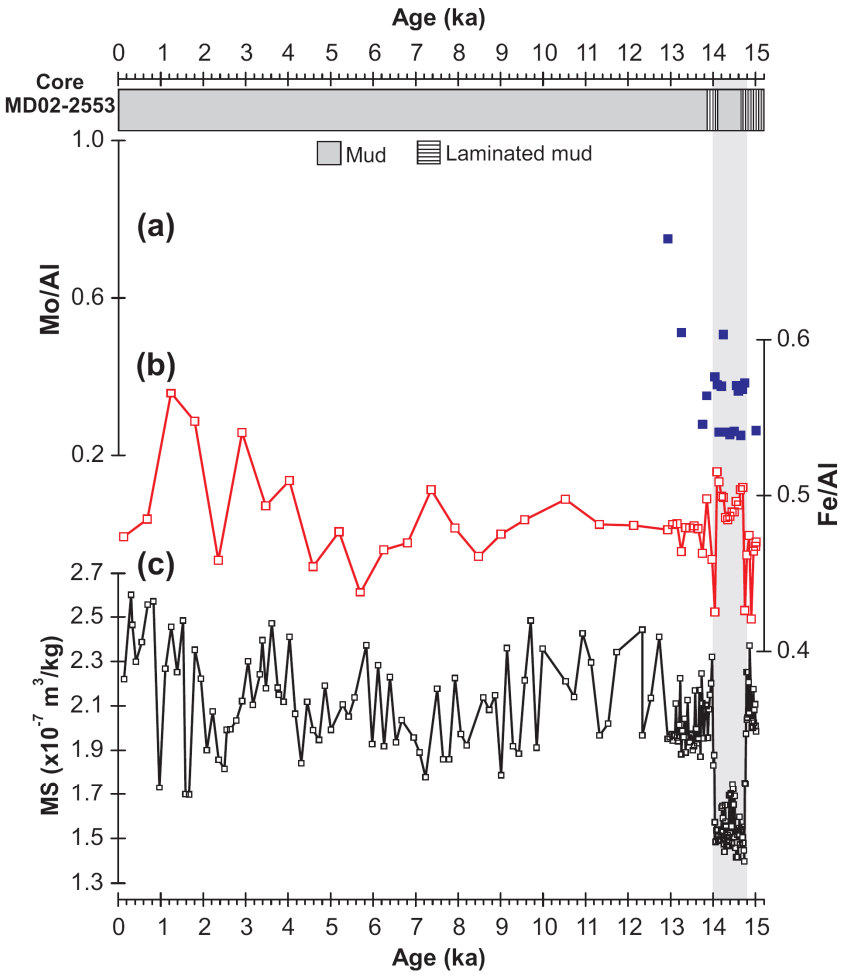

Fig. 2.21. Comparison between magnetic susceptibility (MS) values and Al-normalized abundances of Fe and Mo from the Pigmy Basin. Note the low MS values during the meltwater spike interval (shaded band).

On the other hand, Fig. 2.21c shows that the MS values are quite low during the main meltwater discharge episode, although the grain size and mineralogical proxies indicate a strong supply of terrigenous material (e.g., Figs. 2.6 - 2.7). It is noteworthy also that these low values correspond exactly with a high Fe/Al and Mo/Al ratios and with a break in laminations (Fig 2.17). This could be discussed in terms of redox conditions. When oxygen levels decrease and other electron acceptors are required for organic matter degradation, magnetite-like iron – which is the dominant magnetic mineral in the Pigmy Basin sediments (King, 1986) – is reduced to Fe(II), which subsequently yields low MS values (e.g., Bloemendal et al., 1992).

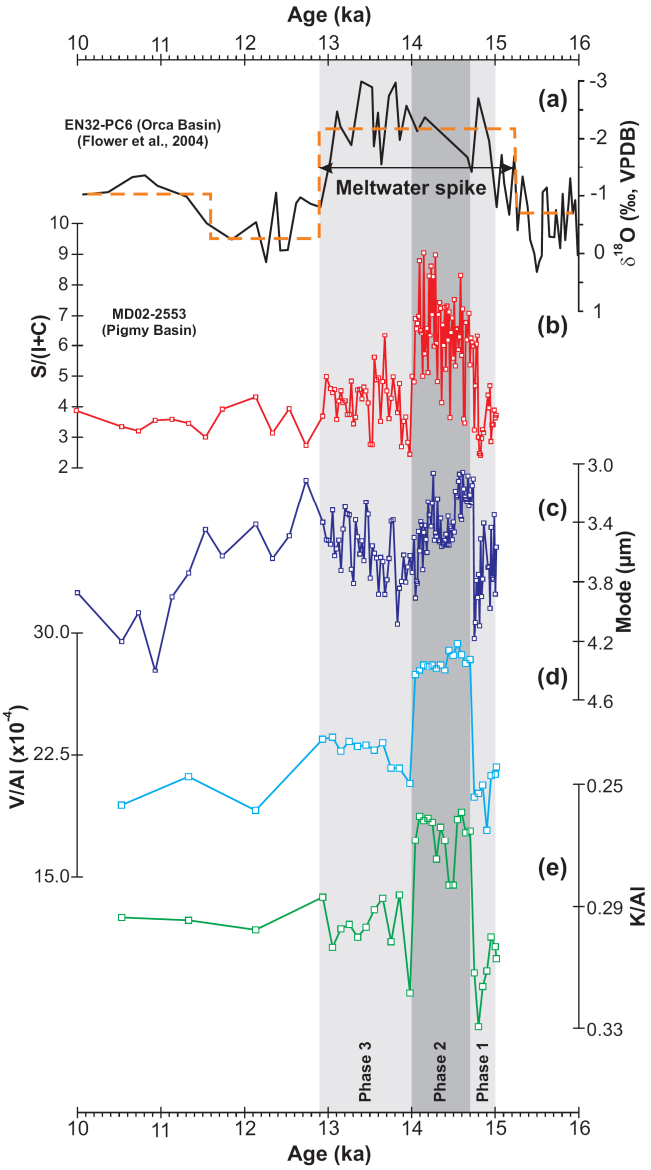

Fig. 2.22. Deglacial proxy records during 16–10 ka interval. (**a**) The $\delta^{18}O$ foraminifer records from Orca Basin core EN32-PC6 (Flower et al., 2004). Sedimentary records in the Pigmy Basin: (**b**) clay mineral ratio S/(I+C), (**c**) grain-size mode (µm), (**d**) V/Al ratio, and (**e**) K/Al from core MD02-2553. Shaded bands represent the three distinct phases of erosion of the meltwater spike here proposed.

During the meltwater spike, most sedimentological and geochemical proxies display a peculiar stair-step pattern (eg., Fig. 2.8, and Figs. 2.6-2.8), which suggests more specifically, that the meltwater spike occurred in three distinct phases of erosion, with a maximum of erosion between 14.7 and 14 ka (Fig. 2.22). These phases are described briefly as follows:

1.- Phase 1 (15-14.7 ka): During this early erosive phase, mineralogical [S/(I+C)<4.9] and geochemical (relatively high Ti/Al and K/Al values and low Fe/Al and V/Al) proxies indicate a mixed provenance of detrital particles, i.e. mainly from the north-western province (smectite) but with some contribution of the north-eastern province (illite and chlorite), suggesting that meltwater originated from almost all the southern margin of the LIS - from the southwest of James glacial lobe to the eastern margin of Lake Erie (Fig. 2.16). Grain-size distribution (mode ~3.8 µm, high %sortable-silt) indicates that erosional processes of the main Mississippi River channel were rather important during the early phase of the Meltwater Spike.

2.- Phase 2 (14.7-14 ka): This second phase represents the climax of midcontinental erosion, and is characterized by a strong increase in smectite content (up to 86 %) at the expense of illite + chlorite, which suggest a dominant origin from NW North America for detrital particles, reflecting meltwater outflow from the rapid retreat of the southwestern LIS margin (Fig. 2.16). Note that the low Ti/Al, Th/Al, K/Al, La/Al, Y/Al and Total REE/Al ratios during this phase (Fig. 2.12) suggest a significantly reduced contribution of the northeast cratonic province (Fig. 2.16), and therefore also pinpoint the north-western province (high V/Al ratio) as the main detrital contributor during this phase. The decreasing in the grain-size mode (down to 3.1µm) suggest an increasing in the supplied of fine-grained sediment to the GOM, as a result of the more intense deglacial megafloods erosion over the clay-rich terrace deposits along upper Mississippi River tributaries (Knox, 1996; Rittenour et al., 2007).

3.- Phase 3 (14-12.9 ka): This third phase displays mineralogical and geochemical characteristics similar to those of Phase 1, which suggests a re-start of contributions from the northeast province as the LIS was withdrawn from its southern extent (Fig. 2.16). The still high sedimentation rate (200 cm/ka) though lower than in Phase 2, the slightly coarser mode, and the higher proportion of sortable-silt suggest that this phase corresponds to the late phase of the meltwater spike with reduced erosional processes.

To summarize, using a strategy pioneered by Brown and Kennett (1998), Sionneau (2008) and Sionneau et al. (in revision), which uses clay mineralogy as a tracer of geographic provenance in North America, in combination with other terrigenous proxies (sediment grain-size, elemental geochemistry) in Pigmy Basin (core MD02-2553), this part of the research allowed to identify with more detail the time-dependent shifting location of the LIS ice melting lobes during the main meltwater discharge episode (15-12.9 ka). These changes in the dynamics of LIS are summarized in three different phases of erosion that added valuable insights to previously published data (e.g., Sionneau et al., in revision), since to enable better understanding of the history of meltwater input into the GOM.

Sedimentary regime during the Holocene and variability of Mississippi River runoff

The linkages between deglacial meltwater episodes originating from the southern margin of the LIS and the Pigmy Basin sedimentary record (core MD02-2553) suggest that subsequent changes in Holocene Mississippi River discharge, unrelated to LIS melting history, may also be recorded in this core. However, unlike the last deglaciation, the detrital sedimentary record of the Mississippi River discharges within the GOM through the Holocene has been so far poorly investigated (e.g., Brown et al., 1999) although it may provide a high-resolution data on the long-term paleohydrologic changes over North America, and allows to investigate the links between ocean-atmosphere dynamics and continental flooding. These last aspects are discussed briefly in this section.

During the early Holocene, the Mississippi River discharge capacity was significantly reduced, as evidenced in the Pigmy Basin record by a decrease of the sedimentation rate from about 200 to 36-25 cm/ka (Fig. 2.6), likely due to a drastic decrease in the glacial erosional processes linked to the decaying LIS. In the neighboring Orca Basin this is reflected by more positive *G. ruber* $\delta^{18}O$ values (~0‰) compared to the deglaciation values (Flower et al., 2004; Fig. 2.22a).

Consequently, a major modification of the sedimentary regime occurs in the Pigmy Basin during the Pleistocene/Holocene transition. This transition is characterized by the general increase of the carbonate contents ($CaCO_3$), reaching values around 21%, whereas the TOC concentrations and C/N ratio are rather low (Fig. 2.8), suggesting an increased in the autochthonous biogenic contribution as the terrigenous input progressively diminished. This increase in biogenic productivity probably is related to warmer sea-surface temperature (SST) evidenced in the Orca Basin (Flower et al., 2004).

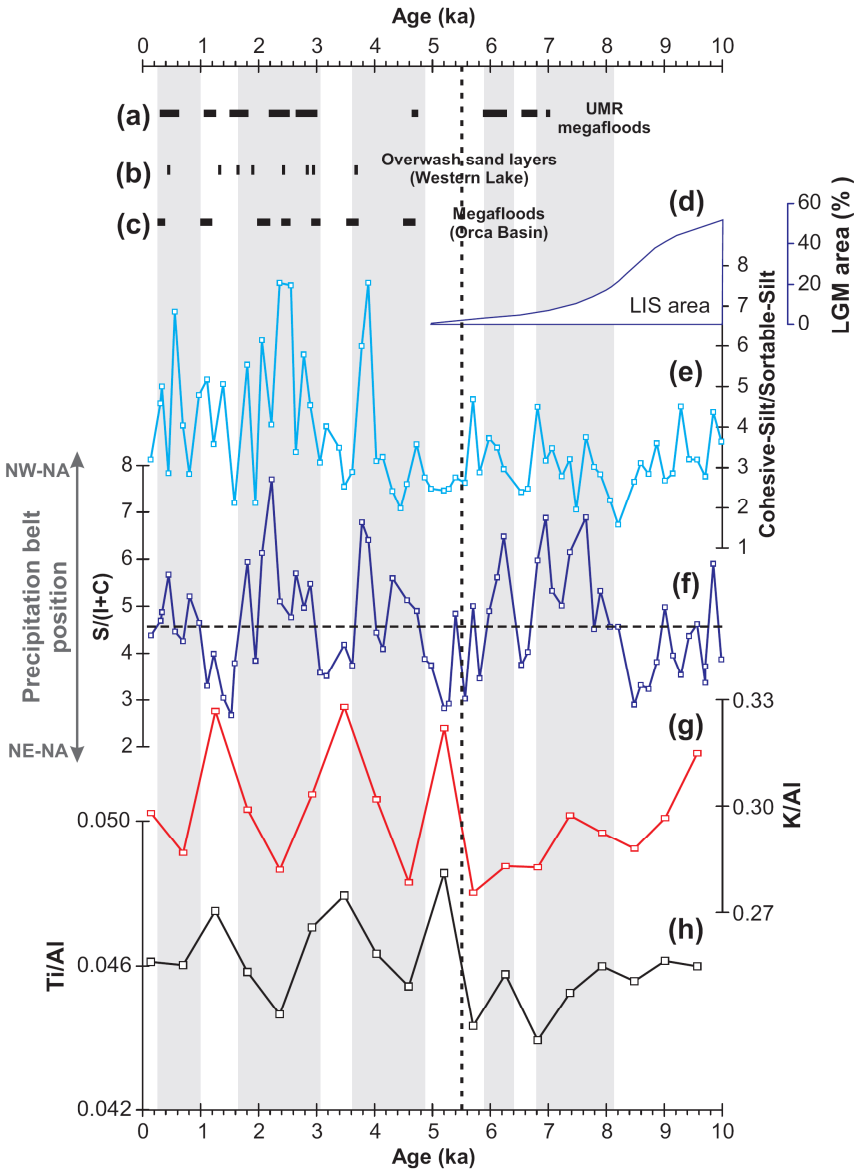

Fig. 2.23. Comparison of the multi-proxy record from the Pigmy Basin (core MD02-2553) with: (**a**) Upper Mississippi River (UMR) channel megafloods episodes (Knox, 2003); (**b**) overwash sand layers from Western Lake, Gulf Coast (Liu and Fearn, 2000); (**c**) megafloods on the Mississippi River identified by Brown et al. (1999) in the Orca Basin; (**d**) the area of the Laurentide ice sheet (LIS) as a fraction of the area during the last glacial maximum (LGM), adapted from Shuman et al. (2005); (**e-g**) sedimentological and geochemical proxies from the core MD02-2553. The smectite-rich intervals are indicated in shaded bands. The two-step of changes in the sedimentation regime inferred around of 5.5 ka also is indicated (dotted lines).

On the other hand, sedimentological and geochemical signatures indicate that early Holocene detrital sedimentation in Pigmy Basin was directly controlled by the LIS extent changes (Fig.2.19d), whereas that the oscillations of cohesive smectite-rich intervals associated with high geochemical variability characterize of mid to late Holocene sedimentation (Fig.2.19e-h). This notable shift in the sedimentation regime probably was due to (1) that the ice-sheet probably filtered and smoothed some of the high-frequency climatic variability during the early Holocene (e.g., Mayewski et al., 2004), and (2) a rapid

atmospheric reorganization following the LIS collapse (e.g., Shuman et al., 2002), likely triggers strong hydrological changes over central North America during the mid to late Holocene. Indeed, Knox (2000, 2003), working in the upper Mississippi valley, found relatively few large floods before 7 ka (Fig. 2.23a).

During the mid to late Holocene, after the final collapse of the LIS, mineralogical and geochemical records evidenced fluctuations in the Mississippi River sedimentation patterns (Fig. 2.23). They likely reflect oscillations between the two dominant terrigenous sources, smectite and illite + chlorite provinces (Fig. 2.19), linked to the meridian moisture transfer towards the North American continent and, to the successive migrations of the main precipitation belt over the Mississippi River watershed (Fig. 2.17). Within this context, the smectite-rich intervals in the Pigmy Basin point out specific terrigenous supply from the NW Mississippi River watershed, suggesting enhanced precipitations and moisture influx from the GOM toward central North America (Fig. 2.17b). These intervals coincide with large Mississippi floods (Fig. 2.23a) described in central North America (Knox, 2000, 2003) and catastrophic hurricanes (Fig. 2.22b) evidenced in the Gulf Coast Western Lake (Liu and Fearn, 2000). Contrastingly, repetitive enrichments in illite and chlorite suggest successive eastward migrations of main precipitation belt (Fig. 2.17a) consistent with documented evidences of increase aridity over central North America (Nordt et al., 2008) and development of more humid conditions along the Atlantic margin (Willard et al., 2005; Springer et al., 2008). In addition, the smectite-rich intervals characterized in the Pigmy Basin are in close general agreement with the intervals punctuated in Orca Basin by relatively coarse siliciclastic grain-size peaks, planktonic faunal turnovers, and negative $\delta^{13}C$ excursions of planktonic foraminifers *G. ruber* and *G. sacculifer*, which are interpreted by Brown et al. (1999) as episodes of megafloods on the Mississippi River (Fig. 2.23c). The correlations between continental and marine records indicate that these megafloods events represent regional-scale changes in the hydrologic cycle over North America.

To sum up, the sedimentological and geochemical results here obtained provide a solid record of detrital inputs delivered into GOM by the Mississippi River during the last 15 ka, and adds another “brick” in the histories edifice of the (1) dynamics and timing of deglacial meltwater discharge (meltwater spike) and, (2) episodes of Holocene megafloods in North America. These two climatic episodes will be discussed more widely in the next sections, following the style and format of a scientific paper.

References

Aharon, P., 2003. Meltwater flooding events in the Gulf of Mexico revisited: Implications for rapid climate changes during the last deglaciation. Paleoceanography 18(4), PA1079. doi: 10.1029/2002PA000840.

Bard, E., 1988. Correction of accelerator mass spectrometry 14C ages measured in planktonic foraminifera: paleoceanographic implications. Paleoceanography 3(6), 635-645.

Bloemendal, J., King, J.W., Hall, F.R., Doh, S.-J., 1992. Rock magnetism of Late Neogene and Pleistocene deep-sea sediments: relationship to sediment source, diagenetic processes, and sediment lithology. Journal of Geophysical Research 97 (B4), 4361-4375.

Bouma, A.H., Stelting, C.E., Leg 96 sedimentologists, 1986. Seismic stratigraphy and sedimentary processes in Orca and Pigmy Basin. In Initial Reports of the Deep-Sea Drilling Project. Leg 96. Bouma, A.H., Coleman, J.M., Meyer, A.W., et al., (Eds), Washington D.C., U.S. Government Printing Office. pp. 563-576 doi:10.2973/dsdp.proc.96.128.1986.

Brown, P., Kennett, J.P., Ingram, B.L., 1999. Marine Evidence for Episodic Holocene Megafloods in North America and the Northern Gulf of Mexico. Paleoceanography, 14(4), 498-510.

Brown, P.A. and Kennett, J.P., 1998. Megaflood erosion and meltwater plumbing changes during last North American deglaciation recorded in Gulf of Mexico sediments. Geology 26, 599-602.

Bryant, W.R., Bryant, J.R., Feeley, M.R., Simmons, G.R., 1990. Physiographic and bathymetric characteristics of the continental slope, Northwest Gulf of Mexico. Geo-Marine Letters 10, 182–199.

Dyke, A.S., 2004. An outline of North American deglaciation with emphasis on central and northern Canada. In Ehlers, J., Gibbard, P.L., (Eds), Quaternary Glaciations - Extent and Chronology, Part II. Elsevier B.V., Amsterdam, pp. 373-424.

Elderfield, H., Upstill-Goddard, R., Sholkovitz, ER., 1990. The rare earth elements in rivers, estuaries and coastal seas and their significance to the composition of ocean water. Geochimica et Cosmochimica Acta 54, 971-991.

Flower, B.P., Hastings, D.W., Hill, H.W., Quinn, T.M., 2004. Phasing of deglacial warming and laurentide ice sheet meltwater in the Gulf of Mexico. Geology 32, 597-600.

Goldstein, S.J., Jacobsen, S.B., 1988. Rare earth elements in river waters. Earth and Planetary Science Letters 89, 35-47.

Gromet, L.P., Dymek, R.F., Haskin, L.A., Korotev, R.L., 1984. The North American shale composite: its compilation, major and trace element characteristics. Geochimica et Cosmochimica Acta 48, 2469–3482.

Grossman, J., 2009. National Geochemical Atlas: The geochemical landscape of the conterminous United States derived from stream sediment and other solid sample media analyzed by the National Uranium Resource Evaluation (NURE) program. U.S. Geological Survey Open-File Report 98-622.
Online at http://tin.er.usgs.gov/geochem/about.php?group=Analyses+by+ICP%2FAcid+dissolution
(Revised 2009-04-01)

Gustavsson, N., Bølviken, B., Smith, D.B., Severson, R.C., 2001. Geochemical landscapes of the conterminous United States - New map presentations for 22 elements. U.S. Geol. Survey Prof. Paper, 1648. U.S. Department of the Interior.

Hughen, K.A., Baillie, M.G.L., Bard, E., Beck, J.W., Bertrand, C.J.H., Blackwell, P.G., Buck, C.E., Burr, G.S., Cutler, K.B., Damon, P.E., Edwards, R.L., Fairbanks, R.G., Friedrich, M., Guilderson, T.P., Kromer, B., McCormac, G., Manning, S., Ramsey, C.B., Reimer, P.J., Reimer, R.W., Remmele, S., Southon, J.R., Stuiver, M., Talamo, S., Taylor, F.W., van der Plicht, J.,Weyhenmeyer, C.E., 2004. Marine04 marine radiocarbon age calibration, 0–26 cal kyr BP. Radiocarbon 46, 1059-1086.

Jasper, J.P., Gagosian, R.B., 1990. The sources and deposition of organic-matter in the Late Quaternary Pigmy Basin, Gulf of Mexico. Geochimica et Cosmochimica Acta 54, 1117-1132.

King, J.W., 1986. Paleomagnetic and rock-magnetic stratigraphy of Pigmy Basin, Deep Sea Drilling Project Site 619, Leg 96. In Bouma, A. H., Coleman, J. M., Meyer, A. W., et al., Init. Repts. DSDP, 96: Washington (U.S. Govt. Printing Office), 677-684.

Knox, J.C., 1996. Late Quaternary Upper Mississippi River alluvial episodes and their significance to the Lower Mississippi River system. Engineering Geology 45, 263-285.

Knox, J.C., 2000. Sensitivity of Modern and Holocene floods to climate change. Quaternary Science Reviews 19, 439- 457.

Knox, J.C., 2003. North American palaeofloods and future floods: Responses to climate change. In: K.J. Gregory and G. Benito, Editors, Palaeohydrology: Understanding Global Change, J. Wiley and Sons, Chichester (2003), pp. 143-164.

Leventer, A., Williams, D.F., Kennett, J.P., 1983. Relationships between anoxia, glacial meltwater and microfossil preservation in the Orca Basin, Gulf of Mexico. Marine Geology 53, 23-40.

Licciardi, J.M., Teller, J.T., Clark, P.U., 1999. Freshwater routing by the Laurentide ice sheet during the last deglaciation. In Clark, P.U., et al., eds., Mechanisms of global climate change at millennial time scales. American Geophysical Union Geophysical Monograph 112, pp. 177-201.

Liu, K.B., Fearn, M., 2000. Reconstruction of prehistoric landfall frequencies of catastrophic hurricanes in Northwestern Florida from lake sediment records. Quaternary Research 54, 238-245.

Marchitto, T.M. and Wei, K.Y., 1995. History of Laurentide meltwater flow to the Gulf of Mexico during the last deglaciation, as revealed by reworked calcareous nannofossils. Geology 23, 779-782.

Mayewski, P.A., Rohling, E.E., Stager, J.C., Karlen,W., Maasch, K.A., Meeker, L.D.,Meyerson, E.A., Gasse, F., vanKreveld, S.,Holmgren, K., Lee-Thorp, J., Rosqvist, G., Rack, F., Staubwasser, M., Schneider, R.R., Steig, E.J., 2004. Holocene climate variability. Quaternary Research 62, 243-255.

Meckler, A.N., C.J. Schubert, P.A. Hochuli, B. Plessen, D. Birgel, B.P. Flower, K.-U. Hinrichs, and Haug, G.H., 2008. Glacial to Holocene terrigenous organic matter input to sediments from Orca Basin, Gulf of Mexico- a combined optical and biomarker approach. Earth and Planetary Science Letters 272, 251-263.

Nordt, L., Von Fischer, J., Tieszen, L., Tubbs, J., 2008. Coherent changes in relative C4 plant productivity and climate during the late Quaternary in the North American Great Plains. Quaternary Science Reviews 27, 1600-1611.

Nürnberg, D., Ziegler, M., Karas, C., Tiedemann, R., Schmidt M.W., 2008. Interacting Loop Current variability and Mississippi River discharge over the past 400 kyr. Earth and Planetary Science Letters 272, 278-289.

Poore, R.Z., Verardo, S., Caplan, J., Pavich, K., Quinn, T., in press. Planktic foraminiferal relative abundance trends in the Gulf of Mexico Holocene sediments: Records of climate variability. In Holmes, C., (Ed.), Gulf of Mexico, its origins, waters, biota, and human impacts. Univ Texas Press.

Rittenour, T.M., Blum, M.D., Goble, R.J., 2007. Fluvial evolution of the lower Mississippi River valley during the last 100 k.y. glacial cycle: response to glaciation and sea-level change. Geological Society of America Bulletin 119, 586-608.

Sionneau, T., 2008. Transferts Continent – Océan : Enregistrement du dernier cycle climatique par les sédiments terrigènes du Golfe du Mexique. PhD thesis, Université Lille 1. 377 p. online at http://tel.archives-ouvertes.fr/tel-00366377/fr/

Sionneau, T., Bout-Roumazeilles, V., Biscaye, P.E., van Vliet-Lanoë, B., Bory, A., 2008. Clay-mineral distributions in and around Mississippi River watershed and Northern Gulf of Mexico: Sources and transport patterns. Quaternary Science Reviews 27, 1740-1751.

Sionneau, T., Bout-Roumazeilles, V., Flower, B.P., Bory, A., Tribovillard, N., Kissel, C., Van Vliet-Lanoë, B., Montero-Serrano, J.C., in revision. On the provenance of freshwater pulses in the Gulf of Mexico during the last deglaciation: Evidence from grain size and clay mineralogy. Quaternary Research.

Shuman, B., Bartlein, P., Logar, N., Newby, P., Webb III, T., 2002. Parallel climate and vegetation responses to the early-Holocene collapse of the Laurentide Ice Sheet. Quaternary Science Reviews 21, 1793-1805.

Shuman, B., Bartlein, P., Webb III, T., 2005. The magnitudes of millennial- and orbital-scale climatic change in eastern North America during the Late Quaternary. Quaternary Science Reviews 24, 2194-2206.

Springer, G.S., Rowe, H.D., Hardt, B., Edwards, R.L., Cheng, H., 2008. Solar forcing of Holocene droughts in a stalagmite record from West Virginia in east-central North America. Geophysical Research Letters 35, L17703, doi:10.1029/2008GL034971.

Stuiver, M., Reimer, P.J., 1993. Extended ^{14}C data-base and revised calib 3.0 ^{14}C age calibration program. Radiocarbon 35, 215-230.

Tarasov, L. and Peltier, W.R., 2005. Arctic freshwater forcing of the Younger Dryas cold reversal. Nature 435, 662-665.

Teller, J.T., Boyd, M., Yang, Z.R., Kor, P.S.G., Fard, A.M., 2005. Alternative routing of Lake Agassiz overflow during the Younger Dryas: new dates, paleotopography, and a reevaluation. Quaternary Science Reviews 24, 1890-1905.

Tribovillard, N., Algeo, T., Lyons, T.W., Riboulleau, A., 2006. Trace metals as paleoredox and paleoproductivity proxies: an update. Chemical Geology 232, 12-32.

Tribovillard, N., Bout-Roumazeilles, V., Algeo, T.J., Lyons, T., Sionneau, T., Montero-Serrano, J.C., Riboulleau, A., Baudin, F., 2008. Paleodepositional conditions in the Orca Basin as inferred from organic matter and trace metal contents. Marine Geology 254, 62-72.

Tribovillard, N., Bout-Roumazeilles, V., Sionneau, T., Montero-Serrano, J.C., Riboulleau, A., Baudin, F., 2009. Does a strong pycnocline impact organic-matter preservation and accumulation in an anoxic setting? The case of the Orca Basin, Gulf of Mexico. Comptes Rendus Geosciences 341, 1-9.

Tripsanas, E.K., Bryant, W.R., Slowey, N.C., Bouma, A.H., Karageorgis, A.P., Berti, D., 2007. Sedimentological history of Bryant Canyon area, northwest Gulf of Mexico, during the last 135 kyr (Marine

Isotope Stages 1-6): A proxy record of Mississippi River discharge. Palaeogeography Palaeoclimatology Palaeoecology, 246, 137-161.

Vink, A., Rühlemann, C., Zonneveld, K.A.F., Mulitza, S., Hüls, M., Willems, H., 2001. Shifts in the position of the North Equatorial Current and rapid productivity changes in the western Tropical Atlantic during the last glacial. Paleoceanography 16 (5), 479–490.

Willard, D.A., Bernhardt, C.E., Korejwo, D.A., Meyers, S.R., 2005. Impact of millennial-scale Holocene climate variability on eastern North American terrestrial ecosystems: pollen-based climatic reconstruction. Global and Planetary Change 47, 17-35.

Quaternary Science Reviews xxx (2009) 1–15

Contents lists available at ScienceDirect

Quaternary Science Reviews

journal homepage: www.elsevier.com/locate/quascirev

Section 2.4.2.

Sedimentary evidence of deglacial megafloods in the northern Gulf of Mexico (Pigmy Basin)

Jean Carlos Montero-Serrano [a,*], Viviane Bout-Roumazeilles [a], Nicolas Tribovillard [a], Thomas Sionneau [a], Armelle Riboulleau [a], Aloys Bory [a], Benjamin Flower [b]

[a] Université Lille 1, Laboratoire Géosystèmes, UMR 8157 CNRS, bâtiment SN5, 59655 Villeneuve d'Ascq cedex, France
[b] College of Marine Science, University of South Florida, 140 7th Avenue South, St. Petersburg, FL 33701, USA

ARTICLE INFO

Article history:
Received 22 May 2009
Received in revised form
3 September 2009
Accepted 14 September 2009

ABSTRACT

Cored sediments from the Pigmy Basin, northern Gulf of Mexico, were analyzed in order to better constrain late deglacial and early Holocene paleoenvironmental and sedimentary changes in response to North American climate evolution. Mineralogical and geochemical proxies indicate the succession of two sedimentary regimes: dominantly detrital during the deglaciation (15–12.9 cal ka BP) whereas biogenic contribution relatively increased later on during the Younger Dryas and early Holocene (12.9 and 10 cal ka BP). Geochemical data reveal that the deglacial record mainly reflects variations of terrigenous supply via the Mississippi River rather than modifications of redox conditions in the basin. Specific variations of almost all the parameters measured in this paper are synchronous with the main deglacial meltwater episode (Meltwater Spike) described or modeled in previous marine or continental studies. During this episode, most parameters display "stair-step-like" – pattern variations highlighting three successive steps within the main meltwater flow. Variations in grain-size and clay mineral assemblage recorded in the Pigmy Basin indicate that the erosional regime was very strong on land during the first part of the Meltwater Spike, and then milder, inducing more subtle modifications in the sedimentary regime in this part of the Gulf. Specific geochemical and mineralogical signatures (notably, clay minerals and trace metal geochemistry) pinpoint a dominant origin from NW North America for detrital particles reflecting meltwater outflow from the south-western Laurentide Ice Sheet (LIS) margin during the most intense freshwater discharge. The observed decrease of the sedimentation rate from about 200 to 25 cm/ka at ca 12.9 ka evidenced a drastic decrease of erosional processes during late phase of discharge, consistently with the hypotheses of major reduction of meltwater flow. The major modification at 12.9 cal ka BP is interpreted to result from both modifications of the main Mississippi fluvial regime due to eastward and northward rerouting of meltwater flow at the onset of the Younger Dryas, and the increase of sea-surface temperature linked to insolation. Finally, slight grain-size modifications suggest that some freshwater discharges may have episodically reached the Gulf of Mexico after the Younger Dryas reflecting possible small adjustments of the postglacial hydrological regime.

1. Introduction

It has long been known that the hydrological features of the Gulf of Mexico (GOM) were strongly impacted by the inputs of meltwater from the Laurentide Ice Sheet (LIS) during the last glacial cycle and subsequent deglaciation, since the Mississippi/Missouri watershed represented the main drainage system for the southern LIS meltwater (Kennett and Shackleton, 1975; Leventer et al., 1982; Joyce et al., 1993; Aharon, 2003; Flower et al., 2004). Deglacial meltwater episodes have been extensively documented in the GOM using hydrological proxies (Kennett and Shackleton, 1975; Emiliani et al., 1978; Leventer et al., 1982; Broecker et al., 1989; Flower and Kennett, 1990; Spero and Williams, 1990; Marchitto and Wei, 1995; Aharon, 2003; Flower et al., 2004). Modeling estimates indicate that the water discharge through the Mississippi River has varied by a factor of 5 during the Lateglacial (Teller, 1990), reflecting both the melting history of the LIS and also possible modifications in meltwater drainage pathways. Paleogeographic and ice sheet-volume reconstructions suggest that some of the ice lobe-extent

* Corresponding author. Tel.: +33 3 2043 4395; fax: +33 3 2043 4910.
E-mail addresses: jeanmontero@yahoo.es (J.C. Montero-Serrano), viviane.bout@univ-lille1.fr (V. Bout-Roumazeilles), nicolas.tribovillard@univ-lille1.fr (N. Tribovillard), sionneau.thomas@wanadoo.fr (T. Sionneau), armelle.riboulleau@univ-lille1.fr (A. Riboulleau), aloys.bory@univ-lille1.fr (A. Bory), bflower@marine.usf.edu (B. Flower).

0277-3791/$ – see front matter © 2009 Elsevier Ltd. All rights reserved.
doi:10.1016/j.quascirev.2009.09.011

fluctuations during deglaciation resulted in rapid switches of the meltwater flows pathways from the Mississippi River drainage towards the eastern drainage systems, triggering episodic cooling and warming in the North Atlantic region (Licciardi et al., 1999; Clark et al., 2001).

On the other hand, the detrital sedimentary record (including organic matter sources) of these meltwater discharges within the GOM has been studied in different works, for example in: (a) Orca Basin (Marchitto and Wei, 1995; Brown and Kennett, 1998; Meckler et al., 2008; Sionneau et al., 2008, in revision); (b) Pigmy Basin (Jasper and Gagosian, 1989a, b, 1990; Jasper and Hayes, 1993); and (c) Bryant Canyon (Tripsanas et al., 2007). An important aspect to extract of these studies is that the mineralogy, geochemistry and nature of the terrigenous components transported by the Mississippi River toward the GOM during the meltwater discharges are characteristics of the drainage areas, where the bedrock/soils contain both different clay mineral assemblages (Brown and Kennett, 1998; Sionneau et al., 2008, in revision) and geochemical signatures (Gustavsson et al., 2001). Indeed the mineralogical nature of sediments directly depends on the petrographic characteristics of their source areas (e.g., Bout-Roumazeilles et al., 1999; Sionneau et al., 2008) and they are useful to reconstruct the variability of detrital provenance through time if their main sources are well identified and constrained.

The northern GOM (Fig. 1a) is composed of small intraslope basins (e.g., Pigmy, Orca, La Salle basins) where sedimentation is mainly controlled by terrigenous supply from the Mississippi River and may record specific detrital discharges associated with the LIS melting history (Bout-Roumazeilles and Trentesaux, 2007). In this paper, we report on sedimentological and geochemical variations in terrigenous inputs in core MD02-2553 from the Pigmy Basin in the GOM during the last deglaciation. We chose the Pigmy Basin because it is located at some distance from the Mississippi Delta system. Thus, it collects continuously a smoothed and averaged terrigenous supply from North America and avoids local perturbations linked to the Louisiana slope depositional processes (Aharon, 2003, 2006). Using multiproxy analyses (grain-size, clay mineralogy, magnetic susceptibility, elemental analysis, inorganic geochemistry) on the deglacial terrigenous record of the Pigmy Basin, we aim to determine in detail the timing of continental erosion and sedimentary provenance of the main meltwater discharges, in order to: (1) document the different melting phases of the southern edge of the LIS; and (2) better constrain the history of meltwater input and its terrigenous transfers into the GOM.

2. Pigmy Basin – geological framework

The Pigmy Basin is located on the Louisiana continental slope, about 250 km southwest of the present-day Mississippi Delta, in the northern GOM. The basin is approximately 20 km-long, 7 km-wide, with average depth of 2300 m (Fig. 1b). The structure and bathymetry of the slope are controlled mainly by salt tectonics (Bouma, 1981), with salt domes protruding several hundred meters about the interdiapiric sea floor (Fig. 1b). The Pigmy Basin is defined as a former channel dammed by diapirs, with infilling by bottom transport. Thus sedimentation in the basin is mainly hemipelagic and is strongly linked to the Mississippi River detrital supply (Bouma and Coleman, 1986).

Studies from the Deep-Sea Drilling Project site 619 (Leg 96, Pigmy Basin, Fig. 1b) revealed that the Holocene section displays some intervals nearly devoid of foraminifera. These observations suggest high dilution of the faunal content by rapid influx of terrigenous sediments (Schroeder, 1983; Kohl et al., 1985). Sedimentation rates are higher during glacial isotopic stages (200–300 cm/ka) than during interglacial stages and substages (71–92 cm/ka) because of both increased physical erosion onshore and low sea level characterizing glacial periods. Coleman (1988) evidenced some variability in sediment accumulation during the Holocene, probably resulting from the migration of the main Mississippi River Delta.

Previous studies on the Pigmy Basin revealed glacial–interglacial variability in both the clay composition and terrigenous organic supply (e.g., Tieh et al., 1983; Jasper and Gagosian, 1989a, b, 1990; Jasper and Hayes, 1993). These observations suggest that this major mineral or/and organic terrigenous supply linked to meltwater discharge from the LIS during the deglaciation may have imprinted the Pigmy Basin sedimentary record.

3. Materials and methods

3.1. Materials

The samples were taken from the 10.3 m long core MD02-2553 (Calypso Square). The core was collected in the Pigmy Basin (27°11.01 N, 91°25.00 W) close to DSDP Site 619 (Leg 96, Bouma et al., 1986) during the 2002 Paleoceanography of the Atlantic and Geochemistry (PAGE) cruise of the research vessel Marion Dufresne, as part of the International Marine Past Global Changes Study (IMAGES) program (Fig. 1b). The sediment is mainly composed of massive or faintly laminated greenish gray to dark greenish gray silty to clayey mud throughout the core (Fig. 1c). Slight bioturbation is observed in the sediments. The uppermost 155 cm of the core are composed of sandy to silty clay with foraminifers and coccoliths, whereas the lower part is made up with clays showing foraminifers that become scarce below 400 cm. Dark microlaminations (mm- to cm-scale) are observed between 625–655, 880–946, and 981–1030 cm (Fig. 1c). A homogeneous interval is observed between 655 and 860 cm of the core. Five distinct upward grading, foraminifer-rich, sandy layers interpreted as small turbidites (Meckler, 2006) occurring in the core (298–300, 399–400, 594–596, 614–615, and 974–984 cm). These small turbidites were removed from our calculations because they do correspond to instantaneous processes and will distort the stratigraphic distribution of the proxies (age model).

For this study, the core was evenly sampled every 5 cm between 354 and 1029 cm (yielding a total of 139 samples); this interval corresponds to the deglacial section of the core (see Section 3.2 below). Aliquots of the homogenized sediment samples were rinsed five times to remove salt, dried (40 °C for 48 h) and ground for magnetic susceptibility and geochemical analysis.

3.2. Age model

The chronology of the core MD02-2553 is determined from seven accelerator mass spectrometry (AMS) ^{14}C dates on foraminifera on the studied interval (354–1029 cm) (Table 1; gray dots in Fig. 2). The younger five dates were measured on mixed planktic foraminifers at the CAMS, Lawrence Livermore National Laboratory, USA (Poore et al., in press). The other dates were measured on monospecific *Globigerinoides ruber* (both pink and white varieties) at the Poznan Radiocarbon Laboratory, Poland. All ages were converted into calendar years with the CALIB software (Stuiver and Reimer, 1993, version 5.0.2; http://calib.qub.ac.uk/calib), using the calibration curve Marine04 (Hughen et al., 2004). All AMS ^{14}C ages were corrected using a constant reservoir age of 400 years ($\Delta R = 0$) because it provides consistency with both modern values (Bard, 1988) and with previous paleoceanographic studies from the GOM (e.g., Flower et al., 2004; Meckler et al., 2008; Nürnberg et al., 2008). Reservoir age modifications in the tropical Atlantic Ocean during Late Pleistocene and Holocene are still a matter of debate (Stocker

Please cite this article in press as: Montero-Serrano, J.C., et al., Sedimentary evidence of deglacial megafloods in the northern Gulf of Mexico (Pigmy Basin), Quaternary Science Reviews (2009), doi:10.1016/j.quascirev.2009.09.011

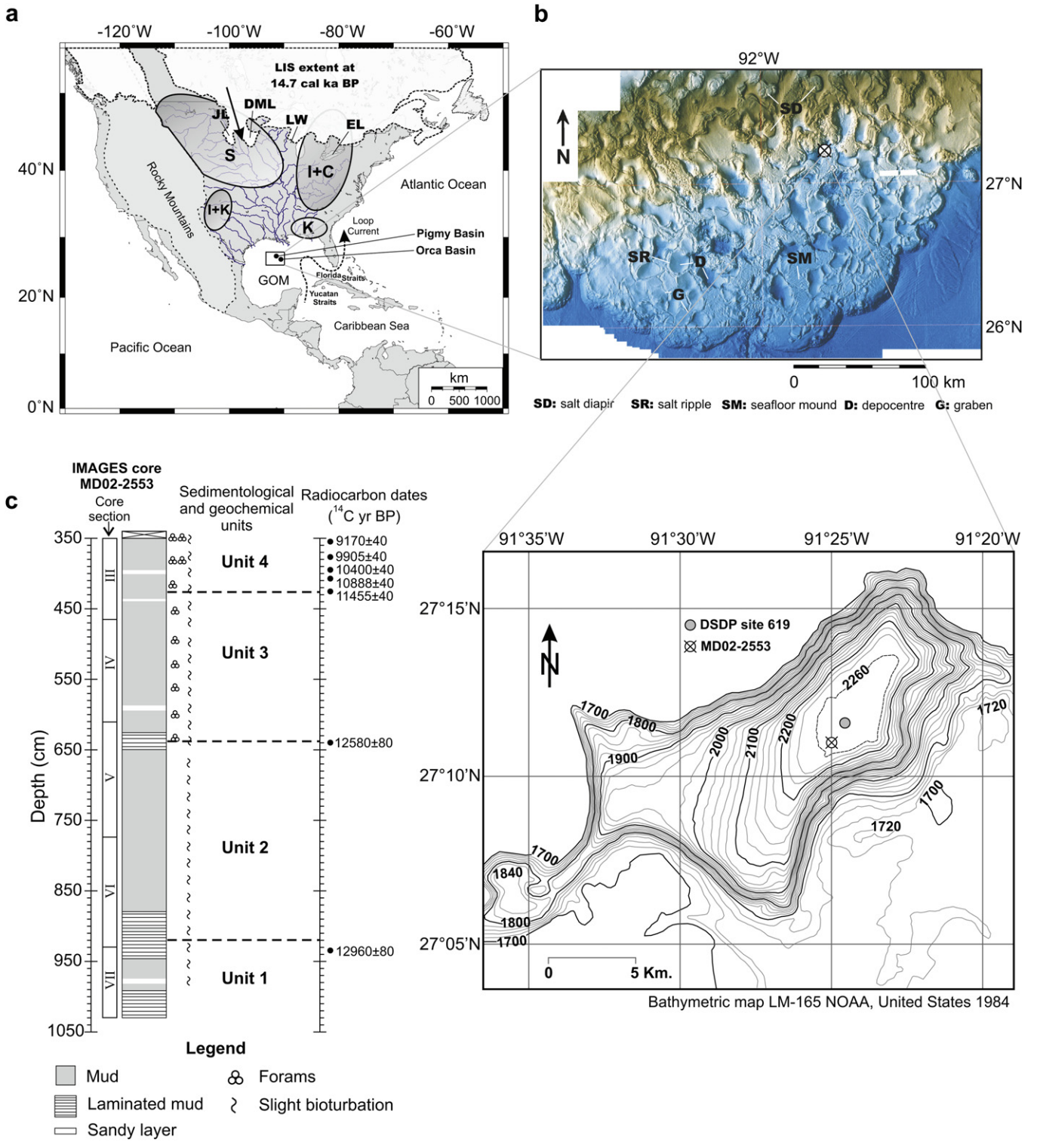

Fig. 1. (a) Map of North America with the extent of the Laurentide Ice Sheet during the last deglaciation (14.7 cal ka BP) (Dyke, 2004) showing the main continental clay mineral provinces (Sionneau et al., 2008); S: smectite, I: illite, C: chlorite, K: kaolinite, GOM: Gulf of Mexico, JL: James glacial lobe, DML: Des Moines glacial lobe, LW: Lake Wisconsin, EL: Erie Lake. (b) Morphological map of the seafloor in the northern Gulf of Mexico (Diegel et al., 1995), and bathymetric map of the Pigmy Basin showing locations of sediment cores MD02-2553 and DSDP 619; contours in meters. (c) Lithological log of core MD02-2553 between 350 and 1050 cm showing the sedimentological and geochemical units defined in this study and radiocarbon ages; Roman numerals in column on far left represent the different core sections.

and Wright, 1996; Rühlemann et al., 2004). However a detailed study of Hughen et al. (1998) indicates that reservoir ages did not change significantly during the last deglaciation. Depth in centimeters was converted to calendar age by linear interpolation between four main calibrated AMS ^{14}C ages at 350.5, 424.5, 640, and 932 cm (black squares in Fig. 2). Linear extrapolation from the radiocarbon date suggests that the age of the core base is approximately 15.1 cal ka BP. Age vs. depth relations in the core MD02-

Table 1
Radiocarbon ages for core MD02-2553.

Lab number or reference	Core depth (cm)	Species	^{14}C AMS Age (ka)	^{14}C Error (±year)	Calibrated age (median, ka BP)	Calibrated error (±year, 1 sigma)
Poore et al. (in press)	350.5	Mixed planktic foraminifers	9.170	40	9.989	89
	375.5		9.905	40	10.810	112
	390.5		10.400	40	11.364	61
	409.5		10.888	40	12.529	81
	424.5		11.455	40	12.956	44
Poz-24558	640.0	*Globigerinoides ruber*	12.580	80	14.034	98
Poz-24559	932.0		12.960	80	14.769	195

2553 indicate linear sedimentation rates ranging from about 200 to 397 cm/ka during the last deglaciation and a significant drop to values of about 25 cm/ka during the early Holocene (dotted line with black squares in Fig. 2). These values are in good agreement with sedimentation rates obtained on: (1) DSDP site 619 of the Pigmy Basin: 300 cm/ka in stage 2 and 92 cm/ka in stage 1 (Jasper and Gagosian, 1990); and (2) core MD02-2552 of the Orca Basin: ca 215 cm/ka during the last deglaciation and ca 65 cm/ka during the early Holocene (Sionneau et al., in revision). The distinct increases in linear sedimentation rates from about 25 to 397 cm/ka at about 12.9, 14, and 14.7 ka appear very large and abrupt, following a stair-step pattern; however, the accumulation is thought to have been continuous because of the lack of sharp lithological breaks or sedimentological indicators of hiatus or mass flow transport in these parts of the core. In addition, the decrease in sedimentation rates from 200 to 25 cm/ka at ca 12.9 ka is consistent with major reduction of meltwater flow (Licciardi et al., 1999; Tarasov and Peltier, 2005; Teller et al., 2005).

3.3. Analytical methods

3.3.1. Grain-size distribution

Grain-size determination was carried out on the carbonate-free fraction of the sediment using a Malvern Mastersizer 2000 laser diffractometer, which has a detection range of 0.02–2000 μm. Sample preparation and optical settings for the Mastersizer 2000 followed Sperazza et al. (2004). Defloculation of the samples was done by successive washing with distilled water after decarbonatation of the sediments with 0.2 M HCl. Samples were split with a 2000 rpm stirrer and disaggregated by 40% ultrasonication (Hydro S dispersion cell) for >60 s during analysis. Sample quantity was adjusted in order to obtain a laser beam obscuration between 12 and 15%. We used a refractive index (RI) value of 1.544 (quartz) and an absorption value of 0.05. The distribution parameters reported here are the mode (μm, most frequent grain-size) and percentage of clays (<2 μm), cohesive-silts (2–10 μm), sortable-silts (10–63 μm) and sands (>63 μm).

3.3.2. Clay mineral analysis

Clay mineral associations were studied using X-ray diffraction following the protocol of Bout-Roumazeilles et al. (1999). In this paper, "clay minerals" refer to the major phyllosilicate minerals within the clay-size fraction (generally less than 2-μm particles). All samples were first decalcified with 0.2 M HCl. Defloculation of clays was achieved by successive washing with distilled water. The clay-size fraction was separated by settling according to Stokes's law, concentrated by centrifugation, and oriented by wet smearing on glass slides. X-ray diagrams were obtained using a Philips PW 1749 diffractometer with CuKα radiation and a Ni filter. A tube voltage of 40 kV and a tube current of 25 mA were utilised. Three X-ray diagrams were performed: air-dried sample (normal run), ethylene–glycol vapour saturation for 12 h (glycol run) and heating at 490 °C during 2 h (heating run). The goniometer scanned from 2.49° to 32.49° 2θ for normal and glycol run and from 2.49° to 14.5° 2θ heating run. Each clay mineral is characterized by its basal layer plus interlayer interval (d) as revealed by XRD analysis (Brown and Brindley, 1980). Smectite (S) is characterized by a peak at 14 Å on the normal run, which expands to 17 Å after saturation by ethylene–glycol and retracts to 10 Å after heating. Illite (I) presents a basal peak at 10 Å on the three runs. Chlorite (C) is characterized by peaks at 14 Å (001), 7 Å (002), 4.75 Å (003) and 3.53 Å (004) on the three runs. Kaolinite (K) is characterized by peaks at 7 Å (001) and 3.58 Å (002) on the normal and glycol runs. Both peaks disappear or are strongly reduced after heating. To distinguish kaolinite from chlorite, the portion of the spectrum containing the basal peaks of kaolinite (002) and chlorite (004) around 3.55 Å is

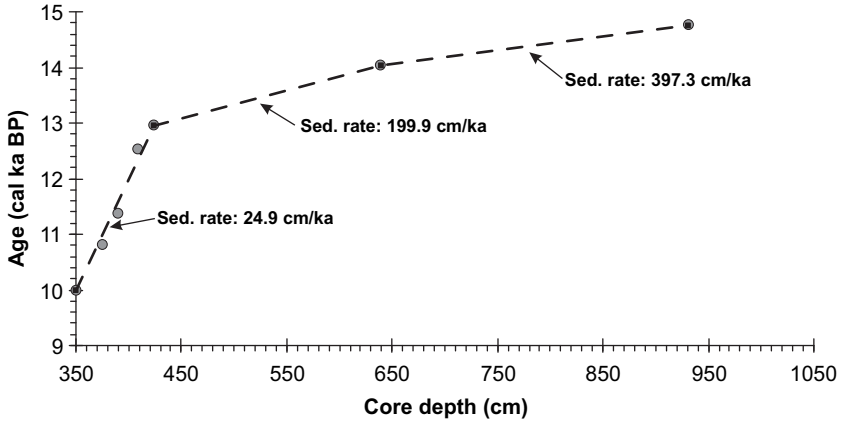

Fig. 2. Age model for core MD02-2553 based on 7 AMS ^{14}C dates (gray dots) from both *Globigerinoides ruber* and mixed planktic foraminifers, converted to calendar ages (see text). Depth in centimeters was converted to calendar age by linear interpolation between the four dates at 350.5, 424.5, 640 and 932 cm (dotted line with black squares).

Please cite this article in press as: Montero-Serrano, J.C., et al., Sedimentary evidence of deglacial megafloods in the northern Gulf of Mexico (Pigmy Basin), Quaternary Science Reviews (2009), doi:10.1016/j.quascirev.2009.09.011

step-scanned in a high-resolution mode following standard procedures described in detail by Petschick et al. (1996). Semi-quantitative estimation of clay mineral abundances is based on peak areas and summed to 100% (S + I + K + C = 100%). Peak area measurements were realized in the glycol runs using the Macintosh MacDiff® 4.2.5 software (Petschick, 2000). The error on the reproducibility of measurements is estimated to be ±5% for each clay mineral.

3.3.3. Rock–Eval pyrolysis

Usual Rock–Eval pyrolysis parameters, namely, total organic carbon content (TOC, wt.%), Tmax (°C), and Hydrogen Index (HI, in mg hydrocarbon per g TOC) were determined with a Delsi Oil Show Analyser (Rock Eval II). The pyrolysis program was adapted to recent sediments, starting with an isothermal stage of 3 min at 180 °C. Then, the pyrolysis oven temperature was raised at 30 °C/min to 600 °C, and held for 3 min at this temperature (see Espitalié et al., 1986 for procedural details and Disnar et al., 2008 for Rock–Eval use for Holocene sediments).

3.3.4. Elemental analysis

Total inorganic carbon (TIC) content was determined as calcium carbonate ($CaCO_3$) percentage using a Bernard calcimeter (measuring the amount of CO_2 released by acid digestion, and based on standard samples of pure $CaCO_3$ – precision <5%).

Total sulfur (S_{total}) and total nitrogen (N_{total}) contents were determined using a Thermo Flash EA1112 CHNSO analyser. The precision is better than 4% for S_{total} and 5% for N_{total}, based on international standards and replicate samples. Though nitrogen may be present in the form of nitrate or ammonium in clay minerals, it is estimated that N_{total} mostly corresponds to organic nitrogen. With this assumption, the C/N ratio (TOC/N_{total}) was calculated as an indication of source of organic matter (OM) in sediments (Jasper and Gagosian, 1990; Meyers, 1997; Meckler et al., 2008). C/N ratio values for organic matter (OM) of marine origin generally range from 4 to 10 because of the high protein content of lower organisms such as phytoplankton and zooplankton (e.g., Meyers, 1997). Higher plant-derived OM gives higher C/N values than those of marine origin OM because it has a high percentage of non-protein materials (e.g., C/N > 15; Meyers, 1997).

3.3.5. Magnetic susceptibility

Magnetic susceptibility (MS) was measured on all discrete samples, using a KLF-4 Agico apparatus. Remnant magnetization was measured on the three-axis using a magnetic field of 300 A/m with a step of 10 A/m. Each sample was measured three times and the mean of these measurements is reported here. MS is normalized by dry mass and expressed as m^3/kg. In Pigmy Basin, the MS measurements are useful for detecting paleoenvironmental changes induced in the magnetic properties of marine sediments (King, 1986).

3.3.6. Inorganic geochemistry

Major, minor, trace and rare earth elements (REE) concentrations were determined on 35 evenly distributed samples (average sample spacing is ~20 cm) by inductively coupled plasma optical emission spectrometry (ICP-OES) and inductively coupled plasma mass spectrometry (ICP-MS), at Activation Laboratories Ltd. (Ancaster, Canada). Samples were mixed with a flux of lithium metaborate ($LiBO_2$) and lithium tetraborate ($Li_2B_4O_7$), and fused in an induction furnace. Molten sample was immediately poured into a solution of 5% nitric acid (HNO_3) containing an internal standard, and mixed continuously until completely dissolved. The analytical accuracy and precision were found to be better than 1–2% for major elements, 5% for REE and 5–10% for the other elements, as checked by international standards and analysis of replicate samples.

Elemental compositions and total REE are normalized to aluminum (Al) to remove the effects of differential dilution of the bulk sediments by the aluminosilicate fraction so that changes in the composition of the lithogenous material can be discerned (see discussion about Al normalization in van der Weijden, 2002, and Tribovillard et al., 2006). In addition, trace metal (TM) concentrations are expressed in terms of enrichment factors (EF_{TM}) where the Al-normalized metal concentration is compared to the average shale values of Wedepohl (1971, 1991): $EF_{TM} = TM/Al_{sample}$: $TM/Al_{average\ shale}$. $EF_{TM} > 1$ suggests enrichment relative to average shale but authigenic enrichments can be suspected when EF_{TM} exceed 5 (Tribovillard et al., 2006). Fractionation between light REE (LREE: La–Nd), medium REE (MREE: Sm–Gd) and heavy REE (HREE: Tb–Lu) was studied by La/Yb and Gd/Yb normalized ratios (Lawrence et al., 2006). Additionally we calculated the distribution of Ce-anomaly ($3Ce_n$: $2La_n + Nd_n$) and Eu-anomaly [Eu_n: $(Sm_n.Gd_n)^{1/2}$] to studied vertical changes in redox conditions. NASC values by Gromet et al. (1984) are used for normalization of the REE.

Al-normalized metal distributions are used as proxies of the detrital sediment sources, complementary to clay mineral proxies. In addition, the REE abundance patterns provide fingerprints associated with detrital fraction of the sediment which in turn represents the bulk composition and stands as proxy for the climate over the source area (e.g., Tanaka et al., 2007).

4. Results

Four main sedimentary units can be identified on the base of the characteristic stair-step patterns of most sedimentological and geochemical proxies (Fig. 3–9). The characteristic stair-step pattern possibly displays the effect of highly variable sedimentation rates (25–397 cm/ka) in Pigmy Basin, and may reveal differences due to clastic dilution and provenance. However, it is necessary to take into consideration that age control rests on interpolation between ^{14}C dates. These units, labelled 1–4 from base to top, are described below.

4.1. Unit 1: 1029–920 cm (15–14.7 cal ka BP)

This unit is mainly characterized by coarsest mode values (ca. 3.8 μm). The proportion of sortable (non-cohesive) silts displays the maximum values of the whole studied interval whereas the fine-cohesive fraction is minimum (Fig. 3). Although smectite is the main component of the clay mineral fraction (ca. 70%), Unit 1 is characterized by enhanced contributions of illite (up to 17%), kaolinite (up to 11%) and chlorite (up to 10%) (Fig. 4). The unit is characterized by intermediate values of TOC associated with a low S_{total} content (Fig. 5). The $CaCO_3$ content (Fig. 5) is slightly higher than average (up to 13%). Unit 1 displays relatively high Ti/Al and K/Al values and low Fe/Al and V/Al (Fig. 9)

4.2. Unit 2: 920–640 cm (14.7–14 cal ka BP)

Unit 2 is characterized by specific sedimentological and geochemical characteristics with low internal variability, associated with a very high sedimentation rate (397 cm/ka). The mode is quite low (down to 3.1 μm) reflecting a high contribution of cohesive particles (up to 95%), whereas MS and $CaCO_3$ content display their lowest values (Figs. 3 and 5). The clay assemblage is markedly dominated by smectite (up to 86%) (Fig. 4). It may be emphasized that the domination of smectite does not result from differential settling processes (Sionneau et al., 2008). High TOC (up to 1.7%) and S_{total} (0.10%) contents and high C/N ratios underline the specificity of Unit 2 (Fig. 5). Moreover the geochemical signature of Unit 2 differs drastically from the other three units. The most remarkable feature is the high V/Al and Fe/Al values associated with depressed

Please cite this article in press as: Montero-Serrano, J.C., et al., Sedimentary evidence of deglacial megafloods in the northern Gulf of Mexico (Pigmy Basin), Quaternary Science Reviews (2009), doi:10.1016/j.quascirev.2009.09.011

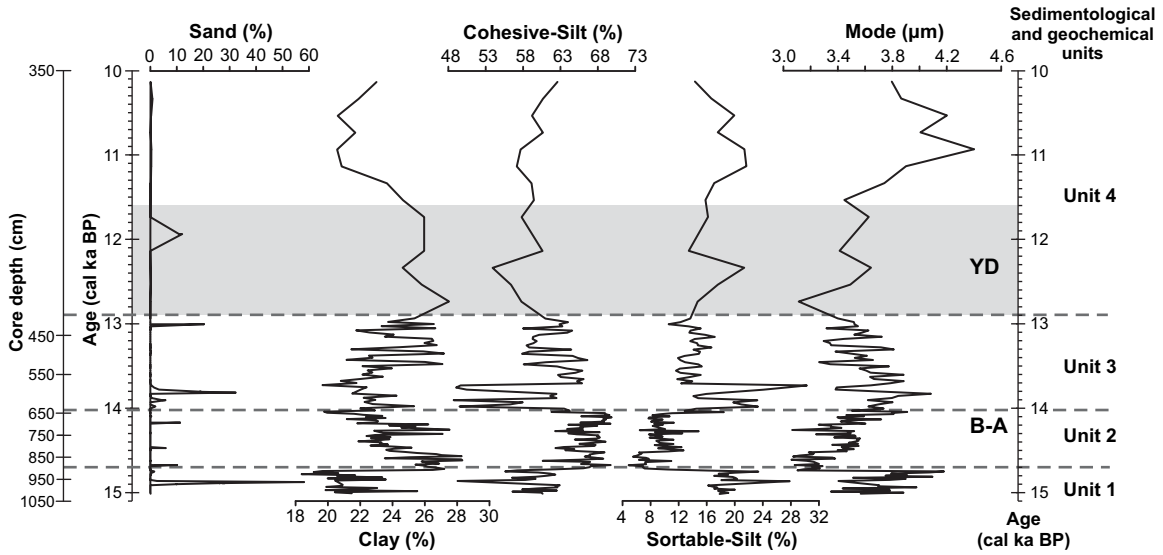

Fig. 3. Grain-size distribution (grain-size classes in %, and mode in μm). The Younger Dryas (YD) from 12.9 to 11.6 ka (shaded) and Bølling–Allerød warming (B–A) from 15.4 to 12.9 ka are indicated.

values of K/Al, Ti/Al, Th/Al, and depletion in most REE (Fig. 9). The peculiar geochemical character of this unit is also obvious on Ti/Al vs. Fe/Al or Th/Al vs. V/Al plots (Fig. 8a,b). Fig. 8c shows that the relatively high contents in V are still strongly correlated to Al concentrations, which points to a terrigenous origin. In addition (La/Yb)n and (Gd/Yb)n ratios show a slight enrichment in LREE and MREE over HREE (Fig. 9).

4.3. Unit 3: 640–424 cm (14–12.9 cal ka BP)

Most geochemical and sedimentological characteristics of this unit are very similar to Unit 1, except for grain-size and $CaCO_3$ distributions that are similar to those of Unit 2 (Figs. 3–9). Some minor discrepancies between Unit 3 and Unit 1 may however be observed: a slightly coarser mode and higher proportion of sortable-silt at the base of Unit 3. Unit 3 is also characterized by an increase of the (La/Yb)n ratio, reflecting slightly enhanced fractionation of LREE (Fig. 9). The sedimentation rate is still high (200 cm/ka) though lower than in Unit 2.

4.4. Unit 4: 424–354 cm (12.9–10 cal ka BP)

The strong decrease of the sedimentation rate is the most prominent feature of Unit 4, also characterized by the increase in grain-size mode and $CaCO_3$ content (up to 22%) (Figs. 3 and 5). The clay fraction is characterized by the increased contribution of illite (up to 15%), kaolinite (up to 12%) and chlorite (up to 10%) at the expense of smectite (Fig. 4). The TOC concentrations and C/N ratio values display a decreasing trend over the interval whereas the S_{total} content is steadily low (Fig. 5). Geochemical parameters would not provide any significant information because elemental analyses were performed only on three samples.

5. Interpretation and discussion

5.1. Main characteristics of sedimentary regimes in the Pigmy Basin

Our mineralogical and geochemical results indicate that sedimentation in the Pigmy Basin is mainly ruled by the terrigenous

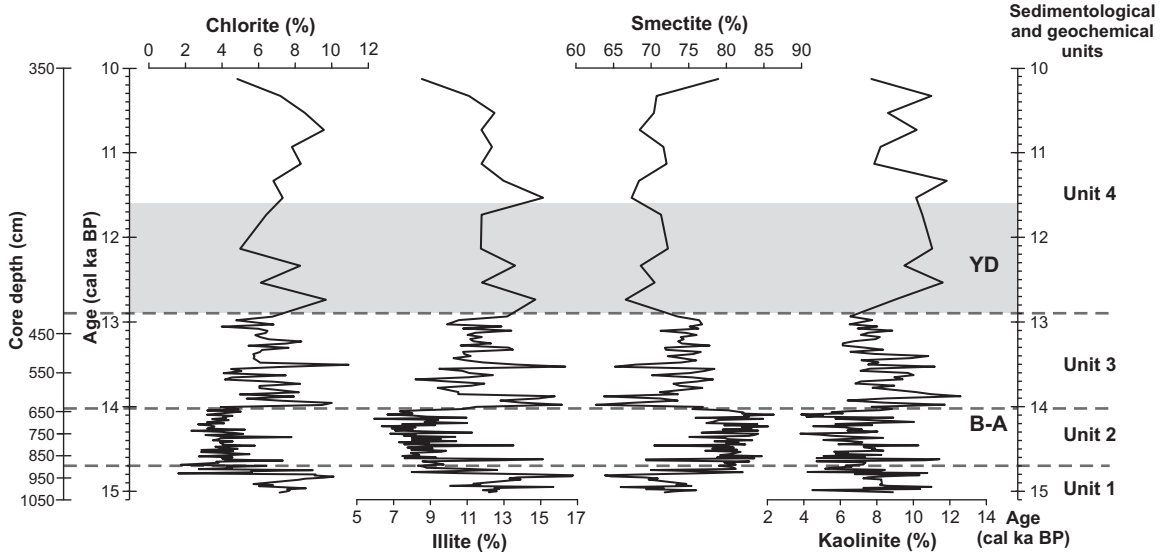

Fig. 4. Clay mineral variations. The Younger Dryas (YD) from 12.9 to 11.6 ka (shaded) and Bølling–Allerød warming (B–A) from 15.4 to 12.9 ka are indicated.

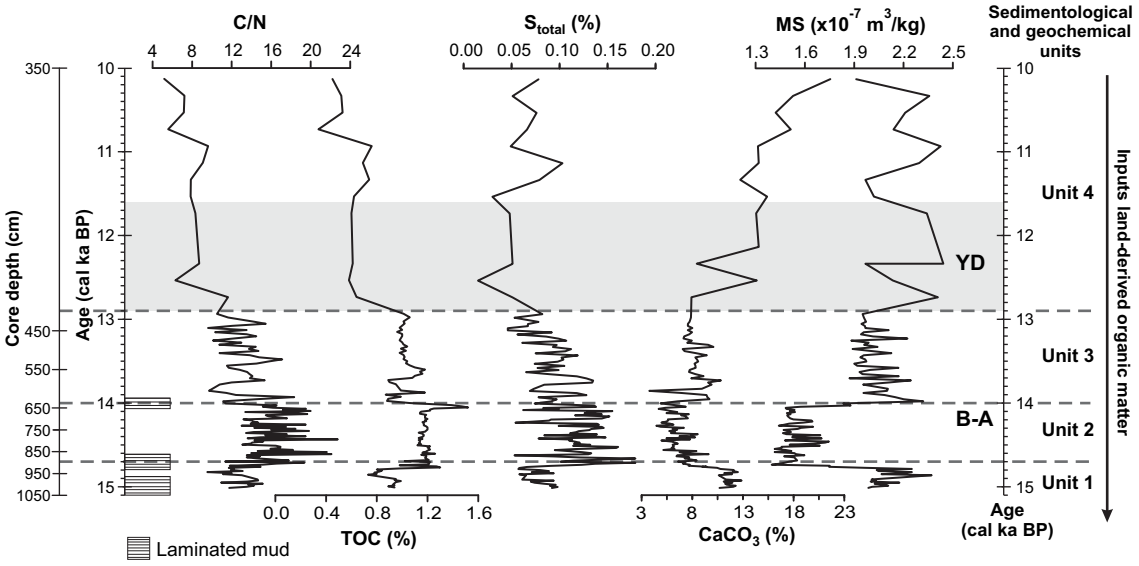

Fig. 5. C/N ratio, TOC, S_{total} and carbonate ($CaCO_3$) concentrations (%), and magnetic susceptibility (MS) values. The Younger Dryas (YD) from 12.9 to 11.6 ka (shaded) and Bølling–Allerød warming (B–A) from 15.4 to 12.9 ka are indicated.

supply over the entire interval (Figs. 3–9) being strictly detrital during the deglaciation (Units 1–3) whereas significant biogenic contribution is observed during the Younger Dryas and early Holocene (Unit 4).

Geochemical proxies highlight a dominant detrital signature and a non-detectable influence of authigenic and diagenetic processes in the Pigmy Basin. Element enrichment factors do not show any significant variations (average, 0.5–2.5), which also indicates that the redox sensitive and/or sulfide-forming trace metals (e.g., V, U, Mo, Cu, Ni, Co) are not authigenically enriched ($EF_{TM} < 5$) (Fig. 7). Accordingly, these trace metals show good correlation with Al concentrations, advocating to a detrital origin (e.g., Fig. 8c). REE normalized patterns, and Ce and Eu anomalies do not show any striking features, except for a general slight enrichment in light REE over HREE evidenced by the (La/Yb)n and (Gd/Yb)n (Fig. 9). The absence of any significant fractionation of REE in the Pigmy Basin sediments, also observed in other basins from the GOM (Flocks and Swarzenski, 2007), points out a highly-mixed detrital source. These results confirm that the terrigenous supply from the Mississippi and Missouri rivers, draining almost half the conterminous USA, mostly controls sedimentation in the GOM. Moreover similar REE distributions are observed in the Pigmy Basin and in Mississippi River suspended loads (Goldstein and Jacobsen, 1988; Elderfield et al., 1990) confirming the dominant influence of the Mississippi River and minor contributions of Mobile, Brazos and Atchtalafaya rivers.

Complementarily, the C/N ratio (up to 15; Fig. 5) and Rock–Eval parameters (Fig. 6) also suggest that organic compounds are mostly of terrigenous origin during the deglaciation whereas they display a higher marine influence in the early Holocene (Unit 4); the samples of Unit 4 show relatively high HI and low Tmax values (Fig. 6b). In addition as indicated by a Tmax vs. HI diagram (Fig. 6a),

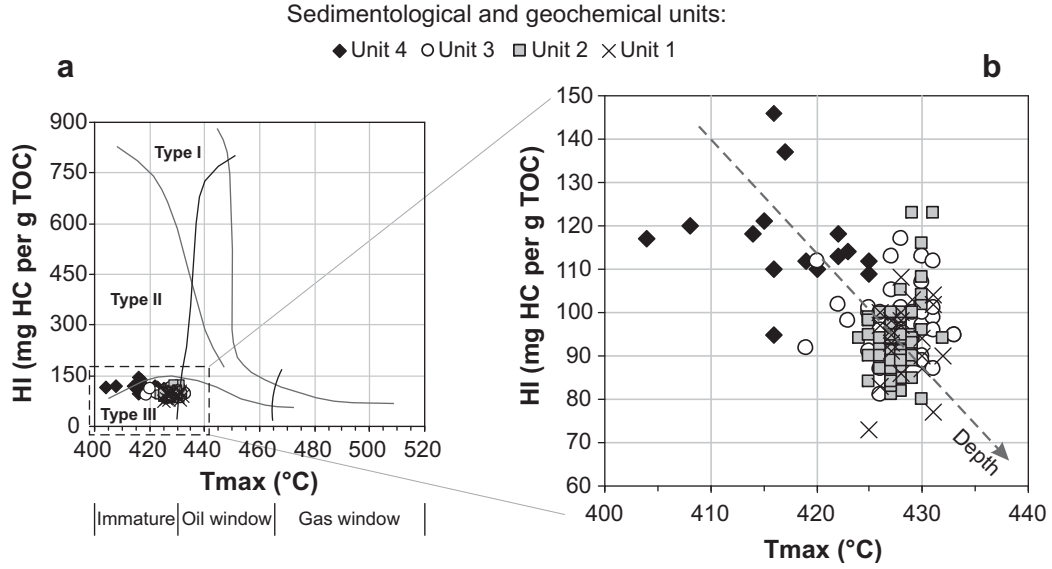

Fig. 6. Rock–Eval pyrolysis parameters. (a) TOC vs. Hydrogen Index (HI), (b) Tmax vs. HI crossplot illustrating the origin and maturation state of the samples. The arrows on (a) and (b) show the general tendency with sample depth below sea floor.

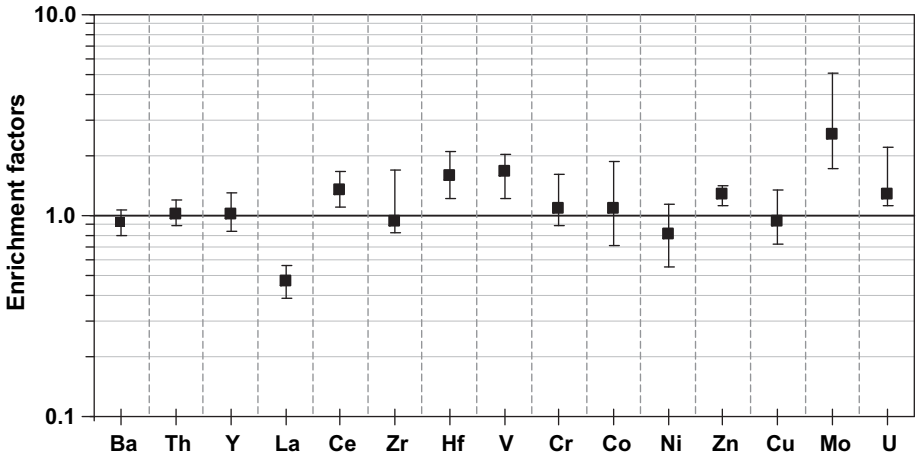

Fig. 7. Comparison of enrichment factor of some trace metals of core MD02-2553 (Pigmy Basin). The extent line of the boxes corresponds to the range of values (min–max) and the boxes to the average value. The horizontal line of the centre indicates the value for which there is no enrichment/depletion with regards to average shale composition.

the studied core contains an immature of type-III OM (terrestrial OM). These observations are in agreement with previous studies on the OM of the Pigmy Basin (Jasper and Gagosian, 1990) and the nearby Orca Basin (Meckler et al., 2008; Tribovillard et al., 2008, 2009; Sionneau et al., in revision).

Under this frame, any variation in the Pigmy Basin sedimentation is then likely to result from modifications of the Mississippi River flow that is largely controlled by meltwater discharges from the LIS during the deglaciation (Fig. 10c, Licciardi et al., 1999).

Several studies provide a detailed record of meltwater discharges in the GOM for the past 20 ka (Marchitto and Wei, 1995; Brown and Kennett, 1998; Aharon, 2003, 2006; Flower et al., 2004; Meckler et al., 2008). Reconstructions suggest that during the Last Glacial Maximum (LGM) most meltwaters originated from the central LIS and were further drained toward the GOM via the Mississippi River (Teller, 1990; Licciardi et al., 1999). On the contrary, during deglaciation ice sheet margin instability and ice lobe fluctuations modified meltwater provenance and caused the main drainage to be repeatedly rerouted eastward (toward the North Atlantic Ocean) or northward (toward the Arctic Ocean). As a consequence discharge fluctuations display different regimes (Teller, 1990; Licciardi et al., 1999) and have likely affected also the provenance of detrital particles (Sionneau et al., in revision).

Over the studied interval, two periods of freshwater discharge are evidenced in $\delta^{18}O$ profiles. The first major discharge occurred during the last deglaciation between 16.5 and 13 cal ka BP as a series of freshwater pulses attributed to the release of glacial meltwater from proglacial Great Lakes and Lake Agassiz (Aharon, 2003; Lewis and Teller, 2006). A minor discharge may have occurred during early Holocene to the GOM resulting from the release of meltwater from Lake Agassiz at 11.4–10.6 cal ka BP (Tripsanas et al., 2007).

In this context, our mineralogical and geochemical results provide new insights the expression of these meltwater episodes in the GOM. A recent study (Sionneau et al., in revision) proposed the use of clay mineralogy to retrace meltwater provenance. Indeed during the last deglaciation, the south margin of the LIS and proglacial lakes encompassed two distinct clay mineral provinces (Fig. 1a). The north-western Mississippi and Missouri river watershed is characterized by high smectite contents, which reflect the composition of Cretaceous, Tertiary and Pleistocene bedrocks associated with a bentonitic or authigenic origin (Sionneau et al.,

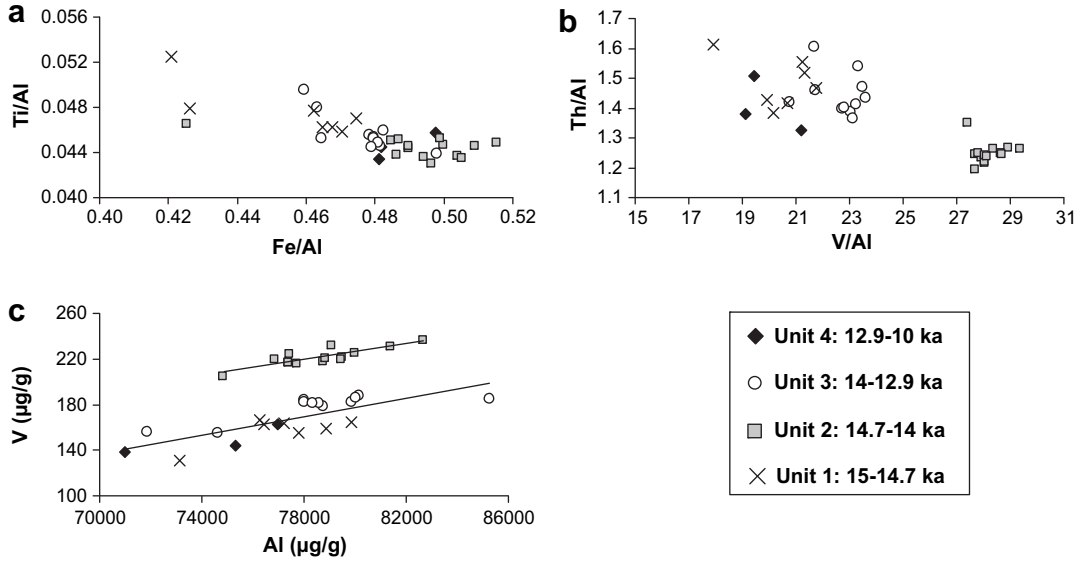

Fig. 8. (a) Ti/Al vs. Fe/Al, (b) Th/Al vs. V/Al, (c) V concentration vs. Al concentration for the studied Pigmy samples.

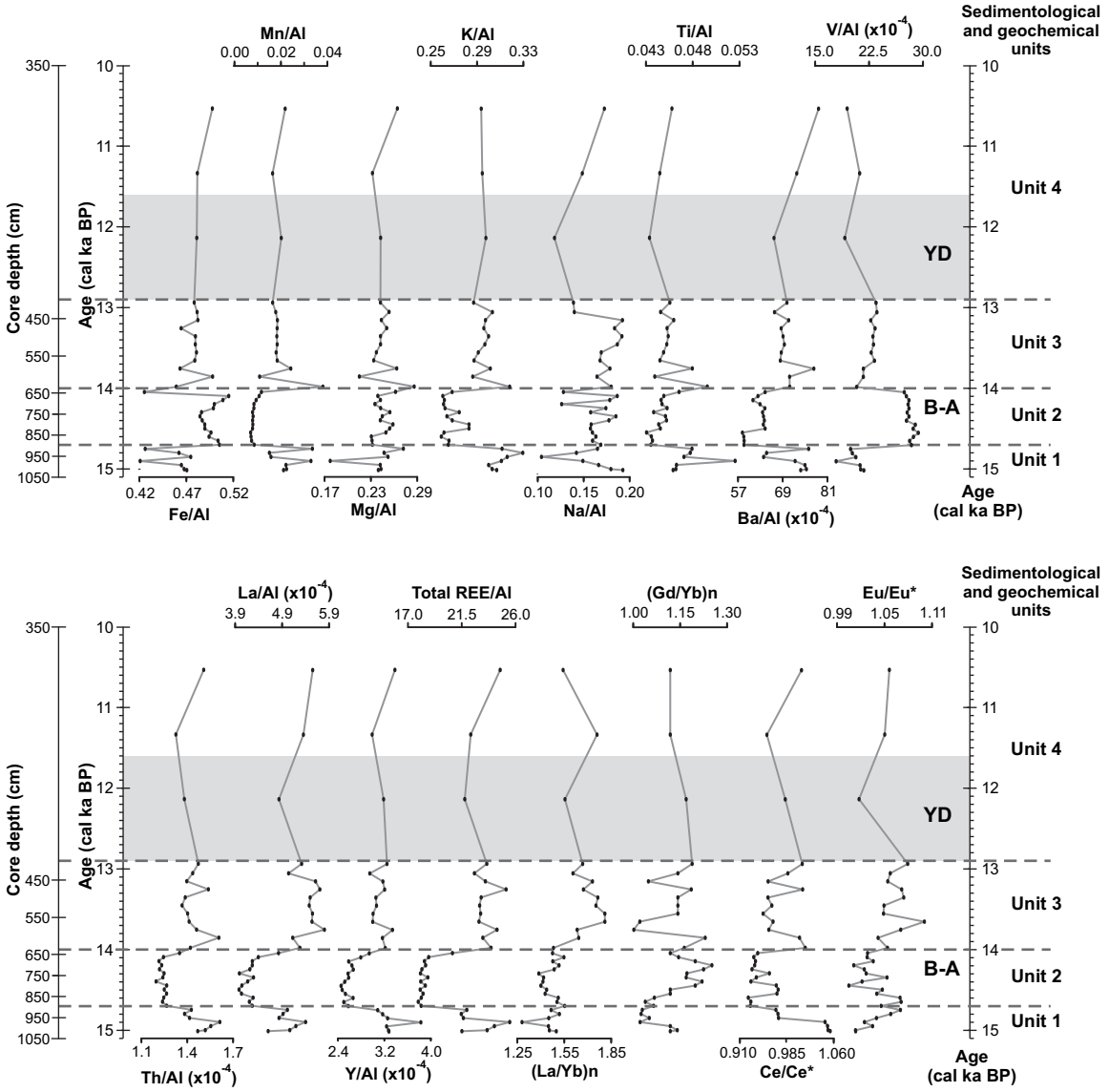

Fig. 9. Al-normalized elemental ratios: major, minor, traces and rare earth (REE) elements. The suffix "n" denotes a NASC-normalized value (Gromet et al., 1984). The Ce and Eu anomalies are shown. The Younger Dryas (YD) from 12.9 to 11.6 ka (shaded) and Bølling–Allerød warming (B–A) from 15.4 to 12.9 ka are indicated.

2008). On the other hand, the northeastern province corresponding to the Great Lakes area and the Ohio and Tennessee river catchment mainly delivers illite and chlorite, resulting from strong physical weathering and erosion of Palaeozoic rocks (Sionneau et al., 2008). The respective contributions of smectite vs. illite and chlorite are thus used to document the origin of deglacial meltwater megafloods (Sionneau et al., in revision).

5.2. The main meltwater discharge episode (15–12.9 cal ka BP)

Previous studies based on deep-sea cores from the GOM (Leventer et al., 1983; Jasper and Gagosian, 1989a, b, 1990; Jasper and Hayes, 1993; Marchitto and Wei, 1995; Brown and Kennett, 1998; Aharon, 2003; Flower et al., 2004; Meckler et al., 2008) and on continental records from North America (e.g., Knox, 1996; Rittenour et al., 2007) evidenced the occurrence of a modest multi-phased surge of glacial meltwater during deglaciation (Figs. 10 and 11). This episode is defined by a major negative $\delta^{18}O$ excursion ($-2.5‰$) between 15.2 and 13 cal ka BP referred to as the Meltwater Spike (Fig. 11a, Leventer et al., 1983; Brown and Kennett, 1998; Flower et al., 2004) and meltwater pulse (MWP-1a) (Fig. 10b, Tarasov and Peltier, 2005) in the GOM, and to meltwater flow (MWF)-3 and MWF-4 on the Louisiana Slope (Fig. 11b, Aharon, 2003).

The sedimentological Units 1–3 defined on core MD02-2553 are synchronous with this Meltwater Spike. The peculiar stair-step pattern of most sedimentological and geochemical proxies provides additional constrains on the synopsis of this major meltwater episode. Our results show that the Meltwater Spike corresponds to three stair-step terrigenous inputs (Units 1–3) with a maximum discharge leading to the deposition of Unit 2 (14.7 and 14 cal ka BP). These three phases are characterized in the Pigmy Basin sediments by distinct mineralogical and geochemical signatures.

In core MD02-2553, the Meltwater Spike is marked by relatively elevated TOC (0.7–1.5%) and S_{total} (0.06–0.18%) concentrations, and high C/N ratio (9.5–22.7) (Fig. 5) consistent with previous observations on the nearby Orca Basin, core MD02-2550 (see Fig. 5 of Meckler et al., 2008). It is noticed that that in spite of the independent age models of the two nearby cores MD02-2553 and MD02-2550, the changes in TOC and C/N distributions for both cores are of the same order (in time and magnitude) with the most

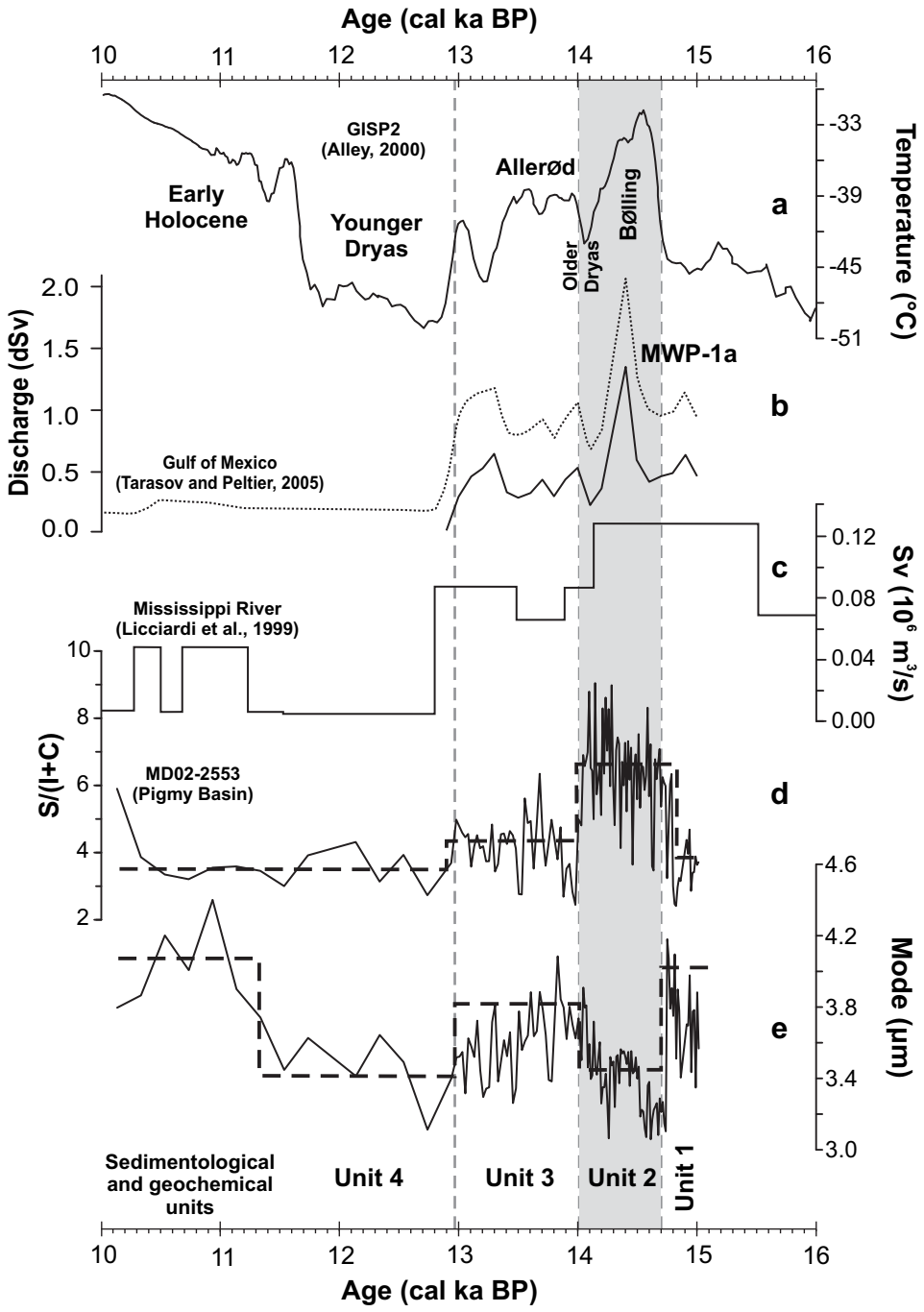

Fig. 10. Comparison of the sedimentological parameters of core MD02-2553 (Pigmy Basin) with ice proxy climate records and meltwater discharge models during 15–10 cal ka BP interval. (a) The Greenland Ice Sheet Project 2 (GISP2) temperature (Alley, 2000). (b) Computed regional drainage chronologies for the Gulf of Mexico (1 dSv = 10^5 m^3/s) (Tarasov and Peltier, 2005); upper bound (fine dotted line) denotes the 1σ upper bound with the additional inclusion of precipitation over ice-free land in the discharge calculation. (c) The meltwater discharge curve for the Mississippi River (Licciardi et al., 1999). Sedimentary records in the Pigmy Basin: (d) clay mineral ratio S/(I + C), and (e) grain-size mode (μm). The sedimentological and geochemical units defined in this study are indicated. Shaded interval indicates the most intense meltwater pulse from the southwest margin of the Laurentide Ice Sheet.

pronounced increase in meltwater flux reflected by $\delta^{18}O$ (−2.5‰). The results of this correlation provide strong support to our interpretations.

Concurrently, the peculiar grain-size distribution characterizing Unit 1 indicates specific supply of coarse particles. Mineralogical and geochemical proxies indicate a mixed provenance of detrital particles, i.e., mainly from the north-western province but with some noticeable contribution of the northeastern province. These results suggest that the Mississippi River received almost all meltwaters from the southwest of James glacial lobe to the eastern margin of Lake Erie (Sionneau, 2008) during the early phase of the Meltwater Spike (Fig. 1a). According to these observations, the deposition of Unit 1 is likely resulting from erosion of the main braided Mississippi River channel rather than from clay-rich terrace deposits along tributaries (Knox, 1996). Our results suggest that Unit 1 may record the initial erosive flood corresponding to the proglacial Lake Wisconsin outburst that occurred at 14.9 cal ka BP (Fig. 1a, Knox, 1996).

Please cite this article in press as: Montero-Serrano, J.C., et al., Sedimentary evidence of deglacial megafloods in the northern Gulf of Mexico (Pigmy Basin), Quaternary Science Reviews (2009), doi:10.1016/j.quascirev.2009.09.011

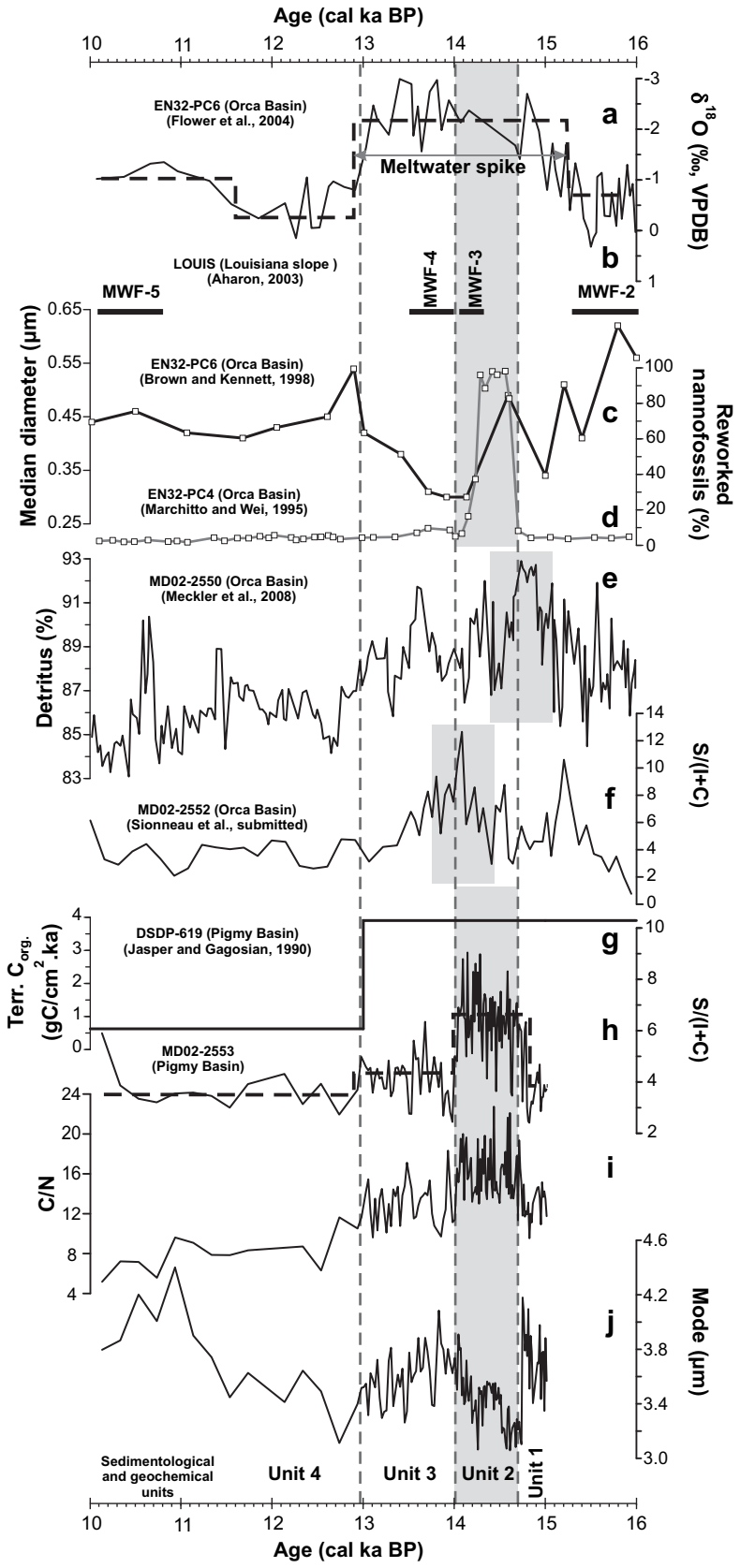

Fig. 11. Comparison of the sedimentological parameters of core MD02-2553 (Pigmy Basin) with proxy records of meltwater discharges of other GOM cores during 15–10 cal ka BP interval. (a) The $\delta^{18}O$ foraminifer records from Orca Basin core EN32-PC6 (Flower et al., 2004). (b) Bold line mark the successions of meltwater floods (MWF 2–5) recognized by Aharon (2003) in Louisiana slope (LOUIS) cores from northern GOM. Proxy records interpreted to represent meltwater flood erosion intensity and provenance records in the Orca Basin cores: (c) siliciclastic grain-size from core EN32-PC6 (Brown and Kennett, 1998), (d) percent reworked calcareous nannofossils as percent of total nannofossil assemblage from core EN32-PC4 (Marchitto and Wei, 1995), (e) percent of detritus from core MD02-2550; a proxy of terrigenous input (Meckler et al., 2008) and, (f) clay mineral ratio S/(I + C) from

Unit 2 displays rather characteristic mineralogical and geochemical compositions: the detrital fraction is typically fine-grained, enriched in smectite and detrital organic matter, and exhibits a peculiar geochemical signature. These characteristics highlight modifications of provenance of the main detrital supply. The clay composition – enriched in smectite at the expense of both illite and chlorite (Fig. 11f,h) – suggests a westward shift of the main outflow from the Great lakes area toward the north-western recessing margin, that is, between the Rocky Mountains and the LIS, encompassing the Mississippi and Missouri provinces. The grain-size data (e.g., decreasing in the grain-size mode) suggest an increasing in the supplied of fine-grained sediment to the GOM in Unit 2 (Figs. 10 and 11), in agreement with terrestrial records showing that deglacial megafloods deeply eroded clay-rich terrace deposits along upper Mississippi River tributaries (Knox, 1996), additionally, the subsequent incision of the Mississippi River tributaries also supplied fine sediment to the fluvial suspended load (Rittenour et al., 2007). Geochemical data, compared with the Al-normalized metal concentrations from the Mississippi drainage area (Gustavsson et al., 2001), give new evidences on the provenance of the detrital fraction during the meltwater episode. Thus, the high V/Al, Fe/Al, (Gd/Yb)n ratios, which cannot be attributed to authigenic/diagenetic processes because of linear relationships between these proxies and Al (Fig. 8), also pinpoint the north-western province as the main detrital contributor during these events (Gustavsson et al., 2001). The low Ti/Al, Th/Al, K/Al, La/Al, Y/Al and Total REE/Al ratios (Figs. 8 and 9) suggest a significantly reduced contribution of the northeast cratonic province. This period of high meltwater supply is also linked with the occurrence of organic layers previously described in the northwest GOM (Tripsanas et al., 2007). The laminations observed in Pigmy Basin may then correspond to: (1) slight stratification in the deep part of the basin as described for the Orca Basin (Tribovillard et al., 2009); or (2) an enhanced oxygen consumption related to increased terrigenous particles flux (organic and mineral) (e.g., Leventer et al., 1983; Meckler et al., 2008). However, there are no geochemical evidences of strong modifications of the redox conditions in the Pigmy Basin that did not undergo oxygen-restricted conditions. On the other hand, in Fig. 5 the MS values are quite low in Unit 2. It is noteworthy also that these low values correspond exactly with a high Fe/Al ratio (Fig. 9) and with a break in laminations (Fig. 1c). This could be discussed in terms of redox conditions. When oxygen levels decrease and other electron acceptors are required for organic matter degradation, magnetite-like iron – which is the dominant magnetic mineral in the Pigmy Basin sediments (King, 1986) – is reduced to Fe(II), which subsequently yields low MS values (e.g., Bloemendal et al., 1992). In summary, our results suggest that Unit 2 corresponds to the most intense meltwater pulse from the southwest margin of the LIS, remobilizing clay-rich terrace deposits from the northwest part of the Mississippi and Missouri river watershed (Knox, 1996). It is synchronous with the most intense period of freshwater discharge as previously described or modeled (Licciardi et al., 1999; Tarasov and Pletier, 2005), which occurred as the LIS was retreating progressively northward. This retreat yielded to the formation of numerous large glacial lakes between the ice margin and former moraines (Teller, 1990), which delivered large amounts of freshwater and sediment when their outlets incised their substratum (Teller et al., 2005; Fisher et al., 2006).

Unit 3 displays mineralogical and geochemical characteristics similar to those of Unit 1, which suggests similar provenance of the detrital supply. The clay composition indicates a re-start of contributions from the northeast province as the LIS was withdrawn from its southern extent. The main discrepancy concerns the grain-size distribution that is mainly fine and cohesive whereas Unit 1 was mostly coarse-grained. We propose that Unit 3 corresponds to the late phase of the Meltwater Spike with reduced erosional processes.

This deglacial megafloods interval characterized in the Pigmy Basin (core MD02-2553) is also supported by contemporaneous spikes observed in proxies of flood erosion intensity (reworked nannofossils, siliciclastic grain-size, clay minerals) from the Orca Basin cores (Fig. 11a,c–f), and by net accumulation rates of sedimentary organic carbon from the Pigmy Basin (DSDP site 619) (Fig. 11g). It is important to emphasize that the difference in the timing of peak meltwater discharge observed in the different sedimentary records most likely reflects uncertainties in the individual core chronologies (e.g., Fig. 11e,f).

To summarize, our sedimentological and geochemical proxies allow differentiating various phases of terrigenous supply originating from different source areas according to the location in the time of the southern edge of LIS ice melting lobes.

5.3. Sedimentary regime during the Pleistocene/Holocene transition (12.9–10 cal ka BP)

Our results reveal that a major modification of the sedimentary regime occurred at 12.9 ka in the Pigmy Basin (Unit 4). The greater abundance of foraminifers in the uppermost part of the core, based in the sedimentological descriptions of the core (Fig. 1c), suggests an increased in the autochthonous biogenic contribution as the terrigenous input progressively diminished. The higher $CaCO_3$ concentration during this interval (Fig. 5) confirms this increase in biogenic productivity probably related to warmer sea-surface temperature (SST) evidenced in the Orca Basin (Flower et al., 2004). Warmer SST may reflect a decreased seasonal influence of cold continental air masses over the GOM as the glacial shoreline retreated over the Louisiana slope (Flower et al., 2004) or may alternatively be controlled by insolation (Ziegler et al., 2008). Our results (notably, C/N ratio and Rock–Eval Pyrolysis) also indicate that the organic matter is mainly of marine origin, in agreement with the proposed increase in productivity and consistently with previous observations in the Pigmy Basin (Jasper and Gagosian, 1990; Jasper and Hayes, 1993) and Orca Basin (Meckler et al., 2008; Tribovillard et al., 2008, 2009; Sionneau et al., in revision).

The reduced terrigenous contribution is confirmed by the low sedimentation rate observed after 12.9 ka (<25 cm/ka) in the Pigmy Basin. The grain-size distribution suggests that the Mississippi River discharge capacity was significantly reduced, especially during the Younger Dryas, in agreement with previous hypothesis (Brown and Kennett, 1998; Licciardi et al., 1999; Teller et al., 2005). The specific clay composition indicates the contribution of the south-eastern province to the sedimentation in the Pigmy Basin after 12.9 ka, as also observed in the sediment from the Orca Basin (Sionneau et al., in revision). All these observations confirm the hypothesis of a modification of the fluvial regime after 12.9 ka in which all meltwater discharges from the LIS are retained in proglacial lakes before entering the Mississippi River. Such

core MD02-2552 (Sionneau et al., in revision). Sedimentary records in the Pigmy Basin: (g) net accumulation rates (gC/cm^2 ka) of terrigenous organic carbon ($C_{org.}$) from core DSDP site 619 (Jasper and Gagosian, 1990), (h) clay mineral ratio S/(I + C), (i) C/N ratio, and (j) grain-size mode (μm) from core MD02-2553 (this study). The sedimentological and geochemical units defined in this study are indicated. The original age model is used in all records with calibration of radiocarbon time scales to calendar years before present using CALIB 5.0.2 (Stuiver and Reimer, 1993) where needed. VPDB – Vienna Peedee belemnite. Shaded interval indicates the most intense meltwater pulse from the southwest margin of the Laurentide Ice Sheet.

Please cite this article in press as: Montero-Serrano, J.C., et al., Sedimentary evidence of deglacial megafloods in the northern Gulf of Mexico (Pigmy Basin), Quaternary Science Reviews (2009), doi:10.1016/j.quascirev.2009.09.011

a mechanism may trap coarse detrital fractions in proximal lakes and damp out any seasonal variations (Bettis et al., 2008).

During the early Holocene (after 11.5 ka), the grain-size distribution suggest modification of the sedimentary regime in the Pigmy Basin (e.g., Fig. 10e) synchronous with evidences of Mississippi River discharge linked to Lake Agassiz overflows (Licciardi et al., 1999; Teller et al., 2002, 2005). In the GOM, these meltwater events are evidenced on the Louisiana slope (MWF-5; Aharon, 2003; Fig. 11b) and Orca Basin (Meckler et al., 2008; Fig. 11e), but are not significantly recorded in other GOM cores (Marchitto and Wei, 1995; Brown and Kennett, 1998; Flower et al., 2004; Sionneau et al., in revision). In this context the absence of any major changes in clay mineral and geochemical records suggest that inflows were of reduced importance and unable to carry significant detrital loads (Sionneau et al., in revision) or alternatively that these detrital inputs correspond to the remobilization of stored glacigenic sediments as the Mississippi River got adjusted to the postglacial hydrologic regime (Knox, 1996; Brown and Kennett, 1998).

6. Summary and conclusions

Our multiproxy record from the Pigmy Basin in the northern GOM reveal large variations in the terrigenous input over the last deglaciation, which are likely associated with the Laurentide Ice Sheet (LIS) melting history and the Mississippi River discharge.

Four main sedimentological units can be distinguished upon their mineralogical and geochemical contents. Geochemical data indicate that sedimentation is mainly terrigenous in the Pigmy Basin, with no detectable authigenic processes, being strictly detrital (Units 1–3) during the deglaciation (15–12.9 cal ka BP) whereas significant biogenic contribution (Unit 4) is observed during the Younger Dryas and early Holocene (12.9–10 cal ka BP). Similarly, organic compounds are mostly terrigenous during the deglaciation whereas they display a higher marine influence in the early Holocene.

Clay mineralogy and rare earth element distribution reveal that sedimentation in the Pigmy Basin is mainly controlled by detrital inputs from the Mississippi River watershed with major contribution of the north-western part and minor supplies from the northeastern province. Most proxies display stair-step pattern suggesting drastic modifications in both hydrodynamic and sediment provenance. These modifications are interpreted to result from changes in the Mississippi River floods caused by LIS meltwater discharges. Over the studied interval both ice sheet margin instabilities and ice lobe fluctuations modified meltwater provenance and caused the main drainage to be repeatedly rerouted eastward or northward, leading to specific stair-step pattern meltwater discharges in the GOM.

A well-known modest surge of glacial meltwater (Melwater Spike or Meltwater Flow) is recorded by the deposition of sedimentological Units 1–3. Our sedimentological data provide new constraints on the synopsis of this major meltwater episode. The Meltwater Spike displays three distinct phases:

- Specific clay mineral and grain-size distributions suggest that meltwater originated from almost all the southern margin of the LIS and that erosion processes of the main Mississippi River channel were rather important during the early phase of the Meltwater Spike. Unit 1 is thus interpreted as the record the initial erosive flood, which may correspond to the proglacial lake Wisconsin outburst (14.9 cal ka BP).
- Unit 2 is characterized by major modifications of provenance of the main detrital supply suggesting a westward shift of the main outflow from the Great lakes area toward the recessing north-western margin. According to geochemical evidences, the organic-rich laminations observed in the Pigmy Basin are interpreted as the result of enhanced detrital particles flux rather than water stratification in the deep part of the basin. Unit 2 records the paroxysmal phase of the meltwater pulse originating from the southwest margin of the LIS while retreating.
- Unit 3 corresponds to the late phase of the Meltwater Spike with reduced erosional processes. The clay composition indicates the onset of contributions from the northeast province as the LIS was withdrawn from its southern extent.

A major modification of the sedimentary regime – increase in biogenic contribution and decrease in terrigenous supply – occurred at ca 12.9 cal ka BP in the Pigmy Basin (Unit 4). These modifications mirrors the average changes in the magnitude of the sedimentation rates from about 200 to 25 cm/ka, which is consistent with major reduction of meltwater flow during this time, and may reveal differences due to clastic dilution. Geochemical and sedimentological proxies suggest an increase in productivity probably related to warmer sea-surface temperature controlling by either seasonality or insolation. The grain-size distribution also suggests that the Mississippi River discharge capacity was significantly reduced, especially during the Younger Dryas whereas specific clay composition (e.g., kaolinite) indicates the contribution of the south-eastern province. These observations confirm a modification of the fluvial regime where all meltwaters were trapped in proglacial lakes before entering the Mississippi River.

During the early Holocene (after 11.5 ka) some minor modifications of the sedimentary regime may reflect episodic Mississippi River discharge linked to Lake Agassiz overflows. But the absence of any major changes in clay mineral and geochemical records suggest that inflows were of reduced importance in agreement with the lack of significant hydrological modifications in the GOM. Alternatively, these detrital inputs may thus correspond to the remobilization of stored glacigenic sediments as the Mississippi River got adjusted to the postglacial hydrologic regime.

Acknowledgements

We thank Yvon Balut, the Institut Paul-Emile Victor (IPEV), the officers and crew of the R/V Marion Dufresne and the IMAGES program for core collection. This study was financially supported by: (1) the UMR Géosystèmes of the Université Lille 1 (France); and (2) the Program Alban, the European Union Program of High Level Scholarships for Latin America, scholarship No. E06D100913VE. We thank the technical staff of the Géosystèmes lab: Léa-Marie Emaille, Laurence Debeauvais, Deny Malengros, Philippe Recourt & Déborah Ponleve. The authors are grateful to François Baudin (Université Pierre et Marie Curie – Paris 6) for performing the Rock–Eval analyses. VBR thanks Laurent Labeyrie for initiating the IMAGES-PAGE cruise. Thanks to the two anonymous reviewers for improving this manuscript through careful review, and to Neil Glasser for his editorial work.

References

Aharon, P., 2003. Meltwater flooding events in the Gulf of Mexico revisited: implications for rapid climate changes during the last deglaciation. Paleoceanography 18 (4), PA1079. doi:10.1029/2002PA000840.

Aharon, P., 2006. Entrainment of meltwaters in hyperpycnal flows during deglaciation superfloods in the Gulf of Mexico. Earth and Planetary Science Letters 241, 260–270.

Alley, R.B., 2000. The Younger Dryas cold interval as viewed from central Greenland. Quaternary Science Reviews 19, 213–226.

Bard, E., 1988. Correction of accelerator mass spectrometry ^{14}C ages measured in planktonic foraminifera: paleoceanographic implications. Paleoceanography 3 (6), 635–645.

Bettis, E.A., Benn, D.W., Hajic, E.R., 2008. Landscape evolution, alluvial architecture, environmental history, and the archaeological record of the Upper Mississippi River Valley. Geomorphology 101, 362–377.
Bloemendal, J., King, J.W., Hall, F.R., Doh, S.-J., 1992. Rock magnetism of Late Neogene and Pleistocene deep-sea sediments: relationship to sediment source, diagenetic processes, and sediment lithology. Journal of Geophysical Research 97 (B4), 4361–4375.
Bouma, A.H., 1981. Depositional sequences in clastic continental slope deposits, Gulf of Mexico. Geo-Marine Letters 1, 115–121.
Bouma, A.H., Coleman, J., 1986. Intraslope basin deposits and relation to continental shelf, northern Gulf of Mexico. American Association of Petroleum Geologists Bulletin 9 (70), 1178.
Bouma, A.H., Stelting, C.E., Leg 96 sedimentologists, 1986. Seismic stratigraphy and sedimentary processes in Orca and Pigmy Basin. In: Bouma, A.H., Coleman, J.M., Meyer, A.W., (Eds.), Initial Reports of the Deep-Sea Drilling Project. Leg 96. Washington D.C., U.S. Government Printing Office, pp. 563–576. doi:10.2973/dsdp.proc.96.128.1986.
Bout-Roumazeilles, V., Trentesaux, A., 2007. Sedimentologic analysis of cores recovered from the RV Marion Dufresne cruise in the Gulf of Mexico, chapter 5, July 2002, PAGE 127 Campaign. In: Winters, W.J., Lorenson, T.D., Paull, C.K. (Eds.), Initial Report of the IMAGES VIII/PAGE 127 Gas Hydrate and Paleoclimate Cruise on the RV Marion Dufresne in the Gulf of Mexico, 2–18 July 2002: U.S. Geological Survey Open-File Report 2004-1358, one DVD. Online at: http://pubs.usgs.gov/of/2004/1358.
Bout-Roumazeilles, V., Cortijo, E., Labeyrie, L., Debrabant, P., 1999. Clay mineral evidence of nepheloid layer contribution to the Heinrich layers in the Northwest Atlantic. Palaeogeography, Palaeoclimatology. Palaeoceanography 146, 211–228.
Broecker, W.S., Kennett, J.P., Flower, B.P., Teller, J.T., Trumbore, S., Bonani, G., Wolfli, W., 1989. Routing of meltwater from the Laurentide Ice-Sheet during the Younger Dryas cold episode. Nature 341, 318–321.
Brown, G., Brindley, G.W., 1980. X-ray diffraction procedures for clay mineral identification. In: Brindley, G.W., Brown, G. (Eds.), Crystal Structures of Clay Minerals and their X-ray Identification. Mineralogical Society, London, pp. 305–359.
Brown, P.A., Kennett, J.P., 1998. Megaflood erosion and meltwater plumbing changes during last North American deglaciation recorded in Gulf of Mexico sediments. Geology 26, 599–602.
Clark, P.U., Marshall, S.J., Clarke, G.K.C., Hostetler, S.W., Licciardi, J.M., Teller, J.T., 2001. Freshwater forcing of abrupt climate change during the last glaciation. Science 293, 283–287.
Coleman, J.M., 1988. Dynamic changes and processes in the Mississippi River delta. Geological Society of America Bulletin 100, 999–1015.
Diegel, F.A., Karlo, J.F., Schuster, D.C., Shoup, R.C., Tauvers, P.R., 1995. Cenozoic structural evolution and tectono-stratigraphic framework of the northern Gulf coast continental margin. In: Jackson, M.P.A., Roberts, D.G., Snelson, S. (Eds.), Salt Tectonics: a Global Perspective: AAPG Memoir 65, pp. 109–151.
Disnar, J.-R., Jacob, J., Morched-Issa, M., Lottier, N., Arnaud, F., 2008. Assessment of peat quality by molecular and bulk geochemical analysis: application to the Holocene record of the Chautagne marsh (Haute Savoie, France). Chemical Geology 254, 101–112.
Dyke, A.S., 2004. An outline of North American deglaciation with emphasis on central and northern Canada. In: Ehlers, J., Gibbard, P.L. (Eds.), Quaternary Glaciations – Extent and Chronology, Part II. Elsevier B.V, Amsterdam, pp. 373–424.
Elderfield, H., Upstill-Goddard, R., Sholkovitz, E.R., 1990. The rare earth elements in rivers, estuaries and coastal seas and their significance to the composition of ocean water. Geochimica et Cosmochimica Acta 54, 971–991.
Emiliani, C., Rooth, C., Stripp, J.J., 1978. Late Wisconsin flood into the Gulf of Mexico. Earth and Planetary Science Letters 41, 159–162.
Espitalié, J., Deroo, G., Marquis, F., 1986. La pyrolyse Rock Eval et ses applications. Revue de l'Institut Français du Pétrole 40 (B), 755–784.
Fisher, T.G., Lowell, T.V., Loope, H.M., 2006. Comment on "Alternative routing of Lake Agassiz overflow during the Younger Dryas: new dates, paleotopography, and a re-evaluation" by Teller et al. Quaternary Science Reviews 25, 1137–1141. 2005.
Flower, B.P., Kennett, J.P., 1990. The Younger Dryas cool episode in the Gulf of Mexico. Paleoceanography 5 (6), 949–961.
Flower, B.P., Hastings, D.W., Hill, H.W., Quinn, T.M., 2004. Phasing of deglacial warming and laurentide ice sheet meltwater in the Gulf of Mexico. Geology 32, 597–600.
Flocks, J., Swarzenski, P., 2007. Sediment collection from Orca and Pigmy Basins, Gulf of Mexico, and analyses for texture and trace-metal concentrations, July 2002, PAGE 127 Campaign. In: Winters, W.J., Lorenson, T.D., Paull, C.K. (Eds.), Initial Report of the IMAGES VIII/PAGE 127 Gas Hydrate and Paleoclimate Cruise on the RV Marion Dufresne in the Gulf of Mexico, 2–18 July 2002: U.S. Geological Survey Open-File Report 2004-1358, one DVD. Online at: http://pubs.usgs.gov/of/2004/1358.
Goldstein, S.J., Jacobsen, S.B., 1988. Rare earth elements in river waters. Earth and Planetary Science Letters 89, 35–47.
Gromet, L.P., Dymek, R.F., Haskin, L.A., Korotev, R.L., 1984. The North American shale composite: its compilation, major and trace element characteristics. Geochimica et Cosmochimica Acta 48, 2469–3482.
Gustavsson, N., Bølviken, B., Smith, D.B., Severson, R.C., 2001. Geochemical Landscapes of the Conterminous United States – New Map Presentations for 22 Elements. U.S. Geol. Survey Prof. Paper, 1648. U.S. Department of the Interior.
Hughen, K.A., Overpeck, J.T., Lehman, S.J., Kashgarian, M., Southon, J.R., Peterson, L.C., Alley, R., Sigman, D.M., 1998. Deglacial changes in ocean circulation from an extended radiocarbon calibration. Nature 391 (6662), 65–68.
Hughen, K.A., Baillie, M.G.L., Bard, E., Beck, J.W., Bertrand, C.J.H., Blackwell, P.G., Buck, C.E., Burr, G.S., Cutler, K.B., Damon, P.E., Edwards, R.L., Fairbanks, R.G., Friedrich, M., Guilderson, T.P., Kromer, B., McCormac, G., Manning, S., Ramsey, C.B., Reimer, P.J., Reimer, R.W., Remmele, S., Southon, J.R., Stuiver, M., Talamo, S., Taylor, F.W., van der Plicht, J., Weyhenmeyer, C.E., 2004. Marine04 marine radiocarbon age calibration, 0–26 cal kyr BP. Radiocarbon 46, 1059–1086.
Jasper, J.P., Gagosian, R.B., 1989a. Glacial–interglacial climatically-forced 13C variations of sedimentary organic matter. Nature 342, 60–62.
Jasper, J.P., Gagosian, R.B., 1989b. Alkenone molecular stratigraphy in an oceanic environment affected by glacial meltwater events. Paleoceanography 4, 603–614.
Jasper, J.P., Gagosian, R.B., 1990. The sources and deposition of organic matter in the late Quaternary Pigmy Basin, Gulf of Mexico. Geochimica et Cosmochimica Acta 54, 1117–1132.
Jasper, J.P., Hayes, J.M., 1993. Refined estimation of marine and terrigenous contributions to sedimentary organic carbon. Global Biogeochemical Cycles 7, 451–461.
Joyce, E.J., Tjalsma, L.R.C., Prutzman, J.M., 1993. North American glacial meltwater history for the past 2.3 m.y.: oxygen isotope evidence from the Gulf of Mexico. Geology 21, 483–486.
Kennett, J.P., Shackleton, N.J., 1975. Laurentide ice sheet meltwater recorded in Gulf of Mexico deep-sea cores. Science 188, 147–150.
King, J.W., 1986. Paleomagnetic and rock-magnetic stratigraphy of Pigmy Basin, Deep Sea Drilling Project Site 619, Leg 96. In: Bouma, A.H., Coleman, J.M., Meyer, A.W., et al. (Eds.), Init. Repts. DSDP, 96. U.S. Govt. Printing Office, Washington, pp. 677–684.
Knox, J.C., 1996. Late Quaternary Upper Mississippi River alluvial episodes and their significance to the Lower Mississippi River system. Engineering Geology 45, 263–285.
Kohl, B., DSDP Leg 96 Shipboard Scientists, 1985. Biostratigraphy and sedimentation rates of the Mississippi Fan. In: Bouma, A.H., Normark, W.R., Barnes, N.E. (Eds.), Submarine Fans and Related Turbidite Systems. Springer-Verlag, New York, pp. 267–273.
Lawrence, M.G., Greig, A., Collerson, K.D., Kamber, B.S., 2006. Rare earth element and yttrium variability in South East Queensland waterways. Aquatic Geochemistry 12, 39–72.
Leventer, A., Williams, D.F., Kennett, J.P., 1982. Dynamics of the Laurentide ice sheet during the last deglaciation: evidence from the Gulf of Mexico. Earth and Planetary Science Letters 59, 11–17.
Leventer, A., Williams, D.F., Kennett, J.P., 1983. Relationships between anoxia, glacial meltwater and microfossil preservation in the Orca Basin, Gulf of Mexico. Marine Geology 53, 23–40.
Lewis, C.F.M., Teller, J.T., 2006. Glacial runoff from North America and its possible impact on oceans and climate, chapter 28. In: Knight, P.G. (Ed.), Glaciers and the Environment. Blackwell Publishing Ltd., Oxford, UK. doi:10.1002/9780470750636.ch28.
Licciardi, J.M., Teller, J.T., Clark, P.U., 1999. Freshwater routing by the Laurentide ice sheet during the last deglaciation. In: Clark, P.U., et al. (Eds.), Mechanisms of Global Climate Change at Millennial Time Scales, 112. American Geophysical Union Geophysical Monograph, pp. 177–201.
Marchitto, T.M., Wei, K.Y., 1995. History of Laurentide meltwater flow to the Gulf of Mexico during the last deglaciation, as revealed by reworked calcareous nannofossils. Geology 23, 779–782.
Meckler, A.N., 2006. Late Quaternary changes in nitrogen fixation and climate variability recorded by sediments from the Gulf of Mexico and the Caribbean Sea. PhD Thesis ETH Zürich N° 16811, p 156. Online at: http://www.up.ethz.ch/people/former/nmeckler/PhD_Meckler.pdf.
Meckler, A.N., Schubert, C.J., Hochuli, P.A., Plessen, B., Birgel, D., Flower, B.P., Hinrichs, K.-U., Haug, G.H., 2008. Glacial to Holocene terrigenous organic matter input to sediments from Orca Basin, Gulf of Mexico – a combined optical and biomarker approach. Earth and Planetary Science Letters 272, 251–263.
Meyers, P.A., 1997. Organic geochemical proxies of paleoceanographic, paleolimnologic and paleoclimatic processes. Organic Geochemistry 27, 213–250.
Nürnberg, D., Ziegler, M., Karas, C., Tiedemann, R., Schmidt, M.W., 2008. Interacting Loop Current variability and Mississippi River discharge over the past 400 kyr. Earth and Planetary Science Letters 272, 278–289.
Petschick, R., 2000. MacDiff 4.2 Manual. MacDiff [Online]. Available from World Wide Web: http://www.geologie.uni-frankfurt.de/Staff/Homepages/Petschick/RainerE.html.
Petschick, R., Kuhn, G., Gingele, F., 1996. Clay mineral distribution in surface sediments of the South Atlantic: sources, transport, and relation to oceanography. Marine Geology 130, 203–229.
Poore, R.Z., Verardo, S., Caplan, J., Pavich, K., Quinn, T., in press. Planktic foraminiferal relative abundance trends in the Gulf of Mexico Holocene sediments: records of climate variability. In: Holmes, C., (Ed.), Gulf of Mexico, its Origins, Waters, Biota, and Human Impacts. Univ Texas Press.
Rittenour, T.M., Blum, M.D., Goble, R.J., 2007. Fluvial evolution of the lower Mississippi River valley during the last 100 k.y. glacial cycle: response to glaciation and sea-level change. Geological Society of America Bulletin 119, 586–608.

Please cite this article in press as: Montero-Serrano, J.C., et al., Sedimentary evidence of deglacial megafloods in the northern Gulf of Mexico (Pigmy Basin), Quaternary Science Reviews (2009), doi:10.1016/j.quascirev.2009.09.011

Rühlemann, C., Mulitza, S., Lohmann, G., Paul, A., Prange, M., Wefer, G., 2004. Intermediate depth warming in the tropical Atlantic related to weakened thermohaline circulation: combining paleoclimate data and modelling results for the last deglaciation. Paleoceanography 19, PA1025. doi: 10.1029/2003PA000948.

Schroeder, C.J., 1983. Changes in Benthic Foraminifer Assemblages across the Holocene/Pleistocene Boundary, Sites 619, 620, 621, 622, and 624, Deep Sea Drilling Project Leg 96. In: Bouma, A.H., Coleman, J.M., Meyer, A.W., et al., (Eds.), Initial Reports of the Deep-Sea Drilling Project. Leg 96. Washington D.C., U.S. Government Printing Office, pp. 631–642. doi:10.2973/dsdp.proc.96.133.1986.

Sionneau, T., 2008. Transferts Continent – Océan: Enregistrement du dernier cycle climatique par les sédiments terrigènes du Golfe du Mexique. PhD thesis. Université Lille 1, p. 377. Online at: http://tel.archives-ouvertes.fr/tel-00366377/fr.

Sionneau, T., Bout-Roumazeilles, V., Biscaye, P.E., van Vliet-Lanoë, B., Bory, A., 2008. Clay mineral distributions in and around Mississippi River watershed and Northern Gulf of Mexico: Sources and transport patterns. Quaternary Science Reviews 27, 1740–1751.

Sionneau, T., Bout-Roumazeilles, V., Flower, B.P., Bory, A., Tribovillard, N., Kissel, C., Van Vliet-Lanoë, B., Montero-Serrano, J.C., in revision for publication. On the provenance of freshwater pulses in the Gulf of Mexico during the last deglaciation: evidence from grain size and clay mineralogy. Quaternary Research.

Sperazza, M., Moore, J.E., Hendrix, M.S., 2004. High-resolution particle size analysis of naturally occurring very fine-grained sediment through laser diffractometry. Journal of Sedimentary Research 74, 736–743.

Spero, H.J., Williams, D.F., 1990. Evidence for seasonal low salinity surface waters in the Gulf of Mexico over the last 16,000 years. Paleoceanography 5, 963–975.

Stocker, T.F., Wright, D.G., 1996. Rapid changes in ocean circulation and atmospheric radiocarbon. Paleoceanography 11 (6), 773–795.

Stuiver, M., Reimer, P.J., 1993. Extended ^{14}C data-base and revised calib 3.0 ^{14}C age calibration program. Radiocarbon 35, 215–230.

Tanaka, K., Akagawa, F., Yamamoto, K., Tani, Y., Kawabe, I., Kawai, T., 2007. Rare earth element geochemistry of Lake Baikal sediment: its implication for geochemical response to climate change during the Last Glacial/Interglacial transition. Quaternary Science Reviews 26, 1362–1368.

Tarasov, L., Peltier, W.R., 2005. Arctic freshwater forcing of the Younger Dryas cold reversal. Nature 435, 662–665.

Teller, J.T., 1990. Volume and routing of late-glacial runoff from the southern Laurentide Ice Sheet. Quaternary Research 34, 12–23.

Teller, J.T., Leverington, D.W., Mann, J.D., 2002. Freshwater outbursts to the oceans from glacial Lake Agassiz and their role in climate change during the last deglaciation. Quaternary Science Reviews 21, 879–887.

Teller, J.T., Boyd, M., Yang, Z.R., Kor, P.S.G., Fard, A.M., 2005. Alternative routing of Lake Agassiz overflow during the Younger Dryas: new dates, paleotopography, and a reevaluation. Quaternary Science Reviews 24, 1890–1905.

Tieh, T.T., Stearns, S.V., Presley, B.J., 1983. Mineralogy and incipient diagenesis of Pigmy Basin sediments, Hole 619, Deep Sea Drilling Project Leg 96. In: Bouma, A.H., Coleman, J.M., Meyer, A.W., et al., (Eds.), Initial Reports of the Deep-Sea Drilling Project. Leg 96. Washington D.C., U.S. Government Printing Office, pp. 631–642. doi:10.2973/dsdp.proc.96.129.1986.

Tribovillard, N., Algeo, T., Lyons, T.W., Riboulleau, A., 2006. Trace metals as paleoredox and paleoproductivity proxies: an update. Chemical Geology 232, 12–32.

Tribovillard, N., Bout-Roumazeilles, V., Algeo, T.J., Lyons, T., Sionneau, T., Montero-Serrano, J.C., Riboulleau, A., Baudin, F., 2008. Paleodepositional conditions in the Orca Basin as inferred from organic matter and trace metal contents. Marine Geology 254, 62–72.

Tribovillard, N., Bout-Roumazeilles, V., Sionneau, T., Montero-Serrano, J.C., Riboulleau, A., Baudin, F., 2009. Does a strong pycnocline impact organic-matter preservation and accumulation in an anoxic setting? The case of the Orca Basin, Gulf of Mexico. Comptes Rendus Geosciences 341, 1–9.

Tripsanas, E.K., Bryant, W.R., Slowey, N.C., Bouma, A.H., Karageorgis, A.P., Berti, D., 2007. Sedimentological history of Bryant Canyon area, northwest Gulf of Mexico, during the last 135 kyr (Marine Isotope Stages 1–6): a proxy record of Mississippi River discharge. Palaeogeography Palaeoclimatology Palaeoecology 246, 137–161.

van der Weijden, C.H., 2002. Pitfalls of normalization of marine geochemical data using a common divisor. Marine Geology 184, 167–187.

Wedepohl, K.H., 1971. Environmental influences on the chemical composition of shales and clays. In: Ahrens, L.H., Press, F., Runcorn, S.K., Urey, H.C. (Eds.), Physics and Chemistry of the Earth. Pergamon, Oxford, pp. 305–333.

Wedepohl, K.H., 1991. The composition of the upper Earth's crust and the natural cycles of selected metals. In: Merian, E. (Ed.), Metals and Their Compounds in the Environment. VCH-Verlagsgesellschaft, Weinheim, pp. 3–17.

Ziegler, M., Nürnberg, D., Karas, C., Tiedemann, R., Lourens, L.J., 2008. Persistent summer expansion of the Atlantic Warm Pool during glacial abrupt cold events. Nature Geoscience 1 (9), 601–605.

Please cite this article in press as: Montero-Serrano, J.C., et al., Sedimentary evidence of deglacial megafloods in the northern Gulf of Mexico (Pigmy Basin), Quaternary Science Reviews (2009), doi:10.1016/j.quascirev.2009.09.011

2.4.3. Changes in precipitation regimes over North America during the Holocene as recorded by mineralogy and geochemistry of the sediments of the Gulf of Mexico*

Abstract

Changes in terrigenous-transfer patterns from North America toward the Gulf of Mexico via the Mississippi River during the Holocene were investigated using sedimentological and geochemical records from the northern Gulf of Mexico (Pigmy Basin). Clay mineralogy and geochemical signatures indicate that detrital sedimentation during the Holocene in the Pigmy Basin originated from both the northern Mississippi and Missouri rivers watershed province and northern Great Lakes area. During the early Holocene, enhanced contribution of illite and chlorite, associated with low elemental variability (e.g., Ti/Al, K/Al) and stable grain-size distribution (e.g., cohesive-silt/sortable-silt) point out to a dominant contribution from the area extending from the Great Lakes to the eastern Mississippi River, suggesting that terrigenous supply was directly controlled by the Laurentide Ice Sheet evolution (LIS) at this time. Mid- and late-Holocene sedimentation, on the other hand, is characterized by repetitive occurrences of cohesive smectite-rich intervals associated with high geochemical variability. These recurring and rapid modifications of erosional processes over this period suggest changes in the hydrological regime via rainfall patterns. Such a modification during the Holocene is likely linked with the rapid atmospheric reorganization following the final collapse of the LIS. Indeed, mineralogical and geochemical proxies indicate east-to-west migrations of the main detrital source (from the Great Lakes and north-eastern province toward the north-western province) associated with Mississippi River megaflood episodes. These modifications of the main detrital sources likely record migrations of the precipitation belt, which are constrained by atmospheric configuration (Jet Stream, Bermuda High and Intertropical Convergence Zone position) and subtropical oceanic hydrological properties (meridional extension of the Atlantic Warm Pool). In the frame of previously published rainfall patterns over the Caribbean and North America, our results highlight some marked modifications of moisture transfer throughout the Holocene. These changes are interpreted as resulting from two atmospheric configurations that have driven alternately the precipitation distribution over North America for the last 10 ka with an apparent cyclicity of ~2.5 ka. The coherent common cyclicity between Gulf of Mexico detrital parameters and Greenland atmospheric proxies over the Holocene suggests that the initial external forcing was rapidly transferred latitudinally through atmospheric processes.

Keywords: Mississippi River, Pigmy Basin, Holocene, atmospheric configuration, clay mineralogy, geochemistry.

* **Montero-Serrano Jean Carlos**, Bout-Roumazeilles Viviane, Sionneau Thomas, Tribovillard Nicolas, Bory Aloys, Flower Benjamin, Riboulleau Armelle. *Changes in precipitation regimes over North America during the Holocene as recorded by mineralogy and geochemistry of the sediments of the Gulf of Mexico*. Global and Planetary Change (under review).

Introduction

The Gulf of Mexico (GOM) is ideally located for studying the relationships between high-latitude climate variability and subtropical hydrology. The hydrological properties of the GOM, that further impacts the Gulf Stream, result from the complex interactions between the inflow of warm tropical waters originating from the Caribbean Sea through the Loop Current, and from evaporation-precipitation budget and North American Rivers freshwater supply (Fig. 2.35a). The warm waters of the GOM, Caribbean Sea, and western tropical North Atlantic constituting the so-called Atlantic Warm Pool (AWP) represent the primary moisture source for North America (Wang and Enfield, 2001). Moisture meridian transfer is constrained by different atmospheric configurations, resulting from the respective position of the Jet Stream, the Bermuda High pressure cell and the Intertropical Convergence Zone (ITCZ) (Fig. 2.35a; Forman et al., 1995; Liu and Fearn, 2000; Knox, 2003; Harrison et al., 2003). The position of the main precipitation belt is therefore likely influenced by both low- and high- latitude forcing. All these oceanic and atmospheric characteristics are seasonally modulated. In the western tropical Atlantic Ocean, the AWP reaches its northern position during boreal summer when the ITCZ is located in its northern position, whereas these tropical waters are restricted to the southeastern GOM during boreal winter when the ITCZ is situated southward (Wang and Enfield, 2001; Poore et al., 2004; Nürnberg et al., 2008; Ziegler et al., 2008).

The hydrological characteristics of the GOM are thus also largely impacted by freshwater outflow from the Mississippi River. The Mississippi and Missouri River watersheds and their tributaries collect runoff from almost half the USA and carry suspended detrital particles that are characteristic of the drained areas. Major Mississippi outflows may modify the sea surface salinity and impact to some extent the thermohaline circulation via the Gulf Stream (Aharon, 2003; Flower et al., 2004). The Holocene climate is characterized by modifications of both atmospheric and oceanic configurations following the final collapse of the Laurentide Ice Sheet (LIS) evolution (Shuman et al., 2002). For instance, the Mississippi River was affected during the late Holocene by megaflood episodes resulting from recurrent modifications of both moisture transfer and precipitation regimes. During these episodes, massive erosion of the alluvial plains promoted the remobilization of fine-grained sediments and their transport toward the GOM via the Mississippi (e.g., Knox, 2000; 2003). These episodes were likely controlled by the atmospheric configuration, and may have resulted in changing the main provenance of the detrital supply and thus its mineralogical characteristics.

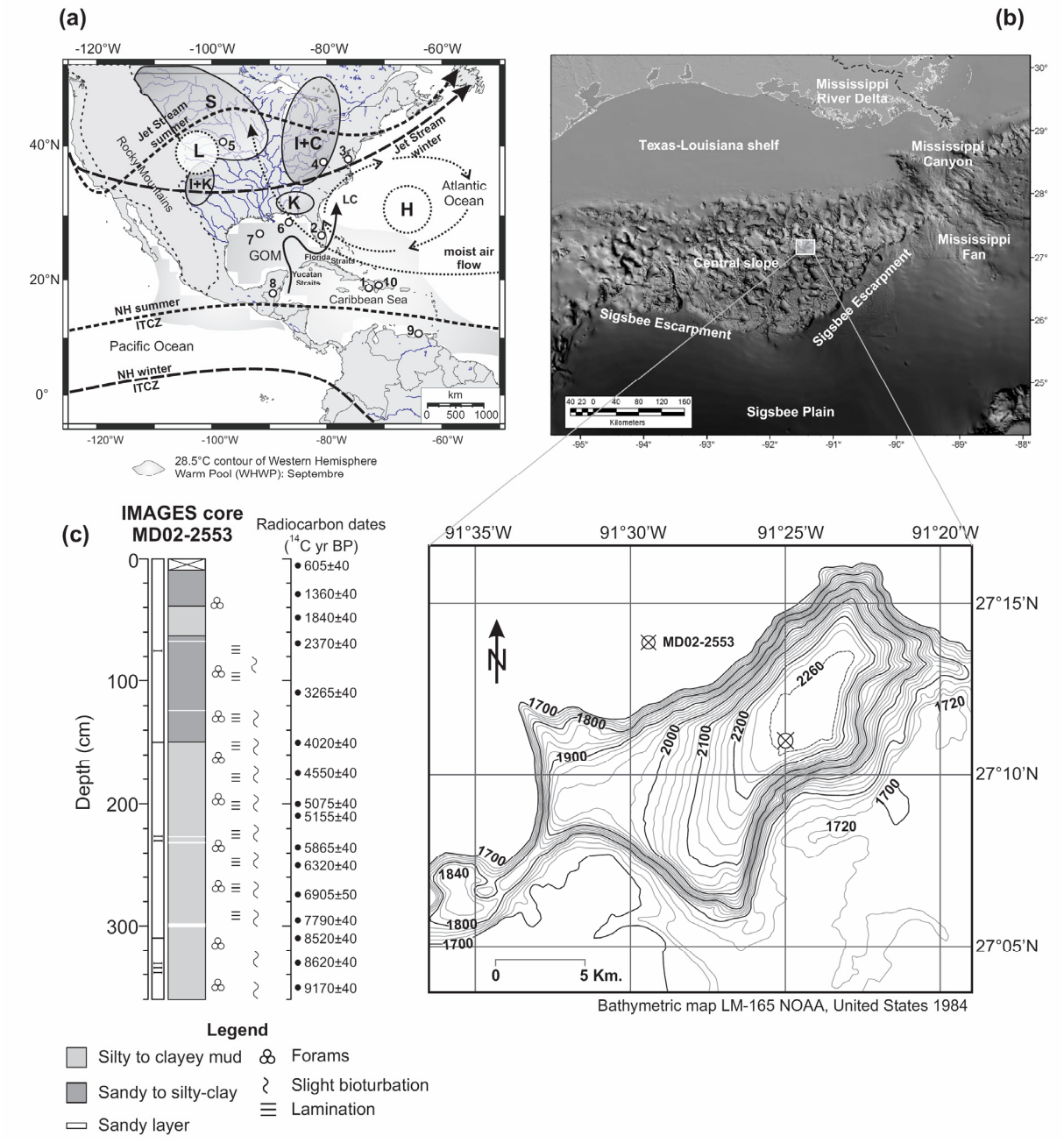

Fig. 2.35. (**a**) Map showing the location of selected localities discussed in this study, the main continental clay-mineral provinces over United States (Sionneau et al., 2008), generalized position of the Intertropical Convergence Zone (ITCZ) for Northern Hemisphere (NH) winter and summer (adapted from Ziegler et al., 2008), the mean configuration of the Jet Stream during winter and summer regimes (adapted from Knox 2000, 2003), and the mean summer position of the Bermuda High and the Thermal Low relative to North America [adapted from Forman et al. (1995) and Liu and Fearn (2000)]. S: smectite, I: illite, C: chlorite, K: kaolinite, GOM: Gulf of Mexico, LC: Loop Current. Numbers at each site are: (1) Lake Miragoane, Haiti; (2) Lake Tulane, Florida; (3) Chesapeake Bay, northeastern of the North America; (4) Buckeye Creek Cave, west Virginia; (5) North American Great Plains, (6) DeSoto Canyon, northeastern GOM; (7) Pigmy Basin, northern GOM; (8) Lake Petén Itzá, northern Guatemala; (9) Cariaco Basin, offshore northern Venezuela; (10) Cordillera Central, Dominican Republic. (**b**) Morphological map of the seafloor in the northern Gulf of Mexico (adapted from Tripsanas et al., 2007), and bathymetric map of the Pigmy Basin showing location of sediment core MD02-2553. Contour in meters. (**c**) Lithological log of core MD02-2553 between 0-360 cm showing the sedimentological characteristics and radiocarbon ages (Poore et al., in press).

Recent studies suggest that variations of the clay-mineral assemblage deposited in the northern GOM mainly reflect changes in the respective contributions of four main mineralogical provinces on land (Fig. 2.35a): (1) the northwestern Mississippi and Missouri rivers watershed characterized by high smectite content (2) the northeastern province mainly delivering illite and chlorite (3) the kaolinite-rich south-eastern part of the United States, and (4) the Brazos River and southwestern Mississippi River watersheds dominated by illite and kaolinite (Sionneau et al., 2008; Sionneau et al., in revision; Montero-Serrano-Serrano et al., in press). The mineralogical and geochemical characteristics of the detrital fraction of the sediment can thus be used to trace the modifications of the main detrital source associated with major flooding episodes and to constrain the main factors triggering such catastrophic events.

In this paper we present a sedimentological and geochemical record of Holocene climate variability for the last 10 ka from Core MD02-2553 recovered in the Pigmy Basin. This basin, situated on the Louisiana continental slope (27°11.01'N, 91°25.00'W, water depth 2,259 m) around 250 km southwest of the present-day Mississippi Delta, is suitably located to record both the terrigenous input from the North American continent and the tropical oceanic influences via the Loop Current (Fig. 2.35a). The basin is approximately 20 km-long, 7 km-wide, and trends northeast to southwest (Fig. 2.35b). Thus, using proxies of terrigenous supply in the Pigmy Basin during the Holocene, the main objectives are: (1) to determine changes in the North American sedimentary provenance throughout the Holocene, (2) to document the main changes in rainfall distribution over North America, and (3) to constrain the links between modifications of both high-latitude and sub-tropical domains, in order to infer possible synoptic scenarios or configurations of the atmosphere-ocean-continent interactions during the Holocene, and to further constrain the Holocene variations in summer moisture transfers across North America.

Materials and methods

Samples and chronology

The samples were taken from the 10.3 m long core MD02-2553 (Calypso Square) collected on the centre of the Pigmy Basin during the 2002 PAGE (Paleoceanography of the Atlantic and Geochemistry) cruise of the research vessel Marion Dufresne, as part of the International Marine Past Global Changes Study (IMAGES) program (Fig. 2.35b). The sediment is mainly composed of massive or faintly laminated silty to clayey mud (Fig. 2.35c).

Black shading related to accumulation of organic material is recurrent throughout the core. The uppermost 155 cm of the core are composed of sandy to silty clay with foraminifers and coccoliths, whereas the lower part contains clays with foraminifers that become scarce below 400 cm. Five distinct upward grading, foraminifer-rich, sandy layers interpreted as small turbidites (Meckler, 2006) occurring in the core (298-300 cm, 399-400 cm, 594-596 cm, 614-615 cm, and at 974-984 cm) have been removed from the record, as they correspond to local sedimentological processes rather than fluvial discharge.

For this study, the sediment samples were taken every 5 cm throughout the upper 359 cm of the core, yielding a total of 79 samples. Aliquots of the homogenized sediment samples were rinsed five times to remove salt, dried (40°C for 48h) and ground for geochemical analysis.

Table 2.3. Radiocarbon ages for core MD02-2553.

Reference	Core depth (cm)	Species	^{14}C AMS Age (ka)	^{14}C Error (± year)	Calibrated age (median, ka BP)	Calibarted error (± year, 1 sigma)
	0		0		0	0
	5.5		0.605	40	0.260	37
	29.5		1.360	40	0.907	49
	48.5		1.840	40	1.370	54
	69.5		2.370	40	1.993	60
	110.0		3.265	40	3.102	71
	150.5		4.020	40	4.029	65
	175.5		4.550	40	4.765	57
Poore et al. (in press)	200.5	Mixed planktic foraminifers	5.075	40	5.428	50
	210.0		5.155	40	5.523	43
	235.5		5.865	40	6.284	47
	250.5		6.320	40	6.783	58
	274.5		6.905	50	7.420	51
	295.5		7.790	40	8.259	52
	310.0		8.520	40	9.157	72
	330.5		8.620	40	9.307	65
	350.5		9.170	40	9.989	89

The chronology for the upper 359 cm of core MD02-2553 is based on sixteen accelerator mass spectrometry (AMS) ^{14}C radiocarbon dates from mixed planktic foraminifers published by Poore et al. (in press) (Table 2.3, Fig. 2.35c). Radiocarbon ages were corrected using a constant 400 yr reservoir age ($\Delta R=0$) and converted to calendar years through the CALIB software (Stuiver and Reimer, 1993; http://calib.qub.ac.uk/calib, version 5.0.2), using the calibration curve Marine04 (Hughen et al., 2004). Calibrated ages were plotted against core depth (Fig. 2.36), and a least squares regression ($r^2=0.996$) indicates a linear

sedimentation rate of 35.9 cm/ka (within the errors of the calibrated dates; 1 ka = 1000 cal yr BP) and a core-top age of 0 yr BP.

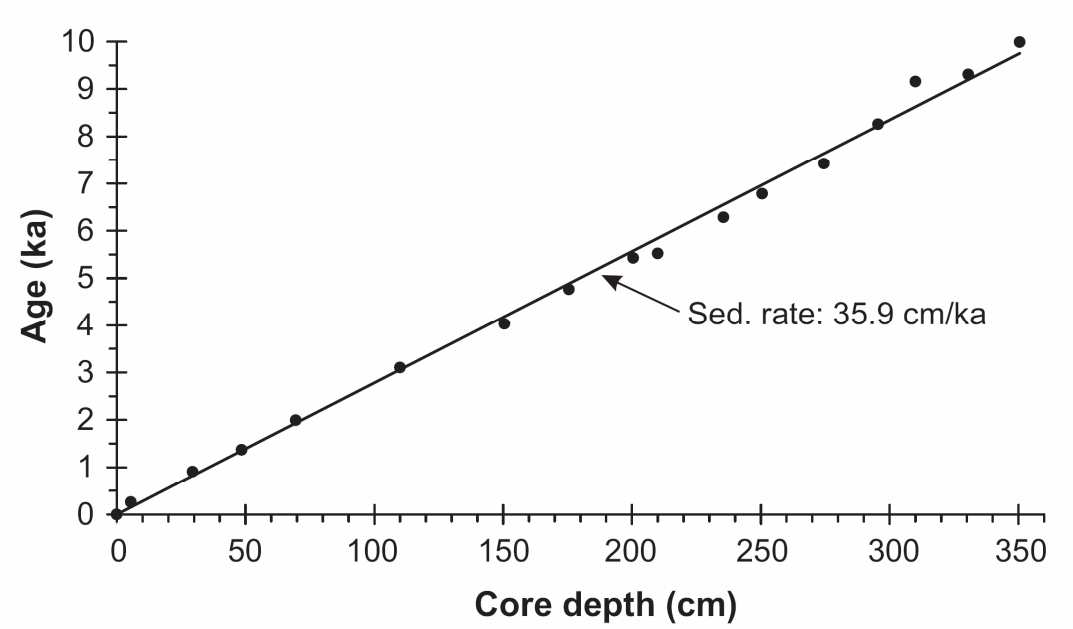

Fig. 2.36. Age model for core MD02-2553 based on 16 AMS ^{14}C dates from mixed planktic foraminifers (Poore et al., in press), converted to calendar ages (Table 2.3). Depth in centimeters was converted to calendar age by linear interpolation (1 ka = 1000 cal yr BP).

Analytical methods

The core MD02-2553 was studied at high resolution (average sample resolution of 5 cm ~ 139 yr) for grain size, clay mineralogy, calcium carbonate (CaCO3), total organic carbon (TOC), and total nitrogen (Ntotal) contents. Rock-Eval pyrolysis and inorganic geochemistry were studied at lower resolutions, with average sample resolution of 259 yr and 555 yr, respectively.

Grain size distribution. Grain size analyses were carried out on the carbonate-free fraction of the sediment, in order to focus on the detrital fraction, using a Malvern Mastersizer 2000 laser diffractometer. Sample preparation and optical settings for the Mastersizer 2000 followed the method described by Montero-Serrano et al. (in press). The distribution parameters reported here are the mode (µm, most frequent grain size) and percentage of clays (<2 µm), cohesive-silts (2-10 µm), sortable-silts (10-63 µm) and sands (>63 µm).

Clay-mineral analysis. Clay-mineral associations were studied using X-ray diffraction following the protocol of Bout-Roumazeilles et al. (1999). The analyses were run from 2.49°

to 32.49° 2θ on a Philips PW 1749 diffractometer (copper anode; 40 kV; 25 mA intensity and 1°2θ/minute speed). Three X-ray diagrams were performed, after air-dried sample, ethylene-glycol vapour saturation for 12 h and heating at 490°C during 2 h. Semi-quantitative estimation of clay-mineral abundances (smectite, illite, chlorite and kaolinite), based on peak areas, was performed using the Macintosh MacDiff® 4.2.5 software (Petschick, 2000). The error on the reproducibility of measurements is estimated to be ±5% for each clay mineral.

Rock-Eval pyrolysis. Usual Rock-Eval pyrolysis parameters, such as the S_2 peak (mg hydrocarbon per g sediment), total organic carbon content (TOC, wt %), Tmax (°C), and Hydrogen Index (HI, in mg hydrocarbon per g TOC) were determined with a Delsi Oil Show Analyser (Rock Eval II). The pyrolysis program was adapted to recent sediments, starting with an isothermal stage of 3 min at 180 °C. Then, the pyrolysis oven temperature was raised at 30 °C/min to 600 °C, and held for 3 min at this temperature (see Espitalié et al., 1986 for procedural details and Disnar et al., 2008 for Rock-Eval use for Holocene sediments).

Elemental analysis. Total inorganic carbon (TIC) content was determined as calcium carbonate ($CaCO_3$) percentage using a Bernard calcimeter and based on standard samples of pure $CaCO_3$ (precision <5%). Total carbon (TC) and total nitrogen (N_{total}) content were determined with a Thermo Flash EA1112 CHNSO analyser. The precision was better than 2% for TC and 5% for N_{total}, based on international standards and replicate samples. For the entire sample set, total organic carbon (TOC) was determined by subtracting inorganic carbon concentrations from total carbon concentrations, because the TOC content obtained by Rock-Eval pyrolysis was studied at lower resolution. Both methods gave consistent results. Though nitrogen may be present in the form of nitrate or ammonium in clay minerals, it is considered that N_{total} mostly corresponds to organic nitrogen. With this assumption, the C/N ratio (TOC/N_{total}) was calculated to indicate the source of organic matter (OM) in sediments (Jasper and Gagosian, 1990; Meyers, 1997; Meckler et al., 2008). C/N ratio values for organic matter (OM) of marine origin generally range from 4 to 10 because of the high protein content of lower organisms such as phytoplankton and zooplankton (e.g., Meyers, 1997). Higher plant-derived OM gives higher C/N values than those of marine origin OM because it has a high percentage of nonprotein materials (e.g., C/N>15; Meyers, 1997).

Inorganic geochemistry. Major, minor, trace and rare earth element (REE) concentrations were determined for 18 samples (average sample spacing is ca. 20 cm) by inductively coupled plasma optical emission spectrometry (ICP-OES) and inductively coupled plasma mass spectrometry (ICP-MS), at Activation Laboratories Ltd. (Ancaster, Canada). Samples were mixed with a flux of lithium metaborate ($LiBO_2$) and lithium

tetraborate ($Li_2B_4O_7$), and fused in an induction furnace. Molten sample was immediately poured into a solution of 5% nitric acid (HNO_3) containing an internal standard, and mixed continuously until completely dissolved. The analytical accuracy and precision were found to be better than 1-2% for major element, 5% for REE and 5-10% for the other elements, as checked by international standards and analysis of replicate samples. Since the carbonate content is not high (<25%) elemental compositions and total REE are normalized to aluminum (Al) to remove the effects of differential dilution of the bulk sediments by the aluminosilicate fraction so that changes in the composition of the lithogenous material can be discerned (see discussion about Al normalization in van der Weijden, 2002, and Tribovillard et al., 2006). In addition, trace metal (TM) concentrations are expressed in terms of enrichment factors (EF_{TM}) where the Al-normalized metal concentration is compared to the average shale values of Wedepohl (1971, 1991): $EF_{TM} = TM/Al_{sample} : TM/Al_{average\ shale}$. $EF_{TM}>1$ suggests enrichment relative to average shale but authigenic enrichments can be considered when EF_{TM} exceed 5 (Tribovillard et al., 2006). Fractionation between light REE (LREE: La-Nd), middle REE (MREE: Sm-Gd) and heavy REE (HREE: Tb-Lu) is retraced by La/Yb and Gd/Yb normalized ratios (Lawrence et al., 2006). NASC values by Gromet et al. (1984) are used for normalization of the REE. Al-normalized metal distributions and the REE abundance patterns are used as proxies of the detrital sediment sources, complementary to clay mineral proxies.

Spectral analyses

We performed time series analysis in order to evidence any cyclicitiy in the Pigmy basin clay-mineral variations and to investigate their correlation with high-latitude climatic records, using the software package AnalySeries 2.0.4 (Paillard et al., 1996; http://www.lsce.ipsl.fr/logiciels/index.php). We used two different spectral analysis methods a non-parametric Multi-Taper method, which provides high spectral resolution even for short time series (Thompson, 1982) and the high confidence Blackman-Tukey method (Blackman and Tukey, 1958) in order to improve accuracy and to prevent any bias due to methodological artefact. All time series were evenly resampled with a 0.145-ka interval and linear trends were removed prior to spectral analysis. The sample interval results in average time-resolution of 0.145 ka (0.028-0.306 ka). Thus the lowest theoretical period (Nyquist period) that could be resolved is always below 0.612 ka (two times maximum sampling period). The multi-taper method (MTM; Ghil et al., 2002) was performed using two tapers and a bandwidth resolution of 3 ka. The Blackman-Tukey cross-spectral analysis (Paillard et al., 1996) was performed

using a Bartlett-type window, high-resolution (50% of the series length) with a resulting 0.30 ka^{-1} bandwidth. Results of the spectral analysis are presented as spectral density. Each frequency band is reported taking as center the observed maximum spectral density for specific band. The mean Blackman-Tuckey coherency and phase were calculated by cross-spectral analysis between the clay-mineral distribution in the Pigmy Basin and GISP2 sea-salt Na record (O'Brien et al., 1995; Mayewski et al., 2004). Coherency is considered significant (at the 99% level) if larger than 0.78. Phases are reported only for the more significant bands (highest spectral density and significant coherency). Phases in radians were converted to kiloyears (one period=360°=2Pi radian) for each of frequency bands.

Results

Sediment characteristics

All samples are characterized by a unimodal grain-size distribution. Vertical changes in the grain-size parameters of the sediment are illustrated in Fig. 2.37. The sediments are mainly fine-grained (3.5µm<mode<5.1µm): 49-70% cohesive-silt, 9-31% sortable-silt, 15-23% clay and 0-5% sand (30% of sand between 298 and 310 cm represent a small turbidite). The cohesive-silt (Fig. 2.37c) shows an increasing trend throughout the Holocene with maximum around the 3-2 ka, while the sortable-silt fraction decreases. Clay content is maximum in the lowermost part of the core (between 10 and 8.5 ka) and shows an upward decreasing trend (Fig. 2.37d), whereas sand and cohesive-silt particles increase.

The clay-mineral fraction is composed of 67-85% smectite, 7-16% illite, 3-10% chlorite and 2-12% kaolinite (Fig. 2.38). The clay-mineral composition displays some characteristic oscillations between smectite-rich intervals (for example between 3.1 and 1.75 ka) and illite + chlorite-rich intervals (for example between 1.7 and 1.1 ka) (Fig. 2.38).

Carbonate content ($CaCO_3$) varies from 11.1 to 24.5% with highest values (>19%) between 4.9-3.6, 3.1-1.7 and 1.1-0.3 ka (Fig. 2.39). The vertical distributions of the values of TOC and C/N are illustrated in Fig. 2.39a-b. TOC content ranges from 0.49 to 1.53% and C/N ratio ranges from 7.7 to 33.9.

In general, the Rock Eval parameters (Tmax and HI) show little variations (supplementary materials, Fig. S-2.1). Tmax values ranges from 386 to 431°C and HI varies from 62 to 146 mg HC/g TOC. The TOC vs. S_2 and Tmax vs. HI crossplots together with C/N values (Fig. 2.39a) suggest predominantly immature type III OM, that is, of terrestrial origin.

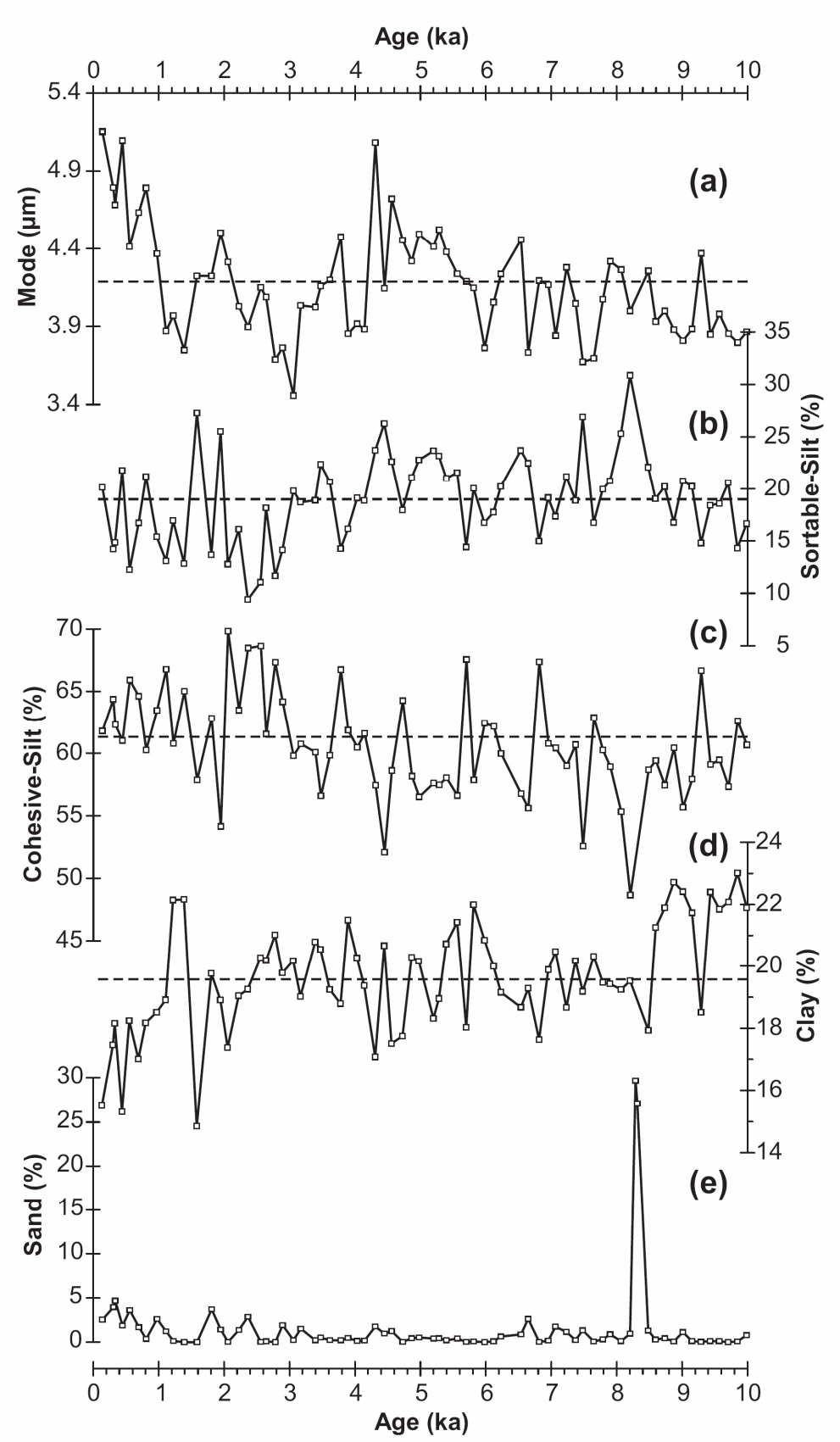

Fig. 2.37. Grain-size distributions (grain-size classes in %, and mode in µm) from Pigmy Basin (core MD02-2553). The horizontal dotted lines indicate the mean concentrations for each grain-size classes.

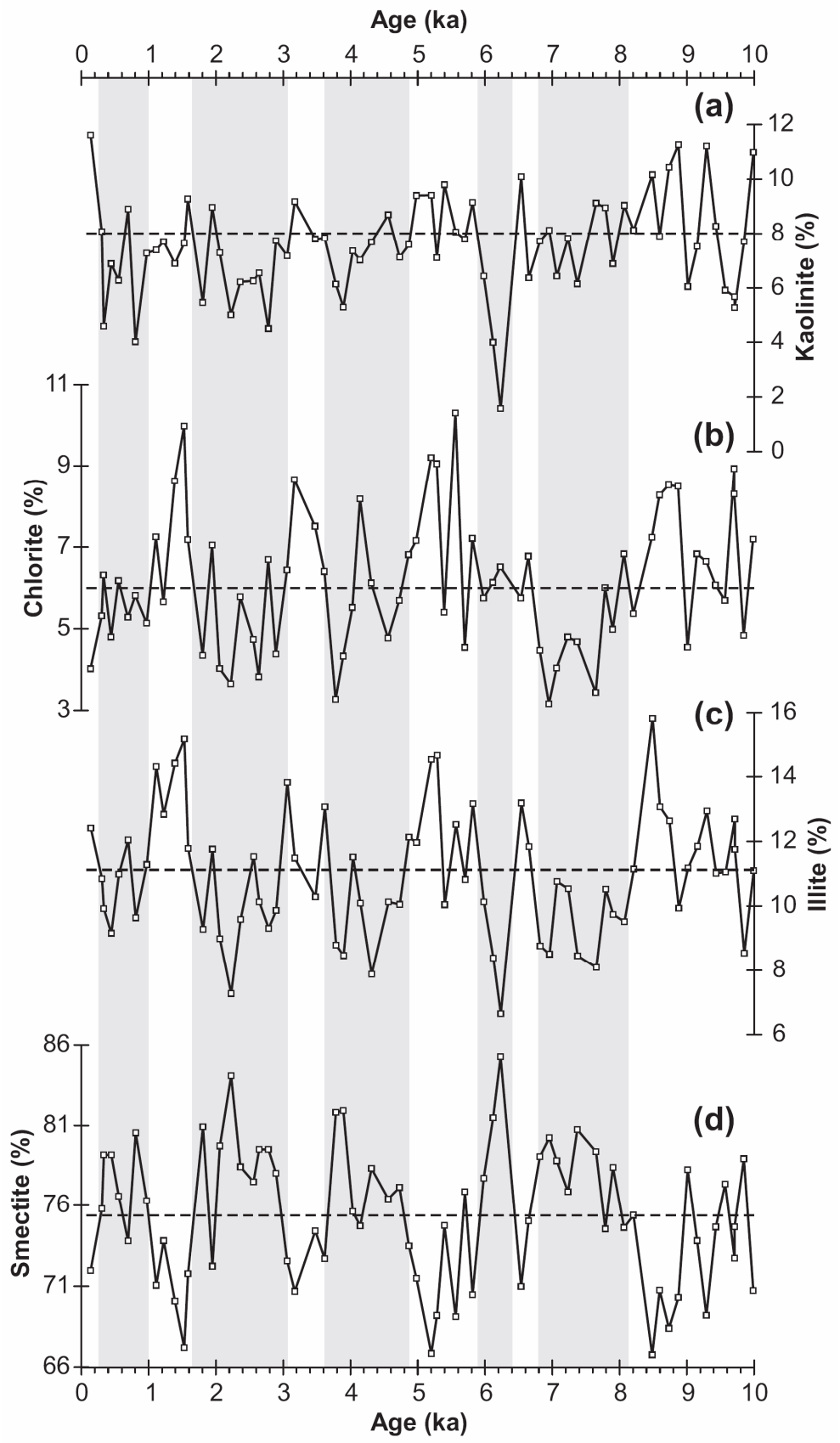

Fig. 2.38. Clay-mineral assemblages from Pigmy Basin (core MD02-2553). The horizontal dotted lines indicate the mean concentrations for each clay mineral. The smectite-rich intervals are indicated in shaded bands.

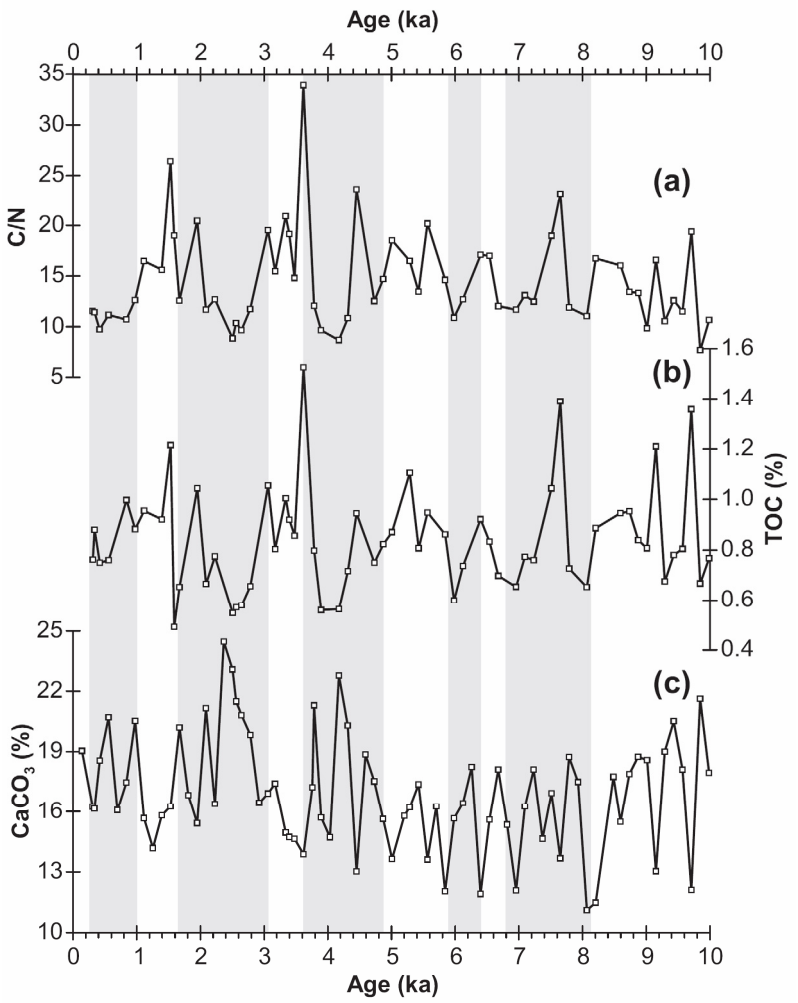

Fig. 2.39. Elemental analyses from Pigmy Basin (core MD02-2553). (**a**) C/N ratio, (**b**) TOC concentrations (%) and (**c**) carbonate ($CaCO_3$). The smectite-rich intervals are indicated in shaded bands.

Elemental geochemistry

All geochemical parameters show rather low variations (supplementary materials, Fig. S-2.2 and Fig. S-2.3). The main variations of both major and trace elements are consistent with the observed clay-mineral oscillations; e.g., K/Al, Mg/Al, Ti/Al and Zn/Al (supplementary materials, Fig. S-2.2) ratios are maximum over the illite + chlorite-rich intervals, whereas V/Al, Ca/Al and Loss on Ignition (LOI, wt %) increase with the smectite. Moreover, increases in Na/Al, Ba/Al, La/Al, Ce/Al and (La/Yb)n characterize the clay-rich interval evidenced by grain-size analyses in the lowermost part of the studied interval (before 8 ka) (Fig. 2.37d).

Trace-metal enrichment factors do not show any significant variations (0.5 to 2.2) (supplementary materials, Fig. S-2.3). NASC-normalized REE patterns do not show any

striking features, except for a general slight enrichment in light REE over HREE evidenced by the (La/Yb)n and (Gd/Yb)n (supplementary materials, Fig. S-2.2).

Interpretation and discussion

Main characteristics of Holocene sedimentary records in the Pigmy Basin

The calcareous biogenic fraction in the Pigmy Basin sediments is relatively low ($CaCO_3$<25%) indicating that the Holocene sedimentation is mostly terrigenous, with a relatively limited, autochthonous biogenic contribution. Furthermore, trace-metal enrichment factors suggest that the authigenic phases in the Pigmy Basin are negligible (supplementary materials, Fig. S-2.3). The absence of any significant REE fractionation when normalized to NASC in Pigmy Basin sediments, as observed in other basins from the GOM (Flocks and Swarzenski, 2007), indicates a highly-mixed detrital source. The similarity of REE distributions in Pigmy Basin sediments when compared with Mississippi River suspended loads (Goldstein and Jacobsen, 1988; Elderfield et al., 1990) indicates the dominant influence of Mississippi River and weak contributions of other rivers (Mobile, Brazos and Atchafalaya). Our results thus suggest that the Pigmy Basin is representative of the sedimentation in the off-shore part of the GOM in that it mainly collects land-derived particles delivered by the Mississippi + Missouri river system that drains almost half of the conterminous USA (Fig. 2.35a). In other words, the Pigmy Basin is an appropriate recorder of the land-to-sea transfer, from North America to the GOM. The C/N ratio (Fig. 2.39a) and Rock-Eval parameters (supplementary materials, Fig. S-2.1) suggest that the organic fraction is also mostly terrigenous, in agreement with similar findings over the deglaciation in the Pigmy Basin (Montero-Serrano et al., in press) and in nearby the Orca Basin (Meckler et al., 2008; Tribovillard et al., 2008, 2009; Sionneau et al., in revision).

Mineralogical and geochemical data both suggest that Holocene detrital sedimentation mainly results from the contributions of two different sources. The first source is characterized by its high smectite content associated mainly with high V/Al ratio and accessorily with high Th/Al ratio and high %LOI whereas the second contributor is enriched in illite and chlorite with high Mg/Al, K/Al, Ti/Al and Zr/Al ratios (supplementary materials, Fig. S-2.2). According to recently published clay-mineral distribution maps (Sionneau et al., 2008), the first end-member corresponds to the northwestern Mississippi and Missouri rivers watershed province and the second one is likely the northeastern Great Lakes province. The low correlation between the variations of illite and kaolinite (correlation coefficient: r<0.2,

n=69) implies that the alternative illite-rich source area from the southwestern illite + kaolinite-rich province (Fig. 2.35a) is not a possible candidate. Instead, the relatively good correlation between illite and chlorite (correlation coefficient: r=0.6, n=69) indicates a common source for illite and chlorite, pointing out to the northeastern province as the main contributor (Fig. 2.35a). In addition, the correspondence of the elemental ratios in the Pigmy Basin characterizing the smectite-rich intervals (mainly high V/Al ratio) with the Al-normalized metal concentrations from the Mississippi drainage area (Gustavsson et al., 2001; Grossman, 2009) is consistent with the hypothesis of specific supply from the northwestern part of the USA, while the elemental ratios observed in the illite- + chlorite-rich intervals (high Mg/Al, K/Al, Ti/Al and Zr/Al ratios) reflect an increase contribution of the northeastern province.

During the early Holocene, the Mississippi River discharge capacity was significantly reduced, as evidenced in the Pigmy Basin record by a decrease of the sedimentation rate from about 200 to 36-25 cm/ka. This decrease is due to a drastic decrease in the glacial erosional processes linked to the decay of the Laurentide Ice Sheet (LIS; Montero-Serrano et al., in press). The modifications of the LIS extent (Fig. 2.41a) played a major role in climate change in the Northern Hemisphere between 10 and 5 ka, resulting in the rapid warming of the Northern Hemisphere interrupted by the cold 8.2 ka event (Mayewski et al., 2004). Consequently, the observed variations in the respective contributions of these two dominant sources during the early Holocene are likely linked to the LIS extent changes.

On the contrary, any major modification of the dominant terrigenous sources that occurred during the late Holocene cannot be driven by the LIS that was considerably reduced by this time. Significant modifications are more likely related to modifications of the continental drainage patterns by the Mississippi and Missouri rivers in response to migrations of the main precipitation belt over North America (Knox, 2000, 2003). The sedimentological and geochemical record of Core MD02-2553 from the Pigmy Basin will thus be further interpreted in relation with the Holocene climatic variability.

LIS influence during early Holocene

The early Holocene is clearly marked by low sedimentological and geochemical variability (Fig. 2.40d; Fig. 2.41j-k). We interpret this feature as resulting from the impact of the LIS on continental climatic variability over the early Holocene. The ice-sheet probably filtered and smoothed some of the high-frequency climatic variability. As a result, continental processes were probably responding slowly to the initial solar forcing because the LIS highly

impacted regional temperatures at least until 8 ka (Mayewski et al., 2004). The northwestern smectite-rich province was the major contributor during the last deglaciation (Montero-Serrano et al., in press), whereas higher contribution of chlorite and illite (Fig. 2.38b-c) and geochemical proxies suggest enhanced contribution of the area extending from the Great Lakes area to the eastern Mississippi River watershed during the early Holocene (10 to 8 ka).

After the collapse of the LIS, rapid reorganization of the atmospheric circulation (Shuman et al., 2002) triggered rapid hydrological changes over central North America during the mid- to late- Holocene (e.g., Liu and Fearn, 2000; Lovvorn et al., 2001; Knox, 2003; Bettis et al., 2008). Consequently, the resulting migration of the precipitation belt might have been responsible for the high variability observed in sedimentological and geochemical proxies.

The variability of Mississippi River runoff after 8 ka

Intervals enriched in both smectite [i.e., S/(I+C)>4.6] and cohesive particles (cohesive-silt/sortable-silt>4.5) characterize mid to late Holocene Pigmy Basin records. These intervals at 6.4-5.9, 4.9-3.6, 3.1-1.7 and 1-0.3 ka (Fig 2.35d,e) coincide with large Mississippi floods (Fig. 2.40a) described in central North America (Knox, 2000, 2003) and catastrophic hurricanes (Fig. 2.40b) evidenced in the Gulf Coast Western Lake (Liu and Fearn, 2000). These Holocene flood episodes and catastrophic hurricanes, occurring as the ice-sheet had almost entirely vanished, likely resulted from heavy rainfall periods over central North America. Additionally, the smectite-rich interval observed in the mid- and late- Holocene in the Pigmy Basin was already described in the Orca Basin (Sionneau, 2008) and interpreted as a period of severe megafloods (Brown et al., 1999; Fig. 2.40c). The correlations between continental and marine records indicate that these megaflood events represent regional-scale changes in the hydrologic cycle over North America.

We do hypothesize that the variability of the Mississippi River regime during the Holocene (i.e., flood episodes) evidenced by both mineralogical and geochemical records reflects primarily variations in the migration of the precipitation belt over the North American continent. According to this scenario, these variations have been controlled by changes in atmospheric circulation patterns and the associated modifications of the meridian moisture transfer from the GOM to the North American continent. This moisture transfer and more generally the hydrological variability directly depend on the evaporation (E) – precipitation (P) balance over the GOM (Knox, 2000; Harrison et al., 2003) where increased evaporation leads to enhanced precipitation over the North American continent (Flannery et al., 2008). As

the E-P balance is linked to insolation, and sensitive to solar irradiance variability (Perry and Hsu, 2000), we also hypothesize that changes in solar variability may ultimately affect rainfall patterns over North America through ocean-atmosphere interactions. We will further test this hypothesis by comparing our records with previously published climate-related records from the Caribbean, GOM and North America.

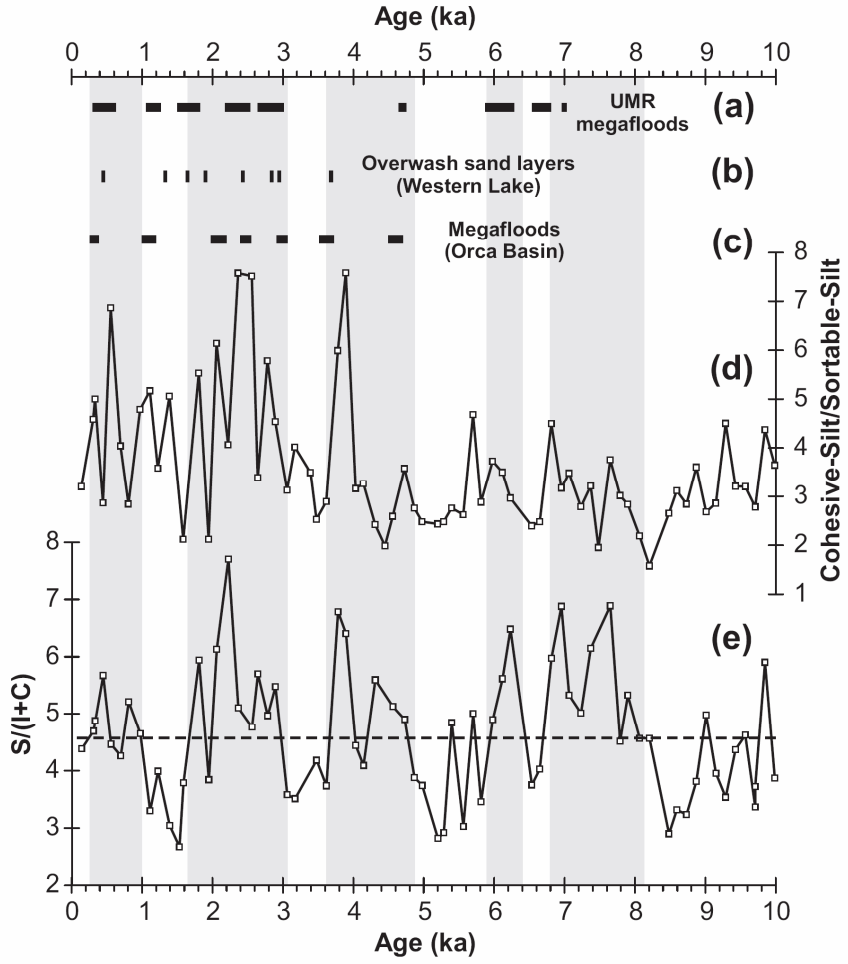

Fig. 2.40. Comparison of the sedimentological parameters of Holocene interval from the Pigmy Basin with terrestrial and marine paleorecords from the GOM, Gulf Coast and central North America. (**a**) Upper Mississippi River (UMR) channel megafloods episodes (Knox, 2003). (**b**) overwash sand layers from Western Lake, Gulf Coast (Liu and Fearn, 2000). (**c**) Megafloods on the Mississippi River identified by Brown et al. (1999) in the Orca Basin; Intervals punctuated by relatively coarse siliciclastic grain-size peaks, planktonic faunal turnovers, and negative $\delta^{13}C$ excursions of planktonic foraminifers *G. ruber* and *G. sacculifer*. Sedimentary records in the Pigmy Basin: (**d**) Cohesive-Silt/Sortable silt ratio. (**e**) smectite/(illite+chlorite) ratio. The smectite-rich intervals are indicated in shaded bands.

Precipitation distribution and atmospheric configuration during the past 8 ka

The interaction of three main air masses controls the general climatic patterns over the North American continent: the warm and moist GOM air-mass, the dry and mild Pacific air-mass, and the dry, cold Arctic air-mass (Knox, 2000). The location of the boundary between

these air masses in North America, and therefore of the main position of the precipitation front, is controlled by the respective position and extension of the Jet Stream, and of the Bermuda High pressure and Thermal Low pressure cells (Forman et al., 1995; Liu and Fearn, 2000; Knox, 2003). In the northwestern Mississippi river watershed, where the smectite-rich intervals are associated with catastrophic paleo-hurricanes and paleo-flooding episodes (Fig. 2.40), present-day average annual precipitation ranges between about 498 and 568 mm with about 70% of the annual amount falling during the warm season from April to September (boreal summer; http://www.rssweather.com/climate/).

Here we attempt to use clay mineral record from the Pigmy Basin to retrace the summer migrations of the precipitation belt over central North America over the mid- to late-Holocene. The contributions of smectite vs. illite and chlorite [S/(I+C) ratio; Fig. 2.41j] from the Pigmy Basin are used to document the continental-scale shift of the precipitation belt over central North America. Similar trends are observed in the clay mineral distributions of the nearby Orca Basin during the Holocene (Sionneau, 2008). This agreement gives support to our interpretations. Additionally, we use previously published palynological, isotopic and geochemical data from both continental and marine series (Hodell et al., 1991; Haug et al., 2001; Willard et al., 2005; Grimm et al., 2006; Kennedy et al., 2006; Nordt et al., 2008; Springer et al., 2008; Mueller et al., 2009) in order to constrain the two proposed configurations of the Holocene variations in summer ocean-continent moisture transfer (Forman et al., 1995; Liu and Fearn, 2000; Knox, 2000, 2003).

Configuration 1. The mineralogical and geochemical signatures of the smectite-rich intervals (8.1-6.8, 6.4-5.9, 4.9-3.6, 3.1-1.7 and 1-0.3 ka, Fig. 2.41i) indicate that the major flood events and catastrophic hurricanes were derived primarily from northwestern Mississippi and Missouri rivers watersheds (Fig. 2.40a-b). These results suggest that the precipitation belt was located over the northwestern province and that main moisture transfer reached the central part of North America during these periods. Organic carbon data (ΔC_4%) on soils form the North American Great Plains (Fig. 2.41g) also indicate an enhanced moisture flux from the GOM toward central North America, whereas the high Sr/Ca ratios from Buckeye Creek Cave (Fig. 2.41e) and the strong increase in the *Quercus* pollen content from the Chesapeake Bay (Fig. 2.41f), in the northeastern region of the North America, suggest the development of drought conditions along the eastern coast of North America. Furthermore, several northeastern USA lakes also experienced low-level during these intervals implying a widespread drought (e.g., Li et al., 2007; Newby et al., 2000; Shuman et al., 2002).

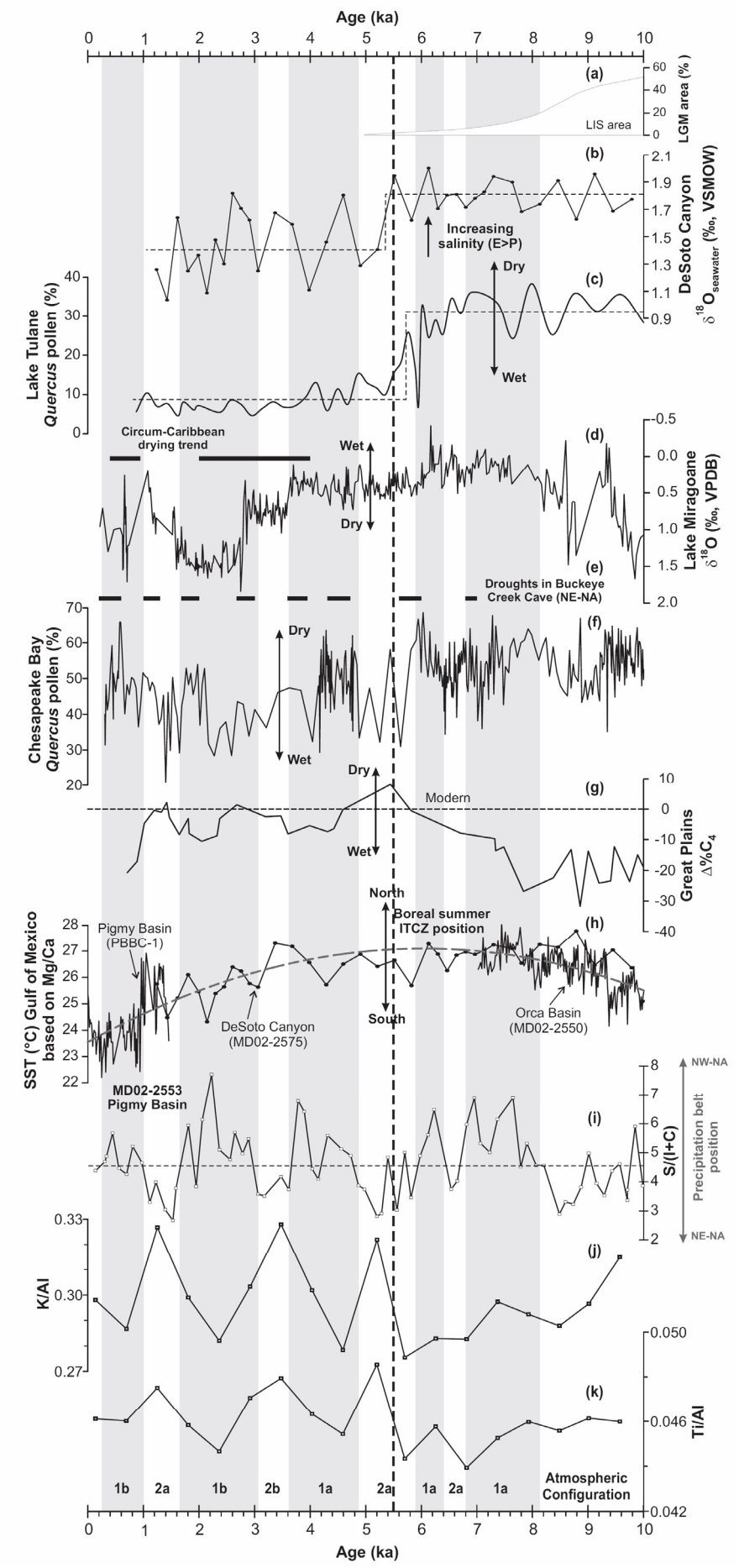

Fig. 2.41. Comparison of the multi-proxy record from the Pigmy Basin (core MD02-2553) with: (**a**) the area of the Laurentide ice sheet (LIS) as a fraction of the area during the last glacial maximum (LGM), adapted from Shuman et al. (2005); (**b**) isotope data from DeSoto Canyon (GOM; Nürnberg et al., 2008); (**c**) palynological records from Lake Tulane (southeastern US; Grimm et al., 2006); (**d**) oxygen isotope data from Lake Miragoane (Haiti; Hodell et al., 1991). Original radiocarbon scale were converted to calendar year scale using CALIB 5.0.2 (Stuiver and Reimer, 1993); (**e**) droughts periods in Buckeye Creek Cave, West Virginia (Springer et al., 2008); (**f**) palynological records from Chesapeake Bay, northeastern USA (Willard et al., 2005); (**g**) isotopic analysis of soil organic carbon ($\Delta\%C_4$) in the North American Great Plains (Nordt et al., 2008). $\Delta\%C_4$ is derived from the equation $\Delta\delta^{13}C_{C4}= \delta^{13}C_{C4\ buried\ soil} - \delta^{13}C_{C4\ modern\ latitudinal}$; see Nordt et al., 2008 for procedural details). Here, positive values indicate that C_4 plants were contributing more carbon to the soil organic pool than today and negative values indicating fewer contributions than today; (**h**) composite records of sea surface temperature (SST, °C) from GOM; core MD02-2550 from LoDico et al. (2006), core MD02-275 from Nürnberg et al. (2008) and core PBBC-1 from Richey et al. (2007); (**i-k**) sedimentological and geochemical proxies from the core MD02-2553. The smectite-rich intervals are indicated in shaded bands. The two-step of changes in the ocean-atmosphere-continent interactions inferred around of 5.5 ka (early Holocene) also is indicated (dotted lines).

According to configuration 1, the moisture distribution evidenced during these intervals implies that the Jet Stream and the Bermuda High were located to their northernmost and southwesternmost positions, respectively, while the low pressure was displaced eastward (configuration 1, Fig. 2.42a) in agreement with configurations proposed by Forman et al. (1995), Liu and Fearn (2000) and Knox (2000, 2003). At present, this synoptic pattern promotes transfer of moist air from the GOM and nearby tropical waters toward the central North America (Knox, 2000, 2003). In addition, the high carbonate content that also characterizes these intervals (Fig. 2.39c) indicates high biogenic productivity. It suggests an intensification of the Atlantic Warm Pool, which promotes the interpretation that warmer waters penetrated into the GOM, favoring evaporation over precipitation – and therefore a greater moisture transport to central North America (configuration 1, Fig. 2.42a).

Configuration 2. The intervals between 6.8-6.4, 5.9-4.9, 3.6-3.1 and 1.7-1 ka are characterized by low S/(I+C) ratio (Fig. 2.41i) indicating low precipitation on the smectite-rich north-western province. This suggests an eastward transfer of the main moisture pattern, which would be consistent with the relative increase in illite and chlorite. Isotopic analysis of organic carbon ($\Delta\%C_4$) from the North American Great Plains (Fig. 2.41g) also indicates dry conditions over the central part of North America. On the contrary, the low Sr/Ca ratios from Buckeye Creek Cave (Fig. 2.41e) and strong decrease in the *Quercus* pollen content from the Chesapeake Bay (Fig. 2.41f) suggest enhanced moisture abundance in the mid-Atlantic region. All these observations enable us to propose a second configuration (configuration 2) of the main moisture transfer over the successive intervals depleted in smectite (Fig. 2.42b). Investigations on the regional hydrologic responses to large-scale atmospheric circulation patterns during the Holocene (e.g., Forman et al., 1995; Liu and Fearn, 2000; Knox, 2000,

2003; Harrison et al., 2003; Goman and Leigh, 2004) suggest that the Jet Stream and the Bermuda High were located to the south and northeast respectively constraining the inflow of moisture along the eastern coast of North America and a reduced flux toward central North America. The reconstructed Jet Stream pattern shown in Fig. 2.42b with a main meridional component and a noticeable zonal component would likely lead to warm and dry summer conditions in the central North America, while increased precipitation and flooding occurred in the eastern area (Knox, 2000, 2003).

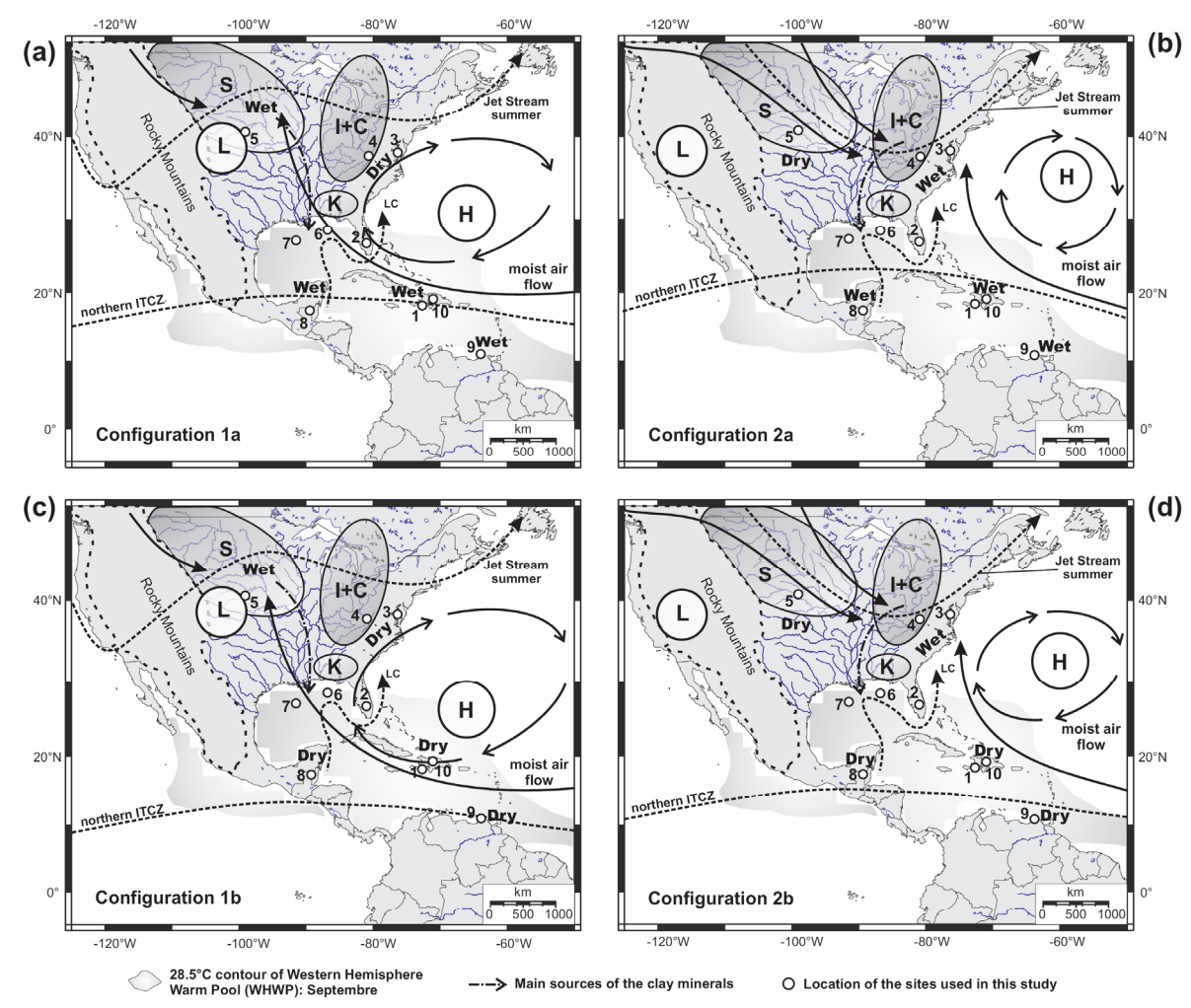

Fig. 2.42. Generalized reconstructions of regional atmospheric circulation patterns during the Holocene summer in the middle-latitude North America and their paleoclimatic implications. (**a**) and (**c**) Configurations during predominant wet periods in central North America (8.1-6.8, 6.4-5.9, 4.9-3.6, 3.1-1.7 and 1-0.3 ka). (**b**) and (**d**) Configurations during predominant dry periods in central North America (6.8-6.4, 5.9-4.9, 3.6-3.1 and 1.7-1 ka). The Jet Streams denote the approximate boundaries of air masses from tropical, pacific and polar-source regions and locations of the areas with the main moisture transfers over the North American continent (adapted from Knox 2000, 2003). The mean summer position of the Bermuda High and the Thermal Low relative to North America are modified from Forman et al. (1995) and Liu and Fearn (2000). Note that the mean latitudinal shifts of the Intertropical Convergence Zone (ITCZ) through the Holocene are monitored using paleoclimate records from the circum-Caribbean region and northern GOM (Fig. 2.41d,h). Numbers at each site are as in Fig. 2.35a.

Configuration modulation. The two proposed configurations are mainly based on GOM and North American records, i.e. related to the position of the Jet Stream and high- and Low- pressure cells. In order to improve these scenarios, we attempt to take into account the variations of the ITCZ that may modulate moisture transfer throughout the Holocene. ITCZ migration can be monitored using paleoclimate records from the circum-Caribbean region and northern GOM (Fig. 2.41d,h) – e.g., the Petén Itzá Lake (northern Guatemala; Mueller et al., 2009); Miragoane Lake (Haiti; Hodell et al., 1991); Cariaco Basin (offshore northern Venezuela; Haug et al., 2001); Cordillera Central (Dominican Republic; Kennedy et al., 2006); Orca Basin (core MD02-2550; LoDico et al., 2006); DeSoto Canyon (core MD02-275; Nürnberg et al., 2008) and Pigmy Basin (core PBBC-1; Richey et al., 2007). During the early Holocene, the ITCZ has a more northerly mean annual position relative to that during the late Holocene (Fig. 2.41h). This position led to enhanced precipitation in the circum-Caribbean region and decreased precipitable water vapour transport (E<P) to the North American continent (Fig. 2.42a-b). However, during the late Holocene, the mean position of the ITCZ was located southward (Fig. 2.41h) promoting drought in the Caribbean region (Fig. 2.42c-d) and increasing the availability of precipitable water vapour (E>P) that was transported to the North American continent. Thus during the past 3 ka, Configuration 1b (Fig. 2.42c) is thought to be responsible of the more important floods events and catastrophic hurricanes that affected central North America (e.g., Liu and Fearn, 2000; Knox, 2000, 2003).

Forcing of the atmosphere-ocean-continent oscillations − teleconnections

The observed link between climatic variability (wet vs. dry periods), atmospheric configurations and clay mineral record are further evaluated using spectral analysis (Fig. 2.43). The clay mineral assemblage variations, previously attributed to changes in the precipitation belt over North America, are similar to oscillations evidenced in Holocene glaciochemical records from GISP2 ice core (O'Brien et al., 1995; Mayewski et al., 2004). Clay mineral exhibits variations very similar with maximum sea-salt sodium (ssNa) concentrations (Fig. 2.43a-b). The ssNa in the GISP2 ice core is believed to be an indicator of storminess and sea spray in the atmosphere of the high-latitude region. Thus, the variability of the Mississippi River runoff appears to be correlated with changes in high-latitude atmospheric circulation. Cross-spectral analysis, using the Multi-Taper (Ghil et al., 2002) and Blackman-Tukey methods (Paillard et al., 1996) between the clay-mineral distribution [S/(I+C) ratio] in the Pigmy Basin and GISP2 ssNa record evidenced the same periodicity centered around 2.2-2.5 ka (Fig. 2.43c-d). The two signals are coherent at 99% confidence

level in the 2.5 ka frequency band with an average phase of 1.8±0.3 ka. Smectite-rich intervals in the Pigmy Basin and GISP2 ssNa concentrations are nearly 180 degrees out-of-phase (Fig. 2.43a-b). This relationship reveals that erosional processes in the NW Mississippi River watershed have been in antiphase with periods of intense atmospheric circulation in Greenland. Consequently, these results suggest a link between large-scale atmospheric circulation changes in the high-latitude North Atlantic and the hydrological and erosional changes in the North American continent.

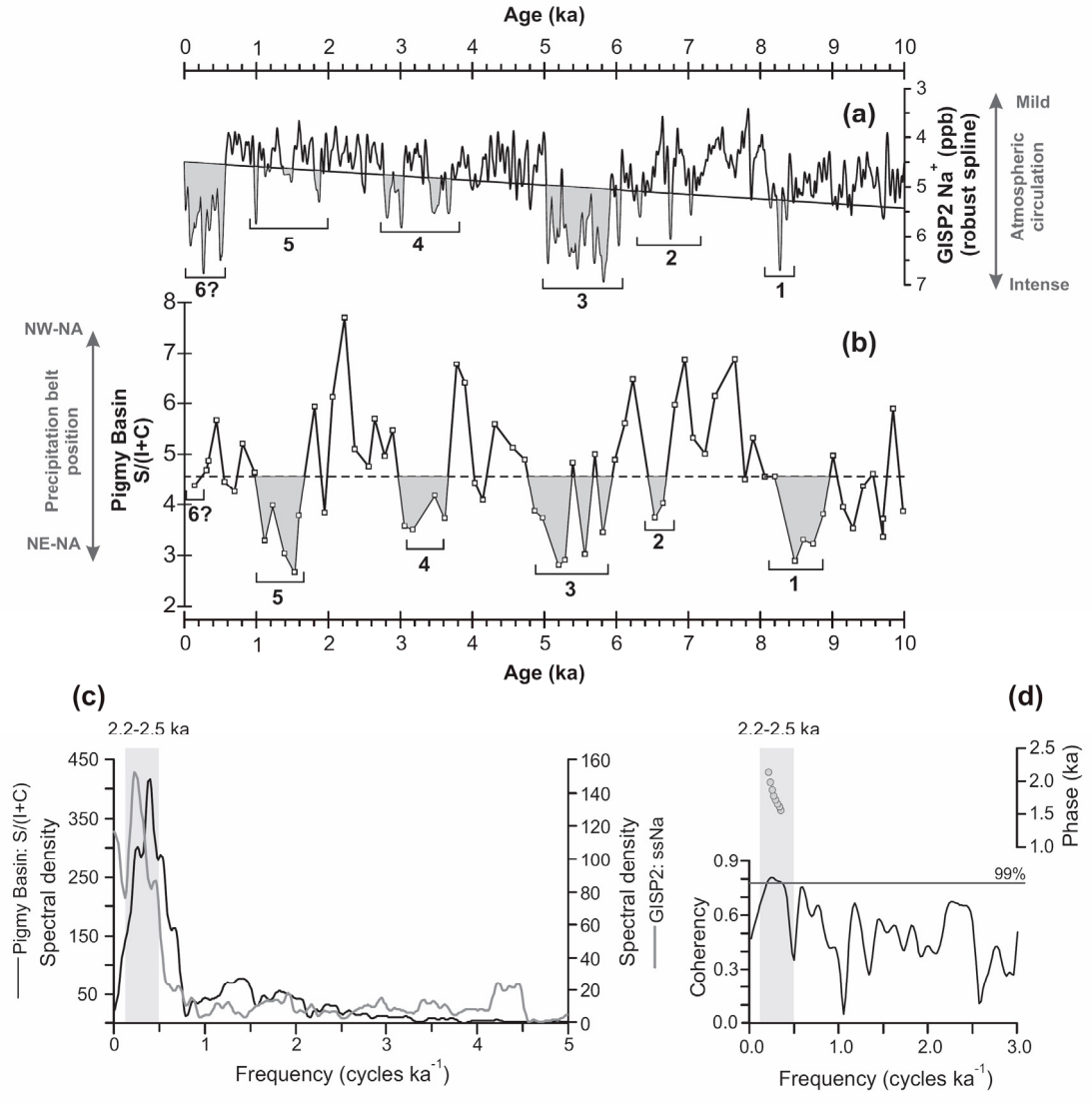

Fig. 2.43. (**a**) Holocene glaciochemical record from GISP2 ice (O'Brien et al., 1995; Mayewski et al., 2004) compared with (**b**) clay-mineral distribution [S/(I+C) ratio] from Pigmy Basin. Numbers in (**a**) and (**b**) represent tentative correlations between the illite + chlorite-rich intervals of core MD02-2553 (Pigmy Basin) and intervals with high concentrations of GISP2 sea-salt sodium (ssNa; shaded values from O'Brien et al., 1995). NW-NA: northwestern North America, NE-NA: northeastern North America. Spectral analysis: (**c**) Multi-Taper spectral analysis of the S/(I+C) ratio and GISP2 sea-salt sodium (ssNa). (**d**) Cross-spectral analysis, based on Blackman-Tukey method, between the S/(I+C) ratio and GISP2 ssNa record. Lower panel: Coherency spectrum. Upper panel: Phase. All periodicities significant above 99% are labeled.

The 2.5 ka periodicity also characterized ice rafted debris (IRD) occurrences in North Atlantic marine sediments (Bond et al., 2001), the $\delta^{18}O$ record in GISP2 ice core (Alley et al., 1997), and solar irradiance cycles (Stuiver et al., 1995). The correspondence between our sedimentological data and North Atlantic paleoclimate records may be due to modulation of atmospheric dynamics by solar forcing (e.g., Debret et al., 2007; in press).

Summary and Conclusions

Sedimentological and geochemical investigations of Holocene sediments from the Pigmy basin (GOM) indicate that both mineral and organic sedimentation are dominantly terrigenous and are mainly supplied by the Mississippi River. Clay mineral composition (smectite vs. illite + chlorite) indicates that early Holocene detrital sedimentation is characterized by an enhanced contribution of the area extending from Great Lakes to eastern Mississippi River provinces corresponding to the southern edge of the Laurentide Ice Sheet (LIS). Moreover, low geochemical (e.g., Ti/Al, K/Al) and grain-size (e.g., cohesive-silt/sortable-silt) variability over the early Holocene suggests persistent influence of the LIS that smoothed high-frequency climatic forcings. Contrastingly, mid and late-Holocene sedimentation is marked by a high geochemical variability (Ti/Al, K/Al) and by repetitive occurrences of smectite-rich intervals characterized by both cohesive grain-size and peculiar geochemical signatures. Indeed, rapid atmospheric reorganization following the LIS collapse likely triggered the hydrological changes observed during the late Holocene. After the final collapse of the LIS, sedimentation is characterized by recurrent occurrences of smectite-rich intervals associated with documented catastrophic hurricanes in the Gulf Coast and flooding episodes of the Mississippi River. Their geochemical and mineralogical signatures point out to specific terrigenous supply from the NW Mississippi river watershed, suggesting enhanced precipitations and moisture influx from the GOM toward central North America. Instead, repetitive enrichments in illite and chlorite suggest successive eastward migrations of main precipitation belts, consistent with documented evidences of increased aridity over central North America and development of more humid conditions along the Atlantic margin.

The comparison of our data with previously published records from central and eastern North America, GOM and circum-Caribbean region provides evidence of modifications of the main moisture transfer to the North America and of the associated precipitation belt over the mid- and late-Holocene. Our sedimentological records evidence two main atmosphere-ocean configurations that alternatively predominated throughout the Holocene:

(1) A northern position of the Jet Stream and southwest migration of the Bermuda High promote the influx of moisture over central North America which may trigger catastrophic hurricanes and flooding of the Mississippi River about 8.1-6.8, 6.4-5.9, 4.9-3.6, 3.1-1.7 and 1-0.3 ka ago. On the opposite, the northeastern provinces experienced dry conditions.

(2) A southern position of the Jet Stream associated with a northeastward displacement of the Bermuda High constrained the main moisture flux along the Atlantic margin about 6.8-6.4, 5.9-4.9, 3.6-3.1 and 1.7-1 ka ago.

Oscillations of these two configurations promoted the repetitive occurrence of drought/flooding over the northwestern Mississippi River through the Holocene. These two configurations correlate with both continental and oceanic records in North America and the Caribbean, and take into account the mean position of the ITCZ and AWP that modified moisture balance (E-P) over the GOM and ultimately affected the hydrologic variability over the North American continent. The previously discussed aspects suggest thus that during the Holocene the main moisture flux trajectories and migrations of the precipitation belt over North America were mainly constrained by the respective positions of the Jet Stream and Bermuda High modulated by displacements of both ITCZ and AWP.

Spectral analysis evidences a coherent common cyclicity of 2.5 ka between mineral proxies from Pigmy Basin and Greenland sea-salt sodium record suggesting a tight chronological connection between atmospheric circulation changes in the high-latitude North Atlantic and the hydrological and erosional changes in the North American continent. The close connection between the climate forcing and the erosional response of North America indicates that the “driving belt” cannot be the ocean because it would induce a time lag between climatic responses recorded in high latitudes and in the GOM. Our study thus confirmed the major role of the atmosphere as a vector of rapid climatic variability.

Acknowledgements

We thank Yvon Balut, the Institut Paul-Emile Victor (IPEV), the officers and crew of the R/V Marion Dufresne and the IMAGES program for core collection. This study was financially supported by: (1) the UMR Géosystèmes of the Université Lille 1 (France), and (2) the Programme Alban, the European Union Programme of High Level Scholarships for Latin America, scholarship No. E06D100913VE. We thank the technical staff of the Géosystèmes lab: Léa-Marie Emaille, Laurence Debeauvais, Deny Malengros, Philippe

Recourt & Déborah Ponleve. VBR thanks Laurent Labeyrie for initiating the IMAGES - PAGE cruise. The authors are grateful to François Baudin (Université Pierre et Marie Curie - Paris 6) for performing the Rock-Eval analyses. Thanks also to Richard Poore, Debra Willard, Eric Grimm, Lee Nordt, Dirk Nürnberg, Paul Mayewski and David Hodell for providing data. Lastly, this manuscript benefited from the reviews and suggestions of Anna Nele Meckler.

Supplementary materials

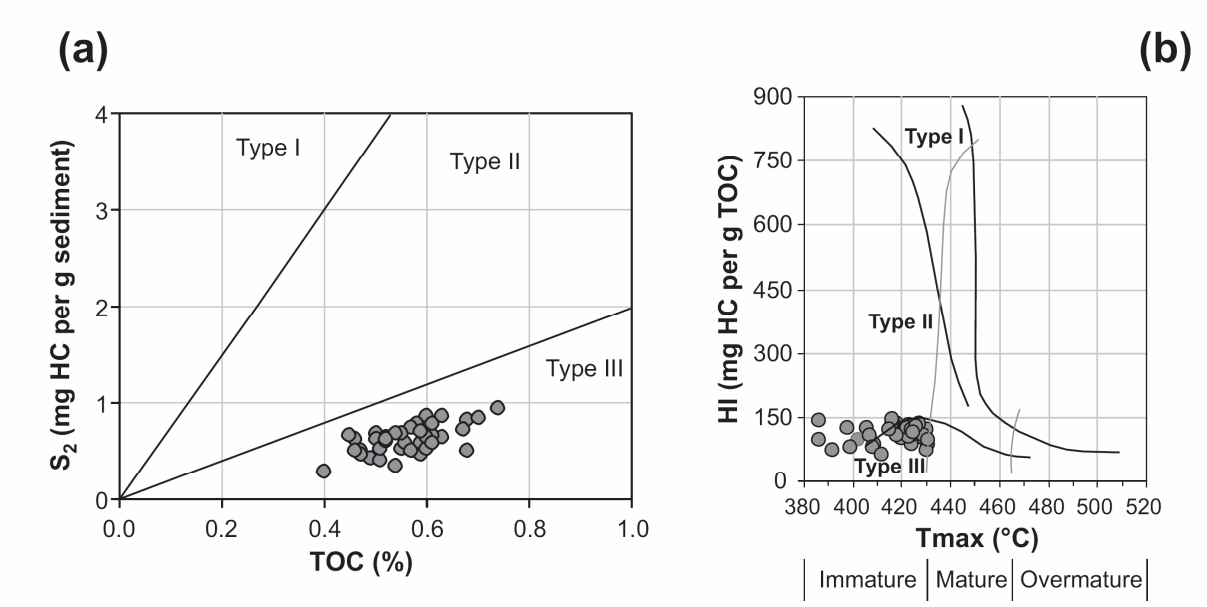

Fig. S-2.1. Rock-Eval pyrolysis parameters. (**a**) TOC vs. S_2 and (**b**) Tmax vs. HI crossplot illustrating the origin and maturation states of the organic matter.

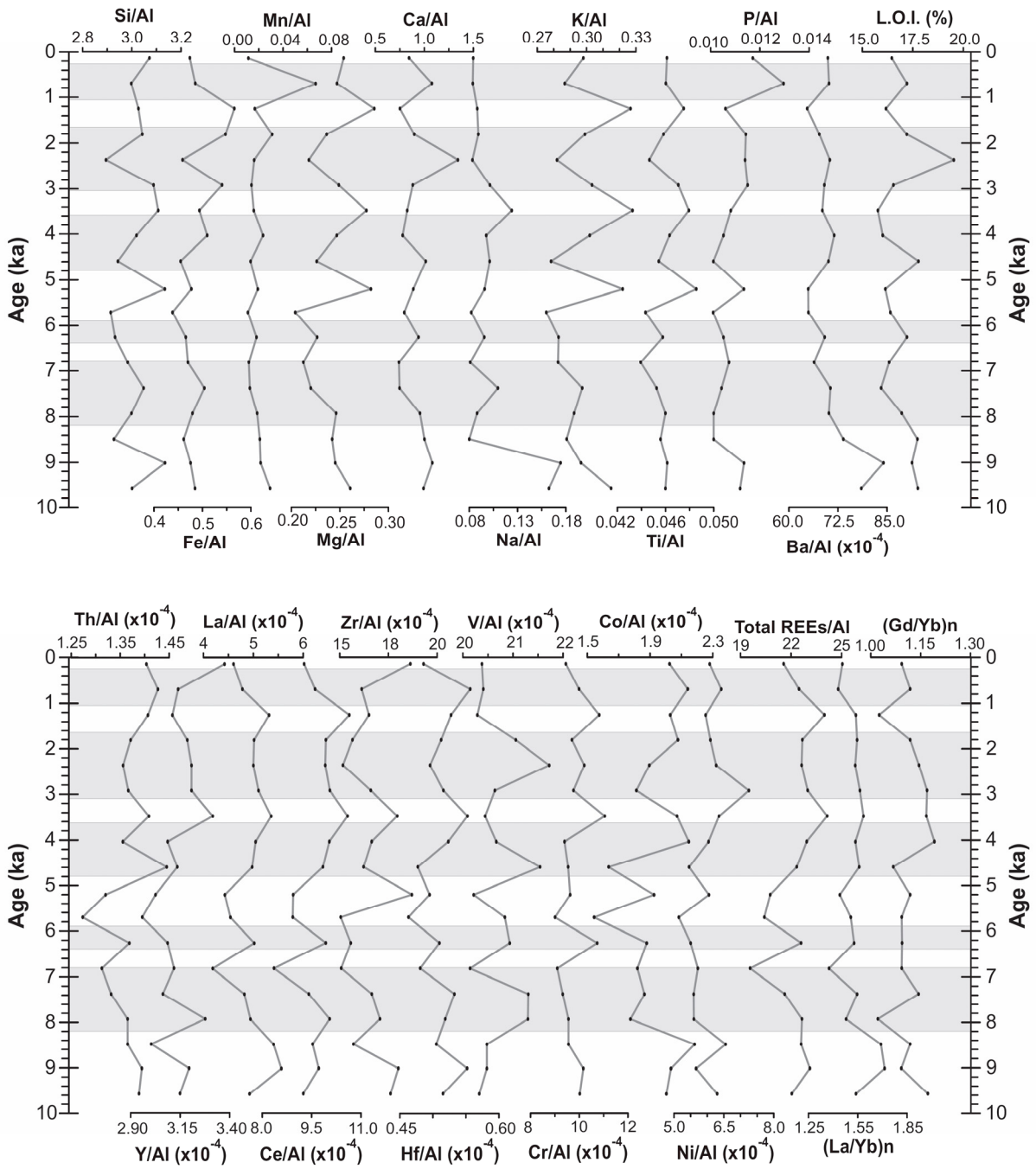

Fig. S-2.2. Al-normalized elemental ratios: major, minor, traces and rare earth (REE) elements. The suffix "n" denotes a NASC-normalized value (Gromet et al., 1984). LOI: Loss on Ignition. The smectite-rich intervals are indicated in shaded bands.

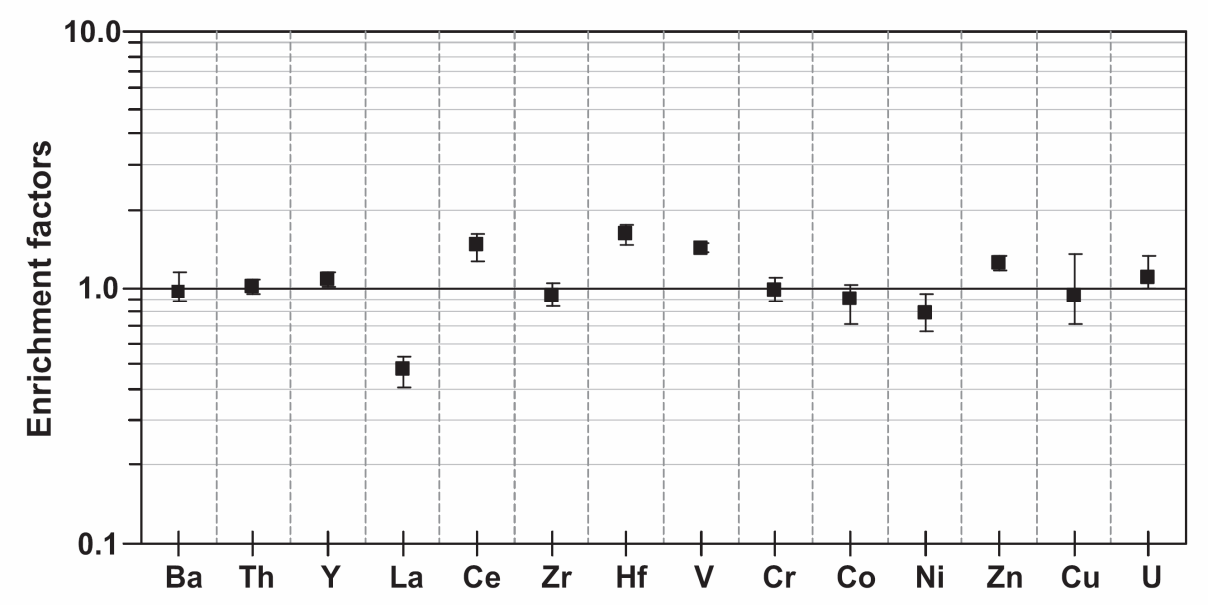

Fig. S-2.3. Comparisons of the enrichment factor of selected trace metals of core MD02-2553 (Pigmy Basin). The extent line of the boxes corresponds to the range of values (min-max) and the boxes to the average value. The horizontal line EF = 1 indicates the value for which there is no enrichment/depletion with regards to average shale composition.

References

Aharon, P., 2003. Meltwater flooding events in the Gulf of Mexico revisited: Implications for rapid climate changes during the last deglaciation. Paleoceanography 18(4), PA1079. doi: 10.1029/2002PA000840.

Alley, R.B., Mayewski, P.A., Sowers, T., Stuiver, M., Taylor, K.C., Clark, P.U., 1997. Holocene climatic instability: A prominent, widespread event 8200 yr ago, Geology 25, 483-486.

Bettis, E.A., Benn, D.W., Hajic, E.R., 2008. Landscape evolution, alluvial architecture, environmental history, and the archaeological record of the Upper Mississippi River Valley. Geomorphology 101, 362-377.

Blackman, R.B., Tukey, J.W., 1958. The measurement of power spectra from the point of view of communication engineering. Dover Publications, 190 pp.

Bond, G., Kromer, B., Beer, J., Muscheler, R., Evans, M., Showers, W., Hoffmann, S., Lotti-Bond, R., Hajdas, I., Bonani, G., 2001. Persistent solar influence on North Atlantic climate during the Holocene. Science 294, 2130-2136.

Bout-Roumazeilles, V., Cortijo, E., Labeyrie, L., Debrabant, P., 1999. Clay-mineral evidence of nepheloid layer contribution to the Heinrich layers in the Northwest Atlantic. Palaeogeography, Palaeoclimatology, Palaeoceanography 146, 211-228.

Brown, P., Kennett, J.P., Ingram, B.L., 1999. Marine Evidence for Episodic Holocene Megafloods in North America and the Northern Gulf of Mexico. Paleoceanography, 14(4), 498-510.

Debret, M., Bout-Roumazeilles, V., Grousset, F.E., Desmet, M., McManus, J.F., Massei, M., Sebag, D., Petit, J.R., Copard, Y., Trenteseaux, A., 2007. The origin of the 1500-year climate cycles in Holocene North-Atlantic records. Climate of the Past 3, 569-575.

Debret, M., Sebag, D., Crosta, X., Massei, N., Petit, J.-R., Chapron, E., Bout-Roumazeilles, V., in press. Evidence from wavelet analysis for a mid-Holocene transition in global climate forcing. Quaternary Science Reviews.

Disnar, J-R., Jacob, J., Morched-Issa, M., Lottier, N. and Arnaud, F., 2008. Assessment of peat quality by molecular and bulk geochemical analysis: Application to the Holocene record of the Chautagne marsh (Haute Savoie, France). Chemical Geology 254, 101-112.

Elderfield, H., Upstill-Goddard, R., Sholkovitz, ER., 1990. The rare earth elements in rivers, estuaries and coastal seas and their significance to the composition of ocean water. Geochimica et Cosmochimica Acta 54, 971-991.

Espitalié, J., Deroo, G., and Marquis, F., 1986. La pyrolyse Rock Eval et ses applications. Revue de l'Institut Français du Pétrole 40(B), 755-784.

Forman, S.L., Oglesby, R., Markgraf, V., Stafford, T., 1995. Paleoclimatic significance of late Quaternary eolian deposition on the Piedmont and High Plains, central United States. Global and Planetary Change 11, 35-55.

Flannery, J.A., Richey, J.N., Meckler, A.N., Hollander, D.J., 2008. A 1400 Year Multi-Proxy Record of Hydrologic Variability in the Gulf of Mexico: Exploring Ocean-Continent Linkages During the Late Holocene. Poster Presentation, 2008 ASLO Ocean Sciences Meeting. online at: http://www.marine.usf.edu/PPBlaboratory/pages_students/flannery (Revised 2009-04-01)

Flower, B.P., Hastings, D.W., Hill, H.W., Quinn, T.M., 2004. Phasing of deglacial warming and laurentide ice sheet meltwater in the Gulf of Mexico. Geology 32, 597-600.

Flocks, J., Swarzenski, P., 2007. Sediment collection from Orca and Pigmy Basins, Gulf of Mexico, and analyses for texture and trace-metal concentrations, July 2002, PAGE 127 Campaign. In: Winters, W.J., Lorenson, T.D., Paull, C.K. (Eds.), Initial Report of the IMAGES VIII/PAGE 127 Gas Hydrate and Paleoclimate Cruise on the RV Marion Dufresne in the Gulf of Mexico, 2–18 July 2002: U.S. Geological Survey Open-File Report 2004-1358, one DVD. online at http://pubs.usgs.gov/of/2004/1358/.

Ghil, M., Allen, M.R., Dettinger, M.D., Ide, K., Kondrashov, D., Mann, M.E., Robertson, A.W., Saunders, A., Tian, Y., Varadi, F., Yiou, P., 2002. Advanced spectral methods for climatic time series. Reviews of Geophysics 40, 1003, doi:10.1029/2000RG000092.

Goman, M., Leigh, D.S., 2004. Wet early to middle Holocene conditions on the upper coastal plain of North Carolina. Quaternary Research 61, 256-264.

Goldstein, S.J., Jacobsen, S.B., 1988. Rare earth elements in river waters. Earth and Planetary Science Letters 89, 35-47.

Grimm, E.C., Watts, W.A., Jacobson Jr., G.L., Hansen, B.C.S., Almquist, H.R., Dieffenbacher-Krall, A.C., 2006. Evidence for warm wet Heinrich events in Florida, Quaternary Science Reviews 25, 2197-2211.

Gromet, L.P., Dymek, R.F., Haskin, L.A., Korotev, R.L., 1984. The North American shale composite: its compilation, major and trace element characteristics. Geochimica et Cosmochimica Acta 48, 2469–3482.

Grossman, J., 2009. National Geochemical Atlas: The geochemical landscape of the conterminous United States derived from stream sediment and other solid sample media analyzed by the National Uranium Resource Evaluation (NURE) program. U.S. Geological Survey Open-File Report 98-622.
Online at http://tin.er.usgs.gov/geochem/about.php?group=Analyses+by+ICP%2FAcid+dissolution
(Revised 2009-04-01)

Gustavsson, N., Bølviken, B., Smith, D.B., Severson, R.C., 2001. Geochemical landscapes of the conterminous United States - New map presentations for 22 elements. U.S. Geol. Survey Prof. Paper, 1648. U.S. Department of the Interior.

Haug, G.H., Hughen, K.A., Sigman, D.M., Peterson, L.C., Roehl, U., 2001. Southward migration of the intertropical convergence zone through the Holocene. Science 293, 1304-1308.

Harrison, S.P., Kutzbach, J.E., Liu, Z., Bartlein, P. J., Otto-Bliesner, B., Muhs, D.,Prentice, I. C., and Thompson, R. S. (2003). Mid-Holocene climates of the Americas: a dynamical response to changed seasonality. Climate Dynamics 20, 663-688.

Hodell, D.A., Curtis, J.H., Jones, G.A., Higuera-Gundy, A., Brenner, M., Binford, M.B., Dorsey, K.T., 1991. Reconstruction of the Caribbean climate change over the past 10,500 years. Nature 352, 790-793.

Hughen, K.A., Baillie, M.G.L., Bard, E., Beck, J.W., Bertrand, C.J.H., Blackwell, P.G., Buck, C.E., Burr, G.S., Cutler, K.B., Damon, P.E., Edwards, R.L., Fairbanks, R.G., Friedrich, M., Guilderson, T.P., Kromer, B., McCormac, G., Manning, S., Ramsey, C.B., Reimer, P.J., Reimer, R.W., Remmele, S., Southon, J.R., Stuiver, M., Talamo, S., Taylor, F.W., van der Plicht, J.,Weyhenmeyer, C.E., 2004. Marine04 marine radiocarbon age calibration, 0–26 cal kyr BP. Radiocarbon 46, 1059-1086.

Jasper, J.P., Gagosian, R.B., 1990. The sources and deposition of organic-matter in the Late Quaternary Pigmy Basin, Gulf of Mexico. Geochimica et Cosmochimica Acta 54, 1117-1132.

Kennedy, L.M., Horn, S.P., Orvis, K.H., 2006. A 4000-yr record of fire and forest history from Valle de Bao, Cordillera Central, Dominican Republic. Palaeogeography, Palaeoclimatology, and Palaeoecology 231, 271-290.

Knox, J.C., 2000. Sensitivity of Modern and Holocene floods to climate change. Quaternary Science Reviews 19, 439- 457.

Knox, J.C., 2003. North American palaeofloods and future floods: Responses to climate change. In: K.J. Gregory and G. Benito, Editors, Palaeohydrology: Understanding Global Change, J. Wiley and Sons, Chichester (2003), pp. 143-164.

Lawrence, M.G., Greig, A., Collerson, K.D., Kamber, B.S., 2006. Rare earth element and yttrium variability in South East Queensland waterways. Aquatic Geochemistry 12, 39-72.

Li, Y.X., Yu, Z., Kodama, K.P., 2007. Sensitive moisture response to Holocene millennial-scale climate variations in the Mid-Atlantic region, USA. The Holocene 17, 3-8.

Liu, K.B., Fearn, M., 2000. Reconstruction of prehistoric landfall frequencies of catastrophic hurricanes in Northwestern Florida from lake sediment records. Quaternary Research 54, 238-245.

LoDico, J.M., Flower, B.P., and Quinn, T.M., 2006. Subcentennial-scale climatic and hydrologic variability in the Gulf of Mexico during the early Holocene. Paleoceanography 21, PA3015, doi: 10.1029/2005PA001243.

Lovvorn, M.B., Frison, G.C., Tieszen, L.L., 2001. Paleoclimate and Amerindians: evidence from stable isotopes and atmospheric circulation. Proceedings of the National Academy of Sciences 98, 2485-2490.

Mayewski, P.A., Rohling, E.E., Stager, J.C., Karlen,W., Maasch, K.A., Meeker, L.D.,Meyerson, E.A., Gasse, F., vanKreveld, S.,Holmgren, K., Lee-Thorp, J., Rosqvist, G., Rack, F., Staubwasser, M., Schneider, R.R., Steig, E.J., 2004. Holocene climate variability. Quaternary Research 62, 243-255.

Meckler, A.N., 2006. Late Quaternary changes in nitrogen fixation and climate variability recorded by sediments from the Gulf of Mexico and the Caribbean Sea. PhD Thesis ETH Zürich N° 16811, 156 p. online at http://www.up.ethz.ch/people/former/nmeckler/PhD_Meckler.pdf (Revised 2009-04-01)

Meckler, A.N., C.J. Schubert, P.A. Hochuli, B. Plessen, D. Birgel, B.P. Flower, K.-U. Hinrichs, and Haug, G.H., 2008. Glacial to Holocene terrigenous organic matter input to sediments from Orca Basin, Gulf of Mexico- a combined optical and biomarker approach. Earth and Planetary Science Letters 272, 251-263.

Meyers, P.A., 1997. Organic geochemical proxies of paleoceanographic, paleolimnologic and paleoclimatic processes. Organic Geochemistry 27, 213-250.

Montero-Serrano, J.C., Bout-Roumazeilles, V., Tribovillard, Sionneau, T., Bory, A., Riboulleau, A., Flower, B., in press. Sedimentary evidence of deglacial megafloods in the northern Gulf of Mexico (Pigmy Basin). Quaternary Science Reviews.

Mueller, A.D., Islebe, G.A., Hillesheim, M.B., Grzesik, D.A., Anselmetti, F.S., Ariztegui, D., Brenner, M., Curtis, J.H., Hodell, D.A., Venz, K.A., 2009. Climate drying and associated forest decline in the lowlands of northern Guatemala during the late Holocene. Quaternary Research 71, 133-141.

Newby, P.E., Killoran, P., Waldorf, M.R., Shuman, B.N., Webb, R.S., Webb, T. III., 2000. 14,000 years of sediment, vegetation, and water-level changes at the Makepeace Cedar Swamp, southeastern Massachusetts. Quaternary Research 53, 352-68.

Nordt, L., Von Fischer, J., Tieszen, L., Tubbs, J., 2008. Coherent changes in relative C4 plant productivity and climate during the late Quaternary in the North American Great Plains. Quaternary Science Reviews 27, 1600-1611.

Nürnberg, D., Ziegler, M., Karas, C., Tiedemann, R., Schmidt M.W., 2008. Interacting Loop Current variability and Mississippi River discharge over the past 400 kyr. Earth and Planetary Science Letters 272, 278-289.

O'Brien, S.R., Mayewski, P.A., Meeker, L.D., Meese, D.A., Twickler, M.S., Whitlow, S.I., 1995. Complexity of Holocene climate as reconstructed from a Greenland ice core. Science 270, 1962-1964.

Paillard, D., Labeyrie, L., Yiou, P., 1996. Macintosh program performs time-series analysis, AGU Eos Transactions 77, p. 379.

Perry, C.A., Hsu, K.J., 2000. Geophysical, archaeological, and historical evidence support a solar-output model for climate change. Proceedings of the National Academy of Sciences 97, 12433-12438.

Petschick, R. 2000. MacDiff 4.2 Manual. MacDiff [Online]. Available from World Wide Web: http://www.geologie.uni-frankfurt.de/Staff/Homepages/Petschick/RainerE.html (Revised 2009-04-01)

Poore, R.Z., Quinn, T.M., Verardo, S., 2004. Century-scale movement of the Atlantic Intertropical Convergence Zone linked to solar variability. Geophysical Research Letters 31, L12214, doi: 10.1029/2004GL019940.

Poore, R.Z., Verardo, S., Caplan, J., Pavich, K., Quinn, T., in press. Planktic foraminiferal relative abundance trends in the Gulf of Mexico Holocene sediments: Records of climate variability. In Holmes, C., (Ed.), Gulf of Mexico, its origins, waters, biota, and human impacts. Univ Texas Press.

Richey, J.N., Poore, R.Z., Flower, B.P., Quinn, T.M., 2007. 1400 yr multiproxy record of climate variability from the northern Gulf of Mexico. Geology 35, 423-426.

Sionneau, T., 2008. Transferts Continent – Océan : Enregistrement du dernier cycle climatique par les sédiments terrigènes du Golfe du Mexique. PhD thesis, Université Lille 1. 377 p. online at http://tel.archives-ouvertes.fr/tel-00366377/fr/

Sionneau, T., Bout-Roumazeilles, V., Biscaye, P.E., van Vliet-Lanoë, B., Bory, A., 2008. Clay-mineral distributions in and around Mississippi River watershed and Northern Gulf of Mexico: Sources and transport patterns. Quaternary Science Reviews 27, 1740-1751.

Sionneau, T., Bout-Roumazeilles, V., Flower, B.P., Bory, A., Tribovillard, N., Kissel, C., Van Vliet-Lanoë, B., Montero-Serrano, J.C., in revision. On the provenance of freshwater pulses in the Gulf of Mexico during the last deglaciation: Evidence from grain size and clay mineralogy. Quaternary Research.

Shuman, B., Bartlein, P., Logar, N., Newby, P., Webb III, T., 2002. Parallel climate and vegetation responses to the early-Holocene collapse of the Laurentide Ice Sheet. Quaternary Science Reviews 21, 1793-1805.

Shuman, B., Bartlein, P., Webb III, T., 2005. The magnitudes of millennial- and orbital-scale climatic change in eastern North America during the Late Quaternary. Quaternary Science Reviews 24, 2194-2206.

Springer, G.S., Rowe, H.D., Hardt, B., Edwards, R.L., Cheng, H., 2008. Solar forcing of Holocene droughts in a stalagmite record from West Virginia in east-central North America. Geophysical Research Letters 35, L17703, doi:10.1029/2008GL034971.

Stuiver, M., Reimer, P.J., 1993. Extended ^{14}C data-base and revised calib 3.0 ^{14}C age calibration program. Radiocarbon 35, 215-230.

Stuiver, M., Grootes, P.M., Braziunas, T.F., 1995. The GISP2 $\delta^{18}O$ climate record of the past 16,500 years and the role of the sun, ocean, and volcanoes. Quaternary Research 44, 341-354.

Thompson, D.J., 1982. Spectrum estimation and harmonic analysis. Proc. IEEE 70, 1055-1098.

Tribovillard, N., Algeo, T., Lyons, T.W., Riboulleau, A., 2006. Trace metals as paleoredox and paleoproductivity proxies: an update. Chemical Geology 232, 12-32.

Tribovillard, N., Bout-Roumazeilles, V., Algeo, T.J., Lyons, T., Sionneau, T., Montero-Serrano, J.C., Riboulleau, A., Baudin, F., 2008. Paleodepositional conditions in the Orca Basin as inferred from organic matter and trace metal contents. Marine Geology 254, 62-72.

Tribovillard, N., Bout-Roumazeilles, V., Sionneau, T., Montero-Serrano, J.C., Riboulleau, A., Baudin, F., 2009. Does a strong pycnocline impact organic-matter preservation and accumulation in an anoxic setting? The case of the Orca Basin, Gulf of Mexico. Comptes Rendus Geosciences 341, 1-9.

Tripsanas, E.K., Bryant, W.R., Slowey, N.C., Bouma, A.H., Karageorgis, A.P., Berti, D., 2007. Sedimentological history of Bryant Canyon area, northwest Gulf of Mexico, during the last 135 kyr (Marine Isotope Stages 1-6): A proxy record of Mississippi River discharge. Palaeogeography Palaeoclimatology Palaeoecology, 246, 137-161.

van der Weijden, C.H., 2002. Pitfalls of normalization of marine geochemical data using a common divisor. Marine Geology 184, 167-187.

Wang, C., Enfield, D.B., 2001. The tropical Western Hemisphere warm pool. Geophysical Research Letters 28, 1635-1638.

Wedepohl, K.H., 1971. Environmental influences on the chemical composition of shales and clays. In: Ahrens, L.H., Press, F., Runcorn, S.K., Urey, H.C. (Eds.), Physics and Chemistry of the Earth. Pergamon, Oxford, pp. 305-333.

Wedepohl, K.H., 1991. The composition of the upper Earth's crust and the natural cycles of selected metals. In: Merian, E. (Ed.), Metals and Their Compounds in the Environment. VCH-Verlagsgesellschaft, Weinheim, pp. 3-17.

Willard, D.A., Bernhardt, C.E., Korejwo, D.A., Meyers, S.R., 2005. Impact of millennial-scale Holocene climate variability on eastern North American terrestrial ecosystems: pollen-based climatic reconstruction. Global and Planetary Change 47, 17-35.

Ziegler M., Nürnberg D., Karas C., Tiedemann R., Lourens L.J., 2008. Persistent summer expansion of the Atlantic Warm Pool during glacial abrupt cold events. Nature Geoscience 1(9), 601-605.

Chapter 3

The La Salle Basin: core MD02-2549

3.1. The La Salle Basin – geological setting

The La Salle Basin is a mini-basin part of the Louisiana Slope (Fig. 1.5 and Fig. 3.1). The slope extends from the shelf break to the Sigsbee escarpment with depths ranging from 200 to 3400 m. As mentioned before the basin formation resulted from the movement of the salt sheet under the overburden pressures of the overlying sediment load (Bryant et al., 1990, 1991). Sedimentological processes will be partly controlled by changing slope morphology according to the importance of halokinetic processes in the area. The initial Bryant Canyon gives birth to a series of intraslope basins among which the La Salle, Beaumont and Calcasieu basins. Some processes as sediment failures on the delta front or hyperpynal plumes (Mulder et al., 2003) provoked numerous gravity flows. The canyon is thought to have stopped its activity at the beginning of the last interglacial period as sea-level was rising and sediment being trapped on the continental shelf.

La Salle Basin together with the Calcasieu and Beaumont basins (Fig. 3.1) is one of the basins characterizing the Bryant Canyon area. Seismic investigation of the area evidence that some of these basins are characterized by high slope angle (up to 25°) leading to instabilities and frequent debris-flow or turbidites (as the Calcasieu Basin) whereas La Salle Basin slope angle is low (<0.5°) suggesting lower instability (Silva et al., 2004; Baxter et al., 2003; Tripsanas et al. 2003). Quantitative estimations of such slope instabilities were evaluated in the area. The failures may covered rather huge areas (1.3 to 9.4 km^2) and involve up to 16 km^3 of sediment (Silva et al., 2004; Boll, 2001).

The coring site was prospected using the 3.5 kHz between point 1 (26°22N, 092°33) and point 2 (26°25N, 092°34) at 5 knots speed (Fig. 3.2). The Calypso coring system was used in order to recover a long core covering the complete last climatic cycle. The coring site was located at 26°25.68N and 92°33.94°W at 2049 meters water depth (Fig. 3.2).

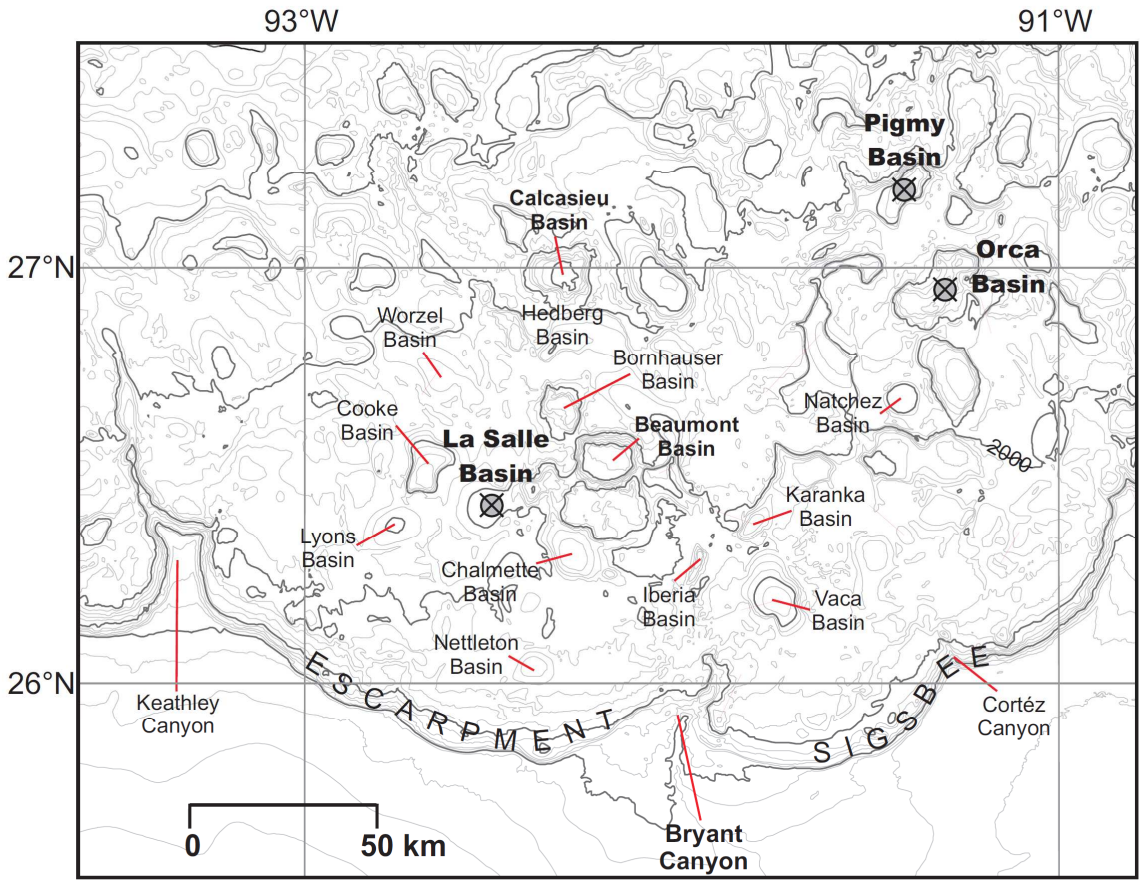

Fig. 3.1. Bathymetric map of the Bryant Canyon area showing the locations of the some mini-basin in the northwest Gulf of Mexico. Contours in meter. Grey circle represent the locations of the cores studied in this dissertation.

The profile evidences the alternations of parallel and semi-transparent seismic reflectors. All reflectors appear to be related to coarser material. One reflector situated circa 15 mbsf suggests a major change in sedimentation. The characteristics of the underlying sediments suggest the occurrence of a massive debris-flow.

The core length is 37,81m for a corer length of 44.80 m. The section IX (1350 to 1500 meters) was not opened because sediment was under-consolidated. This section was lost during the transfer from the ship to the Laboratoire des Sciences du Climat et l'Environnement (LSCE, Gif-sur-Yvette, France) storage.

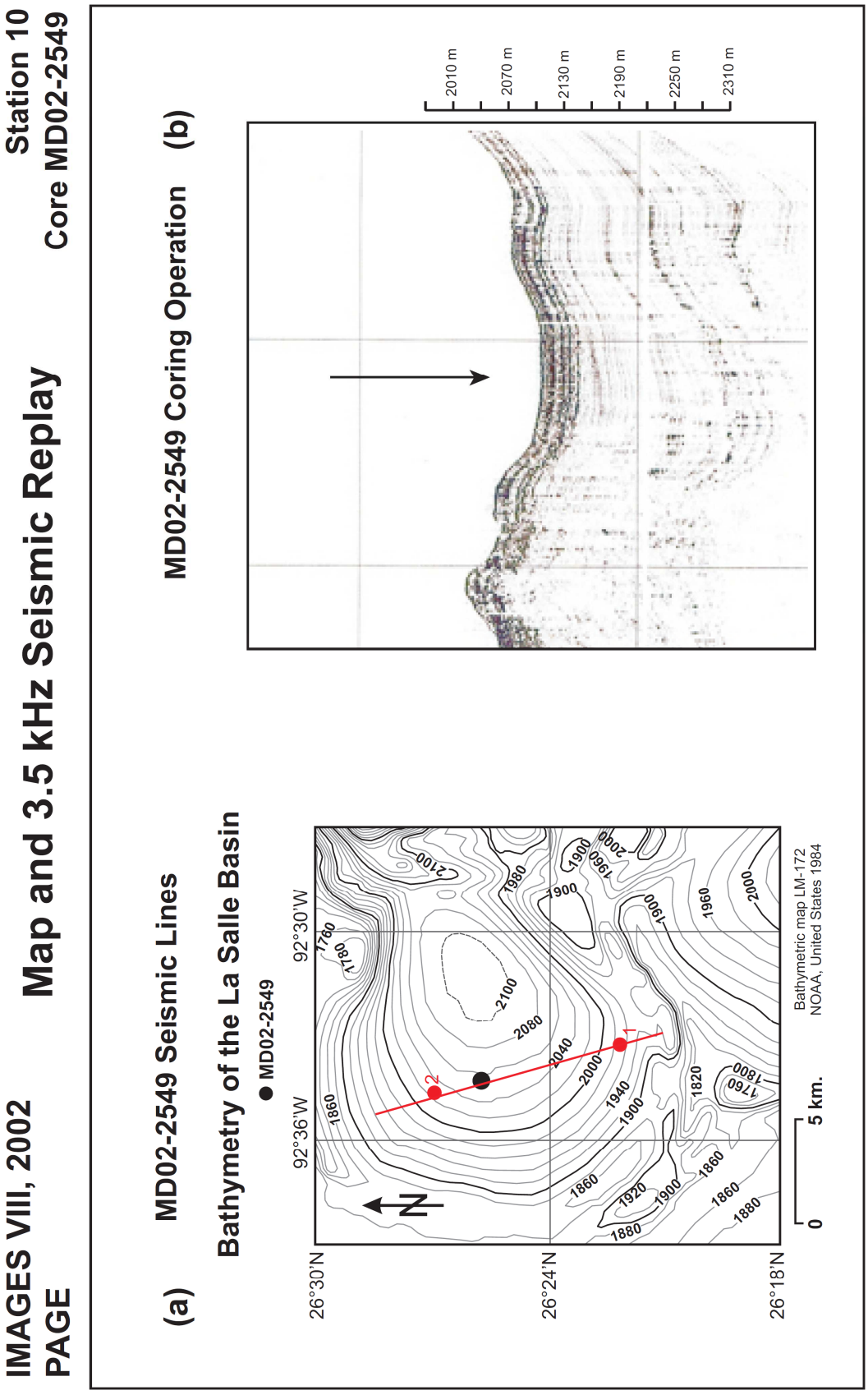

Fig. 3.2. (**a**) Bathymetric map of the La Salle Basin showing location of sediment core MD02-2549, contours in meters. (**b**) Example of 3.5 kHz profile to the main axis of the La Salle Basin.

3.2. Material and sampling

The physical properties were measured using the multisensor core logger (sediment thickness, density, magnetic susceptibility, impedance and fractional porosity) and discrete colour reflectance data were measured with a 2 cm sampling interval.

3.2.1. Physical properties

The uppermost part of the core (0-300 cm) is characterized by high velocity (m/s) (figure m) and low sediment thickness (cm). The magnetic susceptibility (MS) is higher between 400 and 1000 cm (Fig. 3.3). The variations of MS depend on the concentration and on the characteristics of the magnetic minerals contained in the sediments. This result suggests either a higher concentration in magnetic mineral or coarser magnetic particles. The MS displays high amplitude variations between 2200 cm and the base of the core. These high amplitude high frequency variations are not associated with hemipelagic sedimentation and strongly suggest debris flow deposition over the interval. This observation is confirmed by the impedance and fractional porosity evidencing peculiar sedimentary processes below 1500 cm (Fig. 3.3).

The colour reflectivity is in good agreement with physical properties (Fig. 3.4). All parameters (L*, a*, and b*) display a clear modification in sedimentation at 1600 cm. Below 1600 cm, there are very little variations of all parameters whereas the upper part of the core displays classical glacial-interglacial variations. This result is in agreement with the hypothesis of turbiditic deposits below 1600 cm evidenced by seismic observation and physical properties. The uppermost part is characterized by light-coloured, brownish grey sediments that generally characterized the Holocene sedimentation in the GOM. A peculiar interval (high a* and b* parameters and low L*) is situated around 250 cm (Fig. 3.4). The L* parameter shows a light coloured interval from 1100 cm to 1600 cm attributed to the last interglacial period. The a* channel exhibits a strong signal between 500 and 1100 m which is not observed in the L* signal.

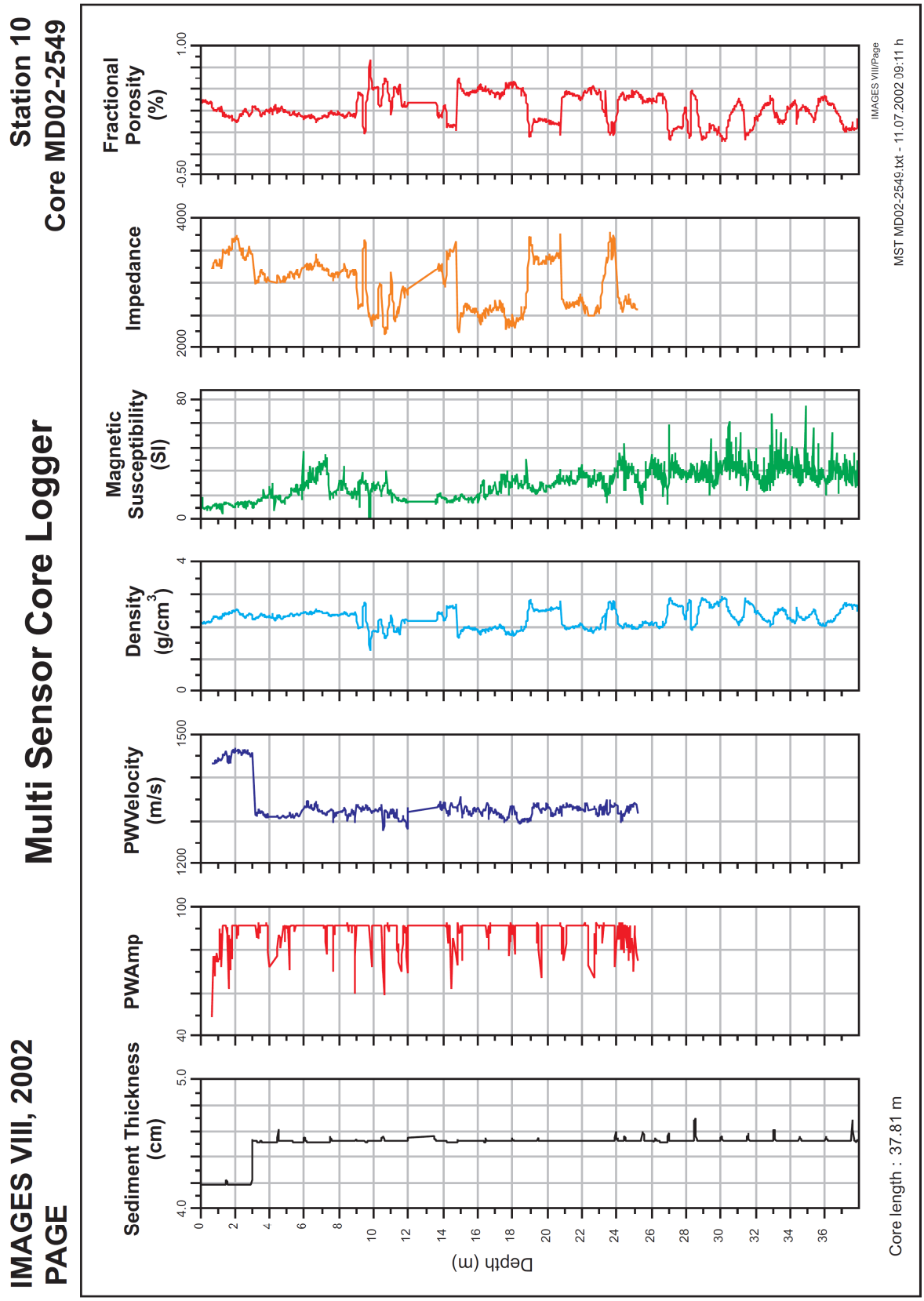

Fig. 3.3. Physical properties measured onboard from the sediment core MD02-2549 (La Salle Basin)

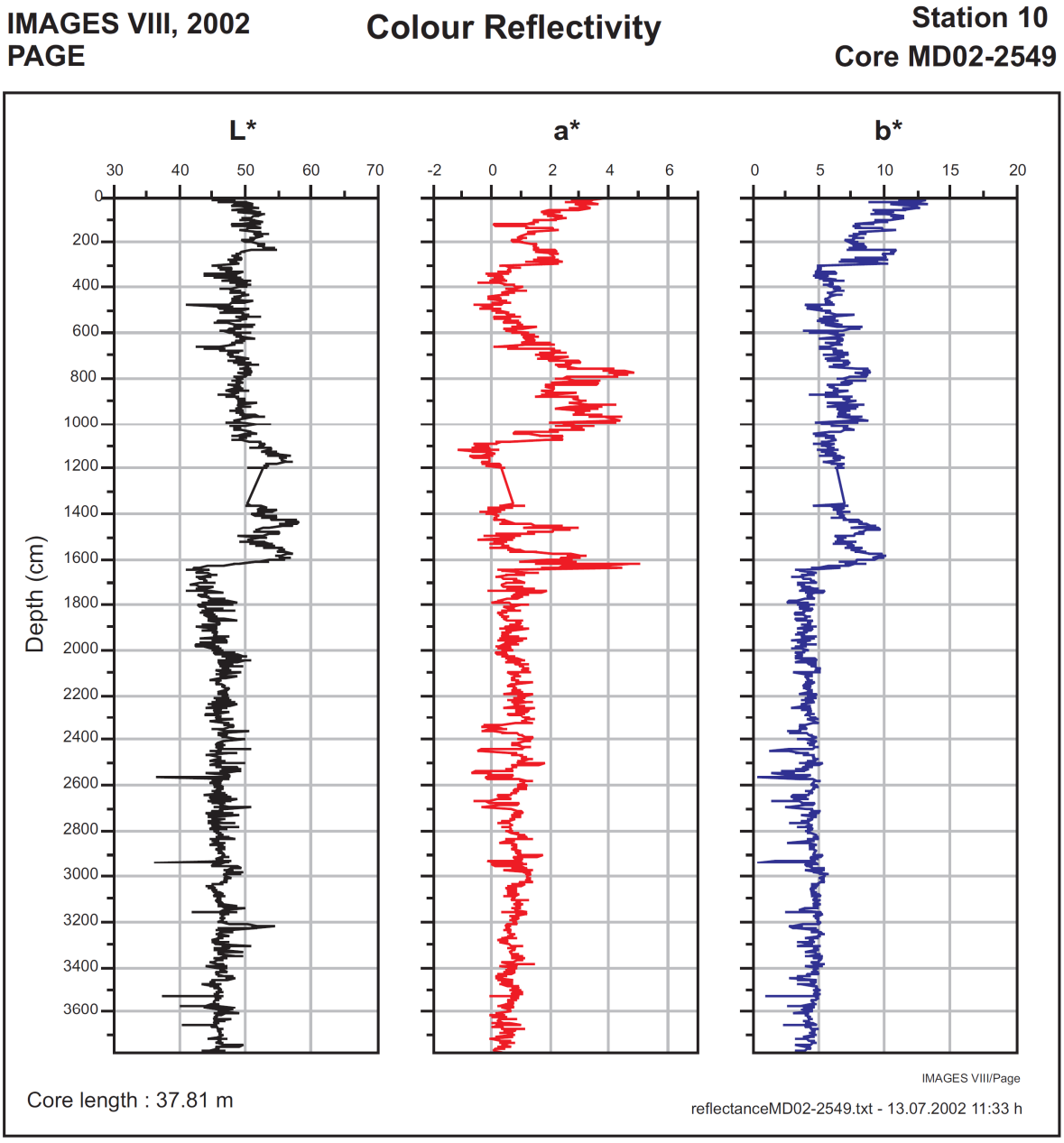

Fig. 3.4. Color reflectance parameters measured onboard from the core MD02-2549 (La Salle Basin). The L* denote lightness or luminance variation, a* denote red/green variation, and b* denote blue/yellow variation.

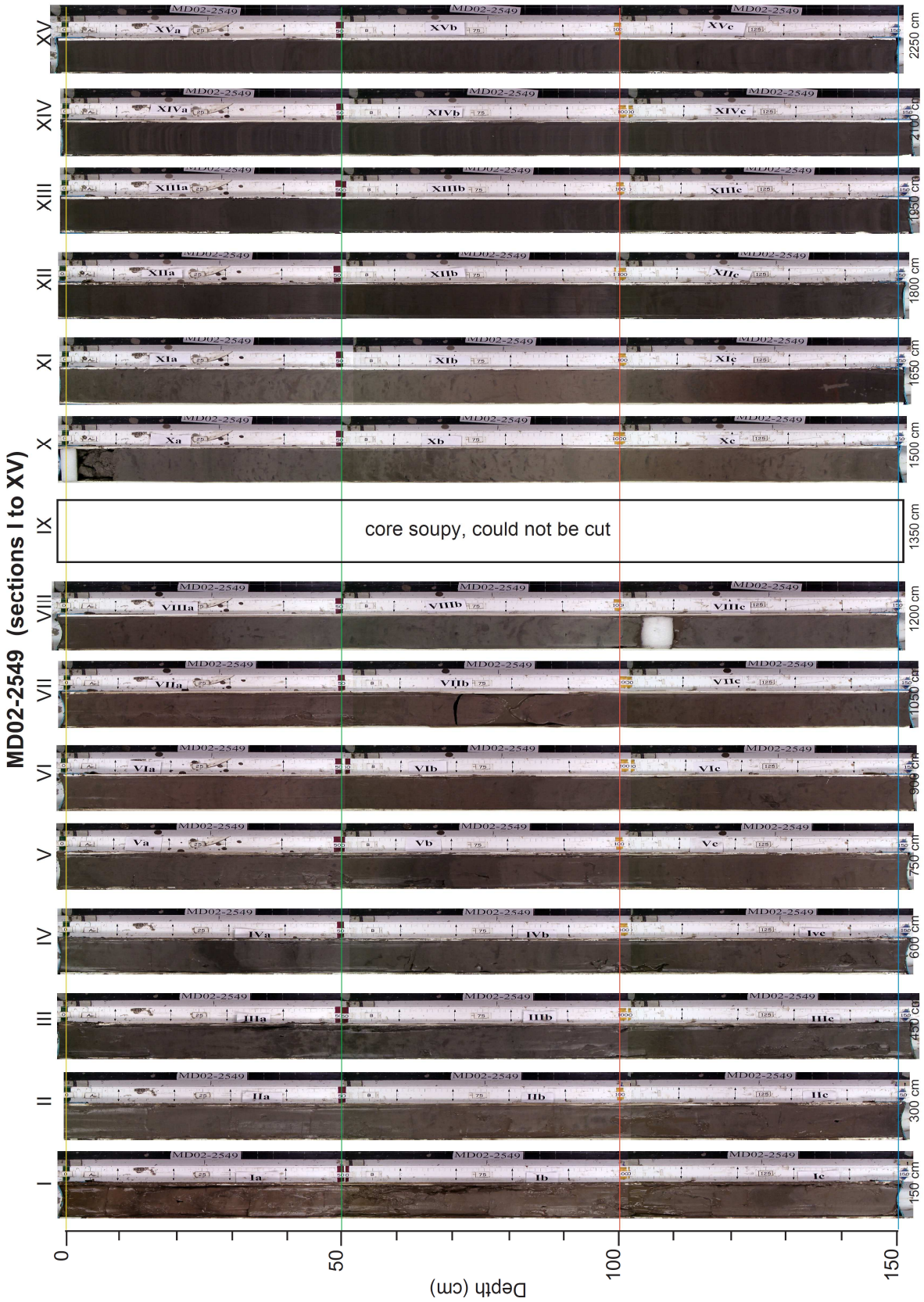

Fig. 3.5. Photomosaic of the core MD02-2549 (La Salle Basin). Brightness differences and contrasting angles in laminations are due to camera angle and lighting.

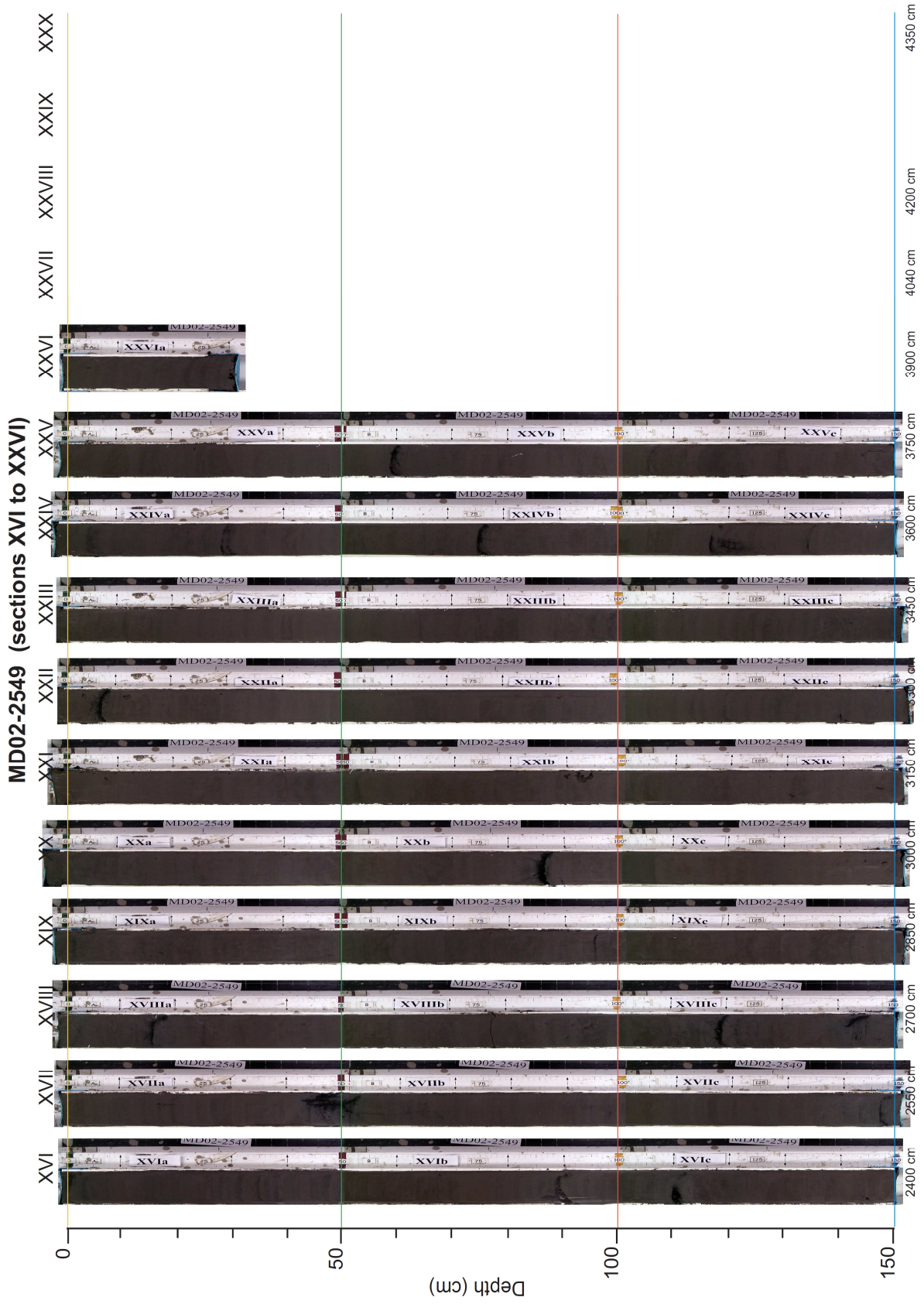

Fig. 3.5. (continued)

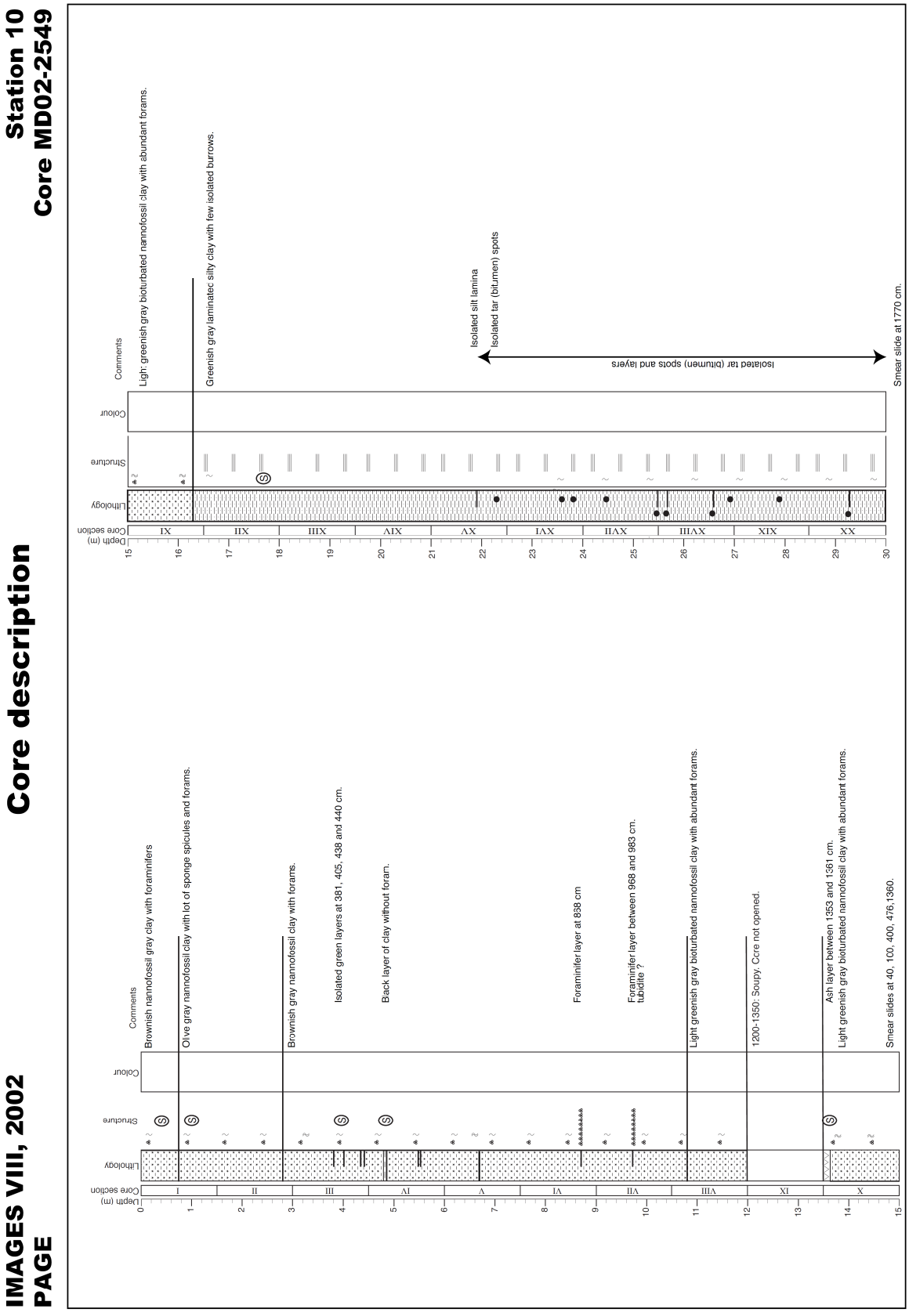

Fig. 3.6. Sedimentological descriptions from the core MD02-2549 (La Salle Basin).

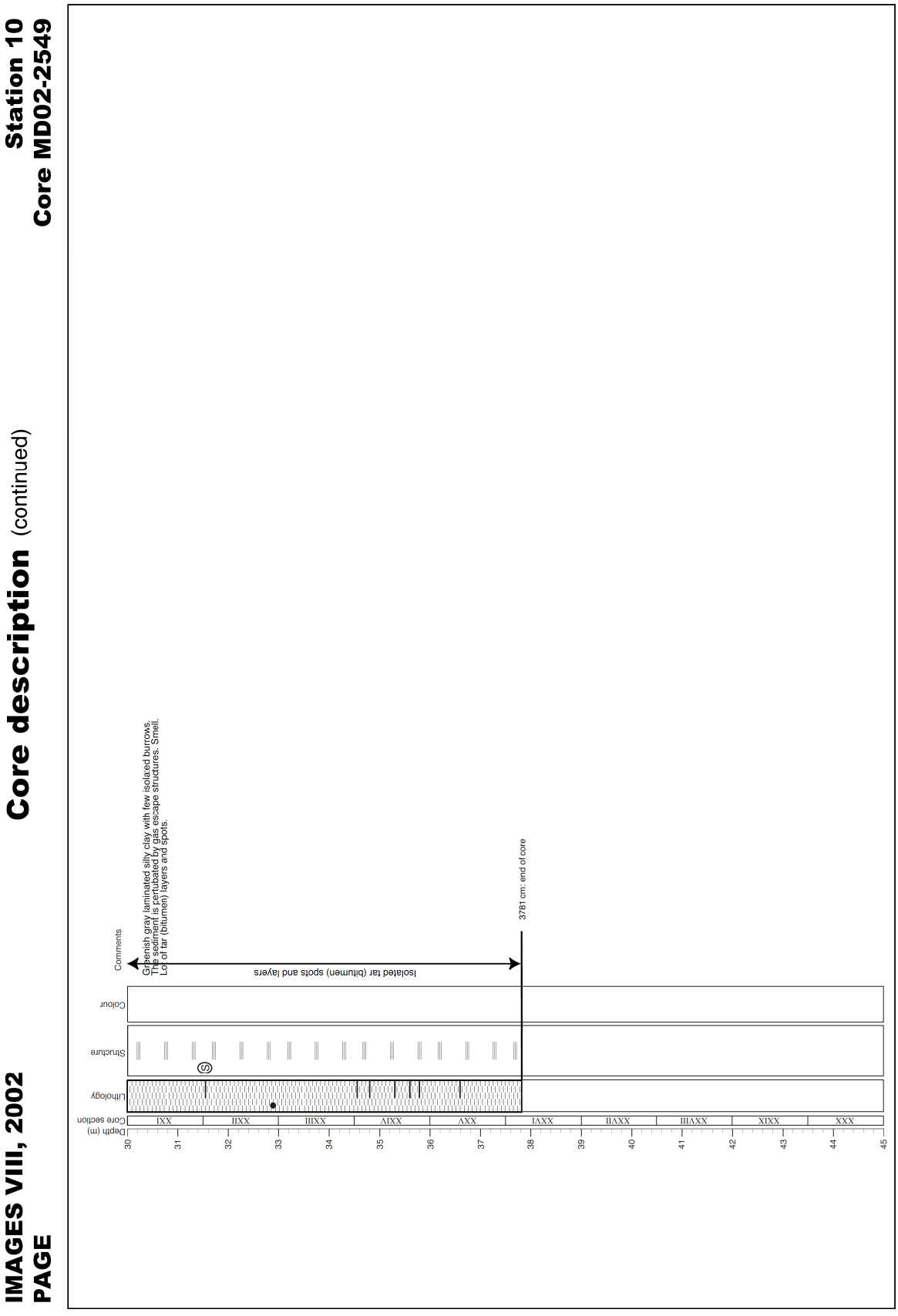

Fig. 3.6. (Continued)

3.2.2. Sedimentological description

The sediment displays two dominant lithologies, with bioturbated brownish, olive or light-greenish grey nannofossil clay with foraminifera between 0 and 1629 cm (Fig. 3.5 and Fig. 3.6) and not bioturbated dark -greenish grey and laminated silt to silty-clay below 1629 cm. The lower part of the core display several isolated tar bitumen. The 1353 to 1629 cm interval is characterized by light-greenish grey clay with abundant foraminifera. It is noteworthy to mention that sedimentation is clearly similar on both side of the missing section. A major ash layer is observed between 1353 and 1361 cm. It could correspond to the Y8 ash layer which is commonly observed in the GOM (Drexler et al., 1980). Some foraminifera-rich intervals occur at 868, 968 and 983 cm. There are interpreted as small turbidites. Some isolated green layers have been described at 381, 405, 438, 440 cm. Reddish coloured layers are frequent between 959 and 1034 cm. Organic matter seems to be more abundant between 0 and 50 cm, 250 and 260 cm, 600-605 cm, 660 and 669 cm, 850-860 cm (Fig. 3.6).

The base of the Holocene was constrained using biostratigraphic indicators (Kennett and Huddlestun, 1972; Beard, 1973). The uppermost part of the core contains abundant *Globorotalia menardii* (warm intervals), decreasing downward and coincident with the last appearance of *Globorotalia inflata* (glacials).

In core MD02-2549, distinct features may be observed and help to reconstruct the stratigraphic frame. The Holocene drape is easily recognized on the density record and MS records (Fig. 3.3), as well as the last glacial inception. The position of the Laschamp excursion helps to constrain MIS 3. The occurrence of the Y8 ash layer dated at 84 ka (Drexler et al., 1980) constrained the limit of MIS 5a (Fig. 3.6).

3.3. Results

3.3.1. Chronostratigraphy

The chronostratigraphy of core MD02-2549 (Table 3.1; Fig. 3.7) is based on the tuning of the calcium carbonate content ($CaCO_3$) and spectral lightness (L*) distribution to the global benthic reference stack LR04 (Lisiecki and Raymo, 2005). The $CaCO_3$ and lightness L* distributions exhibit glacial/interglacial variability in close correspondence with the global benthic reference stack LR04. It is clearly shown from these distributions that the sedimentary record is tightly related to Marine Isotope Stage (MIS) 1-6 (Fig. 3.7). This is

confirmed by (1) the Y-8 ash layer dated at 84 ka (Drexler et al., 1980), (2) the comparison of $\delta^{18}O$ profiles of planktonic foraminifera (*Globogerinoides ruber*) with the nearby core JPC-31 (Bryant Cayon; Tripsanas et al., 2007), and (3) the comparison between the magnetic susceptibility profiles of the cores MD02-2549 and MD02-2575 (DeSoto Cayon; Nürnberg et al., 2008).

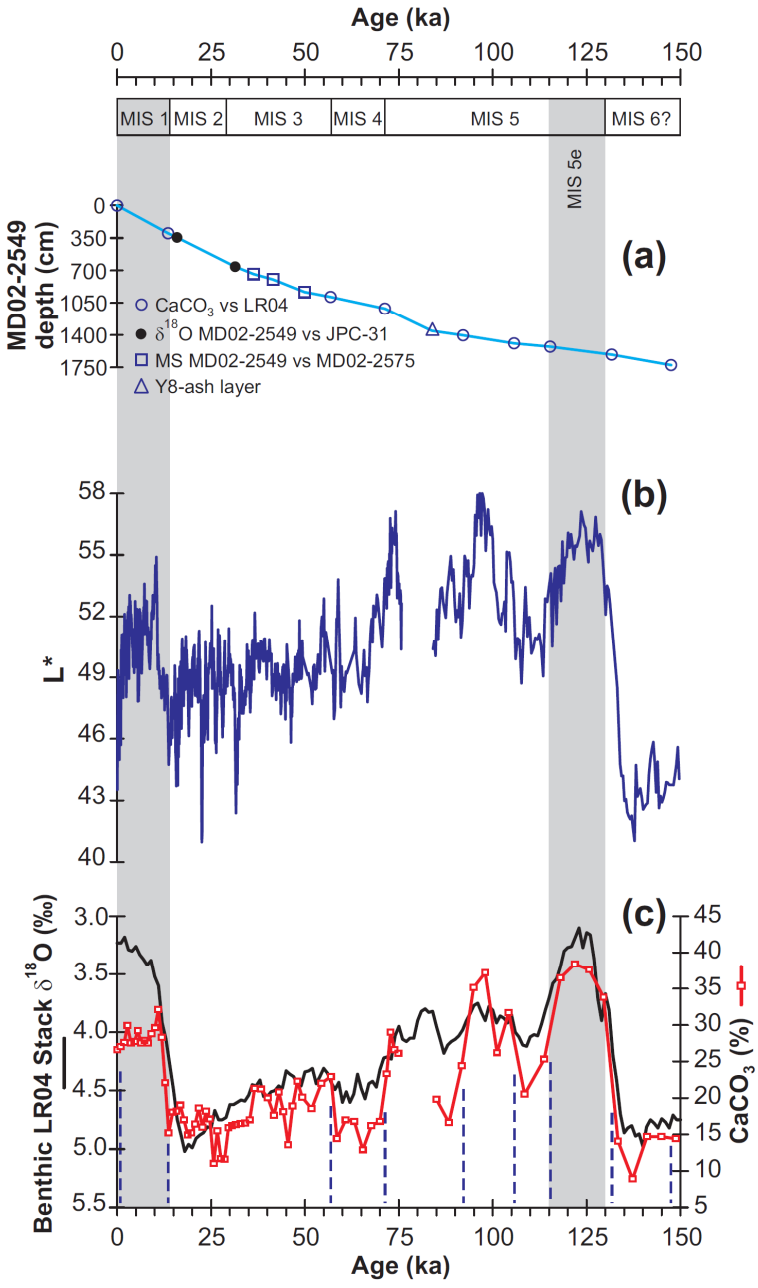

Fig. 3.8. Chronostratigraphy of core MD02-2549 from La Salle Basin. (**a**) The Age-depth relationship suggests continuous and uniform sedimentation over the past 150 ka (see Table 3.1). (**b**) Spectral lightness (L*) distribution from the core MD02-2549. Note the similarity of lightness L* with the carbonate distribution in (**c**). (**c**) Tuning of the calcium carbonate ($CaCO_3$) distribution to the global benthic reference stack LR04 (Lisiecki and Raymo, 2005) (dotted blue lines) used for the chronostratigraphy.

Table 3.1. Age-depth points for core MD02-2549 used to derive chronology shown in Fig. 3.7.

Depth of control points (cm)	Age (ka)	Sedimentation rates (cm/ka)
0.0	0.0	
299.1	13.6	22.0
344.4	16.0	19.0
659.0	31.5	20.3
738.6	36.4	16.3
797.1	41.6	11.3
932.5	50.0	16.1
986.5	56.9	7.8
1112.6	71.3	8.7
1354.4	83.9	19.3
1403.6	92.2	5.9
1490.6	105.8	6.4
1527.2	115.4	3.8
1612.7	131.8	5.2
1725.6	147.6	7.1

Thus, using the Analyseries program (Paillard et al., 1996), 14 age control points were defined for the time period covering MIS 1-6 (listed in Table 3.1). A continuous timescale was obtained by linear interpolation between the age control points (Fig. 3.8a).

The dating of the homogeneous sediment interval between 3780 and 1630 cm was problematic, since it consists of a thick turbidite. However, the location of this interval below MIS 5 (interglacial) sediments indicates that it represents MIS 6 (glacial) deposits. This thick interval can be located in different cores of the Bryant Canyon area (Tripsanas et al., 2007).

3.3.2. Grain size distribution

Grain-size analysis carried out on 363 samples indicates that the sediments of the La Salle Basin are mainly composed of fine-grained cohesive silt (3.1µm<mode<8.9µm). All samples are characterized by a unimodal grain-size distribution. Vertical changes in the grain-size parameters of the sediment are illustrated in Fig. 3.9. The cohesive-silt fraction shows an increasing trend throughout the core, while the sortable-silt fraction decreases (Fig. 3.9c-d). More specifically, the sediments are composed of 49-68% cohesive-silt, 10-36% sortable-silt, 11-27% clay, and 0-6% sand.

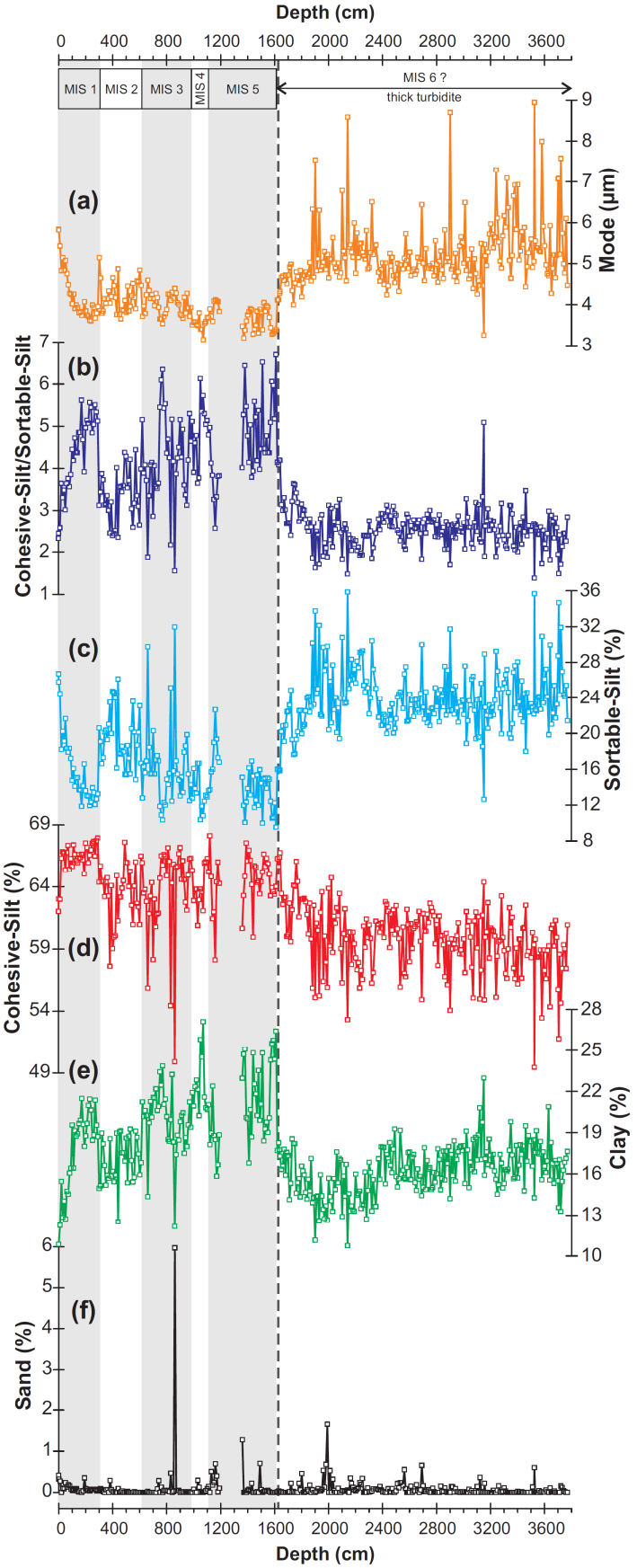

Fig. 3.9. Grain-size distributions (grain-size classes in %, and mode in µm) from the La Salle Basin (core MD02-2549). Shaded bands indicate the MIS 1, 3 and 5. The dotted line represents the upper stratigraphic limit of the thick turbidite.

In general, the grain-size distributions allow to distinguish two intervals with different sedimentological characteristics. In the first interval located between 3770-1630 cm, the proportion of sortable (non-cohesive) silts displays the maximum values of the entire interval whereas the clay fraction is minimum (Fig. 3.9c,e). A final point of interest is that the cohesive-silt/sortable-silt ratio and clay content display rather smooth distributions (Fig. 3.9b,e), which suggests that this unit is composed of a relatively homogeneous detrital material. Contrastingly, the second interval located between 1630-0 cm is characterized by a slight decrease in grain-size mode (down to 3µm) reflecting an increase in the contribution of fine cohesive (up to 68%) and clay particles (up to 27%), whereas the sortable-silt particles decrease (Fig. 3.9c,e). In addition, the cohesive-silt/sortable-silt ratios show a high variability during this unit.

3.3.3. Clay mineral analysis

A total of 362 samples were analyzed by X-ray diffraction to determine the mineralogical assemblage of the La Salle Basin sediments (core MD02-2549). Relative percentages of smectite, illite, chlorite and kaolinite for the entire stratigraphic records of the core MD02-2549 are shown in Fig. 3.10. The description of the results of the clay-mineral would be realized in agreement with the sedimentological observations of the core, since interval 3770-1630 represents a great turbidite, and the interval 1630-0 cm represents variations due to climatic factors (MIS 1-5).

Interval 3770-1630 cm.- The mineral assemblage in the <2 µm-fraction over this interval consists mainly of smectite (20-85%, average 51%), and accessory illite (7-43%, average 24%), chlorite (4-31%, average 14%), and kaolinite (3-21%, average 11%). Overall, the results clearly show that smectite increases and illite + chlorite decrease from 3770 to 1750 cm. Chlorite concentrations show slight similarity with the illite variations, while the kaolinite concentrations in the sediments are highly variable. The smectite/illite+chlorite [S/(I+C)] and kaolinite/chlorite (K/C) ratios display little variability and minimum values.

Interval 1630-0 cm.- Within this interval smectite also dominates the clay-mineral composition with a variable content from 27% to 84% (average 69%). The illite content fluctuates from 6% up to 38% (average 13%). The chlorite concentrations range mainly between 2 and 24% (average 8%). The kaolinite concentration is the most variable, with values mainly between 4% and 19% (average 10%).

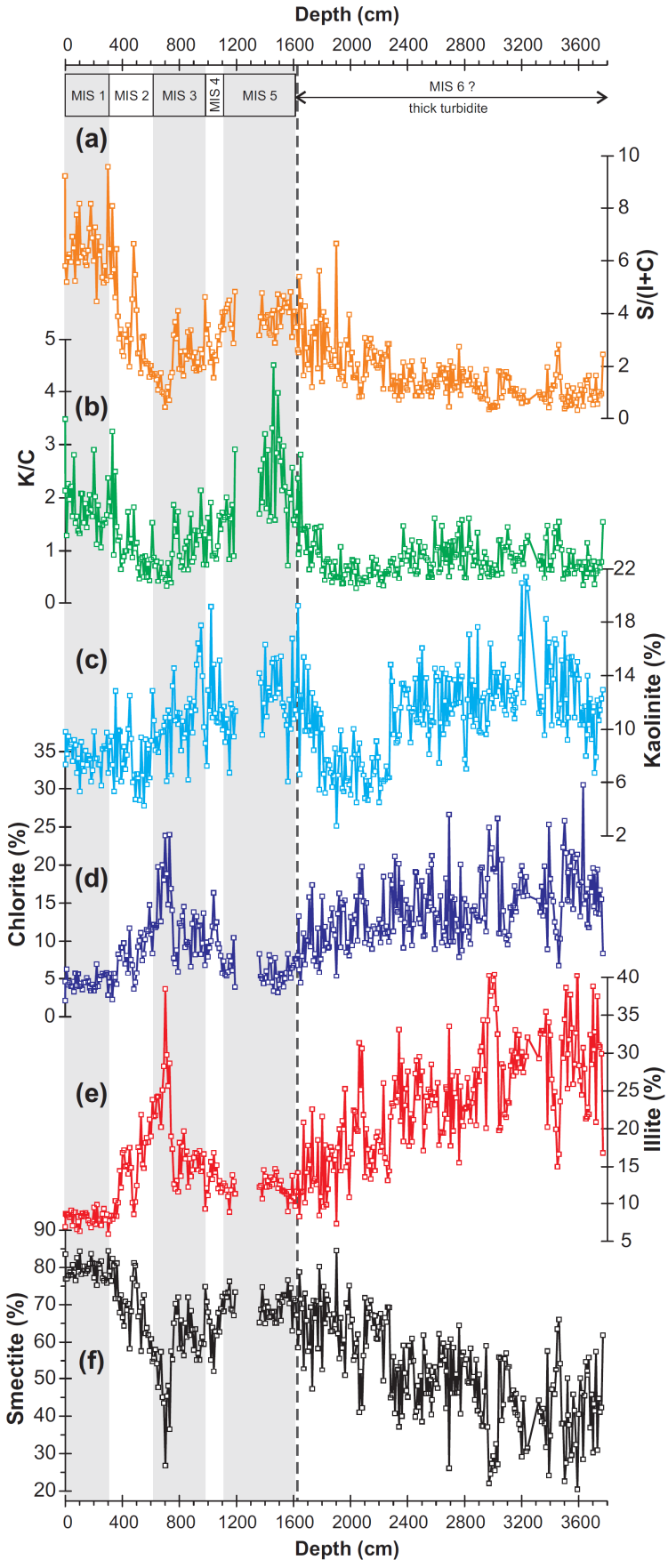

Fig. 3.10. Clay-mineral assemblages from the La Salle Basin (core MD02-2549). Shaded bands indicate the MIS 1, 3 and 5. The dotted line represents the upper stratigraphic limit of the thick turbidite.

The clay-mineral composition display oscillations between smectite-rich interval [S/(I+C)>4; MIS 1], and illite + chlorite intervals [S/(I+C)<4; MIS 2-5] where kaolinite is slightly more abundant (Fig. 3.10). Two remarkable features over this interval are also (1) the noticeable differences in the clay-mineral assemblage between the MIS 1 and MIS 2-5 (Fig. 3.10), and (2) the simultaneous sharp enrichment of the illite + chlorite from MIS 2/3 (~700 cm), whereas smectite strongly decreases. The most significant change in the kaolinite/chlorite ratio is observed during the MIS 5, which the ratio shows a remarkable increase (up to 4, ~1460 cm) reflecting a high contribution of kaolinite during this time.

3.3.4. Bulk analyses: magnetic susceptibility, spectral lightness (L*), calcium carbonate, elemental analysis and Rock-Eval pyrolysis

Magnetic susceptibility (MS) and spectral lightness (L*; generally used as a proxy for the carbonate content of marine sediment, e.g., Balsam et al., 1999) were measured onboard, at a resolution of ~2 cm (Labeyrie et al., 2005). Calcium carbonate, elemental analyses were carried out on 205 samples, whereas the Rock-Eval pyrolysis was measured for 57 samples. Vertical changes in the bulk analyses of the sediment are illustrated in Fig. 3.11. It is important to emphasize that similarly to the Pigmy Basin the calcium carbonate dissolution processes in the La Salle Basin are also negligible. Therefore, the calcium carbonate changes are mainly controlled by opposed autochthonous biogenic productivity and terrigenous dilution.

In general, $CaCO_3$ and lightness L* distributions appear well correlated for the entire interval cored. Similarly, C/N ratio, TOC and MS distributions follow the same trend. The bulk analyses also allow the clear differentiating of the turbidite (3770-1630 cm) from the rest of the core sediments (1630-0 cm).

Interval 3770-1630 cm.- In this interval, the $CaCO_3$ and lightness L* values are quite low, reflecting a low autochthonous biogenic contribution and/or dilution by detrital material, whereas MS, TOC and C/N ratio distributions display their highest values indicating an increase in the terrigenous flux.

Interval 1630-0 cm.- The most significant feature of the bulk analyses (MS, TOC and C/N ratio) variations consists in a drastic shift of magnitudes between about 1000 and 400 cm (MIS 2-3). Within this zone, the major peaks coincide with the highest values of clay fraction and illite + chlorite (MIS 2/3; about Last Glacial Maximum or LGM). The important increase of MS values observed in the glacial stage 2/3 is thus attributed to an increase of the detrital

supply of magnetic minerals. In the same way, the high TOC (up to 1.6%) and C/N ratio (>20) indicating a major supply of terrigenous organic matter (OM).

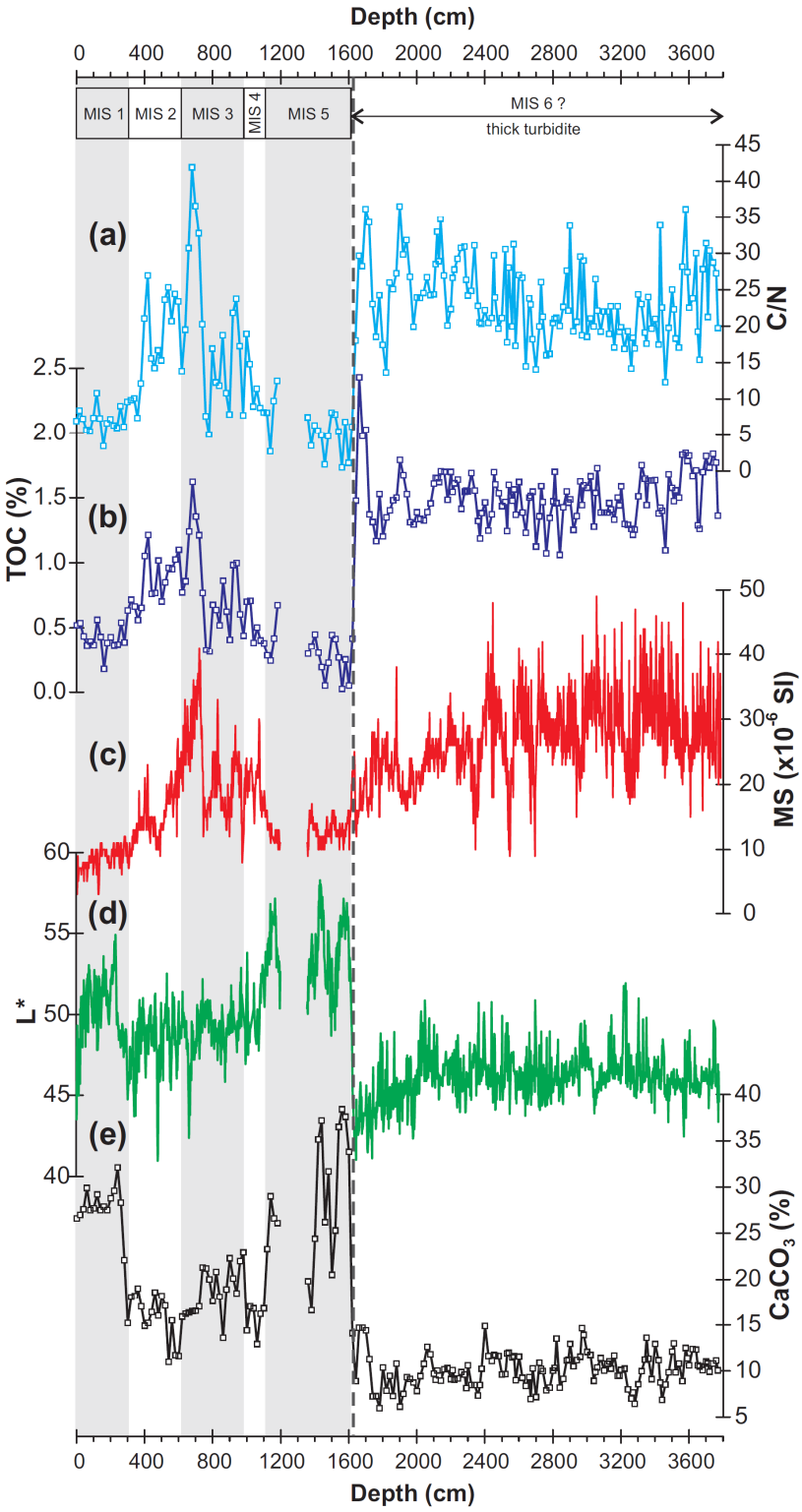

Fig. 3.11. Carbonate ($CaCO_3$), lightness L*, magnetic susceptibility (MS), TOC, C/N ratio distributions from the La Salle Basin (core MD02-2549). Shaded bands indicate the MIS 1, 3 and 5. The dotted line represents the upper stratigraphic limit of the thick turbidite.

The Rock Eval parameters (Tmax and HI) show little variations (Fig. 3.12). Tmax values ranges from 406 to 436°C and HI varies from 14 to 137 mg HC/g TOC. The TOC vs. S_2 and Tmax vs. HI crossplots suggest predominantly immature to mature type III OM, that is, of terrestrial origin. Note that the OM in the interval between 3770-1630 cm is slightly more mature, with respect to the interval between 1630-0 cm.

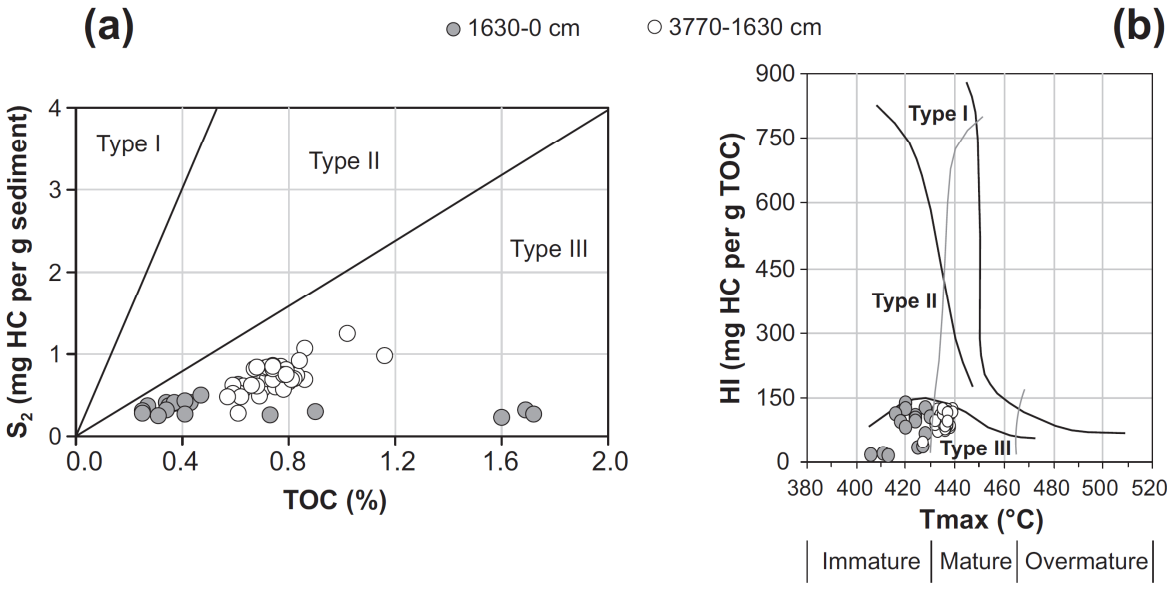

Fig. 3.12. Rock-Eval pyrolysis parameters. (**a**) TOC vs. S_2 and (**b**) Tmax vs. HI crossplot illustrating the origin and maturation states of the organic matter from La Salle Basin (core MD02-2549).

3.3.5. Elemental geochemistry

Major- and trace-elements were measured at low-resolution, on a total of 49 samples, to obtain a broad geochemical signature of the sediments. Element concentrations were normalized to Al in order to exclude a dilution effect by varying carbonate contents. Fig. 3.13 illustrates that the major and trace elements show several variations down core.

Interval 3770-1630 cm.- The thick turbidite shows relatively high Ti/Al, K/Al, Cr/Al, Zr/Al ratios representing heavy minerals, in agreement with the grain-size parameters that indicate a slightly coarser mode and higher proportion of sortable-silts. In addition (La/Yb)n and (Gd/Yb)n ratios show a slight impoverishment in LREE and MREE over HREE.

Interval 1630-0 cm.- Within this interval, the most remarkable feature are the highest Ti/Al, K/Al, Mg/Al, Na/Al, Si/Al, Ce/Al, La/Al values associated with depressed values of V/Al between about 1000 and 400 cm (MIS 2-3; about LGM). The peculiar geochemical character of this last interval is also in agreement with the highest values of clay fraction, illite + chlorite, MS, C/N ratio and TOC.

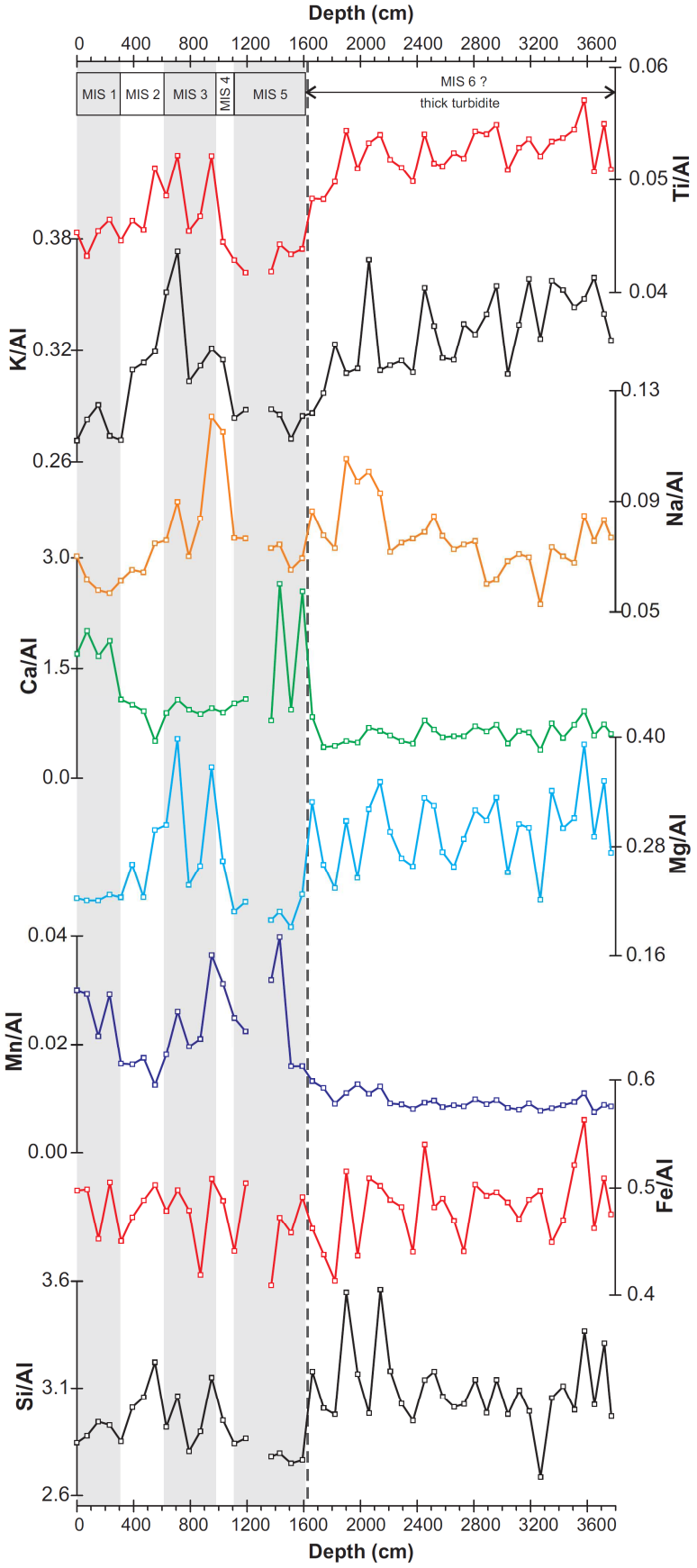

Fig. 3.13. Al-normalized elemental ratios: major, traces and rare earth (REE) elements. Note that the scale of the ratios is expanded. Shaded bands indicate the MIS 1, 3 and 5. The dotted line represents the upper stratigraphic limit of the thick turbidite.

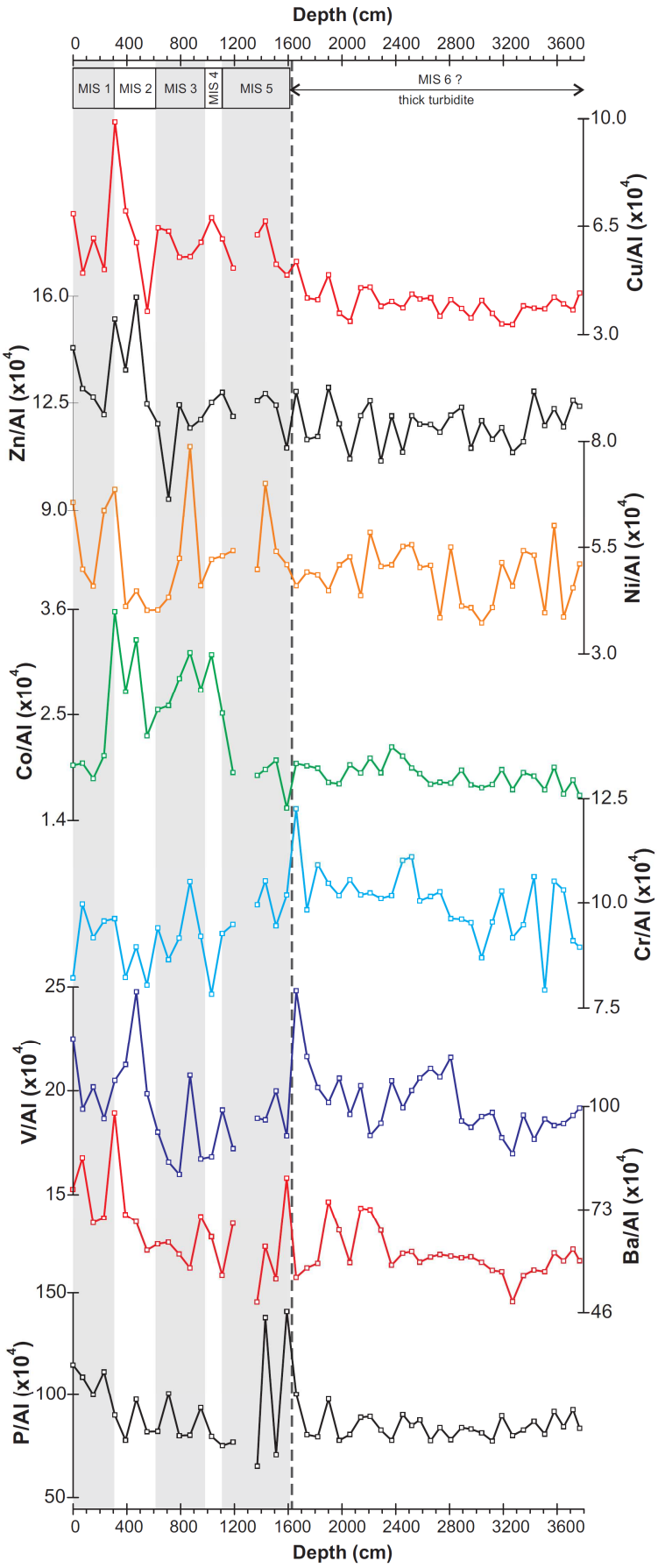

Fig. 3.13. (continued)

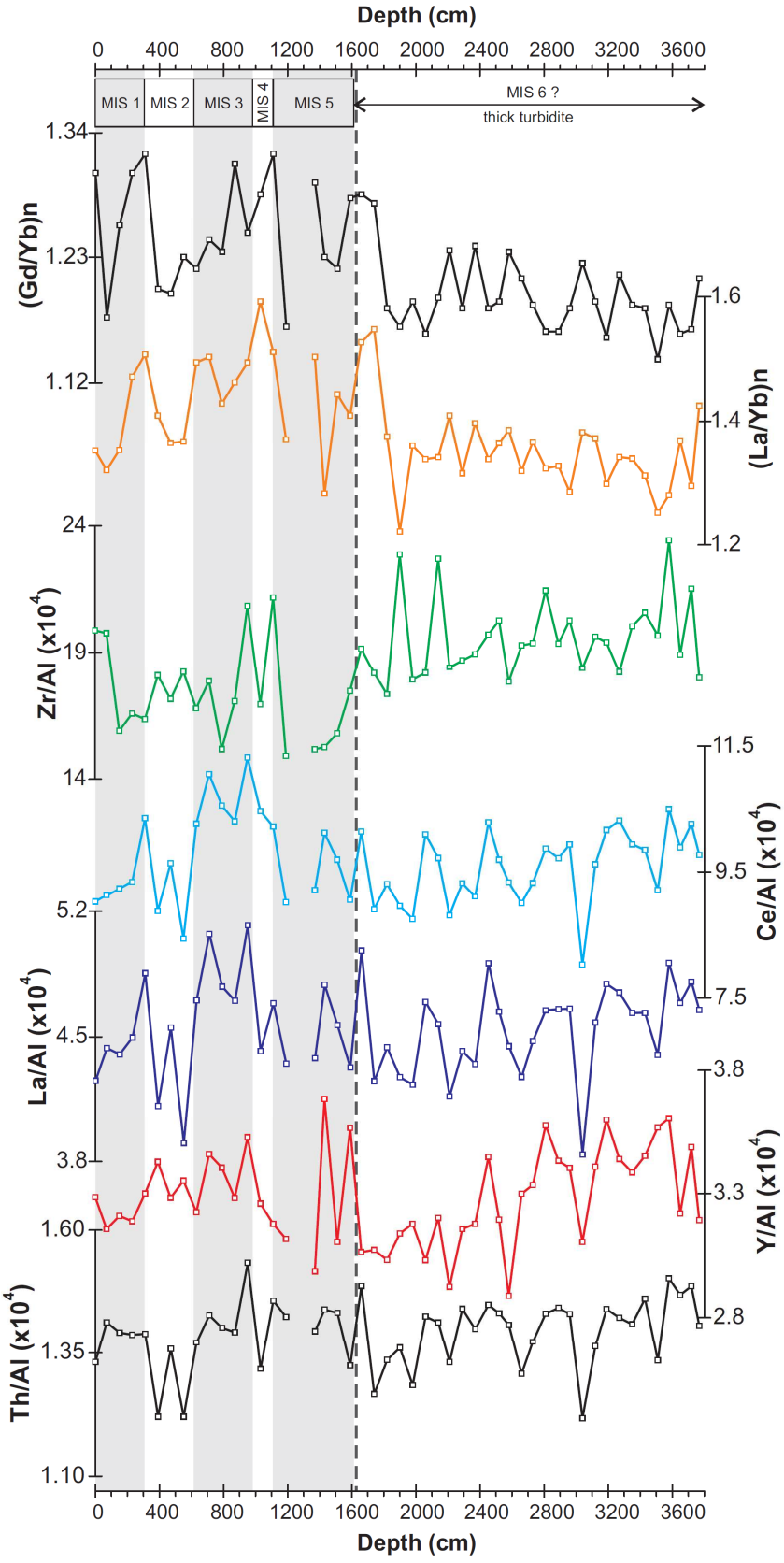

Fig. 3.13. (continued)

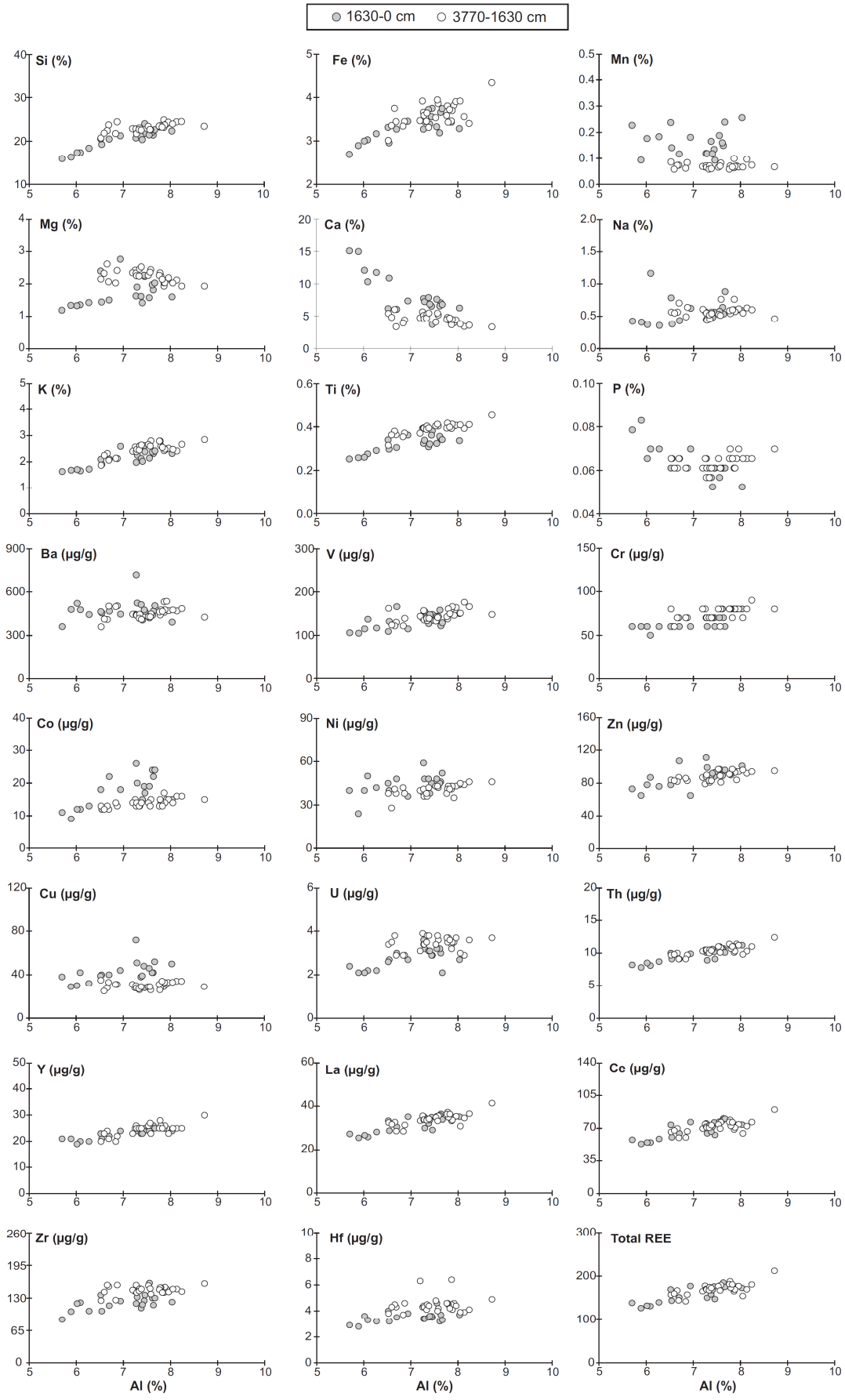

Fig. 3.14. Scatter plots of analyzed elements vs. Al concentrations.

The scatter plots of metal vs. Al concentrations are shown in Fig. 3.14. Major and trace elements show good correlation with Al concentrations, advocating to a detrital origin for these elements. In addition, Ca, mainly associated with carbonates, shows a negative correlation with Al, suggesting a control by dilution process. No relationship between Fe and Ni, Cu, Zn and Co was observed, evidencing no significant incorporation of the trace metals to iron sulfide (e.g., Tribovillard et al., 2006).

Trace-metal enrichment factors do not show any significant variations (average, 0.4 to 2), which also indicates that the redox sensitive and/or sulfide-forming trace metals (e.g., V, U, Cu, Ni, Co) are not authigenically enriched (EF_{TM}<5) (Fig. 3.15).

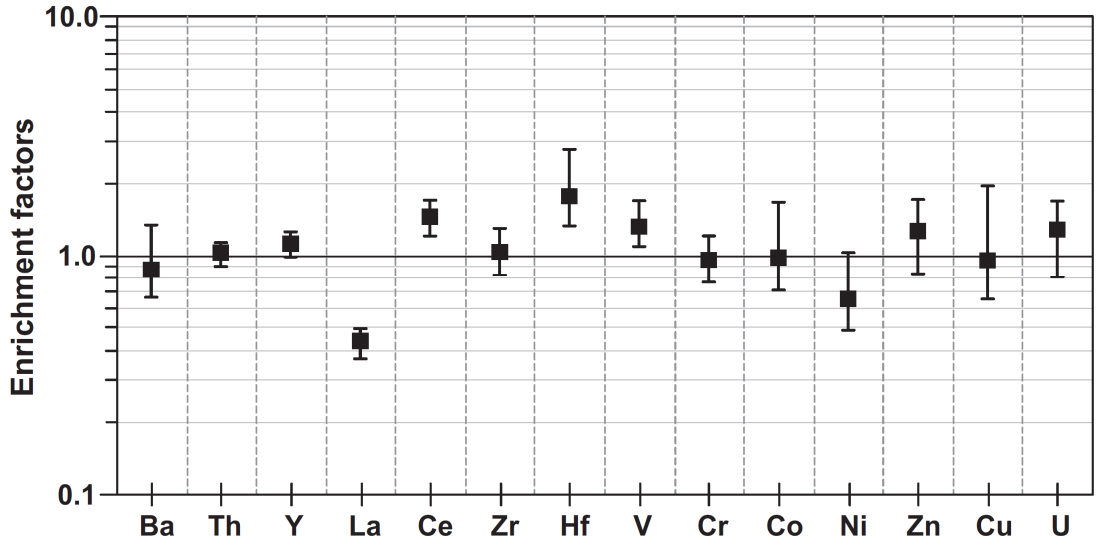

Fig. 3.15. Comparisons of the enrichment factor of selected trace metals of the La Salle Basin (core MD02-2549). The extent line of the boxes corresponds to the range of values (min-max) and the boxes to the average value. The horizontal line EF = 1 indicates the value for which there is no enrichment/depletion with regards to average shale composition.

NASC–normalized REE patterns for the La Salle Basin sediment are shown in Fig. 3.16. The REE patterns exhibit variation typical of the NASC and do not show any striking features, except for a general slight enrichment in light REE (LREE: La-Nd) over heavy REE (HREE: Tb-Lu). The REEs patterns in the La Salle Basin sediments exhibit a similar distribution to the Pigmy Basin sediments and the Mississippi River suspended loads (Fig. 3.16).

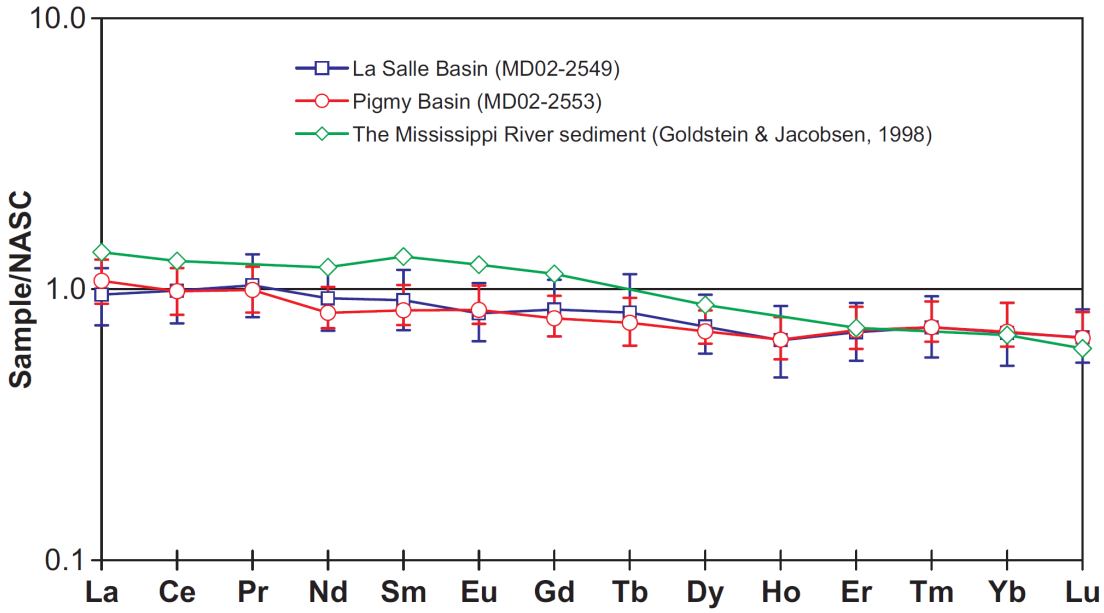

Fig. 3.16. Comparison of REE patterns between the averages of the La Salle and Pigmy basins (this study) and Mississippi River sediments (Goldstein and Jacobsen, 1988; Elderfield et al., 1990). NASC values by Gromet et al. (1984) are used for normalization.

3.4. Interpretations and discussions

3.4.1. Sedimentary regimes in the La Salle Basin over the last climatic cycle (main findings, new insights)

Introduction

The glacial-interglacial history of continental flood runoff is difficult to interpret and document on the North American continent because the past meltwater and megaflood episodes induced erosion that may have modified and/or completely erased the original depositional signatures. Besides, the chronological resolution for terrestrial deposits (e.g., the Mississippi Valley) is lower than for marine counterparts on the continental margin (e.g., Gulf of Mexico). Thus, the best possible way to investigate these flooding events is to look at their marine records. Hemipelagic sediment sequences deposited in the northern Gulf of Mexico (GOM) are indeed ideal for reconstructing continental runoff because terrestrial processes, though very subtle, are recorded continuously in these siliciclastic sediments and at a high resolution due to elevated sedimentation rates (e.g., Brown et al., 1999; Flower et al., 2004; Montero-Serrano et al., in press; Sionneau et al., in revision).

During the last climatic cycle, the modifications in both the quantity and nature of the terrigenous particles eroded and transported by the Mississippi River towards the GOM appear to be constrained by oscillations in high-latitude climate, Laurentide Ice Sheet (LIS) melting dynamics, atmospheric configurations (Jet Stream, Bermuda High and Intertropical Convergence Zone position), subtropical oceanic hydrological properties (meridional extension of the Atlantic Warm Pool) and hydrological regime over North America (e.g., Joyce et al., 1993; Forman et al., 1995; Liu and Fearn, 2000; Knox, 2000, 2003; Flower et al., 2004; Poore et al., 2004; Richey et al., 2007; Nürnberg et al., 2008; Ziegler et al., 2008; Sionneau et al., in revision; Montero-Serrano et al., under review).

In this section are studied the palaeoenvironmental and paleoclimatic signals recorded in the detrital sediment fraction of the core MD02-2549 (26°25.68'N, 92°33.94'W; 2049 m water depth) from La Salle Basin in the northern GOM, covering the last climatic cycle. We chose La Salle Basin because it is located at some distance from the Mississippi Delta system. Thus, it collects continuously a smoothed and averaged terrigenous supply from North America and avoids local perturbations linked to the Louisiana slope depositional processes (e.g., Aharon, 2003, 2006). The objectives are (1) to decipher temporal variations in

terrigenous sediment provenance, and (2) to investigate links between ocean-continent correlations and continental flooding, using mineralogical, granulometric, and geochemical tracers. The interpretation of the data provides a complete reconstruction of the variability of the Mississippi River discharges in response to North American climate evolution during the last climatic cycle, and help to better constrain the history of glacial meltwater and pluvial magaflood events, through terrigenous transfers, into the GOM.

Main characteristics of sedimentary regimes in the La Salle Basin

Organic matter (<3%) and $CaCO_3$ (<38%) are minor but important components, which leaves terrigenous aluminosilicates (detritus) as the major component. A simple calculation assuming that %detritus material=100%−%$CaC0_3$−%TOC, indicates that the detrital fraction in the core range between 62 and 92% (average 84%), indicating that sedimentation is mainly ruled by the terrigenous supply over the entire interval being strictly detrital during the turbidite sedimentation (MIS 6) and MIS 2-4, whereas significant biogenic contribution is observed during the MIS 1 and MIS 5e. Complementarily, trace-metal enrichment factors also highlight a dominant detrital signature and a non detectable influence of authigenic processes in the La Salle Basin (Fig. 3.15). The C/N ratio (Fig. 3.11a) and Rock-Eval parameters (Fig. 3.12) suggest that the organic fraction is also mostly terrigenous, in agreement with similar findings obtained in the Pigmy Basin (see Chapter 2) and in nearby the Orca Basin (Meckler et al., 2008; Tribovillard et al., 2008, 2009; Sionneau et al., in revision).

The absence of any significant REE fractionation when normalized to NASC in La Salle Basin sediments during the last climatic cycle (MIS 1-5), as observed in other basins from the GOM (Flocks and Swarzenski, 2007; see Chapter 2, Pigmy Basin), indicates a highly-mixed detrital source. The similarity of REE distributions in La Salle Basin sediments when compared with Mississippi River suspended loads (Goldstein and Jacobsen, 1988; Elderfield et al., 1990) confirming the dominant influence of Mississippi River and minor contributions of other rivers (Mobile, Brazos and Atchafalaya) during this time. These results thus suggest that the La Salle Basin, similar to Pigmy Basin, is representative of the sedimentation in the off-shore part of the GOM in that it mainly collects land-derived particles delivered by the Mississippi River which receives discharge from Missouri + Ohio rivers system and drains almost half of the conterminous USA. In other words, the La Salle Basin is an appropriate recorder of the land-to-sea transfer, from North America to the GOM, during the last climatic cycle.

Mississippi River discharge during the MIS 6 (3780-1630 cm): turbidity current deposits

More prominent MS values, low $CaCO_3$ concentrations and lightness L* values, and a major enrichment in terrigenous elements such as Al, Si, K, Ti, Cr and Zr as compared to MIS 2-3, suggest a noticeable increase in terrigenous supply to the GOM during the MIS 6. Additionally, the peculiar grain-size distribution characterizing this interval indicates specific supply of coarse particles. These results suggest that the homogeneous interval between 3780 and 1630 cm is likely linked to turbidity current deposits that affected the northwest GOM during the low sea-level stand of MIS 6 (Tripsanas et al., 2007). Indeed, the ancestral Mississippi River delta was located north of Bryant Canyon area during MIS 6 (Fig. 3.17). This led to highly increased supply of terrigenous sediments (transport by gravity flows) to the continental slope and abyssal plain of the northwestern GOM. These interpretations suggest that the detrital signal in this interval cannot be interpreted from the paleoclimatic point of view, but however a sedimentological interpretation is extensively discussed in Tripsanas et al. (2006, 2007).

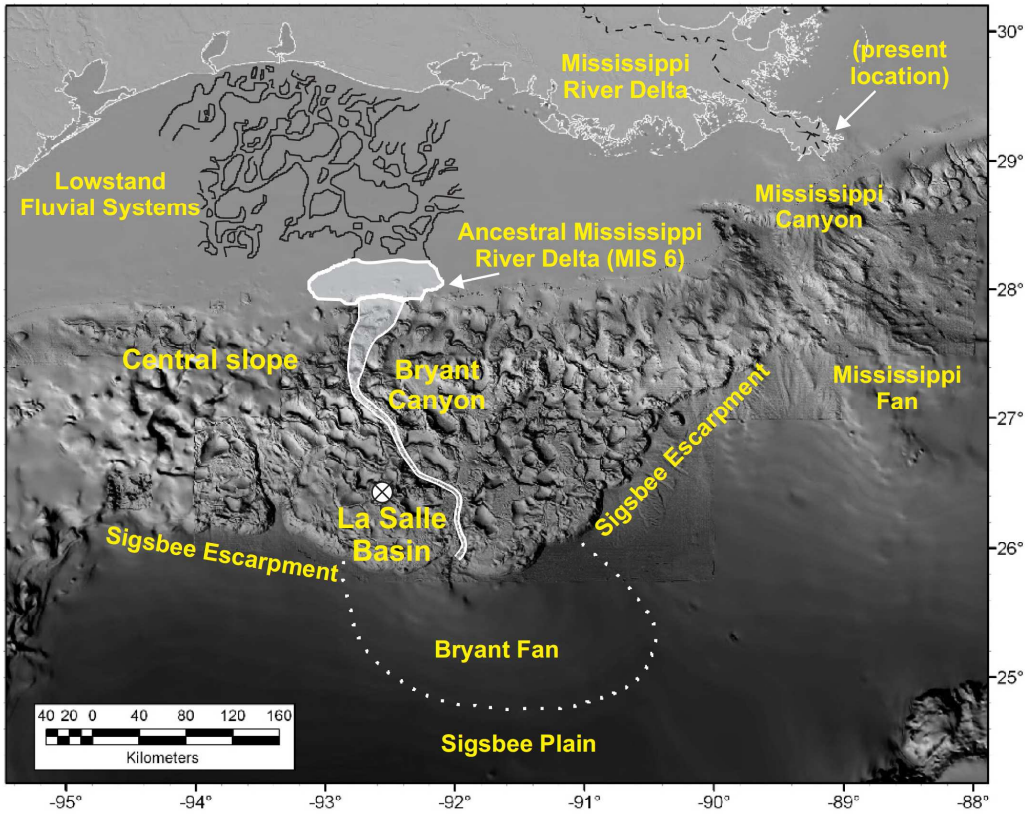

Fig. 3.17. Morphological map of the seafloor in the northern GOM (Tripsanas et al., 2007), displaying the locations of the ancient lowstand fluvial system, the ancestral Mississippi River Delta on the shelf during MIS 6 (adopted from Sutter and Berryhill, 1985), and the La Salle Basin (core MD02-2549).

Conversely, the grain-size data in the La Salle Basin (e.g., decreasing in the grain-size mode) suggest an increasing in the supplied of fine-grained sediment to the GOM upward of 1630 cm (MIS 1-5), in agreement with the shift of the Mississippi River delta to a more easterly location during MIS 5 – to the north of the present Mississippi Canyon (Fig. 3.17) – which caused a dramatic decrease in sediment supply in the northwest GOM, and consequently to the cessation of gravity flows (Tripsanas et al., 2007).

The important point in the previously discussed aspects is that the sedimentary record through the upper 1630 cm of the core MD02-2549 is characterized by the dominance of hemipelagic sedimentation, revealing new sedimentological evidences that the Mississippi River discharges were quickly switched from west to east, up-dip of the present Mississippi Canyon, before and/or during early MIS 5. Additionally, the rather smooth distribution in the grain size mode implies an absence of turbidites and other types of mass gravity flows within this interval.

Variability of the Mississippi River discharges during the last climatic cycle, MIS 1-5 (1630-0 cm): glacial meltwater and pluvial megaflood events

Following the same strategy used in Chapter 2 for the Pigmy Basin (core MD02-2549), which uses high-resolution clay mineral [S/(I+C) and K/C ratios], coupled with geochemical characterization of terrigenous material, as a tracer of geographic provenance in North America during the last deglaciation (e.g., Montero-Serrano et al., in press), **the main aim of this section is to determine at glacial-interglacial time scales the timing of continental erosion and sedimentary provenance of the detrital material delivered to the GOM via the Mississippi River during the last climatic cycle (MIS 1-5)**.

During the last climatic cycle, mineralogical and geochemical data from the La Salle Basin suggest also that detrital sedimentation mainly results from the contributions of two different sources (Fig. 3.18): (1) the northwestern Mississippi and Missouri river watersheds characterized by high smectite content associated mainly with high V/Al ratio, where the eastern part of this province, in the Upper Mississippi River catchment basin between Lakes Superior and Michigan is characterized by locally higher kaolinite content; and (2) the Great Lakes area and eastern Mississippi River watershed (so-called northeastern province) characterized mainly by illite and chlorite-rich sediments with high Mg/Al, K/Al, Ti/Al and Total REE/Al ratios. In general, the low correlation between the variations of illite and kaolinite (correlation coefficient: $r<0.05$, $n=149$; Fig. 3.19a) implies that the alternative illite-

rich source area from the southwestern illite + kaolinite-rich province (Fig. 3.18) is not a possible candidate. In contrast, the relatively good correlation between illite and chlorite (correlation coefficient: r=0.55, n=149; Fig. 3.19b) indicates a common source for illite and chlorite, pointing out the northeastern province as the main contributor (Fig. 3.18).

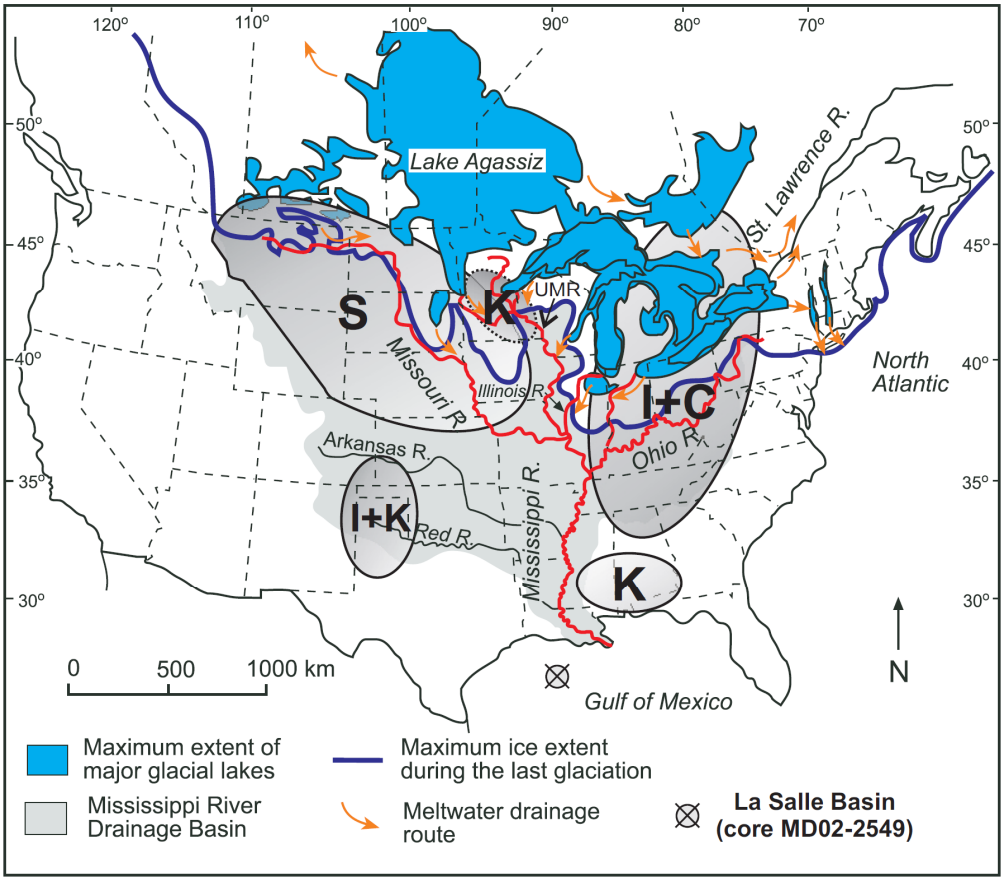

Fig. 3.18. The Mississippi River watershed showing the Last Glacial Maximum extent of the Laurentide Ice Sheet (Dyke, 2004), the maximum extent of glacial lakes and major drainage routes (modified from Rittenour et al., 2007), and the main continental clay mineral provinces (Sionneau et al., 2008); S: smectite, I: illite, C: chlorite, K: kaolinite, UMR: Upper Mississippi River.

Different smectite-rich intervals can be detected on the base of mineralogical proxies during the last 125 ka (gray bands in Fig. 3.20). The smectite-rich intervals – enriched in smectite (>69%), and in sometime in kaolinite (>15%), at the expense of both illite and chlorite (Fig. 3.20) – display rather characteristic mineralogical, sedimentological and geochemical compositions: the detrital fraction is typically fine-grained, impoverished in detrital organic matter, and sometimes high K/C and V/Al ratios. These characteristics during these intervals highlight a provenance of the main detrital supply from the NW Mississippi River watershed (smectite-rich) and accessorily the Upper Mississippi River watershed

(locally high kaolinite content) (Sionneau et al., 2008), suggesting enhanced moisture influx from the GOM toward central North America. However, through the last climatic cycle, these intervals display four distinct characteristics in provenance and erosional landscapes resulting from glacial and fluvial erosion (Fig. 3.21).

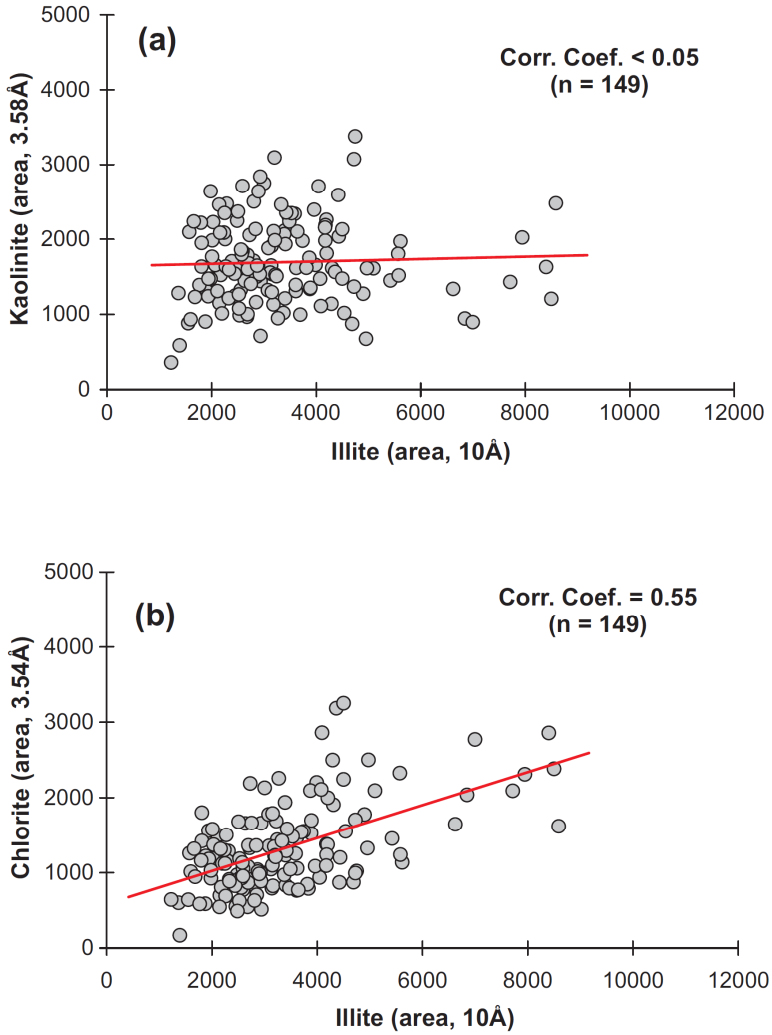

Fig. 3.19. The corresponding relationship between (**a**) illite vs. kaolinite and (**b**) illite vs. chlorite (in counts per second) for the upper 1630 cm (MIS 1-5) of the core M02-2549 from La Salle Basin. Corr. Coef. = Pearson correlation coefficient.

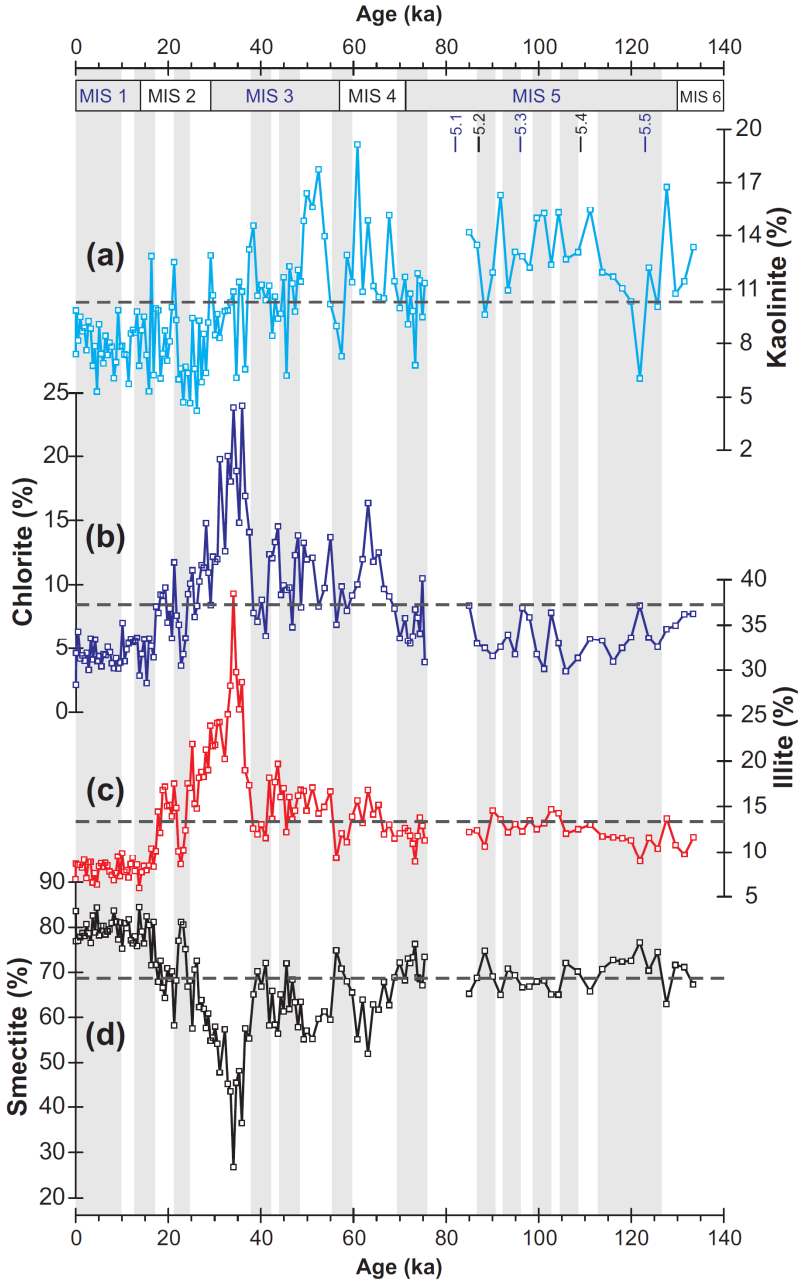

Fig. 3.20. Clay-mineral assemblages from La Salle Basin (core MD02-2549). The horizontal dotted lines indicate the mean concentrations for each clay mineral. The smectite-rich intervals are indicated in gray bands.

Fig. 3.21. (Next page) Comparison of the multi-proxy record from the La Salle Basin (core MD02-2549) with: (**a**) Loess-paleosol records of the Missouri and Mississippi River Valleys (Forman and Pierson, 2002); (**b**) oxygen isotope evidences of meltwater in the northern GOM (Joyce et al., 1990, 1993; Tripsanas et al., 2007); (**c**) Mg/Ca-based sea surface temperature (SST, °C) record in the DeSoto Canyon, core MD02-2575 (Ziegler et al., 2008); (**d-i**) sedimentological and geochemical proxies from the core MD02-2549; (**j**) the cooling episodes related to North Atlantic cold water events (NAC 19-26), Heinrich events (H 1-6) and the Younger Dryas (YD) (Rousseau et al., 2006). The horizontal dotted lines indicate the mean values for each proxy. The smectite-rich intervals are indicated in gray bands (see explanation in the text).

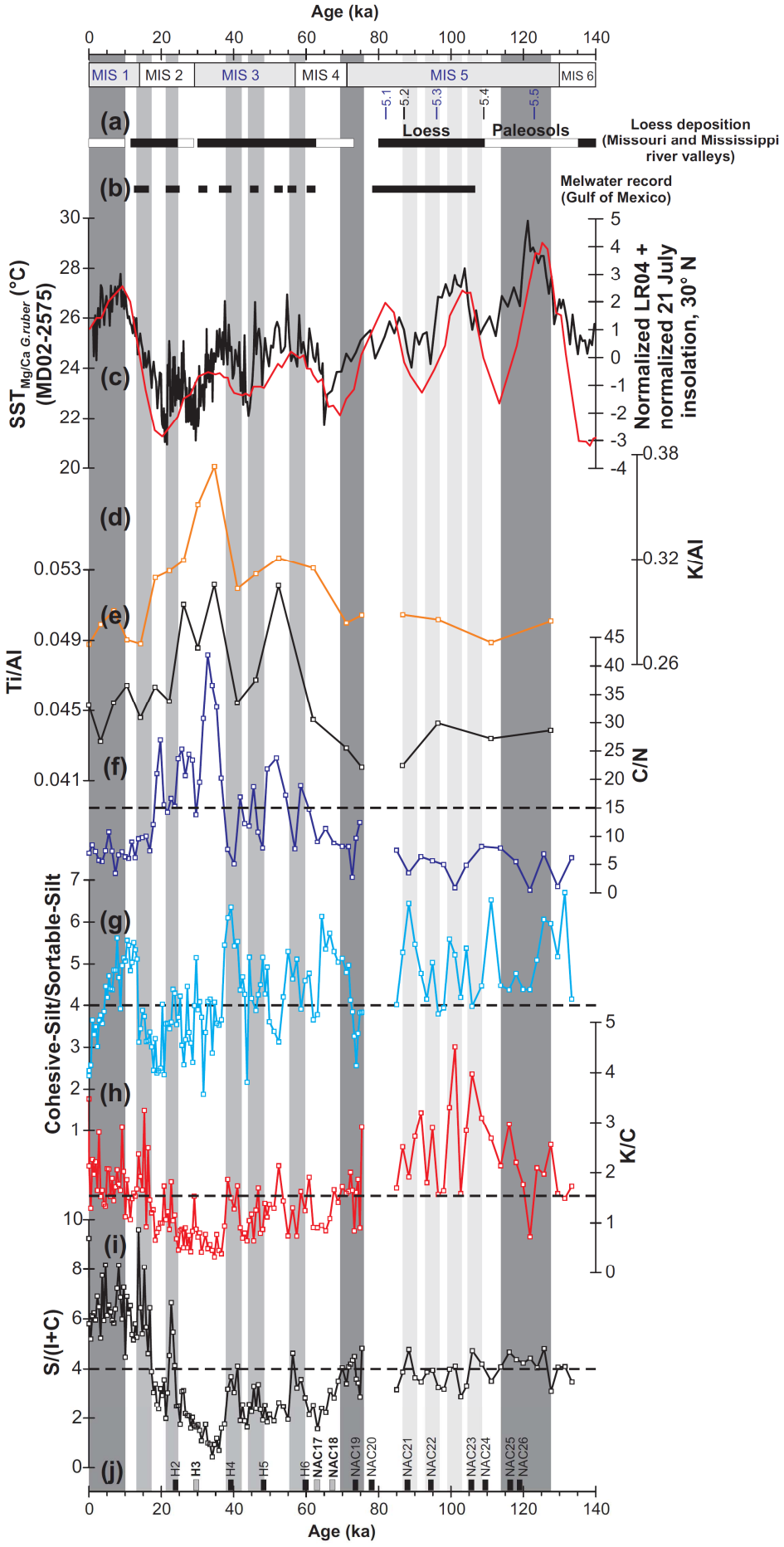

Pluvial megaflood events

Episodes of high continental precipitation and large Mississippi River floods caused the massive erosion of alluvial plains and promoted the remobilization of fine-grained sediment and their transport, via the Mississippi River, toward the GOM (e.g., Brown et al., 1999). Knox (2000, 2003) suggested that extreme floods over North America are commonly associated with large-scale atmospheric circulation patterns. These patterns determine the locations of storm tracks and the locations of air masses responsible for producing high magnitudes of precipitable water vapor and/or rapid temperature changes that contribute to excessive runoff and flooding. Thus, the compositional variations in the relative abundance of clay minerals and chemical composition (organic and mineral) in the GOM sediments may reflect changes in their major source areas over North American continent. It therefore provides insights on the direction of the main moisture vector.

According to these observations, the smectite-rich intervals centred at 120, 73, 5 ka (dark gray bands in Fig. 3.21) may be associated with episodes of high continental precipitation in central North America and large Mississippi River floods (similar to the Holocene, see discussion in section 2.4.3). In fact, any major modification of the dominant terrigenous sources that occurred during these intervals cannot be driven by the LIS that was considerably reduced or absent over the North American continent by these times, (e.g., full interglacial periods 1, 5.1 and 5.5) (Marshall and Clarke, 1999; Marshall et al., 2002). Thus, by similarity with the Holocene, significant modifications are more likely related to modifications of the continental drainage patterns by the Mississippi and Missouri rivers in response to migrations of the main precipitation belt over North America (e.g., Montero-Serrano et al., under review). Consequently, these results suggest that during these periods the precipitation belt was located over the northwestern province and that main moisture transfer reached the central part of North America. Under this hypothesis, high rainfall occurs in NW Mississippi province, promoting the massive erosion of the alluvial plains, and the subsequent remobilization of fine-grained sediments and their transport toward the GOM via the Mississippi (Knox, 1996). These intervals coincide with intervals of little loess deposition and major pedogenic process within the Mississippi and Missouri Valleys (Forman and Pierson, 2002) and eastern Colorado (Muhs et al., 1999) (Fig. 3.21a), which also suggests warmer and moister conditions over the northwestern province during these times.

Globally, during these pluvial megaflood events, negative $\delta^{18}O$ excursions in the sediments of the GOM are not observed, however, negative excursions have been identified in some basins from the northwest GOM (e.g., the Humphrey Basin; Mallarino et al., 2006;

Sionneau, 2008). This is undoubtedly a local phenomenon, because it has not been observed in other basins (e.g., Tripsanas et al., 2007; Nürnberg et al., 2008). The global absence of negative $\delta^{18}O$ excursions associated with these periods in marine records from the northern GOM (Fig. 3.21b) suggests that isotopically light $\delta^{18}O$ signatures of megafloods events were too small and easily dissipated to be recorded by planktonic foraminifera (Joyce et al., 1993; Brown et al., 1999; Tripsanas et al., 2007). To give the large negative $\delta^{18}O$ excursions, similar to the oxygen isotopic spike observed for larger deglacial meltwater flows in the northern GOM (e.g., Aharon, 2003; Flower et al., 2004; Meckler et al., 2008) and cause the associated salinity changes, a freshwater source 5-7 times the volume of the largest historical flood (e.g., Knox, 2000, 2003) would be required, which is unlikely and unreasonable. Note that late Holocene megafloods were derived from isotopically heavy Gulf precipitation, ca. -6‰ relative to standard mean ocean water, rather than isotopically light LIS runoff, ca. -30‰ relative to standard mean ocean water (Brown et al., 1999).

Another remarkable feature in the core MD02-2549 record from La Salle Basin is the noticeable differences in the clay-mineral distribution between the MIS 1 and MIS 5e (Fig. 3.20 and Fig. 3.21h-i). In the MIS 1 the clay assemblage is markedly dominated by smectite [75-84%; S/(I+C) up to 9.2], indicating that the detrital fraction was derived primarily from northwestern Mississippi and Missouri rivers watersheds (Fig. 3.18). In contrast, although the smectite is still the main component of the clay-mineral fraction [70-77%; S/(I+C) up to 4.8], MIS 5e is characterized by enhanced contributions of illite (up to 14%), kaolinite (up to 17%) and chlorite (up to 8%), suggesting a mixed provenance of detrital particles, i.e. mainly from the north-western province but with a notable contribution of the north-eastern province (Fig. 3.18). Nevertheless, note that the differences with the MIS 5e are based on 7 samples. According to these evidence, and assuming that the same drainage pattern persisted during the last climatic cycle with an increased long-term Mississippi River discharge due to glacial ice sheet fluctuations (Galloway et al., 2000; Galloway, 2005; Tripsanas et al., 2007; Rittenour et al., 2007; M. Blum, personal communication, 2009), the differences between MIS 1 and MIS 5e could be interpreted as noticeable modifications of the erosion regime over the North American continent, that are linked to the recurrent migrations of the precipitation belt over the continent (see discussion in section 3.4.2). These migrations are mainly constrained by the respective positions of the Jet Stream and Bermuda High modulated by displacements of both Intertropical Convergence Zone or ITCZ and Atlantic Warm Pool or AWP (e.g., Montero-Serrano et al., under review). Thus, these results suggest that the disagreement between MIS 1

and MIS 5e is due to notable differences in the configuration of atmospheric circulation patterns during these warm periods. These differences are probably caused to the greater seasonal temperature variations in the Northern Hemisphere during the MIS 5e (Denton et al., 2005), related to differences in orbital parameters compared to today (greater obliquity and eccentricity). It is important to emphasize that this interpretation is a viable mechanism to explain the unexpected disagreement in terrigenous sources between the MIS 1 and MIS 5e in the sedimentary record from La Salle Basin. However, a high-resolution study must be carried out to better constrain the sedimentary dynamic of the Mississippi River during MIS 5e.

Meltwater events

During the glacial (i.e., full glacial MIS 2 and MIS 4) and subglacial (i.e. colder periods within interglacials 5b, 5d) conditions, mineralogical and geochemical proxies suggest that terrigenous supply variations were directly controlled by the Laurentide Ice Sheet evolution (LIS). Thus, the modifications in the terrigenous proxies (notably, clay mineral) are interpreted to result from changes in the Mississippi River floods caused by LIS meltwater discharges.

Atypical sub-glacial sedimentation (MIS 5b–5d, high smectite and kaolinite).- the intervals centred at 106, 101, 93 and 88 ka (light gray bands in Fig. 3.20) are enriched in smectite and relatively high in kaolinite content and cohesive particles, indicating a mixed provenance of detrital particles, i.e. mainly from the NW Mississippi River watershed but with some noticeable contribution of the Upper Mississippi River watershed (Fig. 3.18). During this intervals (MIS 5d–5b) the sea-level fall of about 50-60 m within a time of general high sea-level (Cutler et al., 2003; Lambeck and Chappell, 2001), largely reflecting the the expansion of the LIS over the North America continent. Within this frame, mineralogical signature likely reflects a regional southward expansion of the LIS, which is extended to at least the headwaters of the Upper Mississippi and Missouri rivers, in the north central North America during the MIS 5d–5b interval (Miller and de Vernal, 1992; Marshall and Clarke, 1999; Marshall et al., 2002). According to these observations, the deposition of these intervals resulting from glacial erosion of the clay-rich terrace deposits along Upper Mississippi River tributaries (Knox, 1996). These interpretations are in agreement with Joyce et al. (1990, 1993), Tripsanas et al. (2007) and Forman and Pierson (2002), who, through high-resolution $\delta^{18}O$ records from the GOM and dating of loess deposits in Mississippi River Valley, indicated meltwater inputs within the Mississippi River basin from ca. 110 to 75 ka.

Typical glacial sedimentation (MIS 2-4, high illite and chlorite).- during full glacial periods MIS 2-4 (~70-10 ka), the La Salle Basin sedimentation is characterized by lower S/(I+C) ratios (Fig. 3.21) indicating a maximum contribution in illite+chlorite (high K/Al, Ti/Al), and accessorily in kaolinite. This strongly suggests that sedimentation in the northern GOM was mainly influenced by hydrological and erosional processes affecting the Great Lakes area and eastern Mississippi River watershed, during the intervals centred at 63, 51, 43, 30 and 20 ka (Fig. 3.21). Palynological data from Florida (Grimm et al., 2006), MS and clay-mineral data from western North Atlantic (Keigwin et al., 1998; Bout-Roumazeilles et al., 1999; Çağatay et al., 2002), and MS data from northeastern GOM (Nürnberg et al., 2008) also indicate increased the moisture transfers along the USA Atlantic coast. This eastward shift of the main moisture pattern from the NW Mississippi River watersheet toward the northeastern province may be interpreted as resulting from the impact of the LIS on continental climatic variability (e.g., Montero-Serrano et al., under review); indeed the southeastern edge of the LIS reached a great extension and elevation during these periods (Marshall and Clarke, 1999; Marshall et al., 2002; Kleman et al., 2002). Thus, the impact of LIS on atmospheric circulation is characterized by a stronger anticyclone over the ice sheet, a stronger trough and cold air over the east side of North America, a sharper storm track in the North Atlantic, and more precipitation in the southeastern periphery of the LIS (e.g., Otto-Bliesner et al., 2006; Abe-Ouchi et al., 2007). Runoff will promote the subsequent remobilization of glacial tills that are further carried as suspended loads through the eastern Mississippi River fluvial systems to the GOM, in agreement with the La Salle Basin grain-size distribution that indicates specific supply of coarse particles during the illite- and chlorite-rich intervals.

Furthermore, during the full glacial stages (MIS 2-4), and more notably between MIS 2/3 (Last Glacial Maximum or LGM), the detrital sedimentation displays an increased delivery in the contribution of illite and chlorite (up to 55% of the clay mineral association), terrigenous organic matter (C/N>15), coarse particles (mode>4µm), and fine-grained magnetic minerals, mainly magnetite and hematite which likely controls the magnetic susceptibility distribution (Keigwin et al., 1998) (Fig. 3.22). The sedimentological descriptions of the core (see section 3.2.2) and the generally high values of color reflectance a* (red variation) in the La Salle Basin sediments (Fig. 3.4), also suggest the presence the reddish coloured layers during MIS 2-4. These reddish layers, which indicate the presence of hematite and possibly other iron hydroxides (Giosan et al., 2002), are derived from the Permo-Carboniferous deposits of the Appalachian Chain (Keigwin et al., 1998).

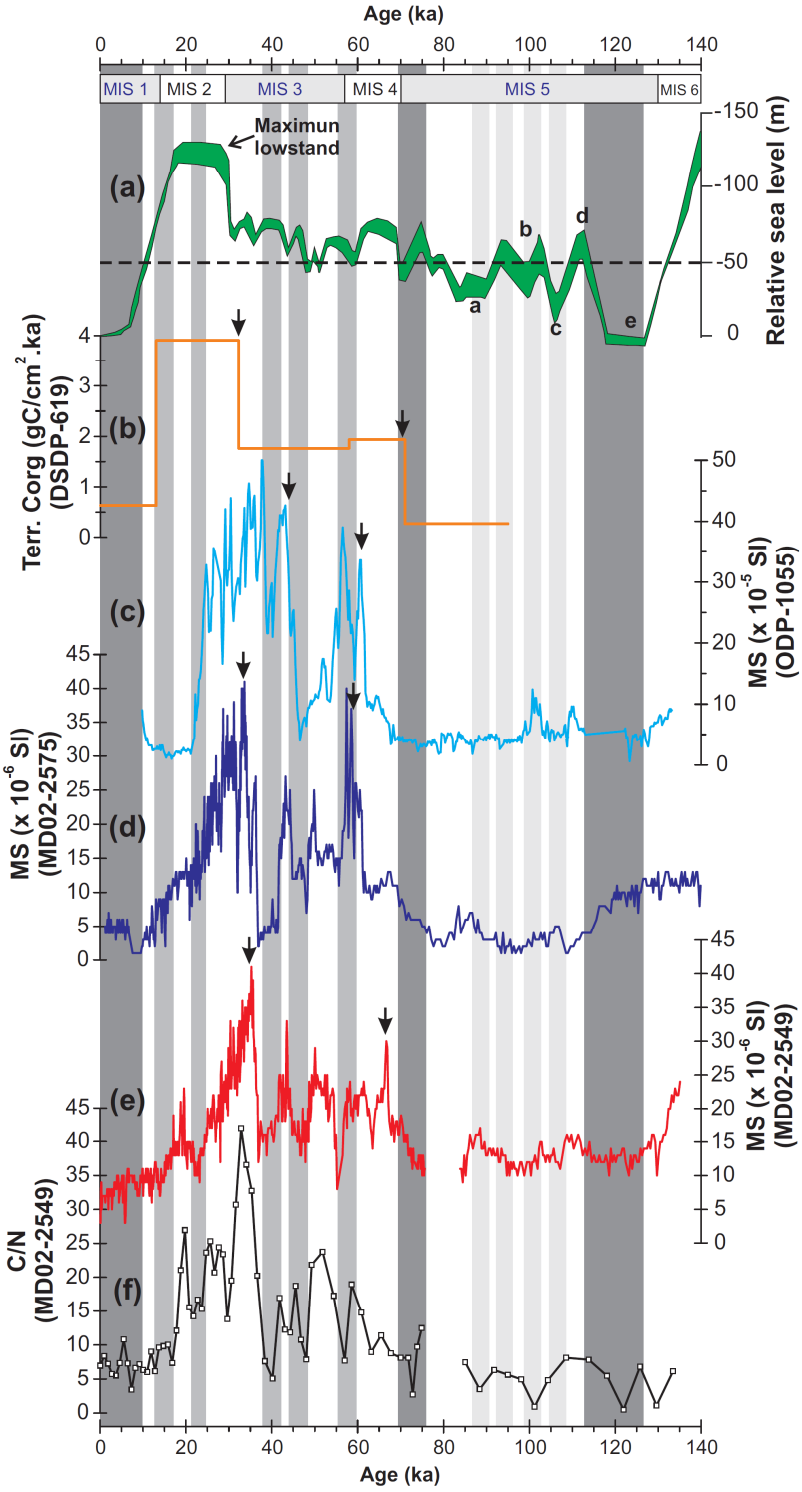

Fig. 3.22. Comparison of the sedimentological parameters from GOM and northwestern Atlantic for last 150 ka. (**a**) Sea level change through the last glacial cycle (Lambeck and Chappell, 2001). The dotted line represents the global sea level at ca. 11.5 ka and indicates the possible threshold for LIS within UMR basin (Dyke and Prest, 1987); (**b**) net accumulation rates (gC/cm^2.ka) of terrigenous organic carbon ($C_{org.}$) from core DSDP site 619 (Jasper and Gagosian, 1990); (**c**) MS from ODP-1055, NW-Atlantic (Keigwin et al., 1998); (**d**) MS from MD02-2575, NE-GOM (Nürnberg et al., 2008); (**e**) MS from MD02-2549; (**f**) C/N ratio from MD02-2549. The smectite-rich intervals are indicated in shaded bands. The arrows indicate the tentative correlation between the different paleorecords. Note that the difference in the timing of different peaks observed in the sedimentary records most likely reflects uncertainties in the individual core chronologies.

These results suggest that the Mississippi River received large amount of terrigenous materials resulting from maximal glacial erosion in northeastern North America (illite- and chlorite-rich province). Note that terrigenous inputs (e.g., MS, C/N ratio) derived from glacial erosion also are connected with the periods of lowest sea level during MIS 2-4 (Fig. 3.22a).

According to these observations, the variations in the sedimentary regime in the La Salle Basin during full glacial periods (MIS 2-4) may be interpreted to relate to the advances and retreats of the southeastern edge of the LIS linked to the Dansgaard-Oeschger (D-O) cycles, and which becomes maximum during around the LGM (Marshall et al., 2002; Kleman et al., 2002), in agreement with previous observations on the DeSoto Cayon (Nürnberg et al., 2008), Pigmy Basin (Jasper and Gagosian, 1990) and northwestern Atlantic (Keigwin et al., 1998) (Fig. 3.22a-c).

Lastly, over this interval of the typical glacial sedimentation (~70-10 ka), the illite- and chlorite-rich background sedimentation is interrupted by episodic smectite-rich intervals centred at 57, 46, 40, 21, 14 ka (medium gray bands in Fig. 3.21), which suggest a sporadic westward shift the main detrital source toward the northwestern Mississippi province. These bursts are interpreted as both brief re-advances and melting phases of the southwest margin of the LIS, which encompass the Mississippi and Missouri provinces, during times of maximal ice-sheet extension. These episodic smectite-rich events are also in line with meltwater inputs recorded in the northern GOM sediments (Joyce et al., 1990, 1993; Flower et al., 2004; Tripsanas et al., 2007, Montero-Serrano et al., in press; Sionneau et al., in revision), and with an extensive loess deposition from glacial outwash in the Missouri and Mississippi River Valleys dated around 60-30 ka (Forman and Pierson, 2002) (Fig. 3.21a-b).

Correlation with the North Atlantic cold water events

Outside of the glacial-interglacial oscillations, other climatic factors of second order can also modify the erosional processes over the continent and to produce changes in the main provenance of detrital particles. The North Atlantic cold water and Heinrich events are some of these climatic factors. Concomitantly, various studies document that abrupt climate changes in the high-latitude North Atlantic had a significant impact in the tropical and sub-tropical climate (e.g., Peterson et al., 2000; Haug et al., 2001; Lea et al., 2003; Hodell et al., 2008) nevertheless the mechanisms and dynamics of these effects are still in discussion (e.g., Chiang et al., 2003; Ziegler et al., 2008).

On the other hand, recent studies suggest that variations of the main detrital sources recorded in the northern GOM sediments mainly reflect changes in the moisture vector

direction across North America (e.g., Forman et al., 1995; Liu and Fearn, 2000; Knox, 2000, 2003; Montero-Serrano et al., under review). This moisture vector is mainly constrained by atmospheric configuration (Jet Stream, Bermuda High and ITCZ position) and subtropical oceanic hydrological properties (meridional extension of the AWP).

Within this frame, the smectite-rich intervals appears to be coeval with the cooling episodes related to North Atlantic cold water (NAC: 19, 21, 22, 23, 24, 25, 26) and Heinrich events (H: 2, 4, 5, 6) (Fig. 3.21j). However, it is important to consider that the uncertainties of the age model generated for the La Salle Basin is about 1000 yr, which is major that the duration of these cold events (~500 yr). Taking into account this slight imprecision, the key to interpret this coevality is most likely linked to modulation of moisture transfer by the ITCZ (e.g., Poore et al., 2003, 2004). Indeed, the smectite-rich intervals during these cold events coincide with both GOM sea surface temperatures (SST) relatively warm (Fig. 3.21c; Ziegler et al., 2008) and wet phases documented by pollen records from Florida (Lake Tulane; Grimm et al., 2006). These correlations suggest that the ITCZ and AWP in the GOM were seasonally displaced and extended northward during summer, which is translated by an enhanced moisture influx from the GOM toward central North America, and therefore by an increased in the contribution de smectite. Note also that (1) the boreal summer position of the ITCZ and AWP was relatively unaffected by these cold episodes, and (2) the northward extension of the ITCZ in the GOM region during summer is controlled by variations in northern-hemisphere summer insolation (Ziegler et al., 2008) (Fig. 3.21c).

In contrast, only Heinrich event 3 and North Atlantic cold water events 17 and 18 represents an exception in the sedimentary record in the La Salle Basin (Fig. 3.21j), with low S/(I+C) ratio, but this is in line with relatively cold GOM SST (Ziegler et al., 2008), and therefore with a southernmost position of the ITCZ that involves less moisture influx from the GOM toward central North America. The notable disagreement with the Heinrich event 3 is most likely due to greater seasonal temperature variations in the Northern Hemisphere (Denton et al., 2005), due to relatively high northern-hemisphere summer insolation during this time. Several studies suggest that the large increases in seasonal amplitudes are related to fast expansion of the sea ice cover during these cooling events, which causes extreme winter cooling, which are balanced by relatively mild summers (Chiang et al., 2003; Denton et al., 2005; Ziegler et al., 2008). Consequently, a rapid growth of sea ice in conjunction with the intensity of the thermohaline circulation through positive feedbacks, could lead to a southward migration of the ITCZ.

On the other hand, the correlation between low S/(I+C) ratio and the North Atlantic cold water events 17 and 18 (Fig. 3.21i-j) is interpreted to relate with a minimum in the northern-hemisphere summer insolation during MIS 4 which caused a southward migration of the ITCZ (Ziegler et al., 2008) and isolation of the GOM from AWP (Nürnberg et al., 2008). However, how to explain the high pedogenetic activity in the Missouri and Mississippi rivers Valleys with a low S/(I+C) ratio during the full glacial MIS 4? This could be explained in terms of the dynamic effect of the LIS on the climatic conditions. The LIS at ca. 65-60 ka ago extended to at least the headwaters of the Mississippi and Illinois rivers (Marshall and Clarke, 1999; Marshall et al., 2002), the sea-level equivalency of 30-40 m (Peltier, 1994) with the LGM it makes think that approximating an ice sheet of about two thirds to three quarters the volume of the LIS during this time (Klesman et al., 2002). Previous studies based on atmospheric general circulation simulations, pollen records and lake-level data (Kutzbach et al., 1998; Clark et al., 2001; Kaufman et al., 2001; Shuman et al., 2005) suggest that an ice sheet of this size would promote brief developments the monsoonal circulation from increasing moisture availability in central and western North America. Thus, these conditions likely generated an intermittent pedogenetic activity in central North America.

Summary and conclusions

The sedimentological and geochemical results obtained for the La Salle Basin (core MD02-2549) provide a solid record of detrital inputs delivered into Gulf of Mexico (GOM) by the Mississippi River over the past 140 ka (Marine Isotope Stages or MIS 1-6).

The terrigenous proxies obtained in this section reveal new sedimentological evidences that the shift of the Mississippi River delta occurred before MIS 5 as evidenced by the last occurrence of a large gravity-flow deposit in MD02-2549 (interval between 3780 and 1630 cm) in the La Salle Basin.

The clay-mineral assemblage allowed to decipher the variations of moisture transfers across North America during the last glacial period. These moisture transfers had a direct impact (1) on the melting dynamic of the southern edge of Laurentide Ice Sheet (LIS) during full glacial periods and (2) on the position of the main precipitation belt during full interglacial conditions.

Four sedimentary regimes with distinct characteristics in provenance and erosional processes (glacial meltwater and pluvial megaflood events) can be distinguished upon their mineralogical and geochemical contents during the last climatic cycle.

- During extreme warm periods of the MIS 1, 5.a and 5.e, which were characterized by reduced continental ice sheets and major pluvial megaflood erosion over North America, sedimentation is characterized by smectite-rich intervals centred at 120, 73, 5 ka which are associated with high pedogenetic activity in the Missouri and Mississippi River Valleys. This mineralogical signature point out to specific terrigenous supply from the NW Mississippi River watershed, suggesting enhanced precipitations and moisture influx from the GOM toward central North America.
- During cool periods of the MIS 5 (sub-glacial sedimentation, MIS 5b–5d), in particular during the intervals centred at 106, 101, 93 and 88 ka, sedimentation is also enriched in smectite but relatively high in kaolinite indicating a mixed provenance of detrital particles, i.e. mainly from the NW Mississippi River watershed but with some noticeable contribution of the Upper Mississippi River watershed, which probably reflected the southwestward expansion of the LIS margin to at least the headwaters of the Upper Mississippi and Missouri rivers.
- During full glacial periods (typical glacial sedimentation, MIS 2-4), the mineralogical data (illite+chlorite range between 30-60%) suggest that the background terrigenous fraction over the intervals centred at 63, 51, 43, 30 and 20 ka was mainly originating from the Great Lakes area. This suggests that sedimentation in the northern GOM was mainly influenced by hydrological and glacial processes affecting the north-eastern Mississippi River watershed.
- Lastly, over this interval the full glacial conditions (MIS 2-4), the illite- and chlorite-rich background sedimentation is interrupted by five intermittent smectite-rich periods centered at 57, 46, 40, 21, 14 ka, which suggests a westward shift of the main outflow from the Great lakes area toward the recessing north-western margin, probably related to brief re-advances and/or melting phases of the southwest margin of the LIS.

The smectite-rich intervals identified in the La Salle Basin –which are associated with most wet periods in central North America– coincided with the North Atlantic cold water and Heinrich events, when the Intertropical Convergence Zone (ITCZ) and Atlantic Warm Pool (AWP) in the GOM were seasonally displaced and extended northward during summer. These results generally support the hypotheses that summer moisture transfers in the central North America were modulated by displacements of both ITCZ and AWP during the last climatic cycle.

References

Abe-Ouchi, A., Segawa, S. and Saito, F., 2007. Climatic Conditions for modelling the Northern Hemisphere ice sheets throughout the ice age cycle. Climate of the Past 3, 423-438.

Aharon, P., 2003. Meltwater flooding events in the Gulf of Mexico revisited: Implications for rapid climate changes during the last deglaciation. Paleoceanography 18(4), PA1079. doi: 10.1029/2002PA000840.

Aharon, P., 2006. Entrainment of meltwaters in hyperpycnal flows during deglaciation superfloods in the Gulf of Mexico. Earth and Planetary Science Letters 241, 260-270.

Balsam, W.L., Deaton, B.C., Damuth, J.E., 1999. Evaluating optical lightness as a proxy for carbonate content in marine sediment cores, Marine Geology 161, 141-153.

Beard, J.H., 1973. Pleistocene-Holocene boundary and Wisconsin substages in the Gulf of Mexico. In: R.F. Black, R.P. Goldthwait, and H.B. Willman (Editors) The Wisconsin Stage (GSA Memoir 136). GSA, Boulder, CO, 277-297.

Boll, P., 2001. Assessment of Submarine slope Stability in the Gulf of Mexico using Geographic Information Systems. M.Sc. Thesis, Department of Ocean Engineering, University of Rhode Island, Narragansett, RI.

Bout-Roumazeilles, V., Cortijo, E., Labeyrie, L., Debrabant, P., 1999. Clay-mineral evidence of nepheloid layer contribution to the Heinrich layers in the Northwest Atlantic. Palaeogeography, Palaeoclimatology, Palaeoceanography 146, 211-228.

Brown, P., Kennett, J.P., Ingram, B.L., 1999. Marine Evidence for Episodic Holocene Megafloods in North America and the Northern Gulf of Mexico. Paleoceanography, 14(4), 498-510.

Bryant, W.R., Bryant, J.R., Feeley, M.R., Simmons, G.R., 1990. Physiographic and bathymetric characteristics of the continental slope, Northwest Gulf of Mexico. Geo-Marine Letters 10, 182–199.

Bryant, W.R., Lugo, J., Cordova, C. Salvador, A., 1991. Physiography and bathymetry, in Salvador, A., (Ed.), the Gulf of Mexico Basin, The Geology of North America, volume J. The geological Society of America, Boulder, 13-30.

Çağatay, M.N., Keigwin, L.D., Okay, N., Sari, E., Algan, O., 2002. Variability of clay-mineral composition on Caroline Slope (NW Atlantic) during marine isotop stages 1-3 and its paleoceanographic significance. Marine Geology 189, 163-174.

Cutler, K.B., Edwards, R.L., Taylor, F.W., Cheng, H., Adkins, J., Gallup, C.D., Cutler, P.M., Burr, G.S., Bloom, A.L., 2003. Rapid sea-level fall and deep-ocean temperature change since the last interglacial period: Earth and Planetary Science Letters 206, 253– 271.

Chiang, J.C.H., Biasutti, M., Battisti, D.S., 2003. Sensitivity of the Atlantic Intertropical convergence zone to Last Glacial Maximum boundary conditions. Paleoceanography 18, 18-11.

Clark, P.U., Marshall, S.J., Clarke, G.K.C., Hostetler, S.W., Licciardi, J.M., Teller, J.T., 2001. Freshwater forcing of abrupt climate change during the last glaciation. Science 293, 283-287.

Denton, G.H., Alley, R.B., Comer, G.C., Broecker, W.S., 2005. The role of seasonality in abrupt climate change. Quaternary Science Reviews 24, 1159-1182.

Drexler, J.W., Rose, W.I. Jr., Sparks, R.S.J., Ledbetter, M.T., 1980. The Los Chocoyos Ash, Guatemala: a major stratigraphic marker in middle America and in three ocean basins. Quaternary Research 13, 327-345.

Dyke, A.S., Prest, V.K., 1987. Late Wisconsinan and Holocene retreat of the Laurentide Ice Sheet. Geological Survey of Canada, Ottawa, Canada.

Dyke, A.S., 2004. An outline of North American deglaciation with emphasis on central and northern Canada. In Ehlers, J., Gibbard, P.L., (Eds), Quaternary Glaciations - Extent and Chronology, Part II. Elsevier B.V., Amsterdam, pp. 373-424.

Elderfield, H., Upstill-Goddard, R., Sholkovitz, ER., 1990. The rare earth elements in rivers, estuaries and coastal seas and their significance to the composition of ocean water. Geochimica et Cosmochimica Acta 54, 971-991.

Forman, S.L., Pierson, J., 2002. Late Pleistocene luminescence chronology of loess deposition in the Missouri and Mississippi river valleys, United States. Palaeogeography, Palaeoclimatology, Palaeoecology 186, 25-46.

Forman, S.L., Oglesby, R., Markgraf, V., Stafford, T., 1995. Paleoclimatic significance of late Quaternary eolian deposition on the Piedmont and High Plains, central United States. Global and Planetary Change 11, 35-55.

Flocks, J. and Swarzenski, P., 2007. Sediment collection from Orca and Pigmy Basins, Gulf of Mexico, and analyses for texture and trace-metal concentrations, July 2002, PAGE 127 Campaign. In: Winters, W.J., Lorenson, T.D., Paull, C.K. (Eds.), Initial Report of the IMAGES VIII/PAGE 127 Gas Hydrate and Paleoclimate Cruise on the RV Marion Dufresne in the Gulf of Mexico, 2–18 July 2002: U.S. Geological Survey Open-File Report 2004-1358, one DVD. online at http://pubs.usgs.gov/of/2004/1358/.

Flower, B.P., Hastings, D.W., Hill, H.W., Quinn, T.M., 2004. Phasing of deglacial warming and laurentide ice sheet meltwater in the Gulf of Mexico. Geology 32, 597-600.

Galloway, W.E., Ganey-Curry, P., Li, X., and Buffler, R. T., 2000, Cenozoic depositional evolution of the Gulf of Mexico Basin. American Association of Petroleum Geologists Bulletin 84, 1743-1774.

Galloway, W.E., 2005, Gulf of Mexico basin depositional record of Cenozoic North American drainage basin evolution. International Association of Sedimentologists Special Publication 35, 409-423.

Giosan, L., Flood, R.D., Aller, R.C., 2002. Paleoceanographic significance of sediment color on western North Atlantic drifts: I. Origin of color. Marine Geology 189, 43-61.

Goldstein, S.J., Jacobsen, S.B., 1988. Rare earth elements in river waters. Earth and Planetary Science Letters 89, 35-47.

Grimm, E.C., Watts, W.A., Jacobson Jr., G.L., Hansen, B.C.S., Almquist, H.R., Dieffenbacher-Krall, A.C., 2006. Evidence for warm wet Heinrich events in Florida, Quaternary Science Reviews 25, 2197-2211.

Gromet, L.P., Dymek, R.F., Haskin, L.A., Korotev, R.L., 1984. The North American shale composite: its compilation, major and trace element characteristics. Geochimica et Cosmochimica Acta 48, 2469–3482.

Haug, G.H., Hughen, K.A., Sigman, D.M., Peterson, L.C., Roehl, U., 2001. Southward migration of the intertropical convergence zone through the Holocene. Science 293, 1304-1308.

Hodell, D.A., Anselmetti, F.S., Ariztegui, D., Brenner, M., Curtis, J.H., Gilli, A., Grzesik, D.A., Guilderson, T.J., Muller, A.D., Bush, M.B., Correa-Metrio, A., Escobar, J., Kutterolf, S., 2008. An 85-ka record of climate change in lowland Central America. Quaternary Science Reviews 27, 1152-1165.

Jasper, J.P., Gagosian, R.B., 1990. The sources and deposition of organic-matter in the Late Quaternary Pigmy Basin, Gulf of Mexico. Geochimica et Cosmochimica Acta 54, 1117-1132.

Joyce, E.J., Tjalsma, L.R.C., Prutzman, J.M., 1990. High-resolution planktic stable isotope record and spectral analysis the last 5.35 m.y. Ocean Drilling Program site 625, northeast Gulf of Mexico. Paleoceanography 5, 507-529.

Joyce, E.J., Tjalsma, L.R.C., Prutzman, J.M., 1993. North American glacial meltwater history for the past 2.3 m.y.: Oxygen isotope evidence from the Gulf of Mexico. Geology 21, 483-486.

Kaufman, D.K., Forman, S.L., Bright, J., 2001. Age of the Cutler Dam (late Pleistocene) Alloformation, Bonneville Basin. Quaternary Research 56, 322-334.

Keigwin, L.D., Rio, D., Acton, G. et al., 1998. Proc. ODP Init. Rep. 172. ODP, College Station, TX.

Kennett, J.P., Huddlestun, P., 1972. Late Pleistocene paleoclimatology, foraminiferal biostratigraphy, and tephrochronology, Western Gulf of Mexico, Quaternary Research 2, 38-69.

Kolla, V., Perlmutter, M.A., 1993. Timing of Turbidite sedimentation on the Mississippi Fan. American Association of Petroleum Geologists Bulletin 77, 1129-1141.

Kutzbach, J.E., Gallimore, R., Harrison, S., Behling, P., Selin, R., Laarif, F., 1998. Climate and biome simulations for the past 21,000 years. Quaternary Science Reviews 17, 473-506.

Kleman, J., Fastook, J., Stroeven, A.P., 2002. Geologically and geomorphologically constrained numerical model of Laurentide Ice Sheet inception and build-up. Quaternary International 95-96, 87-98.

Knox, J.C., 1996. Late Quaternary Upper Mississippi River alluvial episodes and their significance to the Lower Mississippi River system. Engineering Geology 45, 263-285.

Knox, J.C., 2000. Sensitivity of Modern and Holocene floods to climate change. Quaternary Science Reviews 19, 439- 457.

Knox, J.C., 2003. North American palaeofloods and future floods: Responses to climate change. In: K.J. Gregory and G. Benito, Editors, Palaeohydrology: Understanding Global Change, J. Wiley and Sons, Chichester (2003), pp. 143-164.

Labeyrie, L., Shipboard Scientific Party., 2005. MD127/IMAGES-IX PAGE Cruise Report, 2002. IPEV, in preparation.

Lambeck, K., Chappell, J., 2001. Sea level change through the last glacial cycle. Science 292, 679-686.

Lea, D.W., Pak, D.K., Peterson, L.C., Hughen, K.A., 2003. Synchroneity of tropical and high-latitude Atlantic temperatures over the last glacial termination. Science 301, 1361-1364.

Lisiecki, L.E., Raymo, M.E., 2005. A Pliocene-Pleistocene stack of 57 globally distributed benthic delta 18O records. Paleoceanography 20, PA1003, doi:10.1029/2004PA001071.

Liu, K.B., Fearn, M., 2000. Reconstruction of prehistoric landfall frequencies of catastrophic hurricanes in Northwestern Florida from lake sediment records. Quaternary Research 54, 238-245.

Mallarino, G., Beaubouef, R.T., Droxler, A.W., Abreu, V., Labeyrie, L., 2006. Sea level influence on the nature and timing of a minibasin sedimentary fill (northwestern slope oft he Gulf of Mexico). American Association of Petroleum Geologists Bulletin 90, 1089-1119.

Marshall, S.J., Clarke, G.K.C., 1999. Ice sheet inception. Subgrid hypsometric parametrization of mass balance in an ice sheet model. Climate Dynamics 15, 533-550.

Marshall, S.J., James, T.S., Clarke, G.K.C., 2002. North American Ice Sheet reconstructions at the Last Glacial Maximum. Quaternary Science Reviews 21, 175-192.

Meckler, A.N., C.J. Schubert, P.A. Hochuli, B. Plessen, D. Birgel, B.P. Flower, K.-U. Hinrichs, and Haug, G.H., 2008. Glacial to Holocene terrigenous organic matter input to sediments from Orca Basin, Gulf of Mexico- a combined optical and biomarker approach. Earth and Planetary Science Letters 272, 251-263.

Miller, G.H., de Vernal, A., 1992. Will greenhouse warming lead to Northern Hemisphere ice-sheet growth: Nature 355, 244–246.

Montero-Serrano Jean Carlos, Bout-Roumazeilles Viviane, Sionneau Thomas, Tribovillard Nicolas, Bory Aloys, Flower Benjamin, Riboulleau Armelle, under review. Changes in precipitation regimes over North America during the Holocene as recorded by mineralogy and geochemistry of Gulf of Mexico sediments. Global and Planetary Change.

Montero-Serrano, J.C., Bout-Roumazeilles, V., Tribovillard, Sionneau, T., Bory, A., Riboulleau, A., Flower, B., in press. Sedimentary evidence of deglacial megafloods in the northern Gulf of Mexico (Pigmy Basin). Quaternary Science Reviews.

Muhs, D.R., Swinehart, J.B., Loope, D.B., Aleinikoff, J.N., Been, J., 1999. 200,000 years of climate change recorded in eolian sediments of the High Plains of eastern Colorado and western Nebraska. In: D.R. Lageson, A.P. Lester and B.D. Trudgill, Editors, Colorado and Adjacent Areas: Geological Society of America Field Guide 1, Geological Society of America, Boulder, CO, pp. 71-91.

Mulder, T., Syvitski, J.P.M., Migeon, S., Faugères, J.C., Savoye, B., 2003. Marine hyperpycnal flows: initiation, behaviour and related deposits: A review. Marine and Petroleum Geology 20, 861–882.

Nürnberg, D., Ziegler, M., Karas, C., Tiedemann, R., Schmidt M.W., 2008. Interacting Loop Current variability and Mississippi River discharge over the past 400 kyr. Earth and Planetary Science Letters 272, 278-289.

Otto-Bliesner, B.L., Marshall, S.J., Overpeck, J.T., Miller, G.H., Hu, A., CAPE Last Interglacial Project Members, 2006. Simulating Arctic climate warmth and ice field retreat in the last interglacial. Science 311, 1751–1753.

Paillard, D., Labeyrie, L., Yiou, P., 1996. Macintosh program makes time-series analysis easy. Eos: Transactions American Geophysical Union 77(39), 379-379.

Peltier, W.R., 1994. Ice Age Paleotopography. Science 265, 195-201.

Peterson, L.C., Haug, G.H., Hughen, K.A., Rohl, U., 2000. Rapid changes in the hydrologic cycle of the tropical Atlantic during the last glacial. Science 290, 1947-1951.

Poore, R.Z., Dowsett, H. J., Verardo, S., 2003. Millennial- to century-scale variability in Gulf of Mexico Holocene climate records. Paleoceanography 18(2), 1048, doi:10.1029/2002PA000868.

Poore, R.Z., Quinn, T.M., Verardo, S., 2004. Century-scale movement of the Atlantic Intertropical Convergence Zone linked to solar variability. Geophysical Research Letters 31, L12214, doi: 10.1029/2004GL019940.

Richey, J.N., Poore, R.Z., Flower, B.P., Quinn, T.M., 2007. 1400 yr multiproxy record of climate variability from the northern Gulf of Mexico. Geology 35, 423-426.

Rittenour, T.M., Blum, M.D., Goble, R.J., 2007. Fluvial evolution of the lower Mississippi River valley during the last 100 k.y. glacial cycle: response to glaciation and sea-level change. Geological Society of America Bulletin 119, 586-608.

Rousseau, D.-D., Kukla, G., McManus, J., 2006. What is what in the ice and the ocean?. Quaternary Science Reviews 25, 2025-2030.

Sionneau, T., 2008. Transferts Continent – Océan : Enregistrement du dernier cycle climatique par les sédiments terrigènes du Golfe du Mexique. PhD thesis, Université Lille 1. 377 p.
Online at http://tel.archives-ouvertes.fr/tel-00366377/fr/ (Revised 2009-05-29)

Sionneau, T., Bout-Roumazeilles, V., Biscaye, P.E., van Vliet-Lanoë, B., Bory, A., 2008. Clay-mineral distributions in and around Mississippi River watershed and Northern Gulf of Mexico: Sources and transport patterns. Quaternary Science Reviews 27, 1740-1751.

Sionneau, T., Bout-Roumazeilles, V., Flower, B.P., Bory, A., Tribovillard, N., Kissel, C., Van Vliet-Lanoë, B., Montero-Serrano, J.C., in revision. On the provenance of freshwater pulses in the Gulf of Mexico during the last deglaciation: Evidence from grain size and clay mineralogy. Quaternary Research.

Suter, J.R., Berryhill Jr., H.L., 1985. Late Quaternary shelf-margin deltas, northwest Gulf of Mexico. American Association of Petroleum Geologists Bulletin 69, 77-91.

Shuman, B., Bartlein, P., Webb III, T., 2005. The magnitudes of millennial- and orbital-scale climatic change in eastern North America during the Late Quaternary. Quaternary Science Reviews 24, 2194-2206.

Tribovillard, N., Algeo, T., Lyons, T.W., Riboulleau, A., 2006. Trace metals as paleoredox and paleoproductivity proxies: an update. Chemical Geology 232, 12-32.

Tribovillard, N., Bout-Roumazeilles, V., Algeo, T.J., Lyons, T., Sionneau, T., Montero-Serrano, J.C., Riboulleau, A., Baudin, F., 2008. Paleodepositional conditions in the Orca Basin as inferred from organic matter and trace metal contents. Marine Geology 254, 62-72.

Tribovillard, N., Bout-Roumazeilles, V., Sionneau, T., Montero-Serrano, J.C., Riboulleau, A., Baudin, F., 2009. Does a strong pycnocline impact organic-matter preservation and accumulation in an anoxic setting? The case of the Orca Basin, Gulf of Mexico. Comptes Rendus Geosciences 341, 1-9.

Tripsanas, E.K., Bryant, W.R., Slowey, Kim, J.W., 2006. Marine Isotope Stage 6 Canyon and Spillover Deposits of the Bryant and Eastern Canyon Systems, Northwest Gulf of Mexico: Importance of Fine-Grained Turbidites on a Delta-Fed Prograding Slope. Journal of Sedimentary Research 76, 1012-1034.

Tripsanas, E.K., Bryant, W.R., Slowey, N.C., Bouma, A.H., Karageorgis, A.P., Berti, D., 2007. Sedimentological history of Bryant Canyon area, northwest Gulf of Mexico, during the last 135 kyr (Marine Isotope Stages 1-6): A proxy record of Mississippi River discharge. Palaeogeography Palaeoclimatology Palaeoecology, 246, 137-161.

Ziegler M., Nürnberg D., Karas C., Tiedemann R., Lourens L.J., 2008. Persistent summer expansion of the Atlantic Warm Pool during glacial abrupt cold events. Nature Geoscience 1(9), 601-605.

3.4.2. Mineralogical records of the atmosphere-ocean-continent interactions in the northern Gulf of Mexico during the present and last interglacial period – a first approach*

Abstract

Sedimentological records from La Salle Basin (core MD02-2549) in the northern Gulf of Mexico (GOM) were investigated in order to reconstruct the changes in the atmosphere-ocean-continent interactions in the northern GOM during the present and last interglacial period [Marine Isotope Stages (MIS) 1 and 5e]. Our mineralogical data enable us to track down the origin and changes of the main terrigenous transfers from North America toward the GOM via the Mississippi River. Such modifications of the main detrital sources during the MIS 1 and 5e likely record oscillations of the main trajectories of the moisture flux and migrations of the precipitation belt over North America, themselves constrained by atmospheric configuration (Jet Stream, Bermuda subtropical High and ITCZ position) and subtropical oceanic hydrological properties (extension of the Atlantic Warm Pool). Thus, the respective contributions of smectite vs. illite and chlorite [S/(I+C) ratio] and of kaolinite reveal notable modifications of moisture transfer throughout the MIS 1 and 5e, which can be summarized by two simple atmosphere-ocean coupling synoptic patterns. Finally, a change in the atmospheric configuration, and therefore in the erosion regime over the North American continent, is suggested to explain the remarkable differences in terrigenous sources records in La Salle Basin during the present and last interglacial period.

Keywords: Mississippi River, La Salle Basin, atmospheric configuration, clay mineral, last interglacial, Holocene.

* in preparation as **Montero-Serrano Jean Carlos**, Bout-Roumazeilles Viviane, Tribovillard Nicolas, Sionneau Thomas, Bory Aloys, Flower Benjamin, Riboulleau Armelle. *Mineralogical records of the atmosphere-ocean-continent interactions in the northern Gulf of Mexico during the present and last interglacial period*.

Introduction

The interaction of three main air masses controls the general climatic patterns over the North American continent: the warm and moist GOM air-mass, the dry and mild Pacific air-mass, and the dry, cold Arctic air-mass (eg., Knox, 2003). However, the warm and moist air masses coming from the GOM are the dominant source of moisture over central North America, supplying almost the entire annual precipitation (Yu et al., 1997). The meridian transfer of this moist air masses, and hence precipitation distribution, is constrained by (1) the average atmospheric configuration, resulting from the respective position of the polar Jet Stream, the Bermuda High pressure cell, the Intertropical Convergence Zone (ITCZ), and (2) changes in subtropical oceanic hydrological properties (sea surface temperature or SST, sea surface salinity or SSS) that resulting from the seasonal extension of the warm waters constituting the so-called Atlantic Warm Pool (AWP) (e.g., Forman et al., 1995; Ziegler et al., 2008). All these oceanic and atmospheric characteristics are seasonally modulated. In the western tropical Atlantic Ocean, the AWP reaches its northern position during boreal summer when the ITCZ is located in its northern position, whereas these tropical waters are restricted to the southeastern GOM during boreal winter when the ITCZ is situated southward (Wand and Enfield, 2001; Poore et al., 2004; Wang et al., 2007; Nürnberg et al., 2008; Ziegler et al., 2008).

A large proportion of precipitations falling over North America returns back to the GOM via the Mississippi and Missouri Rivers whose watersheds drain almost half the US. Runoff will promote the remobilization of soils or sediment particulates that are further carried as suspended loads through the previously mentioned fluvial systems. The Mississippi River discharge fluctuations are therefore controlled by oscillations in the precipitation belt between the north-western and eastern parts of the Mississippi River watershed, linked to modifications of both atmospheric configuration and oceanic properties that drive the meridian moisture transfer across North America (Knox, 2003). Subsequently, the mineralogy, geochemistry and nature of the terrigenous components transported by the Mississippi River toward the GOM are characteristics of the drainage areas. These aspects indicate that the terrigenous sediments deposited in the GOM have distinct mineralogical and geochemical signatures characterizing both the petrology of their parent-bedrock (Gustavsson et al., 2001; Sionneau et al., 2008). Thus, variations of the clay-mineral assemblage deposited in the northern GOM may reflect changes in the respective contributions of two main mineralogical provinces (Sionneau et al., 2008): (1) The north-western Mississippi and

Missouri river watershed is characterized by high smectite contents, which reflects the composition of Cretaceous, Tertiary and Pleistocene bedrocks, (2) The northeastern province corresponding to the Great Lakes area and the Ohio and Tennessee rivers catchment mainly delivers illite and chlorite, resulting from strong physical weathering and erosion of Palaeozoic rocks. At present-day terrigenous sedimentation in the northern GOM mainly originates from the northwestern Mississippi and Missouri watershed with minor contribution of the northeastern source area via the Mississippi River (Sionneau et al., 2008). Recent studies in the GOM revealed that their respective contributions have varied during the last climatic cycle, in response to glacial processes and to slight changes in precipitation distributions. The compositional variations in the relative abundance of clay minerals and chemical composition (organic and mineral) in the GOM sediments can thus be used in order to retrace the modifications of the main detrital source (Sionneau et al., 2008; Sionneau et al., in revision; Montero-Serrano et al., in press), and therefore, the variations of the main trajectories of the moisture flux and the migration of the precipitation belt over North America.

On this basis, the GOM is well-situated for investigating changes in both low- and high-latitude atmospheric circulation, and its response on the erosional processes prevailing in continental source areas. Here, we present records of clay mineral assemblage from La Salle Basin sediments (core MD02-2549; 26°25.68'N, 92°33.94'W; 2049 m water depth) during the past 150 ka. This site, situated on the Louisiana continental slope around 400 km southwest of the present-day Mississippi Delta in the northern GOM (Fig. 3.23a), is sensitively located to collect continuously a smoothed and averaged terrigenous supply from the North American continent, via the Mississippi River, as well as record the tropical oceanic response via the Loop Current. From this point of view, the confrontation of our clay mineral records with other marine and continental sequences, provide new insights to decipher the evolution of the atmosphere-ocean-continent interactions in North America through time, and to establish schematic scenarios or models of these interactions with the subtropical hydrology and the high-latitude climatic variability. We focus on the slight changes in the climatic characteristic (e.g., atmospheric configuration) happened between the Marine Isotope Stages (MIS) 1 and 5e, or on the present and last interglacial period, which could be reflected on the terrigenous transfers from the North American continent to the GOM. MIS 1 and 5e are of considerable interest to both paleoclimatologists and climate modeller because these are thought to be the last time global climates were significantly warmer than present, and is a possible analog for future warm climates. This work is intended to provide a basis for

improvement of atmospheric general circulation models that are critical for modelling of future climate.

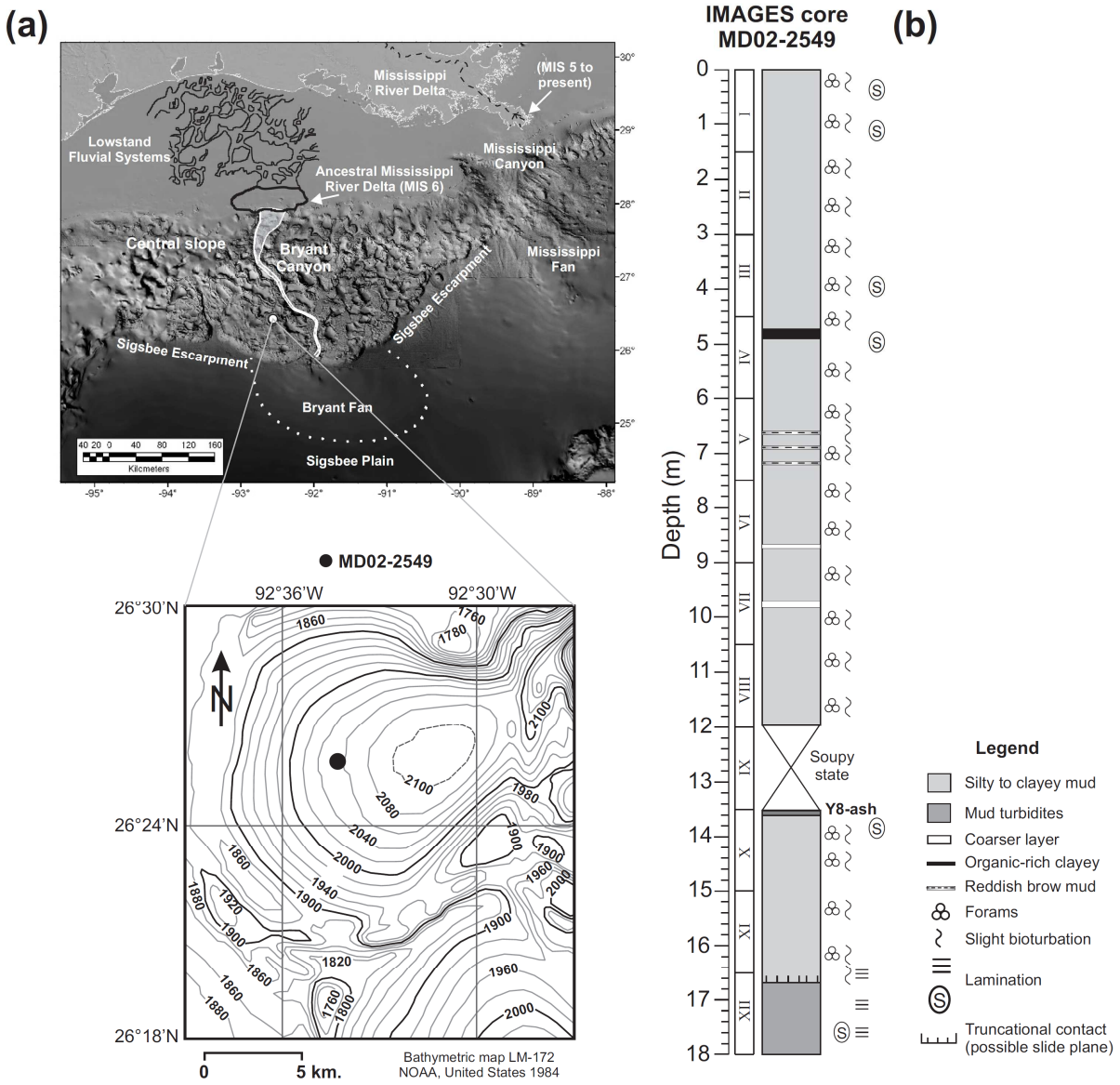

Fig. 3.23. (**a**) Morphological map of the seafloor in the northern GOM (Tripsanas et al., 2007), along with an ancient lowstand fluvial system and an ancestral Mississippi River Delta on the shelf, and bathymetric map of the La Salle Basin showing locations of sediment core MD02-2549. Contour in meters. (**b**) Lithological log of core MD02-2549 between 0-18 m showing the sedimentological characteristics.

Methods

We sampled core MD02-2549 (Calypso II type) collected on the centre of the Salle Basin during the 2002 cruise of the R/V Marion Dufresne, as part of the International Marine Past Global Changes Study (IMAGES) program. The uppermost 1629 cm of the core are composed of massive brownish to light greenish gray silty to clayey mud with foraminifers and slight bioturbations, whereas the lower part contains greenish gray laminated silty clay

with rare biotubations (Fig. 3.23b). Some foraminifer-rich and sandy layers interpreted as small turbidites occur throughout the core at 868, 968 and 983 cm. Ash layer is observed between 1353 and 1361 cm (Fig. 3.23b). Organic-rich clayey and reddish brow muds are observed from 460-480 cm and 660-720 cm, respectively (Fig. 3.23b). The sediment samples were taken every ~10 cm throughout the upper 1750 cm of the core.

The chronostratigraphy of core MD02-2549 (Table 4.1; Fig. 4.2) is based on tuning of the calcium carbonate content ($CaCO_3$) and spectral lightness (L*) distribution to the global benthic reference stack LR04 (Lisiecki and Raymo, 2005). Further support of the age model comes from in the upper part (0-880 m) by the comparison of $\delta^{18}O$ profiles of planktonic foraminifera (*Globogerinoides ruber*) with the nearby core JPC-31 (Bryant Cayon; Tripsanas et al., 2007), the Y8-ash layer (84 ka; Drexler et al., 1980), and by the comparison of magnetic susceptibility profiles with the core MD02-2575 (DeSoto Cayon; Nürnberg et al., 2008). Thus, using the Analyseries program (Paillard et al., 1996), we have defined 14 age control points for the time period covering MIS 1-6 which are listed in Table 4.1. A continuous timescale was obtained by linear interpolation between the age control points (Fig. 3.24a).

Table 3.2. Age-depth points for core MD02-2549 used to derive chronology shown in Fig. 3.24.

Depth of control points (cm)	Age (ka)	Sedimentation rates (cm/ka)
0.0	0.0	
299.1	13.6	22.0
344.4	16.0	19.0
659.0	31.5	20.3
738.6	36.4	16.3
797.1	41.6	11.3
932.5	50.0	16.1
986.5	56.9	7.8
1112.6	71.3	8.7
1354.4	83.9	19.3
1403.6	92.2	5.9
1490.6	105.8	6.4
1527.2	115.4	3.8
1612.7	131.8	5.2
1725.6	147.6	7.1

Clay-mineral associations (smectite, illite, kaolinite and chlorite) were studied using X-ray diffraction following established protocols (Bout-Roumazeilles et al., 1999). Grain size analyses, report here as mode (μm) grain-size, were carried out on the carbonate-free fraction

of the sediment using a Malvern Mastersizer 2000 laser diffractometer. Sample preparation and optical settings for the Mastersizer 2000 followed Montero et al. (in press).

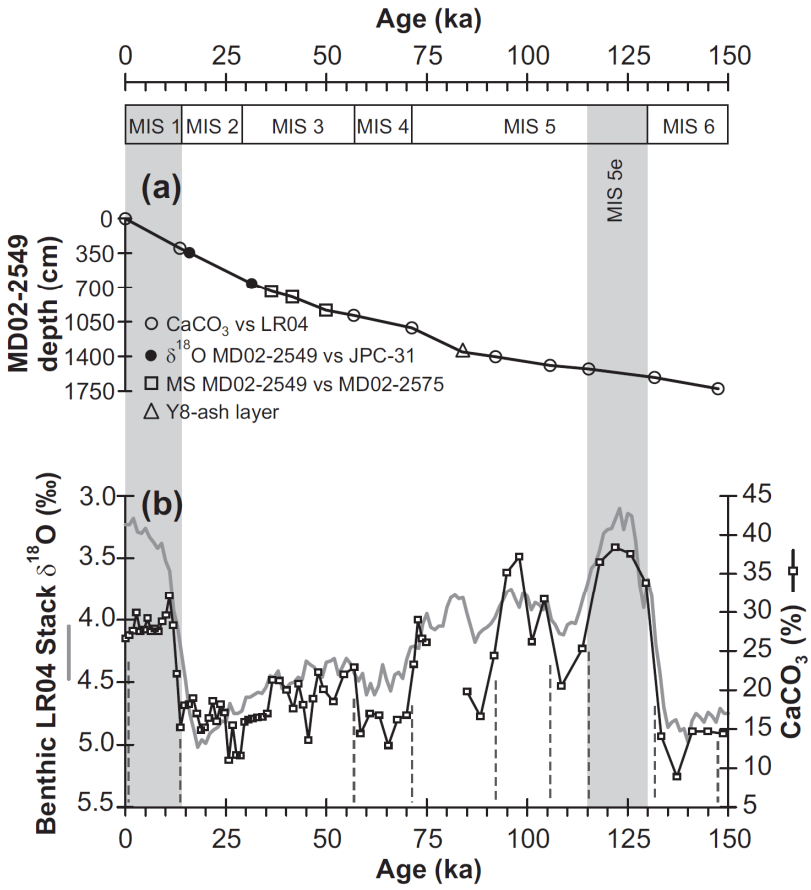

Fig. 3.24. Chronostratigraphy of core MD02-2549 from the La Salle Basin. (**a**) The Age-depth relationship suggests continuous and uniform sedimentation over the past 150 ka (see Table 3.2). (**b**) Tuning of the calcium carbonate ($CaCO_3$) distribution to the global benthic reference stack LR04 (Lisiecki and Raymo, 2005) (grey line) used for the chronostratigraphy.

Results and discussion

Clay mineral and mode grain-size distributions from core MD02-2549 are illustrated in Fig. 3.25-3.26. One remarkable feature of the record is the noticeable differences in the clay-mineral distribution between the MIS 1 and MIS 5e (Fig. 3.25-3.26). In the MIS 1 the clay assemblage is markedly dominated by smectite [77-84%; S/(I+C) up to 9.2], where sediment is typically silty (4.5µm<grain-size mode<5.5µm; Fig. 3.26b). In contrast, although smectite is the main component of the clay-mineral fraction [63-76%; S/(I+C) up to 4.8], MIS 5e is characterized by enhanced contributions of illite (up to 14%), kaolinite (up to 17%) and chlorite (up to 8%), where the detrital fraction is slightly finer (grain-size mode<4µm; Fig.

3.26b). Furthermore, the S/(I+C) ratios is kept constant about 3.1 and 4.8 during all MIS 5 (Fig. 3.26d).

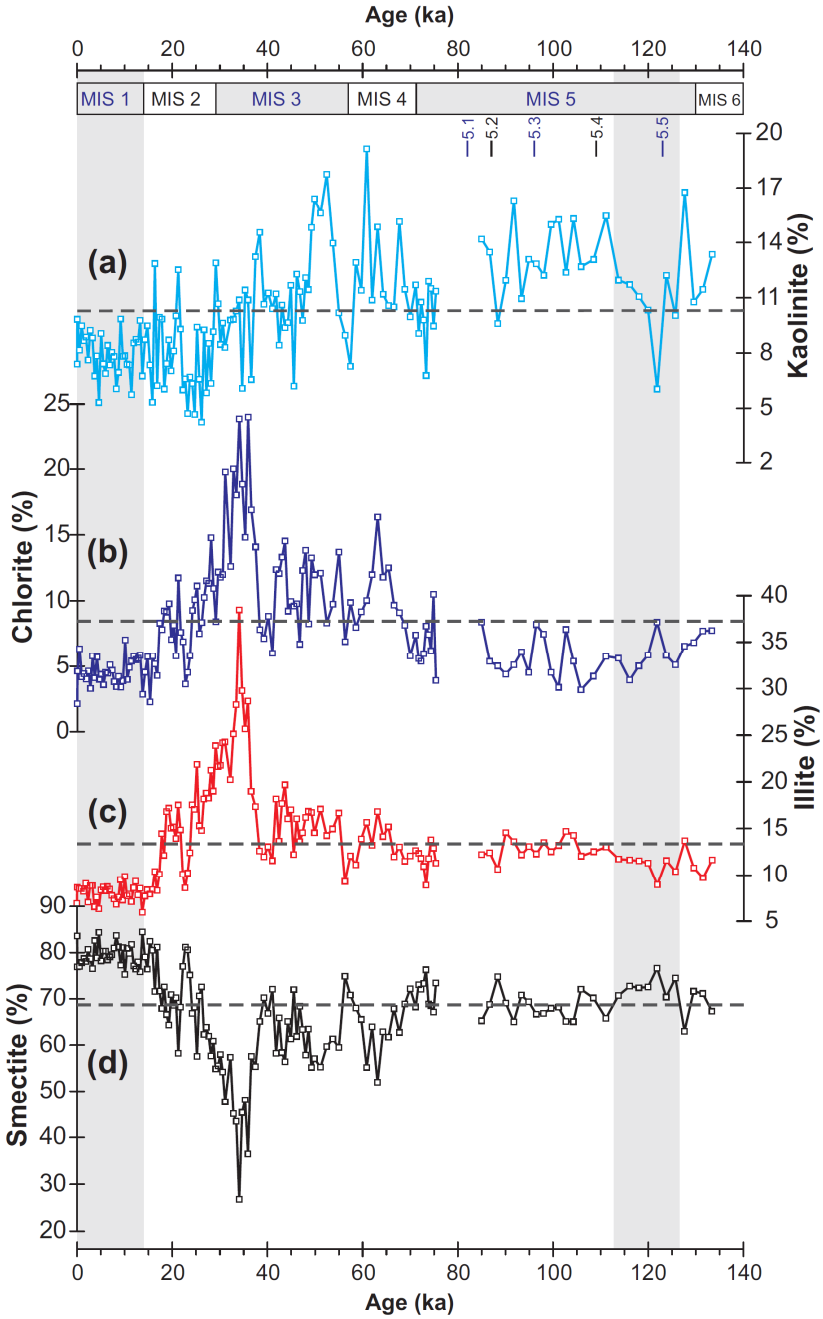

Fig. 3.25. Clay-mineral assemblages from the La Salle Basin (core MD02-2549). The horizontal dotted lines indicate the mean concentrations for each clay mineral.

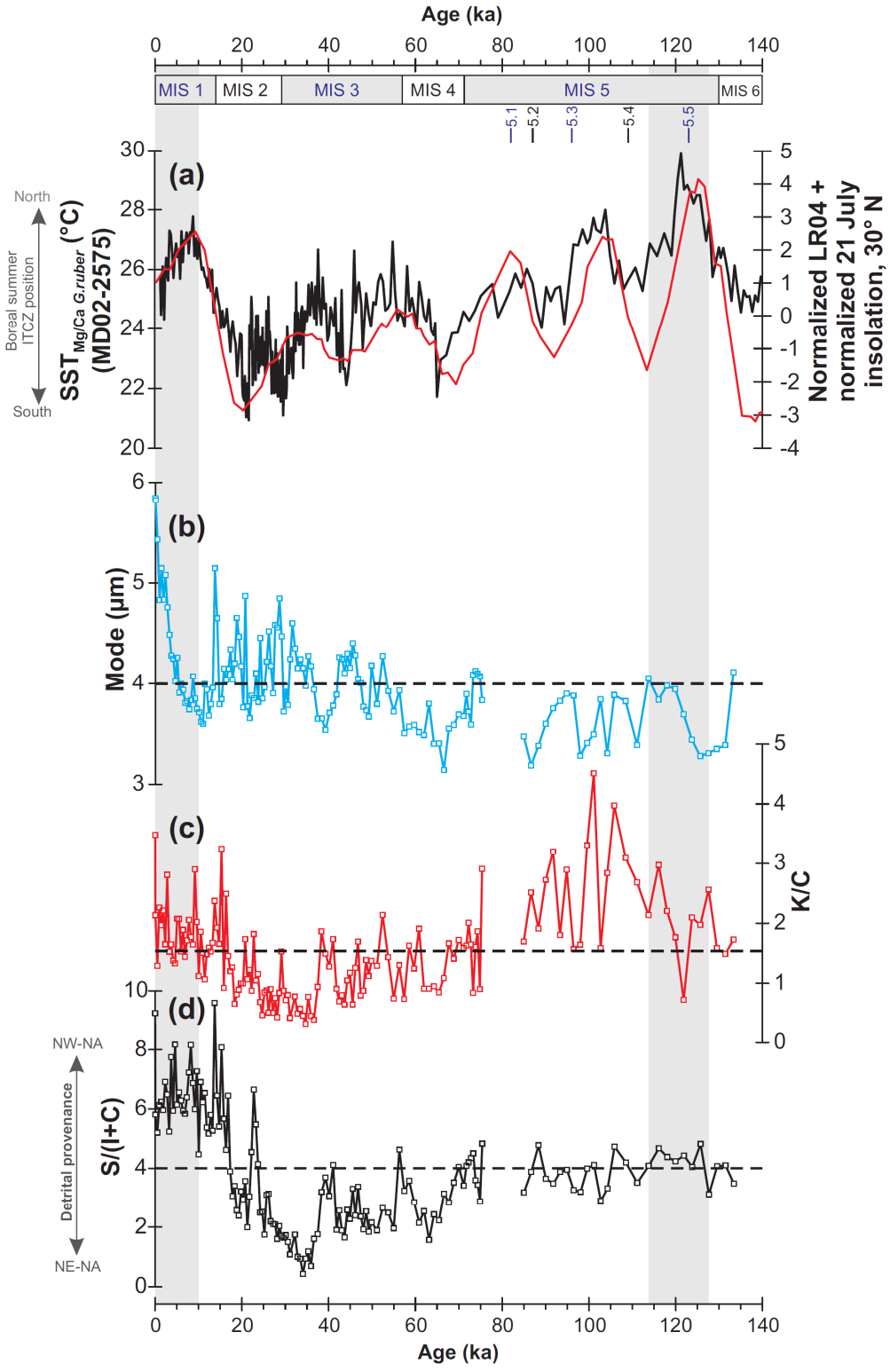

Fig. 3.26. Sedimentological parameters from the La Salle Basin (core MD02-2549) for last 150 ka. (**a**) Mg/Ca-based SST (°C) record from MD02-2575 (Ziegler et al., 2008) and the sum of the normalized LR04 stack (representing here glacial/interglacial-related North American ice volume variability) and the normalized 21 July insolation at 30°N (grey line). (**b**) Grain-size mode. (**c**) Calculated kaolinite/chlorite ratio (K/C). (**d**) Calculated smectite/illite+chlorite ratio [S/(I+C)]. The horizontal dotted lines indicate the mean values for each proxy.

Overall, the responses of low- and high-latitude regions to global warming during the last interglacial period (MIS 5e ~125 ka) have been actively debated. It has been considered that the last interglacial is not a perfect analogous to the present interglacial period (the Holocene), i.e. climate was ≥2°C warmer than present (Otto-Bliesner et al., 2006), and sea level was 4-6 m higher than present (Thompson and Goldstein, 2005). Although other works emphasize that the global mean sea surface temperatures was not thought to have been significantly higher than in the Holocene, hence the thermal expansion difference from today was small (e.g., Overpeck et al., 2006). In this context, our mineralogical data [e.g., S/(I+C) ratio] also reveal notable differences between the present and last interglacial period. Several hypothesis and/or factors could explain this disagreement:

(1) Changes in the fluvial architecture of the Mississippi River, location of the main river discharges and sea-level stand: the Mississippi River watershed currently drains North America between the Rocky and Appalachian Mountains to the northern GOM. Recent works on the evolution of the Mississippi River suggest that this fluvial architecture has been kept during the last climatic cycle, after that during MIS 5 both the Ohio and Missouri rivers assembled the Mississippi in the northern Mississippi valley (Rittenour et al., 2007; M. Blum, personal communication, 2009), and that the discharges of the Mississippi River switched – due to sea-level rise at MIS 5 – from a location north of the Bryant Canyon to updip of the present Mississippi Canyon (Tripsanas et al., 2007). Therefore, differences due to changes in the fluvial architecture could be discarded.

(2) The presence of great turbidites in the stratigraphic records: the sedimentation – dominated by hemipelagic sediments – is thought to have been continuous because of the lack of sharp lithological breaks or sedimentological indicators of hiatus or mass flow transport (e.g., turbidites) in these parts of the core. In addition, Tripsanas et al. (2007) suggest that the sea-level rise at MIS 5 led to confinement of river-sourced sediments to the widespread continental shelf of the northwest GOM, and consequently to the cessation of gravity flows, providing further support to our interpretation.

(3) Differences in the glacial activity during the MIS 2 and 6: based on the evolution of the southern margin of the Laurentide Ice Sheet (LIS) from 19.1 to 12.9 ka (Dyke, 2004; Sionneau et al., in revision), and the main continental clay mineral provinces of North America (Sionneau et al., 2008), we hypothesize that the MIS 2 ice advance in the Dakotas and Iowa region (e.g., Des Moines and James glacial lobes) could be probably more extensive than during the MIS 6, exposing more smectite-rich glacial till over the Missouri River basin during the subsequent southern LIS retreat, increasing thus the amount of the

smectite-rich sediments that the Missouri and Mississippi rivers could transport to the GOM during the MIS 1. Much of the region where these glacier lobes advanced contains Cretaceous Pierre Shale Formation, which is rich in smectite (T. Rittenour, personal communication, 2009). Although this hypothesis could explain the disagreement in the clay-mineral composition between the MIS 1 and 5e, we lack of continental evidences that confirm if MIS 2 and 6 glacial lobes activities influenced the exposed sediment in the Missouri River basin enough to cause the observed changes in the clay-mineral assemblage. This dynamic in the glacial erosion is difficult to interpret over the North American continent because the glacier ice advance/retreat or megaflood induced erosion could modify and/or completely erase the original depositional signature.

Another variant is that mineralogical discrepancies may also reflect some differences in the available terrigenous stock produced during the previous glacial periods. Actually, the extension of the LIS during stage 6 was probably different when compared to stage 2. The total ice-volume was similar but it seems that the European ice-sheet was more extended during stage 6 (J. McManus, personal communication, 2009). This observation implies that the other ice-sheet must have been reduced in Antarctic, in the Barents Sea or even the LIS even if there are few evidences so far. Nevertheless the magnetic susceptibility in the northeastern GOM (DeSoto Canyon) displays a rather different signal during MIS 6 compared with the others full glacial periods (Nurnberg et al., 2008) suggesting reduced terrigenous supply into the GOM due to discharges. This observation is in agreement with the hypothesis of a modification of the available detrital stock, with typical primary clay mineral being stocked on the continent during MIS 6 due to the low fluvial discharge and being remobilized during deglaciation, explaining the smectite-depleted MIS 5e. However, we thought that other factors, such as the atmospheric configuration may also play an important role in the erosional processes over North America during these times.

(4) Modifications of the erosion regime over the North American continent: according to present-day atmospheric configurations, we also hypothesize that the hydrologic variability, and therefore, the modifications of the erosion regime recorded over the North American continent during MIS 1 and 5e are directly dependent of the migration of the precipitation belt over the continent, which affect two distinct clay-mineral provinces (i.e. northwestern and northeastern provinces). Thus, this hypothesis seems to be most probable to explain the remarkable differences in terrigenous sources between the MIS 1 and 5e. Variations in atmospheric circulation, position and intensity of the Bermuda high, Jet Stream, ITCZ and AWP, can provide a coherent mechanism that can control the amount of moisture

transport to and precipitation over the North American continent. This disagreement, notably in the configuration of atmospheric circulation patterns during these time, is most likely due to greater seasonal temperature variations in the Northern Hemisphere (Denton et al., 2005) during the MIS 5e, related to changes in orbital parameters from today (greater obliquity and eccentricity), and additionally, to positive feedback mechanisms potentially link rapid growth of sea ice with the intensity of the thermohaline circulation (Ziegler et al., 2008).

Consequently, the respective contributions of smectite vs. illite and chlorite [S/(I+C) ratio] and of kaolinite from La Salle Basin were thus used to document the continental-scale shifts of the moisture transferences over North America during the MIS 1 and 5e. Additionally, we consider several previously published isotopic, palynological, sedimentological and loess-paleosol data from both continental and marine records (see below) in order to retrace the interglacial variations in the main ocean-continent moisture transfer trajectories over the North American continent (Fig. 3.27).

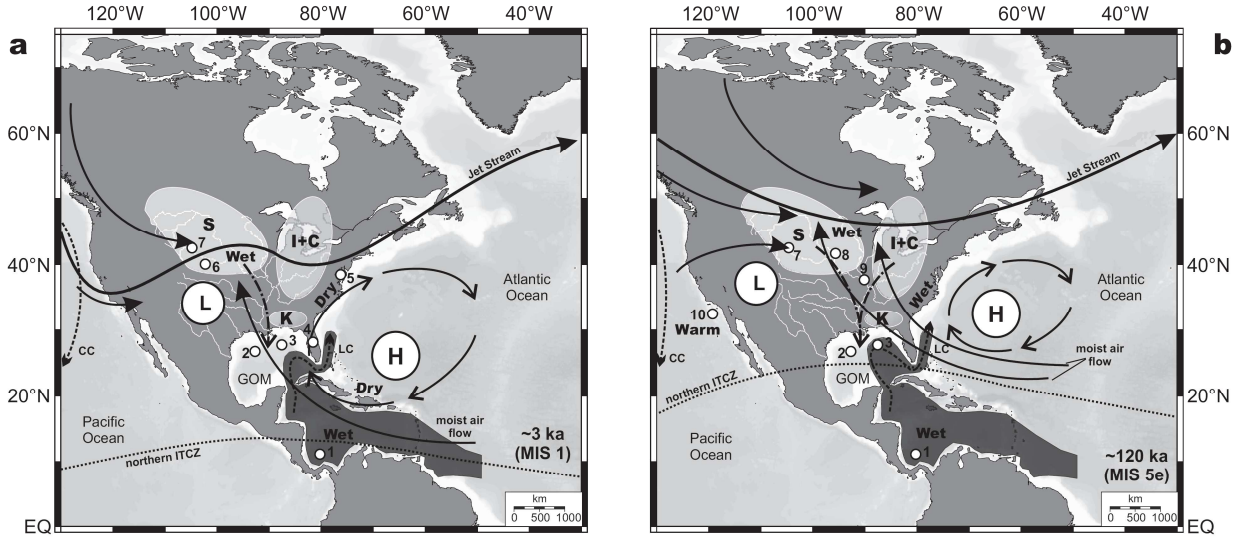

Fig. 3.27. Schematic reconstructions of the atmosphere-ocean-continent interactions from middle-latitude North America during the present and last interglacial period, and their paleoclimatic implications. (**a)** Configuration during predominant wet periods in central North America (MIS 1). (**b**) Configuration during around 120 ka (MIS 5e). Note the anomalous wet period happened largely of North America. The Jet Streams denote the approximate boundaries of air masses from tropical, pacific and polar-source regions and locations of the areas with the main moisture transfers over the North American continent. The generalized position of the AWP and ITCZ for Northern Hemisphere summer in the time also is indicated (Nürnberg et al., 2008; Ziegler et al., 2008). Numbers at each sites show location of selected localities discussed in this study: (1) western Caribbean Sea (ODP-999; Schmidt et al., 2004), (2) La Salle Basin (MD02-2549), (3) DeSoto Canyon (MD02-2575; Nürnberg et al., 2008; Ziegler et al., 2008), (4) Lake Tulane (Florida; Grimm et al., 2006), (5) Chesapeake Bay (northeastern of the North America; Willard et al., 2005), (6) North American Great Plains (Nordt et al., 2008), (7) northern High Plains and Colorado Piedmont (Forman et al., 1995; Muhs et al., 1999), (8) Missouri valley (Forman and Pierson, 2002), (9) Mississippi River valley (Forman and Pierson, 2002), (10) tropical Pacific (ODP-1014; Yamamoto et al., 2007).

− **MIS 1**. During the present interglacial period, the La Salle Basin terrigenous sedimentation show a strong increase in the relative content of smectite [S/(I+C) up to 9.2; Fig. 3.26d]. According to this mineralogical signature, MIS 1 is characterized by major modifications of provenance of the main detrital supply suggesting a westward shift of the main outflow from the north-eastern Mississippi watershed toward the north-western area, encompassing the Mississippi and Missouri provinces. This result suggests that the main moisture transfer reached the central part of North America during this time, in agreement with a northward propagation of the AWP and paleo-ITCZ position (Fig. 3.26a; Ziegler et al., 2008). In absence of agents, such as the LIS or meltwater discharges, and by comparison with present-day atmospheric configurations, the Jet Stream and the Bermuda High must have been located to the north and southwest respectively, while the low pressure was displaced eastward (Fig. 3.27a) in agreement with models proposed by Forman et al. (1995) and Knox (2003). This synoptic pattern will promote transfer of moist air from the GOM and nearby tropical waters toward the central North America. The reconstructed Jet Stream pattern is thus characterized mainly by a strong meridional component (north-south) (Fig. 3.27a). At present-day this configuration would involve strong precipitations and flooding in the central North America (Knox, 2003). This reconstruction is supported by organic carbon data (ΔC_4%) on soils form the North American Great Plains (Nordt et al., 2008) which indicate an enhanced moisture flux from the GOM toward central North America, whereas the strong decrease in the *Quercus* pollen content from the southeastern (Lake Tulane; Grimm et al., 2006) and northeastern (Chesapeake Bay; Willard et al., 2005) region of the North America (Fig. 3.27a) suggest the development of drought conditions along the eastern coast of North America. In addition, sea surface salinity from Caribbean region also indicates wet conditions during this time (Schmidt et al., 2004).

− **MIS 5e**. Our mineralogical proxies [S/(I+C)<4.8; Fig. 3.26d] indicate a mixed provenance of detrital particles or a differential contributions by the Missouri vs. Ohio rivers, during the last interglacial period (~127-116 ka), i.e. mainly from the north-western Mississippi River watershed but with one notably contribution of the north-eastern Mississippi watershed. These results suggest a simultaneous enhanced moisture flux across east to central North America, during this time. Loess-paleosol records of the Mississippi and Missouri basins (Forman and Pierson, 2002) and eastern Colorado (Muhs et al., 1999), and notably the Sangamon paleosols – interglacial soil with weathering characteristics comparable to the modern-day soil (Muhs et al., 2001), which can be traced from Indiana to Great Plains (Ruhe, 1974a,b) – also suggest a simultaneous increased precipitation across east to central

North America during the last interglacial period. From this point of view, we suggested that the Jet Stream and the Bermuda High were situated to the northernmost and slightly to the northeast of their present-day positions, respectively (Fig. 3.27b). This synoptic pattern is likely conducive for routing moist air from the tropical Atlantic, east Caribbean region and northeastern GOM toward both the eastern and central part of North America (Fig. 3.27b). The Jet Stream pattern is characterized by a main meridional component but with a strong zonal (west-east) westerly circulation (Pacific air-mass) that tends to suppress the magnitudes of precipitation and large floods in the continent interior because it serves as a wedge minimizing the collision between warm, moist air from more tropical source regions and cold, dry air from Canadian source regions (Fig. 3.27b). It is worth noting that this zonal westerly circulation tends to be associated with strong El Niño development in the tropical Pacific during this time (Yamamoto et al., 2007). Forman et al. (1995) emphasize that moisture from the Atlantic Ocean does generally not penetrate into the central North America. However, an anomalously strong high pressure situated over the western Atlantic could propagate an easterly low-level Atlantic moisture flux, perhaps linked to that the AWP and paleo-ITCZ reached their maximum latitudinal positions in response to higher boreal summer insolation during this time (Fig. 3.26a; Ziegler et al., 2008), explains why the moisture transfer from the tropical Atlantic, east Caribbean region and northeastern GOM penetrate into central North America as suggested by our model. Our interpretations are also in agreement with (1) the paleoclimatic interpretations inferred on the Sangamon paleosols extension, which reflect during all MIS 5 a longer, warmer, or wetter last interglacial period over almost all Mississippi River watershed region (Ruhe, 1974a,b; Muhs et al., 1999; Hall and Anderson, 2000), and (2) wet periods in the Caribbean region (Schmidt et al., 2004).

Conclusions

The comparison of our dataset with previously published results and with the Holocene configuration (Montero et al., under review) enables us to propose two synoptic atmosphere-ocean patterns which may explain the observed discrepancies in clay-mineral assemblages between the MIS 5e and Holocene, and may reconciliate some apparently conflicting findings on stage 5e. Furthermore, these models support the hypothesis over the strong link between high-latitude climate processes and subtropical marine hydrology during the last climatic cycle. Within this context, we suggest that interglacial atmosphere-ocean-continent interactions, recorded in the northern GOM, are closely connected to the general

location of the Jet Stream, Bermuda subtropical high, ITCZ and AWP, confirming the major role of the atmosphere as a vector of rapid climatic variability. Finally, these new insights raise several questions that are still under debate.

Acknowledgements

We thank Yvon Balut, the Institut Paul-Emile Victor (IPEV), the officers and crew of the R/V Marion Dufresne and the IMAGES program for core collection. We thank the technical staff of the Géosystèmes lab for their laboratory assistance. We also thank Daniel Muhs, Michael Blum and Tammy Rittenour for their comments and suggestions. Funding for this research was provided by: (1) the UMR Géosystèmes of the Université Lille 1 (France), and (2) the Programme Alban, the European Union Programme of High Level Scholarships for Latin America, scholarship No. E06D100913VE. VBR thanks Laurent Labeyrie for initiating the IMAGES -PAGE cruise.

References

Baxter, C.D.P., King, J.W., Silva, A.J., Bryant, W.R., 2003. Investigation of the age of submarine slope failures in the Gulf of Mexico. Proceedings of the 13th International Offshore and Polar Engineering Conference, Honolulu, HI, May 25–30, pp. 1132–1139.

Bout-Roumazeilles, V., Cortijo, E., Labeyrie, L., Debrabant, P., 1999. Clay-mineral evidence of nepheloid layer contribution to the Heinrich layers in the Northwest Atlantic. Palaeogeography, Palaeoclimatology, Palaeoceanography 146, 211-228.

Denton, G.H., Alley, R.B., Comer, G.C., Broecker, W.S., 2005. The role of seasonality in abrupt climate change. Quaternary Science Reviews 24, 1159-1182.

Drexler, J.W., Rose, W.I. Jr., Sparks, R.S.J., Ledbetter, M.T., 1980. The Los Chocoyos Ash, Guatemala: a major stratigraphic marker in middle America and in three ocean basins. Quaternary Research 13, 327-345.

Dyke, A.S., 2004. An outline of North American deglaciation with emphasis on central and northern Canada. In Ehlers, J., Gibbard, P.L., (Eds), Quaternary Glaciations - Extent and Chronology, Part II. Elsevier B.V., Amsterdam, pp. 373-424.

Forman, S.L., Pierson, J., 2002. Late Pleistocene luminescence chronology of loess deposition in the Missouri and Mississippi river valleys, United States. Palaeogeography, Palaeoclimatology, Palaeoecology 186, 25-46.

Forman, S.L., Oglesby, R., Markgraf, V., Stafford, T., 1995. Paleoclimatic significance of late Quaternary eolian deposition on the Piedmont and High Plains, central United States. Global and Planetary Change 11, 35-55.

Gustavsson, N., Bølviken, B., Smith, D.B., Severson, R.C., 2001. Geochemical landscapes of the conterminous United States - New map presentations for 22 elements. U.S. Geol. Survey Prof. Paper, 1648. U.S. Department of the Interior.

Grimm, E.C., Watts, W.A., Jacobson Jr., G.L., Hansen, B.C.S., Almquist, H.R., Dieffenbacher-Krall, A.C., 2006. Evidence for warm wet Heinrich events in Florida, Quaternary Science Reviews 25, 2197-2211.

Grossman, J., 2009. National Geochemical Atlas: The geochemical landscape of the conterminous United States derived from stream sediment and other solid sample media analyzed by the National Uranium Resource Evaluation (NURE) program. U.S. Geological Survey Open-File Report 98-622. Online at http://tin.er.usgs.gov/geochem/about.php?group=Analyses+by+ICP%2FAcid+dissolution (Revised 2009-04-01)

Hall, R.D., Anderson, A.K., 2000. Comparative soil development of Quaternary paleosols of the central United States. Palaeogeography, Palaeoclimatology, Palaeoecology 158, 109-145.

Knox, J.C., 2003. North American palaeofloods and future floods: Responses to climate change. In: K.J. Gregory and G. Benito, Editors, Palaeohydrology: Understanding Global Change, J. Wiley and Sons, Chichester (2003), pp. 143-164.

Lisiecki, L.E., Raymo, M.E., 2005. A Pliocene-Pleistocene stack of 57 globally distributed benthic delta 18O records. Paleoceanography 20, PA1003, doi:10.1029/2004PA001071.

Montero-Serrano, J.C., Bout-Roumazeilles, V., Tribovillard, Sionneau, T., Bory, A., Riboulleau, A., Flower, B., in press. Sedimentary evidence of deglacial megafloods in the northern Gulf of Mexico (Pigmy Basin). Quaternary Science Reviews.

Muhs, D.R., Bettis III, E.A., Been, J., McGeehin, J.P., 2001. Impact of Climate and Parent Material on Chemical Weathering in Loess-derived Soils of the Mississippi River Valley. Soil Science Society of America Journal 65, 1761-1777.

Muhs, D.R., Swinehart, J.B., Loope, D.B., Aleinikoff, J.N., Been, J., 1999. 200,000 years of climate change recorded in eolian sediments of the High Plains of eastern Colorado and western Nebraska. In: D.R. Lageson, A.P. Lester and B.D. Trudgill, Editors, Colorado and Adjacent Areas: Geological Society of America Field Guide 1, Geological Society of America, Boulder, CO, pp. 71-91.

Nordt, L., Von Fischer, J., Tieszen, L., Tubbs, J., 2008. Coherent changes in relative C4 plant productivity and climate during the late Quaternary in the North American Great Plains. Quaternary Science Reviews 27, 1600-1611.

Nürnberg, D., Ziegler, M., Karas, C., Tiedemann, R., Schmidt M.W., 2008. Interacting Loop Current variability and Mississippi River discharge over the past 400 kyr. Earth and Planetary Science Letters 272, 278-289.

Otto-Bliesner, B.L., Marshall, S.J., Overpeck, J.T., Miller, G.H., Hu, A., CAPE Last Interglacial Project Members, 2006. Simulating Arctic climate warmth and ice field retreat in the last interglacial. Science 311, 1751–1753.

Overpeck, J.T., Otto-Bliesner, B.L., Miller, G.H., Muhs, D.R., Alley, R.B., Kiehl, J.T., 2006. Paleoclimatic Evidence for Future Ice-Sheet Instability and Rapid Sea-Level Rise". Science 311, 1747 – 1750.

Paillard, D., Labeyrie, L., Yiou, P., 1996. Macintosh program makes time-series analysis easy. Eos: Transactions American Geophysical Union 77(39), 379-379.

Poore, R.Z., Quinn, T.M., Verardo, S., 2004. Century-scale movement of the Atlantic Intertropical Convergence Zone linked to solar variability. Geophysical Research Letters 31, L12214, doi: 10.1029/2004GL019940.

Richey, J.N., Poore, R.Z., Flower, B.P., Quinn, T.M., 2007. 1400 yr multiproxy record of climate variability from the northern Gulf of Mexico. Geology 35, 423-426.

Rittenour, T.M., Blum, M.D., Goble, R.J., 2007. Fluvial evolution of the lower Mississippi River valley during the last 100 k.y. glacial cycle: response to glaciation and sea-level change. Geological Society of America Bulletin 119, 586-608.

Ruhe, R.V., Hall, R.D., Camepa, A.P., 1974a. Sangamon paleosols of southwestern Indiana, U.S.A. Geoderma 12, 191-200.

Ruhe, R.V., 1974b. Sangamon paleosol and Quaternary environments in Midwestern United States. In: W.C. Mahaney, Editor, Quaternary Environments: Proceedings of a Symposium. First York University Symposium on Quaternary Research, York University, Toronto, ON, pp. 53-167.

Sionneau, T., Bout-Roumazeilles, V., Flower, B.P., Bory, A., Tribovillard, N., Kissel, C., Van Vliet-Lanoë, B., Montero-Serrano, J.C., in revision. On the provenance of freshwater pulses in the Gulf of Mexico during the last deglaciation: Evidence from grain size and clay mineralogy. Quaternary Research.

Sionneau, T., Bout-Roumazeilles, V., Biscaye, P.E., van Vliet-Lanoë, B., Bory, A., 2008. Clay-mineral distributions in and around Mississippi River watershed and Northern Gulf of Mexico: Sources and transport patterns. Quaternary Science Reviews 27, 1740-1751.

Silva, A.J., Baxter, C.D.P, LaRosa, P.T., Bryant, W.R., 2004. Investigation of mass wasting on the continental slope and rise. Marine Geology 203, 355-366.

Schmidt, M.W., Spero, H. J., Lea, D.W., 2004. Links between salinity variation in the Caribbean and North Atlantic thermohaline circulation. Nature 428, 160-163.

Thompson, W.G., Goldstein, S.L., 2005. Open-system coral ages reveal persistent suborbital sea-level cycles. Science 308, 401-404.

Tripsanas, E.K., Bryant, W.R., Prior, D.B., Phaneuf, B.A., 2003. Interplay between salt activities and slope instabilities, Bryant Canyon area, northwest Gulf of Mexico. In: Locat, J., Mienert, J. (Eds.), Submarine Mass Movements and Their Consequenses, 307–315.

Tripsanas, E.K., Bryant, W.R., Slowey, N.C., Bouma, A.H., Karageorgis, A.P., Berti, D., 2007. Sedimentological history of Bryant Canyon area, northwest Gulf of Mexico, during the last 135 kyr (Marine Isotope Stages 1-6): A proxy record of Mississippi River discharge. Palaeogeography Palaeoclimatology Palaeoecology, 246, 137-161.

Wang, C., Enfield, D.B., 2001. The tropical Western Hemisphere warm pool. Geophysical Research Letters 28, 1635-1638.

Wang, X., Auler, A.S., Edwards, R.L., Cheng, H., Cristalli, P.S., Smart, P.L., Richards, D.A., Shen, C.C., 2004. Wet periods in northeastern Brazil over the past 210 kyr linked to distant climate anomalies. Nature 432, 740-743.

Willard, D.A., Bernhardt, C.E., Korejwo, D.A., Meyers, S.R., 2005. Impact of millennial-scale Holocene climate variability on eastern North American terrestrial ecosystems: pollen-based climatic reconstruction. Global and Planetary Change 47, 17-35.

Yamamoto, M., Yamamuro,M., Tanaka, Y., 2007. The California current system during the last 136,000 years response of the North Pacific High to precessional forcing. Quaternary Science Reviews 26, 405-414.

Yu, Z., Andrews, J.H., Eicher, U., 1997. Middle Holocene dry climate caused by change in atmospheric circulation patterns: evidence from lake levels and stable isotopes. Geology 25, 251-254.

Ziegler M., Nürnberg D., Karas C., Tiedemann R., Lourens L.J., 2008. Persistent summer expansion of the Atlantic Warm Pool during glacial abrupt cold events. Nature Geoscience 1(9), 601-605.

Chapter 4

Synthesis

Comparison with other sedimentological records from the northern Gulf of Mexico − transect from west to east

To gain insight into the regional and local characters of sedimentological and paleoclimatic signatures interpreted in the Pigmy and La Salle basins (Chapters 2 and 3), this section intends to compare the clay minerals [S/(I+C) ratio] and magnetic susceptibility (MS) records obtained in this dissertation with the mineralogical, magnetic susceptibility and oxygen isotope data from sediments collected in the northern GOM during the 2002 and 2003 cruises of the research vessel Marion Dufresne (MD127-IMAGES and MD132-PICASSO). More specifically, the comparison was carried out through a west to east transect (Fig. 4.1): MD03-2641 (Humphrey Basin; Mallarino et al., 2006; Sionneau, 2008), MD02-2552 (Orca Basin; Sionneau, 2008), MD02-2549 (La Salle Basin; this study), MD02-2553 (Pigmy Basin; this study) and MD02-2575 (DeSoto Canyon; Nümberg et al., 2008). According to their respective locations, these cores likely collect continuously an averaged terrigenous supply from North America.

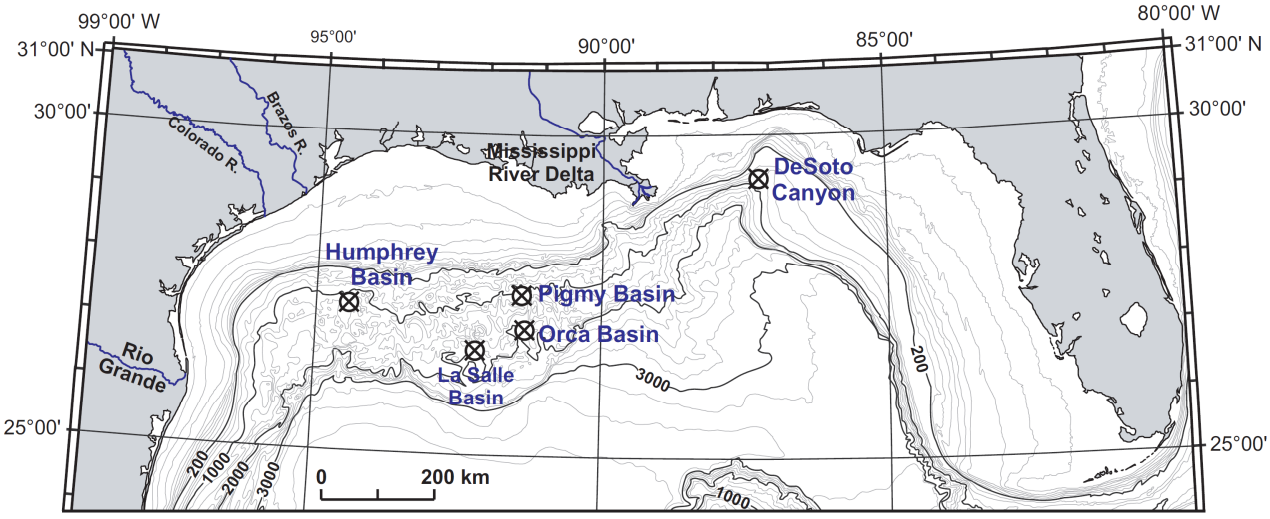

Fig. 4.1. Map showing the location of the GOM sediment cores discussed in this section. Transect from west to east: Humphrey, La Salle, Orca and Pigmy basins, and DeSoto Canyon.

The respective accumulation rates of the different cores are compared over the last climatic cycles. Some basic observations can be deduced from the depth-age relationships observed for the different cores (Fig. 4.2):

– In general, three different sedimentation dynamics can be observed along the studied transect. The DeSoto Canyon and Salle Basin show low and similar sedimentation rates. It suggests that these areas are not directly submitted to the sediment plume from the Mississippi River delta. By contrast, The Pigmy and Orca basins display high and similar sedimentation rates, suggesting a direct feeding by the Mississippi River sediment plume. This observation allows constraining the main Mississippi plume pattern and confirms the main westward dissipation of the plume resulting from the general westward surface circulation onto the northern continental shelf. On the other hand, the Humphrey Basin shows rather different sedimentation rates compared with the other basins of the transect. This fact probably evidences an additional influence of the Brazos, Colorado and Río Grande rivers originating from the southwestern USA through the Brazos-Trinity canyon (e.g., Mallarino et al., 2006).

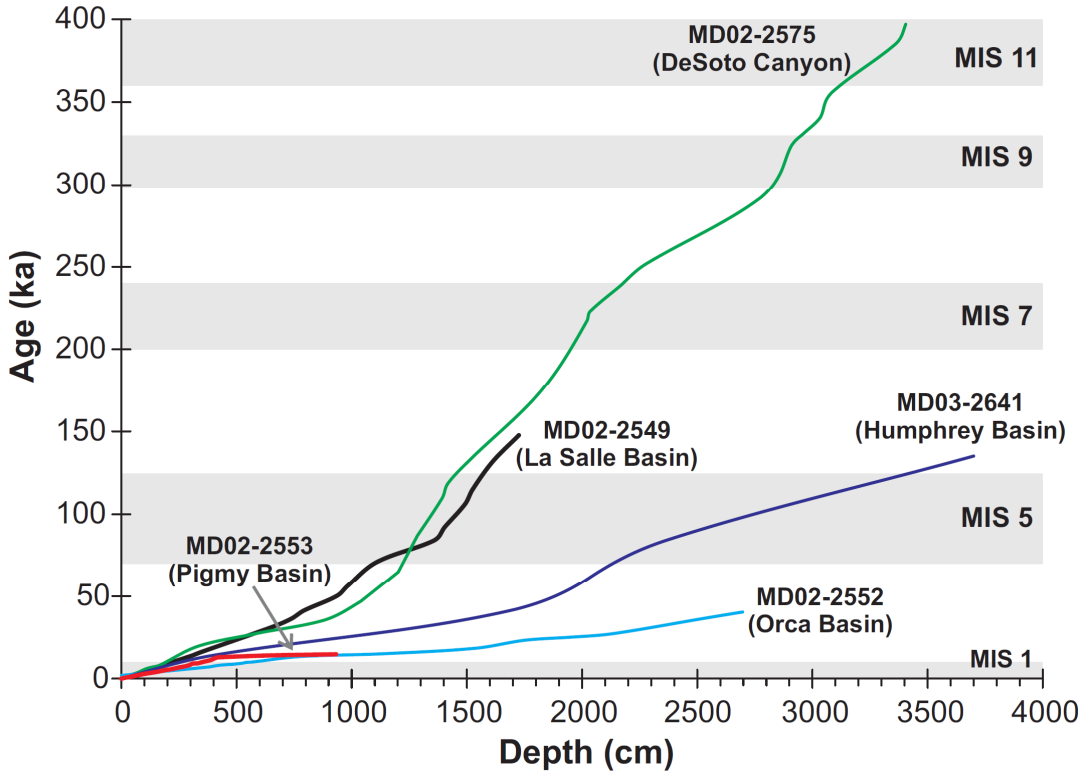

Fig. 4.2. The depth-age relationship of the GOM sediment cores discussed in this section.

- The high sedimentation rates of the Pigmy and Orca basins allow to carry out high-resolution climate studies over the MIS 3, last deglaciation and the Holocene, whereas the low sedimentation rates in the DeSoto Canyon and La Salle Basin provide ideals records for climate studies at the glacial/interglacial timescale.
- Lastly, only the DeSoto Canyon sedimentation offers a uniform and continuous record of the Mississippi River discharges over the past 400 ka (MIS 11) whereas the western sites seem to be influenced by gravity transport before MIS6.

Some characteristic proxies have been used for inter-comparison between the different cores. The magnetic susceptibility, which displays a global signature over the GOM has been chosen, as well as, $\delta^{18}O$ isotopic record when available and/or the S/(I+C) mineralogical record. The data are presented according to their own depth, in order to highlight the sedimentary significance of each record. Moreover, specific time-slice (MIS 5, MIS 3, MIS 1 or Holocene) as well as stratigraphic markers (Y8 ash layer) are underlined in order to help time-correspondence. The comparison between the different sedimentological records of this transect through the northern GOM is shown in Fig. 4.3 and 4.4. In order to facilitate the comparison, the interpretations are presented in succesive climatic period (Marine Isotope Stages or MIS).

The MIS 6/5 boundary (~130 ka; Termination II)

In the transect studied, this transition can be identified in the Humphrey, La Salle and DeSoto cores (Fig. 4.2). However, in the Humphrey and La Salle basins the MIS 6 is characterized by non-hemipelagic sedimentation as indicated by the high MS values and physical properties (Bout-Roumazeilles and Trentesaux, 2007; Laj et al., 2004) (Fig. 4.3d-e). This interval appears especially thick (~2200 cm) in the La Salle Basin displaying unrealistic sedimentation rates. This interval is interpreted to represent turbidity current deposits (e.g., Mallarino et al., 2006; Tripsanas et al., 2007), resulting from the ancestral drainage of the Mississippi River north of the La Salle Basin during this time. It led to highly increased supply of terrigenous sediments toward the continental slope of the northwestern GOM. By contrast, the NE area of the gulf was experienced a decreased terrigenous input over this time-slice. Consequently, the sedimentation in the northeastern part of the GOM was mainly hemipelagic, as suggested by the less prominent MS excursions when compared to glacial MIS 2-3 values in the DeSoto Canyon (Nümberg et al., 2008).

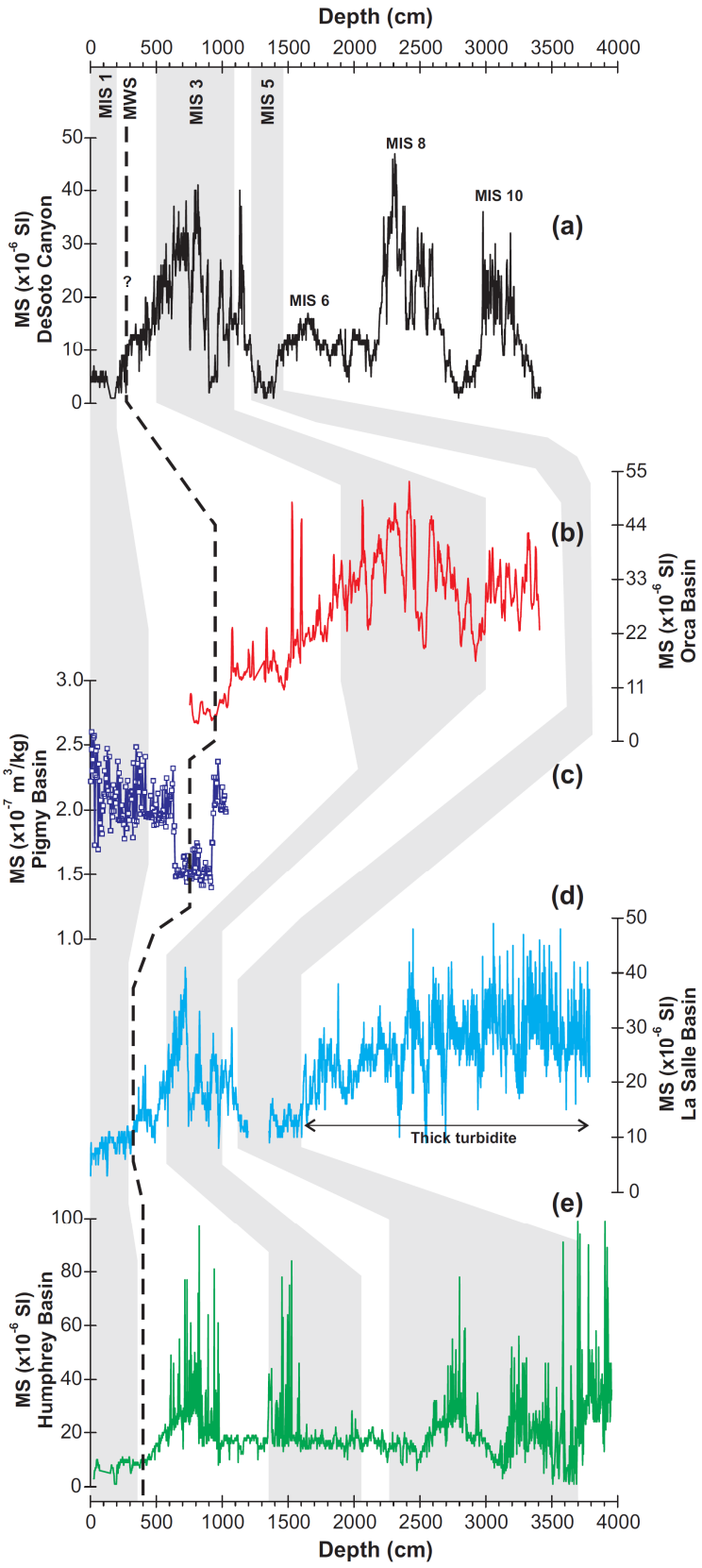

Fig. 4.3. Comparison between magnetic susceptibility (MS) from sediments collected in the northern GOM. (**a**) MS data from the DeSoto Canyon (core MD02-2575; Nürnberg et al., 2008). (**b**) MS data from the Orca Basin (core MD02-2552; Sionneau, 2008). (**c-d**) MS data from the Pigmy (core MD02-2553) and La Salle (core MD02-2549) basins (this study). (**e**) MS data from the Humphrey Basin (core MD03-2641; Sionneau, 2008). The shaded bands indicate the tentative correlation between the different cores. MWS: meltwater spike (15 to 12.9 cal ka BP; Flower et al., 2004).

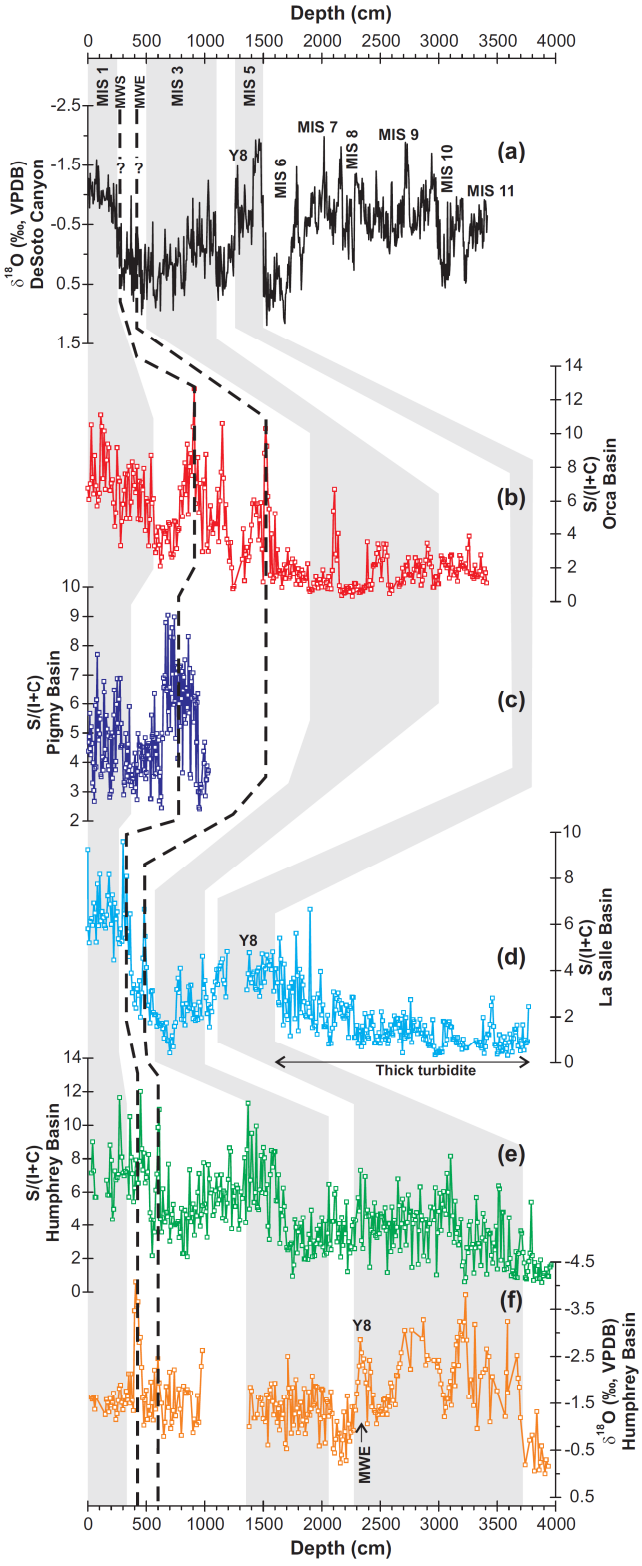

Fig. 4.4. Comparison between mineralogical and oxygen isotope data from sediments collected in the northern GOM. (**a**) Oxygen isotope data (*G. ruber*) from the DeSoto Canyon (core MD02-2575; Nürnberg et al., 2008). (**b**) Mineralogical data from the Orca Basin (core MD02-2552; Sionneau, 2008). (**c-d**) Mineralogical data from the Pigmy (core MD02-2553) and La Salle (core MD02-2549) basins (this study). (**e-f**) Mineralogical and oxygen isotope (*G. ruber*) data from the Humphrey Basin (core MD03-2641; Sionneau, 2008). The shaded bands indicate the tentative correlation between the different cores. The Y8 ash layer is dated at 84 ka (Drexler et al., 1980). MWS: meltwater spike (15 to 12.9 cal ka BP; Flower et al., 2004). MWE: meltwater event (e.g., Aharon, 2003; Sionneau, 2008).

During the early stages of the last sea level highstand (MIS 5; Lambeck and Chappell, 2001), the Mississippi River discharge quickly switched from west to east, up-dip of the present Mississippi Canyon, causing both a dramatic decrease in the sediment supply into the NW GOM and the initiation of dominantly hemipelagic sedimentation in the La Salle Basin (see Chapter 3). Additionally, the difference in the MS values between the MIS 6-7 and MIS 2-3 in the DeSoto Canyon is noteworthy. It could be interpreted as differences in the total detrital supply during these two glacial periods reflecting rather areal different extension of the LIS on the North American continent during these two full glacial periods. Indeed, a reduced extension of the LIS during MIS 6 compared with the Last Glacial Maximun (LGM), likely allowed reduce glacial erosion on the Mississippi River drainage area resulting in a generally lesser discharge in detrital material during the full-glacial MIS 6, in agreement with the hypothesis discussed in section 3.4.2.

MIS 5 (~125-70 ka)

This interval can be identified in the Humphrey and La Salle basins and DeSoto Canyon, due to the presence of the ash layer Y8 (Fig. 4.4a,d,f) which was deposited ca. 84 ka ago and is observed across the entire GOM (Drexler et al., 1980). In the Humphrey Basin and DeSoto Canyon the $\delta^{18}O$ record display lighter values (-1.5 – -3‰) suggesting interglacial conditions (MIS 5). The $\delta^{18}O$ values lighter than -2‰ in the Humphrey Basin also point out a meltwater event, synchroneous with the ash layer Y8. This meltwater event is only identified in this basin suggesting a local influence. Equivalently, the La Salle Basin shows high $CaCO_3$ content and high lightness L* values, with respect to the MIS 2-4 (see Chapter 3), indicating also a significant biogenic contribution, which is characteristic of the MIS 5. On the other hand, this interval is relatively thick in the Humphrey Basin and displays high MS values (Fig. 4.3e and 4.4e-f), with respect to the La Salle Basin and DeSoto Canyon. Mallarino et al. (2006) emphasized that the Humphrey Basin was affected during this time by sandy turbidity currents as a consequence of a temporary sea-level fall of about 50-60 m occurring within a time of general high sea-level (early MIS 5; Lambeck and Chappell, 2001), in agreement with sedimentological and geochemical properties of core MD03-2641 (Fig. 4.3e and 4.4e-f; Sionneau, 2008). The important point is that during the MIS 5 the cores MD02-2549 (La Salle Basin) and MD02-2575 (DeSoto Canyon) recorded hemipelagic sedimentation, with the absence of mass gravity flows (i.e., turbidity currents). These aspects suggest that the La Salle Basin and DeSoto Canyon area are ideal sites for paleoclimate studies, allowing the

comparison between the present and last interglacial periods (see section 3.4.2.). The rather smooth distribution of clay mineral [S/(I+C)>4] in the Humphrey and La Salle basins implies few modifications in the detrital source, with a major contribution of the NW Mississippi River watershed (smectite-rich province).

MIS 4 (~70-50 ka)

The MIS 4 is characterized in the La Salle and Orca basins and DeSoto Canyon by high MS excursions indicating a greater contribution of detrital material during this glacial period. This excursion is not identified in the Humphrey Basin, in agreement with interpretations of Sionneau (2008) that indicate a low contribution of terrigenous material at this time. This observation confirms the peculiar character of sedimentation within the Humphrey Basin. In the Humphrey and DeSoto areas, the light isotopic values characterizing MIS 5 are followed by a drastic shift toward more positive values of about -0.5‰ reflecting the MIS 4 glacial conditions (Fig. 4.4a,f). In the La Salle and Orca basins, although smectite is the main component of the clay-mineral fraction, this interval is characterized by enhanced contributions of illite and chlorite [relatively low S/(I+C) ratio] (Fig. 4.4b,d). Contrastingly, the clay mineral distribution in the Humphrey Basin shows few variations with respect to the MIS 5 (Fig. 4.4e).

MIS 3 (~50-25 ka)

The last glacial period is characterized in the northern GOM sediments (notably, the La Salle and Orca basins and DeSoto Canyon) by high MS excursions (Fig. 4.3a,b,d), which reflects an increased detrital input from the GOM via the Mississippi River. The La Salle and Orca basins display low S/(I+C) values (Fig. 4.4b,d) reflecting a major contribution of illite+chlorite. These aspects support the interpretation that during the MIS 3, the Mississippi River received large amounts of terrigenous materials resulting from maximal glacial erosion in northeastern North America (see section 3.4.1). By contrast, the Humphrey Basin also shows in the late MIS 3 high MS excursions (Fig. 4.3e), and high S/(I+C) values (Fig. 4.4e), suggesting that the sedimentary processes that predominated in this basin are notably different from those affecting the other GOM basins studied here. Mallarino et al. (2006) and Sionneau (2008) indicate that this interval in the Humphrey Basin is characterized by short hemipelagic sedimentation in the early MIS 3, and nonhemipelagic sedimentation (sandy turbidites) in the late MIS 3, which reflects the progressive fall of the sea-level during the MIS 3 (Lambeck and

Chappell, 2001). According to this evidence and similarly with the MIS 5, the high MS excursions in the Humphrey Basin during the MIS 3 are interpreted to relate mass-gravity flows, which can easily overprint the paleoclimatic signal delivered by the Mississippi River detrital inputs.

MIS 2 (~25-10 ka) and sedimentary evidence of deglacial megafloods

The MIS 2 can be identified, by its peculiar mineralogical and isotopic signatures, in all the studied sediment cores of the W-E GOM transect (Fig. 4.3 and 4.4). The MS values display a characteristic upward decreasing tendency during the MIS 2. The La Salle and Orca basins show slight MS excursions whereas major MS excursions are observed in the Humphrey Basin. These excursions are probably associated with the maximum glacial erosion during the last glacial maximum (LGM), altogether with the lowest sea level (Lambeck and Chappell, 2001). In the Humphrey Basin, this interval specifically represents a turbidite sandy deposit (Mallarino et al., 2006; Sionneau, 2008) as suggested by the high MS values (Fig. 4.3e). Conversely, hemipelagic sedimentation predominated in the La Salle, Pigmy and Orca basins, and the DeSoto Canyon during the MIS 2.

On the other hand, sedimentological (clay-minerals and MS) and geochemical ($\delta^{18}O$) proxies from the Humphrey, La Salle, Orca and Pigmy basins show evidences of meltwater discharges from the LIS through the Mississippi River. These episodes are however not recorded in the DeSoto Canyon (Fig. 4.4). According to these evidences, deglacial meltwater events described farther west apparently did not affected the northeastern GOM (see the dotted lines in Fig. 4.4), implying that meltwater routing from the LIS via the Mississippi River must not have affected the northward oceanic heat transport throughout the Atlantic Ocean, in agreement with the interpretations realised by Nümberg et al. (2008). The clay composition - enriched in smectite at the expense of both illite and chlorite (Fig. 4.4b-e) – from the La Salle, Pigmy, Orca, and accessorily, Humphrey basins suggests that these deglacial meltwater events during the MIS 2 are originating from NW Mississippi River watershed (smectite-rich province). Note that the meltwater spike (15-12.9 ka; Flower et al., 2004) is marked by a lightest value of $\delta^{18}O$ in the Humphrey Basin, and by the clay mineralogy [S/(I+C) ratio] (Fig. 4.4e-f). It indicates a westward vanishing of terrigenous discharge from the Mississippi River. Concurrently, the low MS values characterizing the meltwater spike in the Pigmy Basin (Fig. 4.3c), which was interpreted as reflecting an

enhanced oxygen consumption related to increased terrigenous particles flux (see section 2.4.2), is undoubtedly a local phenomenon, because it has not been observed in other basins.

MIS 1 (10-0 ka)

The uppermost part of all the cores is characterized by a hemipelagic drape as indicated by the low MS values (Fig. 4.3), and relatively light values of $\delta^{18}O$ (Fig. 4.3a). Specific mineralogical signatures (high smectite content; Fig. 4.4b-d) pinpoint a dominant origin from NW North America for detrital particles, which is less evident in the Humphrey Basin (Fig. 4.4e). As previously discussed, the Pigmy and Orca basins seem to be the sites of the W-E transect studied here the more suitable for carrying out high-resolution studies on the Holocene climate variability.

To sum up, the comparison between sedimentological and geochemical proxies from sediment cores collected in the northern GOM reveals that the La Salle, Pigmy and Orca basins, and DeSoto Canyon at a lesser extent, are ideally located to decipher the variability of the Mississippi River discharges during the last climatic cycle. The fact that the Humphrey Basin is affected by several mass-gravity flows, and receives an additional influence of the Brazos, Colorado and Río Grande rivers suggests that the paleoclimatic signal recorded through the Mississippi River is masked during a large part of the last climatic cycle. Finally, these comparisons suggest that the sedimentological and geochemical variations identified and interpreted in the Pigmy and La Salle basins (Chapters 2 and 3) are representative of the Quaternary climatic variability over the North American continent.

References

Aharon, P., 2003. Meltwater flooding events in the Gulf of Mexico revisited: Implications for rapid climate changes during the last deglaciation. Paleoceanography 18(4), PA1079. doi: 10.1029/2002PA000840.

Bout-Roumazeilles, V., Trentesaux, A., 2007. Sedimentologic analysis of cores recovered from the RV Marion Dufresne cruise in the Gulf of Mexico, chapter 5, July 2002, PAGE 127 Campaign. In: Winters, W.J., Lorenson, T.D., Paull, C.K. (Eds.), Initial Report of the IMAGES VIII/PAGE 127 Gas Hydrate and Paleoclimate Cruise on the RV Marion Dufresne in the Gulf of Mexico, 2-18 July 2002: U.S. Geological Survey Open-File Report 2004-1358, one DVD. Online at http://pubs.usgs.gov/of/2004/1358/.

Drexler, J.W., Rose, W.I. Jr., Sparks, R.S.J., Ledbetter, M.T., 1980. The Los Chocoyos Ash, Guatemala: a major stratigraphic marker in middle America and in three ocean basins. Quaternary Research 13, 327-345.

Flower, B.P., Hastings, D.W., Hill, H.W., Quinn, T.M., 2004. Phasing of deglacial warming and laurentide ice sheet meltwater in the Gulf of Mexico. Geology 32, 597-600.

Laj, C., Labeyrie, L., Kissel, C., 2004. Le rapport de campagne à la mer MD 132/P.I.C.A.S.S.O.—IMAGES XI à bord du Marion Dufresne. OCE/2004/02.

Lambeck, K., Chappell, J., 2001. Sea level change through the last glacial cycle. Science 292, 679-686.

Mallarino, G., Beaubouef, R.T., Droxler, A.W., Abreu, V., Labeyrie, L., 2006. Sea level influence on the nature and timing of a minibasin sedimentary fill (northwestern slope oft he Gulf of Mexico). American Association of Petroleum Geologists Bulletin 90, 1089-1119.

Nürnberg, D., Ziegler, M., Karas, C., Tiedemann, R., Schmidt M.W., 2008. Interacting Loop Current variability and Mississippi River discharge over the past 400 kyr. Earth and Planetary Science Letters 272, 278-289.

Sionneau, T., 2008. Transferts Continent – Océan : Enregistrement du dernier cycle climatique par les sédiments terrigènes du Golfe du Mexique. PhD thesis, Université Lille 1. 377 p.
Online at http://tel.archives-ouvertes.fr/tel-00366377/fr/ (Revised 2009-05-29)

Tripsanas, E.K., Bryant, W.R., Slowey, Kim, J.W., 2006. Marine Isotope Stage 6 Canyon and Spillover Deposits of the Bryant and Eastern Canyon Systems, Northwest Gulf of Mexico: Importance of Fine-Grained Turbidites on a Delta-Fed Prograding Slope. Journal of Sedimentary Research 76, 1012-1034.

Chapter 5

Summary, main conclusions and outlook

The sedimentological and geochemical characteristics of sediments collected in the northern GOM (MD02-2553 and MD02-2549) during the 2002 cruise of the research vessel Marion Dufresne (MD127 - IMAGES: International Marine Past Global Changes Study programs) were studied in order to reconstruct the variability of past terrigenous supply through the Mississippi River system in response to climatic forcings. Three periods were especially considered: (1) the Holocene (0-10 ka), (2) the last deglaciation punctuated by rapid severe climatic events (10-15 ka) and (3) the last climatic cycle (0-140 ka). These timesclices offer the opportunity to study both millennial and sub-millennial variabilities as well as glacial-interglacial oscillations. The results highlight variations in the contribution and nature of terrigenous particles eroded and transported by the Mississippi River towards the GOM interpreted as changing origin in response to climate influences. **The modifications of provenance were predominantly linked to glacial processes during glacial periods (orbital variability) and Terminations whereas migration of the precipitation belt resulting from changing moisture transfer patterns became a dominant process during ice-free intervals (millennial variability).**

5.1. Last deglaciation – Termination I

During the last termination, rapid changes of the Laurentide Ice Sheet (LIS) triggered major meltwater flows which were evidenced in the GOM through their imprints on hydrological proxies (Kennett and Shackleton, 1975; Emiliani et al., 1978; Leventer et al., 1982; Broecker et al., 1989; Spero and Williams, 1990; Flower and Kennett, 1990; Marchitto and Wei, 1995; Aharon, 2003; Flower et al., 2004; Tripsanas et al., 2007). Clay-mineral assemblages and elemental geochemistry from Pigmy Basin (core MD02-2553) provide new insights on the progress of deglacial meltwater episodes, and bring additional constraints on their provenance. **In core MD02-2553, clay minerals and major elements enabled us to track down the provenance of the detrital material delivered to the GOM via the Mississippi River during the main deglacial meltwater episode referred as to Meltwater**

Spike (13-15.2 cal ka BP, e.g., Flower et al., 2004; Meckler et al., 2008). The high- resolution mineralogical and geochemical records evidence **a multiphased event, with significant variations in provenance**:

- **During the early phase** (Phase 1), mineralogical and geochemical proxies indicate a mixed provenance of detrital particles, i.e. mainly from the north-western province (smectite) but with some contribution of the north-eastern province (illite and chlorite). These results suggest that melting had an effect on a large part of the southern margin of the LIS. Grain-size distribution indicates that erosional processes were rather important in the main Mississippi River channel during the early phase of the Meltwater Spike. According to these results, this **first phase is interpreted as the initial erosive flood** possibly resulting from the proglacial lake Wisconsin outburst (14.9 cal ka BP);

- **The second phase** (Phase 2) is characterized by a major modification in detrital provenance recorded by abundant smectite, which implies a main northwestern origin encompassing the Mississippi and Missouri provinces. It suggests a westward shift of the main outflow toward the recessing northwestern margin. Moreover, geochemical evidences reveal that the organic-rich laminations observed in the Pigmy Basin likely result from enhanced detrital particles flux rather than from deep water stratification as previously suggested (Tripsanas et al., 2007; Meckler et al., 2008). According to our dataset, **this second phase may correspond to the most intense freshwater discharge resulting from the rapid retreat of the southwestern LIS margin**;

- Grain-size distribution suggests **reduced erosional processes** during **the third phase** (Phase 3). The clay mineral assemblage composition indicates progressively growing contributions of the northeast province as the LIS was withdrawn from its southern extent.

The sedimentological record from core MD02-2553 also evidences a major modification of the sedimentary regime occurring after the meltwater spike at ca. 12.9 cal ka BP. This major modification is associated with a drastic reduction of the sedimentation rates (from about 200 to 25 cm/ka), which gives support to the proposed decreasing meltwater supply toward the GOM after the meltwater spike. Simultaneously, the enhanced biogenic contribution may reflect warmer sea-surface temperature resulting from increasing seasonality and/or insolation.

5.2. Holocene

The **Holocene** sedimentary record from Pigmy Basin (core MD02-2553) evidences **contrasting interactions between atmosphere-ocean-continent** during the early and late Holocene. This discrepancy indicates that the ice-sheet likely filtered and smoothed some of the high-frequency climatic variability during the early Holocene whereas the rapid atmospheric reorganization following the LIS collapse triggered rapid hydrological changes over central North America during the late Holocene.

After the final collapse of the LIS, mineralogical and geochemical records evidenced fluctuations of the Mississippi River discharge. They likely reflect alternations between at least two dominant terrigenous sources - the smectite-rich NW Mississippi watershed, and the illite- and chlorite-rich Great Lakes province and NE Mississippi watershed- interpreted as successive migrations of the main precipitation belt over North America. The timing of these migrations is consistent with previously documented catastrophic hurricanes in the Gulf Coast (Liu and Fearn, 2000) and flooding episodes of the Mississippi River in central North America (Knox, 2000, 2003).

These data provide additional informations to those previously published on the North American continent, Caribbean region and GOM. Their confrontation allows documenting the variations of the main moisture flux trajectories over North America and of the associated precipitation belt during the mid- and late Holocene. These interpretations support the hypothesis (e.g., Forman et al., 1995; Liu and Fearn, 2000; Knox, 2003), that **two main atmosphere-ocean configurations, successively controlling moisture transfer and precipitation distribution over North America throughout the Holocene:**

(1) A northern position of the Jet Stream and southwest migration of the Bermuda High promote the influx of moisture over central North America which may trigger **catastrophic hurricanes and flooding of the Mississippi River** during about 8.1-6.8, 6.4-5.9, 4.9-3.6, 3.1-1.7 and 1-0.3 ka ago. By contrast, the northeastern provinces experienced dry conditions.

(2) A southern position of the Jet Stream associated with a northeastward displacement of the Bermuda High constrained the **main moisture flux along the Atlantic margin** during about 6.8-6.4, 5.9-4.9, 3.6-3.1 and 1.7-1 ka ago.

These configurations allow correlating both continental and oceanic records in North America and the Caribbean, which are interconnected by the mean position of the Intertropical Convergence Zone and Atlantic Warm Pool. As a whole, these postulated shifts

in atmospheric as well as oceanic configuration promote the repetitive occurrence of drought/flooding over the northwestern Mississippi River through the Holocene.

These simple patterns highlight the **importance of atmospheric configuration on terrigenous supply through modifications of moisture transfer**, in turn conditioning precipitations, and thereby erosion. In addition, the coherency between the Pigmy Basin clay mineral records and the Holocene glaciochemical records (proxies sensitive to rapid atmospheric change) from GISP2 suggests a **very quick link between atmospheric circulation changes in the high latitude North Atlantic and the hydrological and erosional changes in the North American continent.** This synchronism underlines the major role played by the atmosphere compared with the ocean in the moisture transfers over North America, because processes involving the ocean would have induced a time lag between the respective records of the high latitudes and GOM settings.

To summarize, the Pigmy Basin sedimentary record suggests that the variations of the Mississippi River supply is mainly controlled by glacigenic processes resulting from the decaying LIS during the early Holocene, whereas atmosphere-ocean interactions become the main forcing during late Holocene once the LIS had collapsed. As depicted by the synoptic configurations, these atmosphere-ocean coupling concerns (1) the evaporation-precipitation budget in the GOM and the Caribbean sea; (2) moisture transfer resulting from the combination of hydrologic and atmospheric characteristics (extension of the Atlantic Warm Pool, Jet-Stream and ITCZ latitudinal position, Bermuda High pressure location, etc) and (3) the distribution of continental precipitations as forced by atmospheric configuration.

5.3. Last climatic cycle

The late Quaternary detrital sediment record of the core MD02-2549 from the La Salle Basin in the northern GOM provides insights into the **variability of terrigenous sediment provenance related to North American regional climate changes during the last 140 ka**. Clay mineralogy and geochemical signatures thus indicate that detrital sediments mainly originated from both the northern Mississippi and Missouri rivers watershed province (smectite-rich intervals) and northern Great Lakes area and NE Mississippi watershed (illite- and chlorite-rich intervals) during the entire last climatic cycle. The MD02-2549 results were compared with recent synthetic studies using (1) numerical models of ice thickness and North American freshwater runoff (Marshall and Clarke, 1999; Marshall et al., 2002; Kleman et al.,

2002), (2) meltwater record based on marine records of the GOM (Joyce et al., 1990, 1993; Tripsanas et al., 2007), and (3) dating of loess-paleosol deposits in Mississippi River Valley (Forman and Pierson, 2002), as a chronological and conceptual framework to guide the interpretations of the variability of the Mississippi River discharges in response to changes in the glacial and pluvial magaflood erosion over North America through the last glacial cycle.

Additionally, the **variability of the Mississippi River runoff –notably during the smectite-rich periods– appears to be correlated with the North Atlantic cold water events, when the Intertropical Convergence Zone (ITCZ) and Atlantic Warm Pool (AWP) in the GOM were seasonally displaced and extended northward during summer.** Perhaps a more vigorous Loop Current, before and during these cold episodes, may have raised sea surface temperatures and evaporation in the GOM during these times, leading to increased of the moisture transfers to central North America, and therefore a most intense freshwater discharge (meltwater, precipitations, megafloods) to the GOM, via the Mississippi River.

To sum up, the terrigenous proxies from the **La Salle Basin reveal new sedimentological evidences that the shift of the Mississippi River delta occurred before MIS 5**. These proxies also suggest that **provenance is highly variable on glacial-interglacial time scales** and that **different erosional process (glacial and rainfall) controlled both the flux and the provenance of detrital material delivered toward the GOM**:

(1) During MIS 5 (~125-70 ka), mineralogical proxies indicate a mixed provenance of detrital particles, i.e. mainly from the NW Mississippi River watershed (smectite) but with noticeable contribution of the Upper Mississippi River province (kaolinite). This result suggests that the environmental conditions during MIS 5 were rather different from present-day (available sedimentary load, erosion, runoff, precipitation distribution, etc…).

(2) During MIS 2-4 (~70-10 ka) important modification in detrital provenance are evidenced by a maximum contribution in illite+chlorite, and accessorily in kaolinite, which implies a main northeastern origin encompassing the Great Lakes area and eastern Mississippi River watershed. This glacial period is interrupted by episodic smectite-rich events, which suggest a sporadic westward shift the main detrital source toward the northwestern Mississippi province. These alternations are likely related to Dansgaard-Oeschger events (stadials/interstadials), but their respective causality is still debating.

(3) The Holocene MIS 1 (~10-0 ka) displays the maximum input in smectite, suggesting the dominant contribution from the NW Mississippi River watershed was triggered by the collapse of the LIS.

Finally, further high-resolution investigations are necessary to understand the apparent teleconnections between both the erosional processes in the NW Mississippi River watershed and the latitudinal migration of ITZC (and its impact on moisture transfer), and their relationships with the North Atlantic cold climatic events described during the last climatic cycle.

5.4. Comparison of the Holocene and Eemian records – a first approach

The core MD02-2549 from La Salle Basin in the northern GOM records the last climatic cycle. **It thus offers the opportunity to compare the sedimentological signatures of the two last interglacial intervals: i.e. the Holocene versus the MIS 5e**. In that context, this section refocused attention on atmosphere-ocean-continent interactions over the Holocene and MIS 5e. The respective clay-mineral compositions are unexpectedly different when comparing MIS 1 and MIS 5e, with distinct S/(I+C) ratios. Such a difference may result from several environmental modifications among which: (1) modification of the available terrigenous stock due to different extensions of the LIS southern margin during MIS 2 and MIS 6, (2) a westward migration of the Mississippi River paleodelta causing differential settling phenomenon, (3) modification of the upstream Mississippi and Missouri Rivers drainage patterns due to isostatic adjustment, and (4) modifications of provenance due to changing precipitation distribution likely linked to changes in the atmospheric configuration and moisture transport. These new insights raise several questions which are still under debate. **Nevertheless, according to recently evidenced relationships between Holocene atmospheric configuration and terrigenous supply, altogether with other evidences of altered hydrological regime during MIS 5e,** we propose a synoptic atmosphere-model which may explain the observed discrepancies in terrigenous supply and reconciliate apparent conflicting findings about MIS 5e.

5.5. Comparison to other continental and marine paleoclimate records

The long-term sedimentological and geochemical trends interpreted in the Pigmy and La Salle records from the northern GOM are similar to the trends of the several continental (e.g., Upper Mississippi River channel, North American Great Plains, Buckeye Creek Cave) and marine (e.g., Orca Basin and DeSoto Canyon) paleoclimate records. This demonstrates that regional changes in the distribution of Mississippi River sediments in the northern GOM do not appear to be the dominant factor for the observed sedimentological and geochemical variability. By contrast, these modifications are likely driven by climatic forcings at both millennial and orbital timescale.

The comparison of the multiproxy records generated within this dissertation, with previously published continental and marine records allowed to provide new evidences and insights on:

1. The influence of the LIS evolution on the variations of the main detrital sources and the major modifications of the sedimentary regime of the Mississippi River during the glacial periods and terminations of the last climatic cycle.
2. The modifications of the main moisture transfer toward North America and their relationship with the migration of the associated precipitation belt during the Holocene.
3. The connection through the Holocene between large-scale atmospheric circulation changes in the high-latitude North Atlantic and the hydrological and erosional changes in the North American continent.
4. The noticeable different of the Mississippi River discharges between the Holocene and Eemian periods.
5. The magnitude of the paleoclimatic signal recorded through the Mississippi River in the terrigenous sediments of the northern GOM. Indeed the basins located in the NW GOM (e.g., Humphrey Basin) recorded a notable influence of the Brazos, Colorado and Río Grande rivers originating from the southwestern USA, and therefore the climatic signal of the Mississippi was likely masked. On the other hand, the basins located in the NE GOM (e.g., DeSoto Canyon) apparently were not affected by the deglacial meltwater input through the Mississippi River.

In summary, this PhD-thesis illustrates the use of the detrital fraction (clay mineralogy, grain-size and geochemistry) as a reliable proxy for retracing variations in both main terrigenous provenance and continental hydrological regime complementary with paleoceanographic proxies reflecting the main surface- and deep-sea characteristics (sea-surface temperature or SST, sea surface salinity or SSS, $\delta^{18}O$).

The reconstruction of continental areas successively accepted to erosion gives new insights on the continental hydrological system response to climatic forcings through glacial activity or precipitation distribution. In particular, our results are informative on the dynamical component of the atmospheric configuration, i.e. the moisture transfer from the GOM toward the North American continent, which is so far still speculative on the studied timescale.

5.6. Outlook for future works

The multi-proxy records produced on cores MD02-2553 and MD02-2549 give some new insights on the relationship between the LIS growth/decay phases and the Mississippi River variability during the last climatic cycle and depict some of the atmosphere-ocean-continent interactions at mid- and high latitudes. Several questions are still debated and further research may actually give clues on the moisture transfer dynamic and processes between the GOM and North America during the last climatic cycle:

A.- The mineralogical records from both the Orca (core MD02-2552) and Pigmy (MD02-2553) basins evidenced a series of specific detrital inputs linked to freshwater discharges -referred as to Meltwater flows (Aharon et al., 2003, 2006) or Meltwater Spike (Flower et al., 2004) - occurring during the last deglaciation (Montero Serrano et al., in press; Sionneau et al., in revision). Similar signal is observed in clay mineralogy and oxygen isotopic data in core MD02-2549 from the La Salle Basin, but the chronological frame of the uppermost part of the core is not yet constrained enough (Fig. 5.1). Further work will allow producing a detailed chronological framework for core MD02-2549 (La Salle Basin) by measuring some accelerator mass spectrometry (AMS) ^{14}C radiocarbon dates on planktonic foraminifera. Thus the comparison of the climatic and detrital records from the three cores would be achieved on their own chronological scale.

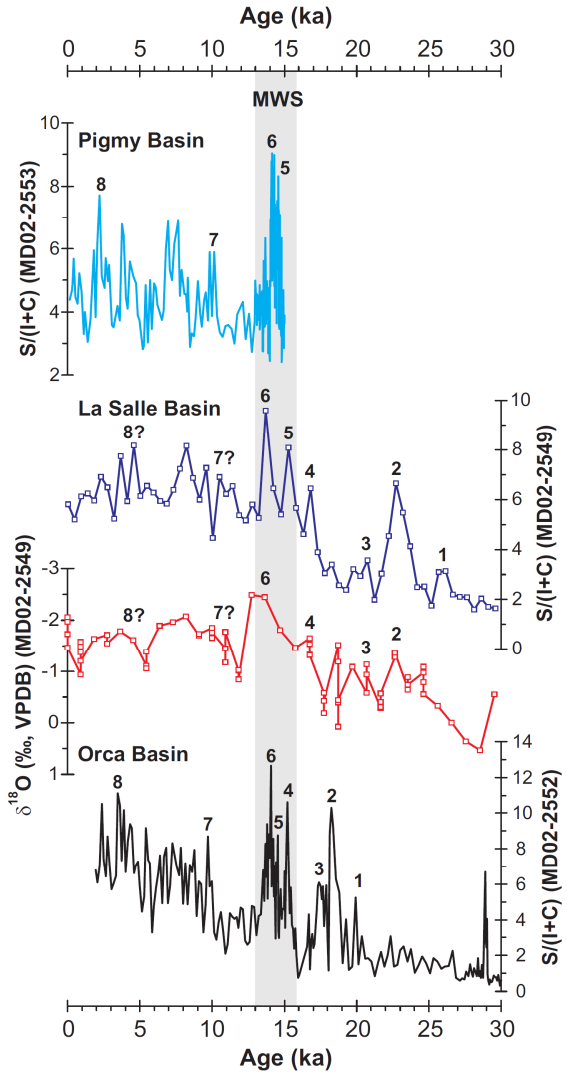

Fig. 5.1. Comparison of the clay mineral ratios S/(I+C) from Orca, La Salle and Pigmy basins (Montero-Serrano et al., in press). Also showing the stable oxygen isotope ($\delta^{18}O$ in ‰ VPDB) records of *G. rubber* from La Salle Basin (core MD02-2549). Orca Basin data from Sionneau et al. (in revision). MWS: Meltwater Spike (Flower et al., 2004). Although it is not possible to assume synchronism due to chronological imprecision, several general variations or peaks (meltwater flows) can be tentatively correlated (Arabic numerals) between the different cores.

B.- The mineralogical variations observed in core MD02-2549 during MIS 3 (Fig. 5.2) suggest a link with the Dansgaard-Oeschger (D-O) oscillations characterizing the last climatic cycle. These observations raise the questions of both relationship and respective timing of high-latitude climatic events (Fig 5.2f), advance/retreat phases of the LIS, moisture transfer (Fig 5.2a), atmospheric configuration (Fig 5.2b) and terrigenous supply toward the GOM via the Mississippi River system during MIS 3 (Fig 5.2c-e). Similar trends were evidenced by a high-resolution mineralogical study of core MD02-2552 from the Orca basin (Fig. 5.2c; Meunier, 2009; Sionneau et al., in preparation). So far, the sampling resolution of core MD02-2549 is too low to allow further interpretations. In that context, a high-resolution

mineralogical study of the MIS 3 interval will be performed shortly in order to document with details the links between high-latitude processes and terrigenous transfers toward the GOM. These new results will also confirm (or not) the apparent synchronicity between the terrigenous supply toward GOM and North GRIP D-O oscillations. In that case, it would imply that the climatic forcing was initiated or transferred through atmospheric processes rather than through ocean transport which would likely result in a lag between both records.

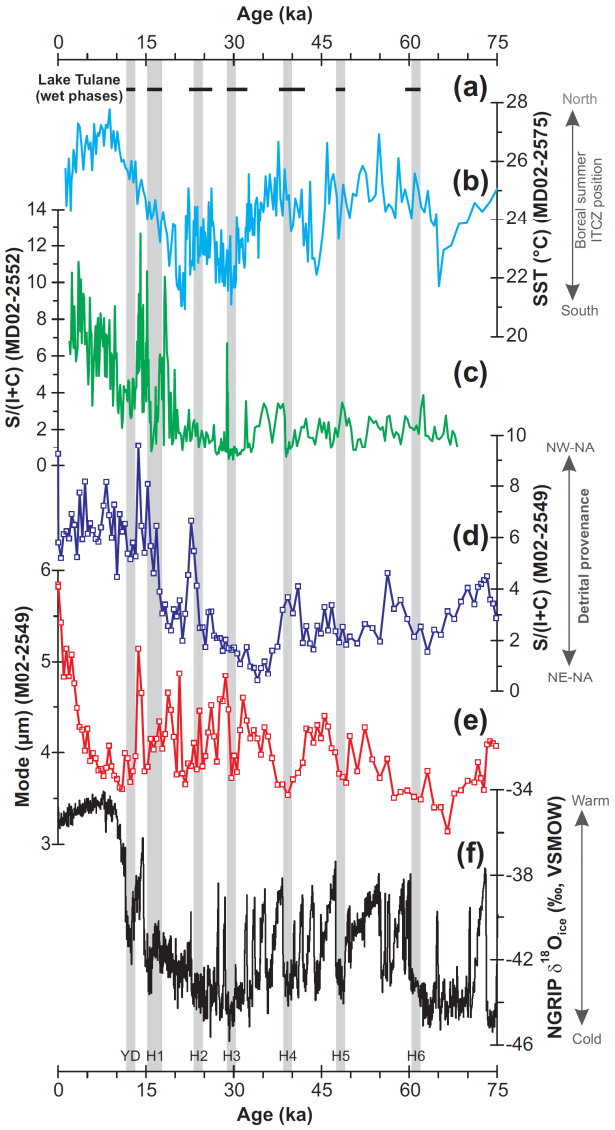

Fig. 5.2. Comparison of the sedimentological parameters from the La Salle Basin with paleoclimatic records from NGRIP and GOM. **a,** Wet phases in Florida (Lake Tulane) based on palynological data (Grimm et al., 2006). **b**, SST record from MD02-2575. **c**, S/(I+C) ratio from MD02-2549 (La Salle Basin). **d**, S/(I+C) ratio from MD02-2552 (Orca Basin; Meunier, 2009; Sionneau et al., in preparation). **e**, Mode grain-size from MD02-2549 (La Salle Basin). **f**, $\delta^{18}O_{ice}$ from Greenland ice core North GRIP (North Greenland Ice Core Project Members, 2004). The grey vertical bars mark the North Atlantic Heinrich events (H1-H6) and Younger Dryas (YD).

C.- Up to now, we mainly focused on the terrigenous fraction, because it provides valuable informations on sediment provenance during the major climate modifications over the last climatic cycle (i.e. Meltwater Flow, Mississippi megafloods, terminations, interglacial intervals, etc). Nevertheless, our interpretations are meaningless without the use of the paleoceanographic proxies produced by other research groups (e.g., Jasper and Gagosian, 1990; Brown and Kennett, 1999; Flower et al., 2004; Poore et al., 2004, 2005; Hill et al., 2006; LoDico et al., 2006; Tripsanas et al., 2007; Meckler et al., 2008; Nürnberg et al., 2008). In that sense, a joint work on cores MD02-2553 and MD02-2549 − from the Pigmy and La Salle basins respectively − focusing on sea-surface temperature (SST based on Mg/Ca *G. ruber*) and oxygen isotope composition of seawater ($\delta^{18}O_{SW}$, approximating sea surface salinity, SSS) reconstructions would nicely complement the available dataset. It would provide informations on the hydrological impact of massive freshwater discharge (meltwater, precipitations and megafloods) from the Mississippi River on the GOM sea-surface main properties (Fig. 5.3).

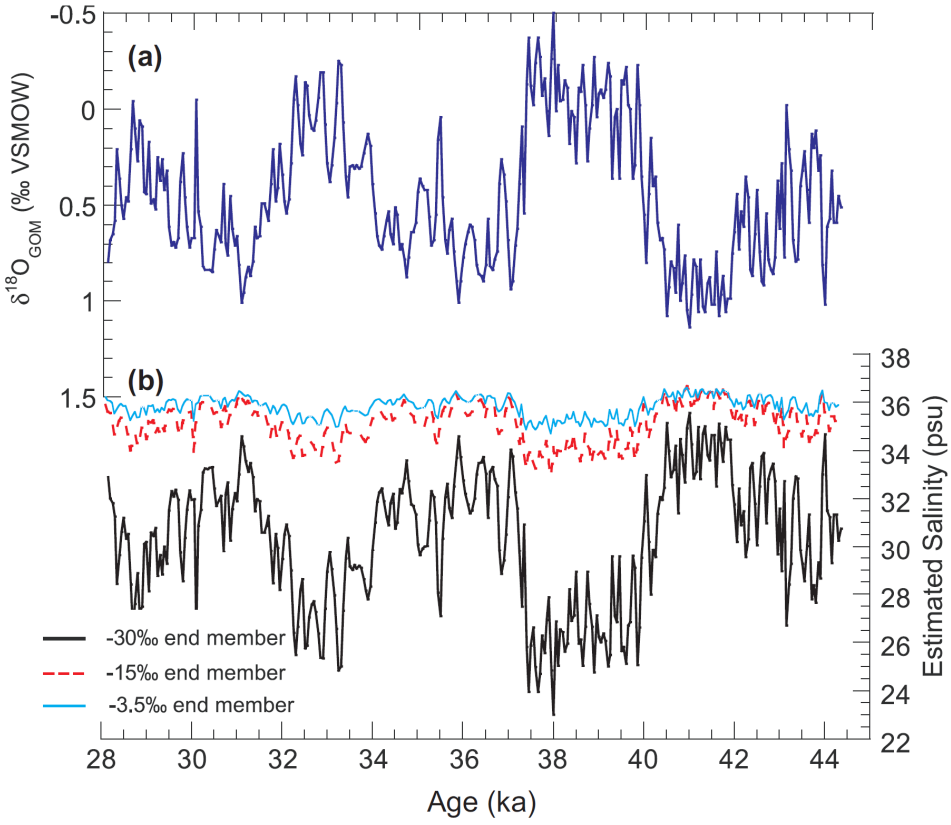

Fig. 5.3. GOM sea surface salinity (SSS) reconstructions from 28 to 45 ka (adopted from Hill et al., 2006). SSS is based on the conversion of $\delta^{18}O_{GOM}$ to salinity using a mixing model with three possible end-member compositions for freshwater input: (**a**) $\delta^{18}O_{GOM}$ and (**b**) estimated salinity. The most conservative estimate for salinity changes indicates a substantial meltwater contribution to $\delta^{18}O_{sw}$ in the GOM.

D.- In order to retrace the North American southwest (SW) monsoon activity, it will be interesting to count the abundance of the planktonic foraminifera *G. sacculifer* in core MD02-2549 (La Salle Basin) and MD03-2641 (Humphrey Basin) as it was done for the core MD02-2553 from the Pigmy basin by Poore et al. (2005) (Fig. 5.4). Indeed, *G. sacculifer* is a good record of the SW monsoon activity on millennial and sub-millennial timescales (Poore et al., 2005). It would indicate if there is any correlation between the sedimentological events evidenced by clay mineralogy, grain-size distribution or geochemistry and periods of enhanced precipitations on the SW part of North America, and to evaluate the influence of the monsoon system over a rather long transect.

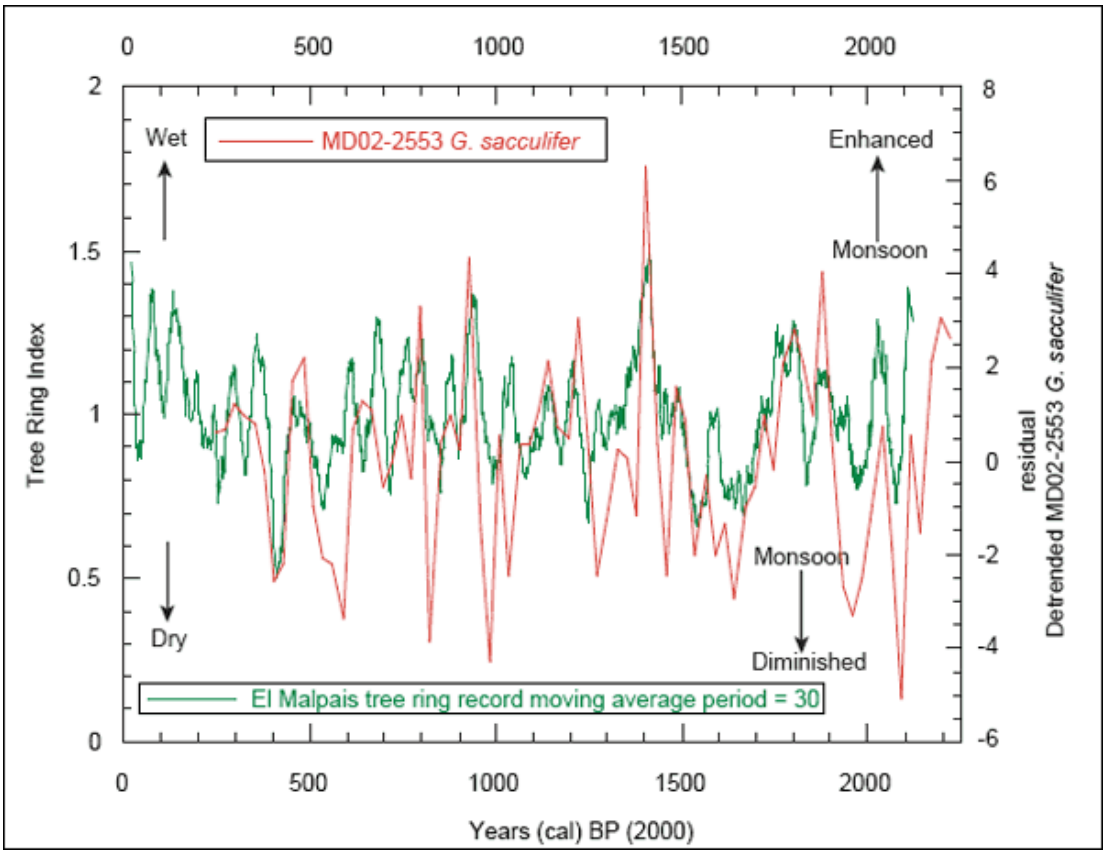

Fig. 5.4. Comparison of time-series of standard tree-ring width index developed from living trees and subfossil wood at El Malpais National Monument in west-central New Mexico and relative abundance of *G. sacculifer* in core MD02-2553 from the Pigmy Basin in the northern Gulf of Mexico (adopted from Poore et al., 2005). The MD02-2553 record has been detrended to remove low-frequency variability. Time scale is in calendar years before present (BP; before 2000). Each record is plotted against its own independent chronology. Development of the El Malpais chronology is outlined in Grissino-Mayer (1996). Chronology for the MD02-2553 % *G. sacculifer* time-series (Poore et al., 2004) is based on 8 AMS ^{14}C dates that were calibrated to calendar years with the OxCal Program (Ramsey, 2001). Larger tree-ring index values represent increased annual precipitation. Increased *G. sacculifer* relative abundance values represent more northerly average position of the ITCZ, which results in enhanced monsoon circulation.

E.- Our discrimation of major detrital provinces is mainly based on the clay mineral distribution maps produced by Sionneau et al. (2008), supported by geochemical data (major, trace elements and rare-earth elements). This approach provides rather satisfying regional provenance. In that frame, radiogenic isotopes would help to pinpoint the provenance of detrital inputs associated with various events (megafloods, meltwater pulses) or to assess changing provenance during the Holocene. An important characteristic of the continental crust is that different regions are characterized by distinct Sr-Nd-Pb isotope signatures depending on age and thermo-tectonic evolution. This has allowed previous workers to successfully document the changing isotopic signatures and, by implication, terrigenous source (Grousset et al., 1988; Revel et al., 1996; Gwiazda et al., 1996; Innocent et al., 1997; Winter et al., 1997; Fagel et al. 2002; Abouchami & Zabel, 2003; Grousset & Biscaye, 2005). This approach will help not only to constrain the different sources but also to estimate their respective contributions through time.

F.- A recent study carried out in the anoxic Orca Basin (core MD02-2552) shows that organic-matter (OM) may be degraded within the water column when it is retained durably at the pycnocline (Tribovillard et al., 2009). These authors suggest that high productivity coupled to strictly anoxic conditions cannot guarantee significant OM accumulation if a marked pycnocline strongly slows down organic-particle settling, and maintains OM in protracted contact with O_2-bearing water. Thus, these results may apply to any basin characterized by a sharp density contrast within its water mass. The Orca, Pigmy and La Salle basins are very close to each other. It is inferred that they collect an OM that has exactly the same origin, a mixture of marine and land-derived organic products, as observed by Meckler et al. (2008) and Tribovillard et al. (2009). Thus it would be interesting to study how the same types of OM can accumulate in basins with contrasting depositional conditions: in one case (Orca Basin), an anoxic bottom water mass favours OM preservation but the presence of the a strong pycnocline delays the OM settling; in the second case (Pigmy and La Salle basins), the ventilated water column must not favours OM preservation but a high sedimentation rate can help OM accumulation. The results of such a study must help us to better constrain the key factors intervening in the process of OM storage in sediments. In order to fulfil this objective, the organic fraction (palynofacies and Rock-Eval pyrolysis) of the cores MD02-2553 and MD02-2549 is currently studied.

References

Abouchami, W. and Zabel, M., 2003. Climate forcing of the Pb isotope record of terrigenous input into the Equatorial Atlantic. Earth and Planetary Science Letters 213, 221-234.

Aharon, P., 2003. Meltwater flooding events in the Gulf of Mexico revisited: Implications for rapid climate changes during the last deglaciation. Paleoceanography 18(4), PA1079. doi: 10.1029/2002PA000840.

Aharon, P., 2006. Entrainment of meltwaters in hyperpycnal flows during deglaciation superfloods in the Gulf of Mexico. Earth and Planetary Science Letters 241, 260-270.

Broecker, W.S., Kennett, J.P., Flower, B.P., Teller, J.T., Trumbore, S., Bonani, G., Wolfli, W., 1989. Routing of meltwater from the Laurentide Ice-Sheet during the Younger Dryas cold episode. Nature 341, 318-321.

Brown, P., Kennett, J.P., Ingram, B.L., 1999. Marine Evidence for Episodic Holocene Megafloods in North America and the Northern Gulf of Mexico. Paleoceanography, 14(4), 498-510.

Emiliani, C., Rooth, C., and Stripp, J.J., 1978. Late Wisconsin flood into the Gulf of Mexico. Earth and Planetary Science Letters 41, 159-162

Fagel, N., Innocent, C., Gariépy, C., Hillaire-Marcel, C., 2002. Sources of Labrador Sea sediments since the Last Glacial Maximum inferred from Nd-Pb isotopes. Geochimica Cosmochimica Acta 66, 2569-2581.

Flower, B.P., Kennett, J.P., 1990. The Younger Dryas cool episode in the Gulf of Mexico. Paleoceanography 5(6), 949-961.

Flower, B.P., Hastings, D.W., Hill, H.W., Quinn, T.M., 2004. Phasing of deglacial warming and laurentide ice sheet meltwater in the Gulf of Mexico. Geology 32, 597-600.

Forman, S.L., Oglesby, R., Markgraf, V., Stafford, T., 1995. Paleoclimatic significance of late Quaternary eolian deposition on the Piedmont and High Plains, central United States. Global and Planetary Change 11, 35-55.

Grimm, E.C., Watts, W.A., Jacobson Jr., G.L., Hansen, B.C.S., Almquist, H.R., Dieffenbacher-Krall, A.C., 2006. Evidence for warm wet Heinrich events in Florida, Quaternary Science Reviews 25, 2197-2211.

Grissino-Mayer, H.D., 1996. A 2129-year reconstruction of precipitation for northwestern New Mexico, USA, in Dean, J.S., et al., eds., Tree rings, environment, and humanity, Tucson, University of Arizona, p. 191–204.

Grousset, F.E., Biscaye, P.E., Zindler, A., Prospero, J., Chester, R., 1988. Neodymium isotopes as tracers in marine sediments and aerosols: North Atlantic. Earth and Planetary Science Letters 87, 367-378.

Grousset, F.E., Biscaye, P.E., 2005. Tracing dust sources and transport patterns using Sr, Nd and Pb isotopes. Chemical Geology 222, 149-167.

Gwiazda, R.H., Hemming, S.R., Broecker, W.S., 1996. Tracking the sources of icebergs with lead isotopes: the provenance of ice-rafted debris in Heinrich layers 2. Palaeoceanography 11, 77-93.

Hill, H.W., Flower, B.P., Quinn, T.M., Hollander, D.J., Guilderson, 2006. Laurentide Ice Sheet meltwater and abrupt climate change during the last glaciation, Paleoceanography 21, PA1006, doi:10.1029/2005PA001186.

Innocent, C., Fagel, N., Stevenson, R.K., Hillaire-Marcel, C., 1997. Sm-Nd signature of sediments and deep current changes in the NW North Atlantic since the Last Glacial Maximum. Earth and Planetary Science Letters 146, 607-625.

Jasper, J.P., Gagosian, R.B., 1990. The sources and deposition of organic-matter in the Late Quaternary Pygmy Basin, Gulf of Mexico. Geochimica et Cosmochimica Acta 54, 1117-1132.

Kennett, J.P., Shackleton, N.J., 1975. Laurentide ice sheet meltwater recorded in Gulf of Mexico deep-sea cores. Science 188, 147-150.

Knox, J.C., 2000. Sensitivity of Modern and Holocene floods to climate change. Quaternary Science Reviews 19, 439- 457.

Knox, J.C., 2003. North American palaeofloods and future floods: Responses to climate change. In: K.J. Gregory and G. Benito, Editors, Palaeohydrology: Understanding Global Change, J. Wiley and Sons, Chichester (2003), pp. 143-164.

Leventer, A., Williams, D.F., Kennett, J.P., 1982. Dynamics of the Laurentide ice sheet during the last deglaciation: evidence from the Gulf of Mexico. Earth and Planetary Science Letters 59, 11-17.

Liu, K.B., Fearn, M., 2000. Reconstruction of prehistoric landfall frequencies of catastrophic hurricanes in Northwestern Florida from lake sediment records. Quaternary Research 54, 238-245.

LoDico, J.M., Flower, B.P., and Quinn, T.M., 2006. Subcentennial-scale climatic and hydrologic variability in the Gulf of Mexico during the early Holocene. Paleoceanography 21, PA3015, doi: 10.1029/2005PA001243.

Marchitto, T.M., Wei, K.Y., 1995. History of Laurentide meltwater flow to the Gulf of Mexico during the last deglaciation, as revealed by reworked calcareous nannofossils. Geology 23, 779-782.

Meckler, A.N., C.J. Schubert, P.A. Hochuli, B. Plessen, D. Birgel, B.P. Flower, K.-U. Hinrichs, and Haug, G.H., 2008. Glacial to Holocene terrigenous organic matter input to sediments from Orca Basin, Gulf of Mexico- a combined optical and biomarker approach. Earth and Planetary Science Letters 272, 251-263.

Meunier G., 2009. Relations entre la variabilité climatique sur le continent nord-américain et les modifications des apports terrigènes dans le Golfe du Mexique au cours du stade isotopique 3. Mémoire de Master 1 – Géosciences de l'environnement, Université Lille 1, Science de la Terre, 31 p.

Montero-Serrano, J.C., Bout-Roumazeilles, V., Tribovillard, Sionneau, T., Bory, A., Riboulleau, A., Flower, B., in press. Sedimentary evidence of deglacial megafloods in the northern Gulf of Mexico (Pigmy Basin). Quaternary Science Reviews.

North Greenland Ice Core Project Members, 2004. High-resolution record of Northern Hemisphere climate extending into the Last Interglacial period. Nature 431, 147-151.

Nürnberg, D., Ziegler, M., Karas, C., Tiedemann, R., Schmidt M.W., 2008. Interacting Loop Current variability and Mississippi River discharge over the past 400 kyr. Earth and Planetary Science Letters 272, 278-289.

Poore, R.Z., Quinn, T.M., Verardo, S., 2004. Century-scale movement of the Atlantic Intertropical Convergence Zone linked to solar variability. Geophysical Research Letters 31, L12214, doi: 10.1029/2004GL019940.

Poore, R.Z., Pavich, M.J., Grissimo-Mayer, H.D., 2005. Record of the North American monsoon from Gulf of Mexico sediment cores. Geology 33, 209-212.

Ramsey, C.B., 2001, Development of the radiocarbon calibration program: Radiocarbon 43, 355–363.

Revel, M., Sinko, J.A., Grousset, F.E., Biscaye, P., 1996. Sr and Nd isotopes as tracers of North Atlantic lithic particles: Paleoclimatic implications. Palaeoceanography 11, 95-113.

Richey, J.N., Poore, R.Z., Flower, B.P., Quinn, T.M., 2007. 1400 yr multiproxy record of climate variability from the northern Gulf of Mexico. Geology 35, 423-426.

Sionneau, T., Bout-Roumazeilles, V., Flower, B.P., Bory, A., Tribovillard, N., Kissel, C., Van Vliet-Lanoë, B., Montero-Serrano, J.C., in revision. On the provenance of freshwater pulses in the Gulf of Mexico during the last deglaciation: Evidence from grain size and clay mineralogy. Quaternary Research.

Spero, H. J., Williams, D.F., 1990. Evidence for seasonal low salinity surface waters in the Gulf of Mexico over the last 16,000 years. Paleoceanography 5, 963-975.

Tribovillard, N., Bout-Roumazeilles, V., Sionneau, T., Montero-Serrano, J.C., Riboulleau, A., Baudin, F., 2009. Does a strong pycnocline impact organic-matter preservation and accumulation in an anoxic setting? The case of the Orca Basin, Gulf of Mexico. Comptes Rendus Geosciences 341, 1-9.

Tripsanas, E.K., Bryant, W.R., Slowey, N.C., Bouma, A.H., Karageorgis, A.P., Berti, D., 2007. Sedimentological history of Bryant Canyon area, northwest Gulf of Mexico, during the last 135 kyr (Marine Isotope Stages 1-6): A proxy record of Mississippi River discharge. Palaeogeography Palaeoclimatology Palaeoecology, 246, 137-161.

Winter, B.L., Johnson, C.M., Clark, D.L., 1997. Strontium, neodymium, and lead variations of authigenic and silicate sediment components from the Late Cenozoic Arctic Ocean: Implications for sediment provenance and the source of trace metals in seawater. Geochimica Cosmochimica Acta 61, 4181-4200.

General appendix

Appendix A.1

On the provenance of freshwater pulses in the Gulf of Mexico during the last deglaciation: Evidence from grain size and clay mineralogy*

Thomas Sionneau [a,b], Viviane Bout-Roumazeilles [a], Benjamin Flower [c], Aloys Bory [a,d], Nicolas Tribovillard [a], Catherine Kissel [f], Brigitte Van Vliet-Lanoë [b], **Jean Carlos Montero-Serrano** [a]

[a] Université Lille 1, Laboratoire Géosystèmes, UMR 8157 CNRS, bâtiment SN5, 59655 Villeneuve d'Ascq cedex, France
[b] Institut Universitaire Européen de la Mer, UMR 6538 CNRS, Domaines Océaniques, Place Nicolas Copernic, 29280 Plouzané, France
[c] College of Marine Science, University of South Florida, 140 7th Avenue South, St. Petersburg, FL 33701, USA
[d] Lamont-Doherty Earth Observatory of Columbia University, Palisades, NY, 10964, USA
[e] Laboratoire des Sciences du Climat et de l'Environnement, 91198 Gif-sur-Yvette, France.

Abstract

The clay mineralogy and grain-size of sediments deposited during the last deglaciation in the Orca Basin (Gulf of Mexico) show that the terrigenous-dominated sedimentation, reflecting the high detrital contribution of the illite and chlorite-rich Great lakes area towards the Gulf of Mexico is interrupted by repetitive fine-grained smectite-rich events (SR) originating from the northwestern Mississippi River and Missouri River watersheds. The correlation between the respective timing of the SR, the Laurentide ice-sheet meltwater history -recorded in $\delta^{18}O$ of planktonic foraminifera from the Gulf of Mexico- and the modeled chronology of continental deglacial drainage reveals that the SR occur simultaneously with the major meltwater floods. The comparison of potential source areas for the SR detrital supply (based on recently published clay mineral distribution maps on land) and the Laurentide Ice Sheet margin evolution (as depicted by continental studies) provides additional constrains on the dominant melting areas. This study shows that combining clay mineralogy and grain-size characteristics of sediments deposited in the Orca Basin offers a unique opportunity to link the reconstructed continental glacial history, the modeled drainage patterns, and the marine record of meltwater flows in the Gulf of Mexico.

Keywords: deglaciation, meltwater pulse, Laurentide Ice Sheet, clay minerals, Orca Basin, Mississippi River.

* in revision for Quaternary Research

Appendix A.2

Marine Geology 254 (2008) 62–72

Contents lists available at ScienceDirect

Marine Geology

journal homepage: www.elsevier.com/locate/margeo

Paleodepositional conditions in the Orca Basin as inferred from organic matter and trace metal contents

Nicolas Tribovillard [a,*], Viviane Bout-Roumazeilles [a], Thomas Algeo [b], Timothy W. Lyons [c], Thomas Sionneau [a], Jean Carlos Montero-Serrano [a], Armelle Riboulleau [a], François Baudin [d]

[a] Université Lille 1, Laboratoire Géosystèmes, UMR 8157 CNRS, bâtiment SN5, 59655 Villeneuve d'Ascq cedex, France
[b] Department of Geology, University of Cincinnati, Cincinnati, Ohio 45221-0013, USA
[c] Department of Earth Sciences, University of California, Riverside, CA 92521-0423, USA
[d] Université Pierre & Marie Curie — Paris 6, UMR CNRS 7072 Tectonique, Département de Géologie Sédimentaire, 4 place Jussieu,75252 Paris cedex 05, France

ARTICLE INFO

Article history:
Received 4 October 2007
Received in revised form 21 April 2008
Accepted 28 April 2008

Keywords:
Gulf of Mexico
Holocene
anoxia
euxinia
geochemistry
molybdenum
nickel
chromium
brines

ABSTRACT

The Orca Basin, located in the Gulf of Mexico, is a highly stratified basin that collects sedimentary particles of clastic origin (supplied by the Mississippi River) and of biogenic origin (marine surface productivity). The strong pycnocline induces anoxic bottom conditions that are expected to be favorable to organic matter (OM) accumulation and prone to enrichment of sediments in redox-sensitive trace metals. Here we report on OM and trace metal contents in the upper 750 cm below sea floor (cmbsf) of Core MD02-2552 (mostly Holocene) and deposited under permanently stratified bottom conditions. The organic content is dominated by marine-derived amorphous OM. Contrary to expectations, sedimentary OM in the basin is highly degraded, probably due to a long residence time of organic particles at the basin's basin's halocline at ~2240 m. Also unexpected is the limited sedimentary enrichment of redox-sensitive trace metals. We suggest that the non-enrichment in U and V could be explained by the so-called basin reservoir effect, that is, limited metal availability because of low rates of water renewal in a strongly restricted subpycnoclinal water mass. The non-enrichment in Cu could have the same cause, plus the fact that the relatively degraded OM may not readily form organometallic complexes. However a marked enrichment is observed for Mo, and a moderate one for Ni and Cr, which could be accounted for by sporadic presence of H_2S in bottom waters. Such occurrences of H_2S would not be sufficient to promote a detectable FeS to FeS_2 conversion, but they would induce the capture of Mo in the form of thiomolybdate and accessorily Ni–Cr as Ni–CrO_4 complexes.

1. Introduction

Within the Gulf of Mexico, the Orca Basin is exceptional in that rapid sedimentation (about 1 m/kyr) sustained by high rates of terrigenous clastic input and marine productivity make the basin an excellent recorder of past environmental conditions of sediment deposition (Sheu and Presley, 1986; Sheu, 1990; Van Cappellen et al., 1998; Hurtgen et al., 1999). Its stratified water mass induces anoxic bottom conditions that are potentially favorable to organic-matter preservation and accumulation of redox-sensitive trace metals.

In this paper we report on the quantity and sources of organic matter (OM) in Orca Basin sediments of recent, mostly Holocene age, as well as their trace metal contents (redox-sensitive, productivity-related and/or sulfide-forming elements), with an eye toward depositional conditions that have prevailed in the Orca Basin since the development of strongly stratified conditions at least 8000 yr ago. In the present study, we explore the trace metal contents of the Orca sediments, for which few published data are available.

2. The Orca Basin, description and previous work

The Orca Basin is an intraslope depression in the northern Gulf of Mexico (Fig. 1) characterized by strong water-column stratification (Fig. 2; Sheu, 1990; Van Cappellen et al., 1998; Hurtgen et al., 1999). The origin of the depression is related to regional salt tectonics along the Louisiana continental slope (Trabant and Presley, 1978). Morphologically, the basin is a 400-km^2 elbow-shaped depression with water depths ranging from about 1800 to 2400 m in the deepest portions (Fig. 1). There are two sub-basins separated by a medial saddle. The Orca Basin has a highly stable, anoxic brine pool, and the bottom 200 m of the Orca Basin, including the saddle, are permanently anoxic (Sheu and Presley, 1986; Van Cappellen et al., 1998; Hurtgen et al., 1999; Lyons and Severmann, 2006) and maintain a salinity of >260 g/l due to the dissolution of shallow subsurface salt diapirs (Shokes et al., 1977; Sheu et al., 1987). Geochemical analysis of major components in the Orca Basin brine fingerprint its source to dissolution of the regionally

* Corresponding author.
E-mail address: Nicolas.Tribovillard@univ-lille1.fr (N. Tribovillard).

0025-3227/$ – see front matter © 2008 Elsevier B.V. All rights reserved.
doi:10.1016/j.margeo.2008.04.016

Appendix A.3

Available online at www.sciencedirect.com
ScienceDirect
C. R. Geoscience 341 (2009) 1–9
COMPTES RENDUS GEOSCIENCE
http://france.elsevier.com/direct/CRAS2A/

Geomaterials (Sedimentology)

Does a strong pycnocline impact organic-matter preservation and accumulation in an anoxic setting? The case of the Orca Basin, Gulf of Mexico

Nicolas Tribovillard [a,*], Viviane Bout-Roumazeilles [a], Thomas Sionneau [a], Jean Carlos Montero Serrano [a], Armelle Riboulleau [a], François Baudin [b]

[a] *UMR 8110 CNRS géosystèmes, UFR des Sciences de la Terre, université Lille-1, bâtiment SN5, 59655 Villeneuve d'Ascq cedex, France*
[b] *Département de géologie sédimentaire, UMR 7072 CNRS Tectonique, université Paris-6, 4, place Jussieu, 75252 Paris cedex 05, France*

Received 2 May 2008; accepted after revision 3 October 2008
Available online 11 December 2008

Presented by Jean Dercourt

Abstract

The Orca Basin (an intraslope depression located in the Gulf of Mexico) collects sedimentary particles of terrestrial origin (clastic and organic particles mainly supplied by the Mississippi River) and of marine origin (biogenic productivity). The basin is partly filled with dense brines leached from salt diapirs cropping out on the sea floor, and is permanently stratified. A strong pycnocline induces anoxic bottom conditions, expectedly favorable to organic matter (OM) preservation. Here, we report on OM in the upper 750 cm below sea floor of Core MD02-2552 (Holocene). The organic content is dominated by marine-derived amorphous OM. The organic assemblage is unexpectedly degraded to some extent, which may be accounted for by a relatively long residence time of organic particles at the halocline-pycnocline at ~2240 m. Thus the organic particles are temporarily trapped and kept in contact with the dissolved oxygen-rich overlying water mass. Lastly, the land-derived organic fraction shows co-variations with the land-derived clay mineral supply. ***To cite this article: N. Tribovillard et al., C. R. Geoscience 341 (2009).***

Résumé

Une pycnocline concentrée a-t-elle un impact sur la préservation de la matière organique et sur son accumulation dans un dépôt anoxique ? Le bassin d'Orca, petite dépression située dans le Golfe du Mexique, reçoit des particules sédimentaires d'origine continentale (clastiques et organiques), véhiculées par le Mississippi principalement, et d'origine marine (productivité). Le bassin est partiellement rempli par des saumures issues du lessivage de diapirs salifères affleurant dans les fonds marins. La colonne d'eau y est très fortement stratifiée et le corps d'eau situé sous la halocline-pycnocline est totalement anoxique. Cette anoxie est *a priori* favorable à la préservation de la matière organique (MO). Nous étudions ici le contenu organique des premiers 750 cm de la carotte MD02-2552 déposés au cours de l'Holocène. Le contenu organique est dominé par la MO amorphe d'origine marine. L'état de préservation de la MO est étonnamment mauvais, compte tenu du contexte de dépôt. Cela est dû au fait que la MO est retenue durablement à l'interface de densité à ~2240 m de profondeur, ce qui permet un long séjour dans des conditions encore

* Corresponding author.
E-mail address: Nicolas.Tribovillard@univ-lille1.fr (N. Tribovillard).

1631-0713/$ – see front matter
doi:10.1016/j.crte.2008.10.002

General appendix

Appendix A.4: The Pigmy Basin data (core MD02-2553)

Table A.4.1. Grain-size data of core MD02-2553 from Pigmy Basin.

Depth (cm)	Age (cal ka BP)	Mean grain size (µm)	Mode (µm)	Clay (%, <2µm)	Silt (%, 2-63 µm)	Sand (%, >63 µm)	Cohesive-Silt (%, 2-10 µm)	Sortable-Silt (%, 10-63 µm)
5	0.14	9.81	5.15	15.52	81.94	2.54	61.78	20.16
11	0.31	10.19	4.79	17.46	78.59	3.95	64.35	14.24
12	0.33	11.26	4.68	18.16	77.16	4.68	62.30	14.85
16	0.45	9.48	5.09	15.32	82.80	1.88	61.01	21.79
20	0.56	9.54	4.41	18.24	78.15	3.61	65.90	12.25
25	0.70	8.11	4.63	17.01	81.31	1.68	64.59	16.72
29	0.81	7.51	4.79	18.17	81.47	0.36	60.27	21.20
35	0.97	9.01	4.37	18.51	78.86	2.62	63.47	15.40
40	1.11	6.81	3.87	18.91	79.86	1.23	66.75	13.11
44	1.22	6.28	3.97	22.14	77.73	0.13	60.77	16.96
50	1.39	5.21	3.75	22.16	77.84	0.00	65.00	12.84
57	1.59	8.42	4.22	14.85	85.15	0.00	57.86	27.28
65	1.81	9.93	4.22	19.77	76.51	3.72	62.81	13.69
70	1.95	9.66	4.50	18.90	79.67	1.43	54.15	25.52
74	2.06	5.62	4.31	17.38	82.60	0.02	69.82	12.79
80	2.23	7.72	4.03	19.04	79.59	1.37	63.48	16.11
85	2.36	8.05	3.90	19.25	77.86	2.88	68.47	9.39
92	2.56	5.29	4.15	20.28	79.70	0.02	68.63	11.07
95	2.64	6.61	4.09	20.19	79.72	0.09	61.54	18.18
100	2.78	5.08	3.69	21.01	78.99	0.00	67.32	11.67
104	2.89	7.76	3.76	19.78	78.30	1.92	64.14	14.16
110	3.06	6.89	3.46	20.18	79.61	0.21	59.80	19.81
114	3.17	8.35	4.03	19.02	79.44	1.53	60.74	18.70
122	3.39	6.69	4.02	20.79	79.00	0.21	60.08	18.91
125	3.48	7.90	4.16	20.55	78.93	0.52	56.58	22.35
130	3.62	7.27	4.20	19.25	80.53	0.22	59.84	20.70
136	3.78	6.08	4.48	18.79	81.01	0.20	66.73	14.28
140	3.89	6.98	3.85	21.49	78.03	0.48	61.85	16.18
145	4.03	6.87	3.92	20.27	79.59	0.14	60.46	19.13
149	4.15	6.89	3.88	19.37	80.46	0.17	61.59	18.87
155	4.31	11.57	5.08	17.07	81.16	1.77	57.44	23.72
160	4.45	9.18	4.14	20.67	78.36	0.98	52.09	26.27
164	4.56	8.76	4.72	17.51	81.24	1.25	58.61	22.62
170	4.73	6.50	4.46	17.75	82.22	0.03	64.25	17.97
175	4.87	7.54	4.32	20.30	79.27	0.43	58.16	21.11
179	4.98	7.97	4.49	20.17	79.30	0.53	56.51	22.79
187	5.20	8.11	4.41	18.31	81.28	0.41	57.62	23.67
190	5.29	8.02	4.52	18.95	80.61	0.44	57.46	23.15
194	5.40	7.25	4.38	20.72	79.07	0.21	58.04	21.03
200	5.56	7.53	4.24	21.43	78.17	0.40	56.61	21.56
205	5.70	5.87	4.19	18.03	81.96	0.02	67.54	14.42
209	5.81	6.85	4.15	22.00	77.92	0.08	57.85	20.07
215	5.98	6.23	3.76	20.84	79.16	0.00	62.42	16.74
220	6.12	6.61	4.06	19.99	79.92	0.09	62.14	17.78
224	6.23	7.66	4.24	19.16	80.20	0.64	59.97	20.23
235	6.54	8.59	4.46	18.67	80.46	0.87	56.77	23.69
239	6.65	10.49	3.73	19.28	78.08	2.64	55.61	22.47
245	6.82	6.01	4.19	17.63	82.33	0.04	67.35	14.98
250	6.95	6.93	4.17	19.89	79.94	0.17	60.78	19.16

Appendix A.4: The Pigmy Basin data

Table A.4.1. Grain-size data of core MD02-2553 from Pigmy Basin.

Depth (cm)	Age (cal ka BP)	Mean grain size (µm)	Mode (µm)	Clay (%, <2µm)	Silt (%, 2-63 µm)	Sand (%, >63 µm)	Cohesive-Silt (%, 2-10 µm)	Sortable-Silt (%, 10-63 µm)
254	7.07	10.99	3.84	20.48	77.77	1.75	60.42	17.36
260	7.23	8.44	4.28	18.66	80.17	1.16	58.99	21.18
265	7.37	6.90	4.05	20.18	79.59	0.23	60.69	18.90
269	7.48	9.85	3.67	19.18	79.47	1.34	52.57	26.91
275	7.65	6.35	3.70	20.32	79.60	0.08	62.87	16.74
280	7.79	7.28	4.08	19.47	80.22	0.31	60.25	19.97
284	7.90	7.96	4.32	19.43	79.69	0.89	58.90	20.78
290	8.07	8.10	4.26	19.25	80.64	0.11	55.33	25.31
295	8.21	10.51	4.00	19.53	79.52	0.95	48.66	30.86
305	8.48	8.79	4.26	17.93	80.77	1.31	58.67	22.10
309	8.60	7.11	3.93	21.25	78.45	0.30	59.39	19.06
314	8.74	7.52	4.00	21.89	77.67	0.44	57.45	20.22
319	8.87	6.33	3.88	22.72	77.21	0.08	60.43	16.77
324	9.01	8.64	3.81	22.41	76.44	1.14	55.67	20.78
329	9.15	7.02	3.88	21.73	78.16	0.11	57.92	20.24
334	9.29	6.05	4.37	18.51	81.45	0.04	66.65	14.80
339	9.43	6.71	3.85	22.40	77.50	0.10	59.08	18.42
344	9.57	6.78	3.98	21.85	78.05	0.10	59.46	18.59
349	9.71	6.76	3.85	22.08	77.92	0.00	57.31	20.61
354	9.85	5.91	3.80	23.01	76.91	0.08	62.60	14.32
359	9.99	7.19	3.87	21.90	77.30	0.80	60.66	16.65
364	10.53	7.25	4.20	20.61	79.12	0.28	59.19	19.93
369	10.73	6.55	4.01	21.69	78.22	0.08	60.65	17.57
374	10.93	7.71	4.40	20.57	79.04	0.39	57.66	21.37
379	11.13	7.71	3.90	20.85	78.81	0.34	57.16	21.65
384	11.33	6.44	3.74	23.65	76.20	0.14	59.13	17.07
389	11.53	6.20	3.45	24.65	75.27	0.09	59.45	15.82
394	11.73	6.12	3.63	25.96	73.98	0.06	57.80	16.18
404	12.13	5.54	3.41	25.96	74.04	0.00	60.60	13.44
409	12.33	7.22	3.64	24.63	75.27	0.11	53.92	21.35
414	12.54	6.74	3.49	25.81	73.97	0.23	56.38	17.59
419	12.74	5.77	3.11	27.50	72.48	0.02	57.78	14.70
424	12.94	5.46	3.40	25.36	74.64	0.00	60.98	13.66
429	12.98	5.23	3.52	23.72	76.28	0.00	64.02	12.26
434	13.00	4.87	3.52	26.56	73.44	0.00	62.87	10.57
439	13.03	5.44	3.55	23.32	76.68	0.00	63.25	13.43
444	13.05	6.11	3.32	26.65	73.14	0.21	57.98	15.16
449	13.08	5.49	3.63	21.75	78.25	0.00	64.57	13.69
454	13.10	5.48	3.58	22.57	77.43	0.00	63.91	13.52
459	13.13	5.84	3.52	24.08	75.92	0.00	60.15	15.78
464	13.15	6.17	3.72	23.52	76.48	0.00	59.33	17.16
469	13.18	5.51	3.45	26.44	73.56	0.00	59.28	14.29
474	13.20	5.51	3.30	26.53	73.47	0.00	59.83	13.64
479	13.23	5.71	3.34	25.98	74.02	0.00	59.37	14.65
484	13.25	5.82	3.35	26.74	73.19	0.06	58.47	14.73
489	13.28	6.27	3.72	24.41	75.50	0.09	58.81	16.68
494	13.30	5.65	3.81	21.44	78.56	0.00	64.44	14.11
499	13.33	6.15	3.38	25.91	73.85	0.25	58.80	15.04
504	13.35	5.83	3.50	27.19	72.75	0.06	57.86	14.89

Table A.4.1. Grain-size data of core MD02-2553 from Pigmy Basin.

Depth (cm)	Age (cal ka BP)	Mean grain size (µm)	Mode (µm)	Clay (%, <2µm)	Silt (%, 2-63 µm)	Sand (%, >63 µm)	Cohesive-Silt (%, 2-10 µm)	Sortable-Silt (%, 10-63 µm)
509	13.38	5.36	3.61	22.53	77.47	0.00	64.63	12.83
514	13.40	5.20	3.52	22.77	77.23	0.00	65.34	11.89
519	13.43	5.31	3.66	21.15	78.85	0.00	66.60	12.25
524	13.45	5.28	3.26	26.01	73.99	0.00	61.07	12.92
529	13.48	5.61	3.34	27.09	72.91	0.00	58.08	14.83
534	13.50	5.95	3.78	22.14	77.85	0.01	62.55	15.30
539	13.53	5.25	3.56	23.97	76.03	0.00	63.87	12.16
544	13.55	5.14	3.61	22.46	77.54	0.00	65.93	11.61
549	13.58	5.28	3.64	22.75	77.25	0.00	64.99	12.25
554	13.60	5.99	3.88	22.14	77.82	0.04	62.67	15.15
559	13.63	5.58	3.64	23.41	76.59	0.00	63.03	13.56
564	13.65	5.25	3.67	22.12	77.88	0.00	66.10	11.79
569	13.68	5.84	3.88	20.80	79.16	0.05	65.22	13.94
574	13.70	5.36	3.79	21.77	78.23	0.00	65.89	12.34
579	13.73	10.07	3.64	19.66	79.93	0.40	49.65	30.28
584	13.75	10.59	3.39	22.40	76.20	1.40	49.04	27.16
589	13.78	11.82	3.38	22.07	74.51	3.42	50.45	24.05
599	13.83	6.25	4.08	21.51	78.40	0.09	62.46	15.94
604	13.85	5.74	3.84	24.25	75.72	0.03	61.63	14.09
609	13.88	6.59	3.80	22.21	77.25	0.54	62.47	14.78
614	13.90	18.22	3.62	22.94	71.93	5.13	48.71	23.22
619	13.93	6.68	3.80	22.27	77.73	0.00	57.96	19.77
624	13.95	6.82	3.70	22.77	77.23	0.00	56.26	20.97
629	13.98	9.63	3.62	25.34	72.82	1.84	49.50	23.32
634	14.00	5.80	3.74	22.01	77.98	0.01	63.48	14.50
639	14.03	5.51	3.50	22.92	77.08	0.00	64.24	12.84
644	14.04	6.33	3.91	19.76	80.24	0.00	61.79	18.45
649	14.06	5.25	3.80	19.95	80.03	0.02	68.96	11.07
654	14.07	4.83	3.81	21.61	78.39	0.00	69.03	9.37
659	14.08	4.66	3.46	22.18	77.82	0.00	69.57	8.25
664	14.09	5.41	3.59	23.37	76.49	0.14	65.77	10.72
669	14.11	4.58	3.40	22.35	77.65	0.00	69.85	7.80
674	14.12	4.55	3.42	23.57	76.43	0.00	68.74	7.68
679	14.13	4.94	3.72	21.17	78.83	0.00	69.11	9.72
684	14.14	4.65	3.47	22.96	77.04	0.00	68.59	8.44
689	14.16	4.59	3.42	23.10	76.90	0.00	68.85	8.05
694	14.17	5.22	3.52	23.00	77.00	0.00	65.66	11.34
699	14.18	4.72	3.60	21.81	78.19	0.00	69.70	8.49
704	14.20	4.84	3.26	26.22	73.78	0.00	64.04	9.75
709	14.21	4.62	3.35	23.79	76.21	0.00	67.92	8.29
714	14.22	4.67	3.35	25.42	74.58	0.00	65.65	8.93
719	14.23	4.80	3.43	24.54	75.46	0.00	66.01	9.45
724	14.25	4.86	3.27	26.04	73.96	0.00	63.89	10.07
729	14.26	4.16	3.06	27.53	72.47	0.00	66.02	6.45
734	14.27	5.93	3.52	22.86	77.14	0.00	62.28	14.87
739	14.28	4.70	3.47	23.13	76.87	0.00	68.26	8.62
744	14.30	5.54	3.49	23.40	76.56	0.04	64.04	12.52
749	14.31	4.37	3.24	27.10	72.90	0.00	65.15	7.74
754	14.32	4.72	3.52	22.92	77.08	0.00	68.09	8.99

Appendix A.4: The Pigmy Basin data

Table A.4.1. Grain-size data of core MD02-2553 from Pigmy Basin.

Depth (cm)	Age (cal ka BP)	Mean grain size (µm)	Mode (µm)	Clay (%, <2µm)	Silt (%, 2-63 µm)	Sand (%, >63 µm)	Cohesive-Silt (%, 2-10 µm)	Sortable-Silt (%, 10-63 µm)
759	14.33	4.92	3.53	22.39	77.61	0.00	67.90	9.72
764	14.35	4.50	3.37	23.88	76.12	0.00	68.28	7.85
769	14.36	4.84	3.56	22.66	77.34	0.00	67.85	9.49
774	14.37	5.18	3.54	23.81	76.19	0.00	64.92	11.27
779	14.38	4.68	3.55	23.09	76.91	0.00	68.10	8.81
784	14.40	4.82	3.52	21.88	78.12	0.00	69.04	9.08
789	14.41	4.78	3.48	23.32	76.68	0.00	67.41	9.28
794	14.42	5.13	3.55	23.21	76.79	0.00	65.53	11.26
799	14.43	4.62	3.36	23.72	76.28	0.00	67.70	8.58
804	14.45	4.91	3.55	22.63	77.37	0.00	67.54	9.83
809	14.46	5.37	3.43	24.15	75.85	0.00	63.43	12.42
814	14.47	11.38	3.44	25.18	71.38	3.44	62.33	9.05
819	14.48	5.20	3.52	24.08	75.87	0.05	64.86	11.02
824	14.50	5.61	3.40	23.61	76.35	0.04	63.64	12.71
829	14.51	5.00	3.47	23.81	76.19	0.00	65.72	10.46
834	14.52	4.26	3.19	24.77	75.23	0.00	68.90	6.33
839	14.53	4.33	3.22	25.51	74.49	0.00	67.78	6.71
844	14.55	4.18	3.21	26.71	73.29	0.00	66.90	6.39
849	14.56	4.11	3.12	27.04	72.96	0.00	66.95	6.01
854	14.57	3.98	3.07	28.28	71.72	0.00	66.25	5.47
859	14.59	4.39	3.36	25.07	74.93	0.00	67.59	7.35
864	14.60	4.62	3.38	23.52	76.48	0.00	68.73	7.75
869	14.61	4.12	3.06	28.25	71.75	0.00	65.42	6.33
874	14.62	5.30	3.17	28.32	71.58	0.10	60.62	10.96
879	14.64	4.37	3.22	25.80	74.20	0.00	66.97	7.24
884	14.65	4.31	3.24	26.18	73.82	0.00	66.59	7.23
889	14.66	4.32	3.26	26.89	73.11	0.00	65.74	7.37
894	14.67	3.96	3.08	25.42	74.58	0.00	69.72	4.86
899	14.69	4.32	3.29	25.98	74.02	0.00	67.08	6.95
904	14.70	4.32	3.21	26.19	73.81	0.00	66.89	6.92
909	14.71	4.28	3.27	26.81	73.19	0.00	66.06	7.14
914	14.72	5.08	3.15	27.20	72.76	0.04	62.34	10.42
919	14.74	6.31	3.10	26.49	73.39	0.11	57.20	16.19
924	14.75	9.22	4.18	19.66	78.95	1.39	55.59	23.36
929	14.76	7.88	4.07	19.12	80.07	0.81	60.01	20.06
934	14.77	6.58	3.79	20.64	79.29	0.07	61.59	17.70
939	14.79	7.04	3.91	18.37	81.36	0.27	62.31	19.04
944	14.80	5.99	3.75	21.69	78.31	0.00	61.27	17.04
949	14.81	6.51	4.10	20.57	79.43	0.00	59.72	19.71
954	14.82	6.74	3.51	23.37	76.63	0.00	56.50	20.13
959	14.84	6.82	3.90	19.98	80.02	0.00	59.68	20.34
964	14.85	6.40	3.78	23.59	76.38	0.03	58.30	18.08
969	14.86	11.65	3.40	20.44	77.06	2.49	49.23	27.84
989	14.91	6.00	3.70	20.92	79.08	0.00	62.91	16.18
994	14.93	6.06	3.70	20.86	79.14	0.00	62.35	16.79
999	14.94	6.21	3.98	19.89	80.11	0.00	62.60	17.51
1004	14.95	6.09	3.44	23.05	76.95	0.00	59.90	17.05
1009	14.96	6.76	3.78	22.10	77.90	0.00	57.87	20.03
1014	14.98	6.27	3.78	19.85	80.15	0.00	62.54	17.61
1019	14.99	6.26	3.35	25.53	74.47	0.00	56.56	17.90
1024	15.00	6.63	3.88	20.43	79.57	0.00	60.49	19.09
1029	15.01	6.44	3.57	21.48	78.44	0.08	60.61	17.83

Table A.4.2. Mineralogical data of core MD02-2553 from Pigmy Basin.

Depth (cm)	Age (cal ka BP)	S (%)	I (%)	C (%)	K (%)	S/(I+C)	I 10Å/S 17Å	I5Å/I10Å	Smectite Crystallinity	Illite Crystallinity
5	0.14	72	12	4	12	4.4	0.17	0.34	1.25	0.42
11	0.31	76	11	5	8	4.7	0.14	0.29	0.99	0.30
12	0.33	79	10	6	5	4.9	0.13	0.34	1.03	0.41
16	0.45	79	9	5	7	5.7	0.12	0.40	1.12	0.32
20	0.56	77	11	6	6	4.5	0.14	0.36	1.12	0.46
25	0.70	74	12	5	9	4.3	0.16	0.41	1.33	0.47
29	0.81	81	10	6	4	5.2	0.12	0.29	1.06	0.46
35	0.97	76	11	5	7	4.6	0.15	0.33	0.95	0.32
40	1.11	71	14	7	7	3.3	0.20	0.32	1.16	0.44
44	1.22	74	13	6	8	4.0	0.17	0.26	1.17	0.47
50	1.39	70	14	9	7	3.0	0.21	0.32	1.17	0.44
55	1.53	67	15	10	8	2.7	0.23	0.32	1.21	0.39
57	1.59	72	12	7	9	3.8	0.16	0.41	1.34	0.34
65	1.81	81	9	4	5	5.9	0.11	0.30	1.00	0.37
70	1.95	72	12	7	9	3.8	0.16	0.42	1.22	0.32
74	2.06	80	9	4	7	6.1	0.11	0.35	1.28	0.37
80	2.23	84	7	4	5	7.7	0.09	0.32	1.10	0.36
85	2.36	78	10	6	6	5.1	0.12	0.37	0.99	0.33
92	2.56	77	12	5	6	4.8	0.15	0.31	1.27	0.44
95	2.64	80	10	4	7	5.7	0.13	0.27	1.02	0.52
100	2.78	79	9	7	4	5.0	0.12	0.34	1.06	0.38
104	2.89	78	10	4	8	5.5	0.13	0.38	1.10	0.44
110	3.06	73	14	6	7	3.6	0.19	0.28	1.04	0.38
114	3.17	71	11	9	9	3.5	0.16	0.42	1.13	0.31
125	3.48	74	10	8	8	4.2	0.14	0.35	1.06	0.31
130	3.62	73	13	6	8	3.7	0.18	0.33	1.03	0.36
136	3.78	82	9	3	6	6.8	0.11	0.28	1.03	0.34
140	3.89	82	8	4	5	6.4	0.10	0.35	1.02	0.31
145	4.03	76	12	6	7	4.4	0.15	0.30	1.31	0.46
149	4.15	75	10	8	7	4.1	0.14	0.37	0.92	0.36
155	4.31	78	8	6	8	5.6	0.10	0.48	1.33	0.25
164	4.56	76	10	5	9	5.1	0.13	0.39	1.22	0.34
170	4.73	77	10	6	7	4.9	0.13	0.48	1.54	0.36
175	4.87	73	12	7	8	3.9	0.17	0.36	1.16	0.36
179	4.98	71	12	7	9	3.7	0.17	0.44	1.40	0.35
187	5.20	67	15	9	9	2.8	0.22	0.33	1.32	0.43
190	5.29	69	15	9	7	2.9	0.21	0.39	1.91	0.47
194	5.40	75	10	5	10	4.8	0.13	0.43	1.20	0.33
200	5.56	69	13	10	8	3.0	0.18	0.37	1.01	0.38
205	5.70	77	11	5	8	5.0	0.14	0.32	1.17	0.45
209	5.81	70	13	7	9	3.5	0.19	0.33	1.13	0.39
215	5.98	78	10	6	6	4.9	0.13	0.40	1.23	0.36
220	6.12	81	8	6	4	5.6	0.15	0.40	1.21	0.42
224	6.23	85	7	7	2	6.5	0.08	0.45	1.34	0.68
235	6.54	71	13	6	10	3.7	0.19	0.44	1.46	0.50
239	6.65	75	12	7	6	4.0	0.16	0.32	1.26	0.39
245	6.82	79	9	4	8	6.0	0.11	0.48	1.38	0.31
250	6.95	80	9	3	8	6.9	0.11	0.37	1.00	0.38
254	7.07	79	11	4	6	5.3	0.14	0.30	1.28	0.38
260	7.23	77	11	5	8	5.0	0.14	0.47	1.57	0.39
265	7.37	81	8	5	6	6.1	0.10	0.43	0.98	0.35
275	7.65	79	8	3	9	6.9	0.10	0.47	1.27	0.26
280	7.79	75	11	6	9	4.5	0.14	0.52	1.73	0.38

Appendix A.4: The Pigmy Basin data

Table A.4.2. Mineralogical data of core MD02-2553 from Pigmy Basin.

Depth (cm)	Age (cal ka BP)	S (%)	I (%)	C (%)	K (%)	S/(I+C)	I 10Å/S 17Å	I5Å/I10Å	Smectite Crystallinity	Illite Crystallinity
284	7.90	78	10	5	7	5.3	0.12	0.42	1.00	0.44
290	8.07	75	10	7	9	4.6	0.13	0.54	1.27	0.34
295	8.21	75	11	5	8	4.6	0.15	0.34	1.29	0.34
305	8.48	67	16	7	10	2.9	0.24	0.39	1.31	0.48
309	8.60	71	13	8	8	3.3	0.18	0.33	0.87	0.29
314	8.74	68	13	9	10	3.2	0.18	0.40	0.89	0.30
319	8.87	70	10	8	11	3.8	0.14	0.78	1.26	0.27
324	9.01	78	11	5	6	5.0	0.14	0.27	0.94	0.36
329	9.15	74	12	7	8	4.0	0.16	0.15	0.95	0.29
334	9.29	69	13	7	11	3.5	0.19	0.48	0.82	0.27
339	9.43	75	11	6	8	4.4	0.15	0.34	0.89	0.26
344	9.57	77	11	6	6	4.6	0.14	0.31	0.92	0.34
349	9.71	73	13	9	6	3.4	0.17	0.33	1.00	0.36
349	9.71	75	12	8	5	3.7	0.16	0.33	1.05	0.36
354	9.85	79	9	5	8	5.9	0.11	0.42	0.90	0.27
359	9.99	71	11	7	11	3.9	0.16	0.42	0.86	0.25
364	10.53	70	12	9	9	3.3	0.18	0.37	0.97	0.30
369	10.73	68	12	10	10	3.2	0.17	0.45	1.07	0.25
374	10.93	72	12	8	8	3.6	0.17	0.33	0.86	0.28
379	11.13	72	12	8	8	3.6	0.16	0.34	0.88	0.20
384	11.33	68	13	7	12	3.5	0.19	0.42	0.92	0.32
389	11.53	67	15	7	10	3.0	0.22	0.30	1.02	0.37
394	11.73	71	12	6	10	3.9	0.17	0.40	0.87	0.30
404	12.13	72	12	5	11	4.3	0.16	0.34	0.91	0.29
409	12.33	69	14	8	10	3.1	0.20	0.39	0.87	0.27
414	12.54	70	12	6	12	3.9	0.17	0.43	0.87	0.29
419	12.74	67	15	10	9	2.7	0.22	0.34	0.81	0.26
424	12.94	74	13	7	7	3.7	0.18	0.24	0.82	0.29
429	12.98	76	11	5	8	5.0	0.14	0.39	0.96	0.32
439	13.03	77	10	7	7	4.6	0.13	0.39	0.95	0.28
444	13.05	75	13	4	8	4.5	0.17	0.28	1.06	0.36
449	13.08	76	11	6	7	4.6	0.14	0.33	1.05	0.28
454	13.10	71	13	6	9	3.6	0.19	0.31	1.18	0.33
459	13.13	75	11	6	8	4.2	0.15	0.33	0.83	0.27
464	13.15	76	11	6	7	4.5	0.14	0.36	0.94	0.28
469	13.18	74	12	6	8	4.1	0.16	0.29	0.89	0.29
474	13.20	74	11	7	8	4.2	0.15	0.33	0.88	0.26
479	13.23	74	11	8	7	3.7	0.15	0.36	0.86	0.32
484	13.25	74	12	7	6	3.7	0.17	0.30	1.17	0.34
489	13.28	78	11	5	6	4.8	0.14	0.15	1.03	0.39
494	13.30	72	13	8	7	3.4	0.18	0.31	1.03	0.35
499	13.33	72	13	6	8	3.7	0.19	0.31	0.89	0.31
504	13.35	77	11	6	7	4.5	0.14	0.32	0.88	0.26
509	13.38	76	11	6	8	4.6	0.14	0.27	0.97	0.27
514	13.40	72	11	6	11	4.3	0.15	0.43	0.97	0.34
519	13.43	74	10	6	10	4.6	0.14	0.32	0.93	0.25
524	13.45	76	11	6	7	4.5	0.14	0.31	0.98	0.31
529	13.48	74	12	6	8	4.1	0.16	0.35	0.94	0.28
534	13.50	68	14	11	8	2.8	0.20	0.42	0.87	0.33
539	13.53	65	16	7	11	2.8	0.25	0.36	0.90	0.30
544	13.55	78	9	4	8	5.6	0.12	0.37	0.94	0.29
549	13.58	77	11	5	7	4.9	0.14	0.24	0.88	0.26
554	13.60	75	11	4	10	4.9	0.15	0.35	0.95	0.26

Table A.4.2. Mineralogical data of core MD02-2553 from Pigmy Basin.

Depth (cm)	Age (cal ka BP)	S (%)	I (%)	C (%)	K (%)	S/(I+C)	I 10Å/S 17Å	I5Å/I10Å	Smectite Crystallinity	Illite Crystallinity
559	13.63	70	12	7	10	3.5	0.18	0.41	0.97	0.27
564	13.65	75	11	5	9	4.8	0.15	0.29	0.98	0.33
569	13.68	78	8	4	9	6.3	0.10	0.50	1.15	0.28
574	13.70	76	10	7	7	4.5	0.13	0.35	0.88	0.35
579	13.73	73	12	8	7	3.6	0.16	0.34	0.86	0.27
584	13.75	74	11	6	9	4.3	0.15	0.15	1.11	0.30
589	13.78	77	9	6	8	5.0	0.12	0.41	0.87	0.22
599	13.83	71	11	8	10	3.8	0.15	0.37	0.85	0.29
604	13.85	74	11	5	11	4.8	0.14	0.37	1.02	0.28
609	13.88	64	16	8	13	2.7	0.25	0.34	0.98	0.36
614	13.90	71	15	5	9	3.5	0.21	0.22	0.82	0.35
619	13.93	74	13	7	6	3.7	0.17	0.33	1.00	0.33
624	13.95	68	14	10	8	2.8	0.21	0.38	0.85	0.28
629	13.98	63	16	9	12	2.4	0.26	0.43	0.81	0.29
634	14.00	77	11	4	8	5.0	0.15	0.21	0.95	0.38
639	14.03	75	11	5	9	4.8	0.14	0.26	0.89	0.33
644	14.04	80	8	3	8	6.9	0.11	0.27	0.91	0.32
649	14.06	81	7	5	6	6.6	0.09	0.36	1.01	0.33
654	14.07	82	8	4	6	6.8	0.09	0.30	0.97	0.32
659	14.08	82	8	4	6	7.0	0.10	0.25	1.06	0.32
664	14.09	86	7	3	4	8.8	0.08	0.23	1.03	0.48
669	14.11	82	8	5	5	6.5	0.10	0.31	1.06	0.30
674	14.12	83	9	4	4	6.4	0.11	0.20	1.02	0.42
679	14.13	76	11	4	9	5.0	0.14	0.29	1.26	0.33
684	14.14	85	6	3	6	9.0	0.07	0.39	0.92	0.31
689	14.16	79	9	4	7	5.7	0.12	0.33	1.09	0.34
699	14.18	78	9	3	10	6.6	0.11	0.35	0.87	0.24
704	14.20	77	11	4	8	5.1	0.14	0.25	1.01	0.44
709	14.21	84	7	3	6	8.3	0.09	0.25	0.93	0.36
714	14.22	80	9	3	8	6.3	0.12	0.28	0.99	0.35
719	14.23	86	6	4	5	8.6	0.07	0.33	0.92	0.32
724	14.25	82	8	3	6	7.0	0.10	0.19	1.01	0.35
729	14.26	83	7	3	7	8.3	0.08	0.38	0.99	0.26
734	14.27	80	8	5	7	6.0	0.10	0.42	0.96	0.26
739	14.28	84	7	2	6	9.0	0.08	0.24	1.08	0.33
744	14.30	79	9	4	8	6.1	0.12	0.30	0.96	0.30
749	14.31	77	11	5	7	4.8	0.15	0.25	1.20	0.31
754	14.32	84	7	5	4	7.0	0.08	0.34	0.95	0.30
759	14.33	84	8	3	5	7.4	0.10	0.19	1.03	0.35
764	14.35	83	8	4	6	7.2	0.09	0.31	1.01	0.34
769	14.36	75	10	8	7	4.1	0.14	0.45	1.24	0.33
774	14.37	80	8	4	8	6.7	0.10	0.36	0.89	0.34
779	14.38	80	10	4	6	6.0	0.12	0.22	0.95	0.33
784	14.40	83	8	3	5	7.3	0.10	0.21	0.93	0.30
789	14.41	78	10	5	7	5.2	0.13	0.31	1.25	0.42
794	14.42	82	7	4	7	7.3	0.09	0.36	1.05	0.27
799	14.43	80	9	4	7	6.2	0.11	0.23	0.92	0.36
804	14.45	83	8	4	6	7.1	0.09	0.35	0.97	0.27
809	14.46	70	14	6	10	3.6	0.19	0.16	1.13	0.40
814	14.47	80	9	4	7	6.5	0.11	0.27	1.10	0.32
819	14.48	81	8	4	7	6.9	0.10	0.35	0.99	0.34
824	14.50	78	9	5	8	5.6	0.12	0.33	0.91	0.30
829	14.51	81	8	3	8	7.5	0.10	0.31	0.90	0.35

Appendix A.4: The Pigmy Basin data

Table A.4.2. Mineralogical data of core MD02-2553 from Pigmy Basin.

Depth (cm)	Age (cal ka BP)	S (%)	I (%)	C (%)	K (%)	S/(I+C)	I 10Å/S 17Å	I5Å/I10Å	Smectite Crystallinity	Illite Crystallinity
834	14.52	77	10	5	8	5.3	0.13	0.31	0.89	0.34
839	14.53	82	10	3	6	6.6	0.12	0.21	0.98	0.39
844	14.55	81	8	4	6	6.5	0.10	0.35	0.91	0.31
849	14.56	81	8	6	6	5.9	0.10	0.33	0.86	0.40
854	14.57	79	8	4	8	6.3	0.11	0.42	0.91	0.30
859	14.59	85	7	3	5	8.3	0.09	0.26	0.95	0.45
864	14.60	79	9	5	7	5.7	0.12	0.33	0.98	0.34
869	14.61	84	8	4	5	7.2	0.09	0.26	0.97	0.35
874	14.62	69	15	4	11	3.6	0.22	0.25	1.51	0.48
879	14.64	69	13	7	11	3.5	0.18	0.49	0.97	0.28
884	14.65	83	9	4	5	6.8	0.10	0.21	0.95	0.48
889	14.66	80	9	4	7	6.2	0.11	0.27	0.96	0.37
899	14.69	81	10	2	7	7.1	0.12	0.22	1.03	0.43
904	14.70	79	8	6	6	5.4	0.11	0.38	0.96	0.29
909	14.71	80	9	4	7	6.2	0.11	0.32	0.92	0.35
914	14.72	81	9	5	6	6.1	0.11	0.29	0.93	0.32
919	14.74	81	11	3	5	6.0	0.13	0.19	1.05	0.58
924	14.75	70	13	9	8	3.2	0.18	0.39	0.91	0.30
929	14.76	76	11	6	8	4.7	0.14	0.39	0.86	0.28
934	14.77	82	8	6	4	6.0	0.10	0.32	0.91	0.31
939	14.79	77	11	2	11	6.3	0.14	0.26	1.00	0.27
944	14.80	70	14	9	7	3.0	0.20	0.34	0.95	0.27
949	14.81	64	17	9	10	2.5	0.26	0.33	0.86	0.26
954	14.82	65	17	10	9	2.4	0.26	0.32	0.81	0.29
959	14.84	69	14	10	8	3.0	0.20	0.43	0.99	0.29
964	14.85	71	13	9	7	3.2	0.19	0.38	1.22	0.36
969	14.86	70	14	8	8	3.2	0.20	0.35	0.96	0.25
989	14.91	75	11	6	8	4.4	0.15	0.39	0.95	0.27
994	14.93	73	12	7	8	4.0	0.16	0.35	0.96	0.24
999	14.94	75	10	6	9	4.7	0.13	0.43	1.03	0.28
1004	14.95	66	16	7	11	2.9	0.24	0.32	0.88	0.30
1009	14.96	72	12	9	7	3.4	0.17	0.36	0.93	0.26
1014	14.98	69	13	8	10	3.4	0.18	0.43	0.92	0.25
1019	14.99	76	12	8	4	3.9	0.16	0.31	0.97	0.29
1024	15.00	73	13	8	7	3.6	0.17	0.34	0.86	0.26
1029	15.01	72	12	7	9	3.7	0.17	0.41	0.85	0.26

Table A.4.3. Elemental analysis and C/N ratio (TOC/N_{total}) of core MD02-2553 from Pigmy Basin.

		Elemental analysis				
Depth (cm)	**Age (cal ka BP)**	**N_{total} (%)**	**C_{total} (%)**	**S_{total} (%)**	**TOC (%)**	**C/N ratio**
11	0.31	0.066	2.71	0.00	0.76	11.55
12	0.33	0.077	2.82	0.05	0.88	11.44
15	0.42	0.077	2.98	0.00	0.75	9.74
20	0.56	0.068	3.25	0.00	0.76	11.17
30	0.83	0.093	3.09	0.00	1.00	10.72
35	0.97	0.070	3.35	0.01	0.88	12.62
40	1.11	0.058	2.84	0.00	0.96	16.47
50	1.39	0.059	2.82	0.03	0.92	15.62
55	1.53	0.046	3.17	0.18	1.21	26.40
57	1.59	0.026	4.74	0.09	0.49	18.98
60	1.67	0.052	3.08	0.02	0.65	12.56
70	1.95	0.051	2.89	0.01	1.04	20.45
75	2.09	0.057	3.20	0.00	0.67	11.67
80	2.23	0.061	2.74	0.00	0.77	12.70
90	2.50	0.062	3.32	0.02	0.55	8.84
92	2.56	0.055	3.15	0.00	0.57	10.38
95	2.64	0.060	3.08	0.00	0.58	9.66
100	2.78	0.056	3.04	0.00	0.66	11.73
110	3.06	0.054	2.23	0.01	1.05	19.53
114	3.17	0.052	2.89	0.10	0.80	15.47
120	3.34	0.048	2.80	0.00	1.00	20.92
122	3.39	0.048	2.69	0.00	0.92	19.16
125	3.48	0.058	2.61	0.00	0.86	14.78
130	3.62	0.045	3.19	0.00	1.53	33.91
136	3.78	0.066	3.35	0.00	0.80	12.07
140	3.89	0.058	2.44	0.00	0.56	9.66
150	4.17	0.065	3.30	0.00	0.56	8.67
155	4.31	0.066	3.15	0.00	0.72	10.84
160	4.45	0.040	2.51	0.00	0.94	23.62
170	4.73	0.060	2.85	0.00	0.75	12.51
175	4.87	0.056	2.70	0.00	0.82	14.69
180	5.01	0.047	2.51	0.01	0.87	18.54
190	5.29	0.067	3.05	0.01	1.10	16.49
195	5.42	0.060	2.89	0.00	0.81	13.45
200	5.56	0.047	2.58	0.00	0.95	20.19
210	5.84	0.059	2.31	0.00	0.86	14.61
215	5.98	0.055	2.48	0.00	0.60	10.89
220	6.12	0.058	2.71	0.00	0.74	12.70
230	6.40	0.054	2.35	0.00	0.92	17.07
235	6.54	0.049	2.70	0.00	0.83	17.00
240	6.68	0.058	2.87	0.00	0.70	12.03
250	6.95	0.056	2.10	0.00	0.65	11.68
255	7.09	0.059	2.72	0.00	0.77	13.10
260	7.23	0.061	2.93	0.00	0.76	12.45

Appendix A.4: The Pigmy Basin data

Table A.4.3. Elemental analysis and C/N ratio (TOC/N_{total}) of core MD02-2553 from Pigmy Basin.

		Elemental analysis				
Depth (cm)	**Age (cal ka BP)**	**N_{total} (%)**	**C_{total} (%)**	**S_{total} (%)**	**TOC (%)**	**C/N ratio**
270	7.51	0.055	3.07	0.11	1.04	18.96
275	7.65	0.060	3.03	0.00	1.39	23.16
280	7.79	0.061	2.97	0.00	0.73	11.91
290	8.07	0.059	1.99	0.00	0.65	11.06
295	8.21	0.053	2.26	0.00	0.89	16.73
309	8.60	0.059	2.80	0.10	0.95	16.04
314	8.74	0.071	3.10	0.07	0.95	13.42
319	8.87	0.063	3.09	0.07	0.84	13.32
324	9.01	0.082	3.04	0.08	0.81	9.84
329	9.15	0.073	2.77	0.06	1.21	16.56
334	9.29	0.064	2.96	0.07	0.67	10.54
339	9.43	0.062	3.24	0.11	0.78	12.58
344	9.57	0.070	2.98	0.07	0.81	11.50
349	9.71	0.070	2.81	0.07	1.36	19.39
354	9.85	0.087	3.26	0.08	0.67	7.67
359	9.99	0.072	2.92	0.05	0.77	10.66
364	10.5	0.074	2.96	0.076	1.02	7.2
369	10.7	0.061	3.11	0.066	0.98	5.6
374	10.9	0.079	3.01	0.049	1.27	9.6
379	11.1	0.076	2.91	0.103	1.16	9.1
384	11.3	0.094	2.63	0.079	1.10	7.9
389	11.5	0.079	2.83	0.030	0.98	7.8
394	11.7	0.072	2.71	0.048	0.99	8.3
409	12.3	0.070	2.25	0.051	1.24	8.7
414	12.5	0.092	2.84	0.015	1.11	6.3
419	12.7	0.055	2.12	0.051	1.17	11.6
424	12.9	0.096	2.34	0.082	1.40	10.5
429	13.0	0.091	2.42	0.053	1.47	11.6
439	13.0	0.071	2.44	0.078	1.51	14.2
444	13.1	0.066	2.43	0.067	1.52	15.5
449	13.1	0.083	2.40	0.067	1.49	12.0
454	13.1	0.102	2.44	0.046	1.48	9.6
459	13.1	0.074	2.40	0.046	1.49	13.5
464	13.2	0.093	2.32	0.092	1.36	10.3
469	13.2	0.074	2.48	0.056	1.55	13.5
474	13.2	0.069	2.41	0.086	1.54	14.5
484	13.3	0.097	2.34	0.107	1.38	10.1
489	13.3	0.077	2.37	0.061	1.47	13.0
494	13.3	0.094	2.37	0.097	1.22	10.7
499	13.3	0.072	2.43	0.093	1.22	14.4
504	13.4	0.072	2.34	0.112	1.49	13.8
509	13.4	0.070	2.39	0.106	1.52	14.7
514	13.4	0.091	2.37	0.075	1.36	10.8
519	13.4	0.073	2.36	0.119	1.23	13.8

Table A.4.3. Elemental analysis and C/N ratio (TOC/N_{total}) of core MD02-2553 from Pigmy Basin.

		Elemental analysis				
Depth (cm)	**Age (cal ka BP)**	**N_{total} (%)**	**C_{total} (%)**	**S_{total} (%)**	**TOC (%)**	**C/N ratio**
524	13.5	0.069	2.36	0.102	1.36	14.8
529	13.5	0.059	2.44	0.104	1.42	17.1
534	13.5	0.066	2.45	0.098	1.42	15.8
539	13.5	0.071	2.34	0.074	1.35	14.5
544	13.6	0.092	2.32	0.105	1.32	11.5
549	13.6	0.094	2.55	0.077	1.55	11.7
554	13.6	0.092	2.37	0.099	1.44	12.8
559	13.6	0.084	2.33	0.065	1.41	13.6
564	13.7	0.084	2.32	0.090	1.32	13.8
569	13.7	0.078	2.33	0.118	1.24	14.1
574	13.7	0.078	2.33	0.128	1.38	13.8
579	13.7	0.058	2.53	0.135	1.23	15.3
584	13.8	0.075	2.51	0.134	1.36	12.0
589	13.8	0.088	2.62	0.084	1.43	10.8
604	13.9	0.102	1.68	0.069	1.23	9.7
609	13.9	0.103	2.24	0.118	1.41	11.5
614	13.9	0.070	2.34	0.128	1.21	12.4
619	13.9	0.054	2.60	0.078	1.46	18.3
624	14.0	0.061	2.60	0.097	1.44	14.6
629	14.0	0.079	2.34	0.091	1.55	11.1
634	14.0	0.093	1.94	0.074	1.35	11.4
639	14.0	0.084	2.57	0.136	1.78	16.5
644	14.0	0.097	2.82	0.138	1.93	15.2
649	14.1	0.094	2.62	0.083	1.98	16.2
654	14.1	0.064	2.27	0.099	1.70	19.5
659	14.1	0.071	2.26	0.062	1.62	17.2
664	14.1	0.061	2.19	0.155	1.49	20.0
669	14.1	0.086	2.24	0.131	1.46	13.4
674	14.1	0.061	2.22	0.126	1.57	18.7
679	14.1	0.058	2.22	0.144	1.30	19.7
684	14.1	0.077	2.18	0.116	1.35	15.5
689	14.2	0.075	2.29	0.152	1.40	15.7
699	14.2	0.067	2.22	0.144	1.32	17.6
704	14.2	0.091	2.18	0.091	1.51	13.2
709	14.2	0.084	2.26	0.089	1.59	14.0
714	14.2	0.084	2.25	0.072	1.59	14.2
719	14.2	0.079	2.25	0.054	1.66	14.7
724	14.2	0.084	2.12	0.139	1.43	13.9
729	14.3	0.060	2.28	0.141	1.54	19.5
734	14.3	0.090	2.23	0.099	1.70	13.0
739	14.3	0.068	2.22	0.144	1.63	17.5
744	14.3	0.084	2.15	0.146	1.28	14.3
749	14.3	0.065	2.21	0.133	1.48	18.5
754	14.3	0.075	2.23	0.131	1.45	16.0

Appendix A.4: The Pigmy Basin data

Table A.4.3. Elemental analysis and C/N ratio (TOC/N_{total}) of core MD02-2553 from Pigmy Basin.

		Elemental analysis				
Depth (cm)	**Age (cal ka BP)**	**N_{total} (%)**	**C_{total} (%)**	**S_{total} (%)**	**TOC (%)**	**C/N ratio**
759	14.3	0.060	2.23	0.120	1.54	19.8
764	14.3	0.083	2.14	0.117	1.38	14.2
769	14.4	0.084	2.21	0.111	1.51	13.5
774	14.4	0.066	2.28	0.139	1.25	17.6
779	14.4	0.076	2.22	0.084	1.27	15.4
784	14.4	0.060	2.15	0.136	1.22	19.5
789	14.4	0.078	2.20	0.148	1.21	14.9
794	14.4	0.083	2.22	0.078	1.57	13.6
799	14.4	0.051	2.22	0.113	1.29	22.7
804	14.4	0.079	2.19	0.110	1.59	14.3
809	14.5	0.075	2.22	0.116	1.50	15.2
814	14.5	0.081	2.27	0.121	1.51	14.1
819	14.5	0.081	2.24	0.115	1.45	14.0
824	14.5	0.088	2.15	0.132	1.42	13.1
829	14.5	0.068	2.28	0.114	1.54	16.5
834	14.5	0.072	2.24	0.161	1.50	16.9
839	14.5	0.071	2.24	0.159	1.53	16.9
844	14.5	0.076	2.23	0.116	1.48	15.9
849	14.6	0.067	2.19	0.095	1.57	18.2
854	14.6	0.082	2.27	0.110	1.26	14.6
859	14.6	0.055	2.23	0.124	1.42	21.6
864	14.6	0.083	2.18	0.133	1.33	14.0
869	14.6	0.057	2.25	0.130	1.09	22.1
874	14.6	0.085	2.34	0.053	1.56	13.5
879	14.6	0.080	2.24	0.094	1.47	14.9
884	14.6	0.088	2.21	0.121	1.28	13.5
889	14.7	0.081	2.24	0.179	1.37	14.6
899	14.7	0.068	2.28	0.114	1.27	17.8
904	14.7	0.090	2.20	0.101	1.41	11.3
909	14.7	0.063	2.35	0.179	1.48	19.4
914	14.7	0.073	2.32	0.137	1.47	16.6
919	14.7	0.080	2.50	0.123	1.57	15.1
924	14.7	0.083	2.39	0.091	1.47	11.8
929	14.8	0.085	2.81	0.066	1.69	14.9
934	14.8	0.111	2.87	0.058	1.61	11.7
939	14.8	0.080	2.88	0.057	1.58	12.3
944	14.8	0.067	2.44	0.080	0.99	11.9
949	14.8	0.064	2.58	0.089	1.14	13.1
954	14.8	0.086	2.68	0.071	1.18	9.5
959	14.8	0.065	2.52	0.094	1.18	12.0
964	14.8	0.072	2.47	0.058	1.04	11.1
969	14.9	0.056	2.46	0.065	1.19	13.0
989	14.9	0.065	2.73	0.061	1.37	14.6
994	14.9	0.064	2.67	0.094	1.12	14.7

Table A.4.3. Elemental analysis and C/N ratio (TOC/N_{total}) of core MD02-2553 from Pigmy Basin.

		Elemental analysis				
Depth (cm)	**Age (cal ka BP)**	**N_{total} (%)**	**C_{total} (%)**	**S_{total} (%)**	**TOC (%)**	**C/N ratio**
999	14,9	0,073	2,75	0,070	1,42	13,6
1004	15,0	0,087	2,62	0,074	1,19	10,9
1009	15,0	0,062	2,69	0,084	1,34	15,2
1014	15,0	0,068	2,69	0,096	1,32	13,7
1019	15,0	0,066	2,67	0,090	1,19	14,2
1024	15,0	0,066	2,71	0,098	1,26	13,5
1029	15,0	0,080	2,51	0,092	1,23	11,8

Appendix A.4: The Pigmy Basin data

Table A.4.4. Carbonate ($CaCO_3$) concentrations (%) of core MD02-2553 from Pigmy Basin

Depth (cm)	Age (cal ka BP)	$CaCO_3$ (%)	Depth (cm)	Age (cal ka BP)	$CaCO_3$ (%)
5	0.14	19.0	235	6.54	15.6
11	0.31	16.2	240	6.68	18.1
12	0.33	16.1	245	6.82	15.3
15	0.42	18.6	250	6.95	12.1
20	0.56	20.7	255	7.09	16.3
25	0.70	16.1	260	7.23	18.1
30	0.83	17.5	265	7.37	14.6
35	0.97	20.5	270	7.51	16.9
40	1.11	15.7	275	7.65	13.7
45	1.25	14.2	280	7.79	18.7
50	1.39	15.8	285	7.93	17.5
55	1.53	16.3	290	8.07	11.1
60	1.67	20.2	295	8.21	11.5
65	1.81	16.8	305	8.48	17.8
70	1.95	15.4	309	8.60	15.5
75	2.09	21.2	314	8.74	17.9
80	2.23	16.4	319	8.87	18.8
85	2.36	24.5	324	9.01	18.6
90	2.50	23.1	329	9.15	13.0
92	2.56	21.5	334	9.29	19.0
95	2.64	20.8	339	9.43	20.5
100	2.78	19.8	344	9.57	18.1
105	2.92	16.4	349	9.71	12.1
110	3.06	16.9	354	9.85	21.6
114	3.17	17.4	359	9.99	17.9
120	3.34	14.9	364	10.5	16.2
122	3.39	14.7	369	10.7	17.7
125	3.48	14.6	374	10.9	14.5
130	3.62	13.9	379	11.1	14.6
135	3.76	17.2	384	11.3	12.7
136	3.78	21.3	389	11.5	15.4
140	3.89	15.7	394	11.7	14.3
145	4.03	14.7	409	12.3	8.4
150	4.17	22.8	414	12.5	14.4
155	4.31	20.3	419	12.7	7.9
160	4.45	13.0	424	12.9	7.9
165	4.59	18.9	429	13.0	7.9
170	4.73	17.5	439	13.0	7.7
175	4.87	15.6	444	13.1	7.6
180	5.01	13.6	449	13.1	7.6
187	5.20	15.8	454	13.1	8.0
190	5.29	16.2	459	13.1	7.6
195	5.42	17.4	464	13.2	8.0
200	5.56	13.6	469	13.2	7.7
205	5.70	16.2	474	13.2	7.2
210	5.84	12.0	484	13.3	8.0
215	5.98	15.7	489	13.3	7.5
220	6.12	16.4	494	13.3	9.6
225	6.26	18.2	499	13.3	10.1
230	6.40	11.9	504	13.4	7.1

Table A.4.4. Carbonate ($CaCO_3$) concentrations (%) of core MD02-2553 from Pigmy Basin

Depth (cm)	Age (cal ka BP)	$CaCO_3$ (%)	Depth (cm)	Age (cal ka BP)	$CaCO_3$ (%)
509	13.4	7.2	769	14.4	5.9
514	13.4	8.4	774	14.4	8.5
519	13.4	9.4	779	14.4	8.0
524	13.5	8.3	784	14.4	7.8
529	13.5	8.5	789	14.4	8.3
534	13.5	8.6	794	14.4	5.4
539	13.5	8.2	799	14.4	7.8
544	13.6	8.3	804	14.4	4.9
549	13.6	8.3	809	14.5	6.0
554	13.6	7.7	814	14.5	6.3
559	13.6	7.7	819	14.5	6.6
564	13.7	8.3	824	14.5	6.1
569	13.7	9.1	829	14.5	6.1
574	13.7	7.9	834	14.5	6.2
579	13.7	10.8	839	14.5	6.0
584	13.8	9.6	844	14.5	6.2
589	13.8	9.9	849	14.6	5.1
604	13.9	3.8	854	14.6	8.4
609	13.9	6.9	859	14.6	6.7
614	13.9	9.4	864	14.6	7.1
619	13.9	9.5	869	14.6	9.6
624	14.0	9.7	874	14.6	6.5
629	14.0	6.6	879	14.6	6.4
634	14.0	4.9	884	14.6	7.7
639	14.0	6.6	889	14.7	7.2
644	14.0	7.4	899	14.7	8.4
649	14.1	5.3	904	14.7	6.6
654	14.1	4.7	909	14.7	7.3
659	14.1	5.3	914	14.7	7.1
664	14.1	5.8	919	14.7	7.7
669	14.1	6.5	924	14.7	7.6
674	14.1	5.5	929	14.8	9.3
679	14.1	7.7	934	14.8	10.5
684	14.1	6.9	939	14.8	10.8
689	14.2	7.3	944	14.8	12.1
699	14.2	7.6	949	14.8	12.0
704	14.2	5.6	954	14.8	12.5
709	14.2	5.6	959	14.8	11.2
714	14.2	5.4	964	14.8	11.9
719	14.2	4.9	969	14.9	10.6
724	14.2	5.8	989	14.9	11.3
729	14.3	6.1	994	14.9	12.9
734	14.3	4.5	999	14.9	11.1
739	14.3	4.9	1004	15.0	12.0
744	14.3	7.2	1009	15.0	11.2
749	14.3	6.1	1014	15.0	11.4
754	14.3	6.5	1019	15.0	12.3
759	14.3	5.7	1024	15.0	12.0
764	14.3	6.3	1029	15.0	10.7

Appendix A.4: The Pigmy Basin data

Table A.4.5. Rock-Eval pyrolysis parameters of core MD02-2553 from Pigmy Basin.

Depth (cm)	Age (cal ka BP)	Tmax (°C)	S1 (mg/g)	S2 (mg/g)	TOC (%)	IH (mg HC/g TOC)
5	0.14	402	0.73	0.59	0.61	96
11	0.31	386	0.55	0.58	0.59	98
15	0.42	392	0.77	0.50	0.68	73
30	0.83	418	0.58	0.86	0.63	136
35	0.97	416	0.90	0.95	0.74	128
45	1.25	426	0.48	0.82	0.68	120
50	1.39	424	0.49	0.73	0.67	108
60	1.67	386	0.40	0.86	0.60	143
75	2.09	399	1.02	0.47	0.59	79
80	2.23	430	0.13	0.52	0.55	94
90	2.50	409	0.56	0.43	0.49	87
105	2.92	417	0.15	0.68	0.50	136
110	3.06	430	0.34	0.84	0.70	120
120	3.34	427	0.42	0.78	0.58	134
122	3.39	429	0.65	0.64	0.63	101
135	3.76	431	0.37	0.53	0.60	88
140	3.89	398	0.20	0.65	0.52	125
150	4.17	406	0.55	0.63	0.50	126
155	4.31	407	0.18	0.66	0.61	108
165	4.59	408	0.25	0.41	0.51	80
180	5.01	423	0.61	0.75	0.57	131
195	5.42	425	0.08	0.59	0.56	105
210	5.84	424	0.91	0.50	0.57	87
225	6.26	424	0.39	0.51	0.47	108
255	7.09	412	0.40	0.34	0.54	62
270	7.51	429	0.23	0.64	0.60	106
285	7.93	420	0.37	0.47	0.47	100
300	8.35	430	0.22	0.29	0.40	72
309	8.60	423	0.40	0.53	0.51	103
314	8.74	422	0.30	0.69	0.55	125
319	8.87	416	0.37	0.63	0.46	136
324	9.01	418	0.20	0.50	0.46	108
329	9.15	424	0.31	0.71	0.59	120
334	9.29	426	0.04	0.69	0.54	127
339	9.43	426	0.45	0.78	0.61	127
344	9.57	425	0.26	0.60	0.52	115
349	9.71	431	0.06	0.59	0.61	96
354	9.85	416	0.27	0.66	0.45	146
359	9.99	415	0.24	0.63	0.52	121
364	10.5	417	0.30	0.73	0.53	137
369	10.7	404	0.59	0.40	0.34	117
374	10.9	416	0.30	0.84	0.76	110
379	11.1	423	0.20	0.79	0.69	114
384	11.3	420	0.27	0.82	0.74	110
389	11.5	416	0.69	0.59	0.62	95
394	11.7	408	0.28	0.72	0.60	120
409	12.3	414	0.15	0.69	0.58	118
414	12.5	419	0.14	0.65	0.58	112

Table A.4.5. Rock-Eval pyrolysis parameters of core MD02-2553 from Pigmy Basin.

Depth (cm)	Age (cal ka BP)	Tmax (°C)	S1 (mg/g)	S2 (mg/g)	TOC (%)	IH (mg HC/g TOC)
449	13.1	426	0.17	0.81	1.00	81
454	13.1	426	0.11	0.86	0.98	87
459	13.1	427	0.20	1.13	1.00	113
464	13.2	427	0.14	0.94	0.96	97
469	13.2	425	0.25	0.91	1.00	91
474	13.2	425	0.16	1.01	1.00	101
484	13.3	428	0.28	0.92	0.98	93
489	13.3	428	0.24	0.90	1.00	90
494	13.3	433	0.28	0.96	1.01	95
499	13.3	430	0.23	1.18	1.04	113
504	13.4	430	0.26	0.90	0.99	90
509	13.4	430	0.45	0.92	1.03	89
514	13.4	431	0.16	0.86	0.98	87
519	13.4	430	0.26	0.98	1.01	97
524	13.5	431	0.37	1.01	1.02	99
529	13.5	429	0.33	0.95	1.01	94
534	13.5	430	0.38	1.07	1.04	102
539	13.5	428	0.34	1.04	1.03	100
544	13.6	431	0.69	1.02	1.06	96
549	13.6	426	0.80	1.09	1.10	99
554	13.6	427	1.49	1.14	1.18	96
559	13.6	427	1.18	1.20	1.14	105
564	13.7	428	1.27	1.16	1.16	100
569	13.7	427	1.00	1.06	1.10	96
574	13.7	427	0.80	0.97	1.08	89
579	13.7	429	0.81	0.84	0.89	94
584	13.8	430	0.57	0.90	0.90	100
589	13.8	430	0.47	1.02	0.95	107
604	13.9	419	0.52	0.92	0.99	92
609	13.9	420	0.96	1.33	1.18	112
614	13.9	428	0.71	0.80	0.87	91
619	13.9	431	0.82	1.11	0.99	112
624	14.0	431	0.45	0.90	0.89	101
629	14.0	428	0.14	1.03	0.88	117
634	14.0	426	0.59	1.07	1.06	100
639	14.0	430	0.37	1.62	1.39	116
644	14.0	431	0.28	1.82	1.47	123
649	14.1	429	0.29	1.88	1.52	123
654	14.1	430	0.21	1.36	1.25	108
659	14.1	428	0.40	1.19	1.22	97
664	14.1	429	0.50	1.17	1.22	95
669	14.1	432	0.09	1.09	1.15	94
674	14.1	429	0.12	1.05	1.14	92
679	14.1	429	0.25	0.97	1.14	85
684	14.1	427	0.43	1.02	1.19	85
689	14.2	430	0.31	1.21	1.18	102
699	14.2	425	0.49	1.00	1.18	84
704	14.2	428	0.25	1.07	1.20	89

Appendix A.4: The Pigmy Basin data

Table A.4.5. Rock-Eval pyrolysis parameters of core MD02-2553 from Pigmy Basin.

Depth (cm)	Age (cal ka BP)	Tmax (°C)	S1 (mg/g)	S2 (mg/g)	TOC (%)	IH (mg HC/g TOC)
709	14.2	428	0.25	1.03	1.18	87
714	14.2	429	0.18	1.07	1.19	89
719	14.2	430	0.04	0.93	1.16	80
724	14.2	427	0.18	1.13	1.17	96
729	14.3	430	0.20	1.05	1.17	96
734	14.3	426	0.16	1.13	1.17	89
739	14.3	425	0.22	1.20	1.19	95
744	14.3	426	0.33	1.17	1.20	100
749	14.3	428	0.25	1.18	1.20	98
754	14.3	429	0.60	1.08	1.20	90
759	14.3	425	0.63	1.17	1.19	98
764	14.3	429	0.24	1.19	1.18	100
769	14.4	428	0.26	0.93	1.13	82
774	14.4	428	0.32	1.07	1.16	92
779	14.4	428	0.40	1.10	1.17	94
784	14.4	427	0.60	1.07	1.17	91
789	14.4	428	0.38	0.96	1.16	82
794	14.4	427	0.27	0.96	1.13	84
799	14.4	427	0.23	1.13	1.16	97
804	14.4	427	0.28	0.92	1.13	81
809	14.5	428	0.27	1.13	1.14	99
814	14.5	426	0.30	1.05	1.14	92
819	14.5	427	0.33	0.97	1.13	85
824	14.5	427	0.50	0.96	1.15	83
829	14.5	425	0.10	1.01	1.12	90
834	14.5	429	0.40	1.15	1.22	94
839	14.5	426	0.20	1.09	1.20	90
844	14.5	429	0.13	1.14	1.21	94
849	14.6	428	0.32	1.22	1.22	100
854	14.6	429	0.10	1.12	1.20	93
859	14.6	428	0.23	1.09	1.19	91
864	14.6	427	0.15	1.01	1.16	87
869	14.6	427	0.12	1.19	1.26	94
874	14.6	427	0.09	0.97	1.15	84
879	14.6	426	0.17	1.12	1.19	94
884	14.6	427	0.12	1.14	1.19	95
889	14.7	428	0.18	1.07	1.18	90
899	14.7	428	0.20	1.16	1.21	95
904	14.7	428	0.25	0.91	1.02	89
909	14.7	425	0.19	1.21	1.22	99
914	14.7	425	0.15	1.19	1.21	98
919	14.7	430	0.12	1.27	1.21	104
924	14.7	428	0.30	1.06	0.98	108
929	14.8	426	0.21	1.28	1.27	100
934	14.8	427	0.23	1.24	1.30	95
939	14.8	431	0.17	1.02	0.98	104
944	14.8	431	0.22	0.62	0.80	77
949	14.8	428	0.19	0.82	0.84	97

Table A.4.5. Rock-Eval pyrolysis parameters of core MD02-2553 from Pigmy Basin.

Depth (cm)	Age (cal ka BP)	Tmax (°C)	S1 (mg/g)	S2 (mg/g)	TOC (%)	IH (mg HC/g TOC)
954	14,8	427	0,26	0,79	0,82	96
959	14,8	428	0,25	0,78	0,78	100
964	14,8	428	0,22	0,70	0,80	86
969	14,9	426	0,24	0,61	0,73	83
989	14,9	432	0,12	0,86	0,95	90
994	14,9	427	0,12	0,93	0,94	98
999	14,9	429	0,12	1,02	0,99	103
1004	15,0	426	0,27	0,93	0,95	97
1009	15,0	430	0,08	0,89	0,94	94
1014	15,0	427	0,13	0,85	0,93	91
1019	15,0	427	0,10	0,88	0,94	93
1024	15,0	425	0,08	0,65	0,89	73
1029	15,0	430	0,17	0,82	0,94	87

Appendix A.4: The Pigmy Basin data

Table A.4.6. Magnetic susceptibility (MS) values of core MD02-2553 from Pigmy Basin.

Depth (cm)	Age (cal ka BP)	MS ($\times 10^{-7}$ m^3/kg)
5	0.14	2.22
11	0.31	2.60
12	0.33	2.46
15	0.42	2.30
20	0.56	2.39
25	0.70	2.55
30	0.83	2.57
35	0.97	1.73
40	1.11	2.27
45	1.25	2.46
50	1.39	2.25
55	1.53	2.48
57	1.59	1.70
60	1.67	1.70
65	1.81	2.35
70	1.95	2.22
75	2.09	1.90
80	2.23	2.08
85	2.36	1.86
90	2.50	1.82
92	2.56	1.99
95	2.64	1.99
100	2.78	2.03
105	2.92	2.12
110	3.06	2.30
114	3.17	2.11
120	3.34	2.24
122	3.39	2.40
125	3.48	2.18
130	3.62	2.47
135	3.76	2.18
136	3.78	2.15
140	3.89	2.12
145	4.03	2.41
150	4.17	2.06
155	4.31	1.84
160	4.45	2.12
165	4.59	1.99
170	4.73	1.95
175	4.87	2.19
180	5.01	1.99
190	5.29	2.11
195	5.42	2.05
200	5.56	2.14
210	5.84	2.37
215	5.98	1.93
220	6.12	2.28
225	6.26	1.92
230	6.40	2.23
235	6.54	1.94
240	6.68	2.04
250	6.95	1.96

Depth (cm)	Age (ka)	MS ($\times 10^{-7}$ m^3/kg)
255	7.09	1.89
260	7.23	1.78
270	7.51	2.18
275	7.65	1.86
280	7.79	1.86
285	7.93	2.23
290	8.07	1.97
295	8.21	1.92
309	8.60	2.14
314	8.74	2.08
319	8.87	2.15
324	9.01	1.79
329	9.15	2.36
334	9.29	1.92
339	9.43	1.89
344	9.57	2.22
349	9.71	2.48
354	9.85	1.91
359	9.99	2.36
364	10.5	2.21
369	10.7	2.14
374	10.9	2.43
379	11.1	2.30
384	11.3	1.97
389	11.5	2.02
394	11.7	2.34
409	12.3	2.44
409	12.3	1.97
414	12.5	2.14
419	12.7	2.41
424	12.9	1.95
429	13.0	1.96
439	13.0	1.97
444	13.1	1.94
449	13.1	1.97
454	13.1	1.97
459	13.1	2.11
464	13.2	1.96
469	13.2	1.94
474	13.2	2.01
479	13.2	2.22
484	13.3	1.88
489	13.3	1.99
494	13.3	1.96
499	13.3	2.04
504	13.4	1.89
514	13.4	2.13
519	13.4	1.96
524	13.5	1.94
529	13.5	1.97
534	13.5	1.97
539	13.5	1.90

Table A.4.6. Magnetic susceptibility (MS) values of core MD02-2553 from Pigmy Basin.

Depth (cm)	Age (cal ka BP)	MS ($\times 10^{-7}$ m^3/kg)
544	13.6	1.92
549	13.6	2.17
554	13.6	2.00
559	13.6	1.93
564	13.7	1.95
569	13.7	2.17
574	13.7	1.87
579	13.7	2.25
584	13.8	2.11
589	13.8	1.95
599	13.8	2.11
604	13.9	2.10
609	13.9	1.96
614	13.9	2.09
619	13.9	2.15
624	14.0	2.20
629	14.0	2.32
634	14.0	1.83
639	14.0	1.88
644	14.0	1.57
649	14.1	1.48
654	14.1	1.49
659	14.1	1.54
664	14.1	1.51
669	14.1	1.54
674	14.1	1.49
679	14.1	1.51
684	14.1	1.49
689	14.2	1.50
699	14.2	1.51
704	14.2	1.53
709	14.2	1.64
714	14.2	1.65
719	14.2	1.59
724	14.2	1.50
729	14.3	1.48
734	14.3	1.44
739	14.3	1.65
744	14.3	1.58
749	14.3	1.56
754	14.3	1.47
759	14.3	1.51
764	14.3	1.52
769	14.4	1.47
774	14.4	1.49
779	14.4	1.69
784	14.4	1.53
789	14.4	1.52
794	14.4	1.70
799	14.4	1.55
804	14.4	1.48
629	14.0	2.32

Depth (cm)	Age (ka)	MS ($\times 10^{-7}$ m^3/kg)
809	14.5	1.75
814	14.5	1.72
819	14.5	1.65
824	14.5	1.51
829	14.5	1.69
834	14.5	1.46
839	14.5	1.46
844	14.5	1.42
849	14.6	1.48
854	14.6	1.52
859	14.6	1.42
864	14.6	1.54
869	14.6	1.55
874	14.6	1.60
879	14.6	1.47
884	14.6	1.54
889	14.7	1.54
899	14.7	1.55
904	14.7	1.51
909	14.7	1.48
914	14.7	1.45
919	14.7	1.40
924	14.7	1.75
929	14.8	1.75
934	14.8	1.97
939	14.8	2.25
944	14.8	2.04
949	14.8	2.05
954	14.8	2.25
959	14.8	2.21
964	14.8	2.07
969	14.9	2.37
989	14.9	2.01
994	14.9	2.03
999	14.9	2.00
1004	15.0	2.18
1009	15.0	2.02
1014	15.0	2.08
1019	15.0	2.11
1024	15.0	2.01
1029	15.0	1.99

Appendix A.4: The Pigmy Basin data

Table A.4.7. Major and trace elements abundances (Al-normalized) for the Pigmy Basin (core MD02-2553).

Depth (cm)	Age (ka)	Al (%)	Si/Al	Fe/Al	Mn/Al	Mg/Al	Ca/Al	Na/Al	K/Al	Ti/Al	LOI (%)
5	0.14	7.41	3.07	0.47	0.011	0.25	0.84	0.08	0.30	0.046	16.46
25	0.70	7.01	3.00	0.49	0.067	0.25	1.08	0.08	0.29	0.046	17.21
45	1.25	7.39	3.03	0.57	0.017	0.29	0.75	0.09	0.33	0.048	16.17
65	1.81	7.22	3.04	0.55	0.031	0.24	0.90	0.09	0.30	0.046	17.20
85	2.36	6.86	2.89	0.46	0.016	0.22	1.34	0.08	0.28	0.045	19.53
105	2.92	7.17	3.09	0.54	0.014	0.25	0.88	0.10	0.30	0.047	16.54
125	3.48	7.24	3.11	0.49	0.016	0.28	0.83	0.12	0.33	0.048	15.77
145	4.03	7.45	3.02	0.51	0.023	0.25	0.78	0.10	0.30	0.046	16.01
165	4.59	7.34	2.94	0.45	0.013	0.23	1.01	0.10	0.28	0.045	17.78
187	5.20	7.27	3.13	0.48	0.019	0.28	0.89	0.10	0.32	0.049	16.14
205	5.70	7.77	2.91	0.44	0.011	0.20	0.80	0.08	0.28	0.044	16.39
225	6.26	7.45	2.93	0.47	0.018	0.23	0.94	0.10	0.28	0.046	17.21
245	6.82	7.70	2.98	0.47	0.012	0.21	0.74	0.08	0.28	0.044	16.33
265	7.37	7.51	3.05	0.50	0.013	0.22	0.75	0.11	0.30	0.045	15.93
285	7.93	7.32	3.00	0.48	0.019	0.25	0.96	0.09	0.29	0.046	16.95
305	8.48	7.32	2.93	0.46	0.021	0.24	1.00	0.08	0.29	0.046	17.73
324	9.01	6.89	3.14	0.48	0.021	0.25	1.08	0.17	0.30	0.046	17.46
344	9.57	6.99	3.00	0.48	0.029	0.26	0.99	0.16	0.31	0.046	17.75
364	10.5	7.10	2.99	0.50	0.022	0.26	0.97	0.17	0.29	0.046	17.44
384	11.3	7.70	2.91	0.48	0.016	0.23	0.68	0.15	0.29	0.044	16.12
404	12.1	7.53	2.92	0.48	0.020	0.24	0.81	0.12	0.30	0.043	16.14
424	12.9	8.01	2.93	0.48	0.016	0.24	0.44	0.14	0.29	0.046	14.71
444	13.1	7.80	3.03	0.48	0.018	0.25	0.46	0.14	0.30	0.045	15.05
464	13.2	7.88	3.00	0.48	0.018	0.24	0.46	0.19	0.30	0.046	15.28
484	13.3	7.80	3.01	0.46	0.018	0.25	0.46	0.18	0.30	0.045	15.02
504	13.4	7.86	2.96	0.48	0.018	0.24	0.44	0.19	0.30	0.045	15.11
524	13.5	7.83	2.97	0.48	0.018	0.24	0.45	0.19	0.30	0.045	15.60
544	13.6	7.99	2.94	0.48	0.018	0.24	0.43	0.17	0.29	0.045	14.47
564	13.7	8.00	2.92	0.48	0.018	0.23	0.43	0.17	0.29	0.044	14.71
584	13.8	7.19	3.38	0.46	0.024	0.26	0.59	0.18	0.30	0.048	14.36
604	13.9	8.53	2.82	0.50	0.011	0.22	0.22	0.16	0.29	0.044	13.80
629	14.0	7.46	3.34	0.46	0.038	0.29	0.46	0.18	0.32	0.050	13.78
644	14.0	7.48	3.28	0.43	0.012	0.26	0.48	0.13	0.27	0.047	15.35
664	14.1	7.88	3.15	0.52	0.011	0.24	0.32	0.19	0.26	0.045	14.75
684	14.1	7.74	3.13	0.51	0.009	0.24	0.35	0.18	0.26	0.045	15.19
704	14.2	7.95	3.11	0.50	0.008	0.24	0.32	0.13	0.26	0.045	13.72
724	14.2	7.88	3.13	0.50	0.008	0.24	0.33	0.17	0.26	0.045	13.75
744	14.3	7.77	3.15	0.49	0.008	0.25	0.34	0.16	0.27	0.044	15.03
764	14.3	7.74	3.13	0.48	0.008	0.24	0.34	0.19	0.26	0.045	14.83
784	14.4	7.94	3.12	0.49	0.008	0.24	0.33	0.18	0.27	0.045	14.65
804	14.4	7.74	3.15	0.49	0.008	0.26	0.34	0.16	0.28	0.044	14.36
824	14.5	7.68	3.16	0.49	0.008	0.25	0.34	0.16	0.28	0.045	14.55
844	14.5	7.91	3.03	0.50	0.007	0.25	0.32	0.16	0.26	0.043	15.56
864	14.6	8.27	2.97	0.49	0.007	0.23	0.32	0.16	0.26	0.044	14.73
884	14.6	8.00	2.98	0.50	0.007	0.23	0.32	0.16	0.27	0.044	15.10
904	14.7	8.14	2.97	0.51	0.008	0.23	0.32	0.17	0.27	0.044	14.91
924	14.7	7.78	3.04	0.43	0.034	0.27	0.43	0.16	0.31	0.048	14.66
944	14.8	7.89	2.95	0.46	0.015	0.25	0.53	0.14	0.33	0.048	14.93
964	14.8	7.99	2.96	0.47	0.016	0.25	0.55	0.10	0.32	0.047	14.65
984	14.9	7.31	3.79	0.42	0.033	0.18	0.42	0.15	0.31	0.053	11.79

Table A.4.7. Major and trace elements abundances (Al-normalized) for the Pigmy Basin (core MD02-2553).

Depth (cm)	Age (ka)	P/Al x10^4	Ba/Al x10^4	V/Al x10^4	Cr/Al x10^4	Co/Al x10^4	Ni/Al x10^4	Zn/Al x10^4	Cu/Al x10^4	Mo/Al x10^4	U/Al x10^4
5	0.14	0.012	69.91	20.38	9.45	2.02	6.07	12.82	4.72		0.35
25	0.70	0.013	70.21	20.41	9.99	2.14	6.42	14.13	4.28		0.39
45	1.25	0.011	64.65	20.29	10.82	2.03	5.95	12.71	6.09		0.38
65	1.81	0.011	67.74	21.06	9.70	2.08	6.10	13.02	4.57		0.35
85	2.36	0.011	70.42	21.72	10.21	1.90	6.27	14.00	5.10		0.38
105	2.92	0.012	69.03	20.64	9.76	1.81	7.25	13.39	5.02		0.35
125	3.48	0.011	68.51	20.44	11.05	2.07	6.35	13.54	4.97		0.39
145	4.03	0.011	71.53	20.67	9.39	2.15	6.04	13.02	3.49		0.35
165	4.59	0.010	70.07	21.54	9.54	1.64	5.45	13.63	5.04		0.38
187	5.20	0.011	64.91	20.21	9.63	1.93	6.05	12.51	3.99		0.37
205	5.70	0.010	64.95	20.84	9.00	1.54	5.14	14.15	4.37		0.33
225	6.26	0.011	69.11	20.93	10.74	1.88	5.50	13.15	4.56		0.38
245	6.82	0.011	66.40	20.14	9.10	1.82	5.72	13.64	3.64		0.34
265	7.37	0.010	70.57	21.30	9.32	1.86	5.59	13.05	3.99		0.35
285	7.93	0.010	70.17	21.30	9.56	1.77	5.60	13.38	5.05		0.37
305	8.48	0.010	73.86	20.48	9.56	2.18	6.55	13.52	4.78		0.45
324	9.01	0.011	84.09	20.48	10.17	2.03	5.66	13.22	5.08		0.33
344	9.57	0.011	78.44	20.33	10.02	2.00	6.30	13.46	3.72		0.39
364	10.5	104.54	78.62	19.44	9.86	1.97	6.48	13.24	4.79	0.42	0.42
384	11.3	96.41	72.77	21.18	9.10	2.34	6.63	14.29	5.59		0.43
404	12.1	104.31	66.66	19.12	9.29	2.39	6.11	13.54	4.38		0.41
424	12.9	92.59	70.14	23.46	16.22	2.62	6.49	14.48	5.12	0.75	0.42
444	13.1	106.29	66.79	23.59	10.25	2.82	6.79	14.36	5.13		0.42
464	13.2	99.75	70.60	22.73	10.16	2.67	6.48	14.86	6.10		0.41
484	13.3	95.10	68.58	23.33	11.54	2.69	6.54	14.49	5.13	0.51	0.45
504	13.4	99.95	69.09	23.03	10.18	2.67	6.74	15.14	5.09		0.41
524	13.5	94.72	69.45	23.11	10.21	2.68	6.77	14.43	5.11		0.40
544	13.6	92.90	68.62	22.79	10.02	2.63	6.64	14.27	5.01		0.40
564	13.7	92.71	68.36	23.24	10.00	2.62	6.62	14.37	5.12		0.39
584	13.8	103.23	77.36	21.71	11.13	3.34	7.37	14.61	5.29	0.28	0.45
604	13.9	92.13	70.84	21.70	10.56	2.81	7.74	14.66	5.40	0.35	0.40
629	14.0	99.42	70.89	20.77	10.72	3.08	6.70	13.80	4.42		0.44
644	14.0	93.31	64.27	27.39	12.03	1.87	5.88	12.83	6.81	0.40	0.73
664	14.1	94.21	62.35	27.68	11.43	1.78	5.59	13.08	4.32	0.38	0.42
684	14.1	95.88	61.00	28.04	11.63	1.81	5.69	13.31	3.75	0.26	0.43
704	14.2	93.33	62.90	27.93	12.58	1.89	5.91	13.84	3.77	0.38	0.43
724	14.2	88.61	64.21	28.04	10.15	1.52	5.96	13.70	3.93	0.51	0.38
744	14.3	106.73	63.58	27.80	11.58	1.80	5.92	13.77	3.99		0.41
764	14.3	90.24	63.84	28.04	11.63	1.94	5.95	13.96	4.78	0.26	0.41
784	14.4	87.90	64.07	27.69	11.33	1.89	6.04	13.60	4.03	0.25	0.42
804	14.4	107.09	63.80	28.93	11.62	1.81	6.07	13.56	4.13		0.43
824	14.5	102.22	64.28	28.63	11.71	1.82	5.86	13.40	4.16	0.26	0.42
844	14.5	104.87	58.18	29.34	11.38	1.77	5.69	13.53	3.79	0.38	0.42
864	14.6	89.74	58.55	28.67	12.10	1.69	5.44	12.70	3.63	0.36	0.41
884	14.6	87.32	58.65	28.14	11.25	1.75	5.50	13.01	3.75	0.25	0.40
904	14.7	85.78	58.60	28.38	12.29	1.72	5.28	12.53	3.69	0.37	0.42
924	14.7	95.36	75.96	19.92	10.28	3.98	8.74	14.78	5.01	0.39	0.57
944	14.8	88.55	64.67	20.16	10.14	2.03	5.33	12.43	5.20		0.39
964	14.8	92.90	63.86	20.66	10.02	2.13	5.38	12.40	4.38		0.41
984	14.9	95.47	72.33	17.91	9.57	1.78	4.24	11.89	3.96		0.42

Appendix A.4: The Pigmy Basin data

Table A.4.7. Major and trace elements abundances (Al-normalized) for the Pigmy Basin (core MD02-2553).

Depth (cm)	Age (ka)	Th/Al x10^4	Y/Al x10^4	La/Al x10^4	Ce/Al x10^4	Zr/Al x10^4	Hf/Al x10^4
5	0.14	1.40	3.37	4.60	9.27	18.62	0.49
25	0.70	1.43	3.14	4.78	9.60	16.13	0.56
45	1.25	1.41	3.11	5.32	10.64	16.50	0.53
65	1.81	1.37	3.19	5.01	9.93	15.65	0.51
85	2.36	1.36	3.21	5.00	9.91	15.16	0.50
105	2.92	1.37	3.21	5.10	10.05	16.59	0.52
125	3.48	1.41	3.31	5.36	10.59	17.96	0.55
145	4.03	1.36	3.09	5.05	10.04	16.64	0.52
165	4.59	1.45	3.14	4.98	9.84	16.22	0.48
187	5.20	1.32	3.03	4.43	8.94	18.70	0.50
205	5.70	1.27	2.96	4.54	8.93	15.05	0.46
225	6.26	1.37	3.09	5.02	9.93	15.57	0.51
245	6.82	1.31	3.12	4.18	8.36	15.07	0.48
265	7.37	1.33	3.06	4.82	9.41	16.64	0.53
285	7.93	1.37	3.28	4.94	10.05	17.07	0.52
305	8.48	1.37	3.00	5.41	9.53	15.70	0.51
324	9.01	1.39	3.20	5.56	9.72	18.01	0.55
344	9.57	1.39	3.15	4.92	9.25	17.61	0.52
364	10.5	1.51	3.38	5.55	10.62	17.05	0.54
384	11.3	1.33	2.99	5.35	9.43	15.33	0.47
404	12.1	1.38	3.19	4.83	9.14	15.80	0.49
424	12.9	1.47	3.24	5.32	10.20	16.72	0.49
444	13.1	1.44	2.95	5.04	9.54	16.28	0.50
464	13.2	1.40	3.17	5.61	9.97	16.25	0.50
484	13.3	1.54	3.20	5.70	10.91	16.92	0.50
504	13.4	1.39	3.05	5.50	9.78	15.90	0.48
524	13.5	1.37	3.06	5.48	9.78	15.83	0.49
544	13.6	1.40	3.01	5.55	9.75	15.03	0.48
564	13.7	1.41	3.00	5.54	9.82	15.12	0.47
584	13.8	1.46	3.34	5.80	10.34	21.43	0.64
604	13.9	1.61	3.17	5.13	9.91	15.72	0.47
629	14.0	1.42	3.22	5.28	10.25	22.38	0.63
644	14.0	1.35	2.94	4.82	8.53	16.70	0.53
664	14.1	1.24	2.79	4.39	7.70	15.49	0.50
684	14.1	1.21	2.58	4.26	7.52	15.64	0.49
704	14.2	1.23	2.64	4.26	7.55	15.22	0.49
724	14.2	1.22	2.66	4.21	7.40	16.12	0.43
744	14.3	1.25	2.57	3.99	7.38	15.83	0.49
764	14.3	1.24	2.58	4.29	7.63	15.77	0.49
784	14.4	1.20	2.52	4.17	7.33	15.36	0.48
804	14.4	1.27	2.45	4.04	7.58	17.05	0.52
824	14.5	1.25	2.47	3.98	7.47	16.79	0.51
844	14.5	1.26	2.53	4.03	7.55	15.94	0.49
864	14.6	1.25	2.66	4.28	7.42	15.24	0.47
884	14.6	1.24	2.50	4.20	7.34	14.88	0.49
904	14.7	1.27	2.58	4.26	7.43	14.87	0.48
924	14.7	1.43	3.08	5.01	9.18	17.22	0.55
944	14.8	1.38	3.17	4.92	9.02	17.25	0.53
964	14.8	1.41	3.26	4.83	9.02	17.28	0.54
984	14.9	1.61	3.83	5.40	11.01	30.35	0.66

Table A.4.8. Rare earth elements (REEs) concentrations for the Pigmy Basin (core MD02-2553).

Depth (cm)	Age (ka)	La	Ce	Pr	Nd	Sm	Eu	Gd	Tb	Dy	Ho	Er	Tm	Yb	Lu
5	0.14	34.10	68.70	8.29	27.00	5.30	1.13	4.30	0.70	4.10	0.80	2.40	0.37	2.20	0.34
25	0.70	33.50	67.30	8.15	26.90	5.20	1.11	4.40	0.70	4.10	0.80	2.40	0.36	2.20	0.33
45	1.25	39.30	78.70	9.43	27.50	5.40	1.12	4.40	0.70	4.20	0.80	2.60	0.38	2.40	0.35
65	1.81	36.20	71.70	8.60	25.80	5.00	1.07	4.40	0.70	4.00	0.80	2.50	0.35	2.20	0.32
85	2.36	34.30	68.00	8.20	24.20	4.80	1.03	4.30	0.70	3.80	0.80	2.30	0.34	2.10	0.32
105	2.92	36.60	72.10	8.71	25.70	5.10	1.12	4.60	0.70	4.00	0.80	2.50	0.35	2.20	0.34
125	3.48	38.80	76.70	9.37	27.60	5.40	1.13	4.80	0.70	4.00	0.80	2.50	0.37	2.30	0.34
145	4.03	37.60	74.80	9.11	26.80	5.30	1.12	4.90	0.70	4.10	0.80	2.60	0.37	2.30	0.34
165	4.59	36.50	72.20	8.60	25.50	5.00	1.07	4.20	0.70	4.00	0.80	2.40	0.35	2.20	0.32
187	5.20	32.20	65.00	7.78	25.40	4.90	1.05	4.20	0.70	3.90	0.80	2.30	0.34	2.10	0.32
205	5.70	35.30	69.40	8.42	24.80	4.90	1.04	4.30	0.70	3.80	0.80	2.40	0.34	2.20	0.32
225	6.26	37.40	74.00	8.85	26.40	5.10	1.10	4.50	0.70	4.00	0.80	2.50	0.36	2.30	0.34
245	6.82	32.20	64.30	7.77	25.40	5.00	1.07	4.30	0.70	3.90	0.80	2.30	0.34	2.20	0.32
265	7.37	36.20	70.70	8.60	25.50	5.00	1.08	4.50	0.70	3.90	0.80	2.50	0.36	2.20	0.34
285	7.93	36.20	73.60	8.58	26.10	5.10	1.09	4.20	0.70	4.00	0.80	2.50	0.37	2.30	0.33
305	8.48	39.60	69.80	7.37	27.20	5.20	1.13	4.40	0.70	4.00	0.80	2.40	0.36	2.20	0.34
324	9.01	38.30	66.90	7.10	26.20	5.00	1.09	4.10	0.70	3.90	0.80	2.30	0.34	2.10	0.32
344	9.57	34.40	64.60	7.32	26.50	5.10	1.10	4.40	0.70	4.00	0.80	2.30	0.34	2.10	0.33
364	10.5	39.40	75.40	7.95	29.40	5.60	1.23	4.80	0.80	4.30	0.90	2.50	0.37	2.40	0.35
384	11.3	41.20	72.60	7.68	27.90	5.40	1.15	4.40	0.70	4.10	0.80	2.40	0.35	2.20	0.34
404	12.1	36.40	68.80	7.77	28.50	5.50	1.15	4.60	0.80	4.20	0.80	2.40	0.35	2.20	0.34
424	12.9	42.60	81.70	8.58	31.90	5.90	1.33	5.10	0.80	4.50	0.90	2.60	0.40	2.40	0.36
444	13.1	39.30	74.40	8.30	30.50	5.80	1.24	4.70	0.80	4.50	0.90	2.50	0.37	2.30	0.36
464	13.2	44.20	78.50	8.23	30.60	5.90	1.22	4.50	0.80	4.40	0.80	2.60	0.37	2.40	0.36
484	13.3	44.50	85.10	8.88	32.90	6.20	1.38	5.30	0.80	4.70	0.90	2.70	0.40	2.50	0.39
504	13.4	43.20	76.90	8.16	30.20	5.80	1.26	4.70	0.70	4.40	0.90	2.50	0.36	2.30	0.35
524	13.5	42.90	76.60	8.07	29.60	5.70	1.22	4.70	0.70	4.30	0.80	2.50	0.37	2.30	0.36
544	13.6	44.30	77.90	8.36	30.50	5.80	1.23	4.70	0.70	4.30	0.90	2.60	0.36	2.30	0.36
564	13.7	44.30	78.60	8.21	29.60	5.80	1.22	4.20	0.70	4.40	0.90	2.60	0.37	2.30	0.36
584	13.8	41.70	74.30	7.89	29.10	5.60	1.18	4.30	0.70	4.30	0.90	2.60	0.38	2.40	0.37
604	13.9	43.70	84.50	9.54	34.20	6.60	1.41	5.50	0.90	4.90	1.00	2.80	0.41	2.50	0.38
629	14.0	39.40	76.50	8.18	30.30	5.80	1.30	5.20	0.80	4.40	0.90	2.70	0.39	2.50	0.37
644	14.0	36.10	63.80	7.11	26.20	5.20	1.13	4.60	0.70	4.00	0.80	2.40	0.37	2.30	0.34
664	14.1	34.60	60.60	6.78	24.90	4.90	1.06	4.30	0.70	3.80	0.80	2.30	0.34	2.10	0.33
684	14.1	33.00	58.20	6.47	24.10	4.70	1.07	4.50	0.70	3.70	0.70	2.30	0.34	2.10	0.32
704	14.2	33.90	60.00	6.74	25.20	4.90	1.09	4.70	0.70	3.80	0.80	2.30	0.34	2.10	0.33
724	14.2	33.20	58.30	6.59	24.40	4.70	1.07	4.60	0.70	3.70	0.80	2.30	0.35	2.10	0.32
744	14.3	31.00	57.30	6.68	24.60	4.80	1.06	4.40	0.70	3.90	0.80	2.20	0.32	2.10	0.33
764	14.3	33.20	59.00	6.62	24.80	4.70	1.10	4.60	0.70	3.70	0.80	2.30	0.35	2.20	0.33
784	14.4	33.10	58.20	6.54	24.60	4.70	1.09	4.80	0.70	3.80	0.80	2.30	0.35	2.20	0.33
804	14.4	31.30	58.70	6.86	25.10	4.90	1.06	4.50	0.70	3.90	0.80	2.30	0.32	2.10	0.33
824	14.5	30.60	57.40	6.63	24.30	4.70	1.02	4.00	0.70	3.70	0.70	2.10	0.32	2.00	0.32
844	14.5	31.90	59.70	6.97	25.30	4.90	1.06	4.20	0.70	3.80	0.80	2.30	0.34	2.10	0.33
864	14.6	35.40	61.30	6.87	25.30	4.90	1.09	4.20	0.70	3.90	0.80	2.40	0.35	2.20	0.34
884	14.6	33.60	58.70	6.53	24.40	4.70	1.03	3.90	0.60	3.70	0.70	2.20	0.33	2.10	0.32
904	14.7	34.70	60.50	6.75	25.10	4.90	1.04	4.00	0.70	3.80	0.80	2.30	0.33	2.10	0.33
924	14.7	39.00	71.40	7.78	28.80	5.60	1.22	4.60	0.80	4.50	0.90	2.70	0.39	2.50	0.38
944	14.8	38.80	71.10	7.77	28.40	5.70	1.19	4.40	0.80	4.40	0.90	2.60	0.38	2.40	0.38
964	14.8	38.60	72.00	8.17	30.00	5.90	1.23	4.70	0.80	4.60	0.90	2.60	0.39	2.50	0.38
984	14.9	39.50	80.50	8.10	32.30	6.30	1.33	5.30	0.90	4.70	0.90	3.00	0.45	2.90	0.43

Appendix A.4: The Pigmy Basin data

Appendix A.5: The La Salle Basin data (core MD02-2549)

Table A.5.1. Grain-size data of core MD02-2549 from La Salle Basin.

Depth (cm)	Age (cal ka BP)	Mean grain size (µm)	Mode (µm)	Clay (%, <2µm)	Silt (%, 2-63 µm)	Sand (%, >63 µm)	Cohesive-Silt (%, 2-10 µm)	Sortable-Silt (%, 10-63 µm)
0	0.0	8.74	5.84	10.86	88.72	0.42	62.00	26.71
1	0.0	8.46	5.82	10.86	88.82	0.32	63.02	25.80
11	0.5	8.16	5.43	12.26	87.47	0.27	62.99	24.48
21	1.0	6.54	4.83	15.47	84.53	0.00	66.33	18.20
31	1.4	7.15	5.14	12.83	87.07	0.10	66.83	20.23
41	1.9	6.92	4.83	14.03	85.89	0.08	66.74	19.14
51	2.3	7.61	5.08	12.73	87.04	0.23	65.37	21.67
61	2.8	6.82	4.76	14.74	85.13	0.12	66.79	18.34
71	3.2	6.88	4.49	14.54	85.28	0.19	67.36	17.92
81	3.7	6.90	4.28	16.08	83.76	0.16	65.41	18.35
91	4.1	6.55	4.25	16.42	83.50	0.08	66.29	17.21
101	4.6	5.96	4.02	19.56	80.40	0.04	65.64	14.76
111	5.1	6.31	4.26	16.43	83.49	0.07	67.39	16.10
121	5.5	5.92	3.91	19.15	80.76	0.09	66.64	14.12
131	6.0	6.12	3.99	18.75	81.16	0.09	66.11	15.04
141	6.4	6.00	3.94	18.92	81.05	0.03	65.96	15.09
151	6.9	5.73	3.81	19.67	80.32	0.01	66.60	13.72
161	7.3	5.73	3.82	19.91	80.06	0.04	66.38	13.67
171	7.8	5.19	3.74	21.49	78.51	0.00	66.64	11.86
181	8.2	5.86	3.83	19.60	80.36	0.04	66.21	14.15
191	8.7	6.77	4.07	18.01	81.64	0.35	65.04	16.60
201	9.2	5.89	3.85	18.77	81.14	0.09	67.54	13.61
211	9.6	5.73	3.75	19.68	80.25	0.07	67.18	13.06
221	10.1	5.64	3.71	20.99	78.97	0.04	65.96	13.01
231	10.5	5.44	3.62	21.43	78.53	0.04	66.57	11.96
241	11.0	5.59	3.60	20.64	79.29	0.07	66.99	12.30
251	11.4	5.92	3.99	18.45	81.47	0.08	67.53	13.94
261	11.9	5.80	3.94	18.84	81.10	0.07	67.67	13.43
271	12.3	5.48	3.68	21.35	78.57	0.07	66.50	12.08
281	12.8	5.60	3.80	19.55	80.42	0.04	67.73	12.68
291	13.3	5.75	3.96	18.72	81.22	0.06	67.95	13.27
301	13.7	7.06	5.14	14.96	84.97	0.07	64.36	20.61
311	14.2	6.87	4.65	15.15	84.76	0.09	65.67	19.09
321	14.8	6.29	3.80	18.96	81.01	0.03	64.38	16.62
331	15.3	6.41	3.85	18.19	81.79	0.02	64.51	17.29
341	15.8	6.83	4.15	16.63	83.37	0.00	63.20	20.16
351	16.3	7.26	4.04	15.19	84.75	0.06	64.38	20.36
361	16.8	6.88	4.15	15.91	84.03	0.06	64.74	19.29
371	17.3	7.13	4.34	15.70	84.30	0.00	63.25	21.05
381	17.8	8.10	4.04	18.58	81.13	0.29	57.60	23.53
391	18.3	7.02	4.20	15.85	84.08	0.06	64.09	20.00
401	18.8	7.65	4.65	16.20	83.78	0.02	59.03	24.75
411	19.3	7.64	4.47	15.44	84.56	0.00	59.94	24.62
421	19.8	7.56	4.17	15.93	84.07	0.00	60.06	24.01
431	20.3	6.16	3.76	18.96	81.04	0.00	64.89	16.15
441	20.8	8.39	4.87	12.51	87.40	0.09	61.26	26.14
451	21.3	6.29	3.77	19.07	80.93	0.00	63.16	17.77
461	21.7	6.39	3.65	19.13	80.85	0.01	63.17	17.69
471	22.2	6.64	3.88	17.53	82.44	0.03	63.88	18.56

Appendix A.5: The La Salle Basin data

Table A.5.1. Grain-size data of core MD02-2549 from La Salle Basin.

Depth (cm)	Age (cal ka BP)	Mean grain size (µm)	Mode (µm)	Clay (%, <2µm)	Silt (%, 2-63 µm)	Sand (%, >63 µm)	Cohesive-Silt (%, 2-10 µm)	Sortable-Silt (%, 10-63 µm)
481	22.7	6.36	3.85	17.56	82.44	0.00	64.50	17.94
491	23.2	5.93	4.10	16.95	83.05	0.00	67.61	15.45
501	23.7	5.89	3.82	18.62	81.38	0.00	65.99	15.39
511	24.2	6.64	4.46	15.37	84.60	0.02	65.96	18.64
521	24.7	6.20	3.85	18.74	81.26	0.00	64.02	17.24
531	25.2	5.93	3.96	19.26	80.74	0.00	65.25	15.49
541	25.7	6.79	4.22	16.97	83.03	0.00	62.50	20.53
551	26.2	7.42	4.52	15.43	84.57	0.00	60.96	23.62
561	26.7	6.97	4.18	15.77	84.21	0.01	64.05	20.17
571	27.2	5.82	3.90	19.13	80.87	0.00	66.02	14.85
581	27.6	6.31	4.58	18.67	81.33	0.00	62.64	18.69
591	28.1	6.67	4.56	17.47	82.53	0.00	62.40	20.13
601	28.6	7.19	4.85	15.94	84.06	0.00	60.95	23.11
611	29.1	6.17	4.47	16.83	83.17	0.00	66.49	16.68
621	29.6	5.27	3.72	21.24	78.76	0.00	65.96	12.80
631	30.1	6.05	3.97	20.18	79.82	0.00	63.50	16.32
641	30.6	5.93	3.79	20.61	79.39	0.00	63.77	15.62
651	31.1	6.04	4.25	20.26	79.74	0.00	62.82	16.92
661	31.6	8.83	4.60	14.36	85.61	0.02	55.86	29.75
671	32.2	6.34	4.35	19.72	80.28	0.00	61.83	18.45
681	32.8	5.74	4.15	21.28	78.72	0.00	63.24	15.48
691	33.5	5.87	4.24	20.13	79.87	0.00	64.34	15.53
701	34.1	6.45	4.16	21.57	78.43	0.00	58.13	20.30
711	34.7	5.85	3.98	21.52	78.48	0.00	63.00	15.49
721	35.3	5.96	4.28	22.18	77.82	0.00	60.77	17.04
731	35.9	6.38	4.18	20.62	79.30	0.08	61.77	17.53
741	36.6	6.64	3.94	20.91	78.80	0.28	61.86	16.94
751	37.5	5.34	3.65	23.44	76.56	0.00	64.69	11.87
761	38.4	5.41	3.65	22.46	77.41	0.13	66.51	10.91
771	39.3	5.05	3.54	23.87	76.13	0.00	65.77	10.36
781	40.1	5.58	3.71	21.05	78.90	0.05	66.62	12.28
791	41.0	5.50	3.78	21.44	78.52	0.04	66.50	12.01
801	41.8	6.02	3.89	20.17	79.78	0.05	64.90	14.88
811	42.4	5.89	4.26	18.52	81.45	0.03	67.15	14.30
821	43.1	6.07	4.25	18.38	81.60	0.02	66.07	15.53
831	43.7	8.68	4.11	19.95	79.58	0.47	54.45	25.13
841	44.3	5.40	4.30	23.24	76.76	0.00	64.30	12.46
851	44.9	6.16	4.16	18.32	81.65	0.02	65.84	15.81
861	45.5	6.29	4.40	12.16	81.86	5.97	49.91	31.95
871	46.2	6.42	4.29	17.41	82.55	0.04	65.60	16.94
881	46.8	6.13	4.05	18.81	81.14	0.04	65.68	15.46
891	47.4	6.07	4.00	18.46	81.49	0.05	66.68	14.82
901	48.0	5.61	3.77	19.80	80.20	0.00	67.17	13.03
911	48.6	5.90	3.73	20.26	79.74	0.00	64.60	15.14
921	49.2	5.72	3.67	20.44	79.54	0.02	66.11	13.42
931	49.9	6.45	4.18	17.51	82.49	0.00	64.58	17.91
941	51.2	6.55	3.80	18.63	81.37	0.00	62.76	18.61
951	52.4	6.51	4.28	18.02	81.98	0.00	62.11	19.86
961	53.7	6.03	3.93	19.57	80.41	0.02	64.94	15.47

Table A.5.1. Grain-size data of core MD02-2549 from La Salle Basin.

Depth (cm)	Age (cal ka BP)	Mean grain size (µm)	Mode (µm)	Clay (%, <2µm)	Silt (%, 2-63 µm)	Sand (%, >63 µm)	Cohesive-Silt (%, 2-10 µm)	Sortable-Silt (%, 10-63 µm)
971	55.0	5.49	3.72	21.23	78.76	0.01	66.25	12.50
981	56.3	5.76	3.93	19.40	80.60	0.00	66.32	14.28
991	57.4	5.44	3.51	21.91	78.09	0.00	65.31	12.77
1001	58.6	6.28	3.57	20.95	78.98	0.08	62.88	16.09
1011	59.7	5.62	3.59	22.35	77.65	0.00	63.79	13.86
1021	60.8	5.56	3.52	22.83	77.17	0.00	63.81	13.35
1031	62.0	6.65	3.49	22.15	77.55	0.29	60.88	16.68
1041	63.1	6.46	3.80	20.25	79.63	0.13	62.95	16.67
1051	64.3	4.92	3.40	25.80	74.20	0.00	63.80	10.40
1061	65.4	5.21	3.40	24.51	75.49	0.00	63.61	11.88
1071	66.6	4.92	3.14	27.12	72.88	0.00	62.05	10.83
1081	67.7	5.51	3.55	21.60	78.39	0.01	65.95	12.44
1091	68.9	5.66	3.59	20.82	79.14	0.04	66.05	13.09
1101	70.0	5.70	3.69	20.70	79.22	0.09	66.30	12.91
1111	71.1	5.81	3.67	21.04	78.82	0.14	65.22	13.60
1121	71.8	5.63	3.89	18.15	81.85	0.00	68.14	13.72
1131	72.3	6.69	3.72	18.97	80.53	0.50	64.81	15.72
1141	72.8	6.29	3.59	22.39	77.43	0.18	61.43	16.00
1151	73.3	7.02	4.09	18.80	80.96	0.24	61.96	19.00
1161	73.8	8.25	4.12	18.51	80.79	0.69	58.11	22.68
1171	74.4	7.27	4.10	15.84	83.76	0.40	64.40	19.36
1181	74.9	6.46	4.07	16.69	83.30	0.01	66.00	17.30
1191	75.4	6.47	3.83	18.84	81.05	0.10	64.27	16.78
1361	85.0	7.19	3.47	22.97	75.76	1.28	60.65	15.11
1371	86.7	5.22	3.19	24.72	75.28	0.00	63.29	12.00
1381	88.4	4.80	3.38	25.09	74.91	0.00	64.84	10.07
1391	90.1	5.39	3.60	20.11	79.89	0.00	67.55	12.35
1401	91.8	5.82	3.75	20.00	79.96	0.05	66.10	13.85
1411	93.4	6.35	3.83	16.80	83.12	0.08	66.96	16.16
1421	94.9	5.62	3.90	20.69	79.28	0.03	66.14	13.14
1431	96.5	6.65	3.88	18.69	81.10	0.22	64.18	16.92
1441	98.0	5.86	3.28	24.82	75.18	0.00	59.94	15.24
1451	99.6	5.11	3.41	22.55	77.45	0.00	65.70	11.75
1461	101.2	5.28	3.50	21.83	78.17	0.00	65.60	12.57
1471	102.7	5.96	3.84	20.26	79.72	0.01	64.35	15.38
1481	104.3	5.27	3.31	23.53	76.47	0.00	64.47	12.00
1491	105.9	6.96	3.89	19.91	79.38	0.71	63.42	15.96
1501	108.5	5.92	3.82	21.09	78.84	0.07	64.40	14.44
1511	111.1	4.88	3.39	24.81	75.19	0.00	65.20	9.99
1521	113.7	6.01	4.05	18.42	81.56	0.02	66.65	14.90
1531	116.1	6.03	3.84	19.27	80.69	0.04	65.66	15.04
1541	118.0	5.78	3.98	19.76	80.21	0.03	66.31	13.89
1551	119.9	6.05	3.94	19.02	80.94	0.05	65.88	15.05
1561	121.9	5.92	3.69	20.08	79.91	0.02	65.03	14.88
1571	123.8	5.35	3.44	24.30	75.70	0.00	63.27	12.43
1581	125.7	4.91	3.28	25.52	74.48	0.00	63.93	10.55
1591	127.6	4.95	3.31	25.75	74.25	0.00	63.59	10.66
1601	129.5	5.30	3.35	24.35	75.65	0.00	63.40	12.25

Appendix A.5: The La Salle Basin data

Table A.5.1. Grain-size data of core MD02-2549 from the La Salle Basin.

Depth (cm)	Age (cal ka BP)	Mean grain size (µm)	Mode (µm)	Clay (%, <2µm)	Silt (%, 2-63 µm)	Sand (%, >63 µm)	Cohesive-Silt (%, 2-10 µm)	Sortable-Silt (%, 10-63 µm)
1611	131.5	4.74	3.39	26.42	73.58	0.00	64.02	9.56
1621	133.4	6.17	4.11	17.71	82.28	0.02	66.28	15.99
1631	135.3	6.12	4.12	18.28	81.69	0.03	65.63	16.06
1637	136.5	6.09	4.28	17.77	82.22	0.01	66.40	15.81
1641	137.2	6.01	4.32	17.30	82.70	0.00	66.76	15.94
1651	139.2	6.86	4.67	16.34	83.65	0.01	63.44	20.21
1661	141.1	6.85	4.70	16.58	83.42	0.00	62.58	20.84
1671	143.0	6.55	4.59	17.81	82.19	0.00	63.09	19.10
1681	144.9	6.86	4.72	15.92	84.08	0.00	63.15	20.93
1691	146.8	7.13	4.52	17.57	82.43	0.00	60.01	22.42
1701	148.8	7.04	4.72	17.37	82.63	0.00	60.14	22.50
1711	150.7	7.46	4.91	14.13	85.85	0.02	62.66	23.19
1721		8.07	4.98	15.33	84.45	0.22	59.58	24.87
1731		6.62	4.34	18.56	81.44	0.00	62.13	19.31
1741		6.39	4.00	18.22	81.76	0.03	64.13	17.63
1751		6.29	4.53	18.22	81.78	0.00	64.05	17.73
1761		6.62	4.80	14.61	85.39	0.00	66.06	19.33
1771		6.75	4.69	15.38	84.62	0.00	64.42	20.20
1781		7.62	4.49	15.67	84.11	0.22	61.55	22.56
1791		7.41	4.84	14.35	85.59	0.06	63.00	22.59
1801		7.39	4.19	16.58	82.96	0.46	62.98	19.98
1811		6.93	4.52	16.22	83.78	0.00	62.98	20.80
1821		6.88	4.72	15.95	84.05	0.00	63.07	20.98
1831		7.34	4.80	14.66	85.32	0.02	62.78	22.54
1841		7.66	4.68	14.17	85.76	0.07	61.76	24.00
1851		7.64	4.74	15.62	84.35	0.03	60.19	24.16
1861		7.42	5.03	14.77	85.05	0.18	62.67	22.38
1871		7.29	4.58	17.14	82.86	0.00	59.80	23.07
1881		8.74	6.33	13.92	86.02	0.06	55.86	30.16
1891		7.38	4.67	14.27	85.73	0.00	62.49	23.24
1901		9.40	7.54	11.16	88.84	0.00	55.10	33.74
1911		7.67	4.83	14.36	85.61	0.03	61.07	24.55
1921		7.83	5.12	14.40	85.51	0.09	60.49	25.02
1931		9.17	6.31	12.58	87.39	0.03	55.24	32.14
1941		7.19	4.85	15.94	84.03	0.03	61.91	22.11
1951		7.29	4.93	14.42	85.51	0.07	63.59	21.93
1961		9.57	5.03	13.42	86.05	0.53	56.38	29.67
1971		8.35	5.30	12.75	87.12	0.13	60.04	27.09
1981		9.34	4.86	13.67	85.65	0.68	57.92	27.72
1991		10.91	5.22	12.63	85.71	1.66	55.92	29.80
2001		6.79	4.65	15.69	84.31	0.00	63.87	20.44
2011		8.57	5.12	14.37	85.10	0.53	59.24	25.86
2021		7.00	5.11	14.05	85.95	0.00	64.74	21.20
2031		8.56	5.64	13.27	86.41	0.32	58.73	27.69
2041		7.23	5.02	15.68	84.28	0.04	61.62	22.65
2051		7.46	4.88	14.88	85.12	0.00	61.06	24.06
2061		6.65	4.81	17.60	82.40	0.00	62.30	20.10
2071		7.43	5.02	15.36	84.54	0.10	61.68	22.86
2081		6.57	4.67	17.13	82.87	0.00	63.45	19.42

Table A.5.1. Grain-size data of core MD02-2549 from the La Salle Basin.

Depth (cm)	Age (ka)	Mean grain size (µm)	Mode (µm)	Clay (%, <2µm)	Silt (%, 2-63 µm)	Sand (%, >63 µm)	Cohesive-Silt (%, 2-10 µm)	Sortable-Silt (%, 10-63 µm)
2091		7.42	4.78	17.02	82.98	0.00	59.03	23.95
2101		8.81	6.79	12.90	87.05	0.04	56.27	30.78
2111		7.52	5.30	15.84	84.13	0.03	60.23	23.90
2121		7.45	5.14	14.39	85.58	0.02	62.21	23.37
2131		7.42	4.59	16.71	83.26	0.03	59.79	23.47
2141		9.95	8.59	10.75	89.19	0.06	53.33	35.86
2151		7.63	5.41	14.57	85.43	0.00	60.36	25.07
2161		8.41	5.46	13.30	86.35	0.35	60.33	26.02
2171		8.76	5.28	13.68	86.10	0.22	57.76	28.34
2181		8.22	5.16	13.40	86.48	0.13	60.33	26.15
2191		8.22	5.99	13.29	86.65	0.06	59.41	27.23
2201		7.86	4.77	16.00	83.97	0.03	58.27	25.70
2211		8.43	5.75	14.46	85.46	0.08	57.33	28.14
2221		8.40	5.15	14.57	85.32	0.11	57.91	27.41
2231		8.97	5.49	14.76	85.00	0.23	55.87	29.13
2241		8.87	5.51	13.48	86.33	0.19	57.28	29.05
2251		9.29	5.27	13.81	85.86	0.34	56.56	29.29
2261		7.84	5.19	13.72	86.28	0.00	60.84	25.44
2271		7.64	5.11	16.15	83.83	0.02	59.13	24.69
2281		7.77	5.81	12.72	87.28	0.00	61.39	25.89
2291		7.95	4.87	14.82	85.07	0.11	59.92	25.15
2301		7.12	4.90	16.86	83.13	0.01	60.92	22.21
2311		7.41	5.27	16.12	83.86	0.01	59.85	24.01
2321		8.79	6.51	13.30	86.67	0.03	56.26	30.41
2331		8.25	5.22	15.60	84.32	0.08	57.10	27.22
2351		7.88	5.46	13.64	86.28	0.08	61.22	25.06
2371		7.27	4.79	17.12	82.82	0.06	60.99	21.83
2381		7.77	4.58	15.61	84.25	0.14	60.34	23.91
2391		6.89	4.86	18.00	81.94	0.06	61.05	20.89
2401		6.82	5.02	17.93	82.06	0.01	61.13	20.94
2411		7.10	4.50	17.95	82.03	0.02	59.91	22.12
2421		7.05	5.02	15.29	84.71	0.00	62.78	21.93
2431		6.77	4.24	17.41	82.59	0.00	62.58	20.01
2441		7.09	4.46	17.19	82.73	0.09	62.00	20.73
2454		7.15	5.25	18.29	81.69	0.02	59.11	22.57
2461		7.00	4.95	16.64	83.35	0.01	61.80	21.54
2471		7.45	5.15	16.09	83.82	0.09	60.51	23.31
2481		6.64	4.71	17.82	82.18	0.00	62.13	20.05
2491		6.70	4.54	19.27	80.73	0.00	60.17	20.56
2501		7.11	4.73	15.83	84.14	0.03	62.49	21.65
2511		7.90	5.01	15.07	84.72	0.21	60.61	24.10
2521		7.73	4.33	15.67	84.23	0.11	59.83	24.39
2531		7.80	4.97	19.17	80.59	0.24	55.93	24.66
2551		7.50	4.87	16.28	83.56	0.16	60.75	22.81
2561		9.18	5.13	15.72	83.72	0.55	57.03	26.70
2571		8.22	5.73	15.63	84.28	0.09	56.78	27.50
2581		6.93	5.08	16.47	83.53	0.00	62.16	21.36
2591		6.94	4.88	17.56	82.44	0.00	60.95	21.49
2601		7.39	5.28	17.61	82.39	0.00	57.98	24.41

Appendix A.5: The La Salle Basin data

Table A.5.1. Grain-size data of core MD02-2549 from the La Salle Basin.

Depth (cm)	Age (ka)	Mean grain size (µm)	Mode (µm)	Clay (%, <2µm)	Silt (%, 2-63 µm)	Sand (%, >63 µm)	Cohesive-Silt (%, 2-10 µm)	Sortable-Silt (%, 10-63 µm)
2611		7.62	4.71	15.60	84.24	0.15	61.02	23.22
2621		7.36	4.82	17.23	82.77	0.00	59.04	23.73
2631		7.12	4.87	17.42	82.55	0.03	60.65	21.90
2641		7.49	4.74	15.40	84.57	0.03	60.78	23.78
2651		7.77	4.82	14.82	85.00	0.19	61.16	23.83
2661		7.31	5.15	16.37	83.59	0.04	60.96	22.63
2671		7.14	5.05	15.63	84.37	0.00	62.01	22.36
2681		7.67	5.12	15.83	84.11	0.06	59.62	24.49
2691		9.47	6.44	14.42	84.92	0.65	54.93	29.99
2701		7.53	5.01	15.05	84.79	0.16	61.83	22.96
2711		7.01	4.59	17.91	82.07	0.02	60.45	21.62
2721		7.67	5.37	14.89	85.08	0.03	60.41	24.67
2731		7.07	4.89	16.97	82.97	0.06	61.78	21.19
2741		7.25	4.89	16.34	83.59	0.07	61.11	22.47
2751		6.89	4.95	16.47	83.53	0.00	62.66	20.88
2761		7.29	4.88	14.89	85.11	0.00	62.31	22.80
2771		7.44	5.00	15.01	84.89	0.10	62.01	22.88
2781		7.16	4.70	16.13	83.86	0.01	61.65	22.21
2791		7.63	5.56	15.42	84.58	0.00	59.42	25.16
2801		7.23	4.99	16.03	83.97	0.00	60.96	23.02
2811		7.46	4.55	17.83	82.17	0.00	57.68	24.49
2821		6.90	5.06	17.07	82.93	0.00	61.63	21.30
2831		7.91	5.31	14.85	85.00	0.15	60.04	24.96
2841		7.60	4.85	15.68	84.30	0.02	60.09	24.21
2851		7.30	4.64	17.67	82.30	0.03	59.33	22.98
2861		8.23	5.82	15.56	84.32	0.11	56.77	27.55
2871		7.03	5.05	17.66	82.33	0.01	60.26	22.07
2881		8.05	5.14	16.76	83.24	0.00	56.13	27.11
2891		7.06	5.05	18.00	82.00	0.00	59.46	22.54
2901		8.70	8.70	14.20	85.80	0.00	54.08	31.72
2911		7.37	4.87	17.42	82.44	0.14	59.81	22.62
2921		7.85	4.92	15.89	83.98	0.13	59.00	24.98
2931		7.06	4.69	18.42	81.57	0.01	59.40	22.17
2941		7.85	5.25	15.49	84.42	0.09	59.08	25.34
2951		7.26	4.56	17.06	82.93	0.01	60.06	22.87
2961		6.88	4.80	17.62	82.36	0.02	61.08	21.28
2971		7.23	5.43	17.91	82.09	0.00	58.61	23.48
2981		7.04	5.65	18.03	81.97	0.00	58.93	23.04
2991		7.32	5.51	17.70	82.29	0.01	58.59	23.70
3001		6.89	5.01	18.07	81.93	0.00	59.80	22.13
3011		8.04	6.49	15.31	84.68	0.01	57.10	27.58
3021		6.21	4.83	19.13	80.87	0.00	61.99	18.88
3031		6.82	5.11	17.76	82.24	0.00	60.80	21.43
3041		7.58	4.63	15.02	84.91	0.08	61.23	23.67
3051		7.24	4.71	16.87	83.13	0.00	59.94	23.19
3061		7.90	5.36	16.32	83.64	0.04	57.52	26.12
3071		8.07	4.40	18.52	81.48	0.00	55.08	26.40
3081		7.05	5.12	16.16	83.84	0.00	61.24	22.60
3091		6.34	4.76	18.65	81.35	0.00	61.94	19.40

Table A.5.1. Grain-size data of core MD02-2549 from the La Salle Basin.

Depth (cm)	Age (ka)	Mean grain size (µm)	Mode (µm)	Clay (%, <2µm)	Silt (%, 2-63 µm)	Sand (%, >63 µm)	Cohesive-Silt (%, 2-10 µm)	Sortable-Silt (%, 10-63 µm)
3101		7.62	4.26	17.03	82.82	0.14	59.08	23.74
3111		6.51	4.59	18.83	81.17	0.00	61.58	19.59
3121		7.67	4.47	20.81	78.83	0.36	55.00	23.83
3131		7.65	5.49	17.05	82.93	0.02	57.30	25.64
3141		6.18	4.47	19.76	80.24	0.00	61.70	18.54
3151		5.31	3.25	22.99	77.01	0.00	64.37	12.64
3156		8.90	5.47	15.92	83.86	0.22	54.92	28.94
3161		7.18	5.19	17.11	82.89	0.00	59.94	22.94
3171		7.01	4.96	17.61	82.39	0.00	60.37	22.03
3181		6.67	5.28	16.69	83.31	0.00	62.72	20.59
3191		7.11	5.73	18.55	81.45	0.00	58.26	23.19
3201		6.75	5.97	17.37	82.63	0.00	60.67	21.96
3211		6.97	5.71	16.57	83.43	0.00	60.52	22.92
3221		7.07	5.39	17.44	82.51	0.05	60.42	22.08
3231		7.32	5.65	16.22	83.78	0.00	60.02	23.76
3241		8.29	7.29	15.62	84.38	0.00	55.14	29.24
3251		8.06	6.11	14.53	85.42	0.05	58.42	26.99
3261		7.86	5.53	15.23	84.61	0.16	59.59	25.02
3271		7.20	5.07	17.43	82.55	0.02	59.69	22.87
3281		6.63	4.89	16.79	83.21	0.00	63.25	19.95
3291		7.67	5.68	14.99	84.99	0.02	59.93	25.06
3302		7.81	6.17	15.32	84.57	0.11	58.86	25.71
3311		7.94	5.89	16.31	83.65	0.03	57.03	26.62
3321		7.69	7.09	16.19	83.81	0.00	56.63	27.18
3331		7.23	6.37	16.34	83.66	0.00	59.00	24.66
3341		6.46	5.08	17.74	82.26	0.00	62.31	19.95
3351		6.47	4.64	19.80	80.20	0.00	60.72	19.48
3361		6.76	5.20	17.39	82.61	0.00	61.52	21.09
3371		7.74	6.65	15.67	84.33	0.00	57.46	26.88
3381		7.85	6.92	15.78	84.22	0.00	56.60	27.62
3391		7.05	5.84	18.08	81.92	0.00	59.06	22.86
3401		8.11	6.93	15.72	84.25	0.02	56.19	28.07
3411		7.28	5.09	16.65	83.35	0.00	59.82	23.53
3421		7.01	5.31	18.13	81.86	0.02	59.77	22.09
3431		7.60	5.78	17.43	82.56	0.01	56.65	25.91
3441		6.62	5.47	18.04	81.96	0.00	60.65	21.32
3451		7.48	5.88	14.77	85.23	0.00	60.72	24.51
3461		6.24	4.44	19.50	80.50	0.00	62.50	18.00
3471		7.45	4.93	16.92	83.08	0.00	58.48	24.60
3481		6.95	5.27	18.80	81.20	0.00	58.81	22.39
3501		7.13	5.60	18.37	81.63	0.00	58.30	23.33
3511		7.31	4.91	16.58	83.29	0.13	60.30	22.99
3521		6.95	5.06	18.48	81.52	0.00	59.34	22.18
3525		10.67	8.95	14.27	85.13	0.60	49.47	35.66
3531		6.94	5.55	17.57	82.43	0.00	59.78	22.65
3541		6.86	5.39	19.15	80.85	0.00	58.32	22.53
3551		7.29	5.38	17.57	82.43	0.00	58.35	24.08
3561		7.44	5.32	17.46	82.49	0.04	58.33	24.16
3571		7.08	5.29	18.36	81.64	0.00	58.93	22.72

Appendix A.5: The La Salle Basin data

Table A.5.1. Grain-size data of core MD02-2549 from the La Salle Basin.

Depth (cm)	Age (ka)	Mean grain size (µm)	Mode (µm)	Clay (%, <2µm)	Silt (%, 2-63 µm)	Sand (%, >63 µm)	Cohesive-Silt (%, 2-10 µm)	Sortable-Silt (%, 10-63 µm)
3581		8,76	7,99	15,60	84,38	0,02	53,46	30,93
3591		7,23	5,91	17,62	82,36	0,02	58,92	23,44
3601		7,88	5,44	16,59	83,41	0,01	57,28	26,12
3611		8,30	4,97	16,11	83,83	0,05	56,61	27,22
3621		7,55	4,76	16,96	83,02	0,02	58,88	24,15
3631		6,53	4,71	20,89	79,11	0,00	59,25	19,86
3641		8,78	5,93	15,57	84,32	0,11	54,37	29,96
3651		7,03	4,28	18,30	81,68	0,02	60,65	21,03
3661		7,18	4,89	16,77	83,22	0,01	60,93	22,29
3671		7,88	5,22	15,33	84,64	0,03	59,24	25,40
3681		7,00	4,66	16,97	83,03	0,00	61,29	21,74
3691		7,16	5,21	16,79	83,21	0,00	59,93	23,28
3701		8,06	7,07	15,52	84,48	0,00	55,75	28,73
3705		9,79	7,09	13,56	86,44	0,00	51,78	34,66
3711		7,52	5,23	17,06	82,94	0,00	58,58	24,36
3721		9,18	7,58	13,28	86,56	0,16	54,66	31,90
3731		8,18	5,74	15,46	84,42	0,12	57,45	26,97
3741		7,66	4,99	16,27	83,69	0,04	59,34	24,35
3750		7,53	4,77	16,85	83,14	0,01	59,01	24,13
3760		7,56	6,10	17,14	82,86	0,00	57,43	25,43
3770		6,89	4,47	17,65	82,35	0,00	60,92	21,43

Table A.5.2. Mineralogical data of core MD02-2549 from the La Salle Basin.

Depth (cm)	Age (ka)	S (%)	I (%)	C (%)	K (%)	S/(I+C)	I5Å/I10Å	Smectite Crystallinity	Illite Crystallinity
0	0.0	84	7	2	7	9.25	0.30	1.16	0.41
1	0.0	77	9	5	10	5.81	0.49	0.99	0.29
11	0.5	77	8	6	8	5.20	0.34	0.95	0.34
21	1.0	78	9	4	9	6.13	0.30	0.98	0.40
31	1.4	79	8	4	9	6.24	0.39	1.07	0.36
41	1.9	78	9	4	9	5.96	0.32	0.98	0.37
51	2.3	81	7	5	8	6.91	0.36	1.04	0.31
61	2.8	79	9	3	9	6.49	0.31	1.02	0.33
71	3.2	77	9	6	9	5.23	0.40	1.00	0.32
81	3.7	83	7	4	7	7.75	0.41	1.07	0.33
91	4.1	79	8	6	8	5.93	0.41	1.02	0.26
101	4.6	84	6	4	5	8.17	0.20	1.10	0.37
111	5.1	78	8	4	9	6.14	0.31	1.00	0.33
121	5.5	80	9	4	7	6.55	0.30	1.05	0.34
131	6.0	80	8	5	7	6.28	0.31	0.98	0.35
141	6.4	78	9	4	8	5.94	0.47	1.03	0.38
151	6.9	79	8	5	7	5.83	0.38	1.00	0.33
161	7.3	80	8	5	8	6.39	0.47	1.55	0.26
171	7.8	81	7	4	8	7.23	0.32	0.96	0.31
181	8.2	84	7	3	6	8.16	0.30	1.03	0.37
191	8.7	81	8	4	7	6.87	0.27	1.10	0.23
201	9.2	77	9	3	10	5.99	0.42	1.04	0.40
211	9.6	81	7	4	8	7.27	0.32	0.92	0.34
221	10.1	75	10	7	8	4.47	0.43	0.92	0.38
231	10.5	81	8	4	7	6.90	0.31	1.02	0.31
241	11.0	80	8	5	7	6.23	0.34	0.96	0.35
251	11.4	82	7	5	6	6.53	0.26	1.03	0.36
261	11.9	77	9	6	9	5.37	0.29	1.01	0.30
271	12.3	76	9	5	9	5.16	0.34	1.12	0.34
281	12.8	78	8	6	9	5.80	0.40	1.00	0.27
291	13.3	76	9	6	10	5.27	0.46	1.11	0.29
301	13.7	84	6	3	7	9.59	0.41	1.16	0.29
311	14.2	79	8	5	9	6.45	0.39	1.17	0.40
321	14.8	76	8	6	9	5.41	0.36	1.09	0.34
331	15.3	82	8	2	7	8.08	0.25	1.10	0.47
341	15.8	80	8	6	5	5.67	0.36	1.11	0.45
351	16.3	72	10	5	13	4.61	0.41	1.07	0.38
361	16.8	81	8	4	6	6.45	0.25	1.10	0.41
371	17.3	72	10	8	10	3.89	0.51	1.19	0.32
381	17.8	68	14	8	10	3.05	0.42	1.11	0.29
391	18.3	73	12	9	6	3.40	0.36	0.99	0.29
401	18.8	67	17	9	7	2.56	0.30	1.13	0.39
411	19.3	64	17	10	9	2.39	0.39	1.21	0.33
421	19.8	71	15	7	7	3.21	0.28	1.11	0.40
431	20.3	69	15	8	8	2.94	0.30	1.14	0.42
441	20.8	70	14	6	10	3.56	0.30	1.18	0.36
451	21.3	58	18	12	13	1.99	0.52	1.22	0.28
461	21.7	68	15	8	9	3.04	0.29	1.06	0.36
471	22.2	77	10	7	6	4.54	0.45	1.05	0.30
481	22.7	81	9	4	7	6.65	0.26	1.10	0.35
491	23.2	81	10	5	5	5.47	0.35	1.05	0.44

Appendix A.5: The La Salle Basin data

Table A.5.2. Mineralogical data of core MD02-2549 from the La Salle Basin

Depth (cm)	Age (ka)	S (%)	I (%)	C (%)	K (%)	S/(I+C)	I5Å/I10Å	Smectite Crystallinity	Illite Crystallinity
501	23.7	75	12	6	7	4.13	0.34	1.02	0.44
511	24.2	67	18	9	6	2.49	0.30	0.98	0.41
521	24.7	68	17	10	5	2.51	0.30	1.32	0.40
531	25.2	58	22	11	9	1.74	0.43	1.11	0.44
541	25.7	71	15	7	7	3.10	0.39	1.19	0.37
551	26.2	73	15	8	4	3.14	0.27	0.93	0.41
561	26.7	62	18	10	9	2.19	0.49	1.29	0.33
571	27.2	64	19	12	6	2.10	0.29	1.10	0.42
581	27.6	62	18	11	9	2.09	0.47	1.17	0.35
591	28.1	58	21	15	6	1.60	0.42	1.29	0.44
601	28.6	61	19	11	9	2.03	0.53	1.23	0.34
611	29.1	55	24	8	13	1.70	0.36	1.35	0.39
621	29.6	56	22	12	11	1.64	0.32	1.31	0.33
631	30.1	58	22	12	8	1.73	0.39	1.27	0.38
641	30.6	54	24	12	10	1.50	0.34	1.29	0.35
651	31.1	48	24	20	8	1.08	0.47	1.30	0.37
671	32.2	57	20	13	10	1.75	0.41	1.29	0.37
681	32.8	45	25	20	10	1.00	0.47	1.44	0.37
691	33.5	43	28	18	10	0.94	0.30	1.57	0.31
701	34.1	27	38	24	11	0.43	0.39	0.50	0.32
711	34.7	45	30	19	6	0.93	0.32	1.27	0.50
721	35.3	48	26	15	11	1.19	0.39	1.42	0.38
731	35.9	36	29	24	11	0.69	0.49	1.44	0.42
741	36.6	58	19	17	7	1.60	0.37	1.55	0.42
751	37.5	55	17	14	13	1.76	0.50	1.27	0.41
761	38.4	65	13	8	15	3.19	0.37	0.89	0.34
771	39.3	70	12	7	11	3.68	0.30	1.17	0.39
781	40.1	67	13	9	11	3.06	0.30	1.23	0.44
791	41.0	72	12	6	10	4.11	0.31	1.16	0.45
801	41.8	58	18	12	11	1.91	0.38	1.38	0.42
811	42.4	66	14	12	8	2.56	0.35	1.37	0.33
821	43.1	58	18	13	11	1.88	0.37	1.19	0.38
831	43.7	56	20	15	9	1.65	0.38	1.38	0.39
841	44.3	65	16	9	10	2.58	0.34	1.25	0.46
851	44.9	61	17	10	12	2.27	0.46	1.37	0.40
861	45.5	72	12	10	6	3.30	0.33	1.23	0.36
871	46.2	62	16	10	12	2.39	0.49	1.28	0.33
881	46.8	68	14	7	11	3.37	0.28	1.16	0.39
891	47.4	63	15	12	10	2.36	0.40	1.29	0.39
901	48.0	58	16	14	12	1.93	0.36	1.27	0.28
911	48.6	63	17	8	11	2.53	0.36	1.44	0.46
921	49.2	55	17	13	15	1.84	0.51	1.27	0.33
931	49.9	57	15	12	16	2.15	0.42	1.01	0.29
941	51.2	55	17	12	16	1.89	0.44	1.20	0.36
951	52.4	60	14	8	18	2.64	0.40	1.17	0.34
961	53.7	61	15	10	14	2.48	0.25	1.24	0.37
971	55.0	59	17	14	10	1.96	0.32	1.29	0.36
981	56.3	75	9	7	9	4.63	0.52	1.17	0.28
991	57.4	71	12	10	7	3.23	0.33	1.17	0.38
1001	58.6	68	11	8	13	3.57	0.44	1.18	0.28
1011	59.7	66	14	9	11	2.84	0.48	1.43	0.51

Table A.5.2. Mineralogical data of core MD02-2549 from the La Salle Basin

Depth (cm)	Age (ka)	S (%)	I (%)	C (%)	K (%)	S/(I+C)	I5Å/I10Å	Smectite Crystallinity	Illite Crystallinity
1021	60.8	55	16	10	19	2.15	0.40	1.07	0.36
1031	62.0	64	13	12	11	2.54	0.34	1.23	0.27
1041	63.1	52	17	16	15	1.57	0.43	1.12	0.31
1051	64.3	63	14	12	11	2.42	0.36	1.47	0.36
1061	65.4	62	15	13	11	2.23	0.34	1.18	0.39
1071	66.6	68	12	10	11	3.14	0.34	1.33	0.35
1081	67.7	63	13	9	15	2.83	0.34	1.42	0.35
1091	68.9	69	12	8	11	3.51	0.50	1.21	0.31
1101	70.0	72	12	6	10	4.04	0.39	1.08	0.38
1111	71.1	68	13	7	12	3.40	0.45	0.98	0.33
1121	71.8	73	12	6	9	4.08	0.39	1.22	0.38
1131	72.3	72	12	5	11	4.20	0.40	1.11	0.37
1141	72.8	73	11	6	10	4.34	0.36	1.11	0.38
1151	73.3	76	9	8	7	4.50	0.38	1.33	0.32
1161	73.8	69	12	7	12	3.59	0.48	1.36	0.38
1171	74.4	69	14	6	12	3.43	0.44	1.08	0.34
1181	74.9	67	13	10	9	2.87	0.40	1.22	0.45
1191	75.4	73	11	4	11	4.83	0.39	1.12	0.36
1361	85.0	65	12	8	14	3.17	0.68	1.37	0.32
1371	86.7	69	12	5	13	3.87	0.49	1.19	0.42
1381	88.4	75	11	5	10	4.78	0.33	1.19	0.50
1391	90.1	69	15	4	12	3.64	0.33	1.04	0.42
1401	91.8	65	14	5	16	3.48	0.53	1.45	0.32
1411	93.4	71	12	6	11	3.87	0.40	1.28	0.35
1421	94.9	69	13	5	13	3.94	0.37	1.22	0.44
1431	96.5	67	12	8	13	3.26	0.50	1.20	0.40
1441	98.0	67	13	7	12	3.19	0.50	1.05	0.35
1451	99.6	68	13	5	15	3.99	0.43	1.16	0.37
1461	101.2	68	13	3	15	4.11	0.52	1.25	0.44
1471	102.7	65	15	8	12	2.89	0.49	1.23	0.50
1481	104.3	65	14	5	15	3.31	0.46	1.08	0.41
1491	105.9	72	12	3	13	4.73	0.30	1.13	0.41
1501	108.5	70	13	4	13	4.19	0.33	1.09	0.37
1511	111.1	66	13	6	15	3.51	0.53	1.28	0.36
1521	113.7	71	12	6	12	4.08	0.42	1.12	0.31
1531	116.1	73	12	4	12	4.67	0.30	1.19	0.49
1541	118.0	72	12	5	11	4.38	0.37	1.19	0.37
1551	119.9	73	11	6	10	4.23	0.30	1.22	0.39
1561	121.9	77	9	8	6	4.42	0.39	1.14	0.28
1571	123.8	70	12	6	12	4.04	0.44	1.18	0.29
1581	125.7	74	10	5	10	4.82	0.36	1.23	0.43
1591	127.6	63	14	7	17	3.11	0.51	1.21	0.33
1601	129.5	72	11	7	11	4.07	0.39	1.29	0.37
1611	131.5	71	10	8	11	4.09	0.37	1.34	0.31
1621	133.4	67	12	8	13	3.48	0.33	1.37	0.34
1631	135.3	58	14	8	19	2.62	0.33	0.98	0.35
1637	136.5	63	11	13	13	2.52	0.31	1.21	0.27
1641	137.2	79	8	6	7	5.40	0.30	1.01	0.42
1651	139.2	72	11	4	13	4.49	0.25	1.07	0.57
1661	141.1	69	12	8	11	3.51	0.40	0.94	0.40

Appendix A.5: The La Salle Basin data

Table A.5.2. Mineralogical data of core MD02-2549 from the La Salle Basin

Depth (cm)	Age (ka)	S (%)	I (%)	C (%)	K (%)	S/(I+C)	I5Å/I10Å	Smectite Crystallinity	Illite Crystallinity
1671	143.0	53	21	11	15	1.65	0.37	1.07	0.39
1681	144.9	73	10	7	10	4.28	0.36	0.96	0.44
1691	146.8	66	14	10	10	2.70	0.35	1.04	0.41
1701	148.8	58	18	10	15	2.07	0.38	1.30	0.46
1711	150.7	59	15	16	10	1.89	0.46	1.05	0.44
1721	152.6	69	12	9	10	3.29	0.36	1.02	0.44
1731	154.5	47	23	17	13	1.18	0.27	1.04	0.42
1741	156.4	71	13	7	8	3.48	0.33	1.10	0.45
1751		66	13	8.4	12	3.07	0.37	1.15	0.37
1761		71	13	6.8	9.8	3.68	0.40	0.91	0.45
1771		58	19	12	11	1.92	0.40	1.19	0.44
1781		80	8.4	5.9	5.4	5.62	0.32	0.91	0.36
1791		70	11	7.7	11	3.78	0.43	1.00	0.32
1801		52	22	16	10	1.40	0.44	1.10	0.38
1811		75	9.6	8.8	6.7	4.06	0.32	0.97	0.38
1821		65	18	12	5.2	2.18	0.33	0.95	0.44
1831		73	9.8	9.7	7.7	3.72	0.45	0.90	0.33
1841		71	12	9.1	7.7	3.38	0.32	0.89	0.32
1851		67	16	9.3	7.3	2.66	0.46	0.90	0.40
1861		63	18	13	6.8	2.07	0.37	0.95	0.39
1871		63	17	14	5.6	2.00	0.44	1.09	0.44
1881		67	14	12	6.6	2.60	0.35	0.88	0.36
1891		65	16	11	8.6	2.42	0.48	1.02	0.35
1901		85	7.3	5.4	2.7	6.65	0.34	0.83	0.33
1911		62	17	14	6.6	2.00	0.36	0.90	0.35
1921		56	20	16	8.2	1.53	0.46	1.07	0.32
1931		66	14	9.2	9.9	2.82	0.35	0.97	0.28
1941		58	21	15	5.5	1.62	0.34	1.14	0.32
1951		61	20	14	5.3	1.77	0.43	0.97	0.39
1961		51	25	15	8.4	1.25	0.38	1.20	0.28
1971		70	15	8.6	6.1	2.99	0.31	0.89	0.37
1981		68	16	9.8	6.3	2.65	0.42	0.84	0.40
1991		75	11	8.1	5.8	3.96	0.41	0.87	0.42
2001		64	18	13	5.1	2.09	0.39	0.93	0.40
2011		66	17	9.5	7.8	2.52	0.35	1.09	0.39
2021		55	22	12	10	1.59	0.37	1.31	0.36
2031		56	22	13	8.1	1.57	0.33	1.04	0.39
2041		60	20	16	4.5	1.66	0.33	0.93	0.40
2051		62	20	10	8.1	2.08	0.34	0.98	0.41
2061		41	31	19	9	0.82	0.28	1.04	0.31
2071		52	25	16	7.1	1.26	0.31	1.03	0.35
2081		42	31	20	7.4	0.84	0.37	0.94	0.29
2091		56	22	15	6.6	1.52	0.45	1.03	0.37
2101		72	14	9.8	4.8	3.08	0.39	0.82	0.34
2111		59	20	15	6.1	1.68	0.47	0.92	0.33
2121		66	17	12	4.7	2.30	0.39	0.89	0.37
2131		69	15	9.6	6.1	2.80	0.31	0.87	0.39
2141		71	13	10	5.5	3.05	0.45	0.82	0.34
2151		67	16	9	7.9	2.71	0.39	1.06	0.35
2161		64	18	12	6.7	2.16	0.35	0.91	0.37
2171		67	14	12	6.9	2.57	0.44	0.89	0.31

Table A.5.2. Mineralogical data of core MD02-2549 from the La Salle Basin

Depth (cm)	Age (ka)	S (%)	I (%)	C (%)	K (%)	S/(I+C)	I5Å/I10Å	Smectite Crystallinity	Illite Crystallinity
2181		61	19	11	9.1	2.04	0.35	1.13	0.37
2191		61	20	12	7.9	1.94	0.33	0.89	0.32
2201		64	18	13	4.5	2.04	0.28	1.02	0.30
2211		68	17	9.9	5.6	2.52	0.41	0.90	0.42
2221		64	18	12	6.2	2.12	0.46	0.96	0.35
2231		49	26	18	6.1	1.11	0.43	1.16	0.35
2241		67	16	11	6.2	2.45	0.40	0.93	0.38
2251		65	15	12	7.3	2.38	0.46	1.05	0.37
2261		69	13	11	6.4	2.86	0.39	0.98	0.36
2271		69	14	10	6.4	2.85	0.33	0.91	0.34
2281		45	22	19	15	1.12	0.65	1.05	0.35
2291		46	23	17	14	1.12	0.64	0.97	0.39
2301		56	23	11	9.6	1.63	0.47	1.18	0.39
2311		41	27	21	11	0.85	0.56	0.91	0.38
2321		53	24	14	9	1.42	0.35	1.04	0.29
2331		53	24	14	9.1	1.37	0.43	1.15	0.38
2340		37	33	20	9.6	0.70	0.36	0.96	0.30
2351		54	21	13	12	1.61	0.45	1.00	0.37
2360		40	29	18	13	0.86	0.61	1.15	0.35
2371		59	18	9.2	13	2.15	0.48	1.15	0.37
2381		51	23	12	13	1.45	0.41	1.29	0.41
2391		47	25	15	13	1.15	0.38	1.16	0.31
2401		45	28	14	13	1.07	0.41	1.41	0.38
2411		59	18	12	12	2.01	0.47	1.18	0.31
2421		55	22	14	9	1.51	0.34	1.21	0.38
2431		61	18	9.5	11	2.20	0.39	0.98	0.35
2441		55	21	12	12	1.64	0.44	1.21	0.33
2454		40	27	19	14	0.86	0.45	1.25	0.40
2461		41	29	19	11	0.86	0.38	1.12	0.36
2471		48	24	17	11	1.16	0.49	1.11	0.36
2481		42	30	13	15	1.00	0.40	1.01	0.39
2491		51	26	12	11	1.33	0.38	1.14	0.37
2501		38	28	18	16	0.85	0.48	0.95	0.32
2511		62	17	11	10	2.23	0.37	1.18	0.41
2521		57	20	11	12	1.84	0.50	1.25	0.40
2531		46	24	16	14	1.14	0.50	0.97	0.41
2541		51	24	14	12	1.35	0.32	1.11	0.38
2547		46	25	19	9.6	1.04	0.36	1.33	0.41
2551		54	22	16	8.1	1.40	0.38	1.25	0.32
2561		50	25	15	10	1.24	0.45	1.26	0.33
2566		40	29	20	11	0.83	0.55	1.25	0.37
2571		44	24	21	11	0.98	0.51	1.17	0.28
2581		51	25	14	11	1.30	0.36	1.15	0.38
2591		53	23	9	15	1.66	0.48	1.10	0.39
2601		49	24	14	14	1.29	0.50	1.11	0.38
2611		47	26	13	14	1.22	0.44	1.08	0.41
2621		62	18	12	7.5	2.05	0.39	1.10	0.35
2631		54	20	16	10	1.52	0.57	1.12	0.37
2641		56	19	9.9	15	1.91	0.55	1.36	0.41
2651		60	19	11	9.6	1.94	0.41	1.16	0.37
2661		55	22	11	12	1.68	0.41	1.20	0.40

Appendix A.5: The La Salle Basin data

Table A.5.2. Mineralogical data of core MD02-2549 from the La Salle Basin

Depth (cm)	Age (ka)	S (%)	I (%)	C (%)	K (%)	S/(I+C)	I5Å/I10Å	Smectite Crystallinity	Illite Crystallinity
2669		42	26	18	14	0.96	0.55	1.20	0.32
2671		52	25	12	10	1.38	0.43	1.32	0.42
2681		59	21	9.5	10	1.91	0.35	1.23	0.43
2691		26	34	27	14	0.43	0.60	0.79	0.37
2701		61	18	9.9	12	2.19	0.52	1.17	0.34
2711		46	27	16	11	1.08	0.34	1.21	0.32
2721		58	20	10	12	1.97	0.41	1.10	0.38
2731		46	25	16	14	1.14	0.48	1.13	0.35
2741		51	24	13	12	1.38	0.43	1.05	0.38
2751		46	28	11	15	1.19	0.37	1.07	0.41
2761		65	16	8	12	2.75	0.34	0.97	0.30
2771		41	26	20	14	0.89	0.50	0.86	0.39
2781		56	21	8.8	14	1.89	0.41	1.30	0.38
2791		57	20	12	11	1.80	0.37	1.11	0.42
2801		54	23	16	7.8	1.41	0.34	1.06	0.34
2811		55	23	15	7.1	1.48	0.35	1.04	0.36
2821		49	27	12	12	1.27	0.29	1.16	0.32
2831		49	24	11	17	1.43	0.40	1.25	0.38
2841		58	21	9.7	11	1.90	0.46	1.18	0.40
2851		49	23	14	14	1.31	0.51	1.29	0.37
2861		50	25	14	10	1.28	0.33	1.19	0.26
2871		44	28	15	13	1.05	0.37	1.31	0.28
2881		55	20	13	11	1.63	0.35	1.23	0.33
2891		41	28	13	18	1.01	0.43	1.34	0.37
2901		51	26	13	9.9	1.31	0.28	1.29	0.34
2911		41	30	19	9.8	0.82	0.42	1.37	0.38
2921		37	31	20	12	0.74	0.51	1.00	0.37
2931		37	34	16	12	0.74	0.39	1.16	0.33
2941		47	28	13	13	1.14	0.34	1.01	0.34
2951		59	20	11	9.6	1.88	0.43	1.24	0.34
2961		37	34	18	10	0.71	0.42	1.37	0.43
2971		22	40	25	13	0.34	0.50	0.77	0.41
2981		25	38	22	16	0.41	0.48	1.54	0.39
2991		27	38	22	12	0.45	0.47	1.56	0.41
3001		29	40	19	12	0.50	0.43	0.91	0.32
3011		26	41	20	14	0.42	0.44	1.10	0.33
3021		33	36	19	12	0.59	0.47	1.01	0.40
3031		27	32	26	14	0.46	0.56	0.91	0.35
3041		56	20	11	13	1.82	0.57	1.19	0.35
3051		56	20	11	13	1.79	0.45	1.21	0.46
3061		39	29	21	12	0.79	0.52	0.97	0.41
3071		43	28	14	15	1.02	0.41	1.08	0.37
3081		55	22	11	11	1.68	0.49	1.25	0.36
3091		57	22	10	11	1.79	0.42	1.19	0.38
3101		53	24	9.6	14	1.59	0.38	1.05	0.36
3111		53	23	11	13	1.56	0.43	1.23	0.37
3121		44	28	14	13	1.04	0.47	1.26	0.39
3131		45	30	13	12	1.04	0.42	1.14	0.38
3141		47	27	15	11	1.12	0.38	1.26	0.36
3151		42	30	17	11	0.89	0.43	1.10	0.40
3156		41	33	14	12	0.86	0.41	1.37	0.34

Table A.5.2. Mineralogical data of core MD02-2549 from the La Salle Basin

Depth (cm)	Age (ka)	S (%)	I (%)	C (%)	K (%)	S/(I+C)	I5Å/I10Å	Smectite Crystallinity	Illite Crystallinity
3161		46	27	14	13	1.11	0.46	1.44	0.41
3171		40	29	16	14	0.88	0.49	1.56	0.38
3181		38	32	16	13	0.78	0.45	1.26	0.38
3191		36	28	19	17	0.78	0.63	1.21	0.39
3201		29	30	20	21	0.58	0.52	0.94	0.27
3211		45	27	16	12	1.03	0.39	1.25	0.39
3231		31	30	18	21	0.64	0.56	1.25	0.37
3241		31	32	16	21	0.65	0.46	1.28	0.32
3321		44	29	15	11	0.99	0.47	1.27	0.41
3331		41	33	14	12	0.89	0.31	1.50	0.25
3341		39	33	17	11	0.77	0.48	1.17	0.37
3351		42	33	13	12	0.91	0.40	1.44	0.43
3361		38	33	20	9.6	0.73	0.42	1.39	0.30
3371		32	35	15	18	0.63	0.41	0.67	0.33
3381		58	20	9	13	1.97	0.39	1.03	0.29
3391		24	34	25	16	0.41	0.50	0.58	0.30
3401		35	32	18	15	0.69	0.42	1.32	0.32
3411		47	27	16	10	1.11	0.50	1.08	0.38
3421		48	23	15	14	1.27	0.47	1.36	0.30
3431		46	25	13	17	1.23	0.51	1.31	0.37
3441		52	20	11	16	1.68	0.59	1.06	0.30
3451		63	15	10	11	2.49	0.61	1.26	0.35
3461		66	17	6.8	11	2.82	0.34	1.01	0.41
3471		54	24	10	12	1.60	0.44	1.16	0.45
3481		38	32	15	15	0.81	0.42	1.11	0.30
3491		38	29	22	10	0.74	0.47	0.97	0.37
3501		23	34	26	17	0.38	0.55	0.47	0.24
3511		28	39	22	12	0.46	0.50	1.05	0.37
3521		50	25	15	9.2	1.23	0.38	1.34	0.32
3525		40	30	19	11	0.82	0.50	1.45	0.42
3531		38	32	15	15	0.80	0.51	0.97	0.31
3541		28	38	20	14	0.49	0.50	0.97	0.31
3551		30	33	22	15	0.54	0.42	0.96	0.33
3561		46	26	14	14	1.14	0.53	1.30	0.29
3571		41	29	19	11	0.87	0.45	1.04	0.19
3581		32	33	21	14	0.60	0.52	1.51	0.37
3591		20	43	21	15	0.32	0.47	0.55	0.35
3601		40	28	17	14	0.88	0.52	1.23	0.35
3611		50	26	13	10	1.27	0.35	1.13	0.33
3621		46	24	18	12	1.09	0.52	1.35	0.43
3631		28	31	31	10	0.46	0.56	0.67	0.33
3641		45	28	15	12	1.06	0.45	1.25	0.39
3651		55	21	16	8	1.47	0.52	1.38	0.38
3659		52	22	17	9.6	1.35	0.33	1.20	0.35
3661		51	23	12	14	1.46	0.48	1.20	0.39
3671		56	22	12	10	1.66	0.49	1.20	0.40
3681		37	32	18	12	0.73	0.45	1.19	0.35
3691		46	28	16	9.3	1.02	0.49	1.22	0.37
3701		30	39	20	11	0.52	0.43	1.02	0.33
3705		43	30	15	12	0.96	0.44	1.09	0.39
3711		41	33	19	6.8	0.80	0.36	1.38	0.40

Appendix A.5: The La Salle Basin data

Table A.5.2. Mineralogical data of core MD02-2549 from the La Salle Basin

Depth (cm)	Age (ka)	S (%)	I (%)	C (%)	K (%)	S/(I+C)	I5Å/I10Å	Smectite Crystallinity	Illite Crystallinity
3721		57	21	14	7,9	1,66	0,51	1,36	0,37
3731		31	38	19	12	0,54	0,40	0,75	0,31
3741		45	31	14	11	1,00	0,37	1,21	0,44
3750		41	31	17	11	0,86	0,51	1,49	0,43
3760		42	30	16	12	0,93	0,39	1,27	0,36
3770		62	17	8,4	13	2,45	0,46	1,12	0,34
3721		57	21	14	7,9	1,66	0,51	1,36	0,37
3731		31	38	19	12	0,54	0,40	0,75	0,31
3741		45	31	14	11	1,00	0,37	1,21	0,44
3750		41	31	17	11	0,86	0,51	1,49	0,43
3760		42	30	16	12	0,93	0,39	1,27	0,36
3770		62	17	8,4	13	2,45	0,46	1,12	0,34

Table A.5.3. Carbonate ($CaCO_3$) concentrations (%), Elemental analysis, and C/N ratio (TOC/N_{total}) of core MD02-2549 from the La Salle Basin.

		Bernard calcimeter	Elemental analysis				
Depth (cm)	**Age (ka)**	**$CaCO_3$ (%)**	**N_{total} (%)**	**C_{total} (%)**	**S_{total} (%)**	**TOC (%)**	**C/N ratio**
1	0.0	26.6	0.075	3.72	0.02	0.52	6.95
21	1.0	27.0	0.064	3.78	0.09	0.54	8.38
41	1.9	27.6	0.060	3.75	0.11	0.43	7.24
61	2.8	29.9	0.064	3.95	0.00	0.37	5.70
81	3.7	27.5	0.072	3.70	0.05	0.40	5.50
101	4.6	27.7	0.050	3.70	0.13	0.37	7.35
121	5.5	29.2	0.052	4.06	0.06	0.56	10.80
141	6.4	27.5	0.059	3.73	0.06	0.43	7.29
161	7.3	27.9	0.052	3.52	0.09	0.18	3.43
181	8.2	27.5	0.058	3.68	0.09	0.38	6.61
201	9.2	28.8	0.060	3.88	0.06	0.43	7.16
221	10.1	29.6	0.058	3.92	0.11	0.37	6.31
241	11.0	32.1	0.062	4.22	0.12	0.37	6.00
261	11.9	28.3	0.060	3.94	0.06	0.54	9.01
281	12.8	22.1	0.063	3.04	0.08	0.39	6.15
301	13.7	15.2	0.066	2.46	0.07	0.63	9.59
321	14.8	18.1	0.073	2.88	0.08	0.72	9.82
341	15.8	18.2	0.066	2.85	0.13	0.66	10.05
361	16.8	19.0	0.076	2.84	0.05	0.56	7.36
381	17.8	17.0	0.054	2.69	0.12	0.65	12.10
401	18.8	14.9	0.050	2.84	0.06	1.05	21.03
421	19.8	15.2	0.045	3.04	0.10	1.21	26.95
441	20.8	16.4	0.049	2.73	0.10	0.76	15.56
461	21.7	18.6	0.054	3.00	0.07	0.77	14.25
481	22.7	16.0	0.061	2.94	0.17	1.02	16.68
501	23.7	18.2	0.046	2.89	0.08	0.70	15.28
521	24.7	17.1	0.036	2.90	0.09	0.85	23.62
541	25.7	11.0	0.038	2.28	0.09	0.96	25.31
561	26.7	15.5	0.046	2.81	0.13	0.95	20.68
581	27.6	11.7	0.042	5.32	0.04	1.03	24.42
601	28.6	11.6	0.047	2.49	0.10	1.10	23.41
621	29.6	15.9	0.056	2.68	0.00	0.77	13.82
641	30.6	16.2	0.044	2.81	0.09	0.86	19.51
661	31.6	16.4	0.041	2.92	0.09	1.24	30.72
681	32.8	16.5	0.039	3.04	0.08	1.62	41.93
701	34.1	16.6	0.037	3.31	0.07	1.35	36.60
721	35.3	17.0	0.037	3.25	0.09	1.21	32.77
741	36.6	21.3	0.038	3.32	0.07	0.77	20.24
761	38.4	21.2	0.043	2.88	0.09	0.33	7.61
781	40.1	20.0	0.062	2.71	0.05	0.31	5.07
801	41.8	17.6	0.040	2.79	0.09	0.68	16.91
821	43.1	20.8	0.052	3.13	0.10	0.64	12.27
841	44.3	18.1	0.044	2.69	0.10	0.52	11.81
861	45.5	13.6	0.046	2.50	0.14	0.86	18.74

Appendix A.5: The La Salle Basin data

Table A.5.3. Carbonate ($CaCO_3$) concentrations (%), Elemental analysis, and C/N ratio (TOC/N_{total}) of core MD02-2549 from the La Salle Basin.

		Bernard calcimeter	Elemental analysis				
Depth (cm)	**Age (ka)**	**$CaCO_3$ (%)**	**N_{total} (%)**	**C_{total} (%)**	**S_{total} (%)**	**TOC (%)**	**C/N ratio**
881	46.8	18.9	0.058	2.89	0.17	0.63	10.78
901	48.0	22.3	0.052	3.08	0.06	0.41	7.85
921	49.2	20.1	0.045	3.39	0.04	0.98	21.84
941	51.8	18.5	0.042	3.22	0.11	1.00	23.75
961	54.4	22.0	0.035	3.25	0.17	0.60	17.26
981	57.0	22.9	0.057	3.19	0.13	0.44	7.72
1001	58.6	14.4	0.037	2.42	0.11	0.70	18.93
1021	60.8	17.0	0.048	2.76	0.09	0.71	14.78
1041	63.1	16.8	0.043	2.40	0.09	0.38	8.95
1061	65.4	12.9	0.044	2.05	0.05	0.50	11.40
1081	67.7	16.2	0.046	2.35	0.09	0.40	8.77
1101	70.0	16.8	0.047	2.40	0.10	0.38	8.12
1121	71.8	23.3	0.035	3.08	0.12	0.28	8.10
1141	72.8	29.0	0.089	3.72	0.00	0.24	2.73
1161	73.8	26.6	0.043	3.61	0.10	0.42	9.71
1181	74.9	26.1	0.054	3.80	0.09	0.67	12.47
1361	85.0	19.8	0.040	2.67	0.07	0.30	7.44
1381	88.4	16.6	0.102	2.35	0.07	0.36	3.49
1401	91.8	24.4	0.071	3.37	0.13	0.45	6.32
1421	94.9	35.2	0.054	4.51	0.14	0.30	5.63
1441	98.0	37.2	0.039	4.66	0.07	0.19	4.96
1461	101.2	26.2	0.055	3.14	0.08	0.05	0.91
1481	104.3	31.7	0.047	4.04	0.06	0.23	4.84
1501	108.5	20.5	0.055	2.90	0.06	0.45	8.10
1521	113.7	25.3	0.053	3.45	0.18	0.41	7.83
1541	118.0	36.5	0.049	4.65	0.08	0.27	5.46
1561	121.9	38.4	0.052	4.64	0.08	0.03	0.48
1581	125.7	37.6	0.037	4.76	0.05	0.25	6.80
1601	129.5	33.8	0.045	4.05	0.07	0.05	1.11
1621	133.4	14.1	0.068	2.11	0.01	0.42	6.13
1641	137.2	8.9	0.082	2.54	0.03	1.48	18.02
1661	141.1	14.7	0.082	4.19	0.21	2.43	29.65
1681	144.9	14.7	0.070	3.74	0.22	1.98	28.23
1701	148.8	14.4	0.056	3.75	0.20	2.03	36.19
1721	152.6	11.3	0.040	2.72	0.11	1.37	34.28
1741	156.4	7.2	0.057	2.18	0.11	1.31	23.03
1761		7.3	0.063	2.04	0.16	1.17	18.53
1781		6.0	0.063	2.24	0.10	1.53	24.26
1801		10.4	0.069	2.45	0.11	1.20	17.43
1821		7.9	0.099	2.29	0.05	1.35	13.61
1841		9.5	0.054	2.54	0.11	1.40	25.97
1861		7.3	0.059	2.35	0.11	1.48	25.08
1881		10.8	0.055	2.79	0.13	1.50	27.26

Table A.5.3. Carbonate ($CaCO_3$) concentrations (%), Elemental analysis, and C/N ratio (TOC/N_{total}) of core MD02-2549 from the La Salle Basin.

		Bernard calcimeter	Elemental analysis				
Depth (cm)	**Age (ka)**	**$CaCO_3$ (%)**	**N_{total} (%)**	**C_{total} (%)**	**S_{total} (%)**	**TOC (%)**	**C/N ratio**
1901		6.1	0.049	2.53	0.09	1.79	36.55
1921		7.5	0.056	2.57	0.10	1.67	29.85
1941		9.3	0.048	2.65	0.07	1.53	31.83
1961		9.1	0.049	2.41	0.11	1.31	26.77
1981		8.7	0.065	2.34	0.12	1.29	19.92
2001		7.8	0.058	2.33	0.07	1.39	23.93
2021		9.4	0.056	2.47	0.05	1.34	23.87
2041		10.8	0.054	2.62	0.08	1.33	24.55
2061		12.6	0.052	2.90	0.06	1.39	26.70
2081		11.8	0.060	2.87	0.11	1.46	24.25
2101		9.7	0.066	2.77	0.03	1.61	24.38
2111		9.0	0.058	2.74	0.05	1.65	28.49
2121		10.0	0.050	2.85	0.06	1.65	32.98
2131		9.5	0.056	2.76	0.09	1.62	28.91
2141		8.9	0.049	2.78	0.08	1.70	34.75
2161		10.2	0.063	2.92	0.07	1.70	26.96
2181		10.3	0.074	2.72	0.05	1.48	20.06
2201		9.1	0.076	2.79	0.09	1.70	22.34
2211		10.1	0.058	2.75	0.00	1.54	26.63
2221		9.0	0.058	2.69	0.06	1.61	27.76
2241		9.2	0.056	2.74	0.08	1.64	29.25
2261		9.9	0.046	2.60	0.07	1.41	30.75
2281		9.6	0.050	2.70	0.08	1.55	30.92
2291		8.1	0.059	2.53	0.05	1.56	26.36
2301		10.6	0.064	2.82	0.08	1.55	24.21
2321		8.5	0.068	2.70	0.13	1.69	24.82
2340		8.5	0.050	2.57	0.41	1.56	31.11
2360		7.3	0.058	2.20	3.20	1.32	22.77
2371		8.5	0.058	2.20	0.27	1.19	20.47
2381		10.2	0.068	2.61	0.06	1.38	20.30
2401		14.9	0.066	3.25	0.05	1.46	22.17
2421		11.6	0.061	2.64	0.06	1.25	20.44
2441		11.1	0.065	2.70	0.20	1.37	21.12
2454		11.7	0.057	3.11	0.16	1.70	29.74
2461		11.6	0.067	3.00	0.09	1.60	23.92
2481		11.6	0.078	2.92	0.08	1.53	19.66
2501		9.6	0.068	2.59	0.05	1.43	21.10
2521		9.7	0.048	2.63	0.04	1.47	30.56
2531		11.9	0.070	2.67	0.00	1.24	17.77
2541		12.0	0.057	3.03	0.41	1.60	28.02
2561		11.5	0.074	2.85	0.13	1.48	19.96
2571		11.6	0.050	2.95	0.31	1.56	31.26
2581		9.0	0.079	2.45	0.05	1.37	17.32
2601		11.5	0.060	3.00	0.08	1.62	27.00

Appendix A.5: The La Salle Basin data

Table A.5.3. Carbonate ($CaCO_3$) concentrations (%), Elemental analysis, and C/N ratio (TOC/N_{total}) of core MD02-2549 from the La Salle Basin.

		Bernard calcimeter	Elemental analysis				
Depth (cm)	**Age (ka)**	**$CaCO_3$ (%)**	**N_{total} (%)**	**C_{total} (%)**	**S_{total} (%)**	**TOC (%)**	**C/N ratio**
2621		9.2	0.052	2.50	0.05	1.39	26.64
2641		8.4	0.085	2.23	0.05	1.23	14.49
2661		9.3	0.063	2.62	0.21	1.50	23.80
2669		7.0	0.066	2.35	1.50	1.51	22.95
2681		10.3	0.085	2.78	0.12	1.55	18.19
2701		7.2	0.080	1.98	0.05	1.12	14.06
2721		10.9	0.068	2.66	0.06	1.36	19.95
2731		10.2	0.061	2.82	0.06	1.59	26.05
2741		10.0	0.069	2.67	0.04	1.47	21.27
2761		7.9	0.067	2.02	0.02	1.07	16.00
2781		8.2	0.083	2.32	0.03	1.34	16.19
2801		10.0	0.072	2.68	0.07	1.47	20.44
2811		10.3	0.081	2.94	0.08	1.70	20.96
2821		13.5	0.069	3.08	0.07	1.46	21.13
2841		8.2	0.053	2.04	0.07	1.06	20.01
2861		9.1	0.063	2.52	0.12	1.43	22.63
2881		11.1	0.056	2.88	0.06	1.55	27.62
2891		11.2	0.066	2.81	0.08	1.46	22.14
2901		12.9	0.044	3.04	0.04	1.49	33.81
2921		10.5	0.065	2.51	0.11	1.25	19.27
2941		11.2	0.066	2.70	0.15	1.36	20.58
2961		11.5	0.055	3.01	0.10	1.62	29.53
2971		14.6	0.077	3.20	0.06	1.44	18.73
2981		13.9	0.055	3.26	0.07	1.59	29.00
3001		12.1	0.085	3.02	0.07	1.58	18.53
3021		11.7	0.079	3.07	0.05	1.66	21.07
3041		8.9	0.064	2.35	0.07	1.28	19.97
3051		9.9	0.058	2.72	0.06	1.54	26.48
3061		10.4	0.078	2.97	0.07	1.73	22.14
3081		11.4	0.072	2.75	0.01	1.39	19.25
3101		10.0	0.063	2.59	0.05	1.39	21.99
3121		10.8	0.063	2.68	0.08	1.39	21.99
3131		11.0	0.077	2.78	0.04	1.46	18.94
3141		10.3	0.062	2.64	0.06	1.41	22.74
3161		11.6	0.078	2.73	0.06	1.33	17.09
3181		9.5	0.066	2.64	0.09	1.50	22.75
3191		9.5	0.075	2.58	0.00	1.44	19.22
3201		10.1	0.080	2.80	0.04	1.59	19.83
3221		10.2	0.077	2.53	0.05	1.30	16.86
3241		8.0	0.067	2.25	0.08	1.29	19.30
3261		7.0	0.089	2.10	0.03	1.26	14.16
3271		7.7	0.066	2.14	0.05	1.22	18.41
3281		6.4	0.074	2.03	0.05	1.25	16.95
3302		8.5	0.062	2.54	0.06	1.51	24.36

Table A.5.3. Carbonate ($CaCO_3$) concentrations (%), Elemental analysis, and C/N ratio (TOC/N_{total}) of core MD02-2549 from the La Salle Basin.

		Bernard calcimeter	Elemental analysis				
Depth (cm)	**Age (ka)**	**$CaCO_3$ (%)**	**N_{total} (%)**	**C_{total} (%)**	**S_{total} (%)**	**TOC (%)**	**C/N ratio**
3321		10.0	0.076	2.95	0.03	1.75	23.02
3341		11.2	0.086	2.99	0.01	1.64	19.12
3351		13.6	0.082	3.08	0.05	1.44	17.61
3361		11.3	0.068	2.99	0.07	1.63	23.99
3381		9.1	0.083	2.73	0.03	1.63	19.67
3401		12.9	0.078	3.19	0.04	1.64	20.97
3421		11.2	0.079	2.72	0.04	1.38	17.47
3431		8.7	0.042	2.47	0.03	1.42	33.86
3441		6.8	0.062	2.22	0.09	1.40	22.55
3461		8.5	0.089	2.12	0.05	1.10	12.31
3481		9.9	0.085	2.86	0.05	1.68	19.75
3501		12.1	0.063	3.03	0.08	1.58	25.01
3511		13.0	0.066	3.03	0.06	1.47	22.32
3521		9.9	0.085	2.74	0.08	1.56	18.30
3541		10.8	0.088	2.79	0.04	1.50	17.05
3561		8.9	0.065	2.90	0.09	1.83	28.17
3581		12.5	0.051	3.34	0.10	1.84	36.14
3591		11.4	0.065	3.15	0.10	1.78	27.41
3601		10.6	0.081	3.10	0.06	1.82	22.53
3621		12.4	0.070	3.15	0.09	1.67	23.79
3641		12.3	0.057	3.19	0.07	1.71	30.00
3651		10.6	0.067	2.56	0.06	1.29	19.23
3661		10.5	0.082	2.52	0.07	1.26	15.39
3681		10.1	0.061	2.91	0.05	1.70	27.81
3701		11.0	0.058	3.14	0.05	1.82	31.38
3711		10.8	0.082	3.04	0.05	1.74	21.26
3721		9.9	0.057	2.92	0.06	1.73	30.38
3741		10.8	0.064	3.13	0.10	1.84	28.72
3760		11.1	0.065	3.10	0.09	1.77	27.25
3770		10.1	0.069	2.57	0.09	1.36	19.74

Appendix A.5: The La Salle Basin data

Table A.5.4. Rock-Eval pyrolysis parameters of core MD02-2549 from the La Salle Basin.

Depth (cm)	Age (ka)	Tmax (°C)	S1 (mg/g)	S2 (mg/g)	TOC (%)	IH (mg HC/g TOC)	IO (mg CO_2/g COT)
1	0.0	428	0.01	0.34	0.27	126	1393
11	0.5	420	0.01	0.37	0.27	137	1530
61	2.8	424	0.00	0.40	0.37	108	784
161	7.3	420	0.01	0.31	0.25	124	1664
241	11.0	424	0.00	0.42	0.41	102	644
321	14.8	424	0.01	0.41	0.43	95	716
401	18.8	435	0.00	0.41	0.34	121	444
481	22.7	433	0.00	0.63	0.61	103	367
561	26.7	435	0.01	0.50	0.47	106	366
641	30.6	435	0.01	0.37	0.35	106	511
701	34.1	436	0.00	0.41	0.37	111	330
781	40.1	425	0.00	0.30	0.90	33	449
861	45.5	430	0.01	0.43	0.41	105	624
941	55.8	428	0.00	0.27	0.41	66	488
1021	56.8	427	0.01	0.26	0.73	36	281
1101	68.1	416	0.00	0.28	0.25	112	1080
1181	74.9	418	0.00	0.32	0.34	94	782
1361	84.0	420	0.01	0.25	0.31	81	868
1421	94.9	411	0.00	0.32	1.69	19	285
1481	104.3	413	0.00	0.23	1.60	14	292
1561	121.9	406	0.01	0.27	1.72	16	212
1641	137.2	434	0.00	0.98	1.16	84	161
1721	152.6	433	0.00	1.25	1.02	123	138
1801		437	0.01	0.69	0.86	80	191
1881		436	0.01	0.74	0.83	89	183
1961		438	0.00	0.66	0.80	82	171
2041		437	0.00	0.57	0.70	81	180
2111		438	0.00	0.60	0.75	80	187
2161		438	0.01	0.70	0.82	85	213
2221		436	0.00	0.57	0.78	73	194
2291		437	0.00	0.69	0.81	85	174
2360		427	0.01	0.28	0.61	46	315
2421		437	0.00	0.57	0.63	90	232
2481		439	0.01	1.07	0.86	124	185
2541		434	0.01	0.61	0.63	97	237
2601		434	0.01	0.85	0.77	110	240
2669		433	0.01	0.49	0.69	71	233
2731		438	0.01	0.92	0.84	110	177
2801		437	0.01	0.81	0.79	103	178
2861		437	0.01	0.70	0.72	97	224
2921		432	0.03	0.53	0.61	87	177
2921		435	0.01	0.62	0.59	105	200
2981		437	0.00	0.82	0.67	122	212
3051		437	0.00	0.69	0.74	93	180
3121		435	0.00	0.61	0.68	90	465
3181		437	0.00	0.52	0.59	88	212
3241		436	0.00	0.48	0.62	77	266

Table A.5.4. Rock-Eval pyrolysis parameters of core MD02-2549 from the La Salle Basin.

Depth (cm)	Age (ka)	Tmax (°C)	S1 (mg/g)	S2 (mg/g)	TOC (%)	IH (mg HC/g TOC)	IO (mg CO_2/g COT)
3302		436	0.00	0.62	0.66	94	245
3361		437	0.00	0.83	0.71	117	224
3431		436	0.00	0.48	0.57	84	239
3501		439	0.00	0.86	0.74	116	196
3561		432	0.03	0.75	0.78	96	167
3561		436	0.01	0.84	0.72	117	160
3621		435	0.00	0.82	0.74	111	228
3681		435	0.01	0.84	0.68	124	153
3741		437	0.00	0.85	0.74	115	209
3770		437	0.01	0.75	0.79	95	241

Appendix A.5: The La Salle Basin data

Table A.5.5. Magnetic susceptibility (MS) values of core MD02-2549 from the La Salle Basin.

Depth (cm)	Age (ka)	MS (x 10^{-6} SI)
2	0.1	3
4	0.2	8
6	0.3	9
8	0.4	5
12	0.5	7
14	0.6	7
16	0.7	7
18	0.8	7
20	0.9	7
22	1.0	7
24	1.1	7
26	1.2	6
28	1.3	7
30	1.4	7
32	1.5	7
34	1.5	7
36	1.6	8
38	1.7	7
40	1.8	7
42	1.9	5
44	2.0	8
46	2.1	8
48	2.2	7
50	2.3	7
52	2.4	7
54	2.5	7
56	2.6	8
58	2.6	8
60	2.7	5
62	2.8	6
64	2.9	7
66	3.0	8
68	3.1	7
70	3.2	7
72	3.3	9
74	3.4	9
76	3.5	8
78	3.6	9
80	3.6	9
82	3.7	8
84	3.8	8
86	3.9	10
88	4.0	9
90	4.1	10
92	4.2	10
94	4.3	9
96	4.4	6
98	4.5	7
100	4.6	7
102	4.6	8
104	4.7	8
106	4.8	9
108	4.9	9
110	5.0	9
112	5.1	10
114	5.2	8
116	5.3	6
118	5.4	8
120	5.5	10
122	5.6	7
124	5.6	6
126	5.7	3
128	5.8	3
130	5.9	4
132	6.0	6
134	6.1	9
136	6.2	10
138	6.3	10
140	6.4	11
142	6.5	9
144	6.6	10
146	6.6	11
148	6.7	9
150	6.8	10
152	6.9	10
154	7.0	10
156	7.1	10
158	7.2	10
160	7.3	10
162	7.4	10
164	7.5	10
166	7.6	9
168	7.7	9
170	7.7	9
172	7.8	9
174	7.9	10
176	8.0	9
178	8.1	9
180	8.2	8
182	8.3	9
184	8.4	9
186	8.5	9
188	8.6	9
190	8.7	7
192	8.7	8
194	8.8	8
196	8.9	8
198	9.0	7
200	9.1	7
202	9.2	8
204	9.3	9
206	9.4	10
208	9.5	9
210	9.6	9

Table A.5.5. Magnetic susceptibility (MS) values of core MD02-2549 from the La Salle Basin.

Depth (cm)	Age (ka)	MS (x 10^{-6} SI)
212	9.7	9
214	9.7	10
216	9.8	11
218	9.9	11
220	10.0	7
222	10.1	9
224	10.2	9
226	10.3	9
228	10.4	10
230	10.5	9
232	10.6	10
234	10.7	11
236	10.7	11
238	10.8	11
240	10.9	9
242	11.0	11
244	11.1	11
246	11.2	10
248	11.3	10
250	11.4	8
252	11.5	7
254	11.6	10
256	11.7	10
258	11.8	11
260	11.8	11
262	11.9	8
264	12.0	6
266	12.1	10
268	12.2	8
270	12.3	8
272	12.4	9
274	12.5	9
276	12.6	11
278	12.7	11
280	12.8	12
282	12.8	12
284	12.9	12
286	13.0	11
288	13.1	10
290	13.2	9
292	13.3	11
294	13.4	11
296	13.5	10
298	13.6	8
300	13.7	8
302	13.8	9
304	13.9	7
306	14.0	7
308	14.1	8
310	14.2	11
312	14.3	10
314	14.4	10
316	14.5	9
318	14.6	10
320	14.7	9
322	14.8	9
324	14.9	10
326	15.0	12
328	15.1	10
330	15.3	10
332	15.4	13
334	15.5	13
336	15.6	11
338	15.7	12
340	15.8	12
342	15.9	11
344	16.0	13
346	16.1	12
348	16.2	12
350	16.3	13
352	16.4	14
354	16.5	11
356	16.6	12
358	16.7	13
360	16.8	14
362	16.9	13
364	17.0	13
366	17.1	19
368	17.2	14
370	17.3	13
372	17.4	14
374	17.5	13
376	17.6	15
378	17.7	13
380	17.8	14
382	17.9	14
384	18.0	14
386	18.1	15
388	18.2	13
390	18.3	15
392	18.4	13
394	18.5	15
396	18.5	16
398	18.6	18
400	18.7	21
402	18.8	18
404	18.9	18
406	19.0	19
408	19.1	13
410	19.2	16
412	19.3	18
414	19.4	20
416	19.5	23
418	19.6	21

Appendix A.5: The La Salle Basin data

Table A.5.5. Magnetic susceptibility (MS) values of core MD02-2549 from the La Salle Basin.

Depth (cm)	Age (ka)	MS (x 10^{-6} SI)
420	19.7	13
422	19.8	14
424	19.9	15
426	20.0	13
432	20.3	11
434	20.4	15
436	20.5	14
438	20.6	15
440	20.7	14
442	20.8	15
444	20.9	15
446	21.0	14
450	21.2	12
452	21.3	14
454	21.4	13
456	21.5	15
458	21.6	15
460	21.7	12
462	21.8	14
464	21.9	12
466	22.0	10
468	22.1	12
470	22.2	12
472	22.3	10
474	22.4	11
476	22.5	11
478	22.6	10
480	22.7	10
482	22.8	12
484	22.9	11
486	23.0	13
488	23.1	11
490	23.2	9
492	23.3	13
494	23.4	14
496	23.5	14
498	23.6	13
500	23.7	14
502	23.8	13
504	23.9	13
506	24.0	14
508	24.1	13
510	24.2	14
512	24.3	14
514	24.4	16
516	24.5	15
518	24.6	15
520	24.6	15
522	24.7	15
524	24.8	17
526	24.9	16
528	25.0	20
530	25.1	18
532	25.2	18
534	25.3	18
536	25.4	19
538	25.5	17
540	25.6	19
542	25.7	19
544	25.8	20
546	25.9	19
548	26.0	17
550	26.1	20
552	26.2	21
554	26.3	22
556	26.4	22
558	26.5	21
560	26.6	18
562	26.7	18
564	26.8	17
566	26.9	15
568	27.0	17
570	27.1	17
572	27.2	19
574	27.3	20
576	27.4	20
578	27.5	18
580	27.6	22
582	27.7	22
584	27.8	21
586	27.9	22
588	28.0	12
590	28.1	25
594	28.3	27
596	28.4	22
598	28.5	18
600	28.6	18
602	28.7	21
604	28.8	21
606	28.9	24
608	29.0	23
610	29.1	21
612	29.2	22
614	29.3	25
616	29.4	22
618	29.5	22
620	29.6	20
622	29.7	22
624	29.8	19
626	29.9	29
628	30.0	24
630	30.1	23
632	30.2	23
634	30.3	28

Table A.5.5. Magnetic susceptibility (MS) values of core MD02-2549 from the La Salle Basin.

Depth (cm)	Age (ka)	MS (x 10^{-6} SI)	Depth (cm)	Age (ka)	MS (x 10^{-6} SI)
636	30.4	33	740	36.5	22
638	30.5	27	742	36.7	22
640	30.6	23	744	36.9	12
642	30.7	25	746	37.0	13
644	30.7	26	750	37.4	18
646	30.8	25	752	37.6	17
648	30.9	25	754	37.7	16
650	31.0	32	756	37.9	15
652	31.1	30	758	38.1	16
654	31.2	27	760	38.3	16
656	31.3	23	762	38.5	16
658	31.4	25	764	38.6	16
660	31.5	24	766	38.8	13
662	31.7	23	768	39.0	16
664	31.8	28	770	39.2	17
666	31.9	22	772	39.3	17
668	32.0	26	774	39.5	17
670	32.2	32	776	39.7	17
672	32.3	30	778	39.9	18
674	32.4	33	780	40.1	16
676	32.5	24	782	40.2	16
678	32.7	26	784	40.4	15
680	32.8	27	786	40.6	16
682	32.9	33	788	40.8	18
684	33.0	31	790	40.9	19
686	33.1	36	792	41.1	19
688	33.3	29	794	41.3	19
690	33.4	30	796	41.5	18
692	33.5	27	798	41.6	24
694	33.6	32	800	41.8	25
696	33.8	35	802	41.9	24
698	33.9	31	804	42.0	25
700	34.0	35	806	42.1	23
702	34.1	32	808	42.2	22
704	34.3	32	810	42.4	18
706	34.4	30	812	42.5	18
708	34.5	36	814	42.6	25
710	34.6	33	816	42.7	22
712	34.7	37	818	42.9	23
714	34.9	34	820	43.0	22
716	35.0	34	822	43.1	18
718	35.1	37	824	43.2	19
720	35.2	41	826	43.4	30
722	35.4	36	828	43.5	33
724	35.5	32	830	43.6	30
726	35.6	39	832	43.7	23
728	35.7	31	834	43.9	20
730	35.8	30	836	44.0	22
732	36.0	27	838	44.1	22
734	36.1	29	840	44.2	23
736	36.2	28	842	44.4	19
738	36.3	23	844	44.5	20

Appendix A.5: The La Salle Basin data

Table A.5.5. Magnetic susceptibility (MS) values of core MD02-2549 from the La Salle Basin.

Depth (cm)	Age (ka)	MS (x 10^{-6} SI)
846	44.6	20
848	44.7	16
850	44.9	16
852	45.0	17
854	45.1	17
856	45.2	18
858	45.3	17
860	45.5	16
862	45.6	16
864	45.7	16
866	45.8	16
868	46.0	15
870	46.1	18
872	46.2	18
874	46.3	16
876	46.5	16
878	46.6	13
880	46.7	14
882	46.8	13
884	47.0	15
886	47.1	16
888	47.2	20
890	47.3	15
892	47.5	18
894	47.6	18
896	47.7	17
898	47.8	12
900	47.9	18
902	48.1	15
904	48.2	16
906	48.3	16
908	48.4	20
910	48.6	15
912	48.7	24
914	48.8	23
916	48.9	18
920	49.2	20
922	49.3	25
924	49.4	24
926	49.6	23
928	49.7	22
930	49.8	24
932	50.1	29
934	50.3	23
936	50.6	25
938	50.8	24
940	51.1	23
942	51.3	24
944	51.6	22
946	51.9	23
948	52.1	22
950	52.4	25
952	52.6	20
954	52.9	25
956	53.1	18
958	53.4	19
960	53.7	22
962	53.9	22
964	54.2	23
966	54.4	22
968	54.7	14
970	54.9	16
972	55.2	8
982	56.5	13
984	56.7	18
986	57.0	20
988	57.3	21
990	57.5	17
992	57.5	23
994	57.8	21
996	58.0	22
998	58.2	24
1000	58.4	19
1002	58.7	20
1004	58.9	18
1006	59.1	21
1008	59.4	22
1010	59.6	20
1012	59.8	22
1014	60.0	19
1016	60.3	22
1018	60.5	22
1020	60.7	22
1022	61.0	23
1024	61.2	22
1026	61.4	24
1028	61.6	22
1030	61.9	22
1032	62.1	21
1034	62.3	19
1036	62.6	20
1038	62.8	19
1040	63.0	17
1042	63.2	16
1044	63.5	14
1046	63.7	17
1050	64.2	20
1052	64.4	20
1054	64.6	22
1056	64.8	21
1058	65.1	21
1060	65.3	21
1062	65.5	23
1064	65.8	21

Table A.5.5. Magnetic susceptibility (MS) values of core MD02-2549 from the La Salle Basin.

Depth (cm)	Age (ka)	MS (x 10^{-6} SI)
1066	66.0	23
1068	66.2	23
1070	66.5	27
1072	66.7	30
1074	66.9	29
1076	67.1	21
1078	67.4	18
1080	67.6	17
1082	67.8	16
1084	68.1	19
1086	68.3	18
1088	68.5	15
1090	68.7	17
1092	69.0	18
1094	69.2	18
1096	69.4	16
1098	69.7	16
1100	69.9	18
1102	70.1	19
1106	70.6	17
1108	70.8	15
1110	71.0	16
1112	71.3	15
1114	71.4	15
1116	71.5	16
1118	71.6	16
1120	71.7	14
1122	71.8	13
1124	71.9	13
1126	72.0	13
1128	72.1	14
1130	72.2	13
1132	72.3	14
1134	72.4	14
1136	72.5	12
1138	72.6	12
1140	72.7	11
1142	72.9	12
1144	73.0	14
1146	73.1	12
1148	73.2	12
1150	73.3	12
1162	73.9	11
1164	74.0	12
1166	74.1	11
1168	74.2	13
1170	74.3	12
1172	74.4	13
1174	74.5	13
1176	74.6	13
1178	74.7	11
1180	74.8	13
1182	74.9	12
1184	75.0	10
1186	75.1	11
1188	75.2	13
1190	75.3	12
1192	75.4	10
1194	75.5	11
1196	75.7	11
1354	83.9	11
1356	84.1	11
1358	84.5	9
1360	84.8	13
1362	85.2	10
1364	85.5	13
1366	85.8	14
1368	86.2	16
1370	86.5	15
1372	86.9	14
1374	87.2	15
1376	87.5	16
1378	87.9	16
1380	88.2	16
1382	88.5	17
1384	88.9	14
1386	89.2	14
1388	89.6	15
1390	89.9	13
1392	90.2	13
1394	90.6	14
1396	90.9	14
1398	91.2	13
1400	91.6	14
1402	91.9	13
1404	92.3	13
1406	92.6	14
1408	92.9	12
1410	93.2	12
1412	93.5	14
1414	93.8	13
1416	94.1	13
1418	94.4	13
1420	94.8	10
1422	95.1	12
1424	95.4	10
1426	95.7	12
1428	96.0	11
1430	96.3	12
1432	96.6	11
1434	96.9	11
1436	97.3	10
1438	97.6	11

Appendix A.5: The La Salle Basin data

Table A.5.5. Magnetic susceptibility (MS) values of core MD02-2549 from the La Salle Basin.

Depth (cm)	Age (ka)	MS (x 10^{-6} SI)
1440	97.9	12
1442	98.2	12
1444	98.5	11
1446	98.8	10
1448	99.1	11
1450	99.4	12
1452	99.7	12
1454	100.1	12
1456	100.4	10
1458	100.7	12
1460	101.0	12
1462	101.3	13
1464	101.6	12
1466	101.9	11
1468	102.2	14
1470	102.6	15
1472	102.9	15
1474	103.2	13
1476	103.5	13
1478	103.8	12
1480	104.1	13
1482	104.4	13
1484	104.7	12
1486	105.1	13
1488	105.4	13
1490	105.7	14
1492	106.1	12
1494	106.7	12
1496	107.2	11
1500	108.2	15
1502	108.8	16
1504	109.3	15
1506	109.8	16
1508	110.3	14
1510	110.9	15
1512	111.4	16
1514	111.9	15
1516	112.4	13
1518	113.0	14
1520	113.5	13
1522	114.0	15
1524	114.5	12
1526	115.1	13
1528	115.5	12
1530	115.9	12
1532	116.3	13
1534	116.7	12
1536	117.1	12
1538	117.4	12
1540	117.8	13
1542	118.2	12
1544	118.6	10
1546	119.0	14
1548	119.4	12
1550	119.8	13
1552	120.1	12
1554	120.5	13
1556	120.9	13
1558	121.3	13
1560	121.7	14
1562	122.1	14
1564	122.4	12
1566	122.8	11
1568	123.2	10
1570	123.6	13
1572	124.0	11
1574	124.4	13
1576	124.7	13
1578	125.1	12
1580	125.5	12
1582	125.9	14
1584	126.3	13
1586	126.7	14
1588	127.1	14
1590	127.4	14
1592	127.8	15
1594	128.2	14
1596	128.6	16
1598	129.0	16
1600	129.4	15
1602	129.7	10
1604	130.1	13
1606	130.5	15
1608	130.9	15
1610	131.3	16
1612	131.7	16
1614	132.0	17
1616	132.4	20
1618	132.8	20
1620	133.2	22
1622	133.6	21
1624	134.0	23
1626	134.3	22
1628	134.7	22
1630	135.1	24
1632	135.5	25
1634	135.9	23
1636	136.3	18
1638	136.7	14
1640	137.0	13
1642	137.4	13
1644	137.8	12
1646	138.2	15
1648	138.6	16

Table A.5.5. Magnetic susceptibility (MS) values of core MD02-2549 from the La Salle Basin.

Depth (cm)	Age (ka)	MS (x 10^{-6} SI)
1650	139.0	14
1652	139.3	15
1654	139.7	15
1656	140.1	15
1658	140.5	16
1660	140.9	16
1662	141.3	16
1664	141.6	19
1666	142.0	21
1668	142.4	21
1670	142.8	18
1672	143.2	17
1674	143.6	16
1676	144.0	17
1678	144.3	17
1680	144.7	16
1682	145.1	19
1684	145.5	17
1686	145.9	19
1688	146.3	21
1690	146.6	20
1692	147.0	21
1694	147.4	22
1696	147.8	22
1698	148.2	22
1700	148.6	24
1702	148.9	23
1704	149.3	18
1706	149.7	18
1708	150.1	16
1710	150.5	16
1712	150.9	16
1714	151.3	15
1716	151.6	17
1718	152.0	18
1720	152.4	17
1722	152.8	18
1724	153.2	17
1726	153.6	19
1728	153.9	24
1730	154.3	23
1732	154.7	18
1734	155.1	16
1736	155.5	28
1738	155.9	18
1740	156.2	28
1742		25
1744		25
1746		25
1748		27
1750		28
1752		22

Depth (cm)	Age (ka)	MS (x 10^{-6} SI)
1754		27
1756		23
1758		20
1760		20
1762		24
1764		27
1766		27
1768		26
1770		27
1772		30
1774		24
1776		24
1778		15
1780		15
1782		20
1784		20
1786		24
1788		23
1790		22
1792		20
1794		23
1796		27
1798		23
1800		26
1802		24
1804		25
1806		25
1808		26
1810		24
1812		27
1814		24
1816		22
1818		23
1820		25
1822		28
1824		27
1826		28
1828		22
1830		23
1832		23
1834		21
1836		19
1838		23
1840		23
1842		21
1844		21
1846		23
1848		21
1850		23
1852		25
1854		20
1856		21

Appendix A.5: The La Salle Basin data

Table A.5.5. Magnetic susceptibility (MS) values of core MD02-2549 from the La Salle Basin.

Depth (cm)	Age (ka)	MS (x 10^{-6} SI)	Depth (cm)	Age (ka)	MS (x 10^{-6} SI)
1858		22	1966		22
1860		19	1968		24
1862		22	1970		21
1864		22	1972		23
1866		22	1974		20
1868		24	1976		21
1870		27	1978		22
1872		24	1980		20
1874		23	1982		17
1876		24	1984		17
1878		34	1986		18
1880		38	1988		18
1882		26	1990		17
1884		22	1992		18
1886		24	1994		19
1888		20	1996		22
1890		19	1998		20
1892		22	2000		21
1894		23	2002		21
1896		20	2004		21
1898		20	2006		21
1900		20	2008		21
1902		18	2010		22
1904		18	2012		22
1906		19	2014		20
1908		19	2016		21
1910		17	2018		21
1912		17	2020		19
1914		18	2022		20
1916		22	2024		21
1918		19	2026		22
1920		18	2028		21
1922		19	2030		23
1924		18	2032		23
1926		17	2034		20
1928		19	2036		21
1930		19	2038		23
1932		17	2040		24
1934		16	2042		23
1936		16	2044		22
1938		17	2046		25
1940		17	2048		22
1942		19	2050		24
1944		16	2052		23
1946		18	2054		26
1952		18	2056		27
1954		21	2058		24
1956		21	2060		26
1958		24	2062		23
1960		21	2064		23
1962		18	2066		28
1964		22	2068		22

Table A.5.5. Magnetic susceptibility (MS) values of core MD02-2549 from the La Salle Basin.

Depth (cm)	Age (ka)	MS (x 10^{-6} SI)	Depth (cm)	Age (ka)	MS (x 10^{-6} SI)
2072		25	2178		25
2074		31	2180		26
2076		22	2182		29
2078		26	2184		32
2080		26	2186		26
2082		26	2188		32
2084		24	2190		28
2086		24	2192		26
2088		25	2194		29
2090		27	2196		34
2092		24	2198		26
2094		27	2200		31
2096		25	2202		28
2100		23	2204		30
2102		22	2206		26
2104		25	2208		30
2106		24	2210		27
2108		26	2212		28
2110		25	2214		26
2112		27	2216		26
2114		27	2218		29
2116		26	2220		27
2118		24	2222		26
2120		23	2224		29
2122		24	2226		29
2124		21	2228		26
2126		23	2230		27
2128		27	2232		27
2130		24	2234		24
2132		26	2236		20
2134		24	2238		22
2136		26	2240		21
2138		30	2242		22
2140		25	2244		27
2142		25	2246		22
2144		25	2248		21
2146		22	2250		21
2148		23	2252		24
2150		23	2254		20
2152		23	2256		26
2154		23	2258		23
2156		22	2260		22
2158		25	2262		23
2160		22	2264		24
2162		23	2266		27
2164		23	2268		24
2166		23	2270		27
2168		23	2272		31
2170		24	2274		25
2172		25	2276		23
2174		27	2278		21
2176		26	2280		25

Appendix A.5: The La Salle Basin data

Table A.5.5. Magnetic susceptibility (MS) values of core MD02-2549 from the La Salle Basin.

Depth (cm)	Age (ka)	MS (x 10^{-6} SI)	Depth (cm)	Age (ka)	MS (x 10^{-6} SI)
2282		24	2386		27
2284		23	2388		32
2286		25	2390		29
2288		25	2392		29
2290		28	2394		30
2292		26	2396		29
2294		27	2400		30
2296		27	2402		33
2298		29	2404		29
2300		29	2406		26
2302		24	2408		37
2304		26	2410		34
2306		28	2412		35
2308		29	2414		33
2310		29	2416		33
2312		26	2418		42
2314		25	2420		36
2316		26	2422		31
2318		19	2424		30
2320		24	2426		32
2322		24	2428		34
2324		27	2430		31
2326		20	2432		36
2328		20	2434		40
2330		17	2436		30
2332		14	2438		31
2334		16	2440		25
2336		23	2442		18
2338		16	2444		23
2340		23	2446		48
2342		18	2448		22
2344		10	2450		18
2346		16	2452		30
2348		19	2454		37
2350		19	2456		28
2352		17	2458		33
2354		20	2460		31
2356		15	2462		26
2358		27	2464		26
2360		16	2466		35
2362		17	2468		34
2364		22	2470		32
2366		24	2472		28
2368		26	2474		31
2370		27	2476		33
2372		26	2478		30
2374		22	2480		30
2376		24	2482		32
2378		25	2484		35
2380		28	2486		27
2382		24	2488		28
2384		27	2490		32

Table A.5.5. Magnetic susceptibility (MS) values of core MD02-2549 from the La Salle Basin.

Depth (cm)	Age (ka)	MS (x 10^{-6} SI)	Depth (cm)	Age (ka)	MS (x 10^{-6} SI)
2492		30	2596		34
2494		33	2598		33
2496		31	2600		41
2498		29	2602		37
2500		27	2604		31
2502		25	2606		34
2504		24	2608		38
2506		23	2610		30
2508		26	2612		32
2510		23	2614		27
2512		28	2616		28
2514		28	2618		30
2516		24	2620		39
2518		25	2622		26
2520		22	2624		29
2522		31	2626		29
2524		23	2628		35
2526		20	2630		29
2528		21	2632		34
2530		24	2634		27
2532		21	2636		25
2534		18	2638		25
2536		13	2640		38
2538		22	2642		31
2540		10	2644		26
2542		10	2646		34
2544		11	2648		28
2546		9	2650		25
2548		10	2652		26
2550		16	2654		27
2552		23	2656		35
2554		20	2658		28
2556		24	2660		24
2558		21	2662		21
2560		23	2664		25
2562		24	2666		16
2564		23	2668		29
2566		18	2670		14
2568		36	2672		36
2570		30	2674		25
2572		26	2676		20
2574		31	2678		29
2576		29	2680		26
2578		28	2682		26
2580		26	2684		26
2582		27	2686		22
2584		30	2688		18
2586		27	2690		18
2588		29	2692		13
2590		35	2694		9
2592		33	2696		19
2594		27	2700		23

Appendix A.5: The La Salle Basin data

Table A.5.6. Colour reflectance of sediment core MD02-2549 from the La Salle Basin.

Depth (cm)	Age (ka)	L*	a*	b*
2	0.09	43.52	3.15	11.21
4	0.18	47.89	3.17	12.36
6	0.27	49.33	3.21	12.95
8	0.36	47.74	3.91	13.4
10	0.46	46.88	3.33	12.22
12	0.55	45.27	3.09	11.55
14	0.64	44.98	2.73	11.09
16	0.73	48.48	3.45	13.19
18	0.82	47.69	3.22	12.22
20	0.91	47.88	2.79	10.06
22	1.00	45.7	2.51	10.53
24	1.09	50.33	2.49	8.86
26	1.18	50.12	3.17	11.85
28	1.28	51.1	3.62	13.28
30	1.37	48.09	3.12	12
32	1.46	48.92	3.47	12.72
34	1.55	48.36	2.81	10.42
36	1.64	48	3.21	12.55
38	1.73	51.15	3.01	12.36
40	1.82	49.14	2.98	12.04
42	1.91	49.47	3.18	12.24
44	2.00	52.11	3.36	12.66
46	2.10	51.72	2.62	11.31
48	2.19	51.27	2.77	11.4
50	2.28	50.71	3.28	12.23
52	2.37	51.1	3.41	12.45
54	2.46	48.04	3	11.37
56	2.55	50.44	3	11.61
58	2.64	48.97	2.01	9.09
60	2.73	50.72	1.94	10.28
62	2.82	51.76	1.66	9.19
64	2.91	52.21	1.75	9.54
66	3.01	51.77	1.95	10.26
68	3.10	52.48	2.34	10.81
70	3.19	48.93	2.25	10.66
72	3.28	52.29	1.75	9.52
74	3.37	53.04	1.76	8.93
76	3.46	52.16	2.01	9.9
78	3.55	52.74	1.87	10.13
80	3.64	51.82	2.4	11.56
82	3.73	52.09	2.17	11.06
84	3.83	51.87	1.92	10.45
86	3.92	51.18	2.07	10.65
88	4.01	51.02	2.31	11.17
90	4.10	50.47	2.39	11.44
92	4.19	50.62	2.17	10.67
94	4.28	49.51	2.58	11.13
96	4.37	49.62	2.49	11.45
98	4.46	50.7	1.95	10.5
100	4.55	49.22	2.21	10.51
102	4.65	51.39	1.42	9.24
104	4.74	50.76	1.39	9.56
106	4.83	52.74	1.52	9.22
108	4.92	50.72	1.58	10.08
110	5.01	52.28	1.62	10.23
112	5.10	52.05	1.5	9.69
114	5.19	49.5	1.24	7.78
116	5.28	52.36	1.47	8.9
118	5.37	52.19	1.46	9.24
120	5.47	52.05	1.22	7.78
122	5.56	47.83	0.07	7.94
124	5.65	48.08	0.1	7.82
126	5.74	47.84	0.22	8.15
128	5.83	48.59	0.32	7.53
130	5.92	51.16	1.15	7.53
132	6.01	52.35	1.26	8.37
134	6.10	51.92	1.31	9.45
136	6.19	52.19	1.18	8.09
138	6.29	51.57	1.14	7.68
140	6.38	50.18	2.1	9.82
142	6.47	50.16	2.1	9.83
144	6.56	49.2	2.3	10.89
152	6.92	51.73	1.24	8.22
154	7.01	51.68	1.2	8
156	7.10	52.45	1.39	8.18
158	7.20	51.85	1.46	8.58
160	7.29	53.59	1.3	7.57
162	7.38	51.14	1.21	7.71
164	7.47	52.02	1.23	8.21
166	7.56	51.82	1.19	8.21
168	7.65	51.53	1	7.71
170	7.74	52.77	1.06	7.28
172	7.83	52.16	1.06	7.58
174	7.92	52.74	1.02	7.92
176	8.02	51.36	0.9	7.94
178	8.11	50.58	0.91	7.65
180	8.20	50.66	1.21	8.54
182	8.29	51.46	1.05	7.63
184	8.38	51.08	0.97	7.67
186	8.47	50.12	0.72	7.49
188	8.56	49.75	0.83	7.05
190	8.65	49.66	0.76	7.07
192	8.74	49.41	0.64	6.97
194	8.84	49.89	0.77	7.28
196	8.93	50.39	0.95	8.02
198	9.02	51.26	1.05	7.73
200	9.11	50.84	0.93	7.3
202	9.20	52.14	1.32	7.64
204	9.29	52.21	1.5	8.17
206	9.38	52.25	1.48	7.88
208	9.47	52.37	1.55	8.14
210	9.56	53.04	1.54	8.5
212	9.66	51.89	1.4	7.61
214	9.75	52.1	1.41	7.96

Table A.5.6. Colour reflectance of sediment core MD02-2549 from the La Salle Basin

Depth (cm)	Age (ka)	L*	a*	b*
216	9.84	52.91	1.52	8.48
218	9.93	52.71	1.45	8.53
220	10.02	52.71	1.58	8.6
222	10.11	53.3	1.47	7.86
224	10.20	54.49	1.39	7.23
226	10.29	53.04	1.59	7.84
228	10.38	52.99	1.41	7.52
230	10.48	54.9	1.56	7.17
232	10.57	53.73	1.78	8.68
234	10.66	52.71	1.83	9.19
236	10.75	50.77	2.15	10.88
238	10.84	49.39	2.24	10.76
240	10.93	49.63	2.14	10.56
242	11.02	50.11	2.12	10.68
244	11.11	49.5	1.48	10.48
246	11.20	49.13	2.27	10.71
248	11.29	49.32	1.98	9.93
250	11.39	48.45	2.07	10.23
252	11.48	48.54	2.14	10.05
254	11.57	48.77	2.03	9.88
256	11.66	48.61	2.09	9.95
258	11.75	49.03	2.12	10.16
260	11.84	47.99	2.08	10.02
262	11.93	48.43	2.08	9.97
264	12.02	48.46	2.19	10.21
266	12.11	48.22	1.81	9.23
268	12.21	48.1	1.58	7.71
270	12.30	49.43	1.77	8.31
272	12.39	49.32	1.93	9.41
274	12.48	48.82	2.27	10.28
276	12.57	48.94	2.24	10.23
278	12.66	47.4	1.42	6.67
280	12.75	47.98	2.06	7.56
282	12.84	48.61	2.42	8.72
284	12.93	47.71	1.14	6.58
286	13.03	48.68	2.18	9.51
288	13.12	48.08	1.64	7.89
290	13.21	49.1	2.26	10.23
292	13.30	49.09	2.31	10.07
294	13.39	48.69	2.22	9.67
302	13.77	44.74	0.26	4.9
304	13.88	45.29	0.56	5.45
306	13.99	46.33	0.47	5.22
308	14.09	46	0.69	5.23
310	14.20	46.25	0.69	4.9
312	14.30	45.72	1.03	5.26
314	14.41	47.88	0.61	5.17
316	14.51	48.03	0.58	5.18
318	14.62	47.54	0.55	4.98
320	14.72	46.05	0.68	5.03
322	14.83	47.83	0.64	5.16
324	14.93	47.53	0.56	4.87

Depth (cm)	Age (ka)	L*	a*	b*
326	15.04	46.99	0.64	5.08
328	15.15	47.35	0.46	5.24
330	15.25	47.05	0.23	4.81
332	15.36	49.57	0.26	6.2
334	15.46	48.93	0.25	6.34
336	15.57	45.34	0.59	4.87
338	15.67	44.96	-0.19	5.08
340	15.78	43.7	-0.01	4.77
342	15.88	46.29	0.11	5.12
344	15.99	43.98	0.31	4.61
346	16.09	47.31	-0.13	5.34
348	16.19	43.73	0.21	4.56
350	16.29	48.92	0.35	5.74
352	16.38	45.12	0.37	4.76
354	16.48	47.35	0.4	5.58
356	16.58	45.75	0.08	4.7
358	16.68	49.51	0.13	5.12
360	16.78	47.5	0.49	6.4
362	16.88	48.75	0.26	5.84
364	16.97	49.76	-0.02	5.05
366	17.07	49.31	0.17	5.89
368	17.17	46.5	0.25	5.34
370	17.27	50.57	0.39	6.05
372	17.37	50.9	0.42	6.32
374	17.47	49.14	0.57	7.04
376	17.56	49.87	-0.05	6.04
378	17.66	50.42	0.35	5.95
380	17.76	47.61	-0.49	5.74
382	17.86	49.21	-0.04	5.92
384	17.96	49.58	0.25	6.02
386	18.06	49.81	0.53	6.04
388	18.16	48.4	0.41	5.42
390	18.25	50.23	0.8	5.71
392	18.35	51.02	0.57	5.27
394	18.45	49.62	0.72	5.6
396	18.55	50.33	0.82	5.97
398	18.65	49.65	0.87	6.25
400	18.75	49.24	1.03	6.34
402	18.84	48.95	1.07	6.5
404	18.94	47.87	0.84	6.75
406	19.04	46.68	0.48	6.44
408	19.14	46.14	0.83	6.04
410	19.24	47.52	0.61	6.22
412	19.34	47.79	0.69	6.43
414	19.43	49.35	1.01	6.26
416	19.53	48.96	1.22	6.64
418	19.63	48.47	1.15	6.92
420	19.73	48.2	0.64	6.46
422	19.83	48.21	0.32	5.91
424	19.93	47.58	0.83	5.65
426	20.02	49.67	0.48	5.85
428	20.12	49.98	0.56	5.73

Appendix A.5: The La Salle Basin data

Table A.5.6. Colour reflectance of sediment core MD02-2549 from the La Salle Basin.

Depth (cm)	Age (ka)	L*	a*	b*
430	20.22	49.46	0.53	5.88
432	20.32	50.22	0.6	6.81
434	20.42	50.46	0.43	6.14
436	20.52	50.49	0.37	6.15
438	20.62	50.57	0.38	6.43
440	20.71	48.49	-0.13	5.74
442	20.81	48.11	0.07	5.73
444	20.91	49.35	0.18	5.89
452	21.30	48.76	0.36	5.57
454	21.40	48.04	-0.17	5.48
456	21.50	49.91	0.4	5.65
458	21.60	47.78	0.57	5.82
460	21.70	50.19	0.51	5.5
462	21.80	51.17	0.51	6
464	21.89	51.29	0.49	5.45
466	21.99	49.57	0.42	6.12
468	22.09	49.87	-0.01	5.76
470	22.19	47.93	0.7	5.53
472	22.29	47.87	0.39	5.71
474	22.39	47.67	0.34	6.25
476	22.48	43.05	-0.62	4.09
478	22.58	40.97	-0.51	3.93
480	22.68	41.39	-0.42	4.04
482	22.78	46.28	-0.11	4.46
484	22.88	47.4	0.01	4.45
486	22.98	47.81	0.08	4.84
488	23.07	48.11	0.06	5.15
490	23.17	45.83	-0.06	4.29
492	23.27	46.11	-0.41	4.12
494	23.37	46.28	-0.03	5.13
496	23.47	47.42	0.31	5.29
498	23.57	50.72	0.27	4.33
500	23.67	49.17	0.27	5.36
502	23.76	49.14	0.2	5.76
504	23.86	49.01	0.01	5.78
506	23.96	46.72	0.28	5.2
508	24.06	48.82	0.25	5.91
510	24.16	45.97	0.59	5.79
512	24.26	49.41	0.16	6
514	24.35	49.17	0.29	5.47
516	24.45	49.67	0.48	5.84
518	24.55	49.6	0.51	6.32
520	24.65	49.52	0.69	6.39
522	24.75	50.24	0.7	6.37
524	24.85	50.65	0.8	7.68
526	24.94	49.51	0.63	5.85
528	25.04	49.49	1.02	6.19
530	25.14	50.04	0.93	6.13
532	25.24	52.52	0.53	5.39
534	25.34	48.45	0.04	6.21
536	25.44	50.41	0.2	6.31
538	25.53	50.3	0.09	5.1
540	25.63	49.73	0.66	6.27
542	25.73	50.4	0.55	5.53
544	25.83	48.45	0.66	5.61
546	25.93	49.26	0.5	5.31
548	26.03	48.61	0.96	6.57
550	26.12	45.92	0.5	4.92
552	26.22	45.78	0.42	6.12
554	26.32	46.27	0.91	5.92
556	26.42	45.32	0.51	5.21
558	26.52	46.84	1.03	5.92
560	26.62	47.34	0.93	5.88
562	26.72	48.56	0.9	6.75
564	26.81	49.03	1.11	6.86
566	26.91	51.36	0.88	5.73
568	27.01	50.24	0.86	5.42
570	27.11	48.59	0.94	6.36
572	27.21	50.2	0.7	6.46
574	27.31	51.07	1.16	6.61
576	27.40	50.28	1.1	7.22
578	27.50	48.16	1.54	8.39
580	27.60	49.26	1.09	7.52
582	27.70	48.15	0.59	8.03
584	27.80	48.19	0.93	8.19
586	27.90	47.65	0.42	7.51
588	27.99	47.21	0.86	6.78
590	28.09	46.08	0.69	3.85
592	28.19	48.38	0.84	6.3
594	28.29	46.6	0.49	6.08
596	28.39	47.74	1.27	6.54
598	28.49	49.49	0.96	5.6
602	28.68	50.81	0.65	4.31
604	28.78	48.68	1.12	5.69
606	28.88	48.21	1.01	6.33
608	28.98	49.05	1.28	6.74
610	29.08	49.31	1.06	6.68
612	29.18	49.28	1.49	7.03
614	29.27	49	1.14	6.54
616	29.37	48.56	1.29	6.56
618	29.47	49.04	1.65	6.41
620	29.57	49.58	1.19	6.52
622	29.67	49.29	1.05	6.58
624	29.77	51.41	1.18	5.04
626	29.86	49.56	1.3	6.24
628	29.96	49.24	1.32	6.49
630	30.06	50.12	1.45	6.84
632	30.16	49.83	1.51	6.89
634	30.26	49.88	1.18	6.61
636	30.36	49.65	1.34	6.44
638	30.45	48.62	1.36	6.35
640	30.55	48.83	1.04	6.5
642	30.65	49.32	1.63	6.51
644	30.75	49.58	1.8	6.49

Table A.5.6. Colour reflectance of sediment core MD02-2549 from the La Salle Basin.

Depth (cm)	Age (ka)	L*	a*	b*
646	30.85	49.61	2.03	6.76
648	30.95	47.91	1.49	5.43
650	31.04	48.51	2.17	6.81
652	31.14	48.45	1.73	6.71
654	31.24	47.53	1.81	6.47
656	31.34	48.23	1.18	6.24
658	31.44	45.94	0.18	5.84
660	31.55	44.45	0.06	5.32
662	31.67	42.38	0.22	5.02
664	31.79	44.75	0.88	5.34
666	31.92	44.57	0.85	5.17
668	32.04	43.78	0.54	5.02
670	32.16	46.23	2.07	6.37
672	32.29	46.99	1.92	6.21
674	32.41	46.49	2.18	6.32
676	32.53	45.98	2.01	6.05
678	32.65	49.58	2.11	6.67
680	32.78	48.89	2.09	6.3
682	32.90	49.38	2.38	6.85
684	33.02	48.13	2.05	6.69
686	33.15	49	2.19	6.11
688	33.27	47.24	1.64	6.65
690	33.39	48.17	2.56	7.23
692	33.52	47.53	2.18	6.77
694	33.64	47.24	2.12	7.24
696	33.76	47.6	1.51	5.38
698	33.88	47.96	1.73	6.37
700	34.01	48.34	1.71	6.45
702	34.13	47.66	1.69	6.63
704	34.25	48.52	1.95	6.69
706	34.38	48.06	2.03	6.32
708	34.50	48.92	2.64	7.03
710	34.62	50.6	2.18	5.43
712	34.74	49.96	1.93	5.5
714	34.87	50.3	1.55	5.51
716	34.99	50.29	2.1	6.55
718	35.11	48.4	1.97	6.63
720	35.24	50.01	1.94	5.57
722	35.36	48.18	2.26	6.53
724	35.48	47.3	2.37	6.69
726	35.60	48.42	3	7.3
728	35.73	48.26	3.05	7.11
730	35.85	49.17	2.47	7.38
732	35.97	50.56	2.53	6.88
734	36.10	50.84	2.72	7.12
736	36.22	50.19	2.71	7.23
738	36.34	50.19	2.41	6.56
740	36.50	48.91	2.15	6.51
742	36.68	52.18	2.17	6.1
744	36.86	50.68	2.2	7.1
746	37.04	49.92	2.28	6.57
748	37.21	50.11	2.34	6.94
752	37.57	50.64	2.56	5.79
754	37.75	49.46	2.94	7.99
756	37.92	49.24	2.56	8.59
758	38.10	49.93	3.46	8.33
760	38.28	50.79	3.7	8.75
762	38.46	50.72	4.17	8.86
764	38.63	50.32	3.8	8.49
766	38.81	49.9	3.91	8.99
768	38.99	49.78	3.93	8.37
770	39.17	50.89	4.51	8.77
772	39.34	50.91	4.89	8.88
774	39.52	50.09	4.28	8.74
776	39.70	49.92	4.69	8.94
778	39.88	48.91	3.96	7.8
780	40.05	50.26	4.64	8.84
782	40.23	50.28	4.61	8.76
784	40.41	49.79	4.33	8.17
786	40.59	50.87	4.29	8.28
788	40.77	50.22	4.18	8.69
790	40.94	50.15	4.19	8.59
792	41.12	50.15	4.31	8.49
794	41.30	48.09	2.83	7.35
796	41.48	48.36	2.59	7.38
798	41.63	48.92	2.44	6.88
800	41.75	49.14	2.15	6.67
802	41.88	49.03	2.52	6.63
804	42.00	48.73	2.68	6.32
806	42.13	49.65	2.6	7.01
808	42.25	48.64	2.87	7.08
810	42.37	47.9	3.72	8.68
812	42.50	48.85	3.57	7.53
814	42.62	48.94	3.38	7.29
816	42.75	49.68	2	6.72
818	42.87	48.36	3.08	7.44
820	42.99	48.91	3.22	6.99
822	43.12	49.16	3.63	7.56
824	43.24	48.95	3.56	7.29
826	43.36	48.58	3.18	7.18
828	43.49	48.79	2.32	6.49
830	43.61	47.21	2.25	6.31
832	43.74	47.59	1.82	5.68
834	43.86	49.04	2.09	6.3
836	43.98	49.04	2.07	6.04
838	44.11	49.5	2.13	5.92
840	44.23	48.26	1.83	5.8
842	44.36	49.62	2.13	6.38
844	44.48	49.15	2.17	6.44
846	44.60	49.29	2.12	6.52
848	44.73	48.29	2.1	6.38
850	44.85	46.95	2.08	6.24
852	44.97	49.58	2.06	6.47
854	45.10	47.86	1.86	6.07

Appendix A.5: The La Salle Basin data

Table A.5.6. Colour reflectance of sediment core MD02-2549 from the La Salle Basin.

Depth (cm)	Age (ka)	L*	a*	b*
856	45.22	50.6	1.87	6.12
866	45.84	48.8	2.93	6.3
868	45.97	47.98	2	5.72
870	46.09	47.69	2.01	6.07
872	46.21	48.34	2.12	6.25
874	46.34	45.82	1.68	4.25
876	46.46	48.47	2.22	6.47
878	46.59	47.09	1.47	5.56
880	46.71	48.3	2.56	7.04
882	46.83	49.16	3	7.63
884	46.96	48.64	2.69	7.28
886	47.08	48.92	2.96	6.88
888	47.20	48.89	2.97	7.51
890	47.33	49.16	2.89	7.39
892	47.45	49.99	2.75	6.89
894	47.58	48.86	3.04	7.36
896	47.70	49.45	3.25	7.64
898	47.82	48.78	3.06	7.35
900	47.95	49.5	3.05	7.56
902	48.07	50.15	3.13	7.92
904	48.20	49.54	2.97	7
906	48.32	50.3	2.96	7.05
908	48.44	48.89	2.94	6.51
910	48.57	51.8	2.66	5.7
912	48.69	48.98	3.32	7.33
914	48.81	49.13	4.25	8.53
916	48.94	49.59	4.28	7.83
918	49.06	48.93	3.8	7.29
920	49.19	49.03	2.78	5.69
922	49.31	50.81	3.8	8.04
924	49.43	49.99	3.57	7.6
934	50.72	49.11	2.98	7.13
936	50.98	49.2	2.21	6.37
942	51.75	48.41	3.35	7.41
944	52.00	47.7	3.08	7.38
946	52.26	49.5	3.22	6.8
948	52.52	49.61	2.85	6.52
950	52.77	48.41	3.09	7.12
952	53.03	48.46	3.13	7.05
954	53.29	49.41	3.19	6.6
956	53.54	50.11	2.8	6.48
958	53.80	49.43	3.3	7.48
960	54.06	49.17	3.8	7.07
962	54.32	51.42	3.5	6.96
964	54.57	51.98	3.55	7.25
966	54.83	51.05	3.32	6.38
968	55.09	52.87	3.82	6.7
970	55.34	49.29	4.45	8.31
972	55.60	51.23	3.85	6.71
990	57.30	49.2	1.97	4.73
992	57.53	49.34	4.27	7.62
994	57.76	46.97	3.7	8.09
996	57.99	47.39	3.29	7.02
998	58.21	49.45	2.73	6.07
1000	58.44	51.88	2.75	5.36
1002	58.67	51.81	2.41	5.86
1004	58.90	53.8	2.54	5.21
1006	59.13	51.72	2.76	5.86
1008	59.36	50.09	2.89	6.8
1010	59.59	47.54	2.13	5.92
1012	59.82	49.53	2.98	7.25
1014	60.05	48.41	3.5	7.3
1016	60.27	48.97	2.94	6.97
1018	60.50	48.3	3.06	7.15
1020	60.73	48.84	2.7	6.83
1022	60.96	49.27	3.1	7.21
1024	61.19	49.2	2.85	7
1042	63.25	50.34	0.8	6
1044	63.48	51.93	0.74	4.53
1046	63.71	50.14	1.28	5.4
1052	64.39	48.67	1.68	5.82
1058	65.08	48.2	2.42	6.19
1060	65.31	49	2.41	5.63
1062	65.54	49.44	2.34	6.29
1064	65.76	50.32	2.01	5.51
1066	65.99	49.07	2.23	6.22
1068	66.22	49.2	2.37	6.3
1070	66.45	49.48	2.42	6.13
1072	66.68	47.79	2.12	5.94
1074	66.91	48.78	2.43	6.01
1076	67.14	49.3	1.92	6.45
1078	67.37	50.69	0.61	5.61
1080	67.60	51.44	0.11	5.4
1082	67.82	51.87	0.28	5.6
1084	68.05	50.72	0.2	5.13
1086	68.28	52.52	0.34	5.37
1088	68.51	52.02	0.16	5.79
1090	68.74	51.98	0.17	4.61
1092	68.97	52.32	0.12	5.7
1094	69.20	53.06	-0.62	6.21
1096	69.43	52.82	-0.32	5.65
1106	70.57	50.48	-0.68	6.19
1108	70.80	51.36	-0.3	5.6
1110	71.03	52.37	-0.1	5.95
1112	71.26	53.85	-0.1	5.9
1114	71.40	53.86	-0.04	5.72
1116	71.50	53.29	0.26	6.49
1118	71.61	53.33	0.02	4.95
1120	71.71	53.63	-1.14	6.26
1122	71.81	52.4	-0.42	5.21
1124	71.92	54.35	-0.31	5.87
1126	72.02	53.37	-0.03	5.63
1128	72.13	54.53	-0.66	6.03
1130	72.23	54.69	-0.11	5.94

Table A.5.6. Colour reflectance of sediment core MD02-2549 from the La Salle Basin.

Depth (cm)	Age (ka)	L*	a*	b*
1132	72.33	53.22	0.14	6.39
1134	72.44	53.08	-0.01	6.13
1136	72.54	55.06	-0.18	5.69
1138	72.64	54.21	-0.05	5.46
1140	72.75	56.79	-0.35	6.36
1142	72.85	54.91	0.05	6.76
1144	72.96	53.41	-0.35	4.97
1146	73.06	55.9	-0.72	6.51
1148	73.16	55.08	-0.6	7.03
1150	73.27	56.31	-0.19	6.74
1152	73.37	55.82	-0.04	6.15
1164	73.99	55.51	-0.06	6.73
1166	74.10	56.42	-0.09	5.57
1168	74.20	57.13	-0.08	5.49
1170	74.30	55.68	-0.21	5.66
1172	74.41	56.05	-0.37	5.41
1174	74.51	54.96	-0.25	6.6
1176	74.62	52.9	-0.31	6.29
1178	74.72	54.12	0	5.92
1180	74.82	53.99	0.19	6.37
1182	74.93	53.44	0.28	6.99
1184	75.03	52.94	0.36	6.46
1186	75.13	53.6	0.21	6.9
1188	75.24	52.63	0.23	6.73
1190	75.34	53.07	-0.18	6.6
1192	75.45	53.27	0.4	6.71
1194	75.55	52.99	0.47	6.96
1196	75.65	50.38	0.37	6.31
1198	75.76	52.63	0.34	6.44
1356	84.15	50.78	0.32	4.52
1358	84.49	50.05	1.16	7.33
1360	84.82	52.33	0.35	6.18
1362	85.16	50.85	0.24	5.43
1364	85.50	52.4	0.46	5.93
1366	85.84	53.34	0.62	6.24
1368	86.18	53.41	0.74	6.89
1370	86.51	52.71	0.72	6.69
1372	86.85	52.3	-0.15	6.96
1374	87.19	51.94	0.46	6.75
1376	87.53	53.1	-0.12	6.31
1378	87.87	54.94	0.15	6.71
1384	88.88	53.76	0.3	6.44
1386	89.22	54.29	0.34	7.41
1388	89.56	52.71	-0.43	6.51
1390	89.90	51.74	-0.01	6.7
1392	90.23	52.3	0.17	6.85
1394	90.57	51.97	0.07	6.56
1396	90.91	53.12	-0.23	6.4
1398	91.25	50.98	0.02	6.64
1400	91.59	51.65	0.24	7.04
1402	91.93	53.09	0.16	6.76

Depth (cm)	Age (ka)	L*	a*	b*
1404	92.26	54.95	0.22	6.83
1406	92.57	54.7	0.1	6.54
1408	92.88	53.97	0.18	6.96
1410	93.19	54.73	0.13	6.52
1412	93.51	52.41	0.08	5.89
1414	93.82	53.78	0.22	6.22
1416	94.13	54.02	0.21	7.04
1418	94.44	53.97	0.09	7.16
1420	94.75	54.51	0.14	6.91
1422	95.07	56.95	0.49	7.79
1424	95.38	55.95	0.15	7
1426	95.69	57.93	0.41	8.1
1428	96.00	56.82	0.63	8.2
1430	96.31	58.25	0.34	8.1
1432	96.63	55.95	0.45	7.36
1434	96.94	58	0.61	8.28
1436	97.25	57.77	0.79	8.06
1438	97.56	57.19	0.46	8.65
1440	97.87	55.21	0.29	8.39
1442	98.19	56.5	1.33	8.65
1444	98.50	57.22	1.51	8.88
1446	98.81	56.32	1.43	8.94
1448	99.12	55.98	1.9	8.93
1450	99.43	56.39	2.46	9.46
1452	99.75	55.77	2.37	9.25
1454	100.06	53.66	1.09	7.41
1456	100.37	53.39	2.15	8.86
1458	100.68	53.19	3	9.6
1460	100.99	52.64	2.47	9.48
1462	101.31	51.89	2.56	9.63
1464	101.62	51.7	2.72	9.41
1466	101.93	51.6	2.1	8.89
1468	102.24	52.15	2.07	8.66
1470	102.55	52.16	2.1	8.33
1472	102.87	52.72	1.85	8.45
1474	103.18	51.28	1.68	8.04
1476	103.49	55.15	1.52	8.23
1478	103.80	55.03	1.2	8.51
1480	104.11	55.12	1.48	7.76
1482	104.43	54.65	0.56	8.33
1484	104.74	53.66	0.56	8.46
1486	105.05	53.71	0.13	7.75
1488	105.36	52.74	0.72	7.73
1490	105.67	49.9	-0.28	7.58
1492	106.13	50.93	1.02	7.59
1494	106.66	50.84	0.41	6.9
1496	107.18	48.71	0.27	6.18
1498	107.71	53.43	0.47	6.5
1502	108.76	51.02	0.8	7.16
1504	109.28	51.96	0.76	6.77
1506	109.81	50.17	-0.46	6.91
1508	110.33	50.44	0.73	6.38

Appendix A.5: The La Salle Basin data

Table A.5.6. Colour reflectance of sediment core MD02-2549 from the La Salle Basin.

Depth (cm)	Age (ka)	L*	a*	b*
1510	110.86	50.95	0.13	6.74
1512	111.38	50.84	0.09	6.33
1514	111.91	51.14	0.37	7.17
1516	112.43	50.48	0.33	6.28
1518	112.96	49.06	0.54	7.87
1520	113.48	52.87	0.53	7.35
1522	114.01	52.72	0.07	6.97
1524	114.53	53.49	0.29	7.57
1526	115.06	54.1	0.28	7.45
1528	115.53	50.52	-0.05	6.12
1530	115.91	53.56	0.38	7.33
1532	116.29	54.36	0.42	7.7
1534	116.68	51.63	0.32	7.36
1536	117.06	54.42	0.4	7.15
1538	117.45	54.47	0.63	7.51
1540	117.83	52.76	0.29	7.24
1542	118.22	55.65	0.58	8.12
1544	118.60	53.63	0.37	7.05
1546	118.98	54.87	-0.06	8.35
1548	119.37	54.91	0.62	8.41
1550	119.75	56.08	0.78	7.96
1552	120.14	55.35	0.56	8.06
1554	120.52	56.01	1.02	8.1
1556	120.90	55.44	0.92	7.49
1558	121.29	54.79	1.13	8.54
1560	121.67	55.46	0.58	8.44
1562	122.06	55.41	1.04	7.76
1564	122.44	55.66	1.52	8.71
1566	122.82	55.93	1.45	8.04
1568	123.21	57.12	2.08	8.91
1570	123.59	56.79	2.4	8.8
1572	123.98	56.46	2.56	9.23
1574	124.36	56.31	2.72	9.84
1576	124.75	55.36	3.07	9.74
1578	125.13	54.65	2.91	10.01
1580	125.51	55.32	3.09	9.96
1580	125.51	55.69	3.25	10.12
1582	125.90	55.4	2.58	9.69
1584	126.28	55.2	2.77	9.09
1586	126.67	55.72	3.01	10.03
1588	127.05	56.85	2.64	9.86
1590	127.43	55.95	2.88	9.98
1592	127.82	55.46	2.36	9.5
1594	128.20	56.01	2.36	9.27
1596	128.59	55.75	2.55	9.13
1598	128.97	54.69	2.74	9.23
1600	129.36	53.6	1.87	7.86
1602	129.74	52.09	0.96	7.89
1604	130.12	53.5	0.96	6.9
1606	130.51	53.31	1.7	6.61
1608	130.89	52.65	2.73	7.11
1610	131.28	48.51	4.72	7.71
1620	133.20	46.61	3.8	7.23
1622	133.58	44.76	3.87	7.25
1624	133.97	44.19	2.78	5.89
1626	134.35	44.2	2.43	5.74
1628	134.73	42.98	2.31	5.1
1630	135.12	43.06	1.67	4.47
1632	135.50	42.42	2.15	4.91
1634	135.89	42.23	2.6	5.43
1636	136.27	42.09	4.43	6.71
1638	136.65	42.25	0.63	3.95
1640	137.04	41.62	0.21	3.48
1642	137.42	41.03	0.23	3.25
1644	137.81	44.72	0.34	3.45
1646	138.19	43.19	0.95	3.73
1648	138.58	43.58	0.35	3.57
1652	139.34	43.14	0.49	3.69
1654	139.73	42.56	1.28	4.84
1656	140.11	42.68	0.81	4.46
1658	140.50	42.8	1.64	4.95
1660	140.88	42.87	1.06	4.5
1662	141.26	44.31	0.83	4.18
1664	141.65	45.03	1.17	4.56
1666	142.03	45.48	0.94	4.79
1668	142.42	45.84	0.46	3.65
1670	142.80	44.86	0.61	4.28
1672	143.18	43.39	0.21	3.59
1674	143.57	44.88	0.17	2.91
1676	143.95	42.63	0.15	3.43
1678	144.34	43.21	0.19	3.68
1680	144.72	42.91	0.34	3.89
1682	145.11	43.11	0.37	3.85
1684	145.49	43.42	0.54	4.17
1686	145.87	43.89	0.71	4.22
1688	146.26	43.86	0.88	4.47
1690	146.64	43.76	0.77	4.49
1692	147.03	43.75	0.96	4.64
1698	148.18	44.21	1.16	4.88
1700	148.56	44.76	0.84	3.63
1702	148.95	45.59	0.85	3.99
1704	149.33	44.05	0.49	3.35
1706	149.72	42.99	0.56	3.82
1708		42.99	0.56	3.82
1710		41.72	0.33	3.88
1712		41.49	0.32	3.36
1714		41.94	0.36	3.93
1716		42.37	0.31	3.96
1718		43.08	0.4	3.66
1720		44.89	0.81	3.91
1722		42.83	1.05	4.44
1724		45.1	0.88	4.15
1726		43.85	1.18	4.78
1728		44.05	1.36	5.05

Table A.5.6. Colour reflectance of sediment core MD02-2549 from the La Salle Basin.

Depth (cm)	Age (ka)	L*	a*	b*
1730		43.64	1.51	4.98
1732		42.38	1.07	4.12
1734		43.07	0.52	3.83
1736		42.43	0.53	3.74
1738		41.12	-0.11	3.48
1740		44.07	1.55	5.1
1742		44.72	1.9	5.46
1744		46.76	1.68	5.35
1746		44.19	1.07	4.61
1748		43.8	0.81	4.05
1750		43.78	0.98	4.7
1752		44.16	1.24	4.81
1754		43.6	0.77	4.11
1756		44.2	1.27	4.59
1758		43.77	1.19	4.35
1760		42.93	0.81	4.23
1762		43.24	0.64	4.21
1764		44.55	0.95	4.25
1766		43.95	1.11	4.61
1768		44.11	1.01	4.46
1770		44.91	0.85	4.7
1772		45.28	0.75	4.62
1774		46.85	0.75	4.54
1776		47.06	0.88	4.25
1778		45.69	0.53	3.99
1780		44.75	0.3	3.38
1782		44.34	0.23	3.12
1784		45.85	0.34	3.39
1786		47.39	0.42	2.73
1788		48.85	0	2.7
1790		45.59	0.02	3.14
1792		44.84	0.36	3.48
1794		43.84	0.49	3.84
1796		43.49	0.62	4.28
1798		48.31	0.65	3.35
1802		43.88	1.31	4.72
1804		42.77	0.98	4.28
1806		43.15	0.75	4.28
1808		43.71	0.72	4.02
1810		43.74	0.81	4.18
1812		43.97	0.41	3.52
1814		43.85	0.58	4
1816		46.61	0.62	3.49
1818		44.36	0.51	3.54
1820		46.28	0.71	3.53
1822		45.02	0.77	4.54
1824		46.2	0.78	4.37
1826		48.38	1.04	4.42
1828		45.02	0.89	4.47
1830		43.53	0.35	3.82
1832		44.38	0.51	3.93
1834		44.75	0.35	3.75

Depth (cm)	Age (ka)	L*	a*	b*
1836		42.94	0.32	3.91
1838		45.33	0.21	3.26
1840		44.38	0.35	3.27
1842		45.49	0.4	3.62
1844		43.59	0.3	3.61
1846		44.15	0.36	3.55
1848		43.64	0.28	3.88
1850		44.34	0.47	4.07
1852		44.31	0.45	4.4
1854		44.49	0.58	4.25
1856		45.68	0.33	3.99
1858		44.84	0.51	4.11
1860		44.71	0.47	3.88
1862		44.14	0.41	3.94
1864		44.68	0.48	3.83
1866		46.61	0.41	3.16
1868		48.93	0.54	3.36
1870		46.38	0.68	4.37
1872		45.03	1.06	4.66
1874		44.29	0.88	4.52
1876		46.07	0.96	4.29
1878		45.66	0.81	4.2
1880		45.39	0.98	4.36
1882		46.12	1.04	4.27
1884		46.05	0.96	4.41
1886		44.04	0.6	3.7
1888		43.38	0.82	4.11
1890		44.49	0.63	4.1
1892		44.36	0.7	4.05
1894		45.03	0.59	3.95
1896		45.4	1.08	4.75
1898		45.71	1.11	4.94
1900		42.63	0.49	4.28
1902		45.2	0.48	3.35
1904		44.39	0.26	3.5
1906		45.93	0.79	4.27
1908		44.95	1.26	4.64
1910		45.19	0.74	4.46
1912		44.84	0.44	3.88
1914		44.84	0.62	4.2
1916		43.42	0.45	3.97
1918		45.4	0.61	4.07
1920		45.7	0.66	4.19
1922		44.84	0.39	3.62
1924		44.91	0.35	3.36
1926		45.93	0.38	3.67
1928		45.11	0.44	3.75
1930		45.04	0.63	4.03
1932		45.15	0.36	3.26
1934		45.84	0.5	3.55
1936		45.41	0.46	3.96
1938		45.14	0.35	3.62

Appendix A.5: The La Salle Basin data

Table A.5.6. Colour reflectance of sediment core MD02-2549 from the La Salle Basin.

Depth (cm)	Age (ka)	L*	a*	b*
1940		47.3	0.7	4.31
1942		45.63	0.61	4.06
1944		47.5	0.91	4.82
1946		43.19	0.25	3.71
1948		43.61	0.54	3.91
1952		47.13	1.2	4.79
1954		46.63	0.24	2.99
1956		47.3	0.22	3.22
1958		45.01	0.29	3.91
1960		45.39	0.43	3.41
1962		46.84	1.06	4.4
1964		47.42	0.51	3.38
1966		46.93	0.87	4.21
1968		44.16	0.49	3.55
1970		43.17	0.49	3.92
1972		43.94	0.5	3.82
1974		45.42	0.92	4.82
1976		43.25	0.38	3.98
1978		42.34	0.39	3.62
1980		42.47	0.3	3.61
1982		46.04	0.67	4.2
1984		43.22	0.13	3.38
1986		42.91	0.45	3.82
1988		43.71	0.38	3.22
1990		44.75	0.65	3.56
1992		46.26	0.22	2.87
1994		46.17	0.29	3.07
1996		45.98	0.54	3.67
1998		45.66	0.71	4.26
2000		45.02	0.33	3.77
2002		46.6	0.56	3.94
2004		46.28	0.53	4.09
2006		46.09	0.45	3.86
2008		46.72	0.42	3.92
2010		46.34	0.44	3.47
2012		48.39	0.52	3.93
2014		45.09	0.12	3.3
2016		45.34	0.19	3.51
2018		47.83	0.47	3.76
2020		46.9	0.38	3.63
2022		48.8	0.54	3.79
2024		49.74	0.52	3.24
2026		50.2	0.77	3.16
2028		46.28	0.34	3.42
2030		47.67	0.48	3.85
2032		49.04	0.79	3.73
2034		49.49	0.47	3.16
2036		47.13	0.46	4.15
2038		47.21	0.66	4.08
2040		47.54	0.85	4.75
2042		47.1	1.05	4.84
2044		47.74	0.81	4.44
2046		45.9	0.53	3.93
2048		50.87	1.13	3.96
2050		50.1	0.81	3.85
2052		48.79	0.46	3.24
2054		46.52	0.92	4.74
2056		45.9	1	4.88
2058		46.09	0.8	4.17
2060		46.06	0.79	4.29
2062		47.09	1.28	4.85
2064		47.19	0.85	4.49
2066		48.11	1.01	4.55
2068		46.14	0.97	4.43
2070		46.99	0.93	4.53
2072		49.61	1.02	4.84
2074		49.78	0.95	4.41
2076		46.6	1.1	4.79
2078		46.83	1.1	4.9
2080		47.72	1.22	4.86
2082		46.53	1.2	4.95
2084		47.3	1.27	5.26
2086		47.68	0.99	4.69
2088		47.78	1.16	5
2090		46.23	1.3	5.13
2092		45.54	1.13	4.8
2094		46.66	1.14	4.86
2096		46	1.32	5.19
2098		46.44	1.3	4.99
2102		49.37	0.51	3.13
2104		46.32	0.67	4.06
2106		45.9	0.92	4.54
2108		45.46	0.68	4.34
2110		46.53	0.85	4.36
2112		46.79	0.78	4.29
2114		46.07	0.98	4.66
2116		48.07	0.77	4.12
2118		47.54	0.8	4.17
2120		48.79	0.8	3.99
2122		47.12	0.67	4.09
2124		46.07	0.64	4.35
2126		46.4	0.72	4.24
2128		46.14	0.83	4.35
2130		44.73	0.64	4.13
2132		44.81	0.74	4.52
2134		46.16	0.94	4.46
2136		46.26	0.87	4.47
2138		45.62	0.91	4.42
2140		46.04	0.82	3.99
2142		45.86	0.85	3.97
2144		46.14	1.09	4.31
2146		46.14	1.4	4.72
2148		45.62	0.78	4.45
2150		46.12	0.88	4.34

Table A.5.6. Colour reflectance of sediment core MD02-2549 from the La Salle Basin.

Depth (cm)	Age (ka)	L*	a*	b*
2152		45.56	0.73	4.33
2154		46.42	0.64	4.05
2156		46.96	0.57	3.89
2158		46.34	0.58	3.92
2160		46.9	0.73	4.06
2162		46.28	0.84	4.45
2164		46.96	0.75	4.32
2166		46.87	0.9	4.37
2168		47.13	0.71	3.85
2170		47.55	0.84	4.12
2172		47.72	0.76	4.02
2174		47.21	0.83	4.3
2176		47.19	1.02	4.6
2178		47.11	0.68	4.24
2180		47.11	0.85	4.26
2182		45.81	0.81	4.23
2184		45.64	0.64	4.16
2186		46.63	0.89	4.41
2188		46.65	0.99	4.62
2190		47.22	1.07	4.24
2192		45.65	0.4	3.48
2194		47.24	1.01	4.53
2196		46.05	0.81	4.2
2198		47.35	1.39	4.89
2200		47.15	1.18	4.71
2202		46.34	0.87	4.14
2204		47.39	1.17	4.74
2206		47.14	1.06	4.56
2208		46.8	1.13	4.74
2210		47.62	1.14	4.84
2212		45.17	0.75	4.28
2214		47.31	1.1	4.69
2216		45.66	0.82	4.06
2218		46.95	0.88	4.33
2220		47.83	1.07	4.44
2222		45.63	0.55	3.75
2224		46.62	1.02	4.64
2226		46.99	1.12	4.65
2228		46.25	0.79	4.08
2230		44.93	0.66	4.02
2232		48.38	1.43	4.51
2234		46.39	1.19	4.73
2236		45.04	0.76	3.88
2238		44.24	0.73	3.88
2240		45.42	0.9	4.21
2242		48.74	0.8	3.61
2244		47.6	0.94	3.94
2246		45	1.14	4.43
2248		46.49	0.91	4.01
2254		43.96	0.4	2.9
2256		45.9	0.75	3.43
2258		47.3	1.2	3.78

Depth (cm)	Age (ka)	L*	a*	b*
2260		46.24	1.51	4.48
2262		46.4	0.92	4.25
2264		46.44	1.16	4.28
2266		45.64	0.83	3.68
2268		45.22	1.26	4.37
2270		45.53	1.23	4.5
2272		45.26	0.84	4.21
2274		45.46	0.98	4.48
2276		47.49	0.95	4.5
2278		45.38	0.79	4.32
2280		45.55	0.91	4.43
2282		45.81	1.16	4.71
2284		45.15	1.05	4.62
2286		43.94	0.52	4.11
2288		43.99	0.64	4.03
2290		44.93	1	4.46
2292		46.47	0.93	4.22
2294		46.4	1.03	4.29
2296		45.91	1.05	4.38
2298		46.39	1.23	4.79
2300		46.03	1.29	4.75
2302		46.19	1.28	4.71
2304		45.51	1.25	4.67
2306		45.81	1.29	4.85
2308		45.48	1.5	4.92
2310		46.21	1.42	4.98
2312		48.27	1.13	4.18
2314		44.97	1.15	4.67
2316		44.97	1.16	4.8
2318		46.11	1.22	4.75
2320		44.71	1	4.6
2322		47.03	1.37	4.98
2324		47.1	1.27	5.01
2326		47.13	1.42	5.06
2328		46.9	1.11	4.84
2330		47.59	0.81	4.54
2332		46.74	0.32	4.03
2334		47.27	-0.06	3.96
2336		47.3	-0.28	3.53
2338		48.15	-0.13	3.95
2342		48.08	-0.32	3.54
2344		47.77	-0.26	3.71
2346		47.54	0.18	3.95
2348		46.81	0.42	4.1
2350		44.98	0.18	3.65
2352		46.02	0.53	4.05
2354		45.95	0.41	4.09
2356		45.66	-0.1	3.53
2358		47.12	-0.25	3.7
2360		48.88	-0.36	2.7
2362		48.22	-0.27	2.93
2364		50.73	0.08	2.93

Appendix A.5: The La Salle Basin data

Table A.5.6. Colour reflectance of sediment core MD02-2549 from the La Salle Basin.

Depth (cm)	Age (ka)	L*	a*	b*
2366		46.3	0.55	3.73
2368		46.16	0.82	3.96
2370		45.67	0.32	2.82
2372		46.46	0.78	3.98
2374		47.09	0.9	4.16
2376		47.28	0.97	4.35
2378		45.92	1.08	4.61
2380		46.05	1.09	4.43
2382		46.19	1.02	4.33
2384		47	1.18	4.71
2386		46.62	1.28	4.83
2388		46.27	1.24	4.49
2390		46.85	1.43	4.86
2392		48.84	1.38	4.59
2394		49.79	0.88	3.34
2396		50.13	1.33	3.91
2404		46.61	1.08	4.65
2406		46.95	1.34	4.77
2408		46.59	1.14	4.89
2410		45.65	0.88	4.66
2412		46.79	0.65	4.07
2414		46.24	0.92	4.76
2416		45.79	0.83	4.64
2418		45.72	0.96	4.77
2420		45.38	0.68	4.29
2422		46.91	1	4.72
2424		46.23	0.92	4.66
2426		46.56	0.88	4.54
2428		46.24	1.05	4.78
2430		46.35	1.37	5.07
2432		46.64	1.09	4.74
2434		45.53	1.12	4.8
2436		46.42	1.03	4.65
2438		47.05	1.1	4.54
2440		50.77	0.97	3.56
2442		47.92	0.48	3.64
2444		45.79	-0.36	2.78
2446		46.38	-0.45	1.29
2448		44.55	-0.48	2.16
2450		44.96	-0.24	2.42
2452		45.52	-0.36	2.76
2454		45.81	0.68	3.64
2456		48.82	0.89	3.2
2458		48.75	0.9	3.88
2460		47.51	0.88	4.22
2462		44.1	0.67	3.82
2464		44.15	1.02	4.37
2466		45.78	1.05	4.6
2468		44.78	1.03	4.73
2470		44.73	0.97	4.59
2472		46	1.07	4.65
2474		46.38	1.1	4.77

Depth (cm)	Age (ka)	L*	a*	b*
2476		46.42	1.19	4.77
2478		46.04	1.13	4.74
2480		45.84	0.99	4.65
2482		46.25	1.07	4.66
2484		45.8	1.18	4.9
2486		45.69	1.43	5
2488		45.73	1.25	4.91
2490		44.71	1.09	4.73
2492		45.98	0.89	4.11
2494		45.23	0.91	4.33
2496		46.85	0.93	4.55
2498		45.93	0.85	3.94
2500		46.01	1.13	4.46
2502		49.93	1.09	3.53
2504		45.82	1.84	5.41
2506		44.71	1.61	5.03
2508		45.62	0.82	4.44
2510		45.38	0.65	4.04
2512		45.73	0.72	4.39
2514		46.28	0.67	4.05
2516		45.49	0.89	4.58
2518		46.32	0.85	4.56
2520		47.81	0.72	4.11
2522		48.83	0.72	3.84
2524		48.69	0.64	3.84
2526		47.66	0.63	4.25
2528		49.47	0.45	3.27
2530		46.51	0.58	4.35
2532		48.72	0.74	3.77
2534		49.48	0.35	2.91
2536		45.95	0.19	3.95
2538		48.53	-0.09	3.26
2540		48.68	-0.52	2.17
2542		46.68	-0.71	3.07
2544		47.09	-0.6	3.25
2546		43.85	0	1.48
2554		47.55	-0.17	2.85
2556		47.22	0.29	3.89
2558		47.66	0.77	4.41
2560		47.48	0.64	3.99
2562		47.12	0.35	4.17
2564		47.06	-0.1	3.27
2568		47.71	-0.12	3.6
2570		46.54	0.34	4
2572		46.67	0.29	4.05
2574		46.53	0.93	4.6
2576		46.35	1.2	4.83
2578		46.48	1.26	4.95
2580		46.18	1.4	5.19
2582		44.77	0.95	4.52
2584		45.55	1.17	4.72
2586		44.5	1.1	4.66

Table A.5.6. Colour reflectance of sediment core MD02-2549 from the La Salle Basin.

Depth (cm)	Age (ka)	L*	a*	b*
2588		46.52	1.11	4.81
2590		45.33	1.08	4.69
2592		45.52	1.17	4.61
2594		45.32	0.88	4.51
2596		45.6	0.97	4.66
2598		45.65	1.05	4.79
2600		46.18	1.08	4.93
2602		46.09	1.2	4.94
2604		46.78	1.16	4.93
2606		46.54	1.24	4.98
2608		45.33	1.13	4.8
2610		46.09	0.9	4.61
2612		46.72	1.12	4.69
2614		45.94	1.11	4.8
2616		46.14	1.2	4.78
2618		45.76	0.84	4.57
2620		45.37	0.76	4.45
2622		46.45	0.83	3.94
2624		46.15	0.82	4.5
2626		44.81	0.91	4.59
2628		46.11	0.88	4.37
2630		45.47	0.8	4.53
2632		45.28	0.74	4.28
2634		45.72	0.87	4.39
2636		46.97	0.68	4.25
2638		43.73	0.66	4.26
2640		46.09	0.22	3.39
2642		47.41	0.45	3.87
2644		45.33	0.21	3.04
2646		48.02	0.28	2.92
2648		45.03	0.49	4.09
2650		44.81	0.4	3.93
2652		44.45	0.32	4
2654		44.69	0.51	4.06
2656		44.85	0.67	4.06
2658		45.17	0.55	3.93
2660		45.53	0.59	4.22
2662		48.9	0.19	3.01
2664		46.9	-0.09	3.5
2666		45.38	-0.47	3.09
2668		47.72	-0.33	3.24
2670		47.75	-0.6	1.39
2672		44.41	-0.21	3.5
2674		46.9	-0.1	3.8
2676		45.02	0.2	3.65
2678		45.98	0.59	4.3
2680		45.91	0.93	4.78
2682		46.8	0.89	4.6
2684		46.17	0.79	4.3
2686		46.22	0.7	4.39
2688		46.04	0.25	3.95
2690		47.52	-0.25	2.82
2692		47.53	-0.24	3.26
2694		45.2	-0.3	2.77
2696		50.88	-0.32	2.48
2704		46.89	0.65	4.12
2706		46.24	0.69	4.55
2708		46.36	0.9	4.42
2710		46.3	0.89	4.62
2712		46.66	0.99	5.15
2714		45.02	1.03	5
2716		45.24	1.06	4.99
2718		44.28	0.76	4.43
2720		48.12	0.74	4.28
2722		44.28	0.76	4.6
2724		44.09	0.81	4.5
2726		44.93	1.02	4.92
2728		44.32	0.81	4.47
2730		45.28	0.91	4.82
2732		48.96	0.64	3.62
2734		44.44	1.01	4.87
2736		44.37	0.64	4.46
2738		44.53	0.73	4.54
2740		45.88	0.83	4.61
2742		45.68	0.71	4.47
2744		44.96	0.74	4.53
2746		46.92	0.75	4.16
2748		46.07	0.63	4.32
2750		46.58	0.78	4.52
2752		44.78	0.61	4.28
2754		44.42	0.43	4.08
2756		44.31	0.44	3.97
2758		45.07	0.36	3.63
2760		46.72	0.44	3.98
2762		46.19	0.36	3.93
2764		48.58	0.2	2.84
2766		44.4	0.38	3.98
2768		45.11	0.59	4.31
2770		44.8	0.65	4.36
2772		44.96	0.75	4.58
2774		45.02	0.77	4.49
2776		45.84	0.69	4.3
2778		46.3	0.58	3.93
2780		46.13	0.36	3.91
2782		48.97	0.43	3.35
2784		44.97	0.62	4.29
2786		45.09	0.62	4.4
2788		44.62	0.69	4.55
2790		44.47	0.69	4.38
2792		47.36	0.68	4.09
2794		45.73	0.7	4.58
2796		45.29	0.63	4.29
2798		45.16	0.5	4
2800		46	0.72	4.34

Appendix A.5: The La Salle Basin data

Table A.5.7. Major and trace elements abundances (Al-normalized) for the La Salle Basin (core MD02-2549).

Depth (cm)	Al (%)	Si/Al	Fe/Al	Mn/Al	Mg/Al	Ca/Al	Na/Al	K/Al	Ti/Al	LOI (%)
0	6.1	2.84	0.50	0.186	0.22	1.70	0.19	0.27	0.045	20.79
71	6.0	2.88	0.50	0.029	0.22	2.01	0.06	0.28	0.043	20.84
151	6.5	2.94	0.45	0.022	0.22	1.66	0.06	0.29	0.045	19.74
231	6.3	2.93	0.51	0.029	0.23	1.87	0.06	0.27	0.046	20.86
311	7.3	2.85	0.45	0.016	0.22	1.07	0.06	0.27	0.045	17.36
391	7.3	3.01	0.47	0.016	0.26	1.00	0.07	0.31	0.046	16.27
471	6.7	3.06	0.49	0.017	0.22	0.91	0.06	0.31	0.046	15.79
551	7.5	3.22	0.50	0.012	0.30	0.50	0.07	0.32	0.051	12.62
631	7.4	2.92	0.48	0.018	0.30	0.88	0.08	0.35	0.049	15.21
711	6.9	3.06	0.50	0.026	0.40	1.06	0.09	0.37	0.052	15.98
791	7.6	2.80	0.48	0.020	0.24	0.93	0.07	0.30	0.045	15.70
871	7.6	2.90	0.42	0.021	0.26	0.87	0.08	0.31	0.047	15.63
951	6.5	3.15	0.51	0.036	0.37	0.95	0.12	0.32	0.052	15.44
1031	7.7	2.95	0.49	0.031	0.26	0.89	0.12	0.32	0.044	14.74
1111	7.6	2.84	0.44	0.025	0.21	1.01	0.08	0.28	0.043	16.31
1191	7.4	2.87	0.50	0.022	0.22	1.07	0.08	0.29	0.042	16.69
1371	8.0	2.78	0.41	0.032	0.20	0.78	0.07	0.29	0.042	15.56
1431	5.7	2.80	0.47	0.040	0.21	2.65	0.07	0.29	0.044	23.24
1511	7.4	2.75	0.46	0.016	0.19	0.93	0.07	0.27	0.043	16.27
1591	5.9	2.76	0.49	0.016	0.23	2.54	0.07	0.28	0.044	22.76
1661	6.5	3.18	0.46	0.013	0.33	0.83	0.09	0.29	0.048	16.30
1741	8.1	3.01	0.44	0.012	0.26	0.42	0.08	0.30	0.048	12.79
1821	8.2	2.98	0.41	0.009	0.23	0.44	0.07	0.32	0.050	12.49
1901	6.7	3.55	0.52	0.011	0.31	0.50	0.11	0.31	0.054	12.77
1981	7.9	3.17	0.44	0.013	0.25	0.48	0.10	0.31	0.051	12.64
2061	7.6	2.98	0.51	0.011	0.32	0.68	0.10	0.37	0.053	14.24
2141	6.9	3.56	0.50	0.012	0.35	0.64	0.09	0.31	0.054	14.46
2211	6.8	3.18	0.49	0.009	0.30	0.58	0.07	0.31	0.052	13.95
2291	7.9	3.03	0.48	0.009	0.27	0.50	0.07	0.31	0.051	13.48
2371	7.9	2.95	0.44	0.008	0.26	0.47	0.08	0.31	0.050	13.19
2454	7.3	3.14	0.54	0.009	0.33	0.78	0.08	0.35	0.054	14.94
2521	7.2	3.18	0.48	0.010	0.33	0.66	0.08	0.33	0.051	14.52
2581	8.0	3.06	0.49	0.008	0.27	0.55	0.08	0.32	0.051	13.69
2661	7.9	3.01	0.47	0.009	0.26	0.57	0.07	0.31	0.052	13.97
2731	7.8	3.02	0.44	0.009	0.29	0.57	0.07	0.33	0.052	14.02
2811	7.3	3.14	0.50	0.010	0.32	0.70	0.08	0.33	0.054	14.90
2891	7.3	2.98	0.49	0.009	0.31	0.63	0.06	0.34	0.054	14.38
2961	7.3	3.14	0.50	0.010	0.33	0.72	0.06	0.35	0.055	14.78
3041	8.0	2.98	0.49	0.008	0.25	0.47	0.07	0.31	0.051	13.21
3121	7.3	3.09	0.47	0.008	0.30	0.64	0.07	0.33	0.053	14.28
3191	7.8	2.99	0.49	0.009	0.30	0.62	0.07	0.36	0.054	14.17
3271	8.7	2.69	0.50	0.008	0.22	0.38	0.05	0.33	0.052	12.87
3351	7.4	3.05	0.45	0.008	0.34	0.74	0.07	0.36	0.053	15.19
3431	7.5	3.11	0.47	0.009	0.30	0.54	0.07	0.35	0.054	13.64
3511	7.6	3.00	0.52	0.009	0.31	0.72	0.07	0.34	0.054	14.78
3581	6.7	3.37	0.56	0.011	0.39	0.91	0.08	0.35	0.057	15.79
3651	7.8	3.02	0.46	0.007	0.29	0.58	0.08	0.36	0.051	14.17
3721	6.6	3.31	0.51	0.009	0.35	0.73	0.08	0.34	0.055	14.81
3770	7.8	2.97	0.48	0.009	0.27	0.60	0.08	0.33	0.051	14.49

Table A.5.7. Major and trace elements abundances (Al-normalized) for the La Salle Basin (core MD02-2549)

Depth (cm)	P/Al x104	Ba/Al x104	V/Al x104	Cr/Al x104	Co/Al x104	Ni/Al x104	Zn/Al x104	Cu/Al x104	U/Al x104
0	114.73	78.37	22.51	8.22	1.97	6.57	11.50	6.90	0.36
71	108.79	86.58	19.11	9.97	1.99	4.99	13.29	4.99	0.35
151	100.07	69.56	20.18	9.17	1.83	4.59	18.34	6.11	0.41
231	111.34	70.80	18.66	9.57	2.07	6.38	14.35	5.10	0.35
311	90.02	98.32	20.49	9.63	3.58	6.88	17.88	9.90	0.50
391	77.79	71.71	21.25	8.23	2.74	4.11	13.71	6.99	0.44
471	97.70	69.85	24.78	8.95	3.28	4.48	16.42	5.97	0.45
551	81.93	62.36	19.85	8.05	2.28	4.02	12.07	3.75	0.39
631	82.11	63.97	18.01	9.41	2.55	4.03	14.78	6.45	0.39
711	100.64	64.42	16.57	8.65	2.59	4.32	12.97	6.34	0.39
791	80.00	61.28	15.97	9.17	2.88	5.24	14.40	5.50	0.39
871	80.22	57.64	20.75	10.50	3.15	7.88	13.13	5.51	0.42
951	93.70	71.16	16.72	9.20	2.76	4.60	15.34	5.98	0.40
1031	79.67	65.85	16.82	7.82	3.13	5.22	11.74	6.78	0.27
1111	75.12	55.74	19.07	9.27	2.52	5.30	14.57	6.09	0.42
1191	76.90	69.40	17.21	9.49	1.90	5.42	13.55	5.15	0.42
1371	65.19	48.79	18.67	9.96	1.87	4.98	14.94	6.22	0.34
1431	137.82	63.33	18.60	10.53	1.93	7.02	15.79	6.67	0.42
1511	70.73	54.83	19.99	9.45	2.03	5.40	14.86	5.27	0.42
1591	140.77	81.32	17.83	10.19	1.53	5.09	13.58	4.92	0.36
1661	100.32	55.17	24.83	12.26	1.99	4.60	13.79	5.36	0.52
1741	80.47	57.66	21.64	9.83	1.97	4.92	12.29	4.18	0.36
1821	79.44	58.86	20.14	10.92	1.94	4.85	13.35	4.13	0.44
1901	97.86	75.04	19.43	10.46	1.79	4.48	8.97	4.93	0.43
1981	77.69	67.64	20.60	10.17	1.78	5.09	12.72	3.69	0.43
2061	80.56	59.07	18.86	10.55	1.98	5.27	13.19	3.43	0.47
2141	88.94	73.37	20.23	10.19	1.89	4.37	14.56	4.51	0.42
2211	89.35	72.98	17.84	10.24	2.05	5.85	13.16	4.53	0.42
2291	82.68	67.57	18.44	10.10	1.89	5.05	13.89	3.92	0.44
2371	77.69	58.36	20.47	10.17	2.16	5.09	12.72	4.07	0.41
2454	90.28	61.51	19.17	11.03	2.07	5.52	13.79	3.86	0.54
2521	84.89	61.96	20.01	11.11	1.95	5.56	13.89	4.31	0.43
2581	87.72	59.17	20.60	10.05	1.88	5.03	13.82	4.15	0.46
2661	77.53	60.53	21.06	10.15	1.78	5.08	12.69	4.19	0.44
2731	83.97	61.19	20.65	10.26	1.80	3.85	14.11	3.59	0.47
2811	78.02	60.78	21.59	9.63	1.79	5.50	13.75	4.13	0.47
2891	83.90	60.28	18.54	9.61	1.92	4.12	13.73	3.84	0.47
2961	83.17	60.58	18.24	9.53	1.77	4.08	12.25	3.54	0.52
3041	81.32	59.13	18.76	8.70	1.74	3.73	11.18	4.10	0.37
3121	77.34	56.98	18.95	9.54	1.77	4.09	12.27	3.68	0.48
3191	89.75	56.68	17.74	10.28	1.93	5.14	14.14	3.34	0.45
3271	80.06	48.84	16.97	9.17	1.72	4.59	12.61	3.32	0.42
3351	82.76	55.67	18.83	9.48	1.90	5.42	13.54	3.93	0.51
3431	86.92	57.10	17.66	10.62	1.86	5.31	11.95	3.85	0.45
3511	80.73	56.68	18.63	7.93	1.72	3.96	11.89	3.83	0.50
3581	91.77	61.58	18.32	10.51	1.95	6.01	13.52	4.21	0.57
3651	84.31	59.51	18.42	10.30	1.67	3.86	12.88	3.99	0.48
3721	92.65	62.63	18.80	9.10	1.82	4.55	12.13	3.79	0.53
3770	83.63	59.53	19.16	8.94	1.66	5.11	14.05	4.34	0.46

Appendix A.5: The La Salle Basin data

Table A.5.7. Major and trace elements abundances (Al-normalized) for the La Salle Basin (core MD02-2549)

Depth (cm)	Th/Al x104	Y/Al x104	La/Al x104	Ce/Al x104	Zr/Al x104	Hf/Al x104
0	1.33	3.29	4.26	9.02	19.88	0.54
71	1.41	3.16	4.44	9.12	19.78	0.60
151	1.39	3.21	4.40	9.23	15.90	0.49
231	1.39	3.19	4.50	9.34	16.58	0.51
311	1.39	3.30	4.85	10.36	16.36	0.47
391	1.22	3.43	4.11	8.87	18.10	0.47
471	1.36	3.28	4.55	9.64	17.16	0.52
551	1.22	3.35	3.90	8.43	18.24	0.47
631	1.37	3.23	4.70	10.27	16.80	0.48
711	1.43	3.46	5.07	11.05	17.87	0.55
791	1.40	3.40	4.78	10.55	15.19	0.48
871	1.39	3.28	4.70	10.31	17.07	0.42
951	1.53	3.53	5.12	11.32	20.86	0.61
1031	1.32	3.26	4.42	10.47	16.95	0.43
1111	1.46	3.18	4.69	10.22	21.19	0.61
1191	1.42	3.12	4.35	9.01	14.91	0.47
1371	1.39	2.99	4.38	9.21	15.19	0.46
1431	1.44	3.68	4.79	10.12	15.26	0.51
1511	1.43	3.11	4.57	9.70	15.80	0.49
1591	1.32	3.57	4.33	9.05	17.49	0.48
1661	1.49	3.06	4.98	10.14	19.16	0.58
1741	1.27	3.07	4.25	8.90	18.19	0.48
1821	1.33	3.03	4.44	9.31	17.35	0.50
1901	1.36	3.14	4.28	8.95	22.87	0.64
1981	1.28	3.18	4.23	8.75	17.93	0.81
2061	1.42	3.03	4.69	10.10	18.20	0.55
2141	1.41	3.20	4.57	9.72	22.71	0.67
2211	1.33	2.92	4.17	8.80	18.43	0.54
2291	1.44	3.16	4.42	9.32	18.69	0.58
2371	1.40	3.18	4.35	9.10	18.95	0.57
2454	1.45	3.45	4.91	10.29	19.72	0.59
2521	1.43	3.20	4.64	9.70	20.28	0.88
2581	1.41	2.89	4.45	9.33	17.84	0.55
2661	1.31	3.30	4.28	9.00	19.29	0.52
2731	1.37	3.34	4.48	9.33	19.37	0.58
2811	1.43	3.58	4.65	9.87	21.45	0.61
2891	1.44	3.43	4.66	9.72	19.36	0.59
2961	1.43	3.40	4.66	9.94	20.28	0.61
3041	1.22	3.11	3.84	8.03	18.39	0.48
3121	1.36	3.41	4.58	9.62	19.63	0.56
3191	1.44	3.60	4.79	10.17	19.41	0.59
3271	1.42	3.44	4.75	10.32	18.23	0.56
3351	1.41	3.39	4.63	9.94	20.05	0.60
3431	1.46	3.45	4.63	9.85	20.58	0.64
3511	1.33	3.57	4.40	9.21	19.69	0.53
3581	1.50	3.60	4.91	10.50	23.43	0.68
3651	1.47	3.22	4.69	9.89	18.93	0.59
3721	1.49	3.49	4.81	10.27	21.53	0.65
3770	1.41	3.19	4.65	9.77	18.01	0.54

Table A.5.8. Rare earth elements (REEs) concentrations for La Salle Basin (core MD02-2549).

Depth (cm)	La	Ce	Pr	Nd	Sm	Eu	Gd	Tb	Dy	Ho	Er	Tm	Yb	Lu
0	25.90	54.90	6.60	24.70	4.60	0.92	4.20	0.70	3.60	0.70	1.90	0.28	1.80	0.28
71	26.70	54.90	6.55	24.90	4.80	0.91	4.00	0.60	3.70	0.70	2.00	0.29	1.90	0.29
151	28.80	60.40	7.04	27.00	5.10	0.97	4.50	0.70	3.80	0.70	2.10	0.30	2.00	0.30
231	28.20	58.60	6.98	26.40	4.90	0.96	4.20	0.70	3.70	0.70	2.10	0.30	1.80	0.30
311	35.30	75.30	8.53	32.50	6.10	1.18	5.20	0.80	4.40	0.90	2.50	0.36	2.20	0.34
391	30.00	64.70	7.42	27.90	5.30	0.97	4.30	0.70	3.80	0.70	2.10	0.31	2.00	0.31
471	30.50	64.60	7.39	27.50	5.30	0.98	4.50	0.70	3.90	0.80	2.30	0.33	2.10	0.32
551	29.10	62.90	7.37	27.50	5.20	0.99	4.40	0.70	3.80	0.70	2.20	0.32	2.00	0.32
631	35.00	76.40	8.60	32.90	6.00	1.18	4.80	0.80	4.40	0.80	2.40	0.36	2.20	0.35
711	35.20	76.70	8.85	33.10	6.00	1.13	4.90	0.80	4.40	0.80	2.50	0.35	2.20	0.36
791	36.50	80.60	8.88	34.00	6.40	1.25	5.30	0.90	4.70	0.90	2.60	0.38	2.40	0.37
871	35.80	78.50	7.29	29.20	5.80	1.21	5.40	0.80	4.30	0.80	2.40	0.37	2.30	0.32
951	33.40	73.80	8.32	31.60	5.70	1.08	4.70	0.80	4.20	0.80	2.20	0.34	2.10	0.32
1031	33.90	80.30	8.40	31.10	5.60	1.07	4.60	0.70	4.00	0.80	2.20	0.32	2.00	0.30
1111	35.40	77.20	8.64	32.80	6.10	1.18	5.20	0.80	4.50	0.80	2.40	0.36	2.20	0.34
1191	32.10	66.50	7.81	29.60	5.50	1.05	4.60	0.80	4.20	0.80	2.30	0.34	2.20	0.33
1371	35.20	74.00	8.55	31.70	6.00	1.16	5.10	0.80	4.10	0.80	2.40	0.35	2.20	0.33
1431	27.30	57.70	6.75	26.50	5.00	1.00	4.40	0.70	3.80	0.70	2.20	0.32	2.00	0.28
1511	33.80	71.80	8.24	31.30	5.90	1.09	4.80	0.80	4.10	0.80	2.30	0.36	2.20	0.34
1591	25.50	53.30	6.22	23.60	4.50	0.88	3.90	0.60	3.40	0.60	1.90	0.28	1.70	0.28
1661	32.50	66.20	7.81	29.70	5.30	1.02	4.60	0.70	3.90	0.70	2.10	0.32	2.00	0.31
1741	34.60	72.40	8.42	31.70	5.90	1.11	4.80	0.80	4.10	0.80	2.30	0.34	2.10	0.33
1821	36.60	76.70	8.88	33.70	6.30	1.18	5.30	0.90	4.50	0.90	2.60	0.40	2.50	0.38
1901	28.60	59.90	7.10	27.40	5.20	1.05	4.60	0.70	4.00	0.80	2.30	0.35	2.20	0.33
1981	33.30	68.80	8.21	31.40	5.90	1.15	4.90	0.80	4.40	0.80	2.50	0.38	2.30	0.37
2061	35.60	76.60	8.85	33.80	6.10	1.20	5.20	0.90	4.60	0.90	2.60	0.40	2.50	0.38
2141	31.40	66.80	7.72	29.30	5.60	1.08	4.70	0.80	4.10	0.80	2.40	0.35	2.20	0.35
2211	28.50	60.20	7.01	26.50	5.10	0.97	4.20	0.70	3.70	0.70	2.10	0.31	1.90	0.31
2291	35.00	73.80	8.74	33.10	6.30	1.23	5.30	0.90	4.70	0.90	2.70	0.40	2.50	0.38
2371	34.20	71.60	8.36	31.90	6.00	1.15	5.10	0.80	4.30	0.80	2.50	0.38	2.30	0.36
2454	35.60	74.60	8.76	33.70	6.20	1.20	5.30	0.90	4.60	0.90	2.70	0.40	2.50	0.38
2521	33.40	69.80	8.20	31.00	5.70	1.12	4.90	0.80	4.20	0.80	2.40	0.37	2.30	0.36
2581	35.40	74.30	8.75	33.90	6.30	1.22	5.30	0.80	4.50	0.90	2.60	0.39	2.40	0.38
2661	33.70	70.90	8.40	32.20	6.10	1.12	5.20	0.90	4.40	0.80	2.50	0.38	2.40	0.36
2731	34.90	72.70	8.52	32.80	6.10	1.18	5.10	0.80	4.60	0.90	2.50	0.38	2.40	0.37
2811	33.80	71.80	8.47	32.50	6.00	1.13	5.00	0.80	4.50	0.90	2.50	0.38	2.40	0.36
2891	33.90	70.80	8.33	31.90	6.10	1.15	5.00	0.80	4.60	0.90	2.60	0.39	2.40	0.38
2961	34.20	73.00	8.69	33.40	6.40	1.20	5.30	0.90	4.70	0.90	2.70	0.41	2.50	0.39
3041	30.90	64.60	7.60	29.50	5.50	1.05	4.60	0.80	4.00	0.80	2.30	0.35	2.10	0.33
3121	33.60	70.60	8.33	31.50	5.90	1.13	4.90	0.80	4.40	0.90	2.50	0.38	2.30	0.36
3191	37.30	79.10	9.30	36.10	6.70	1.30	5.60	0.90	4.80	0.90	2.80	0.43	2.70	0.41
3271	41.40	90.00	10.60	40.30	7.50	1.44	6.30	1.10	5.60	1.10	3.10	0.47	2.90	0.44
3351	34.20	73.40	8.59	32.40	6.00	1.15	5.10	0.80	4.40	0.90	2.60	0.39	2.40	0.36
3431	34.90	74.20	8.73	33.70	6.30	1.17	5.30	0.90	4.70	0.90	2.80	0.42	2.50	0.39
3511	33.30	69.70	8.27	31.60	6.00	1.14	5.10	0.80	4.50	0.90	2.50	0.38	2.50	0.37
3581	32.70	69.90	8.28	32.20	5.90	1.12	5.10	0.80	4.40	0.90	2.60	0.38	2.40	0.36
3651	36.40	76.80	8.98	34.40	6.30	1.17	5.20	0.90	4.60	0.90	2.70	0.40	2.50	0.38
3721	31.70	67.70	7.95	29.80	5.60	1.10	4.80	0.70	4.20	0.80	2.50	0.37	2.30	0.36
3770	36.40	76.50	8.91	34.40	6.30	1.21	5.20	0.80	4.60	0.90	2.60	0.39	2.40	0.38

Appendix A.5: The La Salle Basin data

Curriculum Vitae

Jean Carlos MONTERO-SERRANO

Born on the 18th September 1982 in Caracas
Nationality: Venezuelan

Université Lille 1
Laboratoire Géosystèmes (UMR8157-CNRS)
Science de la Terre, bâtiment SN5
France-59655 Villeneuve d'Ascq cedex

Phone: +33 (0)3 20 43 44 87
Mobile: +33 (0)6 74 45 39 10

E-mail : jeanmontero@yahoo.es / jc.montero-serrano@ed.univ-lille1.fr

EDUCATION:

PhD in Geology (Geosciences, Ecology, Palaeontology and Oceanography): Université de Lille 1, France, October 2006- November 2009

Topic Research: *Sedimentary and paleoclimate dynamics of the Gulf of Mexico during the last glacial cycle.* **Supervisors:** Viviane BOUT-ROUMAZEILLES & Nicolas TRIBOVILLARD.

Magister Scientiarum in Geochemistry: Universidad Central de Venezuela, Venezuela, June 2007.

Topic Research: *Organic geochemistry of the Pedregoso Formation (Early Miocene), Falcón Basin, northwest of Venezuela.* **Supervisors:** Manuel MARTINEZ, Armelle RIBOULLEAU & Nicolas TRIBOVILLARD.

Licence in Geochemistry (equivalent to Bachelor degree): Universidad Central de Venezuela, Venezuela, December 2004.

Topic Research: *Determination, characterization and correlation of chemofacies, Cerro Pelado Formation (Miocene), Falcón Basin, Venezuela.* **Supervisors:** José Vicente GUTIERREZ, Manuel MARTINEZ & Carlos YANES.

Studies in Licence of Mathematics: Universidad Central de Venezuela, Venezuela, 3rd year approved.

COURSES:

- Introductory course: The statistical analysis of compositional data. Third compositional data analysis Workshop-CoDaWork'08, University of Girona, Spain, May 26-27, 2008.
- Sedimentology and marine geochemistry: Tools of paleoenvironmental studies. 30 years of the postdegree in Geochemistry. Caracas - Venezuela, November 8-12, 2004.
- AutoCAD 2000 Bidimensional. Instituto de Computación Gráfica Arts. Caracas - Venezuela, November, 2000.

PROFESIONAL EXPERIENCE:

Teaching assistant and research I (half time position):

Universidad Central de Venezuela. Faculty of Sciences. Coordination of Research, October 2005 - October 2006.
Coordinator of Research: Pío ARIAS.
Job description: Database operators, using as tool support the "COORDIN" software, based in object-oriented programming (Visual BASIC and MSQL).

Auxiliary of research

Universidad Central de Venezuela. Earth Sciences Institute. Project CVG TECMIN-UCV, May - October, 2005.
Coordinator of the project: Tommaso TOSIANI & Armado RAMÍREZ.
Job description: *Determination of chemical components in soils developed on limestones, Monagas State, Venezuela*.

Auxiliary of research

Universidad Central de Venezuela. Earth Sciences Institute. Project INTEVEP-UCV, January - May, 2005.
Coordinator of the project: Carlos YANES & Armado RAMÍREZ.
Job description: *Study of line bases environmental in the Deltana Platform, northeast of Venezuela: chemical components of the sediments*.

Professional training in geology

Gold Reserves of Venezuela. Mining Brisas of Cuyuní, Km-88, Bolívar State, Venezuela, September - October, 2003.

Supervisors: José FIRVIDA & Andrés GARCIA.
Job description*: Geological study and environmental monitoring of the mining Brisas of Cuyuní Km-88, Bolívar State, Venezuela.*

TECHNICAL AND ANALYTICAL EXPERIENCES:

- Sample preparation and analyses of major and trace element concentrations by inductively coupled plasma – optical emission spectrometer (ICP-OES) for paleoenvironmental studies in sedimentary sequences.
- Molecular analysis of sedimentary organic matter by: (1) Gas chromatography-mass spectrometry (GC-MS), identifications of molecular markers, and (2) Rock-Eval 6 pyrolysis (vinci technologies).
- Analysis of the carbon (UIC Coulometrics) and sulphur concentrations (LECO SC-432).
- Sedimentological analysis: laser granulometry (MALVERN MASTERSIZER 2000) and semi-quantification of clay minerals by X-ray diffraction (XRD).
- Rock magnetism analysis: measurement of magnetic susceptibility values (KLF-4 AGICO).
- Pick foraminifera for radiocarbon dating.
- Core description (sediment and rocks).
- Geologic mapping and sampling.
- Statistical analysis geo-environnementales variables (compositional data).

COMPUTER EXPERIENCE:

Operating system: Windows
Programming languages: R-code Statistical packages: MVSP, S-PLUS, STATGRAPHICS Plus, STATISTICAL
Mathematical packages: MAPLE, MATHEMATICAL
Design packages: CorelDRAW, Adobe Illustrator, AutoCAD
Mapping software: SURFER V8
Microsoft Office Applications

AWARDS:

- Programme Alßan, high level scholarship programme, N° E06D100913VE, scholarship for PhD studies, October 2006 - September 2009.
- Universidad Central de Venezuela student scholarship, September 1999 – 2004

INTERNATIONAL PUBLICATIONS:

P.1 **Montero-Serrano Jean Carlos**, Bout-Roumazeilles Viviane, Tribovillard Nicolas, Sionneau Thomas, Riboulleau Armelle, Bory Aloys, Flower Benjamin. Sedimentary evidence of deglacial megafloods in the northern Gulf of Mexico (Pigmy Basin). Quaternary Science Reviews (in press).

P.2 **Montero-Serrano Jean Carlos**, Bout-Roumazeilles Viviane, Sionneau Thomas, Tribovillard Nicolas, Bory Aloys, Flower Benjamin, Riboulleau Armelle, Meckler Anna Nele. Changes in precipitation regimes over North America during the Holocene as recorded by mineralogy and geochemistry of Gulf of Mexico sediments. Global and Planetary Change (under review).

P.3 **Montero-Serrano Jean Carlos**, Martínez Manuel, Riboulleau Armelle, Tribovillard Nicolas, Márquez Gonzalo, Gutiérrez José Vicente. Assessment of the oil source-rock potential of the Pedregoso Formation (Early Miocene) in the Falcón Basin of Northwestern Venezuela. Marine and Petroleum Geology (in revision).

P.4 Sionneau Thomas, Bout-Roumazeilles Viviane, Flower Benjamin, Bory Aloys, Tribovillard Nicolas, Kissel Catherine, Van Vliet-Lanoe Brigitte, **Montero-Serrano Jean Carlos.** On the provenance of freshwater pulses in the Gulf of Mexico during the last deglaciation: Evidence from grain size and clay mineralogy. Quaternary Research (in revision).

P.5 **Montero-Serrano Jean Carlos**, Palarea-Albaladejo Javier, Martín-Fernández Josep, Martínez Manuel, Gutiérrez José Vicente. Multivariate analysis applied to chemostratigraphic data: identification of chemofacies and stratigraphic correlation. (in revision).

P.6 **Montero-Serrano Jean Carlos**, Martínez Manuel, Tribovillard Nicolas, Riboulleau Armelle, Garbán Grony, 2009. Geochemical behavior of molybdenum and its isotopes in the sedimentary environment - A bibliographic review. Revista de Biología Marina y Oceanografía 44(2): 263-275.

P.7 Tribovillard Nicolas, Bout-Roumazeilles Viviane, Sionneau Thomas, **Montero-Serrano Jean Carlos**, Riboulleau Armelle, Baudin François, 2009. Does a strong pycnocline impact organic-matter preservation and accumulation in an anoxic setting? The case of the Orca Basin, Gulf of Mexico. C.R. Geoscience 341: 1-9.

P.8 Tribovillard Nicolas, Bout-Roumazeilles Viviane, Algeo Thomas, Lyons Timothy, Sionneau Thomas, **Montero-Serrano Jean Carlos**, Riboulleau Armelle, Baudin François, 2008. Paleodepositional conditions in the Orca Basin as inferred from organic matter and trace metal contents. Marine Geology 254: 62-72.

PUBLICATIONS IN PREPARATION:

P.P.1 **Montero-Serrano Jean Carlos,** Bout-Roumazeilles Viviane, Tribovillard Nicolas, Sionneau Thomas, Bory Aloys, Flower Benjamin, Riboulleau Armelle. Mineralogical records of the atmosphere-ocean-continent interactions in the northern Gulf of Mexico during the present and last interglacial period. (in preparation).

COMMUNICATIONS IN COLLOQUIA:

C.1 **Montero-Serrano Jean Carlos**, Martínez Manuel, Gutiérrez José Vicente, Riboulleau Armelle, Tribovillard Nicolas. Geoquímica de la Formación Pedregoso (Mioceno Temprano), Cuenca de Falcón-Venezuela: condiciones de paleoxigenación, origen y madurez de la materia orgánica. IX Congreso Geológico Venezolano. Caracas, Venezuela, Octobre 2007.

C.2 Martínez Manuel, **Montero-Serrano Jean Carlos**, Gutiérrez José Vicente, González Cesar. Geoquímica Orgánica de las unidades sedimentarias de la Cuenca Central de Falcón. IX Congreso Geológico Venezolano. Caracas, Venezuela, Octobre 2007.

C.3 **Montero-Serrano Jean Carlos**, Martínez Manuel, Gutiérrez José Vicente, Riboulleau Armelle, Tribovillard Nicolas. Geochemistry of the Pedregoso Formation (Early Miocene), Falcon Basin, Venezuela: Paleoredox conditions, origin and maturity of organic matter (P257-WE). 23rd International Meeting on Organic Geochemistry, Torquay, Royaume-Uni, September 2007.

C.4 **Montero-Serrano Jean Carlos**, Martínez Manuel., Gutiérrez José Vicente, Riboulleau Armelle, Tribovillard Nicolas. Distribution of organic matter thermal maturity through the Oligocene-Miocene Central Basin of Falcon, northwestern Venezuela (P5-MO). 23rd International Meeting on Organic Geochemistry, Torquay, Royaume-Uni, September 2007.

C.5 **Montero-Serrano Jean Carlos**, Gutiérrez José Vicente, Martínez Manuel, Barráez Daniel. Application of multivariate methods to identify and correlate chemofacies in the Cerro Pelado Formation (Miocene), Falcon basin, Venezuela. 30 years of the postdegree in Geochemistry. Caracas, Venezuela, 8-12 November, 2004.

LANGUAGES:

Spanish: native language.
French: good knowledge.
English: good knowledge.

REFEREES:

Viviane BOUT-ROUMAZEILLES
Université Lille 1
Laboratoire Géosystèmes (UMR 8157 CNRS)
UFR des Sciences de la Terre – bâtiment SN5
59655 Villeneuve d'Ascq cedex, France
e-mail : viviane.bout@univ-lille1.fr
Phone : +33 (0)3 20 43 43 95 Fax. + 33 (0)3 20 43 49 10

Manuel MARTÍNEZ
Universidad Central de Venezuela
Facultad de Ciencias, Instituto de Ciencias de la Tierra
Caracas, 3895, 1010-A, Venezuela
e-mail : manmarti@gmail.com
Phone : +58 (0) 212 605 14 30 / +58 (0) 212 605 15 71

Nicolas TRIBOVILLARD
Université de Lille 1
Laboratoire Géosystèmes (UMR 8157 CNRS)
UFR des Sciences de la Terre – bâtiment SN5
59655 Villeneuve d'Ascq cedex, France
e-mail : nicolas.tribovillard@univ-lille1.fr
Phone : +33 (0)3 20 43 41 00 Fax. + 33 (0)3 20 43 49 10

Aloys BORY
Université de Lille 1
Laboratoire Géosystèmes (UMR 8157 CNRS)
UFR des Sciences de la Terre – bâtiment SN5
59655 Villeneuve d'Ascq cedex, France
e-mail : aloys.bory@univ-lille1.fr
Phone : +33 (0)3 20 43 41 00 Fax. + 33 (0)3 20 43 49 10

Sedimentary and paleoclimate dynamics of the Gulf of Mexico during the last glacial cycle

Abstract

The objectives of this thesis are to study the sedimentary features of some basins of the Gulf of Mexico (Pigmy and La Salle basins) in order to reconstitute the variability of the detrital input via the Mississippi River during the last climatic cycle. An integrated approach coupling mineralogy, granulometry, and geochemistry (inorganic and organic), within a precise chronostratigraphic framework, allows to progress in the understanding of the relations between the mid- and high-latitude climatic mechanisms and the subtropical hydrology, as well as to propose synoptic models of the ocean-atmosphere coupling. The contrasting mineralogy of the zones drained by the catchment system of the Mississippi River watershed allows constraining the continental zones which will successively feed the sedimentation of the Gulf of Mexico. The modifications of the detrital sources revealed for the last climatic cycle enabled (1) to track down the localization of the zones of destabilization of the southern margin of the Laurentide Ice Sheet and the sequence of sedimentary processes during the freshwater discharges, which characterized the last deglaciation, (2) to highlight modifications of the precipitation front which were associated with episodes of large Mississippi River floods during interglacial times, and therefore, to deduce information on the hydrological regime, and (3) to suggest schematic models of meridian transfer of moisture contrasted during interglacial stages 1 and 5e, suggesting an appreciable difference in the atmospheric configurations. The confrontation of these results with other paleoclimatic records allowed to propose simple models of the atmosphere-ocean-continent interactions recorded in the Gulf of Mexico, which are based on the modifications of both the atmospheric configurations (Jet Stream and ITCZ) and oceanic (extension of Atlantic Warm Pool). These models confirm the major role of the atmosphere as a vector of rapid climatic variability.

Keywords: Gulf of Mexico, Pigmy Basin, La Salle Basin, Pleistocene, Holocene, Laurentide Ice Sheet, Mississippi River, clay mineralogy, geochemistry.

Dynamique sédimentaire et paleoclimate du Golfe du Mexique au cours du dernier cycle glaciaire

Résumé

Les objectifs de cette thèse sont d'étudier la sédimentation dans des sous bassins privilégiés du Golfe du Mexique (Bassin de Pigmy et de La Salle) afin de reconstituer la variabilité des apports détritiques via le fleuve Mississippi au cours du dernier cycle climatique. Une approche intégrée couplant minéralogie, granulométrie, géochimie élémentaire et organique, dans un cadre chronostratigraphique précis, a permis de progresser dans la compréhension des relations entre les mécanismes climatiques de moyenne et haute latitude et l'hydrologie du domaine subtropical et de proposer des schémas d'interprétation du couplage océan-atmosphère. La minéralogie contrastée des zones en érosion drainées par le système fluviatile du bassin versant du Mississippi permet de contraindre les zones continentales qui vont successivement alimenter la sédimentation du Golfe du Mexique. Les modifications des sources détritiques ainsi mises en évidence au cours du dernier cycle climatique ont permis (1) de contraindre la localisation des zones de déstabilisation de la marge Laurentide et l'enchaînement des processus sédimentaires lors des décharges d'eau douce qui caractérisent la dernière déglaciation, (2) de mettre en évidence une modification du front de précipitations associée aux périodes de mégacrue du Mississippi lors des périodes interglaciaires et d'en déduire des informations sur le régime hydrologique et (3) de suggérer des schémas de transferts méridiens d'humidité contrastés lors des stades interglaciaires 1 et 5e, suggérant des configurations atmosphériques sensiblement différentes. La confrontation de ces résultats avec d'autres données paléoclimatiques a alors permis de proposer plusieurs modèles simples pour les interactions océan-atmosphère dans le Golfe du Mexique, basés sur les modifications des configurations atmosphériques (Jet Stream et ITCZ) et océaniques (extension de l'Atlantic Warm Pool) et confirme le rôle majeur de l'atmosphère comme vecteur de la variabilité climatique rapide.

Mots clés: Golfe du Mexique, Pigmy Bassin, La Salle Bassin, Pléistocène, Holocène, calotte de glace Laurentide, fleuve Mississippi, minéralogie des argiles, géochimie.